Department of Spatial Sciences

Precise Multi-GNSS Point Positioning: Theory, Algorithm and Data Analysis

Amir Khodabandeh

This thesis is presented for the Degree of
Doctor of Philosophy
of
Curtin University

March 2015

DECLARATION

To the best of my knowledge and belief this thesis contains no material previously published by any other person except where due acknowledgment has been made. This thesis contains no material which has been accepted for the award of any other degree or diploma in any university.

Amir Khodabandeh
20 March 2015

ABSTRACT

Precise positioning with a global navigation satellite system (GNSS) has found widespread usage in various spatial and Earth science disciplines, such as those in navigation, surveying, geodesy, geophysics, and atmospheric sciences. The basic idea of realizing sub-decimetre- and centimetre-level positioning is to overcome the limited accuracy of the broadcast satellite orbit/clock products and environmental/ instrumental effects through providing external network-derived corrections aiding a single-receiver user. The corrections are obtained by processing GNSS observations of the network stations, thereby representing (adjusted) observations of a single (virtual) point. These corrections can be presented either in the form of observations, or in the form of parameters with physical characteristics. The former approach develops the concept of network-RTK (real-time kinematic) positioning, whereas the latter one establishes the idea of precise point positioning (PPP) and its integer ambiguity resolution-enabled variant, namely, the PPP-RTK. That the single-receiver user needs to incorporate the network-derived corrections into its observation equations highlights the fact that single-receiver precise GNSS-based positioning is always categorized as a *relative* technique, irrespective of the underlying approach providing the corrections. In this thesis we study the principles and intricacies of the new state-of-the-art precise positioning technique, the PPP-RTK. Both its network- and user-components are discussed. Special attention is paid to the estimable satellite phase biases (SPBs), the key parameters realizing single-receiver integer ambiguity resolution. The SPB determination method and real-world multi-GNSS results are presented. The results are then supported by characterizing the role of network integer ambiguity resolution in the precision improvement of the corrections. The dependency of the stated improvement on the number of network stations as well as on the network's geometrical strength is pointed out. Represented as dynamic systems, both the network and user systems of observation equations are to be properly adjusted and filtered over time, in a minimum-mean-squared-error (MMSE) sense. We therefore finally introduce a recursive linear MMSE filter that is capable of processing dynamic systems with unknown state-vector means in general, and the observation equations of the network- and user-components in particular.

ACKNOWLEDGEMENTS

I would like to express my deepest gratitude to my supervisor, Prof Peter J.G. Teunissen, for his professional guidance and scientific support. His strong views on the Estimation Theory and the GNSS Observation Modelling, together with his pioneering research on the mixed-integer models, have inspired me to pursue my interest in these very fields.

I am also thankful to my associate supervisor, Dr Dennis Odijk, for his technical advice and software support. His encouragement and friendly behaviour are highly appreciated.

My appreciation is also forwarded to my teacher, Dr Ali Reza Amiri-Simkooei, and to my colleagues at the Curtin GNSS Research Centre, Dr Nandakumaran Nadarajah, Dr Bofeng Li, Dr Andrea Nardo, Dr Robert Odolinski, Dr Baocheng Zhang, Dr Wei Li, Dr Noor Raziq, Dr Boris Padovan, Dr Paolo Zoccarato, Mr. Balwinder Sing Arora, and Miss Safoora Zaminpardaz for their support.

Finally, I would like to thank my family, especially my parents, for being so patient during this period that I have been abroad.

LIST OF PUBLICATIONS

This PhD thesis by publication comprises 1 single-author, 4 first-author, 4 second-author, and 2 third-author peer-reviewed publications. These articles have been published/accepted in the following journals and proceedings. The reader may be referred to Appendix A for copyright authorization, Appendix B for signed declarations for author contributions to the co-authored publications, and Appendix C for the proof that the publications are all peer-reviewed and have been published/accepted.

1. Teunissen P.J.G. and **Khodabandeh A.** (2014a). Review and Principles of PPP-RTK Methods. Journal of Geodesy, Springer, doi: 10.1007/s00190-014-0771-3.

2. **Khodabandeh A.** and Teunissen P.J.G. (2015). An Analytical Study of PPP-RTK Corrections: Precision, Correlation and User-Impact. Journal of Geodesy, doi: 10.1007/s00190-015-0838-9.

3. **Khodabandeh A.** (2014). Array-aided single-differenced satellite phase bias determination: methodology and results. ION GNSS+, 27:2523–2532. The Institute of Navigation, Florida, USA.

4. **Khodabandeh A.** and Teunissen P.J.G. (2014a). Array-based satellite phase bias sensing: theory and GPS/BeiDou/QZSS results. Meas. Sci. Technol., 25,095801 (11pp). UK.

5. Odijk D., Teunissen P.J.G. and **Khodabandeh A.** (2014). Single-frequency PPP-RTK: theory and experimental results. International Association of Geodesy Symposium (IAG), 139:167–173, Springer.

6. Odijk D., Teunissen P.J.G. and **Khodabandeh A.** (2013). Galileo IOV RTK positioning: standalone and combined with GPS. Survey Review, Maney Publishing. UK.

7. Nadarajah N., **Khodabandeh A.** and Teunissen P.J.G. (2015). Assessing the IRNSS L5-signal in combination with GPS, Galileo, and QZSS L5/E5a-signals for positioning and navigation. GPS Solutions, Springer, doi: 10.1007/s10291-015-0450-8.

8. Teunissen P.J.G. and **Khodabandeh A.** (2014b). Do GNSS parameters always benefit from integer ambiguity resolution? a PPP-RTK Network Scenario. ION GNSS+, 27:590–600. The Institute of Navigation, Florida.

9. **Khodabandeh A.** and Teunissen P.J.G. (2014b). Single-Epoch GNSS Array Integrity: an Analytical Study. International Association of Geodesy Symposium (IAG), Springer, Accepted for publication.

10. Teunissen P.J.G. and **Khodabandeh A.** (2013) BLUE, BLUP and the Kalman filter: some new results. J Geod 87(5):461–473.

11. **Khodabandeh A.** and Teunissen P.J.G. (2014c). A recursive linear MMSE filter for dynamic systems with unknown state vector means. International Journal on Geomathematics, 5:17–31, Springer.

TABLE OF CONTENTS

1 INTRODUCTION

1. 1 Background

Precise positioning with a global navigation satellite system (GNSS) has found widespread usage in various spatial and Earth science disciplines, such as those in navigation, surveying, geodesy, geophysics, and atmospheric sciences. The basic principle of GNSS-based positioning is to measure distances from a to-be-positioned point to satellites of which their position and biases in their signal transmission time are given through broadcast orbits/clocks (Teunissen and Kleusberg 1998, Hofmann-Wellenhof et al. 2008).

The positioning measurement setup is structured by the code observables and\or by the carrier-phase observables. While the code observables—of decimetre level precision—can be used to estimate the position of a single-receiver user in a *real-time* manner, the very precise carrier-phase observables—of millimetre level precision—cannot take a truly active part in estimating the user's position, unless a rather long observational time takes place, see e.g. Leandro et al. (2011) or van Bree and Tiberius (2012). This well-known limitation of the carrier-phase observables stems from two fundamental issues of the GNSS. The first issue lies in the nature of the carrier-phase observables themselves, as they are biased by time-constant ambiguous cycles, namely the ambiguities. In the presence of ambiguities, only the *time-differenced* components of the carrier-phase biases do contribute to positioning, meaning that at least two observational epochs are needed. That the two epochs of the carrier-phase measurements are still *not* capable of substantially contributing to positioning is addressed by the second issue which is described as follows. The geometry of the GNSS satellites, with respect to the receiver's position, is known to change slowly in time (Teunissen 1997). Since the time-differenced carrier-phase measurements are functionally linked to the unknown position by the time-differenced receiver-to-satellite line-of-sight vectors, a long time-span is therefore needed for the time-differences of these vectors to increase, thereby strengthening the stated functional link.

After a sufficient long observational time-span, the very precise phase observables would therefore govern the positioning estimation procedure. Under this assumption, one wonders whether precise positioning, at the sub-decimetre level,

gets feasible or that still some contributing factors are missing. Unfortunately, because of the limited accuracy of the broadcast orbits (up to several meters) and clocks (up to 2 meters), the spectacular precision of the carrier-phase observables would not be taken advantage of (accuracy is quoted from http://igscb.jpl.nasa.gov/components/ prods.html). The limited accuracy of the broadcast products can, however, be mitigated by 1) making use of high spatial dependency of the orbital/clock biases or by 2) a-priori estimating them. The first approach suggests employing an aiding single receiver (or a network of receivers) that are not-too-far from the user. Since not-too-far receivers experience orbital biases of almost the same magnitude, forming differences between observations of the user and those of the network largely reduces the orbital biases and eliminates the clock biases. This builds up the core idea of the GNSS relative positioning techniques, as the user, within this approach, positions itself with respect to the position of the network stations (Blewitt 1989, Frei and Beutler 1990, Teunissen 1993). Upon taking the second approach on the other hand, one utilizes GNSS observations of an external network to estimate the orbital/clock biases and provides the user with improved orbits/clocks. This builds up the core idea of the precise point positioning (PPP) technique, as the user makes use of its own undifferenced observations, but then corrected, among others, by network-derived precise orbital/clock biases (Heroux and Kouba 1995, Zumberge et al. 1997). This approach is deemed to be more favourable, since a) the restriction of not-too-far inter-station distances between the user and the network stations need not necessarily be imposed; b) fewer number of corrections generally need to be sent to the user. The latter is the case since sending the orbital/clock parameters—with knowledge of their behaviour and stability over time—appears to be more efficient than presenting *unlinked-in-time* observations of the network stations as it is often done in the relative positioning techniques (van der Marel 1998).

Despite the aforementioned advantages of the PPP technique, its problem of long observational time-span remains unresolved, thus giving the relative positioning techniques enough room to compete. In fact, the relative positioning techniques are equipped with two important characteristics enabling the possibility of performing *fast* precise positioning. Firstly, forming differences between the observations remove the non-integer satellite phase biases. This, namely, means that the double-differenced (DD) carrier-phase observables are biased by *integer-valued* ambiguities.

Since these unknown DD ambiguities are constrained to be integer, the moment one resolves them, the DD carrier-phase observables act as very precise code observables, realizing fast precise positioning. Secondly, forming differences largely reduces the impact of the differential atmospheric delays on the measurement, as they are highly correlated in space. For short-to-medium inter-station distances, one can then impose constraints on the differential atmospheric parameters, thus strengthening the measurement setup, thereby increasing the probability of correctly resolving the integer DD ambiguities. These form the principles of the network real-time kinematic (RTK) positioning techniques (Frei and Beutler 1990, Teunissen 1993, 1995).

Therefore, while the network PPP outperforms the network-RTK in the sense of providing fewer corrections, the PPP user requires, compared to the RTK-user, a much longer observational time-span—longer than 30 minutes to attain sub-decimetre accuracy (van Bree and Tiberius 2012). One is thus motivated to come up with an idea of *combining* both the PPP and the RTK techniques so that the stated limitations get tackled. This gives rise to a new positioning technique, namely, the PPP-RTK.

1. 2 Literature review

PPP-RTK is integer ambiguity resolution-enabled PPP (Wubbena et al. 2005; Mervart et al. 2008; Teunissen et al. 2010). As stated earlier, with PPP, precise satellite orbits and clocks are provided to enable single-receiver users to compute their positions with decimetre or centimetre accuracy. PPP-RTK extends the PPP corrections by further providing the user with information about the *satellite phase and code biases*. This additional information is then used to tackle the PPP long convergence time by recovering the integerness of the user's ambiguities. Once the user's ambiguities become of an integer nature, one then aims to resolve them, thus speeding up the PPP convergence time. How much time the user needs to be able to successfully fix the recovered ambiguities to their integers largely depends on the strength of the user's measurement setup, e.g. on information about the ionospheric parameters and/or the number of frequencies/visible satellites, see e.g. Teunissen and Khodabandeh (2014a).

Being the key parameters recovering the user's integer ambiguities, satellite phase and code biases would thus take a leading role in the concept of single-receiver integer ambiguity resolution (IAR) and therefore in PPP-RTK. To determine these biases through the network's measurement setup, one is, however, confronted with difficulties in distinguishing them from the integer ambiguities of the carrier-phase observables. The reason lies in the fact that the coefficients, linking these biases and ambiguities to the network's observation equations, experience a *linear dependency*, meaning that the GNSS observables are not capable of determining them in an absolute sense (Teunissen et al. 2010). Instead, linear combinations of the satellite phase/code biases and the ambiguities can be estimated and therefore play the role of their absolute counterparts.

Because of the stated linear dependency between the integer ambiguities and satellite phase biases, several contributions suggest estimating an estimable combination of them as real-valued ambiguities, and then representing the *fractional part* of these ambiguities as the final product recovering the integerness of the user's ambiguities, see e.g. Ge et al. 2008, Geng et al. 2010, Li et al. 2013b. As the first attempt to calibrate the fractional phase biases, Gabor and Nerem (1999, 2002) studied the fractional parts of the between-satellite single-differenced float ambiguities of a large network of receivers. To avoid code multipath effects, they proposed averaging the factional parts of ambiguities over all the network stations. In a similar way, Ge et al. (2008) made use of the international GNSS service (IGS) network stations to estimate the fractional cycle biases (FCBs) and to apply PPP ambiguity resolution, where they also applied station-averaging to reduce the impact of mis-modelled effects. They concluded that the FCBs behave rather stable within 15 minute-intervals, whereas the wide-lane (i.e. between-frequency differenced) FCBs are very stable in time (less than 0.1 cycle change per day). Motivated by the poor precision of the narrow-lane FCBs (i.e. the FCBs accompanied by the narrow-lane wavelength), Geng et al. (2012) proposed improved narrow-lane FCBs that follow by applying network IAR. They argued that the precision of the narrow-lane FCBs gets better after network IAR. Instead of computing the fractional part of the estimated real-valued ambiguities, Bertiger et al. (2010) proposed collecting these ambiguities themselves as corrections for the user. The PPP user can then choose the ambiguities of its preferred station to form differences with its own real-valued ambiguities, thus realizing integer-valued DD ambiguities.

On the other hand, there are contributions that suggest introducing new clock parameters for the carrier-phase observables different from the code clock parameters (de Jong 1998, Laurichesse and Mercier 2007, Collins 2008, Loyer et al. 2012). Within this re-parametrization, a linear combination of the phase and code biases as well as the integer ambiguities are lumped with the carrier-phase clocks. The PPP user would then, next to the orbits and the code clocks, be provided with the stated carrier-phase clocks, recovering the integerness of its ambiguities. Of these types of models meant for PPP-RTK, the integer recovery clock (IRC) model (Laurichesse and Mercier 2007, Laurichesse et al. 2009) and the decoupled satellite clock (DSC) model (Collins 2008, Collins et al. 2008) are quite well-known in the literature.

The stated linear dependency between the GNSS parameters can be well formulated by S-system theory (Baarda 1973, Teunissen 1985) dealing with the *rank-deficient* system of observation equations. The theory allows one to characterize the relation between the estimable combined parameters and the original inestimable parameters. Examples of the theory's applicability to GNSS network undifferenced observation equations can be found in de Jong (1998) and Odijk (2002). The theory's applicability to PPP-RTK is originally introduced by Teunissen et al. (2010), followed further by the contributions of Zhang et al. (2011) and Odijk et al. (2012, 2014b). They showed that the interpretation of the estimable satellite phase biases is such that—once applied—the user's recovered ambiguities automatically become of a DD nature, thus getting integer-valued.

As the final aim of all the PPP-RTK methods discussed above is to recover the integerness of the PPP user's ambiguities, one may infer that the underlying models of the methods are equivalent in principles. Indeed there are some comparative studies between some of these PPP-RTK methods, see e.g. Geng et al. (2010) or Shi and Gao (2013). The stated contributions however, do not make a distinction between the *underlying models* and the *estimation methods*. They therefore come up with a conclusion that the methods studied are theoretically equivalent and will provide equivalent results. This finding is echoed in the publications of, for instance, Bisnath and Collins (2012, p. 378), Shi (2012, p. 89), Li et al. (2013a, p.4), and Zhang and Li (2013, p. 580). The recent contribution of Teunissen and Khodabandeh (2014a) shows, however, that there are noticeable differences between estimation methods employed in the literature (see Chapter 2).

1. 3 Thesis objectives and outline

The main objective of this thesis is to establish a framework developing the principles and intricacies of the new state-of-the-art precise positioning technique, namely, the PPP-RTK. The thesis is considered as one of the first PhD dissertations concerning the multi-GNSS, multi-frequency PPP-RTK concept. Both the network-component and the user-component are discussed. We make use of $\mathcal{S}$-system theory to identify the interpretation of the estimable parameters of different PPP-RTK models. Given the same underlying rank-deficiency of the models, it is shown, for the first time, that the information content in the PPP-RTK corrections of different models must be the same. This implies that the corrections of different models are all related through *one-to-one* transformations (cf. Table 1 in Chapter 2). We show that PPP-RTK is a relative technique through characterizing the role of estimable clocks and phase biases, respectively, as *positional* and *ambiguity* linkages. Next to the models, we also discuss the estimation procedure of the PPP-RTK. Four different estimators of the corrections are presented. They allow one to show how the corrections apply to different user models and why some of the proposed estimation methods cannot be accepted as proper PPP-RTK methods. The estimation procedure is followed by a *closed-form* expression of the (co)variance matrices of the PPP-RTK corrections.

Special attention is paid to the estimable satellite phase biases (SPBs), the key parameters realizing single-receiver integer ambiguity resolution. The SPB determination method and real-world multi-GNSS results are presented. It is shown, for the first time, how the estimable SPBs can be determined by only one *single*-antenna and how they are linked to the well-known code multipath equations. The concept of the array-based SPB determination is introduced in which the role of an external network is taken by an array of antennas mounted on rigid platforms. The results are then supported by characterizing the role of network integer ambiguity resolution in the precision improvement of the corrections. The dependency of the stated improvement on the number of network stations as well as on the network's geometrical strength is pointed out.

Since both the network and user systems of observation equations are to be properly adjusted and filtered over time, their corresponding multi-epoch models need to be represented as a *dynamic system*. Within this context, the unknown estimable parameters would then play the role of the associated *state-vector*. In the

literature, the well-known Kalman filter, as a linear minimum-mean-squared-error (MMSE) filter, is often used to obtain the estimates. The basic assumption of the Kalman filter however, states that the mean of the state-vectors must be known. This is why in the derivation of the Kalman filter, the mean of the initial state-vector is assumed given, see e.g., Sorenson (1966, p. 222), Kailath (1974, p. 148), Maybeck (1979, p.204), Anderson and Moore (1979, p. 15), Stark and Woods (1986, p. 393), Bar-Shalom and Li (1993, p. 209), Kailath et al. (2000, p. 311), Christensen (2001, p. 261), Simon (2006, p. 125), Grewal and Andrews (2008, p. 138). To tackle this shortcoming, we therefore develop a new recursive linear MMSE filter that is capable of processing dynamic systems with unknown state-vector means in general, and the observation equations of the network- and user-components in particular. The new filter encompasses the standard Kalman filter, since it specializes to the Kalman filter in case the state-vector means are known.

The structure of the thesis is organized by the following chapters including papers that cover the objectives discussed below. The conclusions of each chapter can be found in the respective papers. The thesis conclusions can be found at the end of this chapter as to bind the publications into a collective piece of work.

Chapter 2: Review and Principles of PPP-RTK methods

This chapter is covered by the following publication:

- Teunissen P.J.G. and Khodabandeh A. (2014a). Review and Principles of PPP-RTK Methods. Journal of Geodesy, Springer, doi: 10.1007/s00190-014-0771-3.

This paper is the core contribution of the thesis. A framework developing the principles and intricacies of PPP-RTK is presented. This is accompanied by a review of different mechanizations that have been proposed in the literature. By application of $\mathcal{S}$-system theory, the estimable parameters of the different methods are identified and compared. It is shown that PPP-RTK is a relative technique for which the ‘single-receiver user’ integer ambiguities are in fact double-differenced ambiguities. The transformational links between the different methods and their PPP-RTK corrections are given, thereby showing how different PPP-RTK methods can be mixed between network and users. Four different estimators of the PPP-RTK

corrections are presented. It is shown how they apply to the different PPP-RTK models, as well as why some of the proposed estimation methods cannot be accepted as PPP-RTK proper. We determine, for the first time, analytical expressions for the variance matrices of the ambiguity-fixed and ambiguity-float PPP-RTK corrections. This gives important insight into their precision, as well as allows us to discuss which parts of the PPP-RTK correction variance matrix are essential for the user and which are not. This, in turn, enables one to analyse the ambiguity resolution strength of the models by means of analytical expressions of their Ambiguity dilution of precision (ADOP).

Chapter 3: PPP-RTK Corrections and their User-Impact

This chapter is covered by the following publication:

- Khodabandeh A. and Teunissen P.J.G. (2015). An Analytical Study of PPP-RTK Corrections: Precision, Correlation and User-Impact. Journal of Geodesy, doi: 10.1007/s00190-015-0838-9.

This paper provides an analytical study of the quality of the PPP-RTK corrections as well as of their impact on the user ambiguity resolution performance. The best linear unbiased estimator (BLUE) of the corrections is presented in closed-form. This is conducted for both the geometry-free and the geometry-based network scenarios, with and without network ambiguity resolution. The BLUE of the corrections demonstrates how the corrections depend on network parameters such as number of epochs, number of stations, number of satellites, and number of frequencies. Therefore, we are able to describe in a qualitative sense how the user ambiguity resolution performance is driven by the data from the different network scenarios.

Chapter 4: Array-based SPB determination (Part 1: Indexical presentation)

This chapter is covered by the following publication:

- Khodabandeh A. (2014). Array-aided single-differenced satellite phase bias determination: methodology and results. ION GNSS+, 27:2523–2532. The Institute of Navigation, Florida, USA. ***Best Student Paper Award***

This contribution is the first of two parts. We study both the estimability and the estimation components of between-satellite single-differenced (SD) estimable satellite phase biases (SPBs)—the key parameters realizing single-receiver IAR.

Highlighting the code-dominated precision of the SD-SPB corrections, the concept of array-based SPB determination is introduced. The idea is to give the role of the local reference network to an array of antennas, mounted on rigid platforms, that are separated by short distances so that the same ionospheric delay is assumed to be experienced by all the antennas. Closed-form analytical expressions of the single-station as well as the array-based SPB estimators are presented. Upon resolving double-differenced ambiguities of the array's data, the variance of the SD-SPB corrections is shown to be reduced by a factor equal to the number of antennas. This improvement in precision is also confirmed by GPS results. Throughout the text, indexical presentation is employed, well-suited for those acquainted with scalar expressions rather than vectorial expressions.

Chapter 5: Array-based SPB determination (Part 2: Multivariate presentation)

This chapter is covered by the following publication:

- Khodabandeh A. and Teunissen P.J.G. (2014a). Array-based satellite phase bias sensing: theory and GPS/BeiDou/QZSS results. Measurement Science and Technology, 25,095801 (11pp). UK.

This contribution is the second of two parts. Multivariate notation is employed to finalize the concept of array-based SPB determination. The link between the SD-SPB corrections and the code multipath equations is established. As linear combinations of the multipath equations, the SD-SPB corrections can thus be directly affected by the unwanted effects of the multipath. A multi-GNSS analysis is conducted on the basis of real-world data of the three GNSSs GPS, BeiDou and QZSS. Experimental results demonstrate that the integer-recovered ambiguities converge to integers faster, upon increasing the number of antennas aiding the SD-SPB corrections.

Chapter 6: Single-frequency PPP-RTK user performances

This chapter is covered by the following publication:

- Odijk D., Teunissen P.J.G. and Khodabandeh A. (2014). Single-frequency PPP-RTK: theory and experimental results. International Association of Geodesy Symposium (IAG), 139:167–173, Springer.

In this contribution we process the data of a regional GPS network of continuously operating reference stations (CORS) and apply the network-derived corrections to the observations of a single-frequency PPP-RTK user. Next to the precise orbits provided by IGS, the corrections are the estimable satellite clocks, satellite phase biases and ionospheric delays predicted at the approximate location of the user. Experimental results of single-frequency PPP-RTK for both a high-grade geodetic receiver as well as a low-grade mass-market receiver demonstrate that although single-epoch integer ambiguity resolution is not possible, single-frequency ambiguity resolution enabled cm-level PPP is feasible based on an accumulation of less than 10 min of observations plus network corrections on average. The idea is of potential importance for the applicability of mass-market receivers to PPP-RTK.

Chapter 7: GPS+Galileo RTK user performances

This chapter is covered by the following publication:

- Odijk D., Teunissen P.J.G. and Khodabandeh A. (2013). Galileo IOV RTK positioning: standalone and combined with GPS. Survey Review, Maney Publishing. UK.

To gain more insights into the future performance of GPS+Galileo PPP-RTK, this paper is devoted to analysing the observations of the four Galileo In-Orbit Validation (IOV) satellites. Integrated with a GPS data-set, their real-time kinematic positioning capacity is studied. According to the obtained results, integer ambiguity resolution based on the four IOV satellites needs fewer than three minutes when at least observables from three frequencies are used. Combined with data of four GPS satellites even instantaneous (single-epoch) ambiguity resolution is demonstrated, using only two frequencies per constellation (i.e. E1+E5a and L1+L2). We also show that at locations with obstructed satellite visibility, such that positioning based on either GPS-only or Galileo-only becomes impossible or only in a very inaccurate way, combined Galileo+GPS positioning is feasible, within 10 minutes if one frequency of each constellation is used and only 2 minutes time-to-fix the ambiguities based on observations of two frequencies of each constellation. It is furthermore demonstrated that this results in positions with centimetre level accuracy in the horizontal plane and sub-decimetre accuracy in the vertical direction.

Chapter 8: GPS, Galileo, QZSS and IRNSS L5/E5a-signal performance

This chapter is covered by the following publication:

- Nadarajah N., Khodabandeh A. and Teunissen P.J.G. (2015). Assessing the IRNSS L5-signal in combination with GPS, Galileo, and QZSS L5/E5a-signals for positioning and navigation. GPS Solutions, doi: 10.1007/s10291-015-0450 8.

An insight into the future performance of multi-GNSS PPP-RTK using the L5/E5a-signal is considered. The Indian Regional Navigation Satellite System (IRNSS), which is being developed for positioning services in and around India, is the latest addition to the global family of satellite-based navigation systems. As IRNSS only shares the L5-frequency with GPS, the European Galileo, and the Japanese Quasi-Zenith Satellite System (QZSS), it has at least at present a limited interoperability with the existing systems. Noting that the L5- frequency capability is under development even for GPS, this paper assesses the interoperability of the IRNSS L5-signal with the GPS, Galileo, and QZSS L5/E5a-signals for positioning and navigation using real data collected in Perth, Australia. The results show that the IRNSS L5-signal has comparable noise characteristics as that of the other L5/E5a-signals. For single-frequency carrier phase-based positioning and navigation, the results show better ambiguity resolution performance of L5/E5a only processing than that of L1/E1-only processing.

Chapter 9: Impact of IAR on the PPP-RTK network parameters

This chapter is covered by the following publication:

- Teunissen P.J.G. and Khodabandeh A. (2014b). Do GNSS parameters always benefit from integer ambiguity resolution? a PPP-RTK Network Scenario. ION GNSS+, 27:590–600. The Institute of Navigation, Florida.

In this contribution we, for the first time, study the impact of integer ambiguity resolution (IAR) on the precision of PPP-RTK network's estimable parameters. New one-to-one transformations to the parameters have been introduced to ease our analysis. The satellite-/receiver-averaged components of the estimable clocks and phase biases on a particular frequency remain unaffected after network IAR. This is, however, not the case with the precision of the SD clocks and phase biases, including

the essential components of PPP-RTK. We show that the precision improvement of the stated parameters gets larger as the geometry of the model gets weaker. This is, however, not the case with the wide-lane satellite phase biases, since their precision is almost insensitive to the geometry of the model. Supported by numerical results, our analytical expressions show that the precision improvement of the SD satellite clocks and phase biases increases as the number of stations increases. The zero-correlation property between the DD ambiguities and the estimable code biases, served as an additional correction in the multi-frequency PPP-RTK setup, is also pointed out.

Chapter 10: Single-Epoch Integrity Monitoring in Array-based PPP-RTK

This chapter is covered by the following publication:

- Khodabandeh A. and Teunissen P.J.G. (2014b). Single-Epoch GNSS Array Integrity: an Analytical Study. International Association of Geodesy Symposium (IAG), Springer, Accepted for publication.

In this contribution we analyse the integrity of the GNSS array single-epoch model through the so-called uniformly most powerful invariant (UMPI) test-statistics and their corresponding minimal detectable biases (MDBs). The model considered is characterized by multiple receivers/satellites with known coordinates where the multi-frequency carrier-phase and pseudo-range observables are subject to atmospheric (ionospheric and tropospheric) delays, receiver and satellite clock biases, as well as instrumental delays. Highlighting the role played by the model's misclosures, analytical multivariate expressions of a few leading test-statistics together with their MDBs are studied that are further accompanied by numerical results of the three GNSSs GPS, Galileo and BeiDou.

Chapter 11: A recursive MMSE filter (Part 1: Basic Concepts and Principles)

This chapter is covered by the following publication:

- Teunissen P.J.G. and Khodabandeh A. (2013) BLUE, BLUP and the Kalman filter: some new results. Journal of Geodesy, 87(5):461–473

This contribution is the first of two parts. Represented as dynamic systems, both the PPP-RTK network and user systems of observation equations are to be properly adjusted and filtered over time, in a minimum-mean-squared-error (MMSE) sense.

The means of the to-be-predicted state-vector—i.e. the network and user parameters— are generally unknown. In the context of Kalman filtering however, the filter needs to be initialized by the known mean of the state-vector. Motivated by this restrictive assumption, we therefore derive and present a recursive linear MMSE filter for dynamic systems with unknown state-vector means. We commence with the principles of linear unbiased estimators and predictors in the linear models. Highlighting their underlying properties, the best members, i.e. those of the minimum-mean-squared estimation and prediction errors, are identified and entitled as the BLUE and the BLUP, respectively. The recursive forms of the BLUE and BLUP are then presented from the first principles.

Chapter 12: A recursive MMSE filter (Part 2: Relation to the Kalman filter)

This chapter is covered by the following publication:

- Khodabandeh A. and Teunissen P.J.G. (2014c). A recursive linear MMSE filter for dynamic systems with unknown state vector means. International Journal on Geomathematics, 5:17–31, Springer

This contribution is the second of two parts. Further properties of the recursive linear MMSE filter, introduced as the BLUE-BLUP recursion, are presented. The role of the system noise and of the estimation error variance matrix in the joint prediction and estimation of the filter is discussed. We show how the BLUE-BLUP recursion is linked to the standard Kalman filter. In particular, we discuss the fundamentally different roles played by the initialization of the two filters. In case the state-vector means are known, the standard Kalman filter follows as a special case of the new filter.

1. 4 Summary and Conclusions

In this thesis, we discussed the principles of PPP-RTK, together with a comparison of six different PPP-RTK models: two common clock (CC) models, the distinct clocks (DC) model, the integer recover clock (IRC) model, the decoupled satellite clock (DSC) model and the uncalibrated phase delay/fractional cycle bias (UPD/FCB) model. We discussed both their network-component and user-component. Furthermore, by application of $\mathcal{S}$-system theory, we showed how the

corrections of different models are linked to one another through one-to-one transformations. These transformations are given in Table 1 of Chapter 2.

It was shown that the PPP-RTK corrections, next to establishing an *ambiguity* link, also establish a *positional* link between network and user. Through the corrections, the user-positioning parameters become in essence relative positioning parameters between user and network. PPP-RTK is thus a relative positioning method and not one of absolute positioning. The single-receiver 'user' integer ambiguities are thus straightforward *double-differenced* ambiguities and not undifferenced or SD ambiguities as is sometimes stated, see e.g. (Laurichesse et al. 2009) or (Mervart et al. 2013).

We presented four different least-squares PPP-RTK estimators. They are the float and fixed estimators under the *geometry-free* (GF) model and the float and fixed estimators under the *geometry-based* (GB) model. Using the analytical expressions of the variance matrices, it was shown that the precision of the ambiguity-fixed corrections did not differ too much between the GF- and the GB-model. Thus, once ambiguity resolution has been successfully applied, either the GF-based or GB-based corrections can be used. In the impact of ambiguity resolution on their precision, the GF-based and GB-based corrections do differ, however. In case of the GF-model, the variance-improvement due to ambiguity resolution follows the 1-over-*n* rule (*n* being the number of network stations). In case of the GB-model, however, this improvement depends on its model strength. It is larger, the weaker the model is, and it becomes minimum in the geometry-fixed case. In this latter case, the ambiguity-float GB clock solution is already as good as that of the ambiguity-fixed solution.

Next to the PPP-RTK principles, we introduced the concept of array-based SPB determination—the key parameter to perform single-receiver IAR. The aim is to reduce the code-dominated precision of the single-differenced SPB corrections. The dependency of their precision on the number of aiding antennas are characterized by analytical expressions and further affirmed by multi-GNSS numerical results. As to the reliability of the array-based corrections, single-epoch integrity monitoring of an array-based model was also briefly studied. In particular, we showed that as the model gets stronger, one can perform testing on the basis of the single-channel scenario instead.

We concluded the thesis by introducing a new recursive linear MMSE filter that is capable of processing dynamic systems with unknown state-vector means in

general, and the observation equations of the PPP-RTK network- and user-components in particular. We showed how the new filter reduces to the Kalman filter in case the state-vector means are known. More importantly, it was shown that for the new filter the initial estimation variance-matrix of the state-vector need *not* be known, this in contrast to the Kalman filter.

The main contributions of this thesis, which have been made for the first time and are considered to be new, have been highlighted below:

- The transformational links between different PPP-RTK methods and their corrections are determined, thereby showing how different PPP-RTK methods can be mixed between network and users.
- Closed-form expressions of the BLUE and the (co)variance matrices of the PPP-RTK corrections are derived, enabling one to identify which part of the data and the (co)variance matrices takes an active role in the user setup.
- The probability density function (PDF) of the *fractional part* of the satellite phase bias estimator is derived analytically, where no restriction is placed on the type of the PDF of the satellite phase bias estimator.
- It is shown that applying fractional operator gives rise to a biased estimator of the satellite phase biases.
- The concept of single-station PPP-RTK corrections and its array-aided variant is introduced. In particular, it is shown how a single-antenna can provide the estimable satellite phase biases.
- The impact of network integer ambiguity resolution on the precision of the PPP-RTK corrections is studied. The dependency of the precision improvement of the corrections on the number of network stations as well as on the network's geometrical strength is formulated.
- A new recursive linear minimum-mean-squared-error filter is introduced that is capable of handling dynamic systems with *unknown* state-vector means. The standard Kalman filter follows as a special case of the new filter, when the mean of the initial state-vector is a-priori given.
- This thesis is considered as one of the first PhD dissertations concerning the *multi-GNSS, multi-frequency* PPP-RTK concept, where real-world multi-GNSS results are presented.

2 Review and Principles of PPP-RTK methods

This chapter is covered by the following publication:

Teunissen P.J.G. and **Khodabandeh A.** (2014a). Review and Principles of PPP-RTK Methods. Journal of Geodesy, Springer, doi: 10.1007/s00190-014-0771-3.

J Geod
DOI 10.1007/s00190-014-0771-3

ORIGINAL ARTICLE

Review and principles of PPP-RTK methods

P. J. G. Teunissen · A. Khodabandeh

Received: 19 May 2014 / Accepted: 12 October 2014

Abstract PPP-RTK is integer ambiguity resolution-enabled precise point positioning. In this contribution, we present the principles of PPP-RTK, together with a review of different mechanizations that have been proposed in the literature. By application of $\mathcal{S}$-system theory, the estimable parameters of the different methods are identified and compared. Their interpretation is essential for gaining a proper insight into PPP-RTK in general, and into the role of the PPP-RTK corrections in particular. We show that PPP-RTK is a relative technique for which the 'single-receiver user' integer ambiguities are in fact double-differenced ambiguities. We determine the transformational links between the different methods and their PPP-RTK corrections, thereby showing how different PPP-RTK methods can be mixed between network and users. We also present and discuss four different estimators of the PPP-RTK corrections. It is shown how they apply to the different PPP-RTK models, as well as why some of the proposed estimation methods cannot be accepted as PPP-RTK proper. We determine analytical expressions for the variance matrices of the ambiguity-fixed and ambiguity-float PPP-RTK corrections. This gives important insight into their precision, as well as allows us to discuss which parts of the PPP-RTK correction variance matrix are essential for the user and which are not.

Keywords PPP-RTK · Integer ambiguity resolution · Ambiguity dilution of precision (ADOP) · $\mathcal{S}$-bases · Common clock (CC) model · Distinct clock (DC) model · Integer recovery clock (IRC) model · Decoupled satellite clock (DSC) model · Fractional cycle bias (FCB) model · Geometry-free (GF) model · Geometry-based (GB) model

P. J. G. Teunissen · A. Khodabandeh (✉)
GNSS Research Centre, Department of Spatial Sciences,
Curtin University of Technology, Perth, Australia
e-mail: amir.khodabandeh@curtin.edu.au

P. J. G. Teunissen
Department of Geoscience and Remote Sensing,
Delft University of Technology, Delft, The Netherlands
e-mail: p.teunissen@curtin.edu.au

Published online: 13 November 2014

1 Introduction

PPP-RTK is integer ambiguity resolution-enabled precise point positioning (PPP) (Wubbena et al. 2005; Mervart et al. 2008; Teunissen et al. 2010). With PPP, precise satellite orbits and clocks are provided to enable single-receiver users to compute their receiver positions with a high, decimeter or centimeter, accuracy (Zumberge et al. 1997; Kouba and Heroux 2001; Bisnath and Gao 2008). PPP-RTK extends the PPP concept by providing single-receiver users, next to the orbits and clocks, also information about the satellite phase biases. This information, when properly provided, enables recovery of the integerness of the user-ambiguities, thus enabling single-receiver ambiguity resolution thereby reducing the convergence times as compared to that of PPP. The goal of this contribution is to present the principles of PPP-RTK, together with a review of the different mechanizations that have been proposed in the literature.

In recent years, several PPP-RTK methods have been proposed and formulated, see e.g., (Wubbena et al. 2005; Laurichesse and Mercier 2007; Mervart et al. 2008; Collins 2008; Ge et al. 2008; Bertiger et al. 2010; Teunissen et al. 2010; Geng et al. 2012; Lannes and Prieur 2013). These methods differ in the models used, in the corrections applied and/or in the estimation methods employed. Although some comparative studies between some of these different PPP-RTK methods already exist, these studies have not been sufficiently conclusive. The method comparisons of Geng et al. (2010) and Shi and Gao (2013), for instance, do not identify some

of the important differences that exist between the methods. Instead they state that the methods studied are theoretically equivalent and will provide equivalent results. This finding is echoed in the publications of, for instance, Bisnath and Collins (2012, p. 378), Shi (2012, p. 89), Li et al. (2013a, p. 4), and Zhang and Li (2013, p. 580). We will show, however, that there are differences between the methods, even up to the point that some cannot be accepted as proper PPP-RTK methods.

It is the purpose of this contribution to present a framework describing the intricate elements of PPP-RTK, which then are used to identify and describe the differences and similarities of the different methods. We make a distinction between the model formulation used and the estimation method employed. We discuss both the network-component and the user-component. Furthermore, by a careful application of $\mathcal{S}$-system theory (Teunissen 1985), we are in the position to give a clear description of the estimable parameters that are involved in the various different methods. The interpretation of these estimable parameters is essential for gaining a proper insight into PPP-RTK in general, and into the role of the PPP-RTK corrections in particular.

This contribution is organized as follows. After having discussed the basic idea of single-receiver integer ambiguity resolution, three different PPP-RTK models are presented in Sect. 2; two based on different versions of the common clock (CC) model and one based on the distinct clock (DC) model. In Sect. 3, we discuss some of the popular ionosphere-free PPP-RTK models. They are the integer recovery clock (IRC) model (Laurichesse and Mercier 2007; Laurichesse et al. 2009; Laurichesse 2011; Loyer et al. 2012), the Decoupled Satellite Clock (DSC) model (Collins 2008; Collins et al. 2008), and the Uncalibrated Phase Delay/Fractional Cycle Bias (UPD/FCB) model (Ge et al. 2008; Geng 2011). They are compared mutually as well as with the methods of Sect. 2.

In Sect. 4, we discuss the role of the PPP-RTK corrections in establishing the link between the user-parameters and the network-parameters. The corrections are designed to realize integer ambiguities in the user-equations, thus enabling user integer ambiguity resolution. We show that PPP-RTK is a relative positioning method and that these 'single-receiver user' integer ambiguities are straightforward classical *double differenced* (DD) ambiguities and thus not undifferenced ambiguities as is sometimes stated. We also show how the different PPP-RTK corrections are related. This has the important practical implication that it shows how the different PPP-RTK methods can be mixed between network and users.

Section 5 deals with the estimation of the PPP-RTK corrections. Four different estimators of the corrections are discussed. They are the float and fixed estimators under the *geometry-free* (GF) model and the float and fixed estimators under the *geometry-based* (GB) model (Teunissen 1997a). An analytical formulation of their precision is presented, which is then used to compare the performance of the different estimators. It is shown how each of these estimators apply to the different PPP-RTK models. The variance matrices of the individual PPP-RTK corrections are also used to determine the variance matrix of the complete user-corrections. Here, we identify which parts of the PPP-RTK correction variance matrix are essential for the user and which are not. Finally, in Sect. 6, our estimation results are compared to the estimation method as described for FCB. The characteristics of the differences between the PPP-RTK estimators are demonstrated and conclusions on their suitability are drawn.

We make use of the following notation: the expectation and dispersion operators are denoted as $\mathsf{E}(.)$ and $\mathsf{D}(.)$, respectively. In case distributional results are given, the observables are assumed to follow a (multivariate) normal distribution. The identity matrix of order n is denoted as I_n. $\lfloor x \rceil$ denotes the nearest integer to x. If x is a vector, then $\lfloor x \rceil$ is the vector that follows from component-wise integer rounding. The between-satellite single-differenced (SD) combinations are symbolized through $(.)^{ps} = (.)^s - (.)^p$, with s and p being the rover and pivot satellites, respectively. A similar notation is used for between-receiver differences, $(.)_{qu} = (.)_u - (.)_q$, with u and q being the rover and pivot receiver, respectively. The squared norm of a vector, with respect to positive-definite matrix Q, is symbolized by $||.||^2_Q = (.)^T Q^{-1}(.)$.

2 PPP-RTK: from network to user

2.1 Single-receiver integer ambiguity resolution

The idea of single-receiver integer ambiguity resolution (IAR) forms the basis of PPP-RTK. The basic idea of single-receiver IAR is best described by starting with the single-receiver user observation equations. Here and in the following, we will be working with between-satellite single-differenced observation equations, instead of with the undifferenced observation equations. This simplifies our presentation, but does not affect the generality and results of our analyses.

Consider the user's antenna u tracking dual-frequency GNSS data that are transmitted by a rover satellite s and a chosen pivot satellite p. The corresponding between-satellite single-difference (SD) observation equations read then (Hofmann-Wellenhof et al. 2008)

$$\begin{aligned} \Delta\phi^{ps}_{u,j} &= g^{ps\,T}\Delta x_u - \mu_j t^{ps}_u - dt^{ps} + \lambda_j \left(z^{ps}_{u,j} - \delta^{ps}_{,j}\right) \\ \Delta p^{ps}_{u,j} &= g^{ps\,T}\Delta x_u + \mu_j t^{ps}_u - dt^{ps} - d^{ps}_{,j} \end{aligned} \tag{1}$$

where $\Delta\phi^{ps}_{u,j}$ and $\Delta p^{ps}_{u,j}$ denote the SD 'observed-minus-computed' phase and code observables on the frequency band f_j ($j = 1, 2$), respectively. Here and in the follow-

ing, the precise orbital corrections are assumed included in the 'observed-minus-computed' observables. The ν-vector Δx_u contains the user's position increments and/or the zenith tropospheric delay (ZTD). Parameter ν can take the values $\nu = 3$ (position-only model), $\nu = 1$ (ZTD-only model) or $\nu = 4$ (position-plus-ZTD model). Thus, the ν-vector g^{ps} contains the SD receiver-satellite unit vector and/or the SD tropospheric mapping function. The (first-order) SD slant ionospheric delay, experienced on the first frequency, is denoted by ι_u^{ps}. Thus, the frequency-dependent coefficients are defined as the ratio $\mu_j = (f_1^2/f_j^2)$. The SD integer ambiguity $z_{u,j}^{ps} \in \mathbb{Z}$ and the SD satellite phase bias $\delta_{,j}^{ps}$, both expressed in cycles, are linked to the phase observables through the wavelength λ_j. The SD satellite clocks are denoted by dt^{ps}, while the SD satellite code biases are denoted by $d_{,j}^{ps}$. Apart from $z_{u,j}^{ps}$ and $\delta_{,j}^{ps}$, the rest of the quantities are all expressed in units of range. We assume that m satellites are tracked and thus $p, s = 1, \ldots, m$, with $p \neq s$.

If we make use of the more compact dual-frequency vector notation $\Delta\phi_u^{ps} = [\Delta\phi_{u,1}^{ps}, \Delta\phi_{u,2}^{ps}]^T$, $\Delta p_u^{ps} = [\Delta p_{u,1}^{ps}, \Delta p_{u,2}^{ps}]^T$, $\mu = [\mu_1, \mu_2]^T$, $z_u^{ps} = [z_{u,1}^{ps}, z_{u,2}^{ps}]^T$, $\delta^{ps} = [\delta_{,1}^{ps}, \delta_{,2}^{ps}]^T$, and $d^{ps} = [d_{,1}^{ps}, d_{,2}^{ps}]^T$, we may write (1) as

$$\begin{aligned} \Delta\phi_u^{ps} &= e\,\Delta\rho_u^{ps} - \mu\,\iota_u^{ps} - e\,dt^{ps} + \Lambda(z_u^{ps} - \delta^{ps}) \\ \Delta p_u^{ps} &= e\,\Delta\rho_u^{ps} + \mu\,\iota_u^{ps} - e\,dt^{ps} - d^{ps} \end{aligned} \tag{2}$$

where $e = [1, 1]^T$, $\Lambda = \mathrm{diag}(\lambda_1, \lambda_2)$, and

$$\Delta\rho_u^{ps} = g^{ps\,T}\,\Delta x_u \tag{3}$$

The user observation Eq. (2) do not contain enough information to solve for an integer ambiguity resolved user position. This would become possible though, were information about the satellite clocks and satellite biases be given. Using such externally provided information to correct the observations as

$$\begin{aligned} \Delta\phi_u'^{ps} &= \Delta\phi_u^{ps} + e\,dt^{ps} + \Lambda\,\delta^{ps} \\ \Delta p_u'^{ps} &= \Delta p_u^{ps} + e\,dt^{ps} + d^{ps} \end{aligned} \tag{4}$$

results in user-equations that take the form

$$\begin{aligned} \Delta\phi_u'^{ps} &= e\,\Delta\rho_u^{ps} - \mu\,\iota_u^{ps} + \Lambda\,z_u^{ps} \\ \Delta p_u'^{ps} &= e\,\Delta\rho_u^{ps} + \mu\,\iota_u^{ps} \end{aligned} \tag{5}$$

This system is now in a form that can be used to solve for the integer ambiguity resolved user-parameters Δx_u and ι_u. Hence, with externally provided corrections dt^{ps}, δ^{ps}, and d^{ps}, the user system of observation Eq. (5) can be solved as a mixed-integer system of equations, thereby profiting from the integerness of $z_u^{ps} \in \mathbb{Z}^2$ (Teunissen et al. 2010). This is the basic idea of single-receiver, IAR-enabled, positioning.

The question is now whether the above needed parameters dt^{ps}, δ^{ps}, d^{ps} can be determined as such. As we will see, the answer is no. Does this mean that the above basic idea is flawed. The answer is again, fortunately, no. In the following, we will namely show that although a GNSS-network is not capable of providing the 'absolute' parameters dt^{ps}, δ^{ps}, d^{ps}, it is capable of providing *estimable parameters*, that—when applied as corrections—achieve the same goal, namely of enabling the construction of a user system of observation equations that is in mixed-integer form.

We apply $\mathcal{S}$-system theory (Baarda 1973; Teunissen 1985) to solve for the rank-deficient system of observation equations and to allow for a proper interpretation of the estimable parameters. Different sets of estimable parameters, each with their own interpretation, exist. Each such set is defined by the chosen $\mathcal{S}$-basis. By means of the $\mathcal{S}$-transformation, the relation between the original 'absolute' parameters and the estimable parameters is established. Examples of the theory's applicability to GNSS can be found in de Jonge (1998) and Odijk (2002), while examples for PPP-RTK can be found in Teunissen et al. (2010), Zhang et al. (2011), Lannes and Teunissen (2011) and Odijk et al. (2012).

2.2 Common clock (CC-1) model

The externally provided satellite clock and satellite biases will be determined by a GNSS-network. We now show how this network information enables the construction of a user system of observation equations that has the same structure as (5).

2.2.1 Network model

If we replace the user-index u in (2) by $r = 1, \ldots, n$, the resulting system may be considered the dual-frequency n-receiver network system of observation equations. Although in the network case, some or all of the entries of Δx_r, $r = 1, \ldots, n$, may be known, we consider the general case that they are unknown. This difference is of no consequence for the conclusions of our analysis. Furthermore, it is also sufficient for the purpose of this contribution to assume the network to be such that $g_r^s \approx g^s, r = 1, \ldots, n$. This assumption allows the inclusion of small to regional networks in our discussion as well.

With m satellites tracked, the network system of observation equations will have a rank defect of $\nu + 4(m-1)$. Of this defect, ν is due to the linear dependence that exists between the coefficients of Δx_r and dt^{ps}, while $4(m-1)$ is due to the linear dependency among the ionospheric delays, clocks, biases and ambiguities. This latter defect is best demonstrated if we use the geometry-free/ionosphere-free decomposition

$$d^{ps} = [\mu, e] \begin{bmatrix} d^{ps}_{\text{GF}} \\ d^{ps}_{\text{IF}} \end{bmatrix}, \text{ with } [\mu, e]^{-1} = \begin{bmatrix} \mu^T_{\text{GF}} \\ \mu^T_{\text{IF}} \end{bmatrix} \tag{6}$$

to rewrite (2), with u replaced by $r = 1, \ldots, n$,

$$\begin{aligned} \Delta\phi^{ps}_r &= e\,\Delta\rho^{ps}_r - \mu\,\tilde{\iota}^{ps}_r - e\,d\tilde{t}^{ps} + \Lambda(z^{ps}_r - \delta^{ps} - M d^{ps}) \\ \Delta p^{ps}_r &= e\,\Delta\rho^{ps}_r + \mu\,\tilde{\iota}^{ps}_r - e\,d\tilde{t}^{ps} \end{aligned} \tag{7}$$

where $\tilde{\iota}^{ps}_r = \iota^{ps}_r - d^{ps}_{\text{GF}}$, $d\tilde{t}^{ps} = dt^{ps} + d^{ps}_{\text{IF}}$ and $M = \Lambda^{-1}(\mu\mu^T_{\text{GF}} - e\mu^T_{\text{IF}})$. This shows, since only $2(m-1)$ parameters in the combination $z^{ps}_u - \delta^{ps} - Md^{ps}$ are estimable, that the additional defect is indeed $4(m-1)$.

There are many different ways of eliminating the rank defect of the above network system of equations (Teunissen 1985). The ν-defect between Δx_r and dt^{ps} can be eliminated by fixing the parameters of one of the network stations, say Δx_1. Likewise, the $4(m-1)$-defect between ambiguities, code biases and phase biases, can be eliminated by fixing two out of the three types of parameters, say the ambiguities of network station 1 and the code biases. With this choice, the $\mathcal{S}$-basis is thus given as

$$x^{\mathcal{S}}_{\text{CC-1}} = \left[\Delta x^T_1, d^{psT}, z^{psT}_1\right]^T \tag{8}$$

The full-rank network system of observation equations ($r = 1, \ldots, n$) follows then as:

$$\begin{aligned} \Delta\phi^{ps}_r &= e\,\Delta\tilde{\rho}^{ps}_r - \mu\,\tilde{\iota}^{ps}_r - e\,d\tilde{t}^{ps} + \Lambda(\tilde{z}^{ps}_r - \tilde{\delta}^{ps}) \\ \Delta p^{ps}_r &= e\,\Delta\tilde{\rho}^{ps}_r + \mu\,\tilde{\iota}^{ps}_r - e\,d\tilde{t}^{ps} \end{aligned} \tag{9}$$

in which the estimable parameters, denoted using the tilde () symbol, have the following interpretation,

$$\begin{aligned} &\Delta\tilde{x}_r = \Delta x_r - \Delta x_1, r \neq 1 \\ &\tilde{\iota}^{ps}_r = \iota^{ps}_r - \mu^T_{\text{GF}} d^{ps} \\ &d\tilde{t}^{ps} = dt^{ps} + \mu^T_{\text{IF}} d^{ps} - \Delta\rho^{ps}_1 \\ &\tilde{\delta}^{ps} = \delta^{ps} + Md^{ps} - z^{ps}_1 \\ &\tilde{z}^{ps}_r = z^{ps}_r - z^{ps}_1, r \neq 1 \end{aligned} \tag{10}$$

with $\Delta\tilde{\rho}^{ps}_r$ in (9) denoting $g^{psT}\Delta\tilde{x}_r$. The network vector of estimable parameters of the above model is thus given for a SD satellite pair ps and a network station r as

$$x_{\text{CC-1}} = \left[\Delta\tilde{x}^T_r, \tilde{\iota}^{ps}_r, d\tilde{t}^{ps}, \tilde{\delta}^{psT}, \tilde{z}^{psT}_r\right]^T \tag{11}$$

The system (9) is referred to as the *common clock* (CC-1) model, since the phase and code equations have the satellite clock parameter $d\tilde{t}^{ps}$ in common. This model was used in Zhang et al. (2011), Odijk et al. (2012). Another common clock model (CC-2), based on a different $\mathcal{S}$-basis, will be presented in Sect. 2.4.

It is important to recognize that the estimable parameters are not the original parameters, but instead functions of them. The between-satellite estimable slant ionospheric delay $\tilde{\iota}^{ps}_r$, for instance, is a biased version of the actual between-satellite slant ionospheric delay ι^{ps}_r, and the between-satellite estimable integer ambiguity $\tilde{z}^{ps}_r$ is actually a *double-differenced* integer ambiguity, namely z^{ps}_r biased by $-z^{ps}_1$. It is furthermore important to recognize that the interpretation of these estimable parameters depends on the chosen $\mathcal{S}$-basis, i.e., it will change when a different $\mathcal{S}$-basis is chosen (Teunissen 1985). In the next sections, some such cases are described.

2.2.2 User model

With appropriate corrections, one should be able to formulate the user model in mixed-integer form. In case of the above CC-model, the parameters for the corrections are given as

$$x^{\text{corr}}_{\text{CC-1}} = \left[d\tilde{t}^{ps}, \tilde{\delta}^{psT}\right]^T \tag{12}$$

These are not the original 'absolute' satellite clock and satellite biases, dt^{ps} and δ^{ps}, but instead the satellite clock-like and satellite bias-like terms, $d\tilde{t}^{ps}$ and $\tilde{\delta}^{ps}$, of (10). Although they are not the original parameters, they still do the job in ensuring that the user can work with integer ambiguities. With the CC-corrected observations

$$\begin{aligned} \Delta\tilde{\phi}^{ps}_u &= \Delta\phi^{ps}_u + e\,d\tilde{t}^{ps} + \Lambda\tilde{\delta}^{ps} \\ \Delta\tilde{p}^{ps}_u &= \Delta p^{ps}_u + e\,d\tilde{t}^{ps} \end{aligned} \tag{13}$$

the user-equations take, namely, the form

$$\begin{aligned} \Delta\tilde{\phi}^{ps}_u &= e\,\Delta\tilde{\rho}^{ps}_u - \mu\,\tilde{\iota}^{ps}_u + \Lambda\tilde{z}^{ps}_u \\ \Delta\tilde{p}^{ps}_u &= e\,\Delta\tilde{\rho}^{ps}_u + \mu\,\tilde{\iota}^{ps}_u \end{aligned} \tag{14}$$

Note that the structure of these equations is indeed identical to that of (5) and that the user-ambiguities are indeed integer $\tilde{z}^{ps}_u \in \mathbb{Z}^2$. The interpretation of the parameters in (14) is, however, different from those of (5). Through the network-based satellite clock corrections $d\tilde{t}^{ps}$, for instance, the positional link between network and user is established, thus giving, instead of Δx_u in (5), the estimable user parameter vector $\Delta\tilde{x}_u$ in (14).

A similar link between network and user is established for the ambiguities. Note, namely, that the integer 'user' ambiguity $\tilde{z}^{ps}_u$ is in fact a *double-differenced* ambiguity $\tilde{z}^{ps}_u = z^{ps}_u - z^{ps}_1$. In other words, for the ambiguities, the linkage with the network is established through the network-based phase bias correction $\tilde{\delta}^{ps}$, thus enabling the construction of double-differenced integer ambiguities at the user side. This shows that one must be very careful by calling the ambiguity resolution of the user-ambiguities, the fixing of undifferenced or single-differenced integer ambiguities, see e.g., Laurichesse et al. (2009, p. 135) or Mervart et al. (2013, p. 1177). The resolution of these 'user' ambiguities is namely again a resolution of double-differenced ambiguities.

2.3 Distinct clocks (DC) model

Instead of working with the CC-model, one can also work with distinct clocks (DC) models. Using $\mathcal{S}$-system theory, de Jonge (1998) introduced various $\mathcal{S}$-systems for the undifferenced GNSS observation equations. Since his choices give rise to models with common and/or different clocks for different observable types, de Jonge refers to his models as the *distinct clocks* (DC) models, see de Jonge (1998, Chap. 4). Distinct clock models were also used in Odijk (2002) and in Teunissen et al. (2010) for PPP-RTK. The DC-model of de Jonge that we consider in the present contribution uses a common clock for the code observables and two different clocks for the two phase observables.

The DC-model uses the *same* $\mathcal{S}$-basis (8), but a different parametrization. The DC $\mathcal{S}$-basis is, thus, also given as

$$x_{\mathrm{DC}}^{\mathcal{S}} = \left[\Delta x_1^T, d^{psT}, z_1^{psT}\right]^T \tag{15}$$

The CC-to-DC reparametrization is rather simple as it only involves replacing the phase bias by a lumped version of the common clock and phase bias,

$$\begin{bmatrix} d\tilde{t}^{ps} \\ \delta\tilde{t}^{ps} \end{bmatrix} = \begin{bmatrix} 1 & 0 \\ e & \Lambda \end{bmatrix} \begin{bmatrix} d\tilde{t}^{ps} \\ \tilde{\delta}^{ps} \end{bmatrix} \tag{16}$$

Thus, instead of the CC-parametrization $d\tilde{t}^{ps}, \tilde{\delta}^{ps}$, now the DC-parametrization $d\tilde{t}^{ps}, \delta\tilde{t}^{ps}$ is used. Its full-rank network system of observation equations reads therefore

$$\begin{aligned} \Delta\phi_r^{ps} &= e\,\Delta\tilde{\rho}_r^{ps} - \mu\,\tilde{\imath}_r^{ps} - \delta\tilde{t}^{ps} + \Lambda\tilde{z}_r^{ps} \\ \Delta p_r^{ps} &= e\,\Delta\tilde{\rho}_r^{ps} + \mu\,\tilde{\imath}_r^{ps} - e\,d\tilde{t}^{ps} \end{aligned} \tag{17}$$

For a SD satellite pair ps and a network station r, the network vector of estimable parameters is then given as:

$$x_{\mathrm{DC}} = \left[\Delta\tilde{x}_r^T, \tilde{\imath}_r^{ps}, d\tilde{t}^{ps}, \delta\tilde{t}^{psT}, \tilde{z}_r^{psT}\right]^T \tag{18}$$

The PPP-RTK corrections of the DC-model are given as

$$x_{\mathrm{DC}}^{\mathrm{corr}} = \left[d\tilde{t}^{ps}, \delta\tilde{t}^{psT}\right]^T \tag{19}$$

Once these corrections are applied at the user side, the observation equations of the user will again be given by (14). Following the terminology of Laurichesse and Mercier (2007), the correction vector $\delta\tilde{t}^{ps}$ could be called an *integer recovery phase clock* vector as it results in integer double-differenced ambiguities at the user side.

2.4 Common clock (CC-2) model

Instead of using the ambiguities of a reference station as part of the $\mathcal{S}$-basis (cf. 8), one may also choose the phase biases themselves. This will result in real-valued ambiguities that can be used to form the PPP-RTK user-corrections.

2.4.1 Network model

In case the phase biases δ^{ps} replace the ambiguities z_1^{ps} of (8), the $\mathcal{S}$-basis becomes

$$x_{\text{CC-2}}^{\mathcal{S}} = \left[\Delta x_1^T, d^{psT}, \delta^{psT}\right]^T \tag{20}$$

The full-rank network system of observation equations ($r = 1, \ldots, n$) follows then as,

$$\begin{aligned} \Delta\phi_r^{ps} &= e\,\Delta\tilde{\rho}_r^{ps} - \mu\,\tilde{\imath}_r^{ps} - e\,d\tilde{t}^{ps} + \Lambda\,\tilde{a}_r^{ps} \\ \Delta p_r^{ps} &= e\,\Delta\tilde{\rho}_r^{ps} + \mu\,\tilde{\imath}_r^{ps} - e\,d\tilde{t}^{ps} \end{aligned} \tag{21}$$

with the estimable parameters,

$$\begin{aligned} \Delta\tilde{x}_r &= \Delta x_r - \Delta x_1 \\ \tilde{\imath}_r^{ps} &= \iota_r^{ps} - \mu_{\mathrm{GF}}^T d^{ps} \\ d\tilde{t}^{ps} &= dt^{ps} + \mu_{\mathrm{IF}}^T d^{ps} - \Delta\rho_1^{ps} \\ \tilde{a}_r^{ps} &= z_r^{ps} - \delta^{ps} - M d^{ps} \end{aligned} \tag{22}$$

When we compare (10) with (22), we note that $\tilde{\delta}^{ps}$ and $\tilde{z}_r^{ps}$ of (10), and $\tilde{a}_r^{ps}$ of (22), are related as

$$\tilde{a}_r^{ps} = \tilde{z}_r^{ps} - \tilde{\delta}^{ps} \tag{23}$$

We, thus, see that as a consequence of the change of $\mathcal{S}$-basis from z_1^{ps} to δ^{ps} (cf. 8, 20), the $n-1$ *integer* ambiguity vectors $\tilde{z}_r^{ps}$ (recall that $\tilde{z}_{r=1}^{ps} = 0$), together with the phase bias vector $\tilde{\delta}^{ps}$, get replaced by the n *real-valued* ambiguity vectors $\tilde{a}_r^{ps}$ of (22). The network vector of estimable parameters of this model, for a SD satellite pair ps and a network station r, is thus given as

$$x_{\text{CC-2}} = \left[\Delta\tilde{x}_r^T, \tilde{\imath}_r^{ps}, d\tilde{t}^{ps}, \tilde{a}_r^{psT}\right]^T \tag{24}$$

2.4.2 User model

It is now the real-valued ambiguity vector $\tilde{a}_q^{ps}$, that, for some $q \in \{1, \ldots, n\}$, can take over the role of the phase bias $\tilde{\delta}^{ps}$ in forming the corrections for the user,

$$x_{\text{CC-2}}^{\mathrm{corr}} = \left[d\tilde{t}^{ps}, \tilde{a}_q^{psT}\right]^T \tag{25}$$

Note that $\tilde{a}_q^{ps} = -\tilde{\delta}^{ps}$ for $q = 1$ (cf. 23) and $\tilde{a}_q^{ps} = \tilde{z}_q^{ps} - \tilde{\delta}^{ps}$ for $q \neq 1$. Thus, apart from the sign, the real-valued ambiguity $\tilde{a}_q^{ps}$ is either equal to the phase bias or a nonzero integer-shifted version of it. Hence, with the real-valued ambiguity vector $\tilde{a}_q^{ps}$, one should indeed be able to recover ambiguity-integerness at the user side. This is verified when such correction is applied to the user observations.

With the user observations corrected as

$$\begin{aligned} \Delta\tilde{\phi}_u^{ps} &= \Delta\phi_u^{ps} + e\,d\tilde{t}^{ps} - \Lambda\tilde{a}_q^{ps} \\ \Delta\tilde{p}_u^{ps} &= \Delta p_u^{ps} + e\,d\tilde{t}^{ps} \end{aligned} \tag{26}$$

the user-equations take the form

$$\begin{aligned}\Delta\tilde{\phi}_u^{ps} &= e\,\Delta\tilde{\rho}_u^{ps} - \mu\,\tilde{\imath}_u^{ps} + \Lambda\tilde{a}_{qu}^{ps}\\ \Delta\tilde{p}_u^{ps} &= e\,\Delta\tilde{\rho}_u^{ps} + \mu\,\tilde{\imath}_u^{ps}\end{aligned} \tag{27}$$

with integer $\tilde{a}_{qu}^{ps} = z_u^{ps} - z_q^{ps}$. Thus, for $q = 1$, the parametrization of (27) is identical to that of (14), while for $q \neq 1$, the ambiguities are an integer-shifted version of those of (14). Hence, the ambiguity solution of *any* network station $q = 1, \ldots, n$ can be taken to form an admissible user-correction.

3 Ionosphere-free PPP-AR models

In this section, we discuss some further models proposed in the literature. We discuss the Integer Recovery Clock (IRC) model (Laurichesse and Mercier 2007; Laurichesse et al. 2009; Loyer et al. 2012), the Decoupled Satellite Clock (DSC) model (Collins 2008; Collins et al. 2008), and the Uncalibrated Phase Delay/Fractional Cycle Bias (UPD/FCB) model (Ge et al. 2008; Geng and Bock 2013). Since the IRC- and DSC-model are the same, they are discussed under one heading.

3.1 The IRC/DSC-model

The IRC-model has been introduced in Laurichesse and Mercier (2007) and the DSC-model in Collins (2008). The IRC/DSC-model works with ionosphere-free combinations. Thus, instead of working with the four equations of (7), the ionosphere is eliminated first, thereby reducing the four equations to three instead. Although this elimination step is not essential, we include it in the below derivation to better appreciate the choice of parametrization. We show that the IRC/DSC-model uses the *same* $\mathcal{S}$-basis as the CC-model (9) or DC-model (17), but a different parametrization.

3.1.1 Network model

With the wide-lane, narrow-lane and ionosphere-free combinations defined as

$$\begin{aligned}\mu_{\text{WL}} &= \frac{1}{\sqrt{\mu_2} - \sqrt{\mu_1}}[\sqrt{\mu_2}, -\sqrt{\mu_1}]^T,\\ \mu_{\text{NL}} &= \frac{1}{\sqrt{\mu_2} + \sqrt{\mu_1}}[\sqrt{\mu_2}, \sqrt{\mu_1}]^T,\\ \mu_{\text{IF}} &= \frac{1}{\mu_{12}}[\mu_2, -\mu_1]^T,\end{aligned} \tag{28}$$

we have the properties

$$\begin{bmatrix}\mu_{\text{IF}} & 0 & \mu_{\text{WL}}\\ 0 & \mu_{\text{IF}} & -\mu_{\text{NL}}\end{bmatrix} \perp \begin{bmatrix}-\mu\\ \mu\end{bmatrix}, \begin{bmatrix}\mu_{\text{WL}}\\ -\mu_{\text{NL}}\end{bmatrix} \perp \begin{bmatrix}e\\ e\end{bmatrix} \tag{29}$$

with $\mu_{\text{WL}}^T e = 1$. The notation $v \perp w$ means $v^T w = 0$. Hence, if the full-rank 4×3 matrix of (29) is used to form the three ionosphere-free observation combinations $\phi_{r,\text{IF}}^{ps} = \mu_{\text{IF}}^T \phi_r^{ps}$, $p_{r,\text{IF}}^{ps} = \mu_{\text{IF}}^T p_r^{ps}$, and $\phi_{r,WN}^{ps} = \mu_{\text{WL}}^T \phi_r^{ps} - \mu_{\text{NL}}^T p_r^{ps}$, their observation equations follow from (9) as

$$\begin{aligned}\Delta\phi_{r,\text{IF}}^{ps} &= \Delta\tilde{\rho}_r^{ps} - d\tilde{t}^{ps} + \mu_{\text{IF}}^T\Lambda(\tilde{z}_r^{ps} - \tilde{\delta}^{ps})\\ \Delta p_{r,\text{IF}}^{ps} &= \Delta\tilde{\rho}_r^{ps} - d\tilde{t}^{ps}\\ \Delta\phi_{r,WN}^{ps} &= +\mu_{\text{WL}}^T\Lambda(\tilde{z}_r^{ps} - \tilde{\delta}^{ps})\end{aligned} \tag{30}$$

These equations are referred to as 'ionosphere-free' as the ionospheric delay parameters are eliminated from them. These equations are, however, still in the form of the original CC-parametrization. With the IRC/DSC-parametrization

$$\begin{bmatrix}d\tilde{t}^{ps}\\ \delta\tilde{t}_{\text{IF}}^{ps}\\ \tilde{\delta}_W^{ps}\end{bmatrix} = \begin{bmatrix}1 & 0\\ 1 & \mu_{\text{IF}}^T\Lambda\\ 0 & \frac{1}{\lambda_W}\mu_{\text{WL}}^T\Lambda\end{bmatrix}\begin{bmatrix}d\tilde{t}^{ps}\\ \tilde{\delta}^{ps}\end{bmatrix}, \tag{31}$$

the wide-lane transformation

$$\begin{bmatrix}\tilde{z}_{r,1}^{ps}\\ \tilde{z}_{r,W}^{ps}\end{bmatrix} = Z_W\tilde{z}_r^{ps}, \text{ with } Z_W = \begin{bmatrix}1 & 0\\ 1 & -1\end{bmatrix}, \tag{32}$$

thereby recognizing that

$$\begin{bmatrix}\mu_{\text{IF}}^T\Lambda Z_W\\ \mu_{\text{WL}}^T\Lambda Z_W\end{bmatrix} = \begin{bmatrix}\lambda_N & \frac{\lambda_2}{\mu_{12}}\\ 0 & \lambda_W\end{bmatrix} \tag{33}$$

we obtain

$$\begin{aligned}\Delta\phi_{r,\text{IF}}^{ps} &= \Delta\tilde{\rho}_r^{ps} - \delta\tilde{t}_{\text{IF}}^{ps} + \lambda_N\tilde{z}_{r,1}^{ps} + \frac{\lambda_2}{\mu_{12}}\tilde{z}_{r,W}^{ps}\\ \Delta p_{r,\text{IF}}^{ps} &= \Delta\tilde{\rho}_r^{ps} - d\tilde{t}^{ps}\\ \Delta\phi_{r,WN}^{ps} &= \lambda_W(\tilde{z}_{r,W}^{ps} - \tilde{\delta}_W^{ps})\end{aligned} \tag{34}$$

with the narrow-lane and wide-lane wavelengths given as $\lambda_N = (\lambda_1\lambda_2)/(\lambda_2 + \lambda_1)$ and $\lambda_W = (\lambda_1\lambda_2)/(\lambda_2 - \lambda_1)$. Since $\tilde{z}_{r,1}^{ps}$ has the narrow-lane wavelength λ_N as coefficient, it is sometimes referred to as the narrow-lane ambiguity (Beutler et al. 2007). Formally, this is incorrect, since $\tilde{z}_{r,1}^{ps}$ is an L_1 ambiguity, while the narrow-lane ambiguity is defined as the sum of an L_1 and L_2 ambiguity (Wubbena 1989; Allison 1991).

The estimable IRC/DSC-parameters of (34) have the following interpretation,

$$\begin{aligned}\Delta\tilde{x}_r &= \Delta x_r - \Delta x_1\\ d\tilde{t}^{ps} &= dt^{ps} + \mu_{\text{IF}}^T d^{ps} - \Delta\rho_1^{ps}\\ \delta\tilde{t}_{\text{IF}}^{ps} &= dt^{ps} + \mu_{\text{IF}}^T\Lambda(\delta^{ps} - z_1^{ps}) - \Delta\rho_1^{ps}\\ \tilde{\delta}_W^{ps} &= (0,1)Z_W(\delta^{ps} - z_1^{ps}) - \frac{1}{\lambda_W}\mu_{\text{NL}}^T d^{ps}\\ \left.\begin{matrix}\tilde{z}_{r,1}^{ps}\\ \tilde{z}_{r,W}^{ps}\end{matrix}\right\} &= Z_W(z_r^{ps} - z_1^{ps})\end{aligned} \tag{35}$$

For a SD satellite pair ps and a network station r, the network vector of IRC/DSC-estimable parameters is thus given as

$$x_{\text{IRC/DSC}} = \left[\Delta\tilde{x}_r^T,\, d\tilde{t}^{ps},\, [\delta\tilde{t}_{,\text{IF}}^{ps},\, \tilde{\delta}_{,W}^{ps}],\, [\tilde{z}_{r,1}^{ps},\, \tilde{z}_{r,W}^{ps}]\right]^T \tag{36}$$

3.1.2 User model

The PPP-RTK corrections of the IRC/DSC-model are given as

$$x_{\text{IRC/DSC}}^{\text{corr}} = \left[d\tilde{t}^{ps},\, [\delta\tilde{t}_{,\text{IF}}^{ps},\, \tilde{\delta}_{,W}^{ps}]\right]^T \tag{37}$$

The correction $\delta\tilde{t}_{,\text{IF}}{}^{ps}$ is called the *integer recovery phase clock* by Laurichesse and Mercier (2007) and the *decoupled phase clock* by Collins (2008). The correction $\tilde{\delta}_{,W}^{ps}$ denotes the wide-lane, between-satellite differenced estimable phase bias.

With the IRC/DSC-corrected observations

$$\begin{aligned}
\Delta\tilde{\phi}_{u,\text{IF}}^{ps} &= \Delta\phi_{u,\text{IF}}^{ps} + \delta\tilde{t}_{\text{IF}}^{ps} \\
\Delta\tilde{p}_{u,\text{IF}}^{ps} &= \Delta p_{u,\text{IF}}^{ps} + d\tilde{t}^{ps} \\
\Delta\tilde{\phi}_{u,WN}^{ps} &= \Delta\phi_{u,WN}^{ps} + \lambda_W\tilde{\delta}_W^{ps}
\end{aligned} \tag{38}$$

the IRC/DSC user-equations take the form

$$\begin{aligned}
\Delta\tilde{\phi}_{u,\text{IF}}^{ps} &= \Delta\tilde{\rho}_u^{ps} + \lambda_N\tilde{z}_{u,1}^{ps} + \frac{\lambda_2}{\mu_{12}}\tilde{z}_{u,W}^{ps} \\
\Delta\tilde{p}_{u,\text{IF}}^{ps} &= \Delta\tilde{\rho}_u^{ps} \\
\Delta\tilde{\phi}_{u,WN}^{ps} &= \lambda_W\tilde{z}_{u,W}^{ps}
\end{aligned} \tag{39}$$

The Eqs. (34) and (39) are the between-satellite SD network- and user-equations of the IRC/DSC-model. The Eqs. of (34) are the same as those introduced in Collins et al. (2008, p. 1316), be it that in that contribution $\lambda_N\tilde{z}_{u,1}^{ps} + \frac{\lambda_2}{\mu_{12}}\tilde{z}_{u,W}^{ps}$ is explicitly expressed for the GPS frequency bands only, namely as

$$\lambda_I(17\tilde{z}_{u,1}^{ps} + 60\tilde{z}_{u,W}^{ps}), \quad \lambda_I = \frac{2cf_o}{f_1^2 - f_2^2} \tag{40}$$

with $f_o = 10.23$ MHz and c being the velocity of light. Similarly, the Eqs. of (34) are the SD version of those given in Eqs. (3) and (5) of Laurichesse et al. (2009, p. 136, 137), see also Eqs. (4), (5) and (6) of Loyer et al. (2012). The only difference lies in further accounting for the phase center offsets in the first two IF observation equations. This difference is, however, neglected once the estimable wide-lane satellite phase biases are to be determined, see e.g., Eq. (4) in Laurichesse et al. (2009, p. 136) or Eq. (3) in Loyer et al. (2012, p. 993).

3.1.3 The CC-1, DC, and IRC/DSC-models compared

We derived the IRC/DSC-model from the full-rank CC-model (9), by first formulating the ionosphere-free variant of the CC-model and then applying the one-to-one CC-to-IRC/DSC parameter transformation.

The $\mathcal{S}$-basis that we used is $\Delta x_1, d^{ps}, z_1^{ps}$ (cf. 8). In Collins (2008), it is stated however, that the $\mathcal{S}$-basis of the DSC-model is given by the ionosphere-free and narrow-lane code biases, $d_{,\text{IF}}^{ps} = \mu_{\text{IF}}^T d^{ps}$ and $d_{,\text{NL}}^{ps} = \mu_{\text{NL}}^T d^{ps}$, and the ambiguities $z_{1,1}^{ps}$ and $z_{1,W}^{ps}$. Hence, one may think that for the DSC-model in Collins (2008) a different $\mathcal{S}$-basis choice is made than for the CC- or DC-models, (9) and (17), respectively. This is not true, however. As the transformation between d^{ps} and $d_{,\text{IF}}^{ps}, d_{,\text{NL}}^{ps}$ is one-to-one, and also the transformation between z_1^{ps} and $z_{1,1}^{ps}, z_{1,W}^{ps}$ is one-to-one, the DSC-choice in Collins (2008) is identical to the $\mathcal{S}$-basis choice of (9) and (17), respectively, namely $\Delta x_1, d^{ps}, z_1^{ps}$.

We have already shown, with (31) and (32), that the estimable parameters of the IRC/DSC-model stand in one-to-one correspondence with the estimable parameters of the CC-model (9). Additionally, they also stand in one-to-one correspondence with their DC-model counterparts. The estimable IRC/DSC-parameters can namely be expressed in the estimable DC-parameters as

$$\begin{aligned}
\Delta\tilde{x}_r &= \Delta\tilde{x}_r \\
\delta\tilde{t}_{\text{IF}}^{ps} &= \frac{\mu_2}{\mu_{12}}\delta\tilde{t}_{,1}^{ps} - \frac{\mu_1}{\mu_{12}}\delta\tilde{t}_{,2}^{ps} \\
d\tilde{t}^{ps} &= d\tilde{t}^{ps} \\
\tilde{\delta}_{,W}^{ps} &= \frac{1}{\lambda_1}\delta\tilde{t}_{,1}^{ps} - \frac{1}{\lambda_2}\delta\tilde{t}_{,2}^{ps} - \frac{1}{\lambda_W}d\tilde{t}^{ps} \\
\tilde{z}_{r,1}^{ps} &= \tilde{z}_{r,1}^{ps} \\
\tilde{z}_{r,W}^{ps} &= \tilde{z}_{r,1}^{ps} - \tilde{z}_{r,2}^{ps}
\end{aligned} \tag{41}$$

This shows, for instance, that the decoupled phase clock of the IRC/DSC-model, $\delta\tilde{t}_{\text{IF}}^{ps}$, is simply the ionosphere-free version of de Jonge's distinct phase clock of the DC-model, $\delta\tilde{t}_{\text{IF}}^{ps} = \mu_{\text{IF}}^T\delta\tilde{t}^{ps}$.

From the comparison of the CC-1, DC and IRC/DSC-models, one can thus conclude that the IRC/DSC-model is a reparametrized form of both the DC-model (17) and the CC-model (9) using ionosphere-free observations.

3.2 The UPD/FCB-model

Just like the IRC/DSC-model which is obtained as a reparametrized version of the CC-model (9) using ionosphere-free observations, the UPD/FCB-model can be obtained as a reparametrized version of the CC-model (21) using ionosphere-free observations. In case of the UPD/FCB-model, the reparametrization is even simpler as it only involves the wide-lane transformation.

3.2.1 Network model

To derive the UPD/FCB network equations, we first form the ionosphere-free variant of (21) and then apply the wide-lane parameter transformation.

If we apply the full-rank 4×3 matrix of (29) as transformation to (21) to form its three ionosphere-free observation equations, we obtain

$$\begin{aligned} \Delta\phi^{ps}_{r,\mathrm{IF}} &= \Delta\tilde{\rho}^{ps}_{r} - d\tilde{t}^{ps} + \mu^{T}_{\mathrm{IF}}\Lambda\tilde{a}^{ps}_{r} \\ \Delta p^{ps}_{r,\mathrm{IF}} &= \Delta\tilde{\rho}^{ps}_{r} - d\tilde{t}^{ps} \\ \Delta\phi^{ps}_{r,WN} &= +\mu^{T}_{\mathrm{WL}}\Lambda\tilde{a}^{ps}_{r} \end{aligned} \tag{42}$$

With the wide-lane parametrization $\tilde{a}^{ps}_{r} = Z^{-1}_{W}[\tilde{a}^{ps}_{r,1}, \tilde{a}^{ps}_{r,W}]^{T}$, thereby making use of (33), the full-rank network equations of the UPD/FCB-model follow as

$$\begin{aligned} \Delta\phi^{ps}_{r,\mathrm{IF}} &= \Delta\tilde{\rho}^{ps}_{r} - d\tilde{t}^{ps} + \lambda_N\tilde{a}^{ps}_{r,1} + \frac{\lambda_2}{\mu_{12}}\tilde{a}^{ps}_{r,W} \\ \Delta p^{ps}_{r,\mathrm{IF}} &= \Delta\tilde{\rho}^{ps}_{r} - d\tilde{t}^{ps} \\ \Delta\phi^{ps}_{r,WN} &= \lambda_W\tilde{a}^{ps}_{r,W} \end{aligned} \tag{43}$$

Note, although the structure of these equations resembles that of the corresponding IRC/DSC equations (34), that the ambiguities in (34) are integer, whereas in (43) they are not.

For a SD satellite pair ps and a network station r, the network vector of FCB-estimable parameters is thus given as

$$x_{\mathrm{FCB}} = \left[(\Delta\tilde{x}_r)^{T}, d\tilde{t}^{ps}, [\tilde{a}^{ps}_{r,1}, \tilde{a}^{ps}_{r,W}]\right]^{T} \tag{44}$$

The interpretation of these estimable parameters is as given earlier for the CC-model (21), be it that the ambiguities are now in wide-lane form. Hence, in contrast to the ambiguities of the ionosphere-free IRC/DSC-model (cf. 34, 39), the ambiguities of the ionosphere-free UPD/FCB-model are not integer-valued, but real-valued.

3.2.2 User model

As in case of the CC-model (21), next to the estimable satellite clock $d\tilde{t}^{ps}$, the real-valued estimable ambiguities (but now in wide-lane form) of any network station, say $q \in \{1, \ldots, n\}$, can be taken to form the corrections for the user,

$$x^{\mathrm{corr}}_{\mathrm{FCB}} = \left[d\tilde{t}^{ps}, [\tilde{a}^{ps}_{q,1}, \tilde{a}^{ps}_{q,W}]\right]^{T} \tag{45}$$

With the user ionosphere-free observations corrected as

$$\begin{aligned} \Delta\tilde{\tilde{\phi}}^{ps}_{u,\mathrm{IF}} &= \Delta\phi^{ps}_{u,\mathrm{IF}} + d\tilde{t}^{ps} - \lambda_N\tilde{a}^{ps}_{q,1} - \frac{\lambda_2}{\mu_{12}}\tilde{a}^{ps}_{q,W} \\ \Delta\tilde{\tilde{p}}^{ps}_{u,\mathrm{IF}} &= \Delta p^{ps}_{u,\mathrm{IF}} + d\tilde{t}^{ps} \\ \Delta\tilde{\tilde{\phi}}^{ps}_{u,WN} &= \Delta\phi^{ps}_{u,WN} - \lambda_W\tilde{a}^{ps}_{q,W} \end{aligned} \tag{46}$$

the user-equations take the form

$$\begin{aligned} \Delta\tilde{\tilde{\phi}}^{ps}_{u,\mathrm{IF}} &= \Delta\tilde{\rho}^{ps}_{u} + \lambda_N\tilde{a}^{ps}_{qu,1} + \frac{\lambda_2}{\mu_{12}}\tilde{a}^{ps}_{qu,W} \\ \Delta\tilde{\tilde{p}}^{ps}_{u,\mathrm{IF}} &= \Delta\tilde{\rho}^{ps}_{u} \\ \Delta\tilde{\tilde{\phi}}^{ps}_{u,WN} &= \lambda_W\tilde{a}^{ps}_{qu,W} \end{aligned} \tag{47}$$

with the integer *double-differenced* ambiguities $\tilde{a}^{ps}_{qu,1} = z^{ps}_{u,1} - z^{ps}_{q,1}$ and $\tilde{a}^{ps}_{qu,W} = z^{ps}_{u,W} - z^{ps}_{q,W}$. Note that these user-equations are *identical* to the user-equations of the IRC/DSC-model (39), be it that their integer double-differenced ambiguities could differ in their choice of reference station (q vs. 1).

3.2.3 The fractional phase bias (FPB) corrections

Since any integer shift of the real-valued ambiguities in (45) would only result in an integer shift of the corresponding ambiguities in the user-equations, the PPP-RTK corrections remain admissible if the real-valued ambiguities of (45) are replaced by their fractional parts,

$$x^{\mathrm{corr}}_{\mathrm{FPB}} = \left[d\tilde{t}^{ps}, [\mathrm{frac}(\tilde{a}^{ps}_{q,1}), \mathrm{frac}(\tilde{a}^{ps}_{q,W})]\right]^{T} \tag{48}$$

with the fractional operator defined as $\mathrm{frac}(x) = x - \lfloor x \rceil$ (Geng 2011), where $\lfloor x \rceil$ denotes rounding to the nearest integer of x.

Recall from (23) the relation $\tilde{a}^{ps}_{r} = \tilde{z}^{ps}_{r} - \tilde{\delta}^{ps}$. After applying the wide-lane transformation Z_W, this relation becomes,

$$\begin{aligned} \tilde{a}^{ps}_{r,1} &= \tilde{z}^{ps}_{r,1} - \tilde{\delta}^{ps}_{,1} \\ \tilde{a}^{ps}_{r,W} &= \tilde{z}^{ps}_{r,W} - \tilde{\delta}^{ps}_{,W} \end{aligned} \tag{49}$$

Since both $\tilde{z}^{ps}_{r,1}$ and $\tilde{z}^{ps}_{r,W}$ are integer, it follows that

$$\begin{aligned} \mathrm{frac}(\tilde{a}^{ps}_{q,1}) &= -\mathrm{frac}(\tilde{\delta}^{ps}_{,1}) \\ \mathrm{frac}(\tilde{a}^{ps}_{q,W}) &= -\mathrm{frac}(\tilde{\delta}^{ps}_{,W}) \end{aligned} \tag{50}$$

This shows that, apart from their sign, the fractional parts of the real-valued ambiguities are equal to the fractional parts of the phase biases. This is the reason why the set of network- and user-equations, (43) and (47), combined with the correction vector (48), is referred to as the Fractional Cycle Bias (FCB) model (Geng et al. 2010, p. 569). The non-integer phase bias $\tilde{\delta}^{ps}$ is also referred to as the 'Uncalibrated Phase Delay' (UPD) by Ge et al. (2008, p. 389). The network- and user-equations, (43) and (47), together with the corrections (45), i.e., without the use of the fractional operator, is the formulation used by Bertiger et al. (2010).

3.2.4 The FCB corrections

The UPD/FCB method (Ge et al. 2008; Geng et al. 2012) uses a somewhat different version of (43). Using the

identity $\lambda_2/\mu_{12} = \lambda_N\lambda_1/(\lambda_2-\lambda_1)$, we may write $\lambda_N\tilde{a}^{ps}_{r,1} + \frac{\lambda_2}{\mu_{12}}\tilde{a}^{ps}_{r,W} = \frac{\lambda_2}{\mu_{12}}\lfloor\tilde{a}^{ps}_{r,W}\rceil + \lambda_N\tilde{a}^{ps}_{r,c}$, where

$$\begin{aligned}\tilde{a}^{ps}_{r,c} &= \tilde{a}^{ps}_{r,1} + \frac{\lambda_1}{\lambda_2-\lambda_1}\mathrm{frac}(\tilde{a}^{ps}_{r,W}) \\ &= \tilde{z}^{ps}_{r,1} - \tilde{\delta}^{ps}_{,c}\end{aligned} \tag{51}$$

with

$$\tilde{\delta}^{ps}_{,c} = \tilde{\delta}^{ps}_{,1} + \frac{\lambda_1}{\lambda_2-\lambda_1}\mathrm{frac}(\tilde{\delta}^{ps}_{,W}) \tag{52}$$

Hence, (43) can alternatively be expressed as

$$\begin{aligned}\Delta\phi^{ps}_{r,\mathrm{IF}} &= \Delta\tilde{\rho}^{ps}_{r} - d\tilde{t}^{ps} + \frac{\lambda_2}{\mu_{12}}\lfloor\tilde{a}^{ps}_{r,W}\rceil + \lambda_N\tilde{a}^{ps}_{r,c} \\ \Delta p^{ps}_{r,\mathrm{IF}} &= \Delta\tilde{\rho}^{ps}_{r} - d\tilde{t}^{ps} \\ \Delta\phi^{ps}_{r,WN} &= \lambda_W\tilde{a}^{ps}_{r,W}\end{aligned} \tag{53}$$

This leads to the use of the following PPP-RTK corrections

$$x^{\mathrm{corr}}_{\mathrm{FCB}} = \left[d\tilde{t}^{ps}, \left[\mathrm{frac}(\tilde{a}^{ps}_{q,c}), \mathrm{frac}(\tilde{a}^{ps}_{q,W})\right]\right]^T \tag{54}$$

rather than those given in (48). The user observations would then be corrected as

$$\begin{aligned}\Delta\tilde{\tilde{\phi}}'^{ps}_{u,\mathrm{IF}} &= \Delta\phi^{ps}_{u,\mathrm{IF}} + d\tilde{t}^{ps} - \lambda_N\mathrm{frac}(\tilde{a}^{ps}_{q,c}) \\ \Delta\tilde{\tilde{p}}'^{ps}_{u,\mathrm{IF}} &= \Delta p^{ps}_{u,\mathrm{IF}} + d\tilde{t}^{ps} \\ \Delta\tilde{\tilde{\phi}}'^{ps}_{u,WN} &= \Delta\phi^{ps}_{u,WN} - \lambda_W\mathrm{frac}(\tilde{a}^{ps}_{q,W})\end{aligned} \tag{55}$$

These equations show a somewhat more symmetric form than those of (46). Using the definition of the fractional operator, the user observation equations take then the form [compare with (47)]

$$\begin{aligned}\Delta\tilde{\tilde{\phi}}'^{ps}_{u,\mathrm{IF}} &= \Delta\tilde{\rho}^{ps}_{u} + \lambda_N a'^{ps}_{u,1} + \frac{\lambda_2}{\mu_{12}}a'^{ps}_{u,W} \\ \Delta\tilde{\tilde{p}}'^{ps}_{u,\mathrm{IF}} &= \Delta\tilde{\rho}^{ps}_{u} \\ \Delta\tilde{\tilde{\phi}}'^{ps}_{u,WN} &= \lambda_W a'^{ps}_{u,W}\end{aligned} \tag{56}$$

with the integer-valued ambiguities

$$\begin{aligned}a'^{ps}_{u,1} &= \tilde{a}^{ps}_{qu,1} + \lfloor\tilde{a}^{ps}_{q,c}\rceil \\ a'^{ps}_{u,W} &= \tilde{a}^{ps}_{qu,W} + \lfloor\tilde{a}^{ps}_{q,W}\rceil\end{aligned} \tag{57}$$

The Eqs. of (53), with (49), are the SD versions of those given in Eqs. (5) and (14) of Ge et al. (2008, p. 391), see also Eqs. (3) and (5) of Geng and Bock (2013, p. 451). In those contributions, however, the following equivalent expressions are used instead

$$\lambda_N = \frac{\lambda_1 f_1}{f_1+f_2} = \frac{c}{f_1+f_2}; \qquad \frac{\lambda_2}{\mu_{12}} = \frac{\lambda_1 f_1 f_2}{f_1^2 - f_2^2} \tag{58}$$

We already remarked earlier that the ambiguity $\tilde{a}^{ps}_{r,1}$ is sometimes erroneously referred to as the narrow-lane ambiguity because of its λ_N-coefficient in the observation equations (cf. 34). Similarly, it should be understood that the reference to the fractional part of $\tilde{a}^{ps}_{q,c}$ in (53) as the narrow-lane FCB (Ge et al. 2008; Geng et al. 2010, 2012; Geng and Bock 2013) follows the same logic.

3.2.5 The distribution of the fractional phase bias

Although an arbitrary integer shift in the PPP-RTK corrections $\tilde{a}^{ps}_{q}$ or $\tilde{\delta}^{ps}$ is of no concern in sofar that it maintains the integerness of the user-ambiguities, it is important to realize that from a probabilistic point of view the application of the fractional operator to the estimated ambiguity $\hat{\tilde{a}}^{ps}_{q}$ or to the estimated satellite phase bias $\hat{\tilde{\delta}}^{ps}$ will change the statistics of the user-corrected observables. In other words, the probability distribution of the user-corrected observations (46) will change from a multivariate normal distribution to a non-normal distribution if one replaces the estimator $\hat{\tilde{a}}^{ps}_{q}$ by its fractional part $\mathrm{frac}(\hat{\tilde{a}}^{ps}_{q}) = -\mathrm{frac}(\hat{\tilde{\delta}}^{ps})$. The following lemma gives the PDF of the fractional phase bias.

Lemma 1 (PDF of fractional phase bias) *Let $f_{\hat{\delta}}(x)$ be the probability density function of the satellite phase bias estimator $\hat{\delta}$. Then,*

$$f_{\mathrm{frac}(\hat{\delta})}(x) = \sum_{z\in\mathbb{Z}} f_{\hat{\delta}}(x+z)s_0(x) \tag{59}$$

with $\mathcal{P}_0$ the pull-in region and $s_0(x)$ its indicator function ($s_0(x) = 1$ if $x \in \mathcal{P}_0$, $s_0(x) = 0$ otherwise).

Proof Follows from the GNSS ambiguity residual PDF of Teunissen (2002, p. 44). □

For a normally distributed estimated satellite phase bias, the PDF $f_{\mathrm{frac}(\hat{\delta})}(x)$ is determined by the mean and variance of $\hat{\delta}$. The peakedness of the PDF $f_{\mathrm{frac}(\hat{\delta})}(x)$ is driven by the variance of $\hat{\delta}$. The larger the variance, the flatter the PDF, which in the limit becomes a uniform distribution over the pull-in region $\mathcal{P}_0$. The smaller the variance, the more peaked the PDF becomes, with increasing probability mass becoming concentrated at its mean.

Would the mean be integer, as is the case with the mean of the float solution of a double-differenced ambiguity, then the PDF of the fraction would be symmetric with respect to the origin. In case of a non-integer mean, however, the PDF will be asymmetric with respect to the origin. This is the case that applies to the satellite phase bias.

Figure 1 shows some examples for the scalar case. In the scalar case, $\mathcal{P}_0$ is the origin-centered interval of length 1. Figure 1 shows the fractional phase bias PDF $f_{\mathrm{frac}(\hat{\delta})}(x)$ for $\hat{\delta} \sim \mathrm{N}(\mathsf{E}(\hat{\delta}), \sigma^2_{\hat{\delta}})$. The PDF is shown for two different precision levels of the estimated phase bias, $\sigma_{\hat{\delta}} = 0.1$ cycle (blue curve) and $\sigma_{\hat{\delta}} = 0.3$ cycle (green curve). The left panel of the figure shows then the corresponding PDFs for the case the mean of the estimated phase bias would be integer, $\mathsf{E}(\hat{\delta}) \in \mathbb{Z}$,

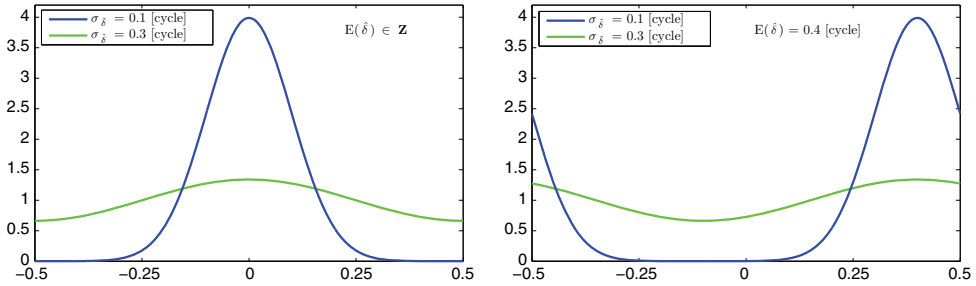

Fig. 1 PDF $f_{\mathrm{frac}(\hat{\delta})}(x)$ of fractional phase bias $\mathrm{frac}(\hat{\delta})$ for $\hat{\delta} \sim \mathrm{N}(\mathsf{E}(\hat{\delta}), \sigma^2_{\hat{\delta}})$. *Left*: $\mathsf{E}(\hat{\delta}) \in \mathbb{Z}$, with $\sigma_{\hat{\delta}} = 0.1$ cycle (*blue curve*) and $\sigma_{\hat{\delta}} = 0.3$ cycle (*green curve*); *Right*: $\mathsf{E}(\hat{\delta}) = 0.4$ cycle, with $\sigma_{\hat{\delta}} = 0.1$ cycle (*blue curve*) and $\sigma_{\hat{\delta}} = 0.3$ cycle (*green curve*)

while in the right panel the two PDFs are shown for a non-integer mean, $\mathsf{E}(\hat{\delta}) = 0.4$ cycle.

The above shows that when use is made of the fractional operator, one has to be very careful when evaluating the statistics and quality of the user-corrected observables. As the user-corrected observables will then in principle fail to be normally distributed, it will affect quality control procedures that are applied at the user side. Only in case sufficient probability mass of the normal distribution of $\hat{\delta}$ is located in the pull-in region $\mathcal{P}_0$, can one hope to be able to approximate the PDF of $\mathrm{frac}(\hat{\delta})$ by that of $\hat{\delta}$. Whether or not this is the case cannot be judged on only the variance $\sigma^2_{\hat{\delta}}$, but requires information about the *unknown* mean $\mathsf{E}(\hat{\delta})$ as well.

3.2.6 The CC-2, IRC/DSC and UPD/FCB-models compared

We derived the UPD/FCB-model from the full-rank CC-model (21), by first formulating the ionosphere-free variant of the CC-model and then applying the one-to-one wide-lane transformation.

The $\mathcal{S}$-basis that we used is $\Delta x_1, d^{ps}, \delta^{ps}$ (cf. 20). In Geng (2011), it is stated, however, that the $\mathcal{S}$-basis of the UPD/FCB-model is given by the ionosphere-free and narrow-lane code biases, $d^{ps}_{,\mathrm{IF}} = \mu^T_{\mathrm{IF}} d^{ps}$ and $d^{ps}_{,\mathrm{NL}} = \mu^T_{\mathrm{NL}} d^{ps}$, and the phase biases $\delta^{ps}_{,1}, \delta^{ps}_{1,W}$. Hence, one may think that for the UPD/FCB-model in Ge et al. (2008), a different $\mathcal{S}$-basis choice is made. This is not true, however, as the transformation between d^{ps} and $d^{ps}_{,\mathrm{IF}}, d^{ps}_{,\mathrm{NL}}$ is one-to-one, and also the wide-lane transformation between δ^{ps} and $\delta^{ps}_{,1}, \delta^{ps}_{1,W}$ is one-to-one. Hence, the $\mathcal{S}$-basis choice is the same, namely $\Delta x_1, d^{ps}, \delta^{ps}$.

We already noted that the IRC/DSC user Eq. (39) are identical to those of UPD/FCB (47) if $q = 1$. Their network equations are quite different, however, compare (34) for IRC/DSC with (43) for UPD/FCB. How is this possible? The reason lies in their PPP-RTK corrections. Although some of the individual parameters that make up their corrections differ, namely

$$\left[\delta\tilde{t}^{ps}_{,\mathrm{IF}}, \tilde{\delta}^{ps}_{,W}\right]_{\mathrm{IRC/DSC}} \; vs \; \left[\mathrm{frac}(\tilde{a}^{ps}_{q,1}), \mathrm{frac}(\tilde{a}^{ps}_{q,W})\right]_{\mathrm{FCB}} \tag{60}$$

the actual corrections that the user observations undergo have the same effect. The user observation corrections for the IRC/DSC-model (cf. 38) and the UPD/FCB-model (cf. 46) satisfy, namely

$$\begin{aligned} \delta\tilde{t}^{ps}_{\mathrm{IF}} &= d\tilde{t}^{ps} - \lambda_N \tilde{a}^{ps}_{q,1} - \frac{\lambda_2}{\mu_{12}} \tilde{a}^{ps}_{q,W} \quad \text{for} \quad q = 1 \\ d\tilde{t}^{ps} &= d\tilde{t}^{ps} \\ \tilde{\delta}^{ps}_{W} &= -\tilde{a}^{ps}_{q,W} \quad \text{for} \quad q = 1 \end{aligned} \tag{61}$$

while for $q \neq 1$, the corrections only make the user-ambiguities of the two models differ by an integer shift.

From the comparison of the CC, IRC/DSC, and UPD/FCB-models, one can thus conclude that the UPD/FCB-model is a reparametrized form of the ionosphere-free version of the CC-model (21), while the IRC/DSC-model is that of the CC-model (9). An overview of the transformational links between the various models is given in Fig. 2.

4 Role of the PPP-RTK corrections

In the previous section, different formulations of the network- and user models were compared. As they could all be derived from the same model, without any change in underlying model assumptions, all the presented formulations are intrinsically the same. Their differences were shown to lie only in (a) the choice of $\mathcal{S}$-basis, (b) in the choice of parameterization, and (c) in the choice of whether or not to eliminate the ionospheric delays.

Since the different formulations are intrinsically the same, their individual set of PPP-RTK corrections are closely linked. In this section, we will have a closer look at these corrections and show how they can be interpreted and transformed.

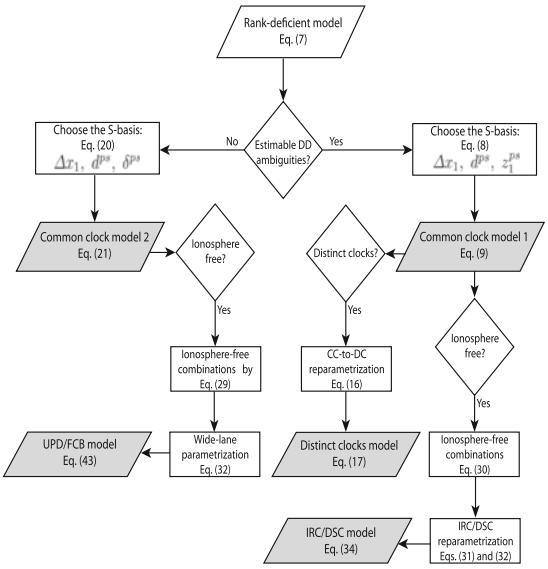

Fig. 2 Diagram illustrating the transformational links between the original rank-deficient model and the PPP-RTK full-rank variants: CC-1 (cf. 9), DC (cf. 17), CC-2 (cf. 21), IRC/DSC (cf. 34), and UPD/FCB (cf. 43)

4.1 The same corrected user observations

When we compare the different *user*-equations, we note that they are essentially the same. This is true for the IRC/DSC and UPD/FCB ionosphere-free user-equations, (39), (47) and (56), since they only differ in a possible integer-shift of their ambiguities. The same holds true for the two sets of CC user-equations, (14) and (27).

The sameness of the user-equations implies, that the corrected user observations themselves are, apart from the presence of integer shifts, also the same. Thus, for the two different CC-corrected user observations, we have

$$\begin{aligned}\Delta\tilde{\phi}_u^{ps} &\overset{(13,26)}{=} \Delta\tilde{\tilde{\phi}}_u^{ps} \pm \Lambda\, z, \quad z \in \mathbb{Z}^2\\ \Delta\tilde{p}_u^{ps} &\overset{(13,26)}{=} \Delta\tilde{\tilde{p}}_u^{ps}\end{aligned} \tag{62}$$

while for the ionosphere-free, IRC/DSC and UPD/FCB, corrected user observations, we have

$$\begin{aligned}\Delta\tilde{\phi}_{u,\mathrm{IF}}^{ps} &\overset{(38,55)}{=} \Delta\tilde{\tilde{\phi}}'^{ps}_{u,\mathrm{IF}} \pm \lambda_N\left(z_1 + \frac{\lambda_1}{\lambda_2-\lambda_1}z_W\right),\ z_1, z_W \in \mathbb{Z}\\ \Delta\tilde{p}_{u,\mathrm{IF}}^{ps} &\overset{(38,55)}{=} \Delta\tilde{\tilde{p}}'^{ps}_{u,\mathrm{IF}}\\ \Delta\tilde{\phi}_{u,WN}^{ps} &\overset{(38,55)}{=} \Delta\tilde{\tilde{\phi}}'^{ps}_{u,WN} \pm \lambda_W z_W\end{aligned} \tag{63}$$

Since BLUE-estimation, i.e., properly weighted least-squares estimation, is intrinsically invariant for differences in choice of (a) $\mathcal{S}$-basis, (b) parameterization, and (c) whether or not some parameters, such as ionospheric delays, are eliminated, the application of a rigorous network adjustment, using any one of the different PPP-RTK methods, must give the same positioning results for the user. Any differences that show up between the results of the different PPP-RTK methods, must then be attributed to the usage of a different nonrigorous estimation procedure. We will revisit this remark in Sect. 6.2.

4.2 Transformation between PPP-RTK corrections

As the user-equations of the user-corrected observations are essentially the same, the different PPP-RTK corrections must contain the same information and hence be related through one-to-one transformations. We have summarized these transformations in Table 1.

For example, if one would like to transform from the IRC/DSC corrections to the CC-1 corrections, then the following transformation applies:

$$\begin{bmatrix} d\tilde{t}^{ps} \\ \tilde{\delta}^{ps}_{,1} \\ \tilde{\delta}^{ps}_{,2} \end{bmatrix}_{\mathrm{CC-1}} = \begin{bmatrix} 1 & 0 & 0 \\ -\frac{1}{\lambda_N} & \frac{1}{\lambda_N} & -\frac{\lambda_1}{\lambda_2-\lambda_1} \\ -\frac{1}{\lambda_N} & \frac{1}{\lambda_N} & -\frac{\lambda_2}{\lambda_2-\lambda_1} \end{bmatrix} \begin{bmatrix} d\tilde{t}^{ps} \\ \delta\tilde{t}^{ps}_{,\mathrm{IF}} \\ \tilde{\delta}^{ps}_{,W} \end{bmatrix}_{\mathrm{IRC/DSC}} \tag{64}$$

These transformations can now be used to operationally link the different PPP-RTK methods and to mix them between network and users. It allows a user to transform the network received corrections to the format that suits his/her user software, or alternatively, as a service to the users, it allows a network server to transform the network corrections to any one of the other formats and thus make any of the different PPP-RTK parametrizations available to the users.

Table 1 PPP-RTK user-corrections in different models

CC 1	CC 2	DC	IRC/DSC	UPD/FCB
$\begin{bmatrix} d\tilde{t}^{ps} \\ \tilde{\delta}^{ps}_{,1} \\ \tilde{\delta}^{ps}_{,2} \end{bmatrix}$	$= \begin{bmatrix} 1 & 0 & 0 \\ 0 & -1 & 0 \\ 0 & 0 & -1 \end{bmatrix} \begin{bmatrix} d\tilde{t}^{ps} \\ \tilde{\tilde{a}}^{ps}_{q,1} \\ \tilde{\tilde{a}}^{ps}_{q,2} \end{bmatrix} + \begin{bmatrix} 0 \\ z_1 \\ z_2 \end{bmatrix}$	$= \begin{bmatrix} 1 & 0 & 0 \\ -\frac{1}{\lambda_1} & \frac{1}{\lambda_1} & 0 \\ -\frac{1}{\lambda_2} & 0 & \frac{1}{\lambda_2} \end{bmatrix} \begin{bmatrix} d\tilde{t}^{ps} \\ \delta\tilde{t}^{ps}_{,1} \\ \delta\tilde{t}^{ps}_{,2} \end{bmatrix}$	$= \begin{bmatrix} 1 & 0 & 0 \\ -\frac{1}{\lambda_N} & \frac{1}{\lambda_N} & -\frac{\lambda_1}{\lambda_2-\lambda_1} \\ -\frac{1}{\lambda_N} & \frac{1}{\lambda_N} & -\frac{\lambda_2}{\lambda_2-\lambda_1} \end{bmatrix} \begin{bmatrix} d\tilde{t}^{ps} \\ \delta\tilde{t}^{ps}_{,IF} \\ \tilde{\delta}^{ps}_{,W} \end{bmatrix}$	$= \begin{bmatrix} 1 & 0 & 0 \\ 0 & -1 & \frac{\lambda_1}{\lambda_2-\lambda_1} \\ 0 & -1 & \frac{\lambda_2}{\lambda_2-\lambda_1} \end{bmatrix} \begin{bmatrix} d\tilde{t}^{ps}, \\ \mathrm{frac}(\tilde{\tilde{a}}^{ps}_{q,c}) \\ \mathrm{frac}(\tilde{\tilde{a}}^{ps}_{q,W}) \end{bmatrix} + \begin{bmatrix} 0 \\ z_c \\ z_W \end{bmatrix}$

The integers $z_1,\ z_2,\ z_c,\ z_W$ may take any integer values

4.3 Interpretation of the PPP-RTK corrections

The PPP-RTK corrections establish a link between the user-parameters and the network-parameters. The corrections are designed to realize integer ambiguities in the user-equations, thus enabling user integer ambiguity resolution. As remarked earlier, the interpretation of these 'user' integer ambiguities is that they are straightforward *double-differenced* (DD) ambiguities.

The presence of z_1^{ps} in the phase bias correction vector of CC-1,

$$\tilde{\delta}^{ps} = \delta^{ps} + Md^{ps} - z_1^{ps} \tag{65}$$

or, in the real-valued ambiguity correction vector of CC-2,

$$\tilde{a}_1^{ps} = z_1^{ps} - \delta^{ps} - Md^{ps} \tag{66}$$

or, in the integer recovery clock and wide-lane phase bias corrections of IRC/DSC,

$$\begin{aligned} \delta\tilde{t}_{\text{IF}}^{ps} &= dt^{ps} + \mu_{\text{IF}}^T \Lambda(\delta^{ps} - z_1^{ps}) - \Delta\rho_1^{ps} \\ \tilde{\delta}_W^{ps} &= (0,1) Z_W (\delta^{ps} - z_1^{ps}) - \frac{1}{\lambda_W} \mu_{\text{NL}}^T d^{ps} \end{aligned} \tag{67}$$

make that the user-ambiguities in all these cases become DD ambiguities between user station u and network station 1.

Next to establishing an ambiguity link between network and user, the PPP-RTK corrections also establish a positional link between network and user. The presence of $\Delta\rho_1^{ps}$ in the satellite clock correction

$$d\tilde{t}^{ps} = dt^{ps} + \mu_{\text{IF}}^T d^{ps} - \Delta\rho_1^{ps} \tag{68}$$

and in the integer recovery clock correction $\delta\tilde{t}_{\text{IF}}^{ps}$ in case of the IRC/DSC method makes that the user-positioning parameters in essence become *relative positioning* parameters between user station u and network station 1. The PPP-RTK method is, thus, a relative positioning method and not one of absolute positioning.

To demonstrate the relative positioning feature of PPP-RTK, consider the special case that the network consists of only *one single station*, i.e., $n = 1$. It then follows from (9), since $\Delta\tilde{\rho}_1^{ps} = 0$ ($\Delta\tilde{x}_1 = 0$) and $\tilde{z}_1 = 0$, that

$$\begin{aligned} \Delta\phi_1^{ps} &= -\mu\, \tilde{\imath}_1^{ps} - e\, d\tilde{t}^{ps} - \Lambda\, \tilde{\delta}^{ps} \\ \Delta p_1^{ps} &= +\mu\, \tilde{\imath}_1^{ps} - e\, d\tilde{t}^{ps}, \quad s = 1, \ldots, m \end{aligned} \tag{69}$$

This is an invertible system of $4(m-1)$ equations in $4(m-1)$ unknowns. After inversion, we get

$$\begin{aligned} \tilde{\imath}_1^{ps} &= +\mu_{\text{GF}}^T \Delta p_1^{ps} \\ d\tilde{t}^{ps} &= -\mu_{\text{IF}}^T \Delta p_1^{ps} \\ \tilde{\delta}^{ps} &= -\Lambda^{-1}[\Delta\phi_1^{ps} + (\mu\mu_{\text{GF}}^T - e\mu\mu_{\text{IF}}^T)\Delta p_1^{ps}] \end{aligned} \tag{70}$$

Substitution of these expressions for $d\tilde{t}^{ps}$ and $\tilde{\delta}^{ps}$ into (13) gives the user observation equations as

$$\begin{aligned} \Delta\tilde{\phi}_u^{ps} &= \Delta\phi_{1u}^{ps} - \mu\mu_{\text{GF}}^T \Delta p_1^{ps} = e\, \Delta\tilde{\rho}_u^{ps} - \mu\, \tilde{\imath}_u^{ps} + \Lambda\tilde{z}_u^{ps} \\ \Delta\tilde{p}_u^{ps} &= \Delta p_{1u}^{ps} + \mu\mu_{\text{GF}}^T \Delta p_1^{ps} = e\, \Delta\tilde{\rho}_u^{ps} + \mu\, \tilde{\imath}_u^{ps} \end{aligned} \tag{71}$$

in which we recognize the DD phase and code observations, $\Delta\phi_{1u}^{ps} = \Delta\phi_u^{ps} - \Delta\phi_1^{ps}$ and $\Delta p_{1u}^{ps} = \Delta p_u^{ps} - \Delta p_1^{ps}$, respectively.

This demonstrates that the PPP-RTK corrected observations are actually DD observations biased with an additional iono-term '$\mu\mu_{\text{GF}}^T \Delta p_1^{ps}$'. This bias term is of no consequence, since it gets fully absorbed in the ionospheric term $\tilde{\imath}_u^{ps}$. It does, therefore, not affect the solution for $\Delta\tilde{x}_u$ (or $\Delta\tilde{\rho}_u^{ps}$) and $\tilde{z}_u^{ps}$. Hence, the PPP-RTK generated solution of the above user model (71) is indeed a relative positioning solution, and one, that will be identical to a standard DD single baseline solution.

In fact, in its ionosphere-free formulation, the bias '$\mu\mu_{\text{GF}}^T \Delta p_1^{ps}$' is eliminated and the observables will consist solely of DD combinations,

$$\begin{aligned} \Delta\tilde{\phi}_{u,\text{IF}}^{ps} &= \Delta\phi_{1u,IF}^{ps} \\ \Delta\tilde{p}_{u,\text{IF}}^{ps} &= \Delta p_{1u,\text{IF}}^{ps} \\ \Delta\tilde{\phi}_{u,WN}^{ps} &= \Delta\phi_{1u,WN}^{ps} \end{aligned} \tag{72}$$

Thus, the only difference between the above PPP-RTK solution and a standard DD single-baseline solution is that with (71) a between-satellite SD ionospheric delay $\tilde{\imath}_u^{ps}$ is estimated, while in the DD single-baseline case, with the absence of '$\mu\mu_{\text{GF}}^T \Delta p_1^{ps}$', this would be the DD ionospheric delay $\tilde{\imath}_{1u}^{ps} = \tilde{\imath}_u^{ps} - \tilde{\imath}_1^{ps}$.

As to the number of correction parameters required, we note that the PPP-RTK method only requires the $3(m-1)$ corrections $d\tilde{t}^{ps}$ and $\tilde{\delta}^{ps}$, while a standard DD approach requires all original $4(m-1)$ phase and code data $\Delta\phi_1^{ps}$ and Δp_1^{ps}.

4.4 On the ionosphere-free formulation

One may wonder what the benefits are of using an ionosphere-free formulation? Surely this is not an improved quality of its solution, since, when rigorously solved, the ionosphere-free model formulations of Sect. 3 give exactly the same solution as when using the original model formulations of Sect. 2. An apparent benefit of this traditional ionosphere-free formulation is that less parameters need to be solved for as all ionospheric delays have been eliminated. But still, if one is not interested in these ionosphere delays, then it is really not needed to have them *a priori* eliminated from the model. If one wants them eliminated, one can simply reduce the normal equations for these ionospheric delays. This has the advantage that one can still work with the original, usu-

ally uncorrelated, observations and their equations, instead of with the correlated ionosphere-free observations.

We find that the ionosphere-free formulation, instead of having clear benefits, has the drawback of lacking flexibility for further model strengthening, see e.g., Teunissen and de Bakker (2012) or Mervart et al. (2013). The inclusion of a dynamic state transition model to capture the temporal smoothness of the ionosphere, for instance, will be problematic with the ionosphere-free model. A similar difficulty exists when one wants to incorporate an ionospheric model to capture both the temporal and spatial characteristics of the ionosphere.

It is well known that the ionosphere-free or ionosphere-float models are relatively weak in the sense of their ambiguity resolution capabilities. Relatively long observation time spans are then needed to achieve successful integer ambiguity resolution (Hernandez-Pajares et al. 2000; Jonkman et al. 2000; Odijk 2002; Odijk et al. 2014a). The lack of any ionospheric information is, in fact, the *bottleneck* for fast ambiguity resolution. Successful ambiguity resolution is achieved much faster when such ionospheric information can be provided to the model. But if such information would be available, it would be cumbersome to include in the ionosphere-free model. Doing so would also defy the whole purpose of an ionosphere-free formulation. This is straightforward, however, with our original model formulations, such as (9) or (21), on the network side, and (14) or (27), on the user side. On the network side, for instance, the inclusion of an ionospheric model would result in a strengthening of the model through the parametrization of the slant delays $\tilde{\imath}_r^{ps}$ into fewer parameters. And on the user side, the model would be strengthened through the provision of a priori information on the ionospheric delays of the user, as was already demonstrated in the PPP-RTK concept of Teunissen et al. (2010) and Odijk et al. (2012, 2014b).

In order for the PPP-RTK concept to be better applicable to a wider range of network and user station separations (i.e., from close to distant), the corrections will have to include ionospheric information. Consider, for instance, the case where BLUP (i.e., least-squares interpolation) is used to predict the ionospheric user delay, say $\tilde{\imath}^{ps}$, from the network delays $\tilde{\imath}_r^{ps}$, $r = 1, \ldots, n$. Then, next to applying $d\tilde{t}^{ps}$ and $\tilde{\delta}^{ps}$, an application of the ionosphere correction gives for the user-equations,

$$\begin{aligned} &\Delta\phi_u^{ps} + \mu\tilde{\imath}^{ps} + e\, d\tilde{t}^{ps} + \Lambda\, \tilde{\delta}^{ps} \\ &\quad = e\tilde{\rho}_u^{ps} - \mu(\tilde{\imath}_u^{ps} - \tilde{\imath}^{ps}) + \Lambda\tilde{z}_u^{ps} \\ &\Delta p_u^{ps} - \mu\tilde{\imath}^{ps} + e\, d\tilde{t}^{ps} = e\tilde{\rho}_u^{ps} + \mu(\tilde{\imath}_u^{ps} - \tilde{\imath}^{ps}) \end{aligned} \tag{73}$$

Hence, at the user side, the biased ionospheric slant delay $\tilde{\imath}_u^{ps}$ is now replaced with its difference to $\tilde{\imath}^{ps}$. This is a flexible formulation as it allows one to a priori weigh the difference $\tilde{\imath}_u^{ps} - \tilde{\imath}^{ps}$ in accordance to the ionospheric prediction error. The smaller the prediction error, the stronger the model and the larger the ambiguity success rate. In the limit, one would have $\tilde{\imath}^{ps} = \tilde{\imath}_u^{ps}$, thus providing a strength that is equivalent to that of an ionosphere-fixed, short baseline model.

5 Estimation of the PPP-RTK corrections

In this section, we discuss 4 different least-squares estimators of the PPP-RTK corrections: the float and fixed estimators under the *geometry-free* (GF) model and the float and fixed estimators under the *geometry-based* (GB) model. The different characteristics of these estimators will also facilitate our discussion of some of the estimation approaches described in the literature.

As the previous sections have shown, there are different forms of network equations one can start from. Hence, the four mentioned estimators can be determined for any of these network equations. The CC-model (9) would have our preference, as its observation equations are already parameterized in integer ambiguities. However, to make an easier link with some of the other approaches, as well as to show how integer ambiguity resolution can be incorporated when the estimated ambiguities are non-integer, we start here from the network equations of the CC-model (21). With this CC-2 model, we discuss the four different estimators for $d\tilde{t}^{ps}$ and $\tilde{a}_q^{ps}$. The corresponding estimators of any of the other forms of corrections can then easily be obtained through the transformations given in Table 1.

5.1 Geometry-free estimation

If we define $\phi_r = [\phi_{r,1}^T, \phi_{r,2}^T]^T \in \mathbb{R}^{2m}$, $\phi_{r,j} = [\Delta\phi_{r,j}^1, \ldots, \Delta\phi_{r,j}^m]^T$, $j = 1, 2$, with a likewise definition for p_r, we can obtain from (21), in vector-matrix form, a uniquely solvable set of equations for station r,

$$\mathsf{E}\begin{bmatrix} (I_2 \otimes D_m^T)\phi_r \\ (I_2 \otimes D_m^T)p_r \end{bmatrix} = \begin{bmatrix} (-\mu, -e, \Lambda) \otimes I_{m-1} \\ (+\mu, -e, 0) \otimes I_{m-1} \end{bmatrix} \begin{bmatrix} \tilde{\imath}_r \\ d\tilde{t}_r \\ \tilde{a}_r \end{bmatrix} \tag{74}$$

where $\otimes$ denotes the Kronecker product (Rao 1973), D_m^T denotes an $(m-1)\times m$ between-satellite differencing matrix, and $\tilde{\imath}_r$, $d\tilde{t}_r$, and $\tilde{a}_r$ denote the vectors of $(m-1)$ between-satellite differenced estimable ionospheric delays, satellite clocks and ambiguities of station r, respectively. Note that $d\tilde{t}^{ps}$ and $\Delta\tilde{\rho}_r^{ps}$ in (21) have been lumped to $d\tilde{t}_r^{ps} = d\tilde{t}^{ps} - \Delta\tilde{\rho}_r^{ps}$ in (74) ($d\tilde{t}_1^{ps} = d\tilde{t}^{ps}$). The system (74) is referred to as *geometry-free* since its design matrix is independent of the receiver-satellite geometry (Teunissen 1997a).

The variance matrix of the observables of (74) is assumed given as

$$\mathsf{D}\begin{bmatrix}(I_2\otimes D_m^T)\phi_r\\(I_2\otimes D_m^T)p_r\end{bmatrix}=c_r^2\begin{bmatrix}C_\phi & 0\\0 & C_p\end{bmatrix}\otimes C_s \tag{75}$$

in which $C_s = D_m^T C_S D_m$, with C_S the co-factor matrix that captures the satellite elevation dependency. The scalar c_r^2 ($r = 1,\ldots,n$) is a receiver-dependent co-factor. In this contribution, we assume all receivers of the same quality and thus $c_r^2 = 1$ for all r. The 2×2 positive-definite matrices C_ϕ and C_p are the co-factor matrices of the phase and code observable types, respectively.

As the design matrix of (74) is square and invertible, the float solution of $d\tilde{t}_r$ and $\tilde{a}_r$ is easily obtained.

Lemma 2 (GF float corrections) *The geometry-free float solutions $d\hat{\tilde{t}}_{r,\mathrm{GF}}$ and $\hat{\tilde{a}}_{r,\mathrm{GF}}$ of (74), and their (co)variance matrices are given as*

$$\begin{aligned}d\hat{\tilde{t}}_{r,\mathrm{GF}} &= -[\mu_{\mathrm{IF}}^T\otimes D_m^T]p_r\\ \hat{\tilde{a}}_{r,\mathrm{GF}} &= +[\Lambda^{-1}\otimes D_m^T][\phi_r-(L\otimes I_{m-1})p_r]\end{aligned} \tag{76}$$

and

$$\begin{aligned}Q^{\mathrm{GF}}_{d\hat{\tilde{t}}_r d\hat{\tilde{t}}_r} &= c_{\hat\rho}^2\otimes C_s\\ Q^{\mathrm{GF}}_{d\hat{\tilde{t}}_r\hat{\tilde{a}}_r} &= c_{\hat\rho}^2 e_\mu^T\Lambda^{-1}\otimes C_s\\ Q^{\mathrm{GF}}_{\hat{\tilde{a}}_r\hat{\tilde{a}}_r} &= \Lambda^{-1}(C_\phi + c_{\hat{\imath}|\rho}^2\mu\mu^T + c_{\hat\rho}^2 e_\mu e_\mu^T)\Lambda^{-1}\otimes C_s\end{aligned} \tag{77}$$

with $L = I_2 - 2\mu\mu_{\mathrm{GF}}^T = -[\mu, e][\mu,-e]^{-1}$, $c_{\hat\rho}^2 = \mu_{\mathrm{IF}}^T C_p\mu_{\mathrm{IF}}$, $c_{\hat{\imath}|\rho}^2 = (\mu^T C_p^{-1}\mu)^{-1}$, $e_\mu = e - (c_{\hat\rho\hat\imath}/c_{\hat\rho}^2)\mu$, $c_{\hat\rho\hat\imath} = \mu_{\mathrm{IF}}^T C_p\mu_{\mathrm{GF}}$.

Proof See Appendix. □

The variance matrix $Q^{\mathrm{GF}}_{\hat{\tilde{a}}_r\hat{\tilde{a}}_r}$ has the typical structure of a geometry-free ambiguity variance matrix (Teunissen 1997c). It has been decomposed such as to clearly show the contribution of the phase and code precision. As shown in the next section, the range-related component that depends on $c_{\hat\rho}^2$ is the part that will be improved when one switches from the geometry-free model to the geometry-based model.

The GF float solution can be obtained on a station-by-station basis. This is not the case for the ambiguity-fixed solution. To the fixed solutions $d\check{\tilde{t}}_r$ and $\check{\tilde{a}}_r$, the data of all network stations contribute. This is a consequence of the fact (cf. 23) that not the station ambiguities $\tilde{a}_r$, but the between-station ambiguities $\tilde{a}_r - \tilde{a}_1 = \tilde{z}_r$ are integer. Hence, it is these double differences that are estimated as integers and not the between-satellite differenced station ambiguities $\tilde{a}_r$. The precision of these estimated station ambiguities, as well as that of the satellite clocks, will benefit, however, from such integer ambiguity resolution.

The GF ambiguity-fixed solution of the satellite clock $d\tilde{t}_r$ and of the real-valued ambiguity vector $\tilde{a}_r$ is given in the following lemma.

Lemma 3 (GF fixed corrections) *The geometry-free fixed solutions $d\check{\tilde{t}}_{r,\mathrm{GF}}$ and $\check{\tilde{a}}_{r,\mathrm{GF}}$ of (74), and their (co)variance matrices are given as*

$$\begin{aligned}d\check{\tilde{t}}_{r,\mathrm{GF}} &= d\hat{\tilde{t}}_{r,\mathrm{GF}} - Q^{\mathrm{GF}}_{d\hat{\tilde{t}}_r\hat{\tilde{a}}_r}Q^{\mathrm{GF}-1}_{\hat{\tilde{a}}_r\hat{\tilde{a}}_r}[\hat{\tilde{a}}_{r,\mathrm{GF}} - \check{\tilde{a}}_{r,\mathrm{GF}}]\\ \check{\tilde{a}}_{r,\mathrm{GF}} &= \check{\tilde{z}}_r + \frac{1}{n}\sum_{j=1}^n[\hat{\tilde{a}}_{j,\mathrm{GF}} - \check{\tilde{z}}_j]\end{aligned} \tag{78}$$

and

$$\begin{aligned}Q^{\mathrm{GF}}_{d\check{\tilde{t}}_r d\check{\tilde{t}}_r} &= Q^{\mathrm{GF}}_{d\hat{\tilde{t}}_r d\hat{\tilde{t}}_r} - \frac{n-1}{n}(c_{\hat\rho}^2 - c_{\check\rho}^2)\otimes C_s \approx \frac{1}{n}Q^{\mathrm{GF}}_{d\hat{\tilde{t}}_r d\hat{\tilde{t}}_r}\\ Q^{\mathrm{GF}}_{d\check{\tilde{t}}_r\check{\tilde{a}}_r} &= \frac{1}{n}Q^{\mathrm{GF}}_{d\hat{\tilde{t}}_r\hat{\tilde{a}}_r}\\ Q^{\mathrm{GF}}_{\check{\tilde{a}}_r\check{\tilde{a}}_r} &= \frac{1}{n}Q^{\mathrm{GF}}_{\hat{\tilde{a}}_r\hat{\tilde{a}}_r}\end{aligned} \tag{79}$$

in which $\check{\tilde{z}}_i$ ($i = 1,\ldots,n$), with $\check{\tilde{z}}_1 = 0$, are the geometry-free integer resolved DD ambiguities of the network. The co-factor $c_{\check\rho}^2$ is given as $c_{\check\rho}^2 = \mu_{\mathrm{IF}}^T(C_\phi^{-1} + L^T C_p^{-1}L)^{-1}\mu_{\mathrm{IF}}$.

Proof See Appendix. □

Note that the difference of the fixed and float solution of $d\tilde{t}_r$ only depends on the ambiguity residual of the station r itself. This is due to the fact that $d\hat{\tilde{t}}_{r,\mathrm{GF}}$ and $\hat{\tilde{a}}_{q,\mathrm{GF}}$ are uncorrelated for $q \neq r$.

Also note, since $\tilde{a}_r = \tilde{z}_r - \tilde{\delta}$ (cf. 23), that the average in the second equation of (78) is the GF fixed solution of the negative phase bias $-\tilde{\delta}$. Thus,

$$\check{\tilde{\delta}}_{\mathrm{GF}} = -\frac{1}{n}\sum_{j=1}^n[\hat{\tilde{a}}_{j,\mathrm{GF}} - \check{\tilde{z}}_j] \tag{80}$$

with variance matrix

$$Q^{\mathrm{GF}}_{\check{\tilde{\delta}}\check{\tilde{\delta}}} = Q^{\mathrm{GF}}_{\check{\tilde{a}}_r\check{\tilde{a}}_r} = \frac{1}{n}Q^{\mathrm{GF}}_{\hat{\tilde{a}}_r\hat{\tilde{a}}_r} \tag{81}$$

where we assumed the ambiguity success rate large enough to neglect the uncertainty in the integer solution $\check{\tilde{z}}_r$.

We return to these equations later when the FCB approach of estimation is discussed. We remark that the average in (80) will generalize to a weighted-average when the station-dependent factors c_r^2 of (75) would be chosen different from 1. This would be the case, for instance, when receivers of different quality would participate in the network.

Lemma 3 shows the GF precision improvement that one can expect to achieve in the clock and ambiguity estimators as a result of successful integer ambiguity resolution. It shows that the gain in precision (approximately) follows the $1/\sqrt{n}$ rule. For the ambiguities, this is due to the network averaging that takes place in computing $\check{\tilde{a}}_{r,\mathrm{GF}}$ (cf. 78) and for the satellite clock $d\check{\tilde{t}}_{r,\mathrm{GF}}$ it follows from using the approximation $c_{\check\rho}/c_{\hat\rho} \approx 0$ (cf. 79).

This $1/\sqrt{n}$ improvement, although significant, is not as spectacular as the two orders of magnitude improvement that

Table 2 GF and GB multi-epoch redundancy table

Redundancy	Float	Fixed
GF	$2(m-1)(k-1)n$	$2(m-1)(kn-1)$
GB	GF $+\,[k(m-1)-v](n-1)$	GF $+\,[k(m-1)-v](n-1)$

Table 3 Variance matrices of the k-epoch *ambiguity-float* GB/GF least-squares PPP-RTK corrections expressed in their single-epoch counterparts

Multi-epoch GB		Single-epoch GB		Multi-epoch GF
$Q^{GB}_{\hat{d\tilde{t}}\hat{d\tilde{t}}}[k]$	=	$\frac{1}{k}Q^{GB}_{\hat{d\tilde{t}}\hat{d\tilde{t}}}[1]+\frac{k-1}{k}\frac{1}{n}c^2_{\tilde{\rho}}C_s$	=	$Q^{GF}_{\hat{d\tilde{t}}\hat{d\tilde{t}}}[k]-\frac{1}{k}\frac{n-1}{n}c^2_{\tilde{\rho}}\tilde{C}_s-\frac{k-1}{k}\frac{n-1}{n}c^2_{\tilde{\rho}}C_s$
$Q^{GB}_{\hat{d\tilde{t}}\hat{\tilde{a}}_1}[k]$	=	$\frac{1}{k}Q^{GB}_{\hat{d\tilde{t}}\hat{\tilde{a}}_1}[1]$	=	$Q^{GF}_{\hat{d\tilde{t}}\hat{\tilde{a}}_1}[k]-\frac{1}{k}\frac{n-1}{n}c^2_{\tilde{\rho}}e^T_\mu\Lambda^{-1}\otimes\tilde{C}_s$
$Q^{GB}_{\hat{\tilde{a}}_r\hat{\tilde{a}}_r}[k]$	=	$\frac{1}{k}Q^{GB}_{\hat{\tilde{a}}_r\hat{\tilde{a}}_r}[1]$	=	$Q^{GF}_{\hat{\tilde{a}}_r\hat{\tilde{a}}_r}[k]-\frac{1}{k}\frac{n-1}{n}c^2_{\tilde{\rho}}\Lambda^{-1}e_\mu e^T_\mu\Lambda^{-1}\otimes\tilde{C}_s$

$Q^{GF}_{\hat{d\tilde{t}}\hat{d\tilde{t}}}[k]=(1/k)Q^{GF}_{\hat{d\tilde{t}}\hat{d\tilde{t}}}[1]+[(k-1)/k]c^2_{\tilde{\rho}}C_s;\ Q^{GF}_{\hat{d\tilde{t}}\hat{\tilde{a}}_1}[k]=(1/k)Q^{GF}_{\hat{d\tilde{t}}\hat{\tilde{a}}_1}[1];\ Q^{GF}_{\hat{\tilde{a}}_r\hat{\tilde{a}}_r}[k]=(1/k)Q^{GF}_{\hat{\tilde{a}}_r\hat{\tilde{a}}_r}[1]$

Table 4 Variance matrices of the k-epoch *ambiguity-fixed* GB/GF least-squares PPP-RTK corrections expressed in their single-epoch counterparts

Multi-epoch GB		Single-epoch GB		Multi-epoch GF
$Q^{GB}_{\check{d\tilde{t}}\check{d\tilde{t}}}[k]$	=	$\frac{1}{k}Q^{GB}_{\check{d\tilde{t}}\check{d\tilde{t}}}[1]+\frac{k-1}{k}\frac{1}{n}c^2_{\tilde{\rho}}C_s$	=	$Q^{GF}_{\check{d\tilde{t}}\check{d\tilde{t}}}[k]-\frac{1}{k}\frac{n-1}{n}c^2_{\tilde{\rho}}\tilde{C}_s-\frac{k-1}{k}\frac{n-1}{n}c^2_{\tilde{\rho}}C_s$
$Q^{GB}_{\check{d\tilde{t}}\check{\tilde{a}}_1}[k]$	=	$\frac{1}{k}Q^{GB}_{\check{d\tilde{t}}\check{\tilde{a}}_1}[1]$	=	$Q^{GF}_{\check{d\tilde{t}}\check{\tilde{a}}_1}[k]$
$Q^{GB}_{\check{\tilde{a}}_r\check{\tilde{a}}_r}[k]$	=	$\frac{1}{k}Q^{GB}_{\check{\tilde{a}}_r\check{\tilde{a}}_r}[1]$	=	$Q^{GF}_{\check{\tilde{a}}_r\check{\tilde{a}}_r}[k]$

$Q^{GF}_{\check{d\tilde{t}}\check{d\tilde{t}}}[k]=(1/k)Q^{GF}_{\check{d\tilde{t}}\check{d\tilde{t}}}[1]+[(k-1)/k]c^2_{\tilde{\rho}}C_s;\ Q^{GF}_{\check{d\tilde{t}}\check{\tilde{a}}_1}[k]=(1/k)Q^{GF}_{\check{d\tilde{t}}\check{\tilde{a}}_1}[1];\ Q^{GF}_{\check{\tilde{a}}_r\check{\tilde{a}}_r}[k]=(1/k)Q^{GF}_{\check{\tilde{a}}_r\check{\tilde{a}}_r}[1]$

one achieves in baseline precision when applying instantaneous ambiguity resolution (Teunissen 1997a). The explanation for this difference lies in the type of parameters considered. As ambiguity resolved single-differenced parameters still require code data for their estimation, the relatively poor code precision prohibits the gain to reach the two orders of magnitude level.

The above results are based on single-epoch solutions. A corresponding multi-epoch solution, based on the time-invariance of $\tilde{a}_r$, can subsequently be obtained. We combine these results with our discussion of the geometry-based model in the next section.

5.2 Geometry-based estimation

Let us first consider the redundancies when comparing the GF-model with the GB-model, see Table 2. The single-epoch GF-model has no redundancy. In the k-epoch case, however, the time-invariance of the $2(m-1)$ ambiguities of each of the n stations, makes the multi-repoch GF-redundancy equal to $2(m-1)(k-1)n$. Would all ambiguities be known, the redundancy would increase further with $2(m-1)n$. However, since ambiguity resolution only affects the integer DD ambiguities, not all, but only $2(m-1)(n-1)$ ambiguities can be considered known. With this increase of redundancy, the ambiguity-fixed, multi-epoch GF-redundancy is equal to $2(m-1)(nk-1)$.

Let us now consider the geometry-based model. With the GB-model, the $(m-1)$-vector $\Delta\tilde{\rho}_r$ of $d\tilde{t}_r=d\tilde{t}-\Delta\tilde{\rho}_r$, $r=2,\ldots,n$, is parametrized in the v-vector $\Delta\tilde{x}_r$. Hence, for the k-epoch case, the $k(m-1)n$ clock parameters of $d\tilde{t}_r$ get replaced by the $k(m-1)$ parameters of $d\tilde{t}$ and the $v(n-1)$ parameters of $\Delta\tilde{x}_r$. The multi-epoch redundancy, for both the ambiguity-float and ambiguity-fixed case, increases therefore by $[k(m-1)-v][n-1]$ when switching from the GF-model to the GB-model (cf. Table 2).

This increase in model strength will show up in the improved precision of the estimated PPP-RTK corrections. To show this clearly, we have determined the variance matrices of their least-squares GB- and GF-estimators under some simplifying assumptions. We followed Teunissen (1997a) and used a time-averaged receiver-satellite geometry matrix G of order $m\times v$, in $\tilde{G}=[G,\ e_m]$, to capture the geometry for the GB-model (e_m is the m-vector of ones). The results are given in Tables 3, 4 and 5, respectively. The proofs of these results can be found in the Appendix.

Table 3 presents the variance matrices of the ambiguity-float GB/GF least-squares PPP-RTK corrections. It shows that all (co)variance matrices, except those of the satellite clocks, follow the 1-over-k rule. For not too large k, however, the same rule applies approximately to the variance matrices of the satellite clocks as well, i.e., $Q^{\mathrm{GB}}_{\hat{d\tilde{t}}\hat{d\tilde{t}}}[k]\approx\frac{1}{k}Q^{\mathrm{GB}}_{\hat{d\tilde{t}}\hat{d\tilde{t}}}$ and $Q^{\mathrm{GF}}_{\hat{d\tilde{t}}\hat{d\tilde{t}}}[k]\approx\frac{1}{k}Q^{\mathrm{GF}}_{\hat{d\tilde{t}}\hat{d\tilde{t}}}$, since $c^2_{\tilde{\rho}}\approx 0$.

Table 5 Impact of integer ambiguity resolution: variance matrices of the ambiguity-fixed GB/GF least-squares PPP-RTK corrections expressed in their ambiguity-float counterparts

Geometry-based	Geometry-free
$Q^{GB}_{\check{d}\check{t}\check{d}\check{t}}[k] = Q^{GB}_{\hat{d}\check{t}\hat{d}\check{t}}[k] - \frac{1}{k}\frac{n-1}{n}(c^2_{\hat{\rho}} - c^2_{\check{\rho}})(C_s - \tilde{C}_s)$	$Q^{GF}_{\check{d}\check{t}_r\check{d}\check{t}_r}[k] = \frac{1}{n}Q^{GF}_{\hat{d}\check{t}_r\hat{d}\check{t}_r}[k] + \frac{n-1}{n}c^2_{\check{\rho}}C_s$
$Q^{GB}_{\check{d}\check{t}\check{a}_1}[k] = Q^{GB}_{\hat{d}\check{t}\hat{a}_1}[k] - \frac{1}{k}\frac{n-1}{n}c^2_{\hat{\rho}}e^T_{\mu}\Lambda^{-1} \otimes (C_s - \tilde{C}_s)$	$Q^{GF}_{\check{d}\check{t}_r\check{a}_r}[k] = \frac{1}{n}Q^{GF}_{\hat{d}\check{t}_r\hat{a}_r}[k]$
$Q^{GB}_{\check{a}_r\check{a}_r}[k] = Q^{GB}_{\hat{a}_r\hat{a}_r}[k] - \frac{1}{k}\frac{n-1}{n}c^2_{\hat{\rho}}\Lambda^{-1}e_{\mu}e^T_{\mu}\Lambda^{-1} \otimes (C_s - \tilde{C}_s) - \frac{1}{k}\frac{n-1}{n}\Lambda^{-1}(C_{\phi} + c^2_{\hat{l}\vert\rho}\mu\mu^T)\Lambda^{-1} \otimes C_s$	$Q^{GF}_{\check{a}_r\check{a}_r}[k] = \frac{1}{n}Q^{GF}_{\hat{a}_r\hat{a}_r}[k]$

In the absence of satellite redundancy, we have $m = \nu + 1$ and therefore $\tilde{C}_s = D^T_m \mathcal{P}^{\perp}_G C_s D_m = 0$. In that case, the ambiguity variance matrix and the ambiguity-clock covariance matrix of the two models are the same. For the variance matrix of the clocks, there is then still a slight difference between the GB- and GF-model, one that can be explained by the assumed time-invariance of $\Delta\tilde{x}_r$. Thus, in the absence of satellite redundancy, the GF-model has approximately the same performance as the GB-model.

Table 4 is the ambiguity-fixed counterpart of Table 3. Again it shows that all (co)variance matrices, except those of the satellite clocks, follow the 1-over-k rule. For not too large k, however, the same rule applies approximately to the ambiguity-fixed variance matrices of the satellite clocks as well, i.e., $Q^{GB}_{\check{d}\check{t}\check{d}\check{t}}[k] \approx \frac{1}{k}Q^{GB}_{\check{d}\check{t}\check{d}\check{t}}$ and $Q^{GF}_{\check{d}\check{t}\check{d}\check{t}}[k] \approx \frac{1}{k}Q^{GF}_{\check{d}\check{t}\check{d}\check{t}}$, since $c^2_{\check{\rho}} \approx 0$. Importantly, we note that

$$Q^{GB}_{\check{a}_r\check{a}_r}[k] = Q^{GF}_{\check{a}_r\check{a}_r}[k] \text{ and } Q^{GB}_{\check{d}\check{t}\check{a}_r}[k] = Q^{GF}_{\check{d}\check{t}\check{a}_r}[k] \tag{82}$$

with

$$Q^{GB}_{\check{d}\check{t}\check{d}\check{t}}[k] \approx Q^{GF}_{\check{d}\check{t}\check{d}\check{t}}[k] \tag{83}$$

for not too large k. Thus, *after* successful integer ambiguity resolution, the GF-based corrections have a quality that is close to their GB-counterparts.

Let us now consider the impact of integer ambiguity resolution per model. In Table 5, the ambiguity-fixed variance matrices of both models are expressed in their ambiguity-float counterparts. The results show that the GF (co)variance matrices, except those of the satellite clocks, follow the 1-over-n rule. For not too large n, however, the same rule applies approximately to the GF variance matrix of the satellite clocks as well, i.e., $Q^{GF}_{\check{d}\check{t}\check{d}\check{t}}[k] \approx \frac{1}{n}Q^{GF}_{\hat{d}\check{t}\hat{d}\check{t}}[k]$, since $c^2_{\check{\rho}} \approx 0$.

In case of the GB-model, the impact of ambiguity resolution differs from that of the GF-model. Here, the impact largely depends on the strength of the GB-model. The weaker the model, the larger the impact of ambiguity resolution is. The model is weakest when there is no satellite redundancy. Then, $m = \nu + 1$ and $\tilde{C}_s = 0$. At the other extreme we have the geometry-fixed case (i.e., $\Delta\tilde{x}_r = 0$ for all r). Then, $\tilde{C}_s = C_s$ and *no* improvement, apart from $Q^{GB}_{\check{a}_r\check{a}_r}[k]$, can be realized. In this case, we have with (82) and (83),

$$\begin{aligned} Q^{GB}_{\check{a}_r\check{a}_r}[k] &= Q^{GB}_{\hat{a}_r\hat{a}_r}[k] - Q = Q^{GF}_{\check{a}_r\check{a}_r}[k] \\ Q^{GB}_{\check{d}\check{t}\check{a}_r}[k] &= Q^{GB}_{\hat{d}\check{t}\hat{a}_r}[k] = Q^{GF}_{\check{d}\check{t}\check{a}_r}[k] \\ Q^{GB}_{\check{d}\check{t}\check{d}\check{t}}[k] &= Q^{GB}_{\hat{d}\check{t}\hat{d}\check{t}}[k] \approx Q^{GF}_{\check{d}\check{t}\check{d}\check{t}}[k] \end{aligned} \tag{84}$$

with $Q = \frac{n-1}{kn}\Lambda^{-1}(C_{\phi} + c^2_{\hat{l}\vert\rho}\mu\mu^T)\Lambda^{-1} \otimes C_s$.

Hence, the ambiguity-float GB clock solution would then already be as good as that of the ambiguity-fixed solutions of either the GB- or GF-model.

5.3 Precision of user-corrected observations

Having the variance matrices of the individual PPP-RTK corrections available, one can now also determine the variance matrix of the complete user-corrections. In (Odijk et al. 2014b), such example is given for the single-frequency PPP-RTK case. Here, we consider as example the dual-frequency GF-model determined corrections. The float corrections that are applied to the user observations are then given as

$$\begin{bmatrix} \hat{c}_{\phi} \\ \hat{c}_p \end{bmatrix} = \left[\begin{bmatrix} e & -\Lambda \\ e & 0 \end{bmatrix} \otimes I_{m-1} \right] \begin{bmatrix} d\hat{\check{t}}_{r,\mathrm{GF}} \\ \hat{\check{a}}_{r,\mathrm{GF}} \end{bmatrix} \tag{85}$$

with a likewise definition in case integer ambiguity resolved corrections $d\check{\check{t}}_{r,\mathrm{GF}}$ and $\check{\check{a}}_{r,\mathrm{GF}}$ are used. The following Lemma gives the variance matrix of these user-corrections for both the ambiguity-float and ambiguity-fixed case.

Lemma 4 (Precision GF User-Corrections) *The variance matrices of the ambiguity-fixed and ambiguity-float PPP-RTK user-corrections are given for a single-epoch as*

$$\mathsf{D}\begin{bmatrix} \check{c}_{\phi} \\ \check{c}_p \end{bmatrix} = \frac{1}{n}\mathsf{D}\begin{bmatrix} \hat{c}_{\phi} \\ \hat{c}_p \end{bmatrix} + \frac{n-1}{n}c^2_{\check{\rho}}\begin{bmatrix} e \\ e \end{bmatrix}\begin{bmatrix} e \\ e \end{bmatrix}^T \otimes C_s \tag{86}$$

and

$$\begin{aligned} \mathsf{D}\begin{bmatrix} \hat{c}_{\phi} \\ \hat{c}_p \end{bmatrix} = \Bigg(&\begin{bmatrix} C_{\phi} & 0 \\ 0 & C_p \end{bmatrix} + c^2_{\hat{l}}\begin{bmatrix} -\mu \\ \mu \end{bmatrix}\begin{bmatrix} -\mu \\ \mu \end{bmatrix}^T \\ &- \begin{bmatrix} -\mu \\ \mu \end{bmatrix}\begin{bmatrix} 0 \\ C_p\mu_{\mathrm{GF}} \end{bmatrix}^T - \begin{bmatrix} 0 \\ C_p\mu_{\mathrm{GF}} \end{bmatrix}\begin{bmatrix} -\mu \\ \mu \end{bmatrix}^T \Bigg) \otimes C_s \end{aligned} \tag{87}$$

with $c^2_{\hat{l}} = \mu^T_{\mathrm{GF}}C_p\mu_{\mathrm{GF}}$.

Proof Follows from using the relevant entries of Tables 3 and 4 in the application of the variance propagation law to (85). □

Two important remarks can now be made about these variance matrices. First, since these variance matrices describe the precision of the user-corrections, all their entries are needed when one wants to perform a statistical validation of the user-corrections themselves (either ambiguity-fixed or ambiguity-float based). For the user-processing, however, not all entries are needed. To understand this, consider the sum-structure of the variance matrices (86) and (87). In them one will recognize rank-one matrices with components that lie in the range-space of the design matrix of the user system of observation equations. These are the rank-one matrices with components $[e^T, e^T]^T$ or $[-\mu^T, \mu^T]^T$ (three in 87 and four in 86). Since they lie in the range-space of the user's design matrix, this part of the variance matrix of the user-corrections will not contribute to the estimation of the user parameters. Hence, for the user-processing, only the following components are of relevance,

$$\frac{1}{n}\begin{bmatrix} C_\phi & 0 \\ 0 & C_p \end{bmatrix} \otimes C_s \quad \text{or} \quad \begin{bmatrix} C_\phi & 0 \\ 0 & C_p \end{bmatrix} \otimes C_s \tag{88}$$

depending on whether the ambiguity-fixed or ambiguity-float corrections are used. Note that this result is consistent with our earlier relative positioning conclusion of PPP-RTK (cf. Sect. 4.3). It thus implies that the $[e^T, e^T]^T$ and $[-\mu^T, \mu^T]^T$ induced correlation present in (86) and (87) can be neglected.

In the first matrix of (88), we see the contribution of the number of network stations, which is analogous to the contribution in the array-aided PPP concept of Teunissen (2012). An increasing number of stations will thus in particular help to reduce the noise contribution of the code measurements.

5.4 Integer ambiguity resolution

5.4.1 ILS, IB and IR

The ambiguity resolved estimators of the previous subsections can only be obtained once integer ambiguity resolution has been performed. We now show how the integer estimators of $\tilde{z}_i$, $i = 2, \ldots, n$, (cf. 78) can be obtained.

Defining the ambiguity matrices $\mathcal{A} = [\tilde{a}_1, \ldots, \tilde{a}_n]$, $\mathcal{Z} = [\tilde{z}_2, \ldots, \tilde{z}_n]$, and using the property $\tilde{a}_r = \tilde{z}_r - \tilde{\delta}$, with $\tilde{z}_r \in \mathbb{Z}^{2(m-1)}$ (cf. 23), we can write

$$\mathcal{Z} = \mathcal{A}D_n \in \mathbb{Z}^{2(m-1)\times(n-1)} \tag{89}$$

with $D_n = [-e_{n-1}, I_{n-1}]^T$ the between-station differencing matrix. The Integer Least-Squares (ILS) estimator of $\mathcal{Z}$ can then be computed as

$$\check{\mathcal{Z}} = \arg \min_{Z \in \mathbb{Z}^{2(m-1)\times(n-1)}} ||\text{vec}(\hat{\mathcal{A}}D_n - Z)||^2_{\mathsf{D}(\text{vec}(\hat{\mathcal{A}}D_n))} \tag{90}$$

with $\mathsf{D}(\text{vec}(\hat{\mathcal{A}}D_n))$ the variance matrix of the float solution $\text{vec}(\hat{\mathcal{A}}D_n)$, obtained from either the GF- or GB-model. The single-epoch version of this variance matrix is given as

$$\mathsf{D}(\text{vec}(\hat{\mathcal{A}}D_n)) = D_n^T D_n \otimes C_{aa} \otimes D_m^T C_S D_m \tag{91}$$

with

$$C_{aa} = \begin{cases} C_{aa}^{\text{GFi}} = \Lambda^{-1}(C_\phi + c^2_{\tilde{l}|\rho}\mu\mu^T)\Lambda^{-1} \\ C_{aa}^{\text{GF}} = C_{aa}^{\text{GFi}} + \Lambda^{-1}(c^2_{\tilde{\rho}} e_\mu e_\mu^T)\Lambda^{-1} \end{cases} \tag{92}$$

in which C_{aa}^{GFi} and C_{aa}^{GF} denote the geometry-fixed and geometry-free ambiguity co-factor matrices, respectively. The geometry-fixed and geometry-free cases are considered, since they represent the two extreme cases of model strength.

The ILS estimator (90) is optimal in the sense that it has the largest possible success rate of all integer estimators (Teunissen 1999). Popular alternatives to ILS are integer bootstrapping (IB) and integer rounding (IR). They are easier to compute than ILS and when the model has sufficient strength their performance can be close to optimal once the decorrelating Z-transformation is applied (Teunissen 1995, 1998).

One can also approximate the ILS solution (90) by approximating the variance matrix. The objective function of (90) decouples, for instance, and becomes easier to minimize, if one neglects the correlation due to differencing. Would one neglect the correlation all together and replace $\mathsf{D}(\text{vec}(\hat{\mathcal{A}}D_n))$ in (90) by a diagonal matrix, then the solution would reduce to ordinary component-wise integer rounding,

$$\check{\tilde{z}}_i = \left\lfloor \hat{\tilde{a}}_i - \hat{\tilde{a}}_1 \right\rceil, \; i = 2, \ldots, n \tag{93}$$

If the underlying model is too weak to achieve high enough success rates for full ambiguity resolution, one can also opt for partial ambiguity resolution. Resolving only wide-lane ambiguities, for instance, is a special case of partial ambiguity resolution (Teunissen 1997d).

5.4.2 Ambiguity dilution of precision

To get an indication of the ambiguity resolution strength of the models, we use the Ambiguity Dilution of Precision (ADOP). This is an easy-to-apply diagnostic measure that was introduced by Teunissen (1997b). The ADOP is defined as the square-root of the ambiguity variance matrix' determinant taken to the power one over the matrix' order. Thus, in case of full ambiguity resolution, with m satellites, n stations and 2 frequencies, it is defined as

$$\text{ADOP} = |\mathsf{D}(\text{vec}(\hat{\mathcal{A}}D_n))|^{\frac{1}{4(m-1)(n-1)}} \quad \text{(cycle)} \tag{94}$$

Since the ADOP is a measure for the average ambiguity precision, the ADOP can also be linked to the probability of correct integer estimation, the ambiguity success rate. As a rule of thumb, ADOP-values smaller than about 0.10 cycle

correspond to ADOP-based success rates larger than 0.999 (Odijk and Teunissen 2008).

If the ADOP-values for full ambiguity resolution are too large, one may also consider partial ambiguity resolution. If we denote the wide-lane-only ambiguity dilution of precision as ADOP_{WL}, then it follows from the definition of the ambiguity dilution of precision that for the dual-frequency case,

$$\text{ADOP}^2 = \text{ADOP}_{L_1|\text{WL}} \times \text{ADOP}_{WL} \quad (\text{cycle}^2) \tag{95}$$

with $\text{ADOP}_{L_1|\text{WL}}$ denoting the wide-lane conditioned L_1-only ambiguity dilution of precision. Thus, if two of the entries in (95) are given, the third follows.

The following lemma gives analytical expressions for the geometry-fixed and geometry-free ADOPs in case of full ambiguity resolution and wide-lane-only ambiguity resolution.

Lemma 5 (Geometry-fixed and Geometry-free ADOPs) *Assuming $C_\phi = \sigma_\phi^2 I_2$ and $C_p = \sigma_p^2 I_2$ (cf. 75), the single epoch, geometry-fixed (GFi) and geometry-free (GF) ADOPs of full ambiguity resolution and wide-lane-only ambiguity resolution are given as*

$$\begin{aligned}
\text{ADOP}^{\text{GFi}} &= c_o \left(\frac{\sigma_\phi \sigma_p}{\lambda_1 \lambda_2}\right)^{\frac{1}{2}} (1+\epsilon)^{\frac{1}{4}} \\
\text{ADOP}^{\text{GF}} &= \text{ADOP}^{\text{GFi}} \left(\frac{1+\epsilon}{\epsilon} + \frac{4(\mu_1+\mu_2)^2}{(1+\epsilon)(\mu_2-\mu_1)^2}\right)^{\frac{1}{4}}
\end{aligned} \tag{96}$$

and

$$\begin{aligned}
\text{ADOP}_{WL}^{\text{GFi}} &= c_o \left(\left(\frac{\sigma_\phi^2}{\lambda_1^2} + \frac{\sigma_\phi^2}{\lambda_2^2}\right) + \frac{\sigma_p^2}{\lambda_W^2} \frac{\mu_2}{\mu_1^2+\mu_2^2}\right)^{\frac{1}{2}} \\
\text{ADOP}_{\text{WL}}^{\text{GF}} &= \text{ADOP}_{\text{WL}}^{\text{GFi}} (1+\gamma)^{\frac{1}{2}}
\end{aligned} \tag{97}$$

with $\epsilon = \sigma_\phi^2/\sigma_p^2$ and

$$c_o = n^{\frac{1}{2(n-1)}} \left(\sum_{s=1}^{m} c_s^{-2} / \prod_{s=1}^{m} c_s^{-2}\right)^{\frac{1}{2(m-1)}} \tag{98}$$

where c_s^2 are the diagonal entries of the elevation-weighting matrix C_S. The scalar γ is approximated as $\gamma \approx (f_1^3 - f_2^3)^2/(f_1^2 f_2^2 (f_1+f_2)^2)$.

Proof Follows from an application of the results of Odijk and Teunissen 2008. The exact value of γ is given in Appendix. □

The Lemma shows that for full ambiguity resolution, the geometry-free ADOP (cf. 96) is about a factor $(\frac{1+\epsilon}{\epsilon})^{\frac{1}{4}} \approx 10$ ($\epsilon \approx 10^{-4}$) larger than the corresponding geometry-fixed ADOP. The Lemma also shows that while the geometry-fixed wide-lane-only ADOP is governed by σ_p/λ_W (cf. 97), its full ambiguity resolution counterpart is governed by $(\sigma_\phi \sigma_p/\lambda_1\lambda_2)^{\frac{1}{2}}$. Hence, for the geometry-fixed case, it does not pay off to do wide-lane-only ambiguity resolution. This changes if one considers the geometry-free model. In that case, wide-lane-only ambiguity resolution has a better success rate performance, since the full ambiguity resolution geometry-free ADOP is about a factor 6 larger than its wide-lane-only counterpart, while the wide-lane-only geometry-free ADOP does not differ too much from its geometry-fixed counterpart.

Table 6 Single-epoch, zenith-referenced ADOP-values for the geometry-fixed and geometry-free scenarios (GPS dual-frequency $L1/L2$)

ADOP (cycle)	Geometry-fixed	Geometry-free
ADOP	0.278	2.787
ADOP_{WL}	0.465	0.497
$\text{ADOP}_{L_1\|WL}$	0.166	15.620

$m = 2; n = 2; \sigma_\phi = 3$ [mm]; $\sigma_p = 30$ [cm]. ADOP refers to full ambiguity resolution; ADOP_{WL} to wide-lane-only ambiguity resolution, while $\text{ADOP}_{L_1|WL}$ refers to L_1 ambiguity resolution assuming the wide-lane ambiguities known

Numerical values for the ADOPs are given in Table 6. They show that full ambiguity resolution requires many epochs in case of the geometry-free model, but only in the order of about ten for the geometry-fixed model. In contrast to full ambiguity resolution, the table also shows that wide-lane-only ambiguity resolution is possible with the geometry-free model. And once the wide-lane ambiguities are known, the geometry-fixed model allows for a reasonable quick resolution of the L_1 ambiguities. This is in contrast to the geometry-free model.

6 The UPD/FCB estimation method revisited

The estimation methods and results presented in the previous sections apply to all the discussed PPP-RTK models. As all the PPP-RTK models considered above are shown to be intrinsically equivalent, a rigorous application of these estimation methods to the different models will, therefore, result in *identical* positioning results. This is also true for the *model* underlying the UPD/FCB method. However, as the UPD/FCB *estimation* method itself differs from the methods of estimation of the previous sections, see e.g., (Ge et al. 2008; Geng et al. 2010, 2011, 2012; Geng and Bock 2013), it is of interest to identify and understand what those differences are.

6.1 The UPD/FCB estimation method

Here, we follow (Ge et al. 2008, p. 392-393) and (Geng et al. 2012, p. 580-582). In the UPD/FCB estimation method,

the sequence of estimating the corrections $d\tilde{t}^{ps}$, $\text{frac}(\tilde{a}^{ps}_{r,c})$ and $\text{frac}(\tilde{a}^{ps}_{r,W})$ (cf. 54) is as follows. First, a geometry-free approach is used to obtain an estimate of the fractional part of the wide-lane ambiguity $\tilde{a}^{ps}_{r,W}$. Then, a geometry-based approach is used to obtain a float estimate of the satellite clock $d\tilde{t}^{ps}$. Finally, a geometry-free approach is used again to obtain an estimate of the fractional part of $\tilde{a}^{ps}_{r,c}$. More specifically, the three steps can be described as follows:

Step 1: The computation of the fractional wide-lane estimate is based on the third equation of the FCB network model (43 or 53):

$$\Delta\phi^{ps}_{r,WN} = \lambda_W \tilde{a}^{ps}_{r,W},\ r = 1, \ldots, n \tag{99}$$

This system is solved on a station-by-station basis, the solutions of which are time-averaged to give the estimates $\hat{\tilde{a}}^{ps}_{r,W}$, $r = 1, \ldots, n$. The fractional parts of them are then station averaged to give [Geng and Bock 2013, p. 451, Eq. (4)],

$$\overline{\text{frac}}(-\tilde{\delta}^{ps}_{,W}) = \frac{1}{n}\sum_{r=1}^{n} \text{frac}(\hat{\tilde{a}}^{ps}_{r,W}) \tag{100}$$

Step 2: The computation of the estimate for $d\tilde{t}^{ps}$ is based on the first two Eqs. of (53),

$$\begin{aligned} \Delta\phi^{ps}_{r,\text{IF}} - \frac{\lambda_2}{\mu_{12}} \lfloor \tilde{a}^{ps}_{r,W} \rceil &= \Delta\tilde{\rho}^{ps}_r - d\tilde{t}^{ps} + \lambda_N \tilde{a}^{ps}_{r,c} \\ \Delta p^{ps}_{r,\text{IF}} &= \Delta\tilde{\rho}^{ps}_r - d\tilde{t}^{ps},\ r = 1, \ldots, n \end{aligned} \tag{101}$$

For $\lfloor \tilde{a}^{ps}_{r,W} \rceil$, the integer $\lfloor \hat{\tilde{a}}^{ps}_{r,W} \rceil$ based on $\hat{\tilde{a}}^{ps}_{r,W}$ of the previous step is used.

The system is solved to obtain $\Delta\hat{\tilde{\rho}}_r$, $d\hat{\tilde{t}}^{ps}$ and $\hat{\tilde{a}}^{ps}_{r,c}$ (Geng et al. 2010, p. 582). Note that this step is not necessary if we have a precise satellite clock product.

Step 3: In this last step, the fractional parts of the 'narrow-lane' ambiguity solutions $\hat{\tilde{a}}^{ps}_{r,c}$, $r = 1, \ldots, n$, of the previous step are taken to compute the station-averaged estimate [Ge et al. 2008; Geng et al. 2012, p. 582, Eq. (11)]

$$\overline{\text{frac}}(-\tilde{\delta}^{ps}_{,c}) = \frac{1}{n}\sum_{r=1}^{n} \text{frac}(\hat{\tilde{a}}^{ps}_{r,c}) \tag{102}$$

Hence, as a result of the above three steps, the PPP-RTK corrections provided are the clocks estimate $d\hat{\tilde{t}}^{ps}$ and the two FCB estimates $\overline{\text{frac}}(-\tilde{\delta}^{ps}_{,c})$ and $\overline{\text{frac}}(-\tilde{\delta}^{ps}_{,W})$, respectively. In the improved narrow-lane FCB method of Geng et al (2012, Sect. 2.3), the computation (102) is replaced by its ambiguity resolved counterpart, through which an improvement in the results, over the method proposed by Ge et al. (2008), was reported.

The above estimators (100) and (102) relate to between-satellite phase biases. Would one work with undifferenced observations, similar estimators can be formulated for the fractional part of the between-receiver phase biases, see e.g., (Li et al. 2013b, 2014).

6.2 Comparison of estimators

We now compare the FCB-estimators (100) and (102) with their corresponding ambiguity resolved satellite phase bias estimator. We start with the wide-lane version (100). Since $\tilde{a}^{ps}_r = \tilde{z}^{ps}_r - \tilde{\delta}^{ps}$ (cf. 23) and thus $\tilde{a}^{ps}_{r,W} = \tilde{z}^{ps}_{r,W} - \tilde{\delta}^{ps}_{,W}$, we have, since $\tilde{z}^{ps}_{r,W} \in \mathbb{Z}$, that $\text{frac}(\tilde{a}^{ps}_{r,W}) = \text{frac}(-\tilde{\delta}^{ps}_{,W})$ for $r = 1, \ldots, n$, and therefore

$$\text{frac}(-\tilde{\delta}^{ps}_{,W}) = \frac{1}{n}\sum_{r=1}^{n} \text{frac}(\tilde{a}^{ps}_{r,W}) \tag{103}$$

Having station-estimators $\hat{\tilde{a}}^{ps}_{r,W}$ of $\tilde{a}^{ps}_{r,W}$ available ($r = 1, \ldots, n$), it is then perhaps 'natural', as is done in the FCB estimation method, to take as estimator of the fraction $\text{frac}(-\tilde{\delta}^{ps}_{,W})$, the station average (100),

$$\overline{\text{frac}}(-\tilde{\delta}^{ps}_{,W}) = \frac{1}{n}\sum_{r=1}^{n} \text{frac}(\hat{\tilde{a}}^{ps}_{r,W}) \tag{104}$$

We now compare this 'natural' estimator with the best estimator of the wide-lane phase bias $\tilde{\delta}^{ps}_{,W}$, i.e., the ambiguity resolved estimator $\breve{\tilde{\delta}}^{ps}_{,W}$. Recall that the integer estimate $\breve{\tilde{z}}^{ps}_j$ in (80) follows from applying integer ambiguity resolution to the GF float solution $\hat{\tilde{z}}_j = \hat{\tilde{a}}_{j,\text{GF}} - \hat{\tilde{a}}_{1,\text{GF}}$. Hence, if integer rounding is used on its wide-lane component to obtain the integer estimate $\breve{\tilde{z}}^{ps}_{j,W} = \lfloor \hat{\tilde{z}}^{ps}_{j,W} \rceil = \lfloor \hat{\tilde{a}}^{ps}_{j,W} - \hat{\tilde{a}}^{ps}_{1,W} \rceil$, it follows from (80) that

$$\begin{aligned} \breve{\tilde{\delta}}^{ps}_{,W} &= -\frac{1}{n}\sum_{j=1}^{n} \left(\hat{\tilde{a}}^{ps}_{j,W} - \lfloor \hat{\tilde{a}}^{ps}_{j,W} - \hat{\tilde{a}}^{ps}_{1,W} \rceil \right) \\ &= -\frac{1}{n}\sum_{j=1}^{n} \left((\hat{\tilde{a}}^{ps}_{j,W} - \hat{\tilde{a}}^{ps}_{1,W}) - \lfloor \hat{\tilde{a}}^{ps}_{j,W} - \hat{\tilde{a}}^{ps}_{1,W} \rceil \right) - \hat{\tilde{a}}^{ps}_{1,W} \\ &= -\frac{1}{n}\sum_{j=1}^{n} \text{frac}(\hat{\tilde{a}}^{ps}_{j,W} - \hat{\tilde{a}}^{ps}_{1,W}) - \hat{\tilde{a}}^{ps}_{1,W} \\ &= -\frac{1}{n}\sum_{j=1}^{n} \text{frac}(\hat{\tilde{z}}^{ps}_{j,W}) - \hat{\tilde{a}}^{ps}_{1,W} \end{aligned} \tag{105}$$

and therefore

$$-\breve{\tilde{\delta}}^{ps}_{,W} = \frac{1}{n}\sum_{j=1}^{n} \text{frac}(\hat{\tilde{z}}^{ps}_{j,W}) + \hat{\tilde{a}}^{ps}_{1,W} \tag{106}$$

This ambiguity resolved estimator of the wide-lane phase bias is made up of two different terms: a station average of the fractions of *double-differenced* float wide-lane ambiguities and the *single-differenced* float wide-lane ambiguity of the reference station 1. Thus, although this estimator is also made up from a station average, its fraction is quite different from the FCB-estimator (104). We, therefore, have the following result.

Lemma 6 (FCB-estimator) *The station-averaged FCB-estimator* $\frac{1}{n}\sum_{r=1}^{n}\text{frac}(\hat{\tilde{a}}_{r,W}^{ps})$ (cf. 100) *is not optimal, since*

$$\overline{\text{frac}}(\tilde{\delta}_{,W}^{ps}) \neq \text{frac}(\breve{\tilde{\delta}}_{,W}^{ps}) \quad \text{for} \quad n > 1 \tag{107}$$

Thus, only in case of a single station, $n = 1$, do we have $\text{frac}(\breve{\tilde{\delta}}_{,W}^{ps}) = \overline{\text{frac}}(\tilde{\delta}_{,W}^{ps})$, since then $-\breve{\tilde{\delta}}_{,W}^{ps} = \hat{\tilde{a}}_{1,W}^{ps}$, because $\hat{\tilde{z}}_{1,W}^{ps} = 0$ by definition. A similar result as (107) also holds true for the estimator (102). Note that in Ge et al. (2008) the estimators $\overline{\text{frac}}(\tilde{\delta}_{,W}^{ps})$ and $\overline{\text{frac}}(\tilde{\delta}_{,c}^{ps})$ are used, while in Geng et al. (2012) the estimators $\overline{\text{frac}}(\tilde{\delta}_{,W}^{ps})$ and improved narrow-lane FCBs are used.

6.3 Unbiasedness

Although the FCB-estimator (100) is not optimal, it could still be a useful estimator if it does what it is supposed to do, namely to guarantee that the user-ambiguities become integer when the estimator is applied as a PPP-RTK correction. Unfortunately, this is not the case either.

This can be understood, if one considers (104) as estimator of (103). Clearly, if $\hat{\tilde{a}}_{r,W}^{ps}$ is an unbiased estimator of $\tilde{a}_{r,W}^{ps}$, then $\overline{\text{frac}}(-\tilde{\delta}_{,W}^{ps})$ is *not* an unbiased estimator of $\text{frac}(-\tilde{\delta}_{,W}^{ps})$, not even of an integer-shifted version of it. Since the frac-operator is nonlinear, the expectation operator and frac-operator do not commute. We, therefore, have the following result.

Lemma 7 (FCB-estimator as PPP-RTK correction) *The station-averaged PPP-RTK correction* $\frac{1}{n}\sum_{r=1}^{n}\text{frac}(\hat{\tilde{a}}_{r,W}^{ps})$ (cf. 100) *of the FCB estimation method fails to recover the integerness of the user-ambiguities, since*

$$\mathsf{E}\left(\overline{\text{frac}}(\tilde{\delta}_{,W}^{ps})\right) \neq \text{frac}(\tilde{\delta}_{,W}^{ps}) + z \quad \text{for some } z \in \mathbb{Z} \tag{108}$$

Using the station average $\frac{1}{n}\sum_{r=1}^{n}\text{frac}(\hat{\tilde{a}}_{r,W}^{ps})$ as estimator for the PPP-RTK correction $\text{frac}(\tilde{a}_{q,W}^{ps}) = -\text{frac}(\tilde{\delta}_{,W}^{ps})$ in (48) or (54) will, thus, bias the user-ambiguities into non-integer values, and thereby undermine the whole purpose of PPP-RTK. Would one use this FCB estimation method and resolve the user-ambiguities as if they are integer, one would in fact propagate their non-integerness as bias into the estimators of the remaining parameters. The following simple example makes this clear.

Example: Consider the model of two observation equations with two unknowns,

$$\mathsf{E}\begin{bmatrix}\phi + a_i\\ p\end{bmatrix} = \begin{bmatrix}1 & 1\\ 1 & 0\end{bmatrix}\begin{bmatrix}\rho\\ z_i\end{bmatrix} \tag{109}$$

with real-valued parameter ρ and integer-valued parameter z_i. For simplicity, we assume the variance matrix of the observables to be a scaled unit-matrix. The ILS solution of ρ follows then as

$$\begin{aligned}\breve{\rho}_i &= \frac{1}{2}\left(\phi + a_i + p - \lfloor \phi + a_i - p \rceil\right)\\ &= \frac{1}{2}\left(\phi + \text{frac}(a_i) + p - \lfloor \phi + \text{frac}(a_i) - p \rceil\right)\end{aligned} \tag{110}$$

The second equation follows from the first, since integer rounding is *integer equivariant*, i.e., $\lfloor x + z \rceil = \lfloor x \rceil + z$ for $z \in \mathbb{Z}$ and thus $\text{frac}(x+z) = \text{frac}(x)$. Hence, the result (110) shows that the ILS solution $\breve{\rho}_i$ remains unchanged when a_i in (109) is replaced by $\text{frac}(a_i)$.

Let us now assume that $i = 1, \ldots, n$ and that we replace a_i in the first equation of (110) by the average $\frac{1}{n}\sum_{i=1}^{n}\text{frac}(a_i)$. The resulting estimator reads then

$$\breve{\rho}' = \frac{1}{2}\left(\phi + \frac{1}{n}\sum_{i=1}^{n}\text{frac}(a_i) + p - \left\lfloor \phi + \frac{1}{n}\sum_{i=1}^{n}\text{frac}(a_i) - p \right\rceil\right) \tag{111}$$

This estimator, however, is a *biased* estimator of ρ. This can be understood as follows. Since the ILS estimators $\breve{\rho}_i$, $i = 1, \ldots, n$, are unbiased estimators of ρ (Teunissen 1999), their average

$$\begin{aligned}\breve{\rho} &= \frac{1}{n}\sum_{i=1}^{n}\breve{\rho}_i\\ &= \frac{1}{2}\left(\frac{1}{n}\sum_{i=1}^{n}\left(\phi + \text{frac}(a_i) + p - \lfloor \phi + \text{frac}(a_i) - p \rceil\right)\right)\end{aligned} \tag{112}$$

is also unbiased, i.e., $\mathsf{E}(\breve{\rho}) = \rho$. Hence, the bias in $\breve{\rho}'$ is given by the expectation of the difference between (111) and (112) as,

$$\begin{aligned}&\mathsf{E}(\breve{\rho}' - \breve{\rho})\\ &= \frac{1}{2}\mathsf{E}\left(\frac{1}{n}\sum_{i=1}^{n}\lfloor \phi - p + \text{frac}(a_i) \rceil - \lfloor \phi - p + \frac{1}{n}\sum_{i=1}^{n}\text{frac}(a_i) \rceil\right)\end{aligned} \tag{113}$$

This bias is nonzero in general. It is zero for $n = 1$ and it is zero for the case that all a_i's can be treated as being equal to an integer-shifted version of the same constant, say $-\delta$. Thus, $a_i = z_i - \delta$ must hold, instead of $\mathsf{E}(a_i) = z_i - \delta$.

7 Conclusions and summary

In this contribution, six different dual-frequency PPP-RTK models were reviewed and compared: two common clock (CC) models, the distinct clocks (DC) model, the integer recover clock (IRC) model, the decoupled satellite clock

(DSC) model and the uncalibrated phase delay/fractional cycle bias (UPD/FCB) model. We discussed both their network-component and user-component. Furthermore, by application of $\mathcal{S}$-system theory, we identified the estimable parameters involved in each of the different methods. The interpretation of these estimable parameters is essential for gaining a proper insight into the principles of PPP-RTK in general, and into the role of the PPP-RTK corrections in particular.

We made a distinction between the model formulation used and the estimation method employed. As to the model formulation, we considered the $\mathcal{S}$-basis choice, the chosen parameterization and the ionospheric delay. From the analyses, it is followed that the CC-1, DC and IRC/DSC-models all use the same $\mathcal{S}$-basis, namely $(\Delta x_1, d^{ps}, z_1^{ps})^T$, and that the IRC/DSC-model is a reparametrized form of both the DC-model and the CC-1 model, using ionosphere-free observations. The IRC/DSC integer recovery or decoupled satellite clock was shown to be the ionosphere-free version of the DC's distinct clock.

All the four models, CC-1, DC and IRC/DSC, have integer ambiguities in their network system of observation equations because of the chosen $\mathcal{S}$-basis. This is not the case with the other two models, the CC-2 model and the (UPD/FCB) model. These two models use $(\Delta x_1, d^{ps}, \delta^{ps})^T$ as $\mathcal{S}$-basis, whereby the (UPD/FCB) model was shown to be a reparametrized form of the ionosphere-free version of the CC-2 model. As we consider the lack of ionospheric information the bottleneck for fast ambiguity resolution, the advantage of working with the original undifferenced formulations over the ionosphere-free formulations was also pointed out.

In the construction of its PPP-RTK corrections, the (UPD/FCB) model makes use of a *fractional* operator. Although it is not essential, the use of this single operator is permitted as it maintains the integerness of the user-ambiguities. However, as it was pointed out, one has to be aware that, from a probabilistic point of view, an application of the fractional operator changes the statistics of the user-corrected observables. Hence, one has to take this into account when evaluating the statistics and quality of the user-corrected observables. This aspect does not yet seem to be fully developed in the applications that make use of the FCB model.

Although the six models provide for different PPP-RTK corrections, an estimability analysis showed their information content to be the same. This implies that they are related through one-to-one transformations. These transformations are given in Table 1. They have the practical implication of showing how the different PPP-RTK methods can be mixed between network and users.

Our estimability analysis also revealed the intrinsic role that is played by the PPP-RTK corrections in establishing the link between user-parameters and network-parameters. It was shown that the single-receiver 'user' integer ambiguities are straightforward double-differenced ambiguities and not undifferenced ambiguities as is sometimes stated. Hence, the integer ambiguity resolution at the PPP-RTK user side is always that of double-differenced ambiguities (or Z-transformed functions thereof).

Similarly, it was shown that the PPP-RTK corrections, next to establishing an *ambiguity* link, also establish a *positional* link between network and user. Through the corrections, the user-positioning parameters become in essence relative positioning parameters between user and network. PPP-RTK is thus a relative positioning method and not one of absolute positioning. This was further demonstrated by showing that one recovers the single-baseline model if one considers the extreme case of a PPP-RTK network consisting of a *single* station only.

As an extension to the review, we presented four different least-squares PPP-RTK estimators. They are the float and fixed estimators under the *geometry-free* (GF) model and the float and fixed estimators under the *geometry-based* (GB) model. As these estimators are generally applicable, they apply to any of the PPP-RTK methods discussed. To understand the precision with which the corrections can be estimated, analytical expressions for their variance matrices were derived. This was done for the CC-2 model, having real-valued ambiguities. With the transformations of Table 1, the corresponding variance matrices of the PPP-RTK corrections for the other models are easily obtained.

Using the analytical expressions of the variance matrices, it was shown that the precision of the ambiguity-fixed corrections did not differ too much between the GF- and the GB-model. Thus, once ambiguity resolution has been successfully applied, either the GF-based or GB-based corrections can be used.

In the impact of ambiguity resolution on their precision, the GF-based and GB-based corrections do differ, however. In case of the GF-model, the variance-improvement due to ambiguity resolution follows the 1-over-n rule (n being the number of network stations). In case of the GB-model, however, this improvement depends on its model strength. It is larger, the weaker the model is, and it becomes minimum in the geometry-fixed case. In this latter case, the ambiguity-float GB clock solution is already as good as that of the ambiguity-fixed solution.

In providing the analytical expressions for the variance matrices of the individual PPP-RTK corrections, we also determined the variance matrix of the complete user-corrections. Here, it was shown that in dependence of its use, not all of its entries need to be known. Although the complete matrix is needed for the statistical validation of the corrections themselves, such is not needed for the actual user-processing. For this latter case, it suffices to neglect the

variance–covariance components that are related to geometry and ionosphere.

We also analyzed the ambiguity resolution strength of the models by means of analytical expressions of their ADOPs. It clearly showed the difference in strength (about a factor of 10) between the geometry-fixed and geometry-free cases. Moreover, it showed that in contrast to the geometry-free model, wide-lane-only ambiguity resolution does not really pay off for the geometry-fixed model.

Our analyses of the ambiguity-float and ambiguity-fixed least-squares PPP-RTK estimators, also facilitated a comparison with the UPD/FCB estimation method. Although the UPD/FCB *model* is as valid as the other models discussed, it was shown that the UPD/FCB *estimation method* cannot be accepted as a proper PPP-RTK estimation method, since it does not do what it is supposed to do, namely to guarantee that the expectation of the user-ambiguity float solution is integer. The reason lies in the fact that the used $\overline{\text{frac}}$-operator (cf. 100) is not a proper frac-operator. Only in two special cases will this operator reduce to that of a proper frac-operator. These two cases are when only a single station is used ($n = 1$) or when the ambiguity-fixed solution $\check{\hat{a}}_r^{ps}$ is used instead of the ambiguity-float solution $\hat{\hat{a}}_r^{ps}$ (cf. 78).

Acknowledgments This work has benefitted from the many fruitful PPP-RTK discussions we had with our colleagues from the Curtin GNSS Research Centre. The first author is the recipient of an Australian Research Council (ARC) Federation Fellowship (project number FF0883188). This work has been done in the context of the Positioning Program Project 1.01 "New carrier phase processing strategies for achieving precise and reliable multi-satellite, multi-frequency GNSS/RNSS positioning in Australia" of the Cooperative Research Centre for Spatial Information (CRC-SI). All this support is gratefully acknowledged.

Appendix

Proof of Lemma 2 As the phase observations in (74) are reserved for the ambiguities $\tilde{a}_r$, the float solutions of $d\tilde{t}_r$ and $\tilde{\iota}_r$ are, respectively, determined as the IF and GF combinations of the code observations only, that is

$$\begin{aligned} d\hat{\tilde{t}}_{r,\text{GF}} &= -[\mu_{\text{IF}}^T \otimes D_m^T]p_r, \\ \hat{\tilde{\iota}}_{r,\text{GF}} &= +[\mu_{\text{GF}}^T \otimes D_m^T]p_r \end{aligned} \tag{114}$$

which gives the first expression of (76). The second expression (76) follows by substituting the preceding equations into

$$\begin{aligned} \hat{\hat{a}}_{r,\text{GF}} &= [\Lambda^{-1} \otimes D_m^T] \\ &\times \left[\phi_r + [e \otimes I_{m-1}]d\hat{\tilde{t}}_{r,\text{GF}} + [\mu \otimes I_{m-1}]\hat{\tilde{\iota}}_{r,\text{GF}}\right], \end{aligned} \tag{115}$$

together with the identity $e\mu_{\text{IF}}^T = I_2 - \mu\mu_{\text{GF}}^T$.

An application of the (co)variance propagation law to (76) gives (77). □

Proof of Lemma 3 Upon resolving the DD ambiguities $\check{\check{z}}_r$ ($r = 1, \ldots, n$), with $\check{\check{z}}_1 = 0$, $2(m-1)(n-1)$ redundant model's misclosures contribute to the estimation procedure, namely

$$t_{\tilde{z}_r} = \hat{\hat{z}}_r - \check{\check{z}}_r, \quad r = 2, \ldots, n \tag{116}$$

According to the least-squares conditional adjustment, the unbiased estimators $\hat{\hat{a}}_{r,\text{GF}}$ and $d\hat{\hat{t}}_{r,\text{GF}}$ are corrected by the above misclosures to provide the best linear unbiased estimators (BLUEs) $\check{\check{a}}_{r,\text{GF}}$ and $d\check{\check{t}}_{r,\text{GF}}$ (Teunissen 2000). Adding the corrections, the BLUEs must remain *unbiased* and get *uncorrelated* with the underlying misclosures, see Teunissen and Khodabandeh (2013, p. 463). The unique corrections must, therefore, fulfill two conditions: (1) they must be zero-mean and (2) their covariances with the misclosures must be identical to those between the float estimators and the misclosures with a negative sign. Proposing the following corrections

$$\begin{aligned} \epsilon_{\tilde{a}_r} &= \check{\check{z}}_r - \hat{\hat{a}}_{r,\text{GF}} + \frac{1}{n}\sum_{j=1}^{n}(\hat{\hat{a}}_{j,\text{GF}} - \check{\check{z}}_j) \\ \epsilon_{d\tilde{t}_r} &= -Q^{\text{GF}}_{d\hat{\tilde{t}}_r\hat{\hat{a}}_r} Q^{\text{GF}-1}_{\hat{\hat{a}}_r\hat{\hat{a}}_r}(\hat{\hat{a}}_{r,\text{GF}} - \check{\check{a}}_{r,GF}) \end{aligned} \tag{117}$$

their zero-mean property follows, respectively, from

$$\begin{aligned} \mathsf{E}(\hat{\hat{a}}_{j,\text{GF}}) &= \check{\check{z}}_j - \check{\delta}, \quad j = 1, \ldots, n \\ \mathsf{E}(\check{\check{a}}_{r,\text{GF}}) &= \mathsf{E}(\hat{\hat{a}}_{r,\text{GF}}), \end{aligned} \tag{118}$$

while the second-property follows, respectively, from

$$\begin{aligned} Q^{\text{GF}}_{\epsilon_{\tilde{a}_r},t_{\tilde{z}_r}} &= -Q^{\text{GF}}_{\hat{\hat{a}}_r,t_{\tilde{z}_r}} \\ Q^{\text{GF}}_{\epsilon_{d\tilde{t}_r},t_{\tilde{z}_r}} &= -Q^{\text{GF}}_{d\hat{\tilde{t}}_r,t_{\tilde{z}_r}} \end{aligned} \tag{119}$$

Accordingly, the fixed solutions are obtained as

$$\begin{aligned} \check{\check{a}}_{r,\text{GF}} &= \hat{\hat{a}}_{r,\text{GF}} + \epsilon_{\tilde{a}_r} \\ d\check{\tilde{t}}_r &= d\hat{\tilde{t}}_r + \epsilon_{d\tilde{t}_r} \end{aligned} \tag{120}$$

which proves (78). Applying the (co)variance propagation law to (78) gives (79). □

Proof of Table 3 We first prove the geometry-free results where again use is made of the GNSS misclosure concept (Khodabandeh and Teunissen 2014). In the k-epoch case, as the ambiguities are assumed constant in time, any (co)variance matrix $Q^{GF}_{\hat{x}\hat{y}}$ is corrected according to the least-squares conditional adjustment as

$$Q^{\text{GF}}_{\hat{x}\hat{y}}[k] = Q^{\text{GF}}_{\hat{x}\hat{y}} - [\frac{k-1}{k}]Q^{GF}_{\hat{x}\hat{\hat{a}}_r} Q^{\text{GF}-1}_{\hat{\hat{a}}_r\hat{\hat{a}}_r} Q^{\text{GF}}_{\hat{\hat{a}}_r\hat{y}} \tag{121}$$

Setting $\hat{y} = \hat{\hat{a}}_r$, the above equation is specialized to

$$Q^{\text{GF}}_{\hat{x}\hat{\hat{a}}_r}[k] = \frac{1}{k}Q^{\text{GF}}_{\hat{x}\hat{\hat{a}}_r} \tag{122}$$

This gives the expressions of $Q^{\text{GF}}_{\hat{\hat{a}}_r\hat{\hat{a}}_r}[k]$ and $Q^{\text{GF}}_{d\hat{\tilde{t}}_r\hat{\hat{a}}_r}[k]$ by setting $\hat{x} = \hat{\hat{a}}_{r,\text{GF}}$ and $\hat{x} = d\hat{\tilde{t}}_{r,\text{GF}}$, respectively. The expression of

$Q^{\mathrm{GF}}_{d\hat{\hat{t}}_r d\hat{\hat{t}}_r}[k]$ follows by setting $\hat{x} = \hat{y} = d\hat{\hat{t}}_r$ in (121), together with the identity

$$Q^{\mathrm{GF}}_{d\hat{\hat{t}}_r \hat{\hat{a}}_r} Q^{\mathrm{GF}-1}_{\hat{\hat{a}}_r \hat{\hat{a}}_r} Q^{\mathrm{GF}}_{\hat{\hat{a}}_r d\hat{\hat{t}}_r} = Q^{\mathrm{GF}}_{d\hat{\hat{t}}_r d\hat{\hat{t}}_r} - c_{\hat{\rho}}^2 C_s \tag{123}$$

We now prove the geometry-based results. To do so, we first formulate the $[k(m-1)-\nu](n-1)$ redundant misclosures brought by the geometry-based model (cf. Table 2). The geometry parametrization $\Delta\tilde{x}_r$ gives $(m-1-\nu)(n-1)$ misclosures as

$$t_{\hat{g}_r} = (D_m^T G)^{\perp T}[\frac{1}{k}\sum_{i=1}^{k}(d\hat{\hat{t}}_{r,\mathrm{GF}}(i) - d\hat{\hat{t}}_{1,\mathrm{GF}}(i))],\ r = 2,\ldots,n \tag{124}$$

while the time-invariance assumption on $\Delta\tilde{x}_r$ gives $(k-1)(m-1)(n-1)$ misclosures as

$$t_{i,r} = [d\hat{\hat{t}}_{r,\mathrm{GF}}(i) - d\hat{\hat{t}}_{1,\mathrm{GF}}(i)] - [d\hat{\hat{t}}_{r,\mathrm{GF}}(1) - d\hat{\hat{t}}_{1,\mathrm{GF}}(1)] \tag{125}$$

for $r = 2,\ldots,n$ and $i = 2,\ldots,k$.

Since the two misclosure vectors $t_{\hat{g}} = [t_{\hat{g}2}^T,\ldots,t_{\hat{g}n}^T]^T$ and $t = [t_{2,2}^T,\ldots,t_{2,n}^T,\ldots,t_{k,n}^T]^T$ are uncorrelated, any (co)variance matrix $Q^{\mathrm{GF}}_{\hat{x}\hat{y}}[k]$ is corrected to $Q^{\mathrm{GB}}_{\hat{x}\hat{y}}[k]$ as

$$\begin{aligned} Q^{\mathrm{GB}}_{\hat{x}\hat{y}}[k] = {} & Q^{\mathrm{GF}}_{\hat{x}\hat{y}}[k] - Q^{\mathrm{GF}}_{\hat{x}t_{\hat{g}}}[k] Q^{-1}_{t_{\hat{g}}t_{\hat{g}}} Q^{\mathrm{GF}}_{t_{\hat{g}}\hat{y}}[k] \\ & - Q^{\mathrm{GF}}_{\hat{x}t}[k] Q^{-1}_{tt} Q^{\mathrm{GF}}_{t\hat{y}}[k] \end{aligned} \tag{126}$$

Accordingly, the expressions of $Q^{\mathrm{GB}}_{\hat{\hat{a}}_r\hat{\hat{a}}_r}[k]$, $Q^{\mathrm{GB}}_{d\hat{\hat{t}}\hat{\hat{a}}_1}[k]$ and $Q^{\mathrm{GB}}_{d\hat{\hat{t}}\hat{\hat{a}}_1}[k]$ follow through the identities

$$\begin{aligned} Q^{\mathrm{GF}}_{\hat{\hat{a}}_r t_{\hat{g}}}[k] Q^{-1}_{t_{\hat{g}}t_{\hat{g}}} Q^{\mathrm{GF}}_{t_{\hat{g}}\hat{\hat{a}}_r}[k] &= \frac{1}{k}\frac{n-1}{n} c_{\hat{\rho}}^2 \Lambda^{-1} e_\mu e_\mu^T \Lambda^{-1} \otimes \tilde{C}_s \\ Q^{\mathrm{GF}}_{d\hat{\hat{t}}t_{\hat{g}}}[k] Q^{-1}_{t_{\hat{g}}t_{\hat{g}}} Q^{\mathrm{GF}}_{t_{\hat{g}}\hat{\hat{a}}_1}[k] &= \frac{1}{k}\frac{n-1}{n} c_{\hat{\rho}}^2 e_\mu^T \Lambda^{-1} \otimes \tilde{C}_s \\ Q^{\mathrm{GF}}_{d\hat{\hat{t}}t_{\hat{g}}}[k] Q^{-1}_{t_{\hat{g}}t_{\hat{g}}} Q^{\mathrm{GF}}_{t_{\hat{g}}d\hat{t}}[k] &= \frac{1}{k}\frac{n-1}{n} c_{\hat{\rho}}^2 \otimes \tilde{C}_s \end{aligned} \tag{127}$$

as well as

$$Q^{\mathrm{GF}}_{d\hat{\hat{t}}t}[k] Q^{-1}_{tt} Q^{\mathrm{GF}}_{td\hat{\hat{t}}}[k] = \frac{k-1}{k}\frac{n-1}{n} c_{\hat{\rho}}^2 \otimes C_s \tag{128}$$

with $Q^{\mathrm{GF}}_{\hat{\hat{a}}_r t}[k] = 0$. □

Proof of Tables 4 and 5 The proof goes along the same lines as the proof of Table 3, so it will not be presented here. □

The exact value of γ The exact value of γ, introduced in Lemma 5, can be stated as

$$\gamma = \frac{(f_1^3 - f_2^3)^2}{f_1^2 f_2^2 (f_1+f_2)^2 + \epsilon\,\eta} \tag{129}$$

with

$$\eta = \left[\frac{f_1+f_2}{f_1-f_2}\right]^2 (f_1^2+f_2^2)(f_1^4+f_2^4) \tag{130}$$

The approximation, given in Lemma 5, follows by neglecting $\epsilon\,\eta$, compared to the first term in the denominator of (129). □

References

Allison T (1991) Multi-observable processing techniques for precise relative positioning. In: Proceedings ION GPS-91. Albuquerque, New Mexico, 11–13 September, pp 715–725

Baarda W (1973) S-transformations and criterion matrices. Tech. rep., Netherlands Geodetic Commission, Publ. on Geodesy, New Series, vol 5(1), Delft

Bertiger W, Desai SD, Haines B, Harvey N, Moore AW, Owen S, Weiss JP (2010) Single receiver phase ambiguity resolution with GPS data. J Geod 84(5):327–337

Beutler G, Bock H, Dach R, Fridez P, Gade A, Hugentobler U, Jaggi A, Meindl M, Mervart L, Prange L, Schaer S, Springer T, Urschl P, Walser P (2007) Bernese GPS software version 5.0. Astron. Inst., Univ. of Bern, Bern, Switzerland

Bisnath S, Collins P (2012) Recent developments in precise point positioning. Geomatica 66(2):103–111

Bisnath S, Gao Y (2008) Current state of precise point positioning and future prospects and limitations. In: Observing our changing earth, IAG Symp 133:615–623

Collins P (2008) Isolating and estimating undifferenced GPS integer ambiguities. In: Proceedings ION NTM, pp 720–732

Collins P, Lahaye F, Heroux P, Bisnath S (2008) Precise point positioning with ambiguity resolution using the decoupled clock model. In: Proceedings of the 21st international technical meeting of the satellite division of the Institute of Navigation (ION GNSS 2008), pp 1315–1322

de Jonge PJ (1998) A processing strategy for the application of the GPS in networks. PhD thesis, Delft University of Technology, Publication on Geodesy, 46, Netherlands Geodetic Commission, Delft

Ge M, Gendt G, Rothacher M, Shi C, Liu J (2008) Resolution of GPS carrier-phase ambiguities in precise point positioning (PPP) with daily observations. J Geod 82(7):389–399

Geng J (2011) Rapid integer ambiguity resolution in GPS precise point positioning. PhD thesis, University of Nottingham, UK

Geng J, Bock Y (2013) Triple-frequency GPS precise point positioning with rapid ambiguity resolution. J Geod 87(5):449–460

Geng J, Meng X, Dodson A, Teferle F (2010) Integer ambiguity resolution in precise point positioning: method comparison. J Geod 84(9):569–581

Geng J, Teferle FN, Meng X, Dodson AH (2011) Towards PPP-RTK: ambiguity resolution in real-time precise point positioning. Adv Space Res 47(10):1664–1673

Geng J, Shi C, Ge M, Dodson AH, Lou Y, Zhao Q, Liu J (2012) Improving the estimation of fractional-cycle biases for ambiguity resolution in precise point positioning. J Geod 86(8):579–589

Hernandez-Pajares M, Juan JM, Sanz J, Colombo OL (2000) Application of ionospheric tomography to real-time GPS carrier-phase ambiguities resolution, at scales of 400–1,000 km and with high geomagnetic activity. Geophys Res Lett 27(13):2009–2012

Hofmann-Wellenhof B, Lichtenegger H, Wasle E (2008) GNSS: global navigation satellite systems: GPS, Glonass, Galileo, and more. Springer, New York

Jonkman N, Teunissen P, Joosten P, Odijk D (2000) GNSS long baseline ambiguity resolution: impact of a third navigation frequency. In: Geodesy Beyond 2000, IAG Symp 121, pp 349–354

Khodabandeh A, Teunissen PJG (2014) Single-epoch GNSS array integrity: an analytical study. IAG Symp 142, accepted for publication

Kouba J, Heroux P (2001) Precise point positioning using IGS orbit and clock products. GPS solut 5(2):12–28

Lannes A, Prieur JL (2013) Calibration of the clock-phase biases of GNSS networks: the closure-ambiguity approach. J Geod 87(8):709–731

Lannes A, Teunissen PJG (2011) GNSS algebraic structures. J Geod 85(5):273–290

Laurichesse D (2011) The CNES real-time PPP with undifferenced integer ambiguity resolution demonstrator. In: Proceedings of the ION GNSS, pp 654–662

Laurichesse D, Mercier F (2007) Integer ambiguity resolution on undifferenced GPS phase measurements and its application to PPP. In: Proceedings of the 20th international technical meeting of the satellite division of the Institute of Navigation (ION GNSS 2007), pp 839–848

Laurichesse D, Mercier F, Berthias J, Broca P, Cerri L, CNES F (2009) Integer ambiguity resolution on undifferenced GPS phase measurements and its application to PPP and satellite precise orbit determination. Navigation 56(2):135–149

Li T, Wang J, Laurichesse D (2013a) Modeling and quality control for reliable precise point positioning integer ambiguity resolution with GNSS modernization. GPS Solut, pp 1–14

Li X, Ge M, Zhang H, Wickert J (2013b) A method for improving uncalibrated phase delay estimation and ambiguity-fixing in real-time precise point positioning. J Geod 87(5):405–416

Li X, Ge M, Lu C, Zhang Y, Wang R, Wickert J, Schuh H (2014) High-rate GPS seismology using real-time precise point positioning with ambiguity resolution. Geoscience and remote sensing, IEEE transactions on, pp 1–15. doi:10.1109/TGRS.2013.2295373

Loyer S, Perosanz F, Mercier F, Capdeville H, Marty JC (2012) Zero-difference GPS ambiguity resolution at CNES-CLS IGS analysis center. J Geod 86(11):991–1003

Mervart L, Lukes Z, Rocken C, Iwabuchi T (2008) Precise point positioning with ambiguity resolution in real-time. In: Proceedings of ION GNSS, pp 397–405

Mervart L, Rocken C, Iwabuchi T, Lukes Z, Kanzaki M (2013) Precise point positioning with fast ambiguity resolution-prerequisites, algorithms and performance. In: Proceedings of ION GNSS, pp 1176–1185

Odijk D (2002) Fast precise GPS positioning in the presence of ionospheric delays. Ph.D. thesis, Delft University of Technology, Publication on Geodesy, 52, Netherlands, Geodetic Commission, Delft

Odijk D, Teunissen PJG (2008) ADOP in closed form for a hierarchy of multi-frequency single-baseline GNSS models. J Geod 82(8):473–492

Odijk D, Teunissen PJG, Zhang B (2012) Single-frequency integer ambiguity resolution enabled GPS precise point positioning. J Survey Eng 138(4):193–202

Odijk D, Arora BS, Teunissen PJG (2014a) Predicting the success rate of long-baseline GPS + Galileo (partial) ambiguity resolution. J Navigat 1–17. doi:10.1017/S037346331400006X

Odijk D, Teunissen PJG, Khodabandeh A (2014b) Single-frequency PPP-RTK: theory and experimental results. IAG Symp Earth Edge: Sci Sustain Planet 139:571–578

Rao CR (1973) Linear statistical inference and its applications, vol 2. Wiley, New Jersey

Shi J (2012) Precise point positioning integer ambiguity resolution with decoupled clocks. PhD thesis, University of Calgary, Canada

Shi J, Gao Y (2013) A comparison of three PPP integer ambiguity resolution methods. GPS Solut (published online)

Teunissen PJG (1985) Generalized inverses, adjustment, the datum problem and S-transformations. In: Grafarend EW, Sanso F (eds) Optimization and design of geodetic networks. Springer, Berlin

Teunissen PJG (1995) The least-squares ambiguity decorrelation adjustment: a method for fast GPS integer ambiguity estimation. J Geod 70(1–2):65–82

Teunissen PJG (1997a) A canonical theory for short GPS baselines. Part I: the baseline precision. J Geod 71(6):320–336

Teunissen PJG (1997b) A canonical theory for short GPS baselines. Part IV: precision versus reliability. J Geod 71(9):513–525

Teunissen PJG (1997c) The geometry-free GPS ambiguity search space with a weighted ionosphere. J Geod 71(6):370–383

Teunissen PJG (1997d) On the GPS widelane and its decorrelating property. J Geod 71(9):577–587

Teunissen PJG (1998) Success probability of integer GPS ambiguity rounding and bootstrapping. J Geod 72(10):606–612

Teunissen PJG (1999) An optimality property of the integer least-squares estimator. J Geod 73(11):587–593

Teunissen PJG (2000) Adjustment theory: an introduction. Delft University Press, series on Mathematical Geodesy and Positioning

Teunissen PJG (2002) The parameter distributions of the integer GPS model. J Geod 76(1):41–48

Teunissen PJG (2012) A-PPP: array-aided precise point positioning with global navigation satellite systems. Signal Process IEEE Trans 60(6):2870–2881

Teunissen PJG, de Bakker PF (2012) Single-receiver single-channel multi-frequency GNSS integrity: outliers, slips, and ionospheric disturbances. J Geod 1–17

Teunissen PJG, Khodabandeh A (2013) BLUE, BLUP and the Kalman filter: some new results. J Geod 87(5):461–473

Teunissen PJG, Odijk D, Zhang B (2010) PPP-RTK: results of CORS network-based PPP with integer ambiguity resolution. J Aeronaut, Astronaut Aviat 42(4):223–229

Wubbena G (1989) The GPS adjustment software package-GEONAP-concepts and models. In: International geodetic symposium on satellite positioning l, Las Cruces, New Mexico, 13–17 March, pp 452–461

Wubbena G, Schmitz M, Bagg A (2005) PPP-RTK: precise point positioning using state-space representation in RTK networks. In: Proceedings of ION GNSS, pp 13–16

Zhang B, Teunissen PJG, Odijk D (2011) A novel un-differenced PPP-RTK concept. J Navig 64(S1):S180–S191

Zhang X, Li P (2013) Assessment of correct fixing rate for precise point positioning ambiguity resolution on a global scale. J Geod 87(6):579–589

Zumberge JF, Heflin MB, Jefferson DC, Watkins MM, Webb FH (1997) Precise point positioning for the efficient and robust analysis of GPS data from large networks. J Geophys Res 102:5005–5017

3 PPP-RTK Corrections and their User-Impact

This chapter is covered by the following publication:

Khodabandeh A. and Teunissen P.J.G. (2015). An Analytical Study of PPP-RTK Corrections: Precision, Correlation and User-Impact. Journal of Geodesy, doi: 10.1007/s00190-015-0838-9.

J Geod
DOI 10.1007/s00190-015-0838-9

ORIGINAL ARTICLE

An analytical study of PPP-RTK corrections: precision, correlation and user-impact

A. Khodabandeh[1] · **P. J. G. Teunissen**[1,2]

Received: 26 March 2015 / Accepted: 21 June 2015

Abstract PPP-RTK extends the PPP concept by providing single-receiver users, next to orbits and clocks, also information about the satellite phase and code biases, thus enabling single-receiver ambiguity resolution. It is the goal of the present contribution to provide an analytical study of the quality of the PPP-RTK corrections as well as of their impact on the user ambiguity resolution performance. We consider the geometry-free and the geometry-based network derived corrections, as well as the impact of network ambiguity resolution on these corrections. Next to the insight that is provided by the analytical solutions, the closed form expressions of the variance matrices also demonstrate how the corrections depend on network parameters such as number of epochs, number of stations, number of satellites, and number of frequencies. As a result we are able to describe in a qualitative sense how the user ambiguity resolution performance is driven by the data from the different network scenarios.

Keywords Global navigation satellite systems (GNSS) · Precise point positioning (PPP) · Integer ambiguity resolution (IAR) · PPP-RTK corrections · Geometry-free (GF) · Geometry-based (GB) · Ambiguity dilution of precision (ADOP)

✉ A. Khodabandeh
amir.khodabandeh@curtin.edu.au

P. J. G. Teunissen
p.teunissen@curtin.edu.au

[1] Department of Spatial Sciences, GNSS Research Centre, Curtin University of Technology, Perth, Australia

[2] Department of Geoscience and Remote Sensing, Delft University of Technology, Delft, The Netherlands

1 Introduction

PPP-RTK is integer ambiguity resolution enabled precise point positioning (PPP) (Wubbena et al. 2005; Mervart et al. 2008). It extends the PPP concept (Heroux and Kouba 1995; Zumberge et al. 1997) by providing single-receiver users, next to the orbits and clocks, also information about the satellite phase and code biases. This information, when properly provided, enables recovery of the integerness of the user ambiguities, thus enabling single-receiver ambiguity resolution, thereby reducing convergence times as compared to that of PPP.

Several PPP-RTK methods have been formulated in recent years, see e.g., (Wubbena et al. 2005; Laurichesse and Mercier 2007; Mervart et al. 2008; Collins 2008; Ge et al. 2008; Bertiger et al. 2010; Teunissen et al. 2010; Geng et al. 2012; Loyer et al. 2012; Geng and Bock 2013; Lannes and Prieur 2013; Banville et al. 2014). For an overview and a critical comparison of these methods, see the review (Teunissen and Khodabandeh 2015). As was demonstrated in (ibid), a careful interpretation of the estimable parameters involved is essential for obtaining a proper insight into the general mechanics of PPP-RTK. It is the goal of the present contribution to take this one step further by providing an analytical study of the multi-frequency PPP-RTK corrections themselves, thereby presenting a precision and correlation analysis that will enable us to demonstrate how the quality of these corrections, as well as their impact on the user parameters, is driven by the information content and adjustment of the external network.

PPP-RTK is founded on the idea of single-receiver integer ambiguity resolution (IAR). This idea, together with the estimability of the associated PPP-RTK corrections, is best described by starting with the single-receiver user observation equations. Consider the user's antenna u tracking

Published online: 21 July 2015

f-frequency GNSS data that are transmitted by a satellite s and a chosen pivot satellite p. The corresponding between-satellite single-difference (SD) observation equations read then (Teunissen and Kleusberg 1998; Hofmann-Wellenhof et al. 2008)

$$\begin{aligned} \Delta\phi^{ps}_{u,j} &= g^{ps\,T}\,\Delta x_u - \mu_j \iota^{ps}_u - dt^{ps} + \lambda_j(z^{ps}_{u,j} - \delta^{ps}_{,j}) \\ \Delta p^{ps}_{u,j} &= g^{ps\,T}\,\Delta x_u + \mu_j \iota^{ps}_u - dt^{ps} - d^{ps}_{,j} \end{aligned} \tag{1}$$

where $\Delta\phi^{ps}_{u,j}$ and $\Delta p^{ps}_{u,j}$ denote the SD 'observed-minus-computed' phase and code observables on the frequency band f_j ($j = 1, \ldots, f$), respectively. Here and in the following, the precise orbital corrections are assumed included in the 'observed-minus-computed' observables. The ν-vector Δx_u contains the user's position increments and/or the zenith tropospheric delay (ZTD). Parameter ν can take the values $\nu = 3$ (position-only model), $\nu = 1$ (ZTD-only model) or $\nu = 4$ (position-plus-ZTD model). Thus, the ν-vector g^{ps} contains the SD receiver-satellite direction vector and/or the SD tropospheric mapping function. The (first-order) SD slant ionospheric delay, experienced on the first frequency, is denoted by ι^{ps}_u. Thus, the frequency-dependent coefficients are defined as the ratio $\mu_j = (f_1^2/f_j^2)$. The SD integer ambiguity $z^{ps}_{u,j} \in \mathbb{Z}$ and the SD satellite phase bias $\delta^{ps}_{,j}$, both expressed in cycles, are linked to the phase observables through the wavelength λ_j. The SD satellite clocks are denoted by dt^{ps}, while the SD satellite code biases are denoted by $d^{ps}_{,j}$. Apart from $z^{ps}_{u,j}$ and $\delta^{ps}_{,j}$, the rest of the quantities are all expressed in units of range. We assume that m satellites are tracked and thus $p, s \in \{h \,|\, h = 1, \ldots, m\}$, with $p \neq s$.

If we make use of the more compact multi-frequency vector notation $\Delta\phi^{ps}_u = [\Delta\phi^{ps}_{u,1}, \ldots, \Delta\phi^{ps}_{u,f}]^T$, $\Delta p^{ps}_u = [\Delta p^{ps}_{u,1}, \ldots, \Delta p^{ps}_{u,f}]^T$, $\mu = [\mu_1, \ldots, \mu_f]^T$, $z^{ps}_u = [z^{ps}_{u,1}, \ldots, z^{ps}_{u,f}]^T$, $\delta^{ps} = [\delta^{ps}_{,1}, \ldots, \delta^{ps}_{,f}]^T$, and $d^{ps} = [d^{ps}_{,1}, \ldots, d^{ps}_{,f}]^T$, we may write (1) as

$$\begin{aligned} \Delta\phi^{ps}_u &= e\,\Delta\rho^{ps}_u - \mu\,\iota^{ps}_u - e\,dt^{ps} + \Lambda(z^{ps}_u - \delta^{ps}) \\ \Delta p^{ps}_u &= e\,\Delta\rho^{ps}_u + \mu\,\iota^{ps}_u - e\,dt^{ps} - d^{ps} \end{aligned} \tag{2}$$

where $e = [1, \ldots, 1]^T$, $\Lambda = \mathrm{diag}(\lambda_1, \ldots, \lambda_f)$, and $\Delta\rho^{ps}_u = g^{ps\,T}\Delta x_u$. The user observation equations (2) do not contain enough information to solve for an integer ambiguity resolved user position. This would become possible though if the information about the satellite clocks, dt^{ps}, and satellite biases, δ^{ps} and d^{ps}, were given. Using such externally provided information to correct the observations as

$$\begin{aligned} \Delta\phi'^{ps}_u &= \Delta\phi^{ps}_u + e\,dt^{ps} + \Lambda\,\delta^{ps} \\ \Delta p'^{ps}_u &= \Delta p^{ps}_u + e\,dt^{ps} + d^{ps} \end{aligned} \tag{3}$$

results in user equations that take the form

$$\begin{aligned} \Delta\phi'^{ps}_u &= e\,\Delta\rho^{ps}_u - \mu\,\iota^{ps}_u + \Lambda\,z^{ps}_u \\ \Delta p'^{ps}_u &= e\,\Delta\rho^{ps}_u + \mu\,\iota^{ps}_u . \end{aligned} \tag{4}$$

This system is now in a form that can be used to solve for the integer ambiguity resolved *user* parameters Δx_u and ι_u. Hence, with externally provided corrections dt^{ps}, δ^{ps}, and d^{ps}, the user system of observation equations (4) can be solved as a mixed-integer system of equations, thereby profiting from the integerness of $z^{ps}_u \in \mathbb{Z}^f$. This is the basic idea of single-receiver, IAR-enabled, positioning.

The operationalization of this basic idea is somewhat more involved however. This is due to the fact that the above needed parameters $dt^{ps}, \delta^{ps}, d^{ps}$ *cannot* be determined as such. GNSS data are namely not capable of providing these 'absolute' parameters, but instead only estimable functions that can *act* as such. These estimable parameters, denoted with a tilde as $d\tilde{t}^{ps}, \tilde{\delta}^{ps}, \tilde{d}^{ps}$, achieve the same goal, namely of enabling the construction of a user system of observation equations that is in mixed-integer form.Thus although they are not the original absolute parameters,

$$d\tilde{t}^{ps} \neq dt^{ps}, \tilde{\delta}^{ps} \neq \delta^{ps}, \tilde{d}^{ps} \neq d^{ps} \tag{5}$$

they still do the job in ensuring that the user can work with integer ambiguities. When they are used to correct the user observations as

$$\begin{aligned} \Delta\tilde{\phi}^{ps}_u &= \Delta\phi^{ps}_u + e\,d\tilde{t}^{ps} + \Lambda\tilde{\delta}^{ps} \\ \Delta\tilde{p}^{ps}_u &= \Delta p^{ps}_u + e\,d\tilde{t}^{ps} + \tilde{d}^{ps} \end{aligned} \tag{6}$$

the user equations take the form

$$\begin{aligned} \Delta\tilde{\phi}^{ps}_u &= e\,\Delta\tilde{\rho}^{ps}_u - \mu\,\tilde{\iota}^{ps}_u + \Lambda\tilde{z}^{ps}_u \\ \Delta\tilde{p}^{ps}_u &= e\,\Delta\tilde{\rho}^{ps}_u + \mu\,\tilde{\iota}^{ps}_u \end{aligned} \tag{7}$$

with integer $\tilde{z}^{ps}_u \in \mathbb{Z}^f$. Thus, the structure of these equations is indeed identical to that of the mixed-integer system (4), be it that the interpretation of the estimable parameters in (7) is different from those of (4). This difference in parameter interpretation is important and it is due to the differences in (5).

It is the goal of the present contribution to provide an analytical study of the *estimable* PPP-RTK corrections $d\tilde{t}^{ps}$, $\tilde{\delta}^{ps}$, and $\tilde{d}^{ps}$, as well as of their impact on the user ambiguity resolution performance. In Sect. 2, we start by introducing single-station PPP-RTK, while in Sect. 3 we warn for the pitfalls that exist when evaluating the PPP-RTK corrections on an individual basis.The results of Sect. 2 are generalized in Sects. 4 and 5, respectively, to the geometry-free (GF) and geometry-based (GB) network case. This is done in network ambiguity-float as well as in network ambiguity-fixed

mode. Next to the insight that is provided by the analytical solutions, the closed form expressions of the variance matrices also demonstrate how the corrections depend on network parameters such as number of epochs, number of stations, number of satellites, and number of frequencies. As a result we are able to describe in a qualitative sense how the user ambiguity resolution performance is driven by the data from the different network scenarios. A summary with conclusions is finally provided in Sect. 6.

2 Single-station PPP-RTK

Although estimators of the PPP-RTK corrections $d\tilde{t}^{ps}$, $\tilde{\delta}^{ps}$, and $\tilde{d}^{ps}$ are usually computed from an external *network*, they can—as the below will show—be obtained from the data of a single station as well.

2.1 Single-station corrections

The observation equations of a single reference station r follow by replacing the user index u in (2) by r,

$$\begin{aligned} \Delta\phi_r^{ps} &= e\,(\Delta\rho_r^{ps} - dt^{ps}) - \mu\,\iota_r^{ps} + \Lambda(z_r^{ps} - \delta^{ps}) \\ \Delta p_r^{ps} &= e\,(\Delta\rho_r^{ps} - dt^{ps}) + \mu\,\iota_r^{ps} - d^{ps}. \end{aligned} \tag{8}$$

These equations are underdetermined as there are $2f$ equations in $3f + 3$ unknowns. The rank defect is $f + 3$. There are many different ways to eliminate a rank defect, each with a different interpretation of the resulting estimable parameters. These different sets of estimable parameters are linked by $\mathcal{S}$-transformations (Baarda 1973; Teunissen 1985). Examples of such different sets in the context of PPP-RTK can be found in Teunissen et al. (2010), Zhang et al. (2011), Lannes and Teunissen (2011), Odijk et al. (2012) and Teunissen and Khodabandeh (2015).

To eliminate the rank defect of the above system (8), we first lump the parameters that have common coefficients,

$$\rho_r^{ps} := \Delta\rho_r^{ps} - dt^{ps},\ a_r^{ps} := z_r^{ps} - \delta^{ps}. \tag{9}$$

As this takes care of $f + 1$ rank defects, there are still 2 defects that need to be taken care of. This will be done by applying the ionosphere-free/geometry-free decomposition of the code bias d^{ps},

$$d^{ps} = [e,\ \mu,\ E]\begin{bmatrix} d_{IF}^{ps} \\ d_{GF}^{ps} \\ \tilde{d}^{ps} \end{bmatrix},\quad \text{with}\quad [e,\ \mu,\ E]^{-1} = \begin{bmatrix} \mu_{IF}^T \\ \mu_{GF}^T \\ E^- \end{bmatrix} \tag{10}$$

where

$$\begin{aligned} \mu_{IF} &= \frac{1}{\mu_2 - \mu_1}[\mu_2, -\mu_1, 0, \ldots, 0]^T \\ \mu_{GF} &= \frac{1}{\mu_2 - \mu_1}[-1, 1, 0, \ldots, 0]^T \\ E^- &= E^T(I_f - e\,\mu_{IF}^T - \mu\,\mu_{GF}^T). \end{aligned} \tag{11}$$

The $f \times (f - 2)$ matrix E is structured by eliminating the first two columns of I_f.

The above decomposition shows that the ionosphere-free and geometry-free combinations d_{IF}^{ps} and d_{GF}^{ps} have the same coefficients as ρ_r^{ps} and ι_r^{ps}, namely e and μ, respectively. Hence, a further lumping can take place, thus taking care of the remaining two rank defects. Substitution of (10) into (8) gives therefore, together with (9), the full-rank single-station model as

$$\begin{aligned} \mathsf{E}(\phi_r^{ps}) &= e\,\tilde{\rho}_r^{ps} - \mu\,\tilde{\iota}_r^{ps} + \Lambda\,\tilde{a}_r^{ps} \\ \mathsf{E}(p_r^{ps}) &= e\,\tilde{\rho}_r^{ps} + \mu\,\tilde{\iota}_r^{ps} - E\,\tilde{d}^{ps} \end{aligned} \tag{12}$$

where

$$\begin{aligned} \tilde{\rho}_r^{ps} &= \rho_r^{ps} - d_{IF}^{ps} \\ \tilde{a}_r^{ps} &= a_r^{ps} + \Lambda^{-1}(e\,d_{IF}^{ps} - \mu\,d_{GF}^{ps}) \\ \tilde{\iota}_r^{ps} &= \iota_r^{ps} - d_{GF}^{ps}. \end{aligned} \tag{13}$$

The estimable parameters in the above system can be interpreted as a biased range $\tilde{\rho}_r^{ps}$, a biased ambiguity $\tilde{a}_r^{ps}$, and a biased ionospheric delay $\tilde{\iota}_r^{ps}$. However, note that with the definitions

$$d\tilde{t}^{ps} := -\tilde{\rho}_r^{ps} \quad \text{and} \quad \tilde{\delta}^{ps} := -\tilde{a}_r^{ps} \tag{14}$$

the 'range' and 'ambiguity' can likewise be interpreted as a biased clock $d\tilde{t}^{ps}$ and a biased phase-bias $\tilde{\delta}^{ps}$, thus giving instead of (13), the estimable parameters

$$\begin{aligned} d\tilde{t}^{ps} &= dt^{ps} + d_{IF}^{ps} - \Delta\rho_r^{ps} \\ \tilde{\delta}^{ps} &= \delta^{ps} - \Lambda^{-1}(e\,d_{IF}^{ps} - \mu\,d_{GF}^{ps}) - z_r^{ps} \\ \tilde{\iota}_r^{ps} &= \iota_r^{ps} - d_{GF}^{ps}. \end{aligned} \tag{15}$$

The corresponding system of observation equations now reads instead of (12),

$$\begin{aligned} \mathsf{E}(\phi_r^{ps}) &= -e\,d\tilde{t}^{ps} - \mu\,\tilde{\iota}_r^{ps} - \Lambda\,\tilde{\delta}^{ps} \\ \mathsf{E}(p_r^{ps}) &= -e\,d\tilde{t}^{ps} + \mu\,\tilde{\iota}_r^{ps} - E\,\tilde{d}^{ps}. \end{aligned} \tag{16}$$

As this is an invertible system of $2f$ equations in $2f$ unknowns per satellite pair ps, its solution follows after inversion as (cf. 10)

$$
\begin{aligned}
d\hat{\tilde{t}}^{ps} &= -\mu_{1F}^T\, p_r^{ps} \\
\hat{\tilde{\delta}}^{ps} &= -\Lambda^{-1}[\phi_r^{ps} + (\mu\, \mu_{GF}^T - e\, \mu_{1F}^T)\, p_r^{ps}] \\
\hat{\tilde{d}}^{ps} &= -E^-\, p_r^{ps} \\
\hat{\tilde{\iota}}_r^{ps} &= +\mu_{GF}^T\, p_r^{ps}.
\end{aligned} \tag{17}
$$

In the following the *user-aiding* functionality of each of these estimators is described.

2.2 The individual corrections applied

To show the effect that each of the PPP-RTK corrections

$$
d\hat{\tilde{t}}^{ps},\ \hat{\tilde{\delta}}^{ps},\ \text{and}\ \hat{\tilde{d}}^{ps} \tag{18}
$$

has, we apply them sequentially to the user observation equations

$$
\begin{aligned}
\mathsf{E}(\phi_u^{ps}) &= e\, \tilde{\rho}_u^{ps} - \mu\, \tilde{\iota}_u^{ps} + \Lambda\, \tilde{a}_u^{ps} \\
\mathsf{E}(p_u^{ps}) &= e\, \tilde{\rho}_u^{ps} + \mu\, \tilde{\iota}_u^{ps} - E\, \tilde{d}^{ps}.
\end{aligned} \tag{19}
$$

2.2.1 Clock $d\tilde{t}^{ps}$ provides positional link

For the expectation of the clock correction we have (cf. 15),

$$
\mathsf{E}(d\hat{\tilde{t}}^{ps}) = d\tilde{t}^{ps} = dt^{ps} + d_{1F}^{ps} - \Delta\rho_r^{ps}. \tag{20}
$$

Application to (19) gives

$$
\begin{aligned}
\mathsf{E}(\phi_u^{ps} + e\, d\hat{\tilde{t}}^{ps}) &= e\, \Delta\rho_{ru}^{ps} - \mu\, \tilde{\iota}_u^{ps} + \Lambda\, \tilde{a}_u^{ps} \\
\mathsf{E}(p_u^{ps} + e\, d\hat{\tilde{t}}^{ps}) &= e\, \Delta\rho_{ru}^{ps} + \mu\, \tilde{\iota}_u^{ps} - E\, \tilde{d}^{ps}
\end{aligned} \tag{21}
$$

with $\Delta\rho_{ru}^{ps} = \tilde{\rho}_u^{ps} - \tilde{\rho}_r^{ps} = \Delta\rho_u^{ps} - \Delta\rho_r^{ps}$ being the double-differenced (DD) geometric/tropspheric delay's increment. This shows, when comparing (21) with (19), that the satellite clock correction has the function to establish a positional link between user u and reference r.

2.2.2 Phase-bias $\tilde{\delta}^{ps}$ provides ambiguity link

Although (21) is solvable for the user's position, it is not yet in mixed-integer form, since $\tilde{a}_u^{ps} \notin \mathbb{Z}^f$. To enable user integer ambiguity resolution, the satellite phase-bias $\tilde{\delta}^{ps}$ is needed. For the expectation of the phase-bias correction we have (cf. 15)

$$
\mathsf{E}(\hat{\tilde{\delta}}^{ps}) = \tilde{\delta}^{ps} = \delta^{ps} + \Lambda^{-1}(\mu\, d_{GF}^T - e\, d_{1F}^T) - z_r^{ps} \tag{22}
$$

Application to (21) gives

$$
\begin{aligned}
\mathsf{E}(\phi_u^{ps} + e\, d\hat{\tilde{t}}^{ps} + \Lambda\hat{\tilde{\delta}}^{ps}) &= e\, \Delta\rho_{ru}^{ps} - \mu\, \tilde{\iota}_u^{ps} + \Lambda\, z_{ru}^{ps} \\
\mathsf{E}(p_u^{ps} + e\, d\hat{\tilde{t}}^{ps}) &= e\, \Delta\rho_{ru}^{ps} + \mu\, \tilde{\iota}_u^{ps} - E\, \tilde{d}^{ps}
\end{aligned} \tag{23}
$$

with $z_{ru}^{ps} = \tilde{a}_u^{ps} - \tilde{a}_r^{ps} = z_u^{ps} - z_r^{ps}$ being the integer-valued double-differenced (DD) ambiguities. This shows that the satellite phase-bias correction has the function of replacing the noninteger user ambiguity $\tilde{a}_u^{ps}$ by the integer DD ambiguity between user u and reference r, $z_{ru}^{ps} \in \mathbb{Z}^f$.

2.2.3 Code-bias $\tilde{d}^{ps}$ exploits multi-frequency code data

Although (23) is in mixed-integer form, it does not yet fully exploit all information in case $f > 2$. The reason being that in each of the last $(f-2)$ code equations of (23), the code-biases $\tilde{d}^{ps}$ are treated as unknown parameters. Hence, to have the multi-frequency user data properly contribute to the user solution, the code-bias corrections need to be provided as well. The resulting user equations then finally read

$$
\begin{aligned}
\mathsf{E}(\phi_u^{ps} - \hat{c}_\phi^{ps}) &= e\, \Delta\rho_{ru}^{ps} - \mu\, \tilde{\iota}_u^{ps} + \Lambda\, z_{ru}^{ps} \\
\mathsf{E}(p_u^{ps} - \hat{c}_p^{ps}) &= e\, \Delta\rho_{ru}^{ps} + \mu\, \tilde{\iota}_u^{ps}
\end{aligned} \tag{24}
$$

with the combined PPP-RTK phase and code corrections, $\hat{c}_\phi^{ps}$ and $\hat{c}_p^{ps}$, given as

$$
\begin{aligned}
\hat{c}_\phi^{ps} &= -e\, d\hat{\tilde{t}}^{ps} - \Lambda\, \hat{\tilde{\delta}}^{ps} \\
\hat{c}_p^{ps} &= -e\, d\hat{\tilde{t}}^{ps} - E\, \hat{\tilde{d}}^{ps}.
\end{aligned} \tag{25}
$$

2.3 Single-baseline RTK

The above has shown that the PPP-RTK corrected user model is in fact a *DD-like* model. The clock correction establishes the geometry in DD-form and the phase-bias correction establishes the ambiguity in DD-form. The question that comes to the fore is therefore how this DD-like model of the PPP-RTK user compares to the more traditional single-baseline model. The latter is given as

$$
\begin{aligned}
\Delta\phi_{ru}^{ps} &= e\, \Delta\rho_{ru}^{ps} - \mu\, \iota_{ru}^{ps} + \Lambda z_{ru}^{ps} \\
\Delta p_{ru}^{ps} &= e\, \Delta\rho_{ru}^{ps} + \mu\, \iota_{ru}^{ps}
\end{aligned} \tag{26}
$$

with $\Delta\phi_{ru}^{ps} = \phi_u^{ps} - \phi_r^{ps}$ and $\Delta p_{ru}^{ps} = p_u^{ps} - p_r^{ps}$. It follows from subtracting (8) from its user version, i.e. with r replaced by u.

A comparison of the PPP-RTK user model (24) with the single-baseline RTK model (26) shows that the two models are identical except for their ionospheric delay parametrization, $\tilde{\iota}_u^{ps}$ vs ι_{ru}^{ps}. For users that are interested in positioning, the performance of the two models (24) and (26) will be the same, both in ambiguity-float as well as in ambiguity-fixed mode. Also their ambiguity-resolution performance will be the same. The ambiguity convergence times of the PPP-RTK user model (24), i.e. its time-to-first-fix, will therefore be

comparable to what one is used to with long baseline ambiguity resolution (Blewitt 1989; Jonkman et al. 2000; Teunissen et al. 2000; Yu et al. 2011; Li et al. 2014).

The difference in ionospheric delay parametrization between (24) and (26) is essential for those users that are interested in ionospheric delay estimation. With the PPP-RTK user model (24) a biased ionospheric delay $\tilde{\iota}_u^{ps} = \iota_u^{ps} - d_{GF}^{ps}$ is obtained, whereas an unbiased DD delay ι_{ru}^{ps} is estimated with the single baseline model (26). In contrast to the single-baseline model, the PPP-RTK user model would thus be able to provide absolute ionospheric delays if d_{GF}^{ps} would be available, e.g. through calibration (Schaer 1999).

2.3.1 Ionospheric delay $\tilde{\iota}_r^{ps}$ to allow for improved IAR

From a positioning perspective, the single-baseline model (26) has the advantage over (24) in that it is parametrized in the *relative* ionospheric delay ι_{ru}^{ps}. Hence, it allows for a further strengthening by making use of the spatial correlation of the ionospheric delays (Odijk 2002; Grejner-Brzezinska et al. 2007; Wielgosz et al. 2008). This is not possible with the PPP-RTK user model (24).

To make this possible, an additional ionospheric correction is needed. As

$$E(\hat{\tilde{\iota}}_r^{ps}) = \tilde{\iota}_r^{ps} = \iota_r^{ps} - d_{GF}^{ps} \tag{27}$$

provision of this ionospheric correction to the user gives

$$\begin{aligned} \mathsf{E}(\phi_u^{ps} - \hat{c}_\phi^{ps} + \mu\,\hat{\tilde{\iota}}_r^{ps}) &= e\,\Delta\rho_{ru}^{ps} - \mu\,\iota_{ru}^{ps} + \Lambda\, z_{ru}^{ps} \\ \mathsf{E}(p_u^{ps} - \hat{c}_p^{ps} - \mu\,\hat{\tilde{\iota}}_r^{ps}) &= e\,\Delta\rho_{ru}^{ps} + \mu\,\iota_{ru}^{ps} \end{aligned} \tag{28}$$

in which the DD ionospheric delay is recognized as $\iota_{ru}^{ps} = \tilde{\iota}_u^{ps} - \tilde{\iota}_r^{ps} = \iota_u^{ps} - \iota_r^{ps}$. Compare (28) with (26). Thus with the ionospheric delay provided as an extra user-correction, the PPP-RTK user model (28) now has the same capabilities as the single baseline model (26). In this contribution though, we restrict attention to the currently more customary case of providing only the PPP-RTK corrections $d\hat{\tilde{t}}^{ps}$, $\hat{\tilde{\delta}}^{ps}$, and $\hat{\tilde{d}}^{ps}$.

3 Pitfalls in analyzing an *individual* correction

3.1 PPP-RTK corrections in combined-form

The above has shown what roles are taken up by the individual PPP-RTK corrections $d\hat{\tilde{t}}^{ps}$, $\hat{\tilde{\delta}}^{ps}$, and $\hat{\tilde{d}}^{ps}$. But what matters, of course, is their combined effect. The comparison between the PPP-RTK model and the single-baseline model has made this clear as well. In the following we will refer to the corrections

$$\begin{aligned} \hat{c}_\phi^{ps} &= -e\,d\hat{\tilde{t}}^{ps} - \Lambda\hat{\tilde{\delta}}^{ps} \\ \hat{c}_p^{ps} &= -e\,d\hat{\tilde{t}}^{ps} - E\hat{\tilde{d}}^{ps} \end{aligned} \tag{29}$$

as the PPP-RTK corrections in combined form. With the aid of (17) it is not difficult to verify that

$$\begin{aligned} \hat{c}_\phi^{ps} &= \phi_r^{ps} + \mu\,\hat{\tilde{\iota}}_r^{ps} \\ \hat{c}_p^{ps} &= p_r^{ps} - \mu\,\hat{\tilde{\iota}}_r^{ps}. \end{aligned} \tag{30}$$

This shows that the combined PPP-RTK corrections represent a biased version of the original reference station observations. This bias explains the presence of the biased ionospheric delay $\tilde{\iota}_u^{ps}$ in the PPP-RTK model (24). It can be eliminated if next to $d\hat{\tilde{t}}^{ps}$, $\hat{\tilde{\delta}}^{ps}$, and $\hat{\tilde{d}}^{ps}$, also the ionospheric delay takes part in the corrections. The combined correction then takes the form

$$\begin{aligned} \hat{\tilde{c}}_\phi^{ps} &= \hat{c}_\phi^{ps} - \mu\,\hat{\tilde{\iota}}_r^{ps} = \phi_r^{ps} \\ \hat{\tilde{c}}_p^{ps} &= \hat{c}_p^{ps} + \mu\,\hat{\tilde{\iota}}_r^{ps} = p_r^{ps} \end{aligned} \tag{31}$$

in which case a complete correspondence with the single-baseline model is obtained. For a quick reference, a brief comparison between the single-station PPP-RTK setup and the single-baseline RTK setup is given in Table 1.

3.2 Individual vs combined corrections

When evaluating the generation of PPP-RTK corrections, it is usually the individual corrections that are judged on quality in the literature, instead of their combined form, see e.g. Li and Zhang (2012), Zhang et al. (2013) and Li et al (2013). Such an analysis of the individual corrections is useful if one wants to study the characteristics and estimation quality of the individual parameters $d\hat{\tilde{t}}^{ps}$, $\hat{\tilde{\delta}}^{ps}$, and $\hat{\tilde{d}}^{ps}$. However, from a PPP-RTK application point of view, such an individual analysis is far from sufficient. It is far better to aim at a qual-

Table 1 User's single-station PPP-RTK setup compared to the standard DD single-baseline setup

	PPP-RTK	Single-baseline
Corrections	$d\hat{\tilde{t}}^{ps},\ \hat{\tilde{\delta}}^{ps},\ \hat{\tilde{d}}^{ps}$	$\phi_r^{ps},\ p_r^{ps}$
Comb.-form	$\hat{c}_\phi^{ps} = -e\,d\hat{\tilde{t}}^{ps} - \Lambda\hat{\tilde{\delta}}^{ps}$ $\hat{c}_p^{ps} = -e\,d\hat{\tilde{t}}^{ps} - E\hat{\tilde{d}}^{ps}$	$-\phi_r^{ps}$ $-p_r^{ps}$
Corrected observations	$\phi_u^{ps} - \hat{c}_\phi^{ps} = \phi_{ru}^{ps} - \mu\hat{\tilde{\iota}}_r^{ps}$ $p_u^{ps} - \hat{c}_p^{ps} = p_{ru}^{ps} + \mu\hat{\tilde{\iota}}_r^{ps}$	$\phi_u^{ps} - \phi_r^{ps} = \phi_{ru}^{ps}$ $p_u^{ps} - p_r^{ps} = p_{ru}^{ps}$
Estimable Parameters	Δx_{ru} z_{ru}^{ps} $\tilde{\iota}_u^{ps} = \iota_u^{ps} - d_{GF}^{ps}$	Δx_{ru} z_{ru}^{ps} $\iota_{ru}^{ps} = \iota_u^{ps} - \iota_r^{ps}$

ity analysis of their combined effect. This is the more so as an analysis restricted to the individual corrections disguises important information that may result in serious pitfalls. Here we give two examples that underline the importance of this viewpoint.

Example 1 (Code-dominated corrections) If we apply the variance propagation law to (17), we obtain the variance matrices of the single-station PPP-RTK corrections as

$$\begin{aligned}
&\mathsf{D}(\hat{\tilde{d}}^{ps}) = 2\,(\mu_{1F}^T C_p \mu_{1F});\rightarrow \text{code-dominated}\\
&\mathsf{D}(\hat{\tilde{\delta}}^{ps}) = 2\,(\Lambda^{-1} C_\phi \Lambda^{-1} + M C_p M^T) \rightarrow \text{code-dominated}\\
&\mathsf{D}(\hat{\tilde{d}}^{ps}) = 2\,(E^- C_p E^{-T});\rightarrow \text{code-dominated}\\
&\mathsf{D}(\hat{\tilde{\imath}}_r^{ps}) = 2\,(\mu_{GF}^T C_p \mu_{GF});\rightarrow \text{code-dominated}
\end{aligned} \tag{32}$$

in which $2\,C_p$ and $2\,C_\phi$ are the cofactor matrices for the satellite-differenced pseudorange and carrier-phase, respectively. This result clearly shows that the precision of the individual corrections is governed by the rather poor precision of the code observations. This seems to be at odds, however, with the quality that the PPP-RTK user-phase corrections are required to have to enable user-ambiguity resolution.

The reason for this apparent inconsistency lies in the *high correlation* that exists between the individual corrections. This becomes clear if we express the phase-bias solution as

$$\hat{\tilde{\delta}}^{ps} = -\Lambda^{-1}\,(\phi_r^{ps} + e\,d\hat{\tilde{t}}^{ps} + \mu\,\hat{\tilde{\imath}}_r^{ps}) \tag{33}$$

This expression shows that the phase-bias solution is indeed highly correlated with the clock- and ionospheric corrections. It is this high correlation that 'repairs' the situation when forming the combined PPP-RTK user-phase correction. Instead of the code-dominated individual corrections, the precise combined correction

$$\hat{\tilde{c}}_\phi^{ps} = -\Lambda\hat{\tilde{\delta}}^{ps} - e\,d\hat{\tilde{t}}^{ps} - \mu\,\hat{\tilde{\imath}}_r^{ps} \tag{34}$$

is obtained, the precision of which will be at the phase-noise level instead of at the code-noise level.

The conclusion reads therefore that the *combined form* of the PPP-RTK corrections should be used for performance evaluation and not the code-noise dominated time series of the individual PPP-RTK corrections. Note that the same conclusion is reached if one would follow the derivation in ionosphere-free form. Hence, the conclusion is not dependent on whether or not the ionospheric correction is provided.

Example 2 (Perfectly known phase-biases) As PPP-RTK users may not always use corrections from one single provider, we now consider a case that can be considered as an example where corrections of two different providers are used. From the first provider, the single-station, the user uses the earlier derived single-station clock- and ionospheric solutions, $d\hat{\tilde{t}}^{ps}$ and $\hat{\tilde{\imath}}_r^{ps}$. And from a second provider the user obtains very precise phase-bias corrections, denoted as $\tilde{\delta}^{ps*}$. For argument-sake the phase biases $\tilde{\delta}^{ps*}$ are assumed so precise that they can be considered non-random for this example.

The corresponding combined corrections now read

$$\begin{aligned}
\hat{\tilde{c}}_\phi^{ps*} &= -e\,d\hat{\tilde{t}}^{ps} - \mu\,\hat{\tilde{\imath}}_r^{ps} - \Lambda\,\tilde{\delta}^{ps*}\\
\hat{\tilde{c}}_p^{ps} &= -e\,d\hat{\tilde{t}}^{ps} + \mu\,\hat{\tilde{\imath}}_r^{ps}.
\end{aligned} \tag{35}$$

Note that while the code-correction $\hat{\tilde{c}}_p^{ps}$ remains unchanged, the phase-correction $\hat{\tilde{c}}_\phi^{ps*}$ differs from its single-station counterpart $\hat{\tilde{c}}_\phi^{ps}$ as,

$$\hat{\tilde{c}}_\phi^{ps*} = \hat{\tilde{c}}_\phi^{ps} + \Lambda\,\varepsilon^{ps} = \phi_r^{ps} + \Lambda\,\varepsilon^{ps} \tag{36}$$

in which $\varepsilon^{ps} = \hat{\tilde{\delta}}^{ps} - \tilde{\delta}^{ps*}$ is zero mean with dispersion $D(\hat{\tilde{\delta}}^{ps})$. Application of the variance propagation law gives

$$\mathsf{D}(\hat{\tilde{c}}_\phi^{ps*}) = \Lambda\,\mathsf{D}(\hat{\tilde{\delta}}^{ps})\,\Lambda - \mathsf{D}(\phi_r^{ps}) \rightarrow \text{code-dominated.} \tag{37}$$

This shows that the provision of the perfectly known phase-bias $\tilde{\delta}^{ps*}$ has turned the previously very precise phase-correction $\hat{\tilde{c}}_\phi^{ps}$ into a *less precise* code-dominated phase-correction $\hat{\tilde{c}}_\phi^{ps*}$.

So what have we gained? Again one should not fall in the trap of making the judgment on the basis of an individual correction. That is, one should consider the PPP-RTK corrections in their combined form. By doing so, one will note the role played by the non-zero correlation between ε^{ps} and the code-corrections $\hat{\tilde{c}}_p^{ps}$.

Indeed, if $\hat{z}_{ru}^{ps}$ and $\hat{z}_{ru}^{ps*}$ denote the two types of float solutions of the user ambiguities based on the two sets of corrections $\hat{\tilde{c}}_\phi^{ps}$, $\hat{\tilde{c}}_p^{ps}$ and $\hat{\tilde{c}}_\phi^{ps*}$, $\hat{\tilde{c}}_p^{ps}$, respectively, then it follows from (36) that ε^{ps} gets fully absorbed in the estimator of the user DD ambiguity z_{ru}^{ps}. Hence, the float solution of all user parameters except the ambiguities remains unchanged, while the user ambiguity solution simply changes as $\hat{z}_{ru}^{ps*} = \hat{z}_{ru}^{ps} - \varepsilon^{ps}$. Since the covariance of $\hat{z}_{ru}^{ps}$ and ε^{ps} is given by $D(\hat{\tilde{\delta}}^{ps})$, application of the variance propagation law gives

$$\mathsf{D}(\hat{z}_{ru}^{ps*}) = \mathsf{D}(\hat{z}_{ru}^{ps}) - \mathsf{D}(\hat{\tilde{\delta}}^{ps}) \tag{38}$$

thus showing that a more precise ambiguity solution is obtained. This shows that despite the poorer precision of the phase-correction ($\hat{\tilde{c}}_\phi^{ps*}$ vs $\hat{\tilde{c}}_\phi^{ps}$), the use of $\tilde{\delta}^{ps*}$ does result in more precise user ambiguities and therefore in an improved ambiguity resolution performance. This again demonstrates

that one should use the combined form of the PPP-RTK corrections, i.e. $\hat{\tilde{c}}_{\phi}^{ps*}, \hat{\tilde{c}}_{p}^{ps}$, for performance evaluation and not the individual corrections.

4 Geometry-free network derived corrections

4.1 Multivariate formulation

So far we restricted ourselves to the observation equations of a single network station r. We now extend the results to n network stations. We use a multivariate formulation and therefore define the undifferenced phase observation vector of station r as $\phi_r = [\phi_{r,1}^T, \ldots, \phi_{r,f}^T] \in \mathbb{R}^{fm}$, $\phi_{r,j} = [\Delta\phi_{r,j}^1, \ldots, \Delta\phi_{r,j}^m]$, $j = 1, \ldots, f$, with a likewise definition for the code observation vector p_r. For the n stations, the network observation matrices are defined as $\Phi = [\phi_1, \ldots, \phi_n]$ and $P = [p_1, \ldots, p_n]$. The compact multivariate formulation of the full-rank, multi-epoch, network observation equations becomes then

$$\begin{aligned} \mathsf{E}((I_f \otimes D_m^T)\,\Phi(i)) &= (e \otimes I_{m-1})\,\tilde{\boldsymbol{\rho}}(i) - (\mu \otimes I_{m-1})\,\tilde{\boldsymbol{\iota}}(i) \\ &\quad + (\Lambda \otimes I_{m-1})\,\tilde{\mathcal{A}} \\ \mathsf{E}((I_f \otimes D_m^T)\,P(i)) &= (e \otimes I_{m-1})\,\tilde{\boldsymbol{\rho}}(i) + (\mu \otimes I_{m-1})\,\tilde{\boldsymbol{\iota}}(i) \\ &\quad - (E \otimes I_{m-1})\,\tilde{d}\,e_n^T \end{aligned} \tag{39}$$

where D_m^T denotes an $(m-1) \times m$ between-satellite differencing matrix. The index i refers to the epoch at which the observations are collected. This system generalizes the single-station system (12). The compact and insightful formulation of (39) is in a large part due to the application of the efficient Kronecker product $\otimes$ (Henderson et al. 1983), which was first introduced for GNSS models in Teunissen (1997a).

Following (ibid), the above model is referred to as *geometry-free* (GF) since no information about the relative receiver-satellite geometry is present in its design matrix. The matrices $\tilde{\boldsymbol{\rho}}(i), \tilde{\boldsymbol{\iota}}(i)$ and $\tilde{\mathcal{A}}$ contain the network's SD estimable non-dispersive delays, ionospheric delays and ambiguities, respectively (Table 2). The SD estimable code biases on the third frequency and beyond are collected in vector $\tilde{d}$.

As we assume the station integer ambiguities z_l^{ps} $(l = 1, \ldots, n)$, the satellite phase biases δ^{ps} and the satellite code biases d^{ps} of the between-satellite single differences to be time-constant, the time-constant estimable parameters of the above full-rank model are the $f(m-1) \times n$ ambiguity matrix $\tilde{\mathcal{A}}$ and the $(f-2)(m-1) \times 1$ code bias vector $\tilde{d}$. As before we take station r as the station to define our estimable satellite clock and estimable satellite phase bias, i.e. $d\tilde{t}^{ps}(i) := -\tilde{\rho}_r^{ps}(i)$ and $\tilde{\delta}^{ps} := -\tilde{a}_r^{ps}$ (cf. 16). The goal is now to derive the estimators for the network-based PPP-RTK corrections and to analyse the improvements that can so be achieved.

The stochastic model of the network's observables is assumed given as

$$\mathsf{D}\begin{bmatrix} (I_f \otimes D_m^T)\,\phi_r(i) \\ (I_f \otimes D_m^T)\,p_r(i) \end{bmatrix} = c_r^2 \begin{bmatrix} C_\phi & 0 \\ 0 & C_p \end{bmatrix} \otimes C_s(i) \tag{40}$$

in which $C_s(i) = D_m^T C_S(i) D_m$, with $C_S(i)$ the $m \times m$ co-factor matrix that captures the satellite elevation dependency at epoch i. The scalar c_r^2 $(r = 1, \ldots, n)$ is a receiver-dependent co-factor. In this study all receivers are assumed to be of the same quality and thus $c_r^2 = 1$ for all r. The $f \times f$ positive-definite matrices C_ϕ and C_p are the co-factor matrices of the phase and code observable types, respectively.

4.2 Geometry-free network redundancy

To identify the relevance of the *network* for PPP-RTK, we need to understand how its redundancy contributes to the best linear unbiased estimator (BLUE) of the PPP-RTK corrections. The network redundancy is defined here as the number of its observations minus the number of its estimable parameters. Would one discard this redundancy, then the network-derived corrections simply follow from the single-station solutions (31). In multivariate form they then read

$$\begin{bmatrix} \hat{\tilde{c}}_\phi(i) \\ \hat{\tilde{c}}_p(i) \end{bmatrix} = \begin{bmatrix} (I_f \otimes D_m^T)\,\phi_r(i) \\ (I_f \otimes D_m^T)\,p_r(i) \end{bmatrix} \tag{41}$$

They can be further improved, however, by exploiting the network redundancy. For the network redundancy, we discriminate between two cases:

Table 2 Network's parameters in index-, vector- and multivariate-forms ($p \neq s$)

	Index-form	Vector-form	Multivariate-form
Non-dispersive SD delays	$\tilde{\rho}_r^{ps} = \rho_r^{ps} - d_{IF}^{ps}$	$\tilde{\rho}_r = [\tilde{\rho}_r^{p1}, \ldots, \tilde{\rho}_r^{pm}]^T$	$\tilde{\boldsymbol{\rho}} = [\tilde{\rho}_1, \ldots, \tilde{\rho}_n]$
Dispersive SD delays	$\tilde{\iota}_r^{ps} = \iota_r^{ps} - d_{GF}^{ps}$	$\tilde{\iota}_r = [\tilde{\iota}_r^{p1}, \ldots, \tilde{\iota}_r^{pm}]^T$	$\tilde{\boldsymbol{\iota}} = [\tilde{\iota}_1, \ldots, \tilde{\iota}_n]$
Estimable SD ambiguities	$\tilde{a}_r^{ps} = a_r^{ps} - Md^{ps}$	$\tilde{a}_r = [[\tilde{a}_{r,1}^{p1}, \ldots, \tilde{a}_{r,1}^{pm}]^T, \ldots, [\tilde{a}_{r,f}^{p1}, \ldots, \tilde{a}_{r,f}^{pm}]^T]^T$	$\tilde{\mathcal{A}} = [\tilde{a}_1, \ldots, \tilde{a}_n]$

$M = \Lambda^{-1}(\mu\,\mu_{GF}^T - e\,\mu_{IF}^T)$

Table 3 Geometry-free network redundancy brought by the ambiguity-float and -fixed scenarios, giving the total size of $2(kn-1)(f-1)(m-1)$

Scenario	Type	Size
(1) single-epoch ($f>2,\ n>1$)	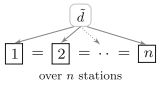	$(f-2)(n-1)(m-1)$
(2) multi-epoch ($f>2,\ k>1$)	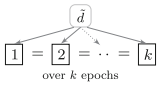	$(k-1)(f-2)(m-1)\,n$
(3) multi-epoch ($k>1$)	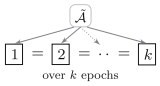	$(k-1)f(m-1)\,n$
# Ambiguity-float		$\{k(f-2)(n-1)+(k-1)(fn+f-2)\}(m-1)$
(4) network-IAR	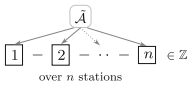	$f\,(n-1)(m-1)$
# Ambiguity-fixed		$2(kn-1)(f-1)(m-1)$

– *Ambiguity float*: the case that the DD ambiguities are treated as real-valued parameters; and
– *Ambiguity fixed*: the case that the DD ambiguities are successfully resolved as integers.

For the geometry-free (GF) network model (39), the ambiguity-float k-epoch redundancy is given as

$$\begin{aligned}&\#\ \mathrm{GF}-\mathrm{float\ redundancy}\\&=\{k(f-2)(n-1)+(k-1)(fn+f-2)\}(m-1)\end{aligned}\tag{42}$$

We now show how this redundancy is built up from the various elements of the network. For a quick reference, a summary of the elements building up the network redundancy is provided in Table 3.

In the single-epoch, multi-frequency case, the network redundancy stems from the fact that all single-station solutions of the estimable code biases $\tilde{d}^{ps}$ have the *same* mean, that is

$$\mathsf{E}(E^{-}p_l^{ps})=-\tilde{d}^{ps},\quad l=1,\ldots,n\tag{43}$$

or

$$\mathsf{E}(E^{-}p_{rl}^{ps})=0,\quad l\neq r\tag{44}$$

In multivariate form this reads as

$$\mathsf{E}((E^{-}\otimes D_m^T)\,P\,D_n)=0\tag{45}$$

in which D_n is the $n\times(n-1)$ between-station differencing matrix. Thus in the single-epoch case the redundancy is $(f-2)(m-1)(n-1)$. Hence, there is no redundancy in the single-station case ($n=1$, see previous section) and no redundancy in case of dual-frequency data ($f=2$).

In case of k epochs, all the additional single-station solutions of $\tilde{d}^{ps}$ (of the second epoch and beyond) have the *same* mean as those of (43). This is the case since the estimable code biases are assumed to be constant in time. This gives an additional redundancy of $(k-1)$ times $(f-2)(m-1)n$. Similarly, an additional redundancy of $(k-1)$ times $f\,(m-1)n$ is then also obtained due to the time constancy of the ambiguity matrix $\tilde{\mathcal{A}}=[\tilde{a}_1,\ldots,\tilde{a}_n]$. Summing these redundancies up gives (42).

Now we consider the ambiguity-fixed network redundancy. It is given as

$$\#\ \mathrm{GF\text{-}fixed\ redundancy}=2(kn-1)(f-1)(m-1)\tag{46}$$

Compare this to the ambiguity-float redundancy (42) and note that it is $f\,(m-1)(n-1)$ larger. This increase in redundancy is due to the successfully resolved integer ambiguities. As the between-station differences of the single-station solutions of the estimable SD ambiguities $\tilde{a}_{ri}^{ps}=\tilde{a}_i^{ps}-\tilde{a}_r^{ps}$ have *integer-valued* means, we have

$$\mathsf{E}(\Lambda^{-1}\phi_{rl}^{ps}+M\,p_{rl}^{ps})=z_{rl}^{ps}\in\mathbb{Z},\quad l\neq r\tag{47}$$

or in multivariate form

$$\mathsf{E}((\Lambda^{-1}\otimes D_m^T)\,\Phi\,D_n+(M\otimes D_m^T)\,P\,D_n)\in\mathbb{Z}^{f(m-1)(n-1)}\tag{48}$$

with $M=\Lambda^{-1}(\mu\mu_{GF}^T-e\mu_{1F}^T)$. Hence, successfully resolving the integer ambiguities results in an additional $f\,(m-1)(n-1)$ condition equations and ditto redundancy. The total ambiguity-fixed redundancy is therefore given by (46). Note that now there already exists redundancy when $k=1$, $f=2$ and $n>1$, this in contrast to the ambiguity-float case (cf. 42). However, for $k=1$, $f=2$, and $n=1$ there is still no redundancy as the single-station case does not enable the formation of integer ambiguities. For $n>1$ such integers can be formed and the redundancy becomes then, for example, for $k=1$, $f=2$ and $n=2$ equal to $2(m-1)$, which is indeed the number of dual-frequency DD ambiguities that can be formed in case of a single baseline.

4.3 The ambiguity-float GF corrections

In this section, we present our analytical analysis of the geometry-free, ambiguity-float network-based PPP-RTK corrections. First we derived the BLUE estimators of the individual PPP-RTK corrections $d\tilde{t}^{ps}$, $\tilde{\delta}^{ps}$ and $\tilde{d}^{ps}$. Their precision is described by the variance-covariance matrices

Table 4 (Co)variance matrices of the ambiguity-float geometry-free (GF) corrections

$$
\begin{aligned}
Q^{GF}_{\hat{d}\hat{d}_{(i)}} &= \left[\tfrac{1}{k} c^2_{\hat{\rho}_2} \otimes \bar{C}_s\right] + \left[c^2_{\hat{\rho}} \otimes (C_s(i) - \tfrac{1}{k}\bar{C}_s)\right] - \left[\tfrac{n-1}{kn} \Delta c^2_{\hat{\rho}} \otimes \bar{C}_s\right] \\
Q^{GF}_{\hat{\delta}\hat{\delta}} &= \left[\tfrac{1}{k} \Lambda^{-1}(C_\phi + [e,-\mu] Q_{[\hat{\rho}_2,\hat{\imath}_2]} [e,-\mu]^T) \Lambda^{-1} \otimes \bar{C}_s\right] \\
&\quad - \left[\tfrac{n-1}{kn} \Lambda^{-1}([e,-\mu] \Delta Q_{[\hat{\rho},\hat{\imath}]} [e,-\mu]^T) \Lambda^{-1} \otimes \bar{C}_s\right] \\
Q^{GF}_{\hat{d}\hat{d}} &= \tfrac{1}{kn}(E^- C_p E^{-T}) \otimes \bar{C}_s \\
Q^{GF}_{\hat{d}\hat{\delta}_{(i)}} &= -\left[\tfrac{1}{k}(c^2_{\hat{\rho}_2} e^T - c_{\hat{\rho}\hat{\imath}_2} \mu^T) \Lambda^{-1} \otimes \bar{C}_s\right] + \left[\tfrac{n-1}{kn}(\Delta c^2_{\hat{\rho}} e^T \right. \\
&\quad \left. - \Delta c_{\hat{\rho}\hat{\imath}} \mu^T) \Lambda^{-1} \otimes \bar{C}_s\right] \\
Q^{GF}_{\hat{d}\hat{d}_{(i)}} &= \tfrac{1}{kn}(\mu^T_{IF} C_p E^{-T}) \otimes \bar{C}_s \\
Q^{GF}_{\hat{\delta}\hat{d}} &= \tfrac{1}{kn} \Lambda^{-1}(M C_p E^{-T}) \otimes \bar{C}_s
\end{aligned}
$$

The ambiguities, phase and code biases are assumed constant over k epochs

$Q_{[\hat{\rho},\hat{\imath}]} = \begin{bmatrix} c^2_{\hat{\rho}} & c_{\hat{\rho}\hat{\imath}} \\ c_{\hat{\rho}\hat{\imath}} & c^2_{\hat{\imath}} \end{bmatrix} = ([e,\mu]^T C_p^{-1}[e,\mu])^{-1}$; $Q_{[\hat{\rho}_2,\hat{\imath}_2]} = \begin{bmatrix} c^2_{\hat{\rho}_2} & c_{\hat{\rho}\hat{\imath}_2} \\ c_{\hat{\rho}\hat{\imath}_2} & c^2_{\hat{\imath}_2} \end{bmatrix} = [\mu_{IF}, \mu_{GF}]^T C_p [\mu_{IF}, \mu_{GF}]$; $\Delta Q_{[\hat{\rho},\hat{\imath}]} = Q_{[\hat{\rho}_2,\hat{\imath}_2]} - Q_{[\hat{\rho},\hat{\imath}]} = \begin{bmatrix} \Delta c^2_{\hat{\rho}} & \Delta c_{\hat{\rho}\hat{\imath}} \\ \Delta c_{\hat{\rho}\hat{\imath}} & \Delta c^2_{\hat{\imath}} \end{bmatrix}$

$Q_{[\check{\phi},\check{p}]} = \begin{bmatrix} c^2_{\check{\phi}} & c_{\check{\phi}\check{p}} \\ c_{\check{\phi}\check{p}} & c^2_{\check{p}} \end{bmatrix} = ([\tilde{e},\tilde{\mu}]^T \text{blkdiag}(C^{-1}_\phi, C^{-1}_p)[\tilde{e},\tilde{\mu}])^{-1}$

as given in Table 4. Note that their covariance matrices are given in the table as well. In the table, additional terms, indicated by the Δ-symbol, show up themselves to characterize the contribution of the multi-frequency code data. Thus when $f = 2$, they vanish, that is, $\Delta Q_{[\hat{\rho},\hat{\imath}]} = 0$. To gain a better insight into the results, let us start with the dual-frequency case, where the (co)variance matrices corresponding to the code biases $\tilde{d}^{ps}$ are absent, as in that case E does not exist by definition. In that case, all the (co)variance matrices, except those of the satellite clocks, follow the 1-over-k rule. For not too large k, almost the same rule applies to the variance matrices of the satellite clocks as well, since $(c_{\check{\rho}}/c_{\hat{\rho}_2}) \approx 0$. Let us now consider the multi-frequency case ($f > 2$). As extra frequencies enter, the precision of the satellite clocks and phase biases improves as their (co)variance matrices decrease by a factor governed by $\Delta Q_{[\hat{\rho},\hat{\imath}]} \neq 0$. Next to those of the satellite clocks and phase biases, however, the (co)variance matrices of the code biases $\tilde{d}^{ps}$ enter. They follow the 1-over-kn rule. Thus, they are largely driven by both the number of epochs k and stations n.

Based on the individual corrections one can construct the BLUE of the combined corrections, $(\hat{c}^T_\phi, \hat{c}^T_p)^T$ (cf. 29) or $(\hat{\tilde{c}}^T_\phi, \hat{\tilde{c}}^T_p)^T$ (cf. 31). As these two correction types are related as

$$
\begin{bmatrix} \hat{c}_\phi \\ \hat{c}_p \end{bmatrix} = \begin{bmatrix} \hat{\tilde{c}}_\phi \\ \hat{\tilde{c}}_p \end{bmatrix} - \begin{bmatrix} -\mu \\ +\mu \end{bmatrix} \iota \tag{49}
$$

both can be used for our analytical analysis of the user PPP-RTK positioning performance. The difference of the two type of corrections lies namely in the range of $(-\mu^T, +\mu^T)^T$ and will therefore be completely absorbed by the ionospheric delays of the user. Hence, their difference will not affect the estimation of user-positioning nor that of user-ambiguity resolution. This can alternatively be understood by noting that both types of corrections have the same ionosphere-free combination. Hence, both corrections lead to an identical ionosphere-free user-correction.

In the following we work with the combined corrections $(\hat{\tilde{c}}^T_\phi, \hat{\tilde{c}}^T_p)^T$. First we present their BLUE and then their variance-covariance matrix. The following two averaging operators will be frequently used in the remainder of this contribution

$$
\begin{aligned}
\text{station-averaging:} (.)_{\bar{r}} &= \frac{1}{n} \sum_{r=1}^{n} (.)_r, \\
\text{epoch-averaging:} (.)(\bar{i}) &= \left[I_f \otimes \left[\sum_{i=1}^{k} C_S^{-1}(i) \right]^{-1} \right] \\
&\quad \times \sum_{i=1}^{k} [I_f \otimes C_S^{-1}(i)]\, (.)(i).
\end{aligned} \tag{50}
$$

We also make use of the notations $(.)_{\bar{r}r} = (.)_r - (.)_{\bar{r}}$ and $(.)(\bar{i}i) = (.)(i) - (.)(\bar{i})$. Thus in the single-station case we have $(.)_{\bar{r}} = (.)_r$, therefore $(.)_{\bar{r}r} = 0$. Likewise, in the single-epoch case we have $(.)(\bar{i}) = (.)(i)$, therefore $(.)(\bar{i}i) = 0$.

Theorem 1 (GF ambiguity-float corrections) *The k-epoch geometry-free ambiguity-float BLUE of the network-derived corrections, at epoch i, is given as*

$$
\begin{bmatrix} \hat{\tilde{c}}_{\phi,\text{GF}}(i) \\ \hat{\tilde{c}}_{p,\text{GF}}(i) \end{bmatrix} = \text{I} - \hat{\text{II}} - \hat{\text{III}} \tag{51}
$$

with

$$
\begin{aligned}
\text{I} &= (I_{2f} \otimes D_m^T) \begin{bmatrix} \phi_r(i) \\ p_r(i) \end{bmatrix} \\
\hat{\text{II}} &= (\mathcal{P}^{\perp}_{[\tilde{e},\tilde{\mu}]} \otimes D_m^T) \begin{bmatrix} \phi_r(\bar{i}i) \\ p_r(\bar{i}i) \end{bmatrix} \\
\hat{\text{III}} &= \begin{bmatrix} 0 \\ (\mathcal{P}^{\perp}_{[e,\mu]} \otimes D_m^T) p_{\bar{r}r}(\bar{i}) \end{bmatrix}
\end{aligned} \tag{52}
$$

and the projectors

$$
\begin{aligned}
&\mathcal{P}_{[e,\mu]} = C_{\hat{p}}\, C_p^{-1}, \;\; \mathcal{P}^{\perp}_{[e,\mu]} = I_f - \mathcal{P}_{[e,\mu]} \\
&\mathcal{P}_{[\tilde{e},\tilde{\mu}]} = C_{[\check{\phi},\check{p}]}\, \text{blkdiag}(C_\phi^{-1}, C_p^{-1}) \\
&\mathcal{P}^{\perp}_{[\tilde{e},\tilde{\mu}]} = I_{2f} - \mathcal{P}_{[\tilde{e},\tilde{\mu}]}
\end{aligned} \tag{53}
$$

where $\tilde{e} = [e^T, e^T]^T$, $\tilde{\mu} = [-\mu^T, \mu^T]^T$, *and*

$$
\begin{aligned}
&C_{\hat{p}} = [e, \mu]\, Q_{[\hat{\rho},\hat{\imath}]}\, [e, \mu]^T,\\
&Q_{[\hat{\rho},\hat{\imath}]} = ([e, \mu]^T C_p^{-1} [e, \mu])^{-1},\\
&C_{[\check{\phi},\check{p}]} = [\tilde{e}, \tilde{\mu}]\, Q_{[\check{\rho},\check{\imath}]}\, [\tilde{e}, \tilde{\mu}]^T\\
&Q_{[\check{\rho},\check{\imath}]} = ([\tilde{e}, \tilde{\mu}]^T \mathrm{blkdiag}(C_\phi^{-1}, C_p^{-1})[\tilde{e}, \tilde{\mu}])^{-1},
\end{aligned}
\tag{54}
$$

Proof See Appendix. □

So as to facilitate its interpretation, the GF-correction (51) has been written in terms of three expressions. The first expression I equals the single-station, single-epoch solution of the previous section (cf. 41), while the second expression $\hat{\mathrm{II}}$ describes the multi-epoch contribution and the third expression $\hat{\mathrm{III}}$ the multi-station contribution. Thus $\hat{\mathrm{II}} = 0$ if $\bar{\imath} = i$ and $\hat{\mathrm{III}} = 0$ if $\bar{r} = r$.

As the two terms, $\hat{\mathrm{II}}$ and $\hat{\mathrm{III}}$, further adjust the single-station solution, they have a zero mean, $\mathsf{E}(\hat{\mathrm{II}}) = \mathsf{E}(\hat{\mathrm{III}}) = 0$. Thus, although the three-term expression (51) provides the BLUE, any of the following combinations provides a LUE and therefore an unbiased estimator of the corrections: I, $\mathrm{I} - \hat{\mathrm{II}}$, and $\mathrm{I} - \hat{\mathrm{III}}$.

Note that the third term not only vanishes for $\bar{r} = r$, but also if $f = 2$, since then $\mathcal{P}_{[e,\mu]} = I_2$ and thus $\mathcal{P}^{\perp}_{[e,\mu]} = 0$. Hence, in the dual-frequency case, not the number of stations, but only the number of epochs contributes to further improving these geometry-free float corrections.

Also note that the third term only contains code data, this in contrast to the first two terms. Hence, if there are more than one station, then only the code data contribute to a further improvement of these GF float corrections.

An important outcome of Theorem 1 is that the combined network correction can indeed be viewed as an *adjusted* version of the observations of a *single* station. Therefore, once the corrections are applied to the PPP-RTK user data, the user corrected observation equations can be interpreted *as if* a single baseline is formed between the user and a network-adjusted reference station.

The precision of the above corrections is obtained after applying the variance propagation law. The result is given in the following lemma.

Lemma 1 (Precision GF ambiguity-float corrections) *The variance matrix of the corrections* (51) *is given as*

$$
\mathsf{D}\left(\begin{bmatrix} \hat{\check{c}}_{\phi,\mathrm{GF}}(i) \\ \hat{\check{c}}_{p,\mathrm{GF}}(i) \end{bmatrix}\right) = \mathsf{D}(\mathrm{I}) - \mathsf{D}(\hat{\mathrm{II}}) - \mathsf{D}(\hat{\mathrm{III}}) \tag{55}
$$

with

$$
\mathsf{D}(\mathrm{I}) = \begin{bmatrix} C_\phi & 0 \\ 0 & C_p \end{bmatrix} \otimes C_s(i)
$$

$$
\begin{aligned}
\mathsf{D}(\hat{\mathrm{II}}) &= P^{\perp}_{[\tilde{e},\tilde{\mu}]} \begin{bmatrix} C_\phi & 0 \\ 0 & C_p \end{bmatrix} \otimes \left[C_s(i) - \frac{1}{k} \bar{C}_s \right]\\
\mathsf{D}(\hat{\mathrm{III}}) &= \frac{n-1}{n} \begin{bmatrix} 0 & 0 \\ 0 & P^{\perp}_{[e,\mu]} C_p \end{bmatrix} \otimes \frac{1}{k} \bar{C}_s
\end{aligned}
\tag{56}
$$

where $\bar{C}_s^{-1} = \frac{1}{k} \sum_{i=1}^{k} C_s^{-1}(i)$.

Proof Follows by an application of the variance propagation law to (51). □

This result shows how the precision of the corrections is driven by the various contributing factors, like precision of observables, number of epochs, number of network stations and the frequencies. In the following we will show the extent to which these contributing factors contribute to the precision of the corrections. We will then also show the impact that these corrections are expected to have on the user's ability to perform successful integer ambiguity resolution.

Role of k, n and f: As the code observables are the less precise observables, it is particularly of interest to understand how the precision of the code correction, $\mathsf{D}(\hat{\check{c}}_{p,\mathrm{GF}}(i))$, benefits from increasing number of epochs k, stations n and/or frequencies f. Note that both $\mathsf{D}(\hat{\mathrm{II}})$ and $\mathsf{D}(\hat{\mathrm{III}})$ depend on k, while only $\mathsf{D}(\hat{\mathrm{III}})$ depends on n. For $k = 1$ the second term vanishes, while for $n = 1$ the third term vanishes. Furthermore, this last term also vanishes if $f = 2$.

A plot of the square root of the mean variance of an individual satellite at zenith [when $c_s(i) = 1$], i.e. $\mathrm{trace}(\mathsf{D}(\hat{\check{c}}^s_{p,\mathrm{GF}}(i)))/f$, is given in Fig. 1. It shows that the impact of the number of stations gets less the larger the number of epochs. This can be understood from the contribution of the third term $\mathsf{D}(\hat{\mathrm{III}})$. Thus only when not too many epochs

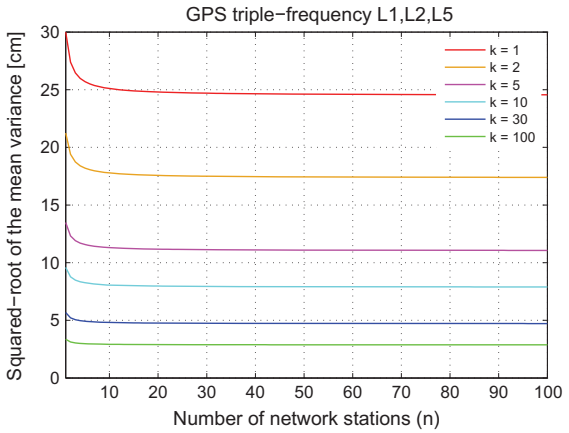

Fig. 1 GPS L1, L2, L5 scenario: the squared-root of the zenith-referenced mean variance of the GF ambiguity-float code corrections as a function of the number of stations n for different number of epochs k ($\sigma_\phi = 3$ [mm], $\sigma_p = 30$ [cm], $c_s = 1$)

Table 5 (Co)variance matrices of the ambiguity-fixed geometry-free (GF) corrections

$$
\begin{aligned}
Q^{GF}_{\check{d}\check{d}_{(i)}} &= \tfrac{1}{n} Q^{GF}_{\hat{d}\hat{d}_{(i)}} + \tfrac{n-1}{n} c^2_{\hat{\rho}}\, \bar{C}_s + \tfrac{n-1}{kn^2} \Delta c^2_{\hat{\rho}} \otimes \bar{C}_s \\
Q^{GF}_{\check{\delta}\check{\delta}} &= \tfrac{1}{n} Q^{GF}_{\hat{\delta}\hat{\delta}} + \tfrac{n-1}{kn^2} \Lambda^{-1}([e,-\mu] \Delta Q_{[\hat{\rho},\hat{\imath}]} [e,-\mu]^T) \Lambda^{-1} \otimes \bar{C}_s \\
Q^{GF}_{\check{d}\check{\delta}} &= Q^{GF}_{\hat{d}\hat{\delta}} \\
Q^{GF}_{d\check{\imath}\check{\delta}_{(i)}} &= \tfrac{1}{n} Q^{GF}_{d\hat{\imath}\hat{\delta}_{(i)}} - \tfrac{n-1}{kn^2} (\Delta c^2_{\hat{\rho}}\, e^T - \Delta c_{\hat{\rho}\hat{\imath}}\, \mu^T) \Lambda^{-1} \otimes \bar{C}_s \\
Q^{GF}_{\check{d}\check{\imath}\check{d}_{(i)}} &= Q^{GF}_{\hat{d}\hat{\imath}\hat{d}_{(i)}} \\
Q^{GF}_{\check{\delta}\check{d}} &= Q^{GF}_{\hat{\delta}\hat{d}}
\end{aligned}
$$

The ambiguities, phase and code biases are assumed constant over k epochs

are used, will the number of stations have a significant effect. For the case of a single station, the third term vanishes, and the variance of the code corrections behaves as $1/k$.

4.4 The ambiguity-fixed GF corrections

We now present our results for the geometry-free ambiguity-fixed network-based PPP-RTK corrections. Again we first derived the BLUE estimators of the individual corrections $d\tilde{\imath}^{ps}$, $\tilde{\delta}^{ps}$ and $\tilde{d}^{ps}$. Their precision is described by the variance-covariance matrices as given in Table 5. To discuss the table, let us start with the dual-frequency case, where the (co)variance matrices corresponding to the code biases $\tilde{d}^{ps}$ are absent and $\Delta Q_{[\hat{\rho},\hat{\imath}]} = 0$. In that case, the (co)variance matrices, corresponding to the satellite phase biases $\tilde{\delta}^{ps}$, are reduced in accordance with the 1-over-n rule. For not too large n, however, almost the same rule applies to the variance matrices of the satellite clocks as well, since $(c_{\check{\rho}}/c_{\hat{\rho}2}) \approx 0$. Let us now consider the multi-frequency case ($f > 2$). It is remarkable to see that the (co)variance matrices, corresponding to the satellite code biases $\tilde{d}^{ps}$, remain *unchanged* after network ambiguity resolution. This is indeed due to the fact that the satellite code biases $\tilde{d}^{ps}$ are *uncorrelated* with the float DD ambiguities (Teunissen and Khodabandeh 2014). Also note, since $\Delta Q_{[\hat{\rho},\hat{\imath}]} \neq 0$ when $f > 2$, that the (co)variance matrices of the satellite clocks and phase biases do not follow the 1-over-n improvement anymore.

Based on the individual corrections one can construct the ambiguity-fixed combined corrections $(\check{\tilde{c}}^T_{\phi}, \check{\tilde{c}}^T_{p})^T$. First we present their estimators and then their variance-covariance matrices.

Theorem 2 (GF ambiguity-fixed corrections) *The k-epoch geometry-free ambiguity-fixed BLUE of the network-derived corrections, at epoch i, is given as*

$$
\begin{bmatrix} \check{\tilde{c}}_{\phi,\mathrm{GF}}(i) \\ \check{\tilde{c}}_{p,\mathrm{GF}}(i) \end{bmatrix} = \mathrm{I} - \check{\mathbb{I}} \tag{57}
$$

with

$$
\begin{aligned}
\mathrm{I} &= (I_{2f} \otimes D^T_m) \begin{bmatrix} \phi_r(i) \\ p_r(i) \end{bmatrix} \\
\check{\mathbb{I}} &= (\mathcal{P}^{\perp}_{[\tilde{e},\tilde{\mu}]} \otimes D^T_m) \begin{bmatrix} \phi_r(\bar{\imath}i) + \tilde{\phi}_{\bar{r}r}(\bar{\imath}) \\ p_r(\bar{\imath}i) + p_{\bar{r}r}(\bar{\imath}) \end{bmatrix}
\end{aligned} \tag{58}
$$

in which the ambiguity-fixed phase data are defined as

$$
\begin{aligned}
\tilde{\phi}_r &= \phi_r \\
\tilde{\phi}_l &= \phi_l - [\Lambda \otimes L]\, \check{z}_{rl}, \quad l \neq r
\end{aligned} \tag{59}
$$

with L being an $m \times (m-1)$ matrix formed by removing the p^{th} column of I_m (given p as the pivot satellite).

Proof See Appendix. □

Compare the above results with that of (51). In particular note that now in the ambiguity-fixed case the time-averaging and the station-averaging have the same contribution to the corrections. In the ambiguity-float case, the contribution from the station-averaging was confined to the code data only (cf. $\hat{\mathbb{I}}$ in 51). In the ambiguity-fixed case, however, also the ambiguity-fixed carrier phase data $\tilde{\phi}_l$ act as pseudorange data and will therefore contribute in a likewise manner in the station-averaging.

The precision of the above corrections is obtained after applying the variance propagation law. The result is given in the following lemma.

Lemma 2 (Precision GF ambiguity-fixed corrections) *The precision of the corrections* (57) *is given as*

$$
\mathsf{D}\left(\begin{bmatrix} \check{\tilde{c}}_{\phi,\mathrm{GF}}(i) \\ \check{\tilde{c}}_{p,\mathrm{GF}}(i) \end{bmatrix} \right) = \mathsf{D}(\mathrm{I}) - \mathsf{D}(\check{\mathbb{I}}) \tag{60}
$$

with

$$
\begin{aligned}
\mathsf{D}(\mathrm{I}) &= \begin{bmatrix} C_{\phi} & 0 \\ 0 & C_p \end{bmatrix} \otimes C_s(i) \\
\mathsf{D}(\check{\mathbb{I}}) &= P^{\perp}_{[\tilde{e},\tilde{\mu}]} \begin{bmatrix} C_{\phi} & 0 \\ 0 & C_p \end{bmatrix} \otimes \left[C_s(i) - \frac{1}{kn} \bar{C}_s \right]
\end{aligned} \tag{61}
$$

where $\bar{C}^{-1}_s = \frac{1}{k} \sum_{i=1}^{k} C^{-1}_s(i)$.

Proof Follows by an application of the variance propagation law to (57). □

Note that the number of epochs and the number of stations now work in tandem, i.e. they contribute in the same way in improving the precision of the corrections. Figure 2 gives a plot of the square root of the mean variance of an individual

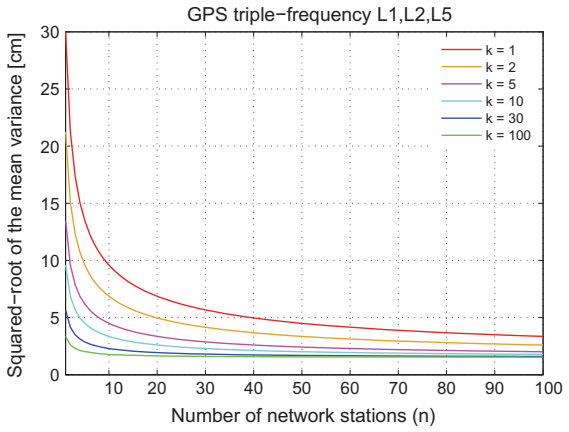

Fig. 2 GPS L1, L2, L5 scenario: the squared-root of the zenith-referenced mean variance of the GF ambiguity-fixed code corrections as a function of the number of stations n for different number of epochs k ($\sigma_\phi = 3$ [mm], $\sigma_p = 30$ [cm], $c_s = 1$)

satellite at zenith, i.e. trace$(\mathsf{D}(\breve{c}^s_{p,\mathrm{GF}}(i)))/f$. Compare the plot with that of Fig. 1. In contrast to the ambiguity-float case, the number of stations now has the *same* impact as that of the number of epochs. The impact of the number of stations gets less the larger the number of epochs, and conversely, the impact of the number of epochs gets less the larger the number of stations.

4.5 Relevance of PPP-RTK corrections for user-IAR

As the goal of PPP-RTK is in first instance not so much to improve the *float* solution of the user-position, but rather to enable user integer ambiguity resolution for obtaining a good *ambiguity-fixed* user-position, we revisit the above BLUE corrections (51) and (57), and identify the part that takes an active role in user integer ambiguity resolution. We first consider the network ambiguity-float case and then the network ambiguity-fixed case.

4.5.1 Network ambiguity-float case

Since any part of the corrections that lies in the range space of $\mathcal{P}_{[\tilde{e},\tilde{\mu}]}$ gets completely absorbed by the user position and user ionospheric delay parameters, one can discard the part $(\mathcal{P}_{[\tilde{e},\tilde{\mu}]} \otimes D_m^T)\left[\phi_r(\bar{i}i)^T,\, p_r(\bar{i}i)^T\right]^T$ in (51) as far as the user-IAR performance is concerned. Hence, for the purpose of user-IAR it then suffices to consider the following simplified corrections

$$\begin{bmatrix} (I_f \otimes D_m^T)\phi_r(\bar{i}) \\ (I_f \otimes D_m^T)p_r(\bar{i}) - (\mathcal{P}^{\perp}_{[e,\mu]} \otimes D_m^T)p_{\bar{r}r}(\bar{i}) \end{bmatrix} \tag{62}$$

instead of the complete BLUE corrections (51). This shows that only the time-averaged network data are of relevance for user-IAR. Note that this simplified correction even simplifies further in the dual-frequency case, since then $P^{\perp}_{[e,\mu]} = 0$.

The variance matrix of the above simplified correction (62) is given as

$$\frac{1}{k}\begin{bmatrix} C_\phi & 0 \\ 0 & (I_f - \frac{n-1}{n}\mathcal{P}^{\perp}_{[e,\mu]})C_p \end{bmatrix} \otimes \bar{C}_s. \tag{63}$$

4.5.2 Network ambiguity-fixed case

In the network ambiguity-fixed case it is the part $(\mathcal{P}_{[\tilde{e},\tilde{\mu}]} \otimes D_m^T)\left[[\phi_r(\bar{i}i) + \phi_{\bar{r}r}(\bar{i})]^T, [p_r(\bar{i}i) + p_{\bar{r}r}(\bar{i})]^T\right]^T$ in (57) that has no role in user integer ambiguity resolution. Hence, for the purpose of user-IAR it then suffices to consider the following simplified corrections

$$(I_{2f} \otimes D_m^T)\begin{bmatrix} \tilde{\phi}_{\bar{r}}(\bar{i}) \\ p_{\bar{r}}(\bar{i}) \end{bmatrix}, \tag{64}$$

This shows that now, next to the time-averaging, also the station-averaging contributes to the user-IAR. The variance-matrix of (64) reads

$$\frac{1}{kn}\begin{bmatrix} C_\phi & 0 \\ 0 & C_p \end{bmatrix} \otimes \bar{C}_s \tag{65}$$

now clearly showing how k and n work in tandem for improved user-IAR.

4.6 User ambiguity dilution of precision

In this subsection, we use the ambiguity dilution of precision (ADOP) measure (Teunissen 1997b) to characterize the role of the network's contributing factors, i.e. the number of epochs k and stations n, as well as the role of the number of frequencies f on the strength of user ambiguity resolution. The ADOP is defined as the square-root of the geometric mean of the ambiguity variance matrix's eigenvalues, thus representing the average ambiguity precision. The smaller the ADOP, the larger the ambiguity success rate. As a rule of thumb, ADOP-values smaller than about 0.10 cycle correspond with success rates larger than 0.999 (Odijk and Teunissen 2008).

The following lemma presents an analytical expressions of the user single-epoch ADOP, once the geometry-free network corrections are applied to the user observations.

Lemma 3 (User single-epoch ADOP: geometry-free network corrections) *Let $C_\phi = \sigma^2_\phi I_f$ and $C_p = \sigma^2_p I_f$, respectively, be the co-factor matrices of the network's phase*

and code observable types in (40), where $C_S(i) \approx \bar{C}_S$. With a likewise structure, let the user phase and code co-factor matrices be given as $C_{\phi_u} = \sigma^2_{\phi_u} I_f$ and $C_{p_u} = \sigma^2_{p_u} I_f$, respectively. The user single-epoch ADOP, based on the k-epoch geometry-free network corrections, reads then

$$\text{ADOP} = c_o \left(\frac{\sigma_{\phi_{u,c}}}{\bar{\lambda}}\right)^{\frac{1}{2}} \left(\frac{\sigma_{p_{u,c}}}{\bar{\lambda}}\right)^{\frac{1}{2}} (1+\epsilon)^{\frac{1}{2f}}\, \epsilon^{\frac{f-2}{4f}} \times \left(\frac{1+\epsilon}{\epsilon} + \frac{4\bar{\mu}^2}{(1+\epsilon)\sigma^2_\mu}\right)^{\frac{v}{2f(m-1)}} \tag{66}$$

where

$$\sigma^2_{\diamond_{u,c}} = \begin{cases} \sigma^2_{\diamond_u} + \frac{1}{k}\sigma^2_\diamond, & \text{network ambiguity} - \text{float} \\ \sigma^2_{\diamond_u} + \frac{1}{kn}\sigma^2_\diamond, & \text{network ambiguity} - \text{fixed} \end{cases} \tag{67}$$

with $\diamond = \{\phi, p\}$, $\epsilon = (\sigma^2_{\phi_{u,c}}/\sigma^2_{p_{u,c}})$, $\bar{\lambda} = \prod_{j=1}^f \lambda_j^{\frac{1}{f}}$, $\bar{\mu} = (1/f)\sum_{j=1}^f \mu_j$, $\sigma^2_\mu = (1/f)\sum_{j=1}^f (\mu_j - \bar{\mu})^2$, and

$$c_o = \left(\sum_{s=1}^m c_s^{-2} \Big/ \prod_{s=1}^m c_s^{-2}\right)^{\frac{1}{2(m-1)}} \tag{68}$$

with c_s^2 being the diagonal entries of the elevation weighting matrix $\bar{C}_S$.

Proof Follows from an application of the results of Odijk and Teunissen (2008). □

The above lemma clearly shows that the number of stations n has *no* role in the user ADOP, when the ambiguity-float network corrections are applied (cf. 67). While in the network ambiguity-float case, the number of epochs k governs the user ADOP, in the network ambiguity-fixed case, both the number of epochs k and stations n work in tandem to reduce the user ADOP. This reduction is, however, bounded by the precision of the user data. For sufficiently large number of epochs and stations, one can *at most* tackle the uncertainty of the network corrections, thereby leaving the precision of the user data to solely govern user ambiguity resolution.

Numerical graphs for the user ADOP, when the ambiguity-fixed network corrections are applied, are given in Fig. 3 (solid lines). It shows the ADOP values decrease as both k and n increase. As one would expect, the ADOPs do not get smaller than certain values, because of the nonzero variances of the user data.

Next to the ADOP values, Fig. 3 also gives the ratio of the ADOP, based on the ambiguity-float network, to the ADOP based on the ambiguity-fixed network (dashed lines). It is observed that these float-to-fixed ratios get larger, the larger the number of stations n. As the number of epochs k increases, their dependency on n gets weaker, though. In the extreme case, when k is large enough, these ratios become all equal to one, meaning that no gain is obtained through replacing the ambiguity-float network corrections by their ambiguity-fixed counterparts.

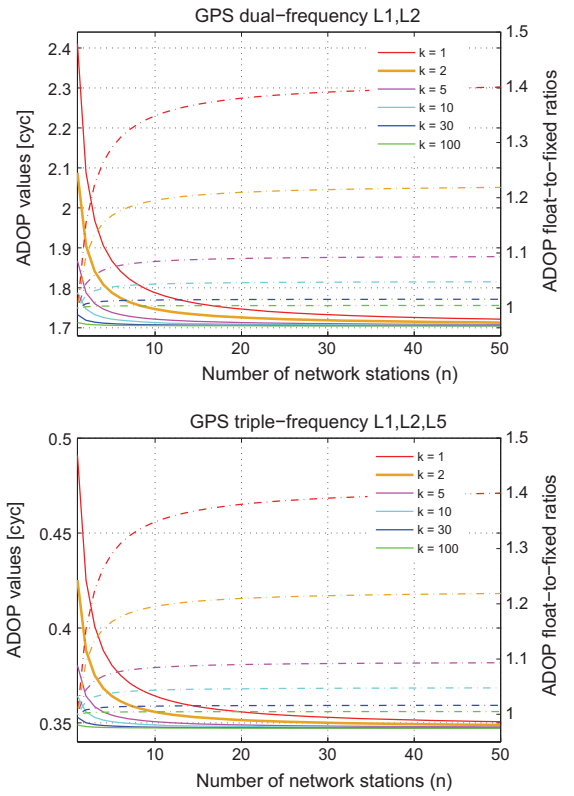

Fig. 3 User single-epoch ADOP values based on the k-epoch geometry-free, ambiguity-fixed network corrections (*solid lines*) as well as their float-to-fixed ratios (*dashed lines*) as a function of the number of stations n. *Top* GPS L1, L2 scenario; *bottom* GPS L1, L2, L5 scenario. The values follow from (66) by setting $m = v + 1 = 5$, $\sigma_{\phi_u} = \sigma_\phi = 3$ [mm], $\sigma_{p_u} = \sigma_p = 30$ [cm], $c_s = 1$

To show the role of the number of frequencies f on the size of the ADOP, let us first make some approximation. Using $\frac{1+\epsilon}{\epsilon} \approx \frac{1}{\epsilon}$ and neglecting $\frac{4\bar{\mu}^2}{(1+\epsilon)\sigma^2_\mu}$ in the last expression of (66), the ADOP is shown to approximately behave as

$$\text{ADOP} \dot{\propto} \epsilon^{\frac{(f-2)(m-1)-2v}{4f(m-1)}} \overset{m=v+1}{=} \epsilon^{\frac{f-4}{4f}} \tag{69}$$

where the notation $\dot{\propto}$ means 'almost proportional to'. In the absence of satellite redundancy ($m = v+1$), the above quantity decreases from $\epsilon^{-1/4} \approx 10$ ($f = 2$) to $\epsilon^{-1/12} \approx 2.15$ ($f = 3$), where $\epsilon \approx 10^{-4}$. Thus, the single-epoch ADOP gets almost 5 times smaller by going from the dual-frequency case to the triple-frequency case. This is in agreement with the numerical results given in Fig. 3. If the number of

Table 6 Extra network redundancy brought by the geometry-based scenario (cf. Table 3)

Scenario	Type	Size
(5) single-epoch ($n > 1$)	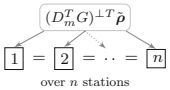	$(m-1-\nu)(n-1)$
(6) multi-epoch ($k > 1,\ n > 1$)	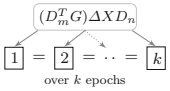	$(k-1)(m-1)(n-1)$
# Extra redundancy		$(k[m-1]-\nu)(n-1)$

satellites m increases, however, the stated ADOP reduction becomes smaller. For instance when the number of satellites increases by ν (i.e. $m = 2\nu+1$), the quantity in (69) decreases from $\epsilon^{-1/8} \approx 3.16$ ($f = 2$) to $\epsilon^0 = 1$ ($f = 3$). In this case, the single-epoch ADOP decreases by almost a factor of 3.

5 Geometry-based network derived corrections

5.1 Extra redundancy by the geometry-based scenario

So far we based our network analysis on the geometry-free model (39), where information about the relative receiver-satellite geometry was *absent* in its design matrix. We now consider the case where the receiver-satellite geometry is incorporated into the model and study the impact such increase in redundancy brings. The underlying model is referred to as *geometry-based* (GB) (Teunissen 1997a).

In the following, we show that the k-epoch redundancy of the GB network model is given by

$$\begin{aligned}&\#\text{GB redundancy}\\ &= \#\text{GFredundancy} + (k[m-1]-\nu)(n-1)\end{aligned} \tag{70}$$

A quick overview of the elements building up the above extra redundancy is provided in Table 6.

Recall from (9) that the ν-vectors Δx_r ($r = 1, \ldots, n$) of the stations' position increments/ZTDs are linked, through $\Delta\rho_r^{ps} = g_r^{psT}\Delta x_r$, to the estimable non-dispersive delays $\tilde{\rho}_r^{ps}$. For the sake of presentation, we assume the network to be such that $g_r^{ps} = g^{ps}$, $r = 1, \ldots, n$. This assumption admits the inclusion of small to regional networks in our discussion. With this in mind, the DD non-dispersive delays $\Delta\rho_{rl}^{ps} = \tilde{\rho}_l^{ps} - \tilde{\rho}_r^{ps} = \Delta\rho_l^{ps} - \Delta\rho_r^{ps}$ can be further parametrized as

$$\Delta\rho_{rl}^{ps} = g^{psT}(\Delta x_l - \Delta x_r) \tag{71}$$

or in the multivariate form as

$$\tilde{\boldsymbol{\rho}}\, D_n = (D_m^T G)\, \Delta X\, D_n \tag{72}$$

with $\Delta X = [\Delta x_1, \ldots, \Delta x_n]$ and the geometry matrix $G = [g^1, \ldots, g^m]^T$.

Equation (72) shows that $(n-1)$ times $(m-1)$ non-dispersive parameters $\tilde{\boldsymbol{\rho}} D_n$ are replaced by $(n-1)$ times ν parameters $\Delta X D_n$, when one switches from the geometry-free model to the geometry-based model. Thus in the single-epoch case, the redundancy increases by $(m-1-\nu)(n-1)$, forming the following condition equations

$$(D_m^T G)^{\perp T}\, \tilde{\boldsymbol{\rho}}\, D_n = 0 \tag{73}$$

where $(D_m^T G)^{\perp}$ denotes an orthogonal complement basis matrix of $D_m^T G$ (Teunissen 2000).

In the k-epoch case, would one assume the relative position increments and ZTDs $(\Delta x_l - \Delta x_r)$ to be time-invariant, all the DD non-dispersive delays $\Delta\rho_{rl}^{ps}(i)$, $i = 2, \ldots, k$ (of the second epoch and beyond) are linked to their first-epoch counterparts in (71). This yields an extra redundancy of $(k-1)$ times $(m-1)(n-1)$. Following Teunissen (1997a), if the time-averaged receiver-satellite geometry is used as approximation, the corresponding condition equations can be written as

$$(\tilde{\boldsymbol{\rho}}(i) - \tilde{\boldsymbol{\rho}}(1))\, D_n = 0, \quad i = 2, \ldots, k \tag{74}$$

Summing the extra redundancies $(m-1-\nu)(n-1)$ and $(k-1)(m-1)(n-1)$ gives (70).

5.2 The ambiguity-float GB corrections

Our analytical analysis of the geometry-based, ambiguity-float network-based PPP-RTK corrections are presented in this section. We first derived the BLUE estimators of the individual PPP-RTK corrections $d\tilde{t}^{ps}$, $\tilde{\delta}^{ps}$ and $\tilde{d}^{ps}$. Their precision is described by the variance-covariance matrices as given in Table 7. The results are linked to their GF counterparts. It is remarkable that the (co)variance matrices, corresponding to the satellite code biases $\tilde{d}^{ps}$, remain

Table 7 (Co)variance matrices of the ambiguity-float geometry-based (GB) corrections. The ambiguities, phase and code biases are assumed constant over k epochs

$$\begin{aligned}
&Q^{GB}_{\hat{d}\hat{t}\hat{d}\hat{t}_{(i)}} = Q^{GF}_{\hat{d}\hat{t}\hat{d}\hat{t}_{(i)}} - \tfrac{n-1}{n}[\tfrac{1}{k}c_{\hat{\rho}}^2\,\tilde{C}_s + c_{\tilde{\rho}}^2\,(C_s(i) - \tfrac{1}{k}\tilde{C}_s)]\\
&Q^{GB}_{\hat{\delta}\hat{\delta}} = Q^{GF}_{\hat{\delta}\hat{\delta}} - \tfrac{n-1}{kn}(c_{\hat{\rho}}^2\,\Lambda^{-1}e_\mu e_\mu^T\Lambda^{-1}) \otimes \tilde{C}_s\\
&Q^{GB}_{\hat{d}\hat{d}} = Q^{GF}_{\hat{d}\hat{d}}\\
&Q^{GB}_{\hat{d}\hat{t}\hat{\delta}_{(i)}} = Q^{GF}_{\hat{d}\hat{t}\hat{\delta}_{(i)}} + \tfrac{n-1}{kn}(c_{\hat{\rho}}^2\,e_\mu^T)\Lambda^{-1} \otimes \tilde{C}_s\\
&Q^{GB}_{\hat{d}\hat{t}\hat{d}} = Q^{GF}_{\hat{d}\hat{t}\hat{d}}\\
&Q^{GB}_{\hat{\delta}\hat{d}} = Q^{GF}_{\hat{\delta}\hat{d}}
\end{aligned}$$

$e_\mu = e - \frac{c_{\hat{\rho}\hat{t}}}{c_{\hat{\rho}}^2}\mu$; $\tilde{C}_s = D_m^T\mathcal{P}_{\tilde{G}}^{\perp}\tilde{C}_S D_m$; $\tilde{G} = [e_m, G]$

unchanged by switching from the GF-model to the GB-model. Thus, the satellite code biases $\tilde{d}^{ps}$ are not only *uncorrelated* with the float DD ambiguities, but also with the relative position increments/ZTDs $(\Delta x_l - \Delta x_r)$. The precision improvement in the satellite clocks and phase biases is governed by matrix $\tilde{C}_s = D_m^T \mathcal{P}_{\tilde{G}}^{\perp} \bar{C}_S D_m$, where $\tilde{G} = [e_m, G]$ (e_m is the m-vector of ones). In the absence of satellite redundancy, we have $m = \nu + 1$ and therefore $\tilde{C}_s = 0$. In that case, the (co)variance matrices, corresponding to the satellite phase biases $\tilde{\delta}^{ps}$, remain unchanged. For the variance matrix of the satellite clocks $d\tilde{t}^{ps}$, there is still a slight improvement, one that can be explained by the assumed time-invariance of $(\Delta x_l - \Delta x_r)$, cf. (74).

Based on the individual corrections we construct the geometry-based, ambiguity-float combined corrections $(\hat{\tilde{c}}_\phi^T, \hat{\tilde{c}}_p^T)^T$. First we present their estimators and then their variance-covariance matrices.

Theorem 3 (GB ambiguity-float corrections) *The k-epoch geometry-based ambiguity-float BLUE of the network-derived corrections, at epoch i, is given as*

$$\begin{bmatrix} \hat{\tilde{c}}_{\phi,\mathrm{GB}}(i) \\ \hat{\tilde{c}}_{p,\mathrm{GB}}(i) \end{bmatrix} = \begin{bmatrix} \hat{\tilde{c}}_{\phi,\mathrm{GF}}(i) \\ \hat{\tilde{c}}_{p,\mathrm{GF}}(i) \end{bmatrix} - \hat{\mathrm{I\!V}} - \hat{\mathrm{V}} \tag{75}$$

with

$$\begin{aligned} \hat{\mathrm{I\!V}} &= ([\mathcal{P}_{[\tilde{e},\tilde{\mu}]} - \mathcal{P}_{\tilde{\mu}}] \otimes D_m^T) \begin{bmatrix} \phi_{\bar{r}r}(\bar{i}i) \\ p_{\bar{r}r}(\bar{i}i) \end{bmatrix} \\ \hat{\mathrm{V}} &= \begin{bmatrix} 0 \\ ([\mathcal{P}_{[e,\mu]} - \mathcal{P}_{\mu}] \otimes D_m^T \mathcal{P}_{\tilde{G}}^{\perp}) p_{\bar{r}r}(\bar{i}) \end{bmatrix} \end{aligned} \tag{76}$$

and the projectors

$$\begin{aligned} &\mathcal{P}_{\mu} = c_{\bar{i}|\rho}^2 \mu \mu^T C_p^{-1} \\ &\mathcal{P}_{\tilde{\mu}} = c_{\bar{i}|\rho}^2 \tilde{\mu} \tilde{\mu}^T \,\mathrm{blkdiag}(C_\phi^{-1}, C_p^{-1}) \\ &\mathcal{P}_{\tilde{G}} = \tilde{G}(\tilde{G}^T C_S^{-1} \tilde{G})^{-1} \tilde{G}^T C_S^{-1}, \;\; \mathcal{P}_{\tilde{G}}^{\perp} = I_m - \mathcal{P}_{\tilde{G}} \end{aligned} \tag{77}$$

where $\tilde{G} = [e_m, G]$, and

$$\begin{aligned} c_{\bar{i}|\rho}^2 &= (\mu^T C_p^{-1} \mu)^{-1}, \\ c_{\bar{i}|\rho}^2 &= (\tilde{\mu}^T \,\mathrm{blkdiag}(C_\phi^{-1}, C_p^{-1})\, \tilde{\mu})^{-1} \end{aligned} \tag{78}$$

Proof See Appendix. □

The GB-correction (75) is linked to its GF counterpart (51) through the *zero-mean* terms $\hat{\mathrm{I\!V}}$ and $\hat{\mathrm{V}}$. The first term $\hat{\mathrm{I\!V}}$ describes the contribution of the additional multi-epoch condition equations of (74). Thus $\hat{\mathrm{I\!V}} = 0$ if $\bar{i} = i$. On the other hand, the second term $\hat{\mathrm{V}}$ describes the contribution of the geometry-based condition equations of (73). Thus $\hat{\mathrm{V}}$ vanishes in the absence of satellite redundancy, i.e. $\hat{\mathrm{V}} = 0$ if $m = \nu + 1$. Also note that both terms are absent when a single network station is considered, i.e. $\hat{\mathrm{I\!V}} = \hat{\mathrm{V}} = 0$ if $\bar{r} = r$.

It should be remarked that the third term $\hat{\mathrm{V}}$ only contains code data. Hence, in the ambiguity-float case, only the code correction $\tilde{c}_p$ benefits from the contribution of the geometry-based condition equations of (73).

The precision of the above corrections is given in the following lemma.

Lemma 4 (Precision GB ambiguity-float corrections) *The variance matrix of the corrections (75) is given as*

$$\mathsf{D}\left(\begin{bmatrix} \hat{\tilde{c}}_{\phi,\mathrm{GB}}(i) \\ \hat{\tilde{c}}_{p,\mathrm{GB}}(i) \end{bmatrix}\right) = \mathsf{D}\left(\begin{bmatrix} \hat{\tilde{c}}_{\phi,\mathrm{GF}}(i) \\ \hat{\tilde{c}}_{p,\mathrm{GF}}(i) \end{bmatrix}\right) - \mathsf{D}(\hat{\mathrm{I\!V}}) - \mathsf{D}(\hat{\mathrm{V}}) \tag{79}$$

with

$$\begin{aligned} \mathsf{D}(\hat{\mathrm{I\!V}}) &= \frac{n-1}{n} [\mathcal{P}_{[\tilde{e},\tilde{\mu}]} - \mathcal{P}_{\tilde{\mu}}] \begin{bmatrix} C_\phi & 0 \\ 0 & C_p \end{bmatrix} \otimes \left[C_s(i) - \frac{1}{k} \bar{C}_s \right] \\ \mathsf{D}(\hat{\mathrm{V}}) &= \frac{n-1}{n} \begin{bmatrix} 0 & 0 \\ 0 & [\mathcal{P}_{[e,\mu]} - \mathcal{P}_{\mu}] C_p \end{bmatrix} \otimes \frac{1}{k} \tilde{C}_s \end{aligned} \tag{80}$$

where $\tilde{C}_s = D_m^T \mathcal{P}_{\tilde{G}}^{\perp} \bar{C}_S D_m$.

Proof Follows by an application of the variance propagation law to (75). □

To evaluate the maximum precision improvement brought by switching to the geometry-based model, we consider the extreme case, namely, the *geometry-fixed* case. The geometry-fixed (GFi) case refers to the situation where all the relative position increments/ZTDs $(\Delta x_l - \Delta x_r), l \neq r$, are assumed known. The GFi (co)variance matrices follow by setting $\tilde{C}_s = \bar{C}_s$ in (79). Figure 4 gives a plot of the square root of the mean variance of an individual satellite at zenith, i.e. $\mathrm{trace}(\mathsf{D}(\hat{\tilde{c}}_{p,\mathrm{GB}}^s(i)))/f$. Compare the plot with its GF-counterpart in Fig. 1. The number of stations n now has a *larger* impact on the precision improvement of the code correction. This is mainly due to the extra condition equations of (73) that link the non-dispersive delays $\tilde{\rho}_r^{ps}$ $(r = 1, \ldots, n)$ to one another. Similar to the GF case, however, the stated impact gets less the larger the number of epochs k.

5.3 The ambiguity-fixed GB corrections

We now present our analytical analysis of the geometry-based, ambiguity-fixed network-based PPP-RTK corrections. The precision of the BLUE estimators of the individual PPP-RTK corrections $d\tilde{t}^{ps}$, $\tilde{\delta}^{ps}$ and $\tilde{d}^{ps}$ is described by

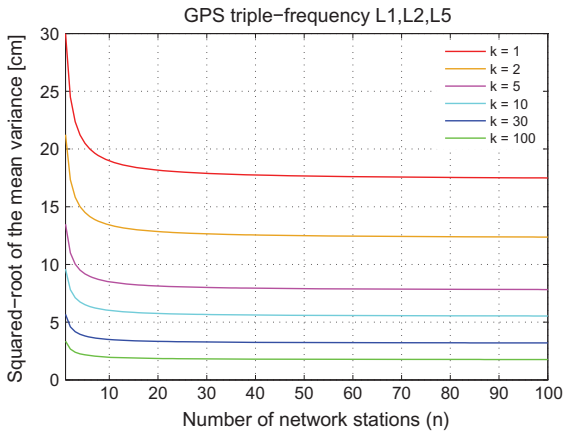

Fig. 4 GPS L1, L2, L5 scenario: the squared-root of the zenith-referenced mean variance of the geometry-fixed, ambiguity-float code corrections as a function of the number of stations n for different number of epochs k ($\sigma_\phi = 3$ [mm], $\sigma_p = 30$ [cm], $c_s = 1$)

Table 8 (Co)variance matrices of the ambiguity-fixed geometry-based (GB) corrections

$$
\begin{aligned}
Q^{GB}_{\check{d}\check{d}\check{\tilde{c}}_{(i)}} &= Q^{GB}_{\hat{d}\hat{d}\hat{\tilde{c}}_{(i)}} - \tfrac{n-1}{kn}(c^2_{\hat\rho} - c^2_{\check\rho})\,(\bar C_s - \tilde C_s)\\
Q^{GB}_{\check{\tilde{\delta}}\check{\tilde{\delta}}} &= Q^{GB}_{\hat{\tilde{\delta}}\hat{\tilde{\delta}}} - \tfrac{n-1}{kn}(c^2_{\hat\rho}\Lambda^{-1}e_\mu e^T_\mu\Lambda^{-1})\,(\bar C_s - \tilde C_s) - Q\\
Q^{GB}_{\check{\tilde{d}}\check{\tilde{d}}} &= Q^{GB}_{\hat{\tilde{d}}\hat{\tilde{d}}}\\
Q^{GB}_{\check{d}\check{\tilde{c}}\check{\tilde{\delta}}_{(i)}} &= Q^{GB}_{\hat{d}\hat{\tilde{c}}\hat{\tilde{\delta}}_{(i)}} + \tfrac{n-1}{kn}(c^2_{\hat\rho}e^T_\mu\Lambda^{-1})\,(\bar C_s - \tilde C_s)\\
Q^{GB}_{\check{d}\check{\tilde{d}}} &= Q^{GB}_{\hat{d}\hat{\tilde{d}}}\\
Q^{GB}_{\check{\tilde{\delta}}\check{\tilde{d}}} &= Q^{GB}_{\hat{\tilde{\delta}}\hat{\tilde{d}}}
\end{aligned}
$$

The ambiguities, phase and code biases are assumed constant over k epochs

$Q = \frac{n-1}{kn}\Lambda^{-1}(C_\phi + c^2_{\tilde\iota|\rho}\mu\mu^T)\Lambda^{-1} \otimes \bar C_s$

the variance-covariance matrices as given in Table 8. The ambiguity-fixed results are expressed in their ambiguity-float counterparts. In contrast to the GF-model, here the impact of ambiguity resolution is dependent on the strength of the GB-model. The stronger the model, the lower the impact of ambiguity resolution. The strongest model follows by the geometry-fixed case. In this extreme case, with $\tilde C_s = \bar C_s$, *no* precision improvement is realized. On the other hand, the impact of ambiguity resolution gets maximum for the weakest model, i.e. when there is no satellite redundancy ($\tilde C_s = 0$ as $m = \nu + 1$).

We now present the geometry-based, ambiguity-fixed combined corrections $(\check{\tilde c}^T_\phi, \check{\tilde c}^T_p)^T$.

Theorem 4 (GB ambiguity-fixed corrections) *The k-epoch geometry-based ambiguity-fixed BLUE of the network-derived corrections, at epoch i, is given as*

$$
\begin{bmatrix} \check{\tilde c}_{\phi,\mathrm{GB}}(i) \\ \check{\tilde c}_{p,\mathrm{GB}}(i) \end{bmatrix} = \begin{bmatrix} \check{\tilde c}_{\phi,\mathrm{GF}}(i) \\ \check{\tilde c}_{p,\mathrm{GF}}(i) \end{bmatrix} - \hat{\mathrm{I}}\check{\mathrm{V}} - \check{\mathrm{V}} \tag{81}
$$

with

$$
\begin{aligned}
\hat{\mathrm{I}}\check{\mathrm{V}} &= ([\mathcal{P}_{[\tilde e,\tilde\mu]} - \mathcal{P}_{\tilde\mu}] \otimes D^T_m) \begin{bmatrix} \phi_{\bar r r}(\bar i i) \\ p_{\bar r r}(\bar i i) \end{bmatrix}\\
\check{\mathrm{V}} &= ([\mathcal{P}_{[\tilde e,\tilde\mu]} - \mathcal{P}_{\tilde\mu}] \otimes D^T_m \mathcal{P}^\perp_{\tilde G}) \begin{bmatrix} \tilde\phi_{\bar r r}(\bar i) \\ p_{\bar r r}(\bar i) \end{bmatrix}
\end{aligned} \tag{82}
$$

where the ambiguity-fixed phase data are given as

$$
\begin{aligned}
\tilde\phi_r &= \phi_r\\
\tilde\phi_l &= \phi_l - [\Lambda \otimes L]\,\check z_{rl}, \quad l \neq r
\end{aligned} \tag{83}
$$

with L being an $m \times (m-1)$ matrix formed by removing the p^{th} column of I_m (given p as the pivot satellite).

Proof See Appendix. □

The GB ambiguity-fixed correction (81) is linked to its GF-counterpart (57) through the *zero-mean* terms $\hat{\mathrm{I}}\check{\mathrm{V}}$ and $\check{\mathrm{V}}$. Compare the results with those of the GB ambiguity-float (75). The first term $\hat{\mathrm{I}}\check{\mathrm{V}}$, due to the multi-epoch condition equations of (74), remains unchanged. This is what one would expect, since the *epoch-differenced* observations $\phi_{\bar r r}(\bar i i)$ and $p_{\bar r r}(\bar i i)$ are uncorrelated with the float ambiguities. The second term $\hat{\mathrm{V}}$ is, however, replaced by its ambiguity-fixed counterpart $\check{\mathrm{V}}$, describing the contribution of the geometry-based condition equations of (73). Next to the code data, the ambiguity-fixed carrier phase data $\tilde\phi_l$ also contribute in a likewise manner to $\check{\mathrm{V}}$.

An application of the variance propagation law to the above corrections gives their precision as presented in the following lemma.

Lemma 5 (Precision GB ambiguity-fixed corrections) *The variance matrix of the corrections* (81) *is given as*

$$
\mathsf{D}\left(\begin{bmatrix} \check{\tilde c}_{\phi,\mathrm{GB}}(i) \\ \check{\tilde c}_{p,\mathrm{GB}}(i) \end{bmatrix}\right) = \mathsf{D}\left(\begin{bmatrix} \check{\tilde c}_{\phi,\mathrm{GF}}(i) \\ \check{\tilde c}_{p,\mathrm{GF}}(i) \end{bmatrix}\right) - \mathsf{D}(\hat{\mathrm{I}}\check{\mathrm{V}}) - \mathsf{D}(\check{\mathrm{V}}) \tag{84}
$$

with

$$
\begin{aligned}
\mathsf{D}(\hat{\mathrm{I}}\check{\mathrm{V}}) &= \frac{n-1}{n}[\mathcal{P}_{[\tilde e,\tilde\mu]} - \mathcal{P}_{\tilde\mu}] \begin{bmatrix} C_\phi & 0 \\ 0 & C_p \end{bmatrix} \otimes \left[C_s(i) - \frac{1}{k}\bar C_s\right]\\
\mathsf{D}(\check{\mathrm{V}}) &= \frac{n-1}{n}[\mathcal{P}_{[\tilde e,\tilde\mu]} - \mathcal{P}_{\tilde\mu}] \begin{bmatrix} C_\phi & 0 \\ 0 & C_p \end{bmatrix} \otimes \frac{1}{k}\tilde C_s
\end{aligned} \tag{85}
$$

Proof Follows by an application of the variance propagation law to (81). □

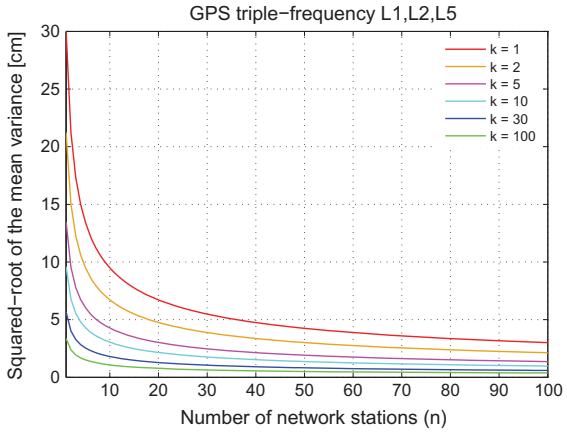

Fig. 5 GPS L1, L2, L5 scenario: the squared-root of the zenith-referenced mean variance of the geometry-fixed, ambiguity-fixed code corrections as a function of the number of stations n for different number of epochs k ($\sigma_\phi = 3$ [mm], $\sigma_p = 30$ [cm], $c_s = 1$)

We again consider the extreme case, the geometry-fixed case, to evaluate the maximum precision improvement brought by switching to the geometry-based model. The stated improvement follows by setting $\tilde{C}_s = \bar{C}_s$ in (84). A plot of the square root of the mean variance of an individual satellite at zenith, i.e. trace$(\mathsf{D}(\check{\tilde{c}}^s_{p,\mathrm{GB}}(i)))/f$, is given in Fig. 5. Compare the plot with its GF-counterpart in Fig. 2. The precision improvement is indeed insignificant. Provided that successful network ambiguity resolution is applied, one should, therefore, not expect a considerable improvement in the precision of the corrections, by switching to the geometry-based model. Once the network's ambiguities are resolved, the GF and GB performances do not differ by much.

5.4 User ADOP improvement by the GB corrections

To evaluate how much switching to the geometry-based model pays off, we again consider the user ADOP to characterize the improvement in the strength of user ambiguity resolution. Since adopting the geometry-based scenario further strengthens the network model, one would expect the user ADOP to get smaller upon replacing the geometry-free corrections by the geometry-based corrections. The maximum reduction in the ADOP follows when the geometry-fixed case is considered. The stated reduction is formulated in the following lemma presenting the user single-epoch ADOP GF-to-GFi ratios.

Lemma 6 (User single-epoch ADOP ratio: from geometry-free to geometry-based network corrections) *Let $C_\phi = \sigma^2_\phi I_f$ and $C_p = \sigma^2_p I_f$, respectively, be the co-factor matrices of the network's phase and code observable types in (40), where $C_S(i) \approx \bar{C}_S$. With a likewise structure, let the user phase and code co-factor matrices be given as $C_{\phi_u} = \sigma^2_{\phi_u} I_f$ and $C_{p_u} = \sigma^2_{p_u} I_f$, respectively. The ratio of the user single-epoch ADOP, based on the k-epoch geometry-free network corrections* (ADOP$_{\mathrm{GF}}$)*, to its geometry-fixed counterpart* (ADOP$_{\mathrm{GFi}}$) *reads then*

$$\frac{\mathrm{ADOP}_{\mathrm{GF}}}{\mathrm{ADOP}_{\mathrm{GFi}}} = \begin{cases} \left(\frac{[1+k\gamma_u][1+kn\gamma_u]+k(n-1)\gamma_u}{[1+k\gamma_u][1+kn\gamma_u]+\tilde{\epsilon}k(n-1)\gamma_u}\right)^{\frac{\nu}{2f(m-1)}}, & \text{net. amb.} - \text{float} \\ 1 & \text{net. amb.} - \text{fixed} \end{cases} \tag{86}$$

with $\gamma_u = (\sigma^2_{p_u}/\sigma^2_p)$, and

$$\tilde{\epsilon} = \frac{\epsilon}{(1+\epsilon) + \frac{4\epsilon\bar{\mu}^2}{(1+\epsilon)\sigma^2_{\bar{\mu}}}} \tag{87}$$

Proof Follows from an application of the results of Odijk and Teunissen (2008). □

The above lemma conveys two important messages. First, after successful network ambiguity resolution, no matter whether the user is provided with the geometry-free corrections or with the geometry-based corrections, in either case, the user ADOP remains the *same* (i.e. ADOP$_{\mathrm{GF}}$ = ADOP$_{\mathrm{GFi}}$).

Second, when the network ambiguity-float scenario is considered, there is a slight reduction in the user ADOP by switching from the geometry-free to the geometry-based corrections. To gain insight into the size of this reduction, we make some approximation. Note that one can neglect $\tilde{\epsilon}\,k(n-1)\gamma_u$, compared to the first term in the denominator of (86). Assuming the user's data to be of the same quality as those of the network receivers (i.e. $\gamma_u = 1$), the first expression of (86) would then takes the following form ($k = 1$)

$$\frac{\mathrm{ADOP}_{\mathrm{GF}}}{\mathrm{ADOP}_{\mathrm{GFi}}} \approx \left[1 + \frac{n-1}{2(n+1)}\right]^{\frac{\nu}{2f(m-1)}} \tag{88}$$

In the absence of satellite redundancy ($m = \nu + 1$), the above ADOP GF-to-GFi ratio becomes around 1.10 (when $f = 2$) and 1.07 (when $f = 3$), would the number of network stations be $n = 100$. When the number of satellites increases by ν (i.e. $m = 2\nu+1$), the above ADOP GF-to-GFi ratio even gets smaller, around 1.05 ($f = 2$) and 1.03 ($f = 3$). In either case, the stated ratio is therefore close to one, meaning that only a slight improvement in the strength of user ambiguity resolution is realized through replacing the ambiguity-float, geometry-free corrections by their geometry-based counterparts. This analysis is consistent with the numerical results that are shown in Fig. 6 (solid lines) for the user-ADOP GF-to-GFi ratios, for the dual- and triple frequency case

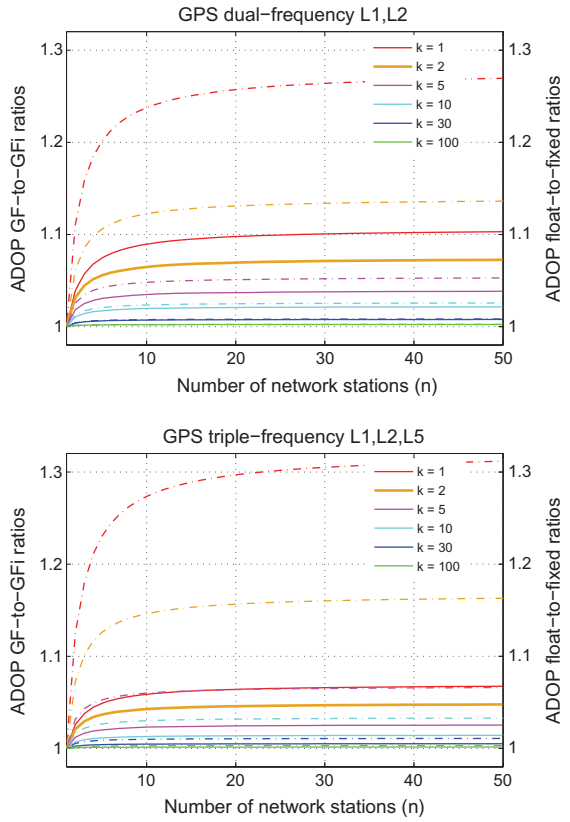

Fig. 6 User ADOP GF-to-GFi ratios (86) of the ambiguity-float network corrections (*solid lines*) as well as the ADOP float-to-fixed ratios of the GFi network corrections (*dashed lines*) as a function of the number of stations n. *Top* GPS L1, L2 scenario; *bottom* GPS L1, L2, L5 scenario. The values follow from (86) by setting $m = \nu + 1 = 5$, $\sigma_{\phi_u} = \sigma_\phi = 3$ [mm], $\sigma_{p_u} = \sigma_p = 30$ [cm], $c_s = 1$

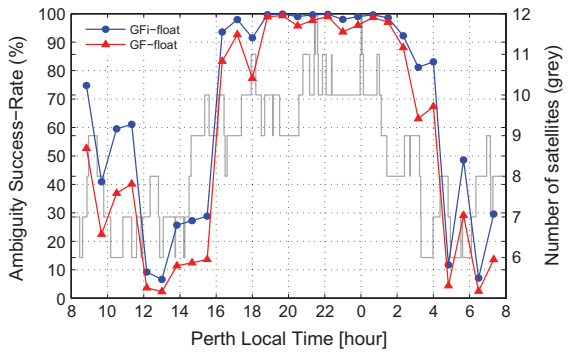

Fig. 7 User ambiguity success rates (%) based on 28 observational groups (each of size 100 epochs) that are corrected by the single-epoch geometry-fixed (GFi) (*blue circles*) and geometry-free (GF) ambiguity-float (*red triangles*) corrections. The number of stations is assumed to be very large, i.e. $n \to \infty$. The number of visible satellites is depicted by the grey lines (GPS L1, L2 scenario: $\sigma_{\phi_u} = \sigma_\phi = 3$ [mm], $\sigma_{p_u} = \sigma_p = 30$ [cm], $\nu = 4$, sampling-interval = 30 s). The ambiguity success rates have been computed using the VISUAL software (Verhagen 2002)

and different number of epochs k and stations n. This is further corroborated by the user ambiguity success rates as shown in Fig. 7, based on the GFi (blue circles) and the GF ambiguity-float (red triangles) corrections. In order to consider the maximum gain in the user-IAR capacity achieved by switching to the GB model, we consider the dual-frequency single-epoch network corrections ($f = 2, k = 1$) where the number of stations is assumed to be very large (i.e. $n \to \infty$). The user corrected data have been partitioned into 28 groups, each of size 100 epochs with the sampling-interval of 30 s. As predicted by the ADOP analysis, Fig. 7 confirms that the user ambiguity success rates based on the GF corrections do not differ too much from their GFi versions.

Although switching from the ambiguity-float, geometry-free network scenario to its geometry-based counterpart does not improve the capacity of user ambiguity resolution by much, one must, however, note that it does play a prominent role in improving the capacity of network ambiguity resolution (Teunissen and Khodabandeh 2015). Furthermore, such a GF-to-GB network switch also improves the float solution of the user position/ZTD, as the clock corrections approximately improve from a 1-over-k rule to a 1-over-kn rule (cf. Table 7 for $\tilde{C}_s = \bar{C}_s$).

Next to the network ambiguity-float, GF-to-GB switch, we also consider the effect of network ambiguity fixing. To compare the user-ambiguity impact of the ambiguity-fixed network corrections with their ambiguity-float counterparts, the user-ADOP float-to-fixed ratios (dashed lines) are shown in Fig. 6 for a GFi-network. The float-to-fixed ratio (dashed lines) is around 1.27 (when $f = 2$) and 1.31 (when $f = 3$) for $k = 1$. When the k-epoch network corrections are applied, the stated ratio does even get smaller as the number of epochs k increases. For instance, the float-to-fixed ratio drops to 1.05 ($f = 2$) and 1.07 ($f = 3$) for $k = 5$.

From the above one may conclude that user ambiguity resolution performance, when based on the PPP-RTK corrections $d\tilde{t}^s, \tilde{\delta}^s$, and $\tilde{d}^s$, will not benefit too much from ambiguity fixing in the network. This does not mean, of course, that network ambiguity resolution has no important role to play. It plays a significant role, for instance, in improving the precision of the estimated ionospheric delays in the network (Teunissen and Khodabandeh 2014).

The reason for the rather modest impact of network ambiguity resolution on the user ambiguity resolution performance lies in the way the user's ionospheric delays are treated. In our formulation, the user's ionospheric delays are treated as unknown, thus resulting in a rather weak model in terms of ambiguity resolution capability. But as was already pointed out in Sect. 2.3.1, one can improve user ambiguity resolution performance significantly if the PPP-RTK corrections would be extended with an ionospheric component, thus enabling the user to make use of the stronger ionosphere-

weighted model. In that case, network ambiguity resolution would improve the provided ionospheric information (Odijk 2002; Grejner-Brzezinska et al. 2004; Mervart et al. 2013; Odijk et al. 2014).

5.5 Corrections' precision relevant to user-IAR

As stated earlier in Sect. 4.5, not all the components of the PPP-RTK corrections contribute to user integer ambiguity resolution. Any part of the corrections that lies in the range space of $\mathcal{P}_{[\tilde{e},\tilde{\mu}]}$ gets fully absorbed by the user position and user ionospheric delay parameters, thus not affecting the estimator of the user ambiguities. This in turn allows one to identify which part of the variance matrix of the corrections is relevant to user-IAR, see e.g. (63) and (65). Drawing a similar analogy to the geometry-free network corrections, the following part of the geometry-based network corrections, relevant to user-IAR, can be considered,

network ambiguity-float case:

$$\begin{bmatrix} (I_f \otimes D_m^T)\phi_r(\bar{i}) \\ (I_f \otimes D_m^T)p_r(\bar{i}) - (\mathcal{P}^{\perp}_{[e,\mu]} \otimes D_m^T)p_{\bar{r}r}(\bar{i}) \\ \quad -([\mathcal{P}_{[e,\mu]} - \mathcal{P}_{\mu}] \otimes D_m^T \mathcal{P}^{\perp}_{\tilde{G}})p_{\bar{r}r}(\bar{i}) \end{bmatrix} \tag{89}$$

network ambiguity-fixed case:

$$(I_{2f} \otimes D_m^T)\begin{bmatrix} \tilde{\phi}_{\bar{r}}(\bar{i}) \\ p_{\bar{r}}(\bar{i}) \end{bmatrix} \tag{90}$$

Compare the above equations with their GF counterparts (62) and (64). This again shows that only the time-averaged network data are of relevance for user-IAR. While the GB ambiguity-fixed part (90) is *identical* to that of the GF ambiguity-fixed case (64), the GB ambiguity-float part (89) differs from its GF version (62). This is due to the difference in their *code* corrections only. The stated code-difference is formed by the projector $\mathcal{P}_{[e,\mu]} - \mathcal{P}_{\mu}$. For the dual-frequency case (i.e. for $\mathcal{P}_{[e,\mu]} = I_f$), this projector is simplified as $\mathcal{P}_{[e,\mu]} - \mathcal{P}_{\mu} = \mathcal{P}^{\perp}_{\mu}$. The projector $\mathcal{P}^{\perp}_{\mu}$ is referred to as the *ionosphere-free* projector, since it nullifies the ionospheric vector μ, i.e. $\mathcal{P}^{\perp}_{\mu}\mu = 0$. Thus in the dual-frequency case, the network ambiguity-float GF-to-GB switch only leads the ionosphere-free code data to contribute to a further improvement of the relevant GF corrections.

The corresponding variance matrices of (89) and (90) are, respectively, given as,

network ambiguity-float case:

$$\begin{aligned} &\tfrac{1}{k}\begin{bmatrix} C_{\phi} & 0 \\ 0 & (I_f - \frac{n-1}{n}\mathcal{P}^{\perp}_{[e,\mu]})C_p \end{bmatrix} \\ &\otimes \tilde{C}_s - \tfrac{n-1}{kn}\begin{bmatrix} 0 & 0 \\ 0 & [\mathcal{P}_{[e,\mu]} - \mathcal{P}_{\mu}]C_p \end{bmatrix} \otimes \tilde{C}_s \end{aligned} \tag{91}$$

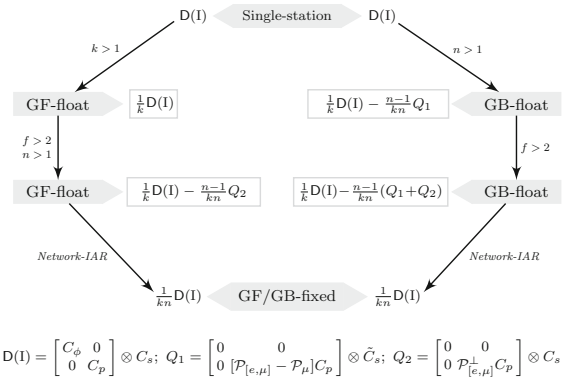

Fig. 8 Diagram linking the parts of the network corrections' variance matrices that determine user ambiguity resolution. With the approximation $C_s(i) = C_s,\ i = 1, \ldots, k$, the role of the number of epochs k and stations n is characterized by switching from the single-station scenario to the GF- and GB-network scenarios

network ambiguity-fixed case:

$$\tfrac{1}{kn}\begin{bmatrix} C_{\phi} & 0 \\ 0 & C_p \end{bmatrix} \otimes \bar{C}_s \tag{92}$$

where an overview of the interactions of the above (co)-variance components with their single-station and geometry-free counterparts is presented by the diagram given in Fig. 8. To highlight the role of the number of epochs k, we make the approximation $C_s(i) = C_s,\ i = 1, \ldots, k$. The diagram commences with the variance matrix of the single-station corrections, i.e. $\mathsf{D(I)}$ (cf. 56). In case of the multi-epoch scenario ($k > 1$), the relevant part of the variance matrix decreases by a factor of k which is identical to that of the dual-frequency GF ambiguity-float (GF-float) model (cf. 63 for $f = 2$). When the multi-frequency GF-float network scenario takes place (i.e. $n > 1$ and $f > 2$), the stated part is reduced further by $[(n-1)/(kn)]Q_2$ (cf. 63). Note that this reduction vanishes when $n = 1$ or when $f = 2$.

On the other side of the diagram, the link between the single-station variance matrix and the GB ambiguity-float (GB-float) variance matrix is considered (cf. 91 for $f = 2$). At least two network stations are needed to realize the GB-float scenario (i.e. $n > 1$). In contrast to the GF-float model, a *single-epoch* reduction ($k = 1$) in the relevant variance matrix can be achieved upon switching to the GB-float model. The stated single-epoch reduction, for the dual-frequency case, is equal to $[(n-1)/n]Q_1$ that is attributed to the contribution of the ionosphere-free code data (cf. 89). Note that this reduction vanishes when $n = 1$ or when $m = \nu + 1$. In case of the multi-epoch scenario ($k > 1$), the reduced variance matrix decreases by a factor of k. Similar to the GF-float model, going from the dual-frequency case to the multi-frequency case ($f > 2$) reduces the GB variance matrix further by $[(n-1)/(kn)]Q_2$ (cf. 91).

After successful network ambiguity resolution, *both* the GF and the GB variance matrices, relevant to user-IAR, get *identical* to $(1/kn)\mathsf{D}(\mathrm{I})$ (cf. 65 and 92). In this case, both the number of epochs k and stations n work in tandem to reduce the relevant variance matrix.

5.6 User corrected data interpreted as DD data

In Sect. 2, an analogy between the single-station PPP-RTK setup and the single-baseline RTK setup was given (cf. Table 1). It was shown that the user corrected data are nothing else but DD observations formed between the user and a single network station. This is the case as the single-station corrections stand in one-to-one correspondence with the single-station observations (cf. 17). On the other hand, through the presentation of Theorems 1–4, the PPP-RTK network corrections were shown to be an *adjusted* version of single-station observations. It is therefore evident that the user's corrected observations, on the basis of the *network* corrections, can also be interpreted as DD observations between the user and the network stations. This notion is visualized in Fig. 9 and made precise via the following theorem.

Theorem 5 (PPP-RTK in DD-form) *Let* $[\phi_u^T(i),\ p_u^T(i)]^T$ *be the user observations at epoch* i*. Also let the* k*-epoch network correction* $[\hat{\tilde{c}}_\phi^T(i), \hat{\tilde{c}}_p^T(i)]^T$ *be a linear unbiased estimator of* $[\tilde{c}_\phi^T(i), \tilde{c}_p^T(i)]^T$*. Then the user corrected observations can always be written as*

$$\begin{bmatrix} (I_f \otimes D_m^T)\,\phi_u(i) \\ (I_f \otimes D_m^T)\,p_u(i) \end{bmatrix} - \begin{bmatrix} \hat{\tilde{c}}_\phi(i) \\ \hat{\tilde{c}}_p(i) \end{bmatrix} = \sum_{q=1}^{k}\sum_{l=1}^{n} W_{q,l}(i) \begin{bmatrix} (I_f \otimes D_m^T)\,\phi_{lu}(q) \\ (I_f \otimes D_m^T)\,p_{lu}(q) \end{bmatrix} \tag{93}$$

for some weight matrices $W_{q,l}(i)$ *satisfying*

$$\sum_{q=1}^{k}\sum_{l=1}^{n} W_{q,l}(i) = I \tag{94}$$

with the DD observations

$$(I_f \otimes D_m^T)\,\phi_{lu}(q) = (I_f \otimes D_m^T)\,[\phi_u(i) - \phi_l(q)]$$
$$(I_f \otimes D_m^T)\,p_{lu}(q) = (I_f \otimes D_m^T)\,[p_u(i) - p_l(q)]$$

Proof Follows by an application of Theorems 1–4. □

According to the above theorem, the user corrected observations can always be viewed as a *weighted-average* of DD observations formed between the user and the network stations. To give an example, consider the user-corrected code observable based on the single-epoch GF-float corrections

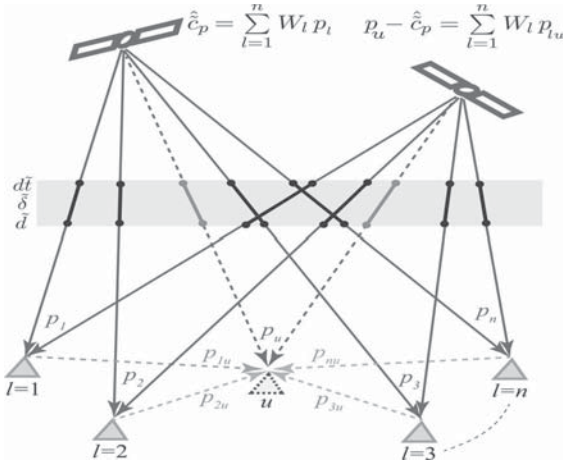

Fig. 9 Illustration of the user corrected observations as a weighted-average of the DD observations formed between the user 'u' and the network stations $l = 1, \ldots, n$

(i.e. $\hat{\mathbb{I}} = 0$ in 51). For one single element of the code correction we may write then

$$\begin{aligned} \hat{\tilde{c}}_{p,\mathrm{GF}}^{ps} &= \mathcal{P}_{[e,\mu]}\, p_{\tilde{r}r}^{ps} + p_{\tilde{r}}^{ps} \\ &= \mathcal{P}_{[e,\mu]}\, p_r^{ps} + \mathcal{P}_{[e,\mu]}^{\perp}\, p_{\tilde{r}}^{ps} \end{aligned} \tag{95}$$

thus forming the user corrected code observations as

$$p_u^{ps} - \hat{\tilde{c}}_{p,\mathrm{GF}}^{ps} = \mathcal{P}_{[e,\mu]}\, p_{ru}^{ps} + \mathcal{P}_{[e,\mu]}^{\perp}\, \frac{1}{n}\sum_{l=1}^{n} p_{lu}^{ps} \tag{96}$$

with the DD observations $p_{lu}^{ps} = p_u^{ps} - p_l^{ps}$. Equation (96) can then be expressed as a weighted-average of p_{lu}^{ps}, $l = 1, \ldots, n$, that is

$$p_u^{ps} - \hat{\tilde{c}}_{p,\mathrm{GF}}^{ps} = \sum_{l=1}^{n} W_l\, p_{lu}^{ps}, \quad \text{with} \quad \sum_{l=1}^{n} W_l = I \tag{97}$$

in which the weight matrices W_l are defined as

$$W_l = \begin{cases} \mathcal{P}_{[e,\mu]} + \frac{1}{n}\mathcal{P}_{[e,\mu]}^{\perp}, & l = r \\ \frac{1}{n}\mathcal{P}_{[e,\mu]}^{\perp}, & l \neq r \end{cases} \tag{98}$$

It therefore follows from the *DD-like* structure of the PPP-RTK user corrected observations that the PPP-RTK setup can be considered equivalent to the more traditional network-RTK setup, be it that their ionospheric parametrization could be different.

6 Summary and conclusions

The contributions of this paper are summarized as follows:

- *Single-station PPP-RTK*: It was shown how a proper set of estimable parameters of a *single station* can act as if they are the satellite clocks and phase/code biases, respectively. In their application to the user observation equations, we characterized the role of each such PPP-RTK correction. The estimable satellite clock $d\tilde{t}$ provides a 'positional link' between the user and reference station, while the estimable satellite phase biases $\tilde{\delta}$ have the function of replacing the noninteger user ambiguity by the integer double-differenced (DD) ambiguity between the user and the reference station. It was also shown that for the *multi-frequency* PPP-RTK setup one needs the additional code bias correction $\tilde{d}$, so as to make optimal use of the user code data on the third frequency and beyond ($f > 2$).
- *Highly correlated PPP-RTK corrections*: It was shown that one should not rely on the quality-judgment of the individual corrections. Instead, the quality of the *combined* version of the corrections must be evaluated. This is because of the high correlation that exists between the individual corrections. By means of some illustrative examples we demonstrated the potential pitfalls of ignoring the stated correlation.
- *Single-station PPP-RTK is single-baseline RTK*: We demonstrated the equivalence between the single-station PPP-RTK setup and the more traditional single-baseline RTK setup (cf. Table 1). It was shown that both formulations are identical except for their ionospheric delay parameters. With the PPP-RTK user model a biased ionospheric delay is obtained, whereas an unbiased DD ionospheric delay is obtained with the single-baseline model.
- *Network redundancy for PPP-RTK*: We identified the network redundancy and its impact on the precision of the PPP-RTK corrections (cf. Tables 3, 6). This was done for both the geometry-free (GF) network model and the geometry-based (GB) network model, with and without network-IAR. The precision impact of the number of epochs k, number of stations n and number of frequencies f was shown for both the individual corrections as well as for their combined form. Furthermore, it was demonstrated that the estimable code biases are *uncorrelated* with the float DD ambiguities and the stations' relative positions/ZTDs. Hence, their (co)variance matrices remain *unchanged* when switching to the geometry-based model and/or when performing integer ambiguity resolution.
- *BLUEs of PPP-RTK corrections*: We derived the best linear unbiased estimators of the PPP-RTK network corrections in analytical form. The BLUEs of the combined corrections are expressed in terms of time- and station-*averaged* network observations and time- and station-*differenced* network observations. Using the conditional least-squares approach, our result is formulated such that it clearly shows how the single-station corrections are further improved by the network information. Therefore, once the corrections are applied to the user data, the user corrected observation equations can be interpreted as if a single baseline is formed between the user and a network-adjusted reference station.
- *Only time-averaged network data relevant for user-IAR*: The closed-form expressions of the BLUE corrections allow one to identify which part of the combined corrections really contributes to user integer ambiguity resolution. For all four network scenarios (i.e. the GF-float, cf. 62, the GF-fixed, cf. 64, the GB-float, cf. 89, and the GB-fixed, cf. 90), it was shown that the network contribution to the float-estimated user ambiguities is only through the time-averaged network data. For the two ambiguity-fixed network scenarios (i.e. GF- and GB-fixed, cf. 64 and 90), the network contribution to the float-estimated user ambiguities becomes even confined to the station-average of the time-averaged network data.
- *Precision impact on user-float position/ZTD*: The GF-to-GB network switch can improve the float solution of the user position/ZTD. This improvement, however, largely depends on the geometrical strength of the GB-model and on whether or not network-IAR is applied. The geometrically stronger the model, the larger the precision improvement becomes. In the strongest case, namely, the geometry-fixed (GFi) case, the precision of the user float position/ZTD, based on the network ambiguity-float corrections, is already as good as that of its network ambiguity-fixed counterpart. In the weakest case, namely, the geometry-free case, the stated precision can almost reach that of the GFi case, would network-IAR be applied (cf. Table 9). Hence, for the variance matrix of the float solution of the user position/ZTD, the network corrections can be ordered as

  $$\text{GF-float} \geq \text{GF-fixed} \approx \text{GFi-float} = \text{GFi-fixed}$$

- *Precision impact on user ambiguities*: In the sense of being able to estimate a more precise user ambiguity, the network corrections of the GB ambiguity-float model outperform their GF ambiguity-float counterpart. For their network ambiguity-fixed versions the situation is different. After performing network-IAR, the user-ambiguity relevant parts of both the GB- and GF-based corrections become *identical*, where now both the number of epochs k and the number of stations n work in tandem to improve the user-ambiguity precision (cf.

Table 9 Precision impact of the network corrections on the user float ambiguities and on the float position/ZTD for the geometry-free (GF) and the geometry-fixed (GFi) network scenarios

Variance matrix relevant to the user ambiguities			Variance matrix relevant to the user-float position/ZTD	
Scenario	Net. ambiguity-float	Net. ambiguity-fixed	Net. ambiguity-float	Net. ambiguity-fixed
GF	$Q^{\mathrm{GF}}_{\mathrm{float}} = \frac{1}{k}\mathsf{D}(\mathrm{I}) - \frac{n-1}{kn} Q_2$	$Q^{\mathrm{GF}}_{\mathrm{fixed}} = \frac{1}{n} Q^{\mathrm{GF}}_{\mathrm{float}}$	$Q^{\mathrm{GF}}_{\mathrm{float}} = \frac{1}{k}(c^2_{\tilde{\rho}} + [k-1]c^2_{\tilde{\rho}}) Q_e + \Delta Q$	$Q^{\mathrm{GF}}_{\mathrm{fixed}} = Q^{\mathrm{GFi}}_{\mathrm{float}} + \frac{n-1}{n} c^2_{\tilde{\rho}}\, Q_e$
GFi	$Q^{\mathrm{GFi}}_{\mathrm{float}} = Q^{\mathrm{GF}}_{\mathrm{float}} - \frac{n-1}{kn}(Q_1 + Q_2)$	$Q^{\mathrm{GFi}}_{\mathrm{fixed}} = Q^{\mathrm{GF}}_{\mathrm{fixed}}$	$Q^{\mathrm{GFi}}_{\mathrm{float}} = \frac{1}{n} Q^{\mathrm{GF}}_{\mathrm{float}} + \frac{n-1}{n} \Delta Q$	$Q^{\mathrm{GFi}}_{\mathrm{fixed}} = Q^{\mathrm{GFi}}_{\mathrm{float}}$

With the approximation $C_s(i) = C_s,\ i = 1, \ldots, k$, the role of the number of epochs k is highlighted. The variance matrices $\mathsf{D}(\mathrm{I})$, Q_1 and Q_2 are given in Fig. 8. The $f \times (f-1)$ matrix B is a basis matrix orthogonal-complement to the f-vector μ, thus forming ionosphere-free combinations $Q_e = (B^T e e^T B \otimes C_s)$; $\Delta Q = Q_{\hat{\tilde{\rho}}\hat{\tilde{d}}} Q^{-1}_{\hat{\tilde{d}}\hat{\tilde{d}}} Q^T_{\hat{\tilde{\rho}}\hat{\tilde{d}}}$; $Q_{\hat{\tilde{\rho}}\hat{\tilde{d}}} = (1/kn)(B^T C_p E^{-T} \otimes C_s)$; $Q_{\hat{\tilde{d}}\hat{\tilde{d}}} = (1/kn)(E^- C_p E^{-T} \otimes C_s)$

Table 9). Hence, for the variance matrix of the user ambiguities, the network corrections can be ordered as

$$\text{GF-float} \geq \text{GB-float} \geq \text{GF-fixed} = \text{GB-fixed}$$

- *Relevance of ionospheric information*: Through our user-ADOP analysis the above improvements were also quantified. It was shown that they are not as significant as would be the case when the user would be able to include ionosphere-weighting in his model. This underlines the importance of being able to include network-based ionospheric information in the corrections, an addition that would then benefit most from using the geometry-based, ambiguity-fixed network model. Without such corrections, the user performance corresponds to that of a long baseline ionosphere float model.
- *PPP-RTK user-parameters are function of DD data*: It was shown that the PPP-RTK user corrected data can always be viewed as a *weighted-average* of the double-differenced (DD) observations that are formed between the user and the network stations. This shows the equivalence between the PPP-RTK formulation and the more traditional network-RTK formulation, be it that their ionospheric parametrizations could be different.
- *Network can at most overcome half the uncertainty of the reference-user data*: Recall that the user corrected model of observation equations can be interpreted as being that of a single baseline formed between the user and network-adjusted reference station. Strengthening the network model would therefore only improve the quality of the reference station's data (i.e. the network corrections), which in the extreme case of perfectly known (i.e. non-random) corrections would still leave the uncertainty of the user data to drive the user positioning performance.

Acknowledgments This work has been done in the context of the Positioning Program Project 1.19 "Multi-GNSS PPP-RTK Network Processing" of the Cooperative Research Centre for Spatial Information (CRC-SI). The second author is the recipient of an Australian Research Council (ARC) Federation Fellowship (Project Number FF0883188). All this support is gratefully acknowledged.

Appendix

Proof of Theorem 1 To prove (51), we apply the least-squares conditional adjustment (Teunissen 2000) to the single-station correction 'I'. Given the GF ambiguity-float network redundancy (Table 3), the following *uncorrelated* sets of misclosures are formed

$$t = (I_{n-1} \otimes E^- \otimes D^T_m)\,[p^T_{12}(\bar{\imath}), \ldots, p^T_{1n}(\bar{\imath})]^T,$$
$$t_l = \left(I_{k-1} \otimes \begin{bmatrix} \Lambda^{-1}, & M \\ 0, & E^- \end{bmatrix} \otimes D^T_m\right) \left[\begin{bmatrix} \phi_l(12) \\ p_l(12) \end{bmatrix}^T, \ldots, \begin{bmatrix} \phi_l(1k) \\ p_l(1k) \end{bmatrix}^T \right]^T \tag{99}$$

$l = 1, \ldots, n$. The first set of misclosures t is due to the fact that all single-station solutions of the estimable code biases $\tilde{d}^{ps}$ have the same mean. The n sets of misclosures t_l are due to the fact that all single-station solutions of the estimable ambiguities $\tilde{a}^{ps}_l$ and code biases $\tilde{d}^{ps}$ are assumed *constant* over k epochs. According to the least-squares conditional adjustment, the GF ambiguity-float network correction (51) is obtained as

$$\begin{bmatrix} \hat{\tilde{c}}_{\phi,\mathrm{GF}}(i) \\ \hat{\tilde{c}}_{p,\mathrm{GF}}(i) \end{bmatrix} = \mathrm{I} - Q_{\mathrm{I},t} Q^{-1}_{tt} t - \sum_{l=1}^{n} Q_{\mathrm{I},t_l} Q^{-1}_{t_l t_l} t_l \tag{100}$$

This, together with the following equalities

$$Q_{\mathrm{I},t} Q^{-1}_{tt} t = \hat{\mathbb{I}}, \quad \text{and} \quad Q_{\mathrm{I},t_l} Q^{-1}_{t_l t_l} t_l = \begin{cases} \hat{\mathbb{I}}, & l = r \\ 0, & l \neq r \end{cases}, \tag{101}$$

completes the proof. □

Proof of Theorem 2 The proof goes along the same lines as the proof of Theorem 1. The GF ambiguity-fixed network correction (57) is obtained through replacing the role of the misclosure vector t in (100) by its higher-dimension counterpart (cf. Table 3)

$$\tilde{t} = \left(I_{n-1} \otimes \begin{bmatrix} \Lambda^{-1}, & M \\ 0, & E^- \end{bmatrix} \otimes D_m^T \right) \times \left[\begin{bmatrix} \tilde{\phi}_{12}(\bar{i}) \\ p_{12}(\bar{i}) \end{bmatrix}^T, \ldots, \begin{bmatrix} \tilde{\phi}_{1n}(\bar{i}) \\ p_{1n}(\bar{i}) \end{bmatrix}^T \right]^T, \quad (102)$$

together with the equality

$$Q_{\mathrm{I},\tilde{t}}\, Q_{\tilde{t}\tilde{t}}^{-1} \tilde{t} = \breve{\mathrm{I}} - \hat{\mathrm{I}} \quad (103)$$

□

Proof of Theorem 3 We apply the least-squares conditional adjustment to the GF ambiguity-float network correction (51). Given the extra redundancy by the geometry-based network model (Table 6), the following sets of misclosures are formed

$$\begin{aligned} t_g &= (I_{n-1} \otimes (D_m^T G)^{\perp T})\, [\hat{\tilde{\rho}}_{12}^T(\bar{i}), \ldots, \hat{\tilde{\rho}}_{1n}^T(\bar{i})]^T, \\ t_{g_{1l}} &= (I_{k-1} \otimes D_m^T)\, [\hat{\tilde{\rho}}_{1l}^T(12), \ldots, \hat{\tilde{\rho}}_{1l}^T(1k)]^T \end{aligned} \quad (104)$$

$l = 2, \ldots, n$. The first set of misclosures t_g is due to the 'geometry-parametrization' of (72). The $(n-1)$ sets of misclosures $t_{g_{1l}}$ are due to the fact that the relative position increments and ZTDs $(\Delta x_l - \Delta x_1)$ are assumed *constant* over k epochs. According to the least-squares conditional adjustment, the GB ambiguity-float network correction (75) is obtained as

$$\begin{bmatrix} \hat{\tilde{c}}_{\phi,\mathrm{GB}}(i) \\ \hat{\tilde{c}}_{p,\mathrm{GB}}(i) \end{bmatrix} = y - Q_{y,t_g} Q_{t_g t_g}^{-1} t_g - Q_{y,t_{g_L}} Q_{t_{g_L} t_{g_L}}^{-1} t_{g_L} \quad (105)$$

with $y = [\hat{\tilde{c}}_{\phi,\mathrm{GF}}^T(i), \hat{\tilde{c}}_{p,\mathrm{GF}}^T(i)]^T$ and $t_{g_L} = [t_{g_{12}}^T, \ldots, t_{g_{1n}}^T]^T$. Equation (75) follows then by substituting

$$Q_{y,t_g} Q_{t_g t_g}^{-1} t_g = \hat{\mathrm{V}}, \quad \text{and} \quad Q_{y,t_{g_L}} Q_{t_{g_L} t_{g_L}}^{-1} t_{g_L} = \hat{\mathrm{I}}\mathrm{V} \quad (106)$$

into (105). □

Proof of Theorem 4 We apply the least-squares conditional adjustment to the GF ambiguity-fixed network correction (57), on the basis of the extra geometry-based misclosures given in (104). The GB ambiguity-fixed network correction (81) follows then through replacing the role of y in (105) by $\tilde{y} = [\check{\tilde{c}}_{\phi,\mathrm{GF}}^T(i), \check{\tilde{c}}_{p,\mathrm{GF}}^T(i)]^T$, together with the equalities

$$Q_{\tilde{y},t_g} Q_{t_g t_g}^{-1} t_g = \check{\mathrm{V}}, \quad \text{and} \quad Q_{\tilde{y},t_{g_L}} Q_{t_{g_L} t_{g_L}}^{-1} t_{g_L} = \check{\mathrm{I}}\mathrm{V} \quad (107)$$

□

References

Baarda W (1973) S-transformations and criterion matrices, vol 5(1). Technical report, Netherlands Geodetic Commission, Publ. on Geodesy, New Series, Delft

Banville S, Collins P, Zhang W, Langley RB (2014) Global and regional ionospheric corrections for faster PPP convergence. Navigation 61(2):115–124

Bertiger W, Desai SD, Haines B, Harvey N, Moore AW, Owen S, Weiss JP (2010) Single receiver phase ambiguity resolution with GPS data. J Geod 84(5):327–337

Blewitt G (1989) Carrier phase ambiguity resolution for the global positioning system applied to geodetic baselines up to 2000 km. J Geophys Res 94(B8):10187–10203

Collins P (2008) Isolating and estimating undifferenced GPS integer ambiguities. In: Proceedings of ION NTM, pp 720–732

Ge M, Gendt G, Rothacher M, Shi C, Liu J (2008) Resolution of GPS carrier-phase ambiguities in precise point positioning (PPP) with daily observations. J Geod 82(7):389–399

Geng J, Bock Y (2013) Triple-frequency GPS precise point positioning with rapid ambiguity resolution. J Geod 87(5):449–460

Geng J, Shi C, Ge M, Dodson AH, Lou Y, Zhao Q, Liu J (2012) Improving the estimation of fractional-cycle biases for ambiguity resolution in precise point positioning. J Geod 86(8):579–589

Grejner-Brzezinska DA, Wielgosz P, Kashani I, Smith DA, Spencer PS, Robertson DS, Mader GL et al (2004) An analysis of the effects of different network-based ionosphere estimation models on rover positioning accuracy. J GPS 3(1–2):115–131

Grejner-Brzezinska DA, Kashani I, Wielgosz P, Smith DA, Spencer PS, Robertson DS, Mader GL (2007) Efficiency and reliability of ambiguity resolution in network-based real-time kinematic GPS. J Surv Eng 133(2):56–65

Henderson HV, Pukelsheim F, Searle SR (1983) On the history of the Kronecker product. Linear Multilinear Algebra 14(2):113–120

Heroux P, Kouba J (1995) GPS precise point positioning with a difference. In: Paper presented at geomatics 95, Ottawa, ON, Canada, 13–15 June

Hofmann-Wellenhof B, Lichtenegger H, Wasle E (2008) GNSS: global navigation satellite systems: GPS, glonass, galileo, and more. Springer, New York

Jonkman N, Teunissen P, Joosten P, Odijk D (2000) GNSS long baseline ambiguity resolution: impact of a third navigation frequency. In: Geodesy beyond 2000, IAG symposium, vol 121, pp 349–354

Lannes A, Prieur JL (2013) Calibration of the clock-phase biases of GNSS networks: the closure-ambiguity approach. J Geod 87(8):709–731

Lannes A, Teunissen PJG (2011) GNSS algebraic structures. J Geod 85(5):273–290

Laurichesse D, Mercier F (2007) Integer ambiguity resolution on undifferenced GPS phase measurements and its application to PPP. In: Proceedings of the 20th international technical meeting of the Satellite Division of The Institute of Navigation (ION GNSS 2007), pp 839–848

Li B, Shen Y, Feng Y, Gao W, Yang L (2014) GNSS ambiguity resolution with controllable failure rate for long baseline network RTK. J Geod 88(2):99–112

Li X, Zhang X (2012) Improving the estimation of uncalibrated fractional phase offsets for PPP ambiguity resolution. J Navig 65(03):513–529

Li X, Ge M, Zhang H, Wickert J (2013) A method for improving uncalibrated phase delay estimation and ambiguity-fixing in real-time precise point positioning. J Geod 87(5):405–416

Loyer S, Perosanz F, Mercier F, Capdeville H, Marty JC (2012) Zero-difference GPS ambiguity resolution at CNES–CLS IGS Analysis Center. J Geod 86(11):991–1003

Mervart L, Lukes Z, Rocken C, Iwabuchi T (2008) Precise Point Positioning with ambiguity resolution in real-time. In: Proceedings of ION GNSS, pp 397–405

Mervart L, Rocken C, Iwabuchi T, Lukes Z, Kanzaki M (2013) Precise point positioning with fast ambiguity resolution-prerequisites, algorithms and performance. In: Proceedings of ION GNSS, pp 1176–1185

Odijk D (2002) Fast precise GPS positioning in the presence of ionospheric delays, vol 52. Ph.D. thesis, Delft University of Technology, Publication on Geodesy, Netherlands, Geodetic Commission, Delft

Odijk D, Teunissen PJG (2008) ADOP in closed form for a hierarchy of multi-frequency single-baseline GNSS models. J Geod 82(8):473–492

Odijk D, Teunissen PJG, Zhang B (2012) Single-frequency integer ambiguity resolution enabled GPS precise point positioning. J Surv Eng 138(4):193–202

Odijk D, Arora BS, Teunissen PJG (2014) Predicting the success rate of long-baseline GPS + Galileo (partial) ambiguity resolution. J Navig 67(3):385–401

Schaer S (1999) Mapping and predicting the Earth's ionosphere using the global positioning system. Ph.D. thesis, University of Bern, Bern, Switzerland

Teunissen P, Jonkman N, Joosten P, Tiberius C (2000) Long baseline 3 frequency differential GNSS. In: Position location and navigation symposium, IEEE 2000, San Diego, CA, pp 7–14. doi:10.1109/PLANS.2000.838277

Teunissen PTG (1985) Generalized inverses, adjustment, the datum problem and S-transformations. In: Grafarend EW, Sanso F (eds) Optimization and design of geodetic networks. Springer, Berlin

Teunissen PJG (1997a) A canonical theory for short GPS baselines. Part I: The baseline precision. J Geod 71(6):320–336

Teunissen PJG (1997b) A canonical theory for short GPS baselines. Part IV: Precision versus reliability. J Geod 71(9):513–525

Teunissen PJG (2000) Adjustment theory: an Introduction. Delft University Press, Series on Mathematical Geodesy and Positioning

Teunissen PJG, Khodabandeh A (2014) Do GNSS parameters always benefit from integer ambiguity resolution? a PPP-RTK network scenario. In: Proceedings of ION GNSS+. Tampa, Florida, pp 590–600

Teunissen PJG, Khodabandeh A (2015) Review and principles of PPP-RTK methods. J Geod 89(3):217–240

Teunissen PJG, Kleusberg A (1998) GPS for geodesy, 2nd edn. Springer, Berlin

Teunissen PJG, Odijk D, Zhang B (2010) PPP-RTK: results of CORS network-based PPP with integer ambiguity resolution. J Aeronaut Astronaut Aviat 42(4):223–229

Verhagen S (2002) Studying the performance of global navigation satellite systems: a new software tool. GPS world 13(6):60–65

Wielgosz P, Krankowski A, Sieradzki R, Grejner-Brzezinska DA (2008) Application of predictive regional ionosphere model to medium range RTK positioning. Acta Geophys 56(4):1147–1161

Wubbena G, Schmitz M, Bagg A (2005) PPP-RTK: precise point positioning using state-space representation in RTK networks. In: Proceedings of ION GNSS, pp 13–16

Yu X, Zhang X, Liu J, Shi J, Cai C, Gao Y (2011) Performance assessment of long-baseline integer ambiguity resolution with different observation models. In: Proceedings of ION GNSS, Portland, pp 688–698

Zhang B, Teunissen PJG, Odijk D (2011) A novel un-differenced PPP-RTK concept. J Navig 64(S1):S180–S191

Zhang X, Li P, Guo F (2013) Ambiguity resolution in precise point positioning with hourly data for global single receiver. Adv Space Res 51(1):153–161

Zumberge JF, Heflin MB, Jefferson DC, Watkins MM, Webb FH (1997) Precise point positioning for the efficient and robust analysis of GPS data from large networks. J Geophys Res 102:5005–5017

4 Array-based SPB determination (Part 1: Indexical presentation)

This chapter is covered by the following publication:

Khodabandeh A. (2014). Array-aided single-differenced satellite phase bias determination: methodology and results. ION GNSS+, 27:2523–2532. The Institute of Navigation, Florida, USA. ***Best Student Paper Award***

Array-aided single-differenced satellite phase bias determination: methodology and results

Amir Khodabandeh
GNSS Research Centre, Department of Spatial Sciences
Curtin University of Technology, Perth, Australia

BIOGRAPHY

Amir Khodabandeh received the MSc degree in Geodesy from University of Tehran, Iran, in 2011. He is currently pursuing the PhD degree at the GNSS Research Centre, Curtin University of Technology. His research interests comprise estimation theory, GNSS precise positioning and GNSS quality control.

ABSTRACT

Integer ambiguity resolution at a single GNSS receiver gets feasible, if network-derived satellite phase biases (SPBs), among other corrections, are a-priori available. In this paper, the concept of array-aided between-satellite single-differenced (SD) SPB determination is introduced which is aimed to reduce the code-dominated precision of SD-SPB corrections. The underlying model is realized by giving the role of the local reference network to an array of antennas, mounted on rigid platforms, that are separated by a few meters only. A closed-form expression of the array-aided SD-SPB corrections is presented, thereby proposing a simple strategy to compute the SD-SPBs. Upon resolving double-differenced ambiguities of the array's data, the variance of the SD-SPB corrections is shown to be reduced by a factor equal to the number of antennas. This improvement in precision is also affirmed by numerical results. Experimental results demonstrate that the user's integer-recovered ambiguities converge to integers faster, upon increasing the number of antennas aiding the SD-SPB corrections. Integrated with the ionospheric corrections, the stated SD-SPB corrections carry over the precision improvement to the user's position as well.

INTRODUCTION

Employing GNSS network-derived orbit/clock corrections, single-station precise point positioning (PPP) has proved to be an efficient technique [1, 2]. Biased by the real-valued (but time-constant) estimable ambiguities, the very precise phase observables would, however, not take a truly active part in estimating the user's position, unless a rather long convergence time takes place—longer than 30 min to attain sub-decimeter level of accuracy [3, 4]. Fast and centimeter level PPP would therefore get feasible, if the ambiguities are successfully resolved to integer values. Unfortunately, because of the presence of the satellite hardware biases in the phase and code data, the estimable between-satellite single-differenced (SD) ambiguities of the PPP user are not of an integer nature. In other words, the integer-valued ambiguities cannot be separated from these biases.

Recent contributions have demonstrated that the stated satellite hardware biases can be properly defined and estimated as the estimable satellite phase biases (also referred to as uncalibrated phase delays or fractional cycle biases), see e.g. [5–13]. Among which, reliable determination of the satellite phase biases (SPBs), on the basis of a local network of reference stations, is also acknowledged [14–16]. Given a-priori network-derived SPBs, the integer property of the user's SD ambiguities is thus recovered, giving rise to single-station integer ambiguity resolution. In this respect, the estimable SPBs are either presented in their undifferenced non-combined form [10, 14, 16], undifferenced combined form [15, 17], between-satellite SD non-combined form [18], between-satellite SD combined form [6, 12], or assimilated into the clocks defining decoupled phase clock parameters [7, 8, 13].

As shown in the contributions by [16, 18], the precision of the non-combined SPB corrections is governed by the code noise. Although significantly shortening the convergence time, PPP ambiguity resolution does therefore still take about 15 min of time to reliably fix the ambiguities to their integers, would no ionospheric corrections be applied [19]. Since a high code-dominated correlation between the SPB corrections and the ionospheric corrections exists, the noise of the code data is, however, canceled out when these two types of corrections are com-

bined to correct the user's phase data. The precision of the user's phase correction is then governed by the phase noise, thereby providing outcomes comparable to the network real-time kinematic solutions [18].

In this paper, the concept of array-aided between-satellite SD-SPB determination is introduced. We convey the idea of SPB determination to the case where the role of the local reference network is taken by an array of antennas, mounted on rigid platforms, that are separated by a few meters only [20, 21]. The objective of this study is twofold. First, an efficient strategy is sought to reduce the code-dominated noise of the SD-SPB corrections, expediting the convergence of the user's integer-recovered ambiguities over time. Second, the user's position improvement is aimed to be realized, once the array-aided SD-SPB corrections are combined with their ionospheric counterparts. We commence with a closed-form analytical expression of the SD-SPB corrections using one single antenna. The contribution of the aiding antennas to the precision of the SD-SPB corrections is then formulated. Upon resolving double-differenced (DD) ambiguities, the code-dominated variance of the SD-SPB corrections is shown to be reduced by a factor equal to the number of antennas. Thus the larger the number of antennas are utilized, the more precise the array-aided SD-SPB corrections become. Presenting a closed-form expression of the array-aided SD-SPB corrections, a simple algorithm to compute them is outlined afterwards. The performance of the proposed methodology is validated by a GPS campaign collecting dual-frequency data.

FULL-RANK MODEL

Consider a reference antenna, say $r = 1$, tracking dual-frequency GNSS data that are transmitted by satellite s and a chosen pivot satellite p. The corresponding between-satellite SD observation equations read then [22]

$$\begin{aligned} \mathsf{E}\{\underline{\phi}^{ps}_{1,j}\} &= \rho^{ps}_1 - \mu_j \iota^{ps}_1 + \lambda_j (a^{ps}_{1,j} - \delta^{ps}_{,j}) \\ \mathsf{E}\{\underline{p}^{ps}_{1,j}\} &= \rho^{ps}_1 + \mu_j \iota^{ps}_1 - d^{ps}_{,j} \end{aligned} \tag{1}$$

where $\underline{\phi}^{ps}_{1,j}$ and $\underline{p}^{ps}_{1,j}$ denote the between-satellite SD phase and code observables on the frequency band f_j ($j = 1,2$), respectively. The non-dispersive parameter ρ^{ps}_1 captures the SD geometric ranges, SD tropospheric delays, as well as the SD satellite clock parameters. The (first-order) SD slant ionospheric delay, experienced on the first frequency, is denoted by ι^{ps}_1. Thus the frequency-dependent coefficients are defined as the ratio $\mu_j = (f_1^2/f_j^2)$. Expressed in cycles, the SD ambiguity is composed of the integer-valued parameter $a^{ps}_{1,j}$ and the SD-SPB $\delta^{ps}_{,j}$ which are linked to the phase observables through the wavelength λ_j. Likewise, the SD satellite code hardware delays are denoted by $d^{ps}_{,j}$. Random variables are indicated by an underscore $(\underline{.})$, and $\mathsf{E}\{.\}$ denotes the expectation operator. We remark, apart from $a^{ps}_{1,j}$ and $\delta^{ps}_{,j}$, that the rest of the quantities have been expressed in units of range.

The observation equations, given in (1), do not represent a full-rank model, in the sense that the parameters involved cannot be separated from one another. It is therefore only possible to estimate combinations of the parameters. These estimable combinations are formed according to the minimum set of parameters which need to be lumped with the remaining parameters so that the underlying rank-deficiency is eliminated [9]. This minimum set of parameters is referred to as an $\mathcal{S}$-basis of the model defining a minimum number of constraints through which the model becomes of full-rank [23, 24].

As shown in [16, 18], the code hardware delays $d^{ps}_{,j}$ and the integer-valued ambiguities $a^{ps}_{1,j}$ can, for instance, be chosen as the $\mathcal{S}$-basis of the model. In doing so, we define the ionosphere-free (IF) and geometry-free (GF) combinations of $d^{ps}_{,j}$ ($j = 1,2$), respectively, as

$$\begin{aligned} d^{ps}_{,IF} &= \tfrac{\mu_2}{\mu_{12}} d^{ps}_{,1} - \tfrac{\mu_1}{\mu_{12}} d^{ps}_{,2}, \\ d^{ps}_{,GF} &= -\tfrac{1}{\mu_{12}} d^{ps}_{,1} + \tfrac{1}{\mu_{12}} d^{ps}_{,2}, \quad \text{with} \quad \mu_{12} = \mu_2 - \mu_1 \end{aligned} \tag{2}$$

On the basis of the above definition, the original code hardware delays stand in *one-to-one* correspondence with their IF and GF counterparts through

$$d^{ps}_{,j} = d^{ps}_{,IF} + \mu_j d^{ps}_{,GF}, \quad j = 1,2 \tag{3}$$

Clearly, the IF component $d^{ps}_{,IF}$ is absorbed by the non-dispersive parameter ρ^{ps}_1, while the GF component $d^{ps}_{,GF}$ is absorbed by the ionospheric delay ι^{ps}_1. This yields the following estimable combinations

$$\tilde{\rho}^{ps}_1 = \rho^{ps}_1 - d^{ps}_{,IF}, \qquad \tilde{\iota}^{ps}_1 = \iota^{ps}_1 - d^{ps}_{,GF} \tag{4}$$

Substituting $\rho^{ps}_1 = \tilde{\rho}^{ps}_1 + d^{ps}_{,IF}$ and $\iota^{ps}_1 = \tilde{\iota}^{ps}_1 + d^{ps}_{,GF}$ into (1), a full-rank model is then structured by lumping $a^{ps}_{1,j}$ with $\delta^{ps}_{,j}$, that is

$$\begin{aligned} \mathsf{E}\{\underline{\phi}^{ps}_{1,j}\} &= \tilde{\rho}^{ps}_1 - \mu_j \tilde{\iota}^{ps}_1 - \lambda_j \tilde{\delta}^{ps}_{,j} \\ \mathsf{E}\{\underline{p}^{ps}_{1,j}\} &= \tilde{\rho}^{ps}_1 + \mu_j \tilde{\iota}^{ps}_1, \end{aligned} \tag{5}$$

where the estimable SD-SPBs take the following form

$$\boxed{\tilde{\delta}^{ps}_{,j} = \delta^{ps}_{,j} - \tfrac{1}{\lambda_j} d^{ps}_{,IF} + \tfrac{\mu_j}{\lambda_j} d^{ps}_{,GF} - a^{ps}_{1,j}} \tag{6}$$

Therefore, the estimable SD-SPBs are composed of the *true* SD-SPBs, the SD satellite code hardware delays and

the SD ambiguities of the reference antenna. When expressed in units of range rather than in cycles, the above estimable SD-SPBs become indeed identical to those presented in [18].

METHODOLOGY

Single-antenna SD-SPB corrections

The number of observations in (5) is as many as the number of estimable parameters. In particular, the number of $\tilde{\delta}_{,j}^{ps}$ is equal to that of $\underline{\phi}_{1,j}^{ps}$ and, at the same time, the estimable SD-SPBs are not present in the code observables. The phase observables are thus fully reserved to determine the estimable SD-SPBs. As a consequence, the estimable parameters $\tilde{\rho}_1^{ps}$ and $\tilde{\imath}_1^{ps}$ are, respectively, determined by the IF and GF combinations of the code observables only, i.e.

$$\begin{aligned} \hat{\underline{\rho}}_1^{ps} &= \underline{p}_{1,IF}^{ps} = \tfrac{\mu_2}{\mu_{12}}\underline{p}_{1,1}^{ps} - \tfrac{\mu_1}{\mu_{12}}\underline{p}_{1,2}^{ps}, \\ \hat{\underline{\imath}}_1^{ps} &= \underline{p}_{1,GF}^{ps} = -\tfrac{1}{\mu_{12}}\underline{p}_{1,1}^{ps} + \tfrac{1}{\mu_{12}}\underline{p}_{1,2}^{ps}, \end{aligned} \tag{7}$$

with notation $\hat{\cdot}$ indicating the estimator of the quantities. Given the above code-based estimators, the single-antenna estimator of the estimable SD-SPBs follows from the first expression of (5), namely

$$\boxed{\hat{\underline{\delta}}_{,j}^{ps} = \tfrac{1}{\lambda_j}(\underline{p}_{1,IF}^{ps} - \mu_j \underline{p}_{1,GF}^{ps} - \underline{\phi}_{1,j}^{ps})} \tag{8}$$

Thus, in addition to the phase observables, the single-antenna SD-SPB estimator is a linear function of the IF and GF code combinations as well.

From single-epoch estimator to multi-epoch estimator

The estimator, given in (8), is based on data of one single epoch, i.e. the SD-SPBs are assumed to be unlinked in time. It is therefore referred to as the single-epoch estimator. In cases where information on the temporal behavior of the parameters, in (1), are assumed given, a joint estimation procedure of the estimable parameters, over time, must be applied [10]. In this study, we only assume the SD-SPBs, the SD satellite code hardware delays, along with the SD ambiguities to behave constant over time. The rest of the parameters are considered to be unlinked in time. Upon these assumptions, the multi-epoch estimator of the estimable SD-SPBs follows by weighted averaging its single-epoch counterparts over epochs, that is

$$\hat{\underline{\delta}}_{,j}^{ps}[k] = \frac{1}{\sum_{i=1}^{k} w_i^{ps}} \sum_{i=1}^{k} w_i^{ps}\, \hat{\underline{\delta}}_{,j}^{ps}(i) \tag{9}$$

where $\hat{\underline{\delta}}_{,j}^{ps}[k]$ denotes the multi-epoch estimator of the SD-SPBs over k epochs. The single-epoch estimator of the SD-SPBs, based on the data of epoch i, is denoted by $\hat{\underline{\delta}}_{,j}^{ps}(i)$. The nonnegative weights w_i^{ps} $(i = 1,\ldots,k)$ capture the dependency of the GNSS data on the satellites' elevation. Here we make use of the exponential elevation weighting strategy [25]. They are, namely, computed as

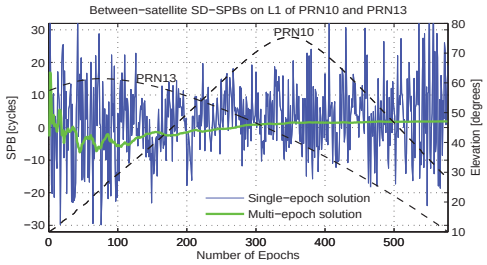

Figure 1. Single-epoch SD-SPB corrections (in blue) compared to its multi-epoch counterparts (in green) over time. Satellites' elevation is depicted in black dashed line.

$$w_i^{ps} = (\frac{1}{w_i^p} + \frac{1}{w_i^s})^{-1}, \tag{10}$$

with

$$w_i^q = [1 + 10\exp(-\frac{\varepsilon_i^q}{10^\circ})]^{-2}, \quad q = p,s \tag{11}$$

where ε_i^q is the elevation of satellite q [degree] at epoch i with respect to the reference antenna.

Fig. 1 shows typical examples of the single-epoch and multi-epoch versions of the SD-SPB corrections. It is observed that the size of the fluctuations of the single-epoch corrections increases as the elevation of the satellites decreases, showing the elevation dependency of the SD-SPB corrections. As the number of epochs increases, the multi-epoch SD-SPB corrections get more stable in time and converge to a constant value.

From non-combined SD-SPBs to combined SD-SPBs

The closed-form expression of (8) enables us to analyze the precision of the single-epoch single-antenna SD-SPB estimator. Consider GPS dual-frequency data where the code observables on both the frequencies are assumed to be uncorrelated and equally precise. Uncorrelated with the code data, the phase observables are also assumed to be uncorrelated and equally precise. Let σ_p and $\sigma_\phi = 0.01\sigma_p$ be the standard deviations of the between-satellite SD code and phase observables *in meters*, respectively. Then an application of the error propagation law to (8) gives

$$\sigma_{\hat{\underline{\delta}}_{,L1}^{ps}} \approx 26.95\,\sigma_p\ [cycle], \quad \sigma_{\hat{\underline{\delta}}_{,L2}^{ps}} \approx 26.75\,\sigma_p\ [cycle] \tag{12}$$

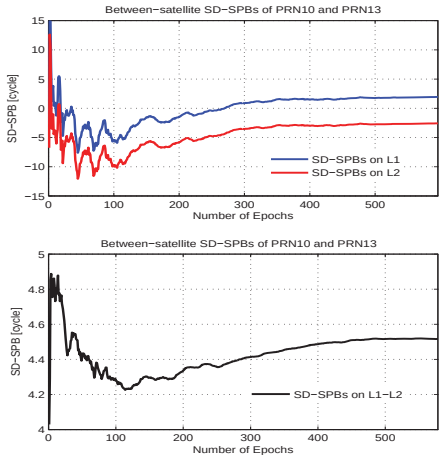

Figure 2. *Top-panel*: Multi-epoch SD-SPB corrections on L1 (in blue) and on L2 (in red). *Bottom-panel*: Multi-epoch SD-SPB corrections on L1-L2, i.e. wide-lane SD-SPB corrections (in black).

with $\sigma_{\tilde{\delta}^{ps}_{,L1}}$ and $\sigma_{\tilde{\delta}^{ps}_{,L2}}$ being, respectively, the standard deviations of the SD-SPBs on L1 and L2. Thus the precision of the non-combined SD-SPBs is heavily dominated by the noise of the code data. The error propagation law also provides us with the *cross-correlation* between the SD-SPBs on L1 and L2. The stated correlation is about 0.9996 which is indeed very significant. As shown in Fig. 2 (top-panel), the signatures of the SD-SPB corrections on both the frequencies are almost the same, corroborating that the SD-SPBs on L1 and L2 are highly correlated.

Of the combined SD-SPBs, we consider the wide-lane SD-SPBs that are defined as the between-frequency difference of the non-combined SD-SPBs (i.e. those on L1-L2). Given the standard deviations of the non-combined SD-SPBs (cf. (12)), together with their cross-correlation, the standard deviation of $\underline{\tilde{\delta}}^{ps}_{,L1-L2} = \underline{\tilde{\delta}}^{ps}_{,L1} - \underline{\tilde{\delta}}^{ps}_{,L2}$ is obtained as

$$\sigma_{\tilde{\delta}^{ps}_{,L1-L2}} \approx 0.83\,\sigma_p \;[cycle] \tag{13}$$

which is about 32 times smaller than those of the SD-SPBs on L1 and L2. The correlation between the SD-SPBs on L1 and L1-L2 is about 0.2581. As shown in Fig. 2 (bottom-panel), the size of the variations of the SD-SPB corrections on L1-L2 is much smaller than that of their non-combined counterparts, while their signature is quite different from that of L1 and L2. In order to appreciate the high correlation between SD-SPBs on L1 and L2, we therefore present those corresponding to L1 and L1-L2 in our further numerical results.

Array-aided SD-SPB corrections

To reduce the code-dominated noise of the SD-SPB corrections (cf. (12)), one may think of including the data of another antenna, say r ($r \neq 1$), for which a similar full-rank model can be formed by replacing subscript 1 with r in (5). As shown in (6), our earlier estimable SD-SPBs depend on the ambiguities of the reference antenna $a^{ps}_{1,j}$. The new full-rank model would, however, offer another form of the estimable SD-SPBs dependent on $a^{ps}_{r,j}$ instead, that is

$$\tilde{\tilde{\delta}}^{ps}_{,j} = \delta^{ps}_{,j} - \frac{1}{\lambda_j} d^{ps}_{,IF} + \frac{\mu_j}{\lambda_j} d^{ps}_{,GF} - a^{ps}_{r,j} \tag{14}$$

where their corresponding estimator reads (cf. (8))

$$\underline{\hat{\tilde{\delta}}}^{ps}_{,j} = \frac{1}{\lambda_j}(\underline{p}^{ps}_{r,IF} - \mu_j \underline{p}^{ps}_{r,GF} - \underline{\phi}^{ps}_{r,j}) \tag{15}$$

Comparing (14) with (6), these new estimable SD-SPBs are related to $\tilde{\delta}^{ps}_{,j}$ through

$$\tilde{\tilde{\delta}}^{ps}_{,j} = \tilde{\delta}^{ps}_{,j} - a^{ps}_{1r,j}, \tag{16}$$

with the DD ambiguities $a^{ps}_{1r,j} = a^{ps}_{r,j} - a^{ps}_{1,j}$.

According to (16), including the data of antenna r results in two additional equations $\underline{\hat{\tilde{\delta}}}^{ps}_{,j}$ ($j = 1,2$), given in (15), at the expense of two *unknown* DD ambiguities $a^{ps}_{1r,j}$ ($j = 1,2$). Therefore, as long as the DD ambiguities are unresolved, the extra antenna r has no contribution to the determination of the SD-SPBs $\tilde{\delta}^{ps}_{,j}$.

Let us, for the moment, assume $a^{ps}_{1r,j}$ to be successfully fixed to their integers $\check{a}^{ps}_{1r,j}$. With (8) and (15), we then arrive at the following equations

$$\begin{aligned} \mathsf{E}\{\underline{\hat{\tilde{\delta}}}^{ps}_{,j}\} &= \tilde{\delta}^{ps}_{,j} \\ \mathsf{E}\{\underline{\hat{\tilde{\delta}}}^{ps}_{,j}\} + \check{a}^{ps}_{1r,j} &= \tilde{\delta}^{ps}_{,j} \end{aligned} \tag{17}$$

in which the first expression characterizes the contribution of the reference antenna $r = 1$, while the second expression characterizes that of the extra antenna $r \neq 1$. Assuming the receivers/antennas of the *same* type, one can simply consider the average of the above two sets of equations as the improved estimator of the SD-SPB corrections $\tilde{\delta}^{ps}_{,j}$. The idea can be generalized to the case where the data of $n-1$ extra antennas $r = 2,\ldots,n$ are incorporated into the model. Given the resolved DD ambiguities, the array-aided SD-SPB estimator $\underline{\check{\tilde{\delta}}}^{ps}_{,j}$ reads then

$$\boxed{\underline{\check{\tilde{\delta}}}^{ps}_{,j} = \tfrac{1}{\lambda_j}(\underline{p}^{ps}_{\bar{r},IF} - \mu_j \underline{p}^{ps}_{\bar{r},GF} - \underline{\phi}^{ps}_{\bar{r},j}) + \check{a}^{ps}_{1\bar{r},j}} \tag{18}$$

Table 1. Information on the location/type/data of the receivers/antennas, date and sampling interval as used in the experiment.

	User data-set	Array data-set
Location:	Curtin Uni. (Lat: 32.01° S, Long: 115.89° E)	South Perth (Lat: 31.98° S, Long: 115.86° E)
Type of receiver/antenna:	Javad TRE_G3T Delta/Javad Grant G3	Javad TRE_G3T Delta/Javad Grant G3
Number of antennas:	1	4
Data:	GPS dual-frequency (C/A, P2, L1, L2)	GPS dual-frequency (C/A, P2, L1, L2)
Date and time:	12 September, 2013 (00:00:00-11:32:00 GPST)	12 September, 2013 (00:00:00-11:32:00 GPST)
Sampling interval:	30 seconds	30 seconds

in which the following quantities are introduced

$$\begin{aligned} \underline{p}^{ps}_{\bar{r},IF} &= \tfrac{1}{n}\sum_{r=1}^{n}\underline{p}^{ps}_{r,IF}, \qquad \underline{p}^{ps}_{\bar{r},GF} = \tfrac{1}{n}\sum_{r=1}^{n}\underline{p}^{ps}_{r,GF} \\ \underline{\phi}^{ps}_{\bar{r},j} &= \tfrac{1}{n}\sum_{r=1}^{n}\underline{\phi}^{ps}_{r,j}, \qquad \breve{a}^{ps}_{1\bar{r},j} = \tfrac{1}{n}\sum_{r=1}^{n}\breve{a}^{ps}_{1r,j} \end{aligned} \tag{19}$$

with $\breve{a}^{ps}_{11,j} = 0$.

Since the array-aided SD-SPB estimator $\underline{\breve{\delta}}^{ps}_{\cdot,j}$ is structured by the average of the data of n antennas, its variance is n times smaller than that of the single-antenna estimator $\underline{\hat{\delta}}^{ps}_{\cdot,j}$, provided that the data of all the antennas are equally precise. Thus their standard deviations are related to one another through

$$\sigma_{\underline{\breve{\delta}}^{ps}_{\cdot,j}} = \frac{1}{\sqrt{n}}\,\sigma_{\underline{\hat{\delta}}^{ps}_{\cdot,j}} \tag{20}$$

Array-based ambiguity-fixing

As stated before, the data of the extra antennas do not contribute to the determination of the SD-SPBs, would the DD ambiguities remain unresolved. This is why one needs the average of the resolved ambiguities $\breve{a}^{ps}_{1r,j}$ $(r = 1,\ldots,n)$ to form the array-aided SD-SPB estimator in (18).

Although GNSS ambiguity-fixing is generally a bit involved, the procedure gets, however, considerably easier if simplified assumptions are placed on the model. Here, we consider an array of antennas separated by a few meters only. In this case, almost the same ionospheric delays are experienced by the antennas, that is $\iota^{ps}_{1r} = \iota^{ps}_{r} - \iota^{ps}_{1} \approx 0$ $(r = 2,\ldots,n)$. Given information on the geometry of the satellites/antennas, the DD geometric ranges are computed, namely $\hat{\underline{\rho}}_{1r} = \hat{\underline{\rho}}_{r} - \hat{\underline{\rho}}_{1}$ $(r = 2,\ldots,n)$. The float DD ambiguities are then obtained as follows

$$\hat{\underline{a}}^{ps}_{1r,j} = \frac{1}{\lambda_j}(\underline{\phi}^{ps}_{1r,j} - \hat{\underline{\rho}}^{ps}_{1r}), \quad r = 2,\ldots,n \tag{21}$$

with $\hat{\underline{a}}^{ps}_{1r,j}$ and $\underline{\phi}^{ps}_{1r,j} = \underline{\phi}^{ps}_{r,j} - \underline{\phi}^{ps}_{1,j}$ being the DD float ambiguities and phase observables, respectively. Having successfully resolved the DD float ambiguities, the algorithmic steps in computing the array-aided SD-SPB corrections have been summarized in Fig. 3.

Input
- SD GNSS data: $\underline{\phi}^{ps}_{r,j}$, $\underline{p}^{ps}_{r,j}$ for $r = 1,\ldots,n;\ j = 1,2$
- DD geometric ranges ρ^{ps}_{1r} for $r = 2,\ldots,n$
- coefficients λ_j and μ_j for $j = 1,2$

Begin
- Form the IF and GF combinations $\underline{p}^{ps}_{r,IF}$ and $\underline{p}^{ps}_{r,GF}$ for $r = 1,\ldots,n$ (cf. (7))
- Compute the float ambiguities $\hat{\underline{a}}^{ps}_{1r,j}$ for $r = 2,\ldots,n;\ j = 1,2$ (cf. (21))
- Resolve $a^{ps}_{1r,j}$ and obtain $\breve{a}^{ps}_{1r,j}$ for $r = 1,\ldots,n;\ j = 1,2,$ with $\breve{a}^{ps}_{11,j} = 0$
- Compute the averages $\underline{\phi}^{ps}_{\bar{r},j}$, $\breve{a}^{ps}_{1\bar{r},j}$, $\underline{p}^{ps}_{\bar{r},IF}$, $\underline{p}^{ps}_{\bar{r},GF}$ for $j = 1,2$ (cf. (19))
- Compute $\underline{\breve{\delta}}^{ps}_{\cdot,j}$ for $j = 1,2$ (cf. (18))

End

Output
- Array-aided SD-SPB corrections $\underline{\breve{\delta}}^{ps}_{\cdot,j}$ $(j = 1,2)$

Figure 3. Algorithmic steps in computing the array-aided SD-SPBs of satellite s, given the pivot satellite p.

NUMERICAL RESULTS

Experiment description

In this section, the methodology discussed above is evaluated by an array-based experiment organized by Curtin University in Perth, Australia. Table 1 presents the information on the collected data. Two GPS dual-frequency data-sets have been collected by 5 Javad receivers of the same type: 1) the array data-set of 4 antennas and 2) the user data-set of 1 antenna. The structure of the array and user has been visualized in Fig. 4. The array was located in Foreshore, South Perth, whereas the user station was set up at Bentley campus of Curtin University. The distance between the reference antenna of the array and the user antenna is about 4 [km]. All the data have been measured above a cut-off elevation of 10° with a sampling interval of 30 seconds. The array data-set is aimed to determine the SD-SPB corrections, while the user data-set is aimed to show the applicability of the stated corrections.

SD-SPB's precision improvement

We first consider the results of the array data-set. To gain some insight into the dependency of the SD-SPBs' preci-

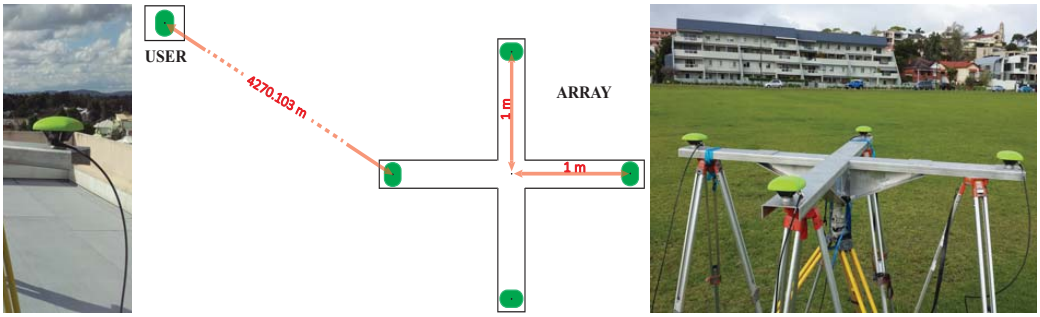

Figure 4. Structure of the user (left) and the array of antennas (right) as used in the experiment. The array is composed of four 1-meter arms. The distance between the user's antenna and the reference antenna of the array is about 4270 meters.

sion on the number of antennas, time-series of the single-epoch SD-SPB estimator have been presented. It is clear that the size of the fluctuations of each time-series gives an impression of the noise of the corresponding SD-SPB corrections. Shown in Fig. 5 are the time-series of the SD-SPB corrections as a function of the number of antennas. The results correspond to PRN23, given PRN13 as the pivot satellite. The noise reduction can be observed as the number of antennas increases from $n = 1$ (red line) to $n = 4$ (green line). This is the case with both the SD-SPBs on L1 and on L1-L2.

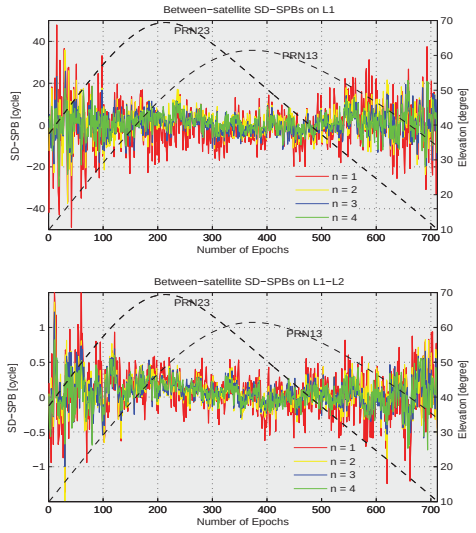

Figure 5. Single-epoch SD-SPB corrections on L1 (*top*) and on L1-L2 (*bottom*) over time as a function of the number of antennas (n). The results correspond to PRN23, given PRN13 as the pivot satellite. Satellites' elevation is depicted in black dashed line.

To quantify the noise of the single-epoch SD-SPB corrections, we make use of the root mean squared error (RMSE) of the time-series. The RMSE of the single-epoch array-aided SD-SPBs are given in Table 2. As shown, the RMSE of the single-antenna SD-SPBs on L1 is computed as 10.89 [cycle] which is almost 32 times larger than that of the SD-SPBs on L1-L2 (0.34 [cycle]). This is in agreement with the theoretical value already inferred from (12) and (13). According to (20), one would expect the ratio of the RMSE of the array-aided SD-SPBs to that of the single-antenna SD-SPBs to be approximated by $(1/\sqrt{n})$. The RMSE ratios have been compared to their theoretical counterparts in Table 2. As shown, the RMSE ratios and the theoretical values do interestingly coincide. In particular, we highlight that the RMSE of the single-epoch SD-SPBs on L1 decreases from 10.89 [cycle] to almost half its value, i.e. 5.52 [cycle].

A similar analysis has been carried out for other pairs of satellites. The results of the analysis are summarized in Fig. 6. The theoretical value $(1/\sqrt{n})$, depicted in green line, serves as reference. As illustrated, the RMSE ratios follow the reference trend dictated by the theoretical value.

Table 2. RMSE of the single-epoch SD-SPB corrections corresponding to PRN13 and PRN23 for different number of antennas. The RMSE ratio has been compared to its theoretical value $(1/\sqrt{n})$.

No. of antennas	$n = 1$		$n = 2$		$n = 3$		$n = 4$	
	L1	L1-L2	L1	L1-L2	L1	L1-L2	L1	L1-L2
RMSE [cycle]	10.89	0.34	7.74	0.23	6.34	0.20	5.52	0.18
RMSE ratio	1.00	1.00	0.71	0.68	0.58	0.59	0.51	0.53
Theoretical value	1.00	1.00	0.71	0.71	0.58	0.58	0.50	0.50

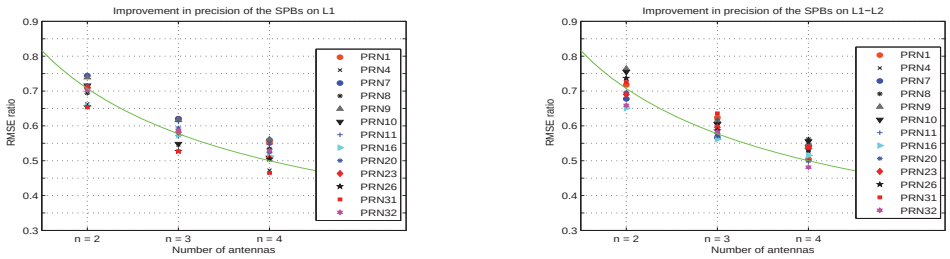

Figure 6. RMSE ratio of the array-aided SD-SPB corrections on L1 (left) and on L1-L2 (right), compared to the theoretical value $(1/\sqrt{n})$ (green line). PRN13 has been taken as the pivot satellite.

Integer recovery of the user's ambiguities

We now turn our attention to the results of the user data-set. Forming the between-satellite SD combinations of the user's observations, the receiver-specific unknown parameters are removed. Like the array data-set, the satellite positions have been computed using the orbits of the IGS. The estimable between-satellite SD satellite clocks and ionospheric delays have been estimated using the array data-set and sent to the user according to the strategy as described in [16, 18]. Since the distance between the array and the user is about 4 [km], correcting the user's data by the same ionospheric delays, estimated at the array's location, is realistically allowed. Corrected by the array-derived satellite clocks and ionospheric delays, the SD observation equations of the user only include the position and real-valued SD ambiguities as unknowns.

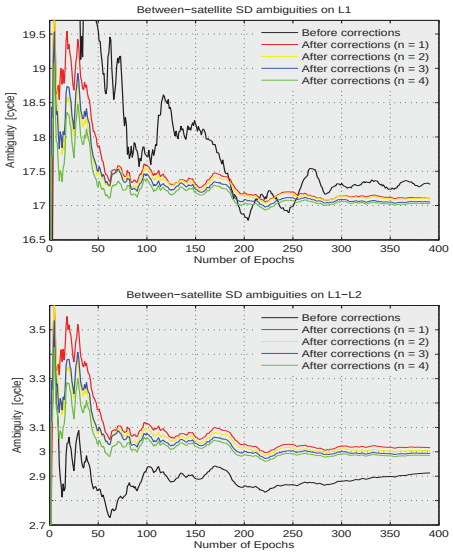

Figure 7. Convergence of the user's SD ambiguities on L1 (*top*) and on L1-L2 (*bottom*) over time. The results correspond to PRN32, given PRN13 as the pivot satellite.

We now evaluate the integer recovery role of the SD-SPB corrections. To do so, we consider the convergence of the user's SD ambiguities over time, once without applying the SD-SPB corrections, and another time with applying the SD-SPB corrections. The corresponding results have been illustrated in Fig. 7. It is clearly visible that the SD ambiguities, without corrections, do not tend to integer values. Corrected by the SD-SPBs however, the integer property of the SD ambiguities is recovered and they do indeed converge to integer values.

In view of the SD-SPBs' precision improvement discussed earlier, one would expect that the array-aided SD-SPBs expedite the ambiguities' convergence compared to the single-antenna SD-SPBs. This has been realized in Fig. 7. For instance, the minimum number of epochs after which the user's SD ambiguities on L1 never exceed half a cycle beyond the integer 17 is computed as $k = 118$ (for $n = 1$). This minimum number of epochs deceases to $k = 103$ (for $n = 2$), $k = 72$ (for $n = 3$), and $k = 44$ (for $n = 4$).

To see the improvement on the estimated user's position, the array-derived ionospheric corrections have been estimated and sent to the user, once based on the data of the reference antenna (i.e. $n = 1$), and another time based on the inclusion of the data of the other antennas (i.e. $n = 2,3,4$). The integer-recovered ambiguities have been then fixed epoch-by-epoch using the LAMBDA method [26]. Fig. 8 shows the North-East scatter of the estimated user's position before ambiguity-fixing (float case) and after ambiguity-fixing (fixed case). The results are accompanied by their corresponding 95% confidence ellipses. In both the float and fixed cases, the improvement occurs by switching from the single-antenna corrections ($n = 1$) to the array-aided corrections ($n = 4$). This is in agreement with the concept of *array-aided precise*

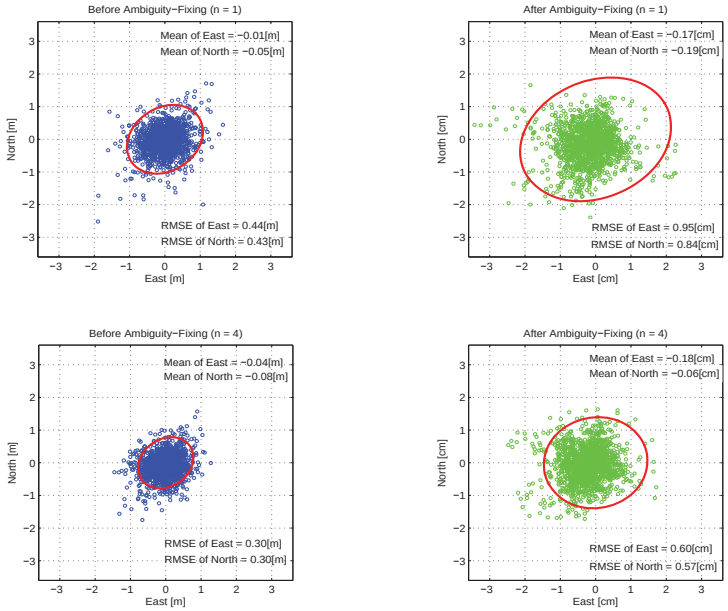

Figure 8. *Top-panel*: North-East position scatter of the user before (left) and after (right) ambiguity-fixing, on the basis of the single-antenna corrections ($n = 1$). *Bottom-panel*: North-East position scatter of the user before (left) and after (right) ambiguity-fixing, on the basis of the array-aided corrections ($n = 4$). The corresponding 95% confidence ellipses are depicted in red lines.

point positioning (A-PPP) which is originally introduced by [20]. In a more quantitative way, Table 3 presents the RMSE of the user's position components as a function of the number of antennas aiding the ionospheric and SD-SPB corrections.

We also remark that the significant improvement in the position upon ambiguity-fixing is due to the high precision of the phase observations which contribute to the model once the integer-recovered ambiguities are successfully resolved. This again confirms the applicability of the array-aided SPBs in recovering the integer property of the user's ambiguities

Table 3. RMSE of the user's position before ambiguity-fixing (*Float*: in centimeters) and after ambiguity-fixing (*Fixed*: in millimeters) based on the array-aided corrections of different number of antennas.

No. of antennas	$n = 1$		$n = 2$		$n = 3$		$n = 4$	
	Float	Fixed	Float	Fixed	Float	Fixed	Float	Fixed
RMSE of East	43.6	9.5	40.2	9.3	34.5	7.6	30.2	6.0
RMSE of North	43.4	8.4	39.2	7.9	34.4	7.1	29.8	5.7
RMSE of UP	98.1	21.2	89.3	19.3	86.7	16.1	83.9	14.0

SUMMARY AND CONCLUSIONS

In this contribution, we introduced the concept of array-aided between-satellite SD-SPBs determination. The underlying model is characterized by data of an array of GNSS antennas, mounted on rigid platforms, that are separated by short distances so that the same ionospheric delay is assumed to be experienced by all the antennas. Forming a full-rank GNSS model, the estimable SD-SPBs were shown to appear, for instance, as a combination of the true SD-SPBs, the SD satellite code hardware delays, and the SD ambiguities of a reference antenna. A closed-form expression of the array-aided SD-SPB corrections was presented through which a simple strategy to compute the SD-SPBs was outlined.

The closed-form expression of the SD-SPB estimator allows us to study the precision of the SD-SPB corrections analytically. In case of GPS dual-frequency data, the high positive correlation between the non-combined SD-SPBs on L1 and on L2 was quantified (about 0.9996), thus highlighting the existence of more precise combined SD-SPBs. It was shown that the standard deviation of the wide-lane SD-SPBs (on L1-L2) is expected to be almost 32 times smaller than that of their non-combined counter-

parts. Moreover, the cross-correlation between the wide-lane SD-SPBs and those on L1 is expected to be about 0.2581.

In order to reduce the code-dominated variance of the SD-SPB corrections, the data of extra antennas are incorporated into the model. As shown, the extra antennas give additional information on the SD-SPBs at the expense of additional unknowns, i.e. the array's DD ambiguities. After resolving the DD ambiguities of the array's data, the extra antennas do contribute to the precision of the SD-SPBs. With n being the number of all contributing antennas, the variance of the array-aided SD-SPB corrections is n times smaller than that of the single-antenna SD-SPB corrections. This precision improvement was also demonstrated by numerical results. As a consequence of which, the integer-recovered ambiguities of the user converge to integer values faster, upon increasing the number of aiding antennas. As a typical example, it was shown that the minimum number of epochs, say k, after which the user's SD ambiguities on L1 never exceed half a cycle beyond an integer was decreased from $k = 118$ (for $n = 1$) to $k = 44$ (for $n = 4$). The precision improvement can also be carried over to the user's position, would the array-aided SD-SPB corrections be accompanied by the ionospheric corrections.

ACKNOWLEDGEMENTS

The array-based experiment was conducted by Dr. N. Raziq and Dr. B. Padovan from Curtin University, Perth, Australia. This support is gratefully acknowledged.

REFERENCES

[1] P. Heroux and J. Kouba, "GPS precise point positioning with a difference," in *Paper presented at Geomatics 95, Ottawa, Canada*, pages 13–15, 1995.

[2] J. F. Zumberge, M. B. Heflin, D. C. Jefferson, M. M. Watkins, and F. H. Webb, "Precise point positioning for the efficient and robust analysis of GPS data from large networks," *J. Geophys. Res.*, vol. 102, pages 5005–5017, 1997.

[3] R. F. Leandro, M. C. Santos, and R. B. Langley, "Analyzing GNSS data in precise point positioning software," *GPS Solut.*, vol. 15, no. 1, pages 1–13, 2011.

[4] R. J. van Bree and C. C. Tiberius, "Real-time single-frequency precise point positioning: accuracy assessment," *GPS Solut.*, vol. 16, no. 2, pages 259–266, 2012.

[5] M. J. Gabor and R. S. Nerem, "Satellite-satellite single-difference phase bias calibration as applied to ambiguity resolution," *Navigation*, vol. 49, no. 4, pages 223–242, 2002.

[6] M. Ge, G. Gendt, M. Rothacher, C. Shi, and J. Liu, "Resolution of GPS carrier-phase ambiguities in precise point positioning (PPP) with daily observations," *J. Geod.*, vol. 82, no. 7, pages 389–399, 2008.

[7] D. Laurichesse, F. Mercier, J. Berthias, P. Broca, L. Cerri, and F. CNES, "Integer ambiguity resolution on undifferenced GPS phase measurements and its application to PPP and satellite precise orbit determination," *Navigation*, vol. 56, no. 2, pages 135–149, 2009.

[8] P. Collins, S. Bisnath, F. Lahaye, and P. Heroux, "Undifferenced GPS ambiguity resolution using the decoupled clock model and ambiguity datum fixing," *Navigation*, vol. 57, no. 2, pages 123–135, 2010.

[9] P. J. G. Teunissen, D. Odijk, and B. Zhang, "PPP-RTK: Results of CORS Network-Based PPP with Integer Ambiguity Resolution," *J. Aeronaut. Astronaut. Aviat.*, vol. 42, no. 4, pages 223–229, 2010.

[10] P. Henkel, Z. Wen, and C. Gunther, "Estimation of satellite and receiver biases on multiple Galileo frequencies with a Kalman filter," in *ION Proceedings of the 2010 International Technical Meeting of The Institute of Navigation, CA*, pages 1067–1074, 2010.

[11] S. Bisnath and P. Collins, "Recent developments in precise point positioning," *Geomatica*, vol. 66, no. 2, pages 103–111, 2012.

[12] J. Geng, C. Shi, M. Ge, A. H. Dodson, Y. Lou, Q. Zhao, and J. Liu, "Improving the estimation of fractional-cycle biases for ambiguity resolution in precise point positioning," *J. Geod.*, vol. 86, no. 8, pages 579–589, 2012.

[13] S. Loyer, F. Perosanz, F. Mercier, H. Capdeville, and J.-C. Marty, "Zero-difference GPS ambiguity resolution at CNES–CLS IGS Analysis Center," *J. Geod.*, vol. 86, no. 11, pages 991–1003, 2012.

[14] Z. Wen, P. Henkel, and C. Gunther, "Reliable estimation of phase biases of GPS satellites with a local reference network," in *ELMAR, 2011 Proceedings, Croatia*, pages 321–324, IEEE, 2011.

[15] X. Li and X. Zhang, "Improving the estimation of uncalibrated fractional phase offsets for PPP ambiguity resolution," *J. Navig.*, vol. 65, no. 03, pages 513–529, 2012.

[16] D. Odijk, P. J. G. Teunissen, and B. Zhang, "Single-frequency integer ambiguity resolution enabled GPS precise point positioning," *J. Surv. Eng.*, vol. 138, no. 4, pages 193–202, 2012.

[17] X. Zhang, P. Li, and F. Guo, "Ambiguity resolution in precise point positioning with hourly data for global single receiver," *Adv. Space Res.*, vol. 51, no. 1, pages 153 – 161, 2013.

[18] D. Odijk, P. J. G. Teunissen, and A. Khodabandeh, "Single-Frequency PPP-RTK: Theory and Experimental Results," *IAG Symp*, vol. 139, pages 167–173, 2014.

[19] X. Li, X. Zhang, and M. Ge, "Regional reference network augmented precise point positioning for instantaneous ambiguity resolution," *J. Geod.*, vol. 85, no. 3, pages 151–158, 2011.

[20] P. J. G. Teunissen, "A-PPP: Array-aided Precise Point Positioning with Global Navigation Satellite Systems," *IEEE Trans. Signal Process*, vol. 60, no. 6, pages 2870–2881, 2012.

[21] A. Khodabandeh and P. J. G. Teunissen, "Single-Epoch GNSS Array Integrity: an Analytical Study," *IAG Symp*, vol. 142, 2015. In press.

[22] B. Hofmann-Wellenhof, H. Lichtenegger, and E. Wasle, *GNSS: Global Navigation Satellite Systems: GPS, Glonass, Galileo, and More*. Springer, New York, 2008.

[23] P. J. G. Teunissen, "Generalized inverses, adjustment, the datum problem and S-transformations," in *Optimization and Design of Geodetic Networks* (E. W. Grafarend and F. Sanso, eds.), pages 11–55, Springer, Berlin, 1985.

[24] P. J. de Jonge, *A processing strategy for the application of the GPS in networks*. PhD thesis, Delft University of Technology, Publication on Geodesy, 46, Netherlands Geodetic Commission, Delft, 1998.

[25] H. J. Euler and C. C. Goad, "On optimal filtering of GPS dual frequency observations without using orbit information," *J. Geod.*, vol. 65, no. 2, pages 130–143, 1991.

[26] P. J. G. Teunissen, "The least-squares ambiguity decorrelation adjustment: a method for fast GPS integer ambiguity estimation," *J. Geod.*, vol. 70, no. 1-2, pages 65–82, 1995.

5 Array-based SPB determination (Part 2: Multivariate presentation)

This chapter is covered by the following publication:

Khodabandeh A. and Teunissen P.J.G. (2014a). Array-based satellite phase bias sensing: theory and GPS/BeiDou/QZSS results. Measurement Science and Technology, 25,095801 (11pp). IOP, UK.

IOP Publishing Measurement Science and Technology
Meas. Sci. Technol. **25** (2014) 095801 (11pp) doi:10.1088/0957-0233/25/9/095801

Array-based satellite phase bias sensing: theory and GPS/BeiDou/QZSS results

A Khodabandeh[1] **and P J G Teunissen**[1,2]

[1] Department of Spatial Sciences, Curtin University of Technology, Perth, Australia
[2] Department of Geoscience and Remote Sensing, Delft University of Technology, Delft, The Netherlands

E-mail: amir.khodabandeh@curtin.edu.au and p.teunissen@curtin.edu.au

Received 28 April 2014, revised 12 June 2014
Accepted for publication 13 June 2014
Published 22 July 2014

Abstract

Single-receiver integer ambiguity resolution (IAR) is a measurement concept that makes use of network-derived non-integer satellite phase biases (SPBs), among other corrections, to recover and resolve the integer ambiguities of the carrier-phase data of a single GNSS receiver. If it is realized, the very precise integer ambiguity-resolved carrier-phase data would then contribute to the estimation of the receiver's position, thus making (near) real-time precise point positioning feasible. Proper definition and determination of the SPBs take a leading part in developing the idea of single-receiver IAR. In this contribution, the concept of array-based between-satellite single-differenced (SD) SPB determination is introduced, which is aimed to reduce the code-dominated precision of the SD-SPB corrections. The underlying model is realized by giving the role of the local reference network to an array of antennas, mounted on rigid platforms, that are separated by short distances so that the same ionospheric delay is assumed to be experienced by all the antennas. To that end, a closed-form expression of the array-aided SD-SPB corrections is presented, thereby proposing a simple strategy to compute the SD-SPBs. After resolving double-differenced ambiguities of the array's data, the variance of the SD-SPB corrections is shown to be reduced by a factor equal to the number of antennas. This improvement in precision is also affirmed by numerical results of the three GNSSs GPS, BeiDou and QZSS. Experimental results demonstrate that the integer-recovered ambiguities converge to integers faster, upon increasing the number of antennas aiding the SD-SPB corrections.

Keywords: GNSS, precise point positioning (PPP), single-receiver integer ambiguity resolution (IAR), single-differenced satellite phase bias (SD-SPB)

(Some figures may appear in colour only in the online journal)

1. Introduction

Precise point positioning (PPP) of a single GNSS receiver has found a widespread usage in various geoscience and atmospheric disciplines [1, 2]. The technique relies on the carrier-phase and code data of a single receiver, profiting from network-derived corrections for satellite orbits, clocks and (sometimes) atmospheric delays [3, 4]. Taking advantage of the millimeter-level precision of the carrier-phase data, the aim is to precisely position the location of a user. Since the carrier-phase data are biased by the real-valued (but time-constant) ambiguities, they would, however, not take a truly active part in estimating the user's position, unless a rather long convergence time takes place—longer than 30 min to attain sub-decimeter level of accuracy [5, 6]. Fast and centimeter level PPP would therefore get feasible, if the ambiguities are successfully resolved to integer values. Unfortunately, because of the presence of the satellite hardware biases in the carrier-phase and code data, the estimable between-satellite single-differenced (SD) ambiguities of the PPP user are not of an integer nature. In other words, the integer-valued ambiguities cannot be separated from these biases.

Recent contributions have demonstrated that the stated satellite hardware biases can be properly defined and estimated as the estimable satellite phase biases (also referred to as uncalibrated phase delays or fractional cycle biases), see

e.g. [7–13]. Given a-priori network-derived SPBs, the integer property of the user's SD ambiguities is thus recovered, giving rise to single-receiver integer ambiguity resolution (IAR). In this respect, the estimable SPBs are either presented in their undifferenced form [14–16], undifferenced between-frequency-combined form [17, 18], between-satellite SD form [19], between-satellite SD between-frequency-combined form [8, 12], or assimilated into the clocks defining decoupled phase clock parameters [9, 10, 13].

As shown in the contributions by [16, 19], the precision of the SPB corrections is governed by the code noise. Although significantly shortening the convergence time, PPP ambiguity resolution does therefore still take about 15 min of time to *reliably* fix the ambiguities to their integers, would no ionospheric corrections be applied [20].

In this paper, the concept of array-based between-satellite SD-SPB determination is introduced. We convey the idea of SPB determination to the case where the role of the local reference network is taken by an array of antennas, mounted on rigid platforms, that are separated by short distances so that the same ionospheric delay is assumed to be experienced by all the antennas [21]. The objective of this study is to develop an efficient strategy to reduce the code-dominated noise of the SD-SPB corrections, expediting the convergence of the user's integer-recovered ambiguities over time. To that end, *closed-form* analytical expressions of the SD-SPB corrections are presented and the dependency of SD-SPB precision on the number of aiding antennas is analyzed. Upon resolving double-differenced (DD) ambiguities, the code-dominated variance of the SD-SPB corrections is shown to be reduced by a factor equal to the *number of antennas*. Thus the larger the number of antennas are utilized, the more precise the array-aided SD-SPB corrections become.

The paper is organized as follows. In section 2, a full-rank model of the single-antenna observation equations is presented. We show that the estimable SD-SPB is, in fact, a combination of the true SD-SPB, the SD satellite code hardware delay, and the SD ambiguity of a reference antenna. Analytical SD-SPB estimators are presented in section 3. We commence with the corrections provided by a single antenna. The insensitivity of the single-antenna SD-SPB corrections to the dispersive and non-dispersive effects is pointed out. In particular, we show that the single-antenna SD-SPB corrections are nothing else, but linear functions of the code multipath equations. The contribution of the aiding antennas to the precision of the SD-SPB corrections is then formulated. It is shown that including the data of the aiding antennas results in the same number of unknowns, i.e. the DD ambiguities. Provided that no further information is available, the contribution of the aiding antennas would thus not make any sense unless the DD ambiguities are successfully resolved. Presenting a closed-form expression of the array-aided SD-SPB corrections, a simple algorithm to compute them is outlined afterwards. Finally in section 4, the performance of the proposed methodology is validated by a GPS/BeiDou/QZSS campaign collecting dual-frequency data.

We make use of the following notation: Random variables are distinguished by an underscore. Thus $\underline{x}$ is random, while x is not. The expectation of $\underline{x}$ is denoted by $E\{\underline{x}\}$, while its standard deviation is denoted by σ_x. The identity matrix and the summation vector (vector of ones) are, respectively, denoted as I and e, where their dimension is indicated by the subscripts. The $\tilde{}$ symbol is used to indicate the estimable combinations, while the $\hat{}$ symbol and $\check{}$ symbol are used to indicate the estimators before and after IAR, respectively. The antenna, satellite and frequency indexes are, respectively, denoted by $r = 1, \ldots, n$; $s = 1, \ldots, m$ and $j = 1, 2$. Throughout the text, we make use of the Kronecker matrix product $\otimes$. For its properties, we refer to, e.g. [22, 23].

2. Single-antenna full-rank model

Consider a reference antenna, say $r = 1$, tracking dual-frequency GNSS data of the rover satellite s, given the pivot satellite $s = 1$. The between-satellite SD observation equations of the satellite pairs $1s$ ($s = 2, \ldots, m$) read then [24]

$$\begin{aligned} E\left\{\underline{\phi}_{1,j}^{1s}\right\} &= \rho_1^{1s} - \mu_j \imath_1^{1s} + \lambda_j\left(a_{1,j}^{1s} - \delta_j^{1s}\right) \\ E\left\{\underline{p}_{1,j}^{1s}\right\} &= \rho_1^{1s} + \mu_j \imath_1^{1s} - d_j^{1s} \end{aligned} \tag{1}$$

where $\underline{\phi}_{1,j}^{1s}$ and $\underline{p}_{1,j}^{1s}$ denote the between-satellite SD phase and code observables on frequency j ($j = 1, 2$), respectively. The non-dispersive parameter ρ_1^{1s} captures the SD geometric ranges, SD tropospheric delays, as well as the SD satellite clock parameters. The (first-order) SD slant ionospheric delay, experienced on the first frequency, is denoted by $\imath_1^{1s}$. Expressed in cycles, the SD ambiguity is composed of the integer-valued parameter $a_{1,j}^{1s}$ and the SD-SPB δ_j^{1s} which are linked to the phase observables through the wavelength Λ_j. Likewise, the SD satellite code hardware delays are denoted by d_j^{1s}. The frequency-dependent coefficients are defined as the ratio $\mu_j = \lambda_j^2 / \lambda_1^2$. We remark, apart from $a_{1,j}^{1s}$ and δ_j^{1s}, that the rest of the quantities have been expressed in units of range.

Multivariate representation

In the remainder of this paper, we make of use the more compact multivariate notation, just for the sake of presentation. In doing so, we define the SD phase observation vector as $\underline{\phi}_1 = \left[\underline{\phi}_{1,1}^T, \underline{\phi}_{1,2}^T\right]^T$, with $\underline{\phi}_{1,j}$ ($j = 1, 2$) being a vector, of size $m - 1$, which contains $\underline{\phi}_{1,j}^{1s}$ ($s = 2, \ldots, m$). The SD code observations vector $\underline{p}_1$ is defined similarly. With these in mind, the multivariate version of (1) can be stated as

$$\begin{aligned} E\left\{\underline{\phi}_1\right\} &= [e_2 \otimes I_{m-1}]\rho_1 - [\mu \otimes I_{m-1}]\imath_1 + [\Lambda \otimes I_{m-1}](a_1 - \delta) \\ E\{\underline{p}_1\} &= [e_2 \otimes I_{m-1}]\rho_1 + [\mu \otimes I_{m-1}]\imath_1 - d \end{aligned} \tag{2}$$

where the vectors ρ_1 and $\imath_1$, of size $m - 1$, contain ρ_1^{1s} and $\imath_1^{1s}$ ($s = 2, \ldots, m$), respectively. The 2×2 diagonal matrix Λ contains the wavelengths λ_j ($j = 1, 2$), while the frequency-dependent vector is defined as $\mu = [\mu_1, \mu_2]^T$. The SD ambiguity vector is defined as $a_1 = \left[a_{1,1}^T, a_{1,2}\right]^T$, with $a_{1,j}$ ($j = 1, 2$) being a vector, of size $m - 1$, which contains $a_{1,j}^{1s}$ ($s = 2, \ldots, m$). The vectors of the SD-SPBs δ and the SD satellite code hardware delays d are defined similarly.

The observation equations, given in (2), do not represent a *full-rank* model, in the sense that the parameters involved cannot be separated from one another. It is therefore only possible to estimate combinations of the parameters. These estimable combinations are formed according to the minimum set of parameters which need to be lumped with the remaining parameters so that the underlying rank-deficiency is eliminated [11]. This minimum set of parameters is referred to as an $\mathcal{S}$-basis of the model defining a minimum number of constraints through which the model becomes of full-rank [25, 26].

As shown in [16, 19], the code hardware delays d and the integer-valued ambiguities a_1 can, for instance, be chosen as the $\mathcal{S}$-basis of the model. In doing so, we define the ionosphere-free (IF) and geometry-free (GF) combinations of d, respectively, as

$$d_{\mathrm{IF}} = \left[\mu_{\mathrm{IF}}^T \otimes I_{m-1}\right] d, \quad \text{with} \quad \mu_{\mathrm{IF}} = \frac{1}{\mu_{12}}[\mu_2, -\mu_1]^T$$
$$d_{\mathrm{GF}} = \left[\mu_{\mathrm{GF}}^T \otimes I_{m-1}\right] d, \quad \text{with} \quad \mu_{\mathrm{GF}} = \frac{1}{\mu_{12}}[-1, 1]^T \quad (3)$$

where $\mu_{12} = \mu_2 - \mu_1$.

On the basis of the above definition, the original code hardware delays stand in *one-to-one* correspondence with their IF and GF counterparts through

$$d = [e_2 \otimes I_{m-1}]\, d_{\mathrm{IF}} + [\mu \otimes I_{m-1}]\, d_{\mathrm{GF}}, \quad (4)$$

since $e_2\mu_{\mathrm{IF}}^T + \mu\mu_{\mathrm{GF}}^T = I_2$.

With the aid of the representation (4), it is evident that the IF component d_{IF} is absorbed by the non-dispersive vector ρ_1, while the GF component d_{GF} is absorbed by the ionospheric delays $\imath_1$. This yields the following estimable combinations

$$\tilde{\rho}_1 = \rho_1 - d_{\mathrm{IF}}, \qquad \tilde{\imath}_1 = \imath_1 - d_{\mathrm{GF}}. \quad (5)$$

Substituting $\rho_1 = \tilde{\rho}_1 + d_{\mathrm{IF}}$ and $\imath_1 = \tilde{\imath}_1 + d_{\mathrm{GF}}$ into (2), a full-rank model is then structured by lumping a_1 with δ, that is

$$E\left\{\underline{\phi}_1\right\} = [e_2 \otimes I_{m-1}]\,\tilde{\rho}_1 - [\mu \otimes I_{m-1}]\,\tilde{\imath}_1 - [\Lambda \otimes I_{m-1}]\,\tilde{\delta}$$
$$E\{\underline{p}_1\} = [e_2 \otimes I_{m-1}]\,\tilde{\rho}_1 + [\mu \otimes I_{m-1}]\,\tilde{\imath}_1, \quad (6)$$

where the estimable SD-SPBs take the following form

$$\tilde{\delta} = \delta - L_p d - a_1, \quad \text{with}$$
$$L_p = \Lambda^{-1}\left(e_2\mu_{\mathrm{IF}}^T - \mu\mu_{\mathrm{GF}}^T\right) \otimes I_{m-1}. \quad (7)$$

Therefore, the estimable SD-SPBs are composed of the *true* SD-SPBs δ, the SD satellite code hardware delays d and the SD ambiguities of the reference antenna a_1. When expressed in units of range rather than in cycles, the above estimable SD-SPBs become indeed identical to those presented in [19].

3. Analytical solution to the SD-SPB corrections

3.1. Single-antenna SD-SPB corrections

The number of observations in (6) is as many as the number of estimable parameters. In particular, the number of $\tilde{\delta}$ is equal to that of $\underline{\phi}_1$ and, at the same time, the estimable SD-SPBs are not present in the code observables. The phase observables are thus fully reserved to determine the estimable SD-SPBs. As a consequence, the estimable parameters $\tilde{\rho}_1$ and $\tilde{\imath}_1$ are, respectively, determined by the IF and GF combinations of the code observables only, i.e.

$$\widehat{\underline{\tilde{\rho}}}_1 = \left[\mu_{\mathrm{IF}}^T \otimes I_{m-1}\right]\underline{p}_1, \qquad \widehat{\underline{\tilde{\imath}}}_1 = \left[\mu_{\mathrm{GF}}^T \otimes I_{m-1}\right]\underline{p}_1. \quad (8)$$

Given the above code-based estimators, the single-antenna estimator of the estimable SD-SPBs follows from the first expression of (6), namely (Appendix A)

$$\widehat{\underline{\tilde{\delta}}} = L_p\underline{p}_1 - L_\phi\underline{\phi}_1, \quad \text{with} \quad L_\phi = \Lambda^{-1} \otimes I_{m-1}. \quad (9)$$

Thus, in addition to the phase observables, the single-antenna SD-SPB estimator is a linear function of the IF and GF code combinations as well.

3.1.1. Relation to the code multipath equations. According to (6), any non-dispersive bias, equally experienced by both the code and phase observations, would be absorbed by the non-dispersive parameter $\tilde{\rho}_1$. Likewise, any dispersive bias, equally experienced by both the code and phase observations, would be absorbed by the dispersive parameter $\tilde{\imath}_1$. This, namely, shows that the SD-SPB estimator is *insensitive* to any non-dispersive and dispersive unmodeled effects. In case unwanted effects only affect, for instance, the code observations however, the outcome of the SD-SPB estimator would change. Of these types of effects, the code multipath is well-known. A traditional diagnostic tool for tracing possible code multipath effects is to check the time-stability of the so-called multipath equations [27]. Using the expressions L_p and L_ϕ, respectively, given in (7) and (9), the code multipath equations can be expressed as [28, p 224]

$$\underline{\eta} = \underline{p}_1 - L_\phi^{-1}L_p\underline{\phi}_1. \quad (10)$$

It is not difficult to verify the identity $L_pL_\phi^{-1}L_p = L_\phi$. With this mind, pre-multiplying the preceding equation by L_p, together with (9), establishes a one-to-one relationship between the SD-SPB estimator and the code multipath as follows

$$\widehat{\underline{\tilde{\delta}}} = L_p\underline{\eta} \Leftrightarrow \underline{\eta} = L_p^{-1}\widehat{\underline{\tilde{\delta}}}. \quad (11)$$

This indeed shows that the SD-SPB corrections are nothing else but linear functions of the code multipath equations. Figure 1 illustrates the SD-SPB corrections on B_1 of BeiDou geostationary satellites C01 and C05 as well as the corresponding SD multipath combinations over time. The adverse effect of the multipath, i.e. the periodic behavior, is clearly observed in both the SD-SPB corrections and the multipath combinations. In other words, the SD-SPB corrections can be directly affected by the code multipath.

3.1.2. From single-epoch estimator to multi-epoch estimator. The estimator, given in (9), is based on data of one single epoch, i.e. the SD-SPBs are assumed to be *unlinked* in time. It is therefore referred to as the *single-epoch* estimator. In cases where information on the temporal behavior of the parameters, in (2), are assumed given, a joint estimation procedure of the estimable parameters, over time, must be applied [14]. In this study, we only assume the SD-SPBs δ, the SD satellite code hardware delays d, along with the SD ambiguities a_1 to behave constant over time.

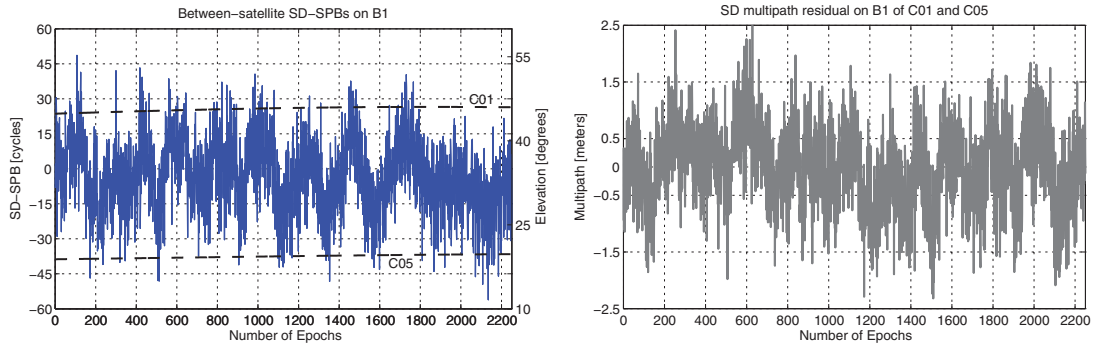

Figure 1. *Left*: SD-SPB corrections on B1 $\left(\underline{\widehat{\breve{\delta}}}_{,B_1}\right)$ corresponding to BeiDou geostationary satellites C01 and C05 over time. Satellites' elevation is depicted in black dashed line. *Right*: the associated SD multipath combinations $\left(\underline{\eta}_{,B_1}\right)$.

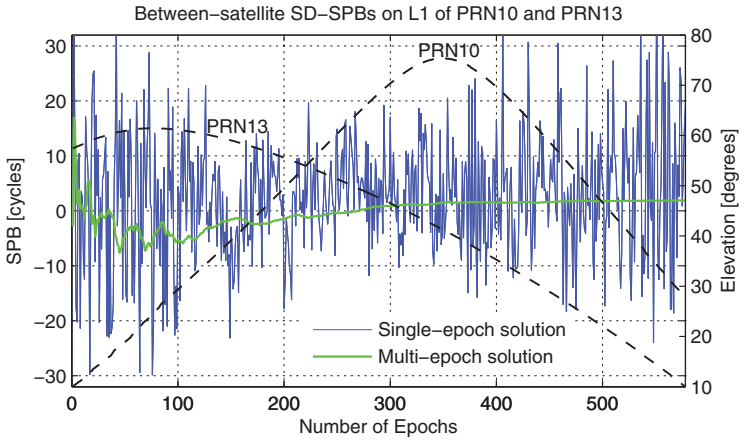

Figure 2. GPS single-epoch SD-SPB corrections $\underline{\widehat{\breve{\delta}}}_{,L_1}(i)$ (in blue) compared to its multi-epoch counterparts $\underline{\widehat{\breve{\delta}}}_{,L_1}[k]$ (in green) over time. Satellites' elevation is depicted in black dashed line.

The rest of the parameters are considered to be unlinked in time. Upon these assumptions, the *multi-epoch* estimator of the estimable SD-SPBs follows by weighted averaging its single-epoch counterparts over epochs, that is

$$\underline{\widehat{\breve{\delta}}}\,[k] = \frac{1}{k}\sum_{i=1}^{k}\left[I_2 \otimes \overline{W}_{[k]}^{-1} W_i\right]\underline{\widehat{\breve{\delta}}}\,(i), \quad \text{with}$$
$$\overline{W}_{[k]} = \frac{1}{k}\sum_{i=1}^{k} W_i \tag{12}$$

where $\underline{\widehat{\breve{\delta}}}\,[k]$ denotes the multi-epoch estimator of the SD-SPBs over k epochs. The single-epoch estimator of the SD-SPBs, based on the data of epoch i, is denoted by $\underline{\widehat{\breve{\delta}}}\,(i)$. The $(m-1) \times (m-1)$ diagonal weight matrices W_i $(i = 1, \ldots, k)$ contain the nonnegative coefficients w_i^{1s} $(s = 2, \ldots, m)$ capturing the dependency of the GNSS data on the satellites' elevation. Here we make use of the exponential elevation weighting strategy [29]. They are, namely, computed as

$$w_i^{1s} = \left(\frac{1}{w_i^1} + \frac{1}{w_i^s}\right)^{-1}, \tag{13}$$

with

$$w_i^s = \left[1 + 10\exp\left(-\frac{\epsilon_i^s}{10^\circ}\right)\right]^{-2}, \quad s = 1, \ldots, m \tag{14}$$

where ϵ_i^s is the elevation of satellite s [degree] at epoch i with respect to the reference antenna.

Figure 2 shows typical examples of the single-epoch and multi-epoch versions of the SD-SPB corrections. It is observed that the size of the fluctuations of the single-epoch corrections increases as the elevation of the satellites decreases, showing the elevation dependency of the SD-SPB corrections. As the number of epochs increases, the multi-epoch SD-SPB corrections get more stable in time and converge to a constant value.

3.1.3. From non-combined SD-SPBs to combined SD-SPBs. The closed-form expression of (9) enables us to analyze the precision of the single-epoch single-antenna SD-SPB estimators. The precision analysis can be conducted for those on the original frequencies (i.e. the non-combined SD-SPBs) as well as for those on a linear combinations of the frequencies (i.e. the combined SD-SPBs). Consider GPS dual-frequency

Table 1. GPS/BeiDou wavelengths λ_j and frequency-dependent coefficients μ_j (dual-frequency scenario).

	L1	L2	B1	B2
λ_j (cm)	19.03	24.42	19.20	24.83
μ_j	1	1.6467	1	1.6724

data where the code observables on both the frequencies are assumed to be uncorrelated and equally precise. Uncorrelated with the code data, the phase observables are also assumed to be uncorrelated and equally precise. Let σ_p and $\sigma_\phi = 0.01\sigma_p$ be the standard deviations of the between-satellite SD code and phase observables *in meters*, respectively. Using the coefficients λ_j and μ_j of GPS/BeiDou systems as given in table 1, an application of the error propagation law to (9) gives

$$\sigma_{\hat{\breve{\delta}},L1} \approx 26.95\sigma_p \text{ [cycle]}, \quad \sigma_{\hat{\breve{\delta}},L2} \approx 26.75\sigma_p \text{ [cycle]}$$
$$\sigma_{\hat{\breve{\delta}},B1} \approx 25.85\sigma_p \text{ [cycle]}, \quad \sigma_{\hat{\breve{\delta}},B2} \approx 25.64\sigma_p \text{ [cycle]}. \quad (15)$$

Thus the precision of the non-combined SD-SPBs is heavily dominated by the noise of the code data. The error propagation law also provides us with the *cross-correlation* between the SD-SPBs on L1/B1 and L2/B2. In case of GPS, the stated correlation is about 0.9996, whereas in case of BeiDou, the correlation is about 0.9918. As shown in figure 3 (left-panel), the signatures of the SD-SPB corrections on both the frequencies are almost the same, corroborating that the SD-SPBs on L1/B1 and L2/B2 are *highly* correlated.

Of the combined SD-SPBs, one can, for instance, consider the *wide-lane* SD-SPBs that are defined as the between-frequency difference of the non-combined SD-SPBs (i.e. those on L1-L2 and on B1-B2). Given the standard deviations of the non-combined SD-SPBs (see (15)), together with their cross-correlation, the standard deviation of the wide-lane SD-SPBs is obtained as

$$\sigma_{\hat{\breve{\delta}},L1-L2} \approx 0.83\sigma_p \text{ [cycle]}, \quad \sigma_{\hat{\breve{\delta}},B1-B2} \approx 0.84\sigma_p \text{ [cycle]} \quad (16)$$

which is roughly 32 times smaller than those of the non-combined SD-SPBs. As shown in figure 3 (right-panel), the size of the variations of the SD-SPB corrections on L1-L2 is much smaller than that of their non-combined counterparts.

3.2. Array-aided SD-SPB corrections

To reduce the code-dominated noise of the SD-SPB corrections (see (15)), one may think of including the data of another antenna, say r ($r \neq 1$), for which a similar full-rank model can be formed by replacing subscript 1 with r in (6). As shown in (7), our earlier estimable SD-SPBs depend on the ambiguities of the *reference* antenna a_1. The new full-rank model would, however, offer *another* form of the estimable SD-SPBs dependent on a_r instead, that is

$$\breve{\tilde{\delta}} = \delta - L_p d - a_r \quad (17)$$

where their corresponding estimator reads (see (9))

$$\underline{\hat{\breve{\delta}}} = L_p \underline{p}_r - L_\phi \underline{\phi}_r \quad (18)$$

Comparing (17) with (7), these new estimable SD-SPBs are related to $\tilde{\delta}$ through

$$\breve{\tilde{\delta}} = \tilde{\delta} - a_{1r}, \quad (19)$$

with the DD ambiguities $a_{1r} = a_r - a_1$.

According to (19), including the data of antenna r results in $2(m-1)$ additional equations $\underline{\hat{\breve{\delta}}}$, given in (18), at the expense of $2(m-1)$ *unknown* DD ambiguities a_{1r}. Therefore, as long as the DD ambiguities are unresolved, the extra antenna r has no contribution to the determination of the SD-SPBs $\tilde{\delta}$.

Let us, for the moment, assume a_{1r} to be successfully fixed to their integers $\breve{a}_{1r}$. With (9) and (18), we then arrive at the following equations

$$\begin{aligned} E\{\underline{\hat{\breve{\delta}}}\} &= \tilde{\delta} \\ E\{\underline{\hat{\breve{\delta}}}\} + \breve{a}_{1r} &= \tilde{\delta} \end{aligned} \quad (20)$$

in which the first expression characterizes the contribution of the reference antenna $r = 1$, while the second expression characterizes that of the extra antenna $r \neq 1$. Assuming the receivers/antennas of the *same* type, one can simply consider the *average* of the above two sets of equations as the improved estimator of the SD-SPB corrections $\tilde{\delta}$. The idea can be generalized to the case where the data of $n-1$ extra antennas $r = 2, \ldots, n$ are incorporated into the model. Given the resolved DD ambiguities, the *array-aided* SD-SPB estimator $\underline{\breve{\tilde{\delta}}}$ reads then

$$\underline{\breve{\tilde{\delta}}} = L_p \underline{p}_{\bar{r}} - L_\phi \underline{\phi}_{\bar{r}} + \breve{a}_{1\bar{r}} \quad (21)$$

in which the following quantities are introduced

$$\underline{p}_{\bar{r}} = \frac{1}{n}\sum_{r=1}^{n} \underline{p}_r, \ \underline{\phi}_{\bar{r}} = \frac{1}{n}\sum_{r=1}^{n} \underline{\phi}_r, \ \breve{a}_{1\bar{r}} = \frac{1}{n}\sum_{r=1}^{n} \breve{a}_{1r} \quad (22)$$

with $\breve{a}_{11} = 0$.

3.2.1. Array-based ambiguity-fixing.

As stated before, the data of the extra antennas do not contribute to the determination of the SD-SPBs, would the DD ambiguities remain unresolved. This is why one needs the average of the resolved ambiguities $\breve{a}_{1r}$ ($r = 1, \ldots, n$) to form the array-aided SD-SPB estimator in (21).

Although GNSS ambiguity-fixing is generally a bit involved, the procedure gets, however, considerably easier if simplified assumptions are placed on the model. Here, we consider an array of antennas, separated by short distances, so that the same ionospheric delay is assumed to be experienced by all the antennas [21], that is $\imath_{1r} = \imath_r - \imath_1 \approx 0$ ($r = 2, \ldots, n$). Given information on the geometry of the satellites/antennas, the DD geometric ranges are computed, namely $\hat{\rho}_{1r} = \hat{\rho}_r - \hat{\rho}_1$ ($r = 2, \ldots, n$). The float DD ambiguities are then obtained as follows [30, p 390]

$$\hat{a}_{1r} = L_\phi \left\{ \underline{\phi}_{1r} - [e_2 \otimes I_{m-1}] \underline{\hat{\rho}}_{1r} \right\}, \quad r = 2, \ldots, n \quad (23)$$

with $\hat{a}_{1r}$ and $\underline{\phi}_{1r} = \underline{\phi}_r - \underline{\phi}_1$ being the DD float ambiguities and phase observables, respectively. Having successfully resolved

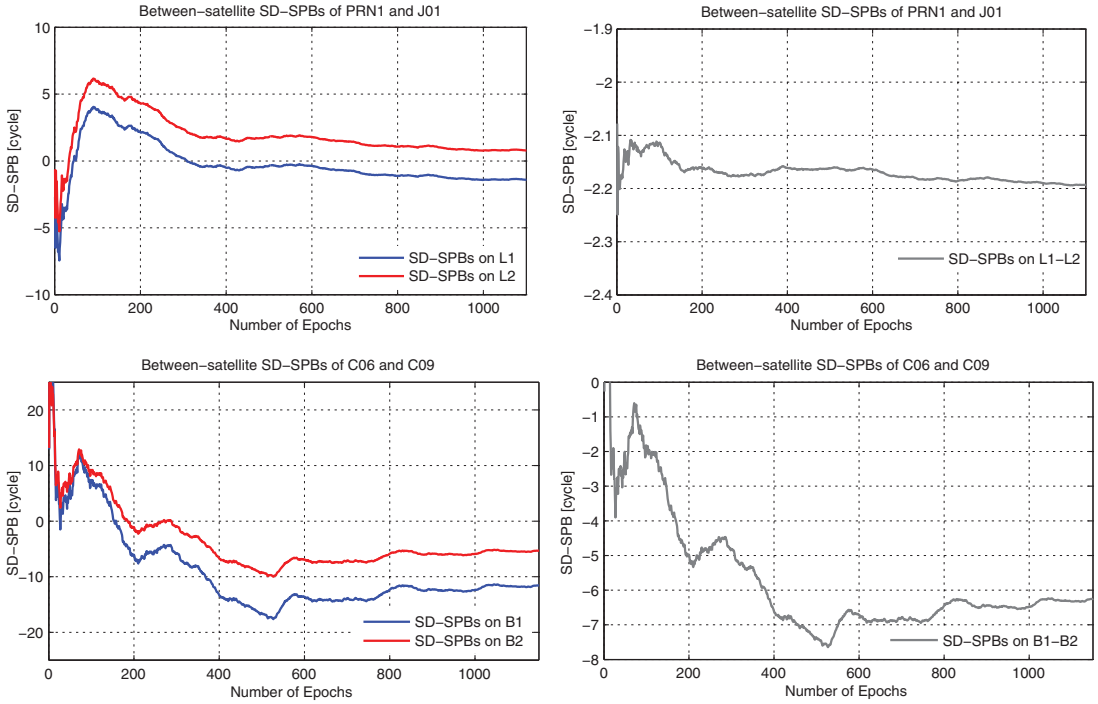

Figure 3. *Top-left*: multi-epoch SD-SPB corrections on L1 (in blue) and on L2 (in red) of GPS. *Top-right*: multi-epoch SD-SPB corrections on L1-L2, i.e. wide-lane SD-SPB corrections (in gray) of GPS. *Bottom-left*: multi-epoch SD-SPB corrections on B1 (in blue) and on B2 (in red) of BeiDou. *Bottom-right*: multi-epoch SD-SPB corrections on B1-B2, i.e. wide-lane SD-SPB corrections (in gray) of BeiDou.

the DD float ambiguities, the algorithmic steps in computing the array-aided SD-SPB corrections have been summarized in figure 4.

3.3. Superiority of the array-aided SD-SPB corrections

3.3.1. Superiority in precision. Since the array-aided SD-SPB estimator $\underline{\check{\hat{\delta}}}$ is structured by the average of the data of n antennas, its variance is n times smaller than that of the single-antenna estimator $\underline{\hat{\delta}}$, provided that the data of all the antennas are equally precise. Thus their standard deviations are related to one another through

$$\sigma_{\check{\hat{\delta}}_{,j}} = \frac{1}{\sqrt{n}}\,\sigma_{\hat{\delta}_{,j}}, \quad j = 1,\ 2. \tag{24}$$

3.3.2. Superiority in expediting the convergence of the user's ambiguities.
As a direct consequence of better precision of the array-aided SD-SPB estimator as compared to its single-antenna counterpart, the integer-recovered user ambiguities converge to their integers faster, would they be corrected by the array-aided SD-SPB corrections. Let k_n be the minimum number of epochs at which the user's ambiguity of the satellite pair $1s$ on frequency j, recovered by the array-aided SD-SPBs, meets certain precision. The ratio of k_n to its corresponding single-antenna version, say k_1, can be formulated as (Appendix A)

$$\frac{k_n}{k_1} = \frac{n\alpha + 1}{n(1+\alpha)}\,\frac{\overline{w}^{1s}_{[k_1]}}{\overline{w}^{1s}_{[k_n]}}, \quad \text{with} \quad \overline{w}^{1s}_{[k_n]} = \frac{1}{k_n}\sum_{i=1}^{k_n} w_i^{1s} \tag{25}$$

where the scalar α denotes the variance-ratio of the data of the user antenna to those of the array's reference antenna.

The preceding equation does in fact show that the reduction in the convergence time $1 - (k_n/k_1)$ depends on the three contributing factors, namely, (1) the elevation of the satellite pair $1s$ characterized by $\left(\overline{w}^{1s}_{[k_1]}/\overline{w}^{1s}_{[k_n]}\right)$, (2) the quality of the user data with respect to the array data characterized by α, and 3) the number of aiding antennas n. As a special case where no elevation weighting is applied (i.e. $\overline{w}^{1s}_{[k_n]} = \overline{w}^{1s}_{[k_1]}$) and the user receiver/antenna is of the same type as the array receiver/antenna (i.e. $\alpha = 1$), the equation is simplified to

$$\frac{k_n}{k_1} = \frac{n+1}{2n} \quad \text{or} \quad 1 - \frac{k_n}{k_1} = \frac{n-1}{2n}. \tag{26}$$

Since $(n-1)/(2n)$ is a monotonically increasing function of n, the more the number antennas are employed, the larger the reduction in the convergence time $1 - (k_n/k_1)$ (thus the faster the convergence time) becomes. In the case where the number of antennas n is large enough, the convergence time can therefore be reduced up to 50%. We remark that the expression (25) is restricted to the ambiguity convergence on a *single* frequency.

Input

- SD GNSS data: $\underline{\phi}_{r,j}$, $\underline{p}_{r,j}$ for $r = 1,\ldots,n;\ j = 1,2$
- DD geometric ranges $\hat{\underline{\rho}}_{1r} = \hat{\underline{\rho}}_r - \hat{\underline{\rho}}_1$ for $r = 2,\ldots,n$
- coefficients λ_j and μ_j for $j = 1,2$

Begin

- Form the IF and GF combinations for $r = 1,\ldots,n$ as:

$$\underline{p}_{r,IF} = \tfrac{\mu_2}{\mu_{12}}\underline{p}_{r,1} - \tfrac{\mu_1}{\mu_{12}}\underline{p}_{r,2}$$
$$\underline{p}_{r,GF} = -\tfrac{1}{\mu_{12}}\underline{p}_{r,1} + \tfrac{1}{\mu_{12}}\underline{p}_{r,2}$$

- Compute the float ambiguities $\hat{\underline{a}}_{1r} = [\hat{\underline{a}}^T_{1r,1},\ \hat{\underline{a}}^T_{1r,2}]^T$ for $r = 2,\ldots,n$ according to (23)
- Resolve a_{1r} and obtain $\check{a}_{1r} = [\check{a}^T_{1r,1},\ \check{a}^T_{1r,2}]^T$ for $r = 1,\ldots,n$, with $\check{a}_{11} = 0$
- Compute the averages $\underline{\phi}_{\bar{r}}$, $\check{a}_{1\bar{r}}$, $\underline{p}_{\bar{r},IF}$, $\underline{p}_{\bar{r},GF}$ over $r = 1,\ldots,n$
- Compute $\check{\underline{\delta}}_{,j} = \frac{1}{\lambda_j}(\underline{p}_{\bar{r},IF} - \mu_j\underline{p}_{\bar{r},GF} - \underline{\phi}_{\bar{r},j}) + \check{a}_{1\bar{r},j}$ for $j = 1,2$

End

Output

- Array-aided SD-SPB corrections $\check{\underline{\delta}} = [\check{\underline{\delta}}^T_{,1},\ \check{\underline{\delta}}^T_{,2}]^T$

Figure 4. Algorithmic steps in computing the array-aided SD-SPBs.

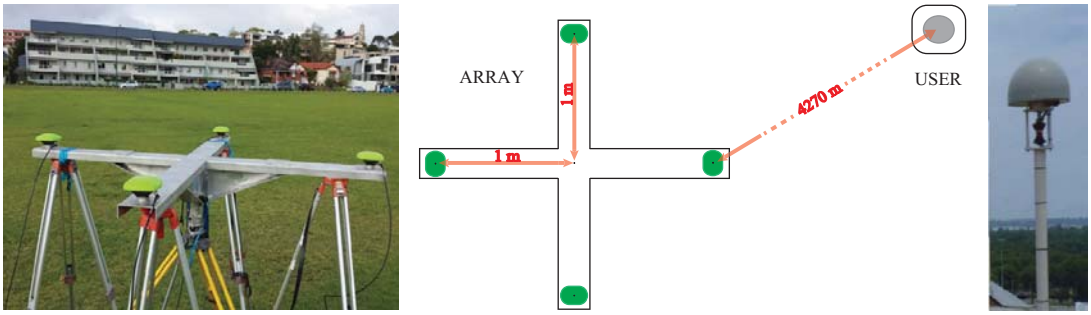

Figure 5. Structure of the array of antennas (left) and the user (right) as used in the experiment. The distance between the user's antenna and the reference antenna of the array is about 4270 m.

The convergence does indeed improve, would information about the ambiguities on both frequencies be considered.

4. Numerical results

4.1. Experiment description

In this section, the methodology discussed above is evaluated by an array-based experiment organized by Curtin University in Perth, Australia on 12 September 2013. Two GPS/BeiDou dual-frequency data-sets have been collected by 5 GNSS receivers: (1) the array data-set of 4 Javad receivers (TRE-G3T Delta) of the same antennas and (2) the user data-set of 1 Trimble receiver (NETR9). The frequencies considered are L1 and L2 (transmitted by GPS) as well as B1 and B2 (transmitted by BeiDou). In one case, the L1/L2 data of the single QZSS satellite J01 is also considered. The structure of the array and user has been visualized in figure 5. The array was located in Foreshore, South Perth, whereas the user station was set up at Bentley campus of Curtin University. The distance between the reference antenna of the array and the user antenna is about 4 km. All the data have been measured above a cut-off elevation of 10° with a sampling interval of 10 s during 00:00:00–11:32:00 in GPS time. The array data-set is aimed to determine the SD-SPB corrections, while the user data-set is aimed to show the applicability of the stated corrections.

4.2. SD-SPB's precision improvement

We first consider the results of the array data-set. To gain some insight into the dependency of the SD-SPBs' precision on the number of antennas, time-series of the single-epoch SD-SPB estimator have been presented. It is clear that the size of the fluctuations of each time-series gives an impression of the noise of the corresponding SD-SPB corrections. Shown in figure 6 are the time-series of the SD-SPB corrections as a function of the number of antennas. The results correspond

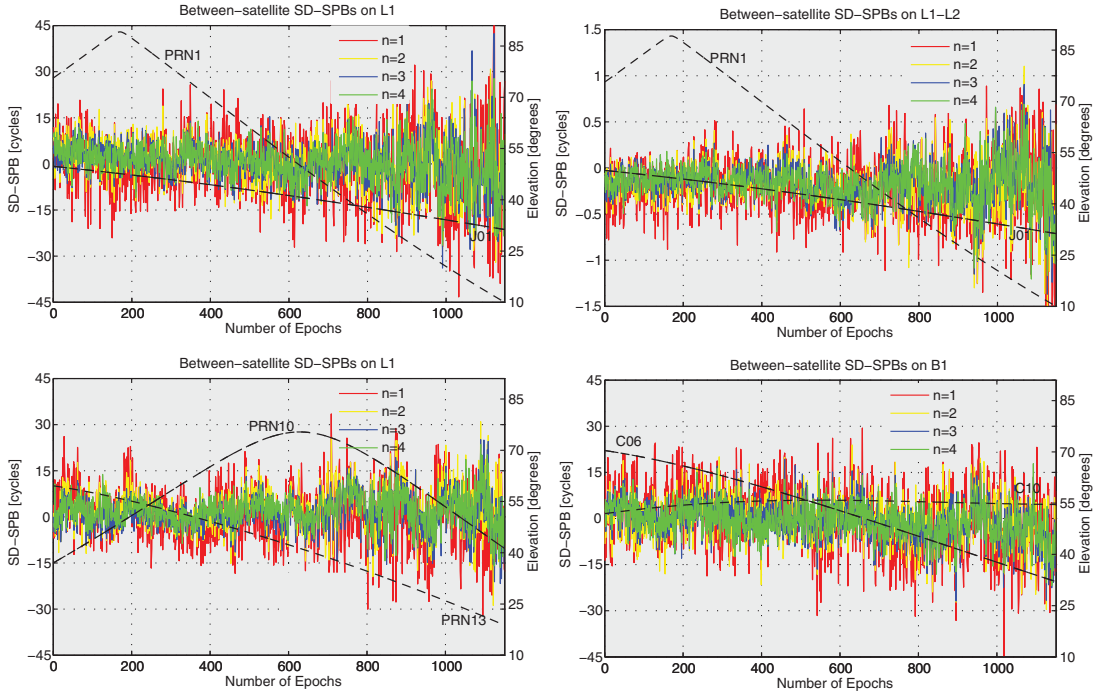

Figure 6. Single-epoch SD-SPB corrections over time as a function of the number of antennas (n); *top-left*: between QZSS and GPS PRN1 on L1; *top-right*: between QZSS and GPS PRN1 on L1-L2; *bottom-left*: between GPS PRN10 and PRN13 on L1; *bottom-right*: between BeiDou C06 and C10 on B1.

Table 2. RMSE of the single-epoch SD-SPB corrections corresponding to GPS PRN10 and PRN13 for different number of antennas. The RMSE ratio has been compared to its theoretical value ($1/\sqrt{n}$).

	$n=1$		$n=2$		$n=3$		$n=4$	
No. of antennas	L1	L1-L2	L1	L1-L2	L1	L1-L2	L1	L1-L2
RMSE [cycle]	10.77	0.36	7.88	0.25	6.42	0.22	5.71	0.19
RMSE ratio	1.00	1.00	0.73	0.69	0.60	0.61	0.53	0.53
Theoretical value	1.00	1.00	0.71	0.71	0.58	0.58	0.50	0.50

Table 3. RMSE of the single-epoch SD-SPB corrections corresponding to BeiDou C06 and C10 for different number of antennas. The RMSE ratio has been compared to its theoretical value ($1/\sqrt{n}$).

	$n=1$		$n=2$		$n=3$		$n=4$	
No. of antennas	B1	B1-B2	B1	B1-B2	B1	B1-B2	B1	B1-B2
RMSE [cycle]	12.05	0.43	8.87	0.31	7.41	0.26	6.53	0.23
RMSE ratio	1.00	1.00	0.74	0.72	0.61	0.60	0.54	0.53
Theoretical value	1.00	1.00	0.71	0.71	0.58	0.58	0.50	0.50

to QZSS satellite J01, GPS satellites PRN1, PRN10, PRN13 and BeiDou satellites C06, C10. In all these cases, these noise reduction can be observed as the number of antennas increases from $n = 1$ (red line) to $n = 4$ (green line).

To quantify the noise of the single-epoch SD-SPB corrections, we make use of the root mean squared error (RMSE) of the time-series. The RMSE of the single-epoch array-aided SD-SPBs of GPS and BeiDou are, respectively, given in tables 2 and 3. As shown, for instance, the RMSE of the single-antenna SD-SPBs on L1 is computed as 10.77 [cycle] which is almost 32 times larger than that of the SD-SPBs on L1-L2 (0.36 [cycle]). This is in agreement with the theoretical value already inferred from (15) and (16). According to (24), one would expect the ratio of the RMSE of the array-aided SD-SPBs to that of the single-antenna SD-SPBs to be approximated by ($1/\sqrt{n}$). The RMSE ratios have been compared to their theoretical counterparts in tables 2 and 3. As shown, the RMSE ratios and the theoretical values, to a large extent, coincide. In case of GPS, the RMSE of the single-epoch SD-SPBs on L1 decreases from 10.77 [cycle] to almost *half* its value,

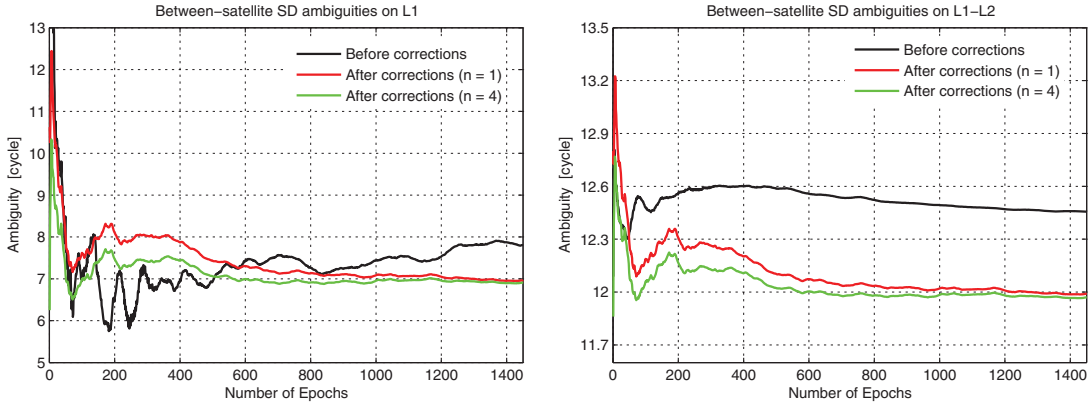

Figure 7. Convergence of the user's SD ambiguities on L1 (*left*) and on L1-L2 (*right*) of GPS over time. The results correspond to PRN10, given PRN13 as the pivot satellite.

Table 4. Reduction in the convergence time of the integer-recovered SD ambiguities $1-(k_n/k_1)$ (percent). The observed results have been computed based on the minimum number of epochs at which the precision of the ambiguities reaches 0.1 [cycle]. The predicted values have been computed using (25).

	$n=2$		$n=3$		$n=4$		$n=10$
No. of antennas	Observed	Predicted	Observed	Predicted	Observed	Predicted	Predicted
GPS: PRN10-PRN13 (L1)	9.5	9.0	13.1	12.3	15.3	15.8	23.9
BeiDou: C06-C10 (B1)	15.5	17.8	24.6	23.5	27.6	26.1	34.3

i.e. 5.71 [cycle]. In case of BeiDou, a similar scenario occurs, i.e. from 12.05 [cycle] to 6.53 [cycle].

4.3. Integer recovery of the user's ambiguities

We now turn our attention to the results of the user data-set. Forming the between-satellite SD combinations of the user's observations, the receiver-specific unknown parameters are removed. Like the array data-set, the satellite positions have been computed using the orbits of the IGS. The estimable between-satellite SD satellite clocks and ionospheric delays have been estimated using the array data-set and sent to the user according to the strategy as described in [16, 19]. Since the distance between the array and the user is about 4 km, correcting the user's data by the *same* ionospheric delays, estimated at the array's location, is realistically allowed. Corrected by the array-derived satellite clocks and ionospheric delays, the SD observation equations of the user only include the position and real-valued SD ambiguities as unknowns.

We now evaluate the integer recovery role of the SD-SPB corrections. To do so, we consider the convergence of the user's SD ambiguities over time, once without applying the SD-SPB corrections, and another time with applying the SD-SPB corrections. The corresponding results have been illustrated in figure 7. It is clearly visible that the SD ambiguities, without corrections, do not tend to integer values. Corrected by the SD-SPBs however, the integer property of the SD ambiguities is recovered and they do indeed converge to integer values.

In view of the SD-SPBs' precision improvement discussed earlier, one would expect that the array-aided SD-SPBs expedite the ambiguities' convergence compared to the single-antenna SD-SPBs. This has been realized in figure 7 where the time-series of the multi-epoch ambiguities, aided by the corrections of four antennas (green lines), goes faster to integers than its counterpart aided by 1 antenna (red lines). More precisely, one can measure the minimum number of epochs k_n through which the precision of the estimated ambiguities reaches a certain value, e.g. 0.1 [cycle], thus computing the reduction in the convergence time $1-(k_n/k_1)$. This observed reduction can also be predicted by the rule given in (25). Both the observed and predicted outcomes have been provided in table 4. In case of GPS, the variance-ratio is taken as $\alpha = 1.3$, while, in case of BeiDou, it is taken as $\alpha = 1.1$. In either case, the convergence time reduces as the number of antennas increases. The rates of the the reduction in the convergence time are different though. In case of BeiDou, the reduction in time is considerable, while in case of GPS, a smaller reduction in time is observed. The reasoning is as follows. As shown in the bottom-panel of figure 6, the elevation of PRN13 of GPS rapidly decreases over time. This makes the elevation-dependent weight $\overline{w}^{1s}_{[k_n]}$ get smaller as the number of epochs increases. Given the ratio $\left(\overline{w}^{1s}_{[k_1]}/\overline{w}^{1s}_{[k_4]}\right)\approx 1.25>1$ in the numerator of (25), the minimum number of epochs k_4 is therefore not significantly smaller than k_1. In case of C06 and C10 of BeiDou however, the weight ratio is smaller than that of the GPS scenario, i.e. $\left(\overline{w}^{1s}_{[k_1]}/\overline{w}^{1s}_{[k_4]}\right)\approx 1.14$, meaning that the reduction in time is mainly governed by the number of antennas n.

It is worth highlighting that the rule, given in (25), enables us to predict the reduction in the convergence time for a larger number of aiding antennas n. For instance, would we make use

of $n = 10$ number of antennas, the reduction becomes about 24 percent for the GPS case, and about 34 percent for the BeiDou case, assuming $\left(\overline{w}^{1s}_{[k_1]} / \overline{w}^{1s}_{[k_4]}\right) = \left(\overline{w}^{1s}_{[k_1]} / \overline{w}^{1s}_{[k_{10}]}\right)$ (see table 4).

5. Conclusions

In this contribution, we introduced the concept of array-based between-satellite SD-SPB determination—the key parameter to perform single-receiver IAR. The underlying model is characterized by data of an array of GNSS antennas, mounted on rigid platforms, that are separated by short distances so that the same ionospheric delay is assumed to be experienced by all the antennas. Forming a full-rank GNSS model, the estimable SD-SPBs were shown to appear, for instance, as a combination of the true SD-SPBs, the SD satellite code hardware delays, and the SD ambiguities of a reference antenna.

A closed-form expression of the array-aided SD-SPB corrections was presented through which a simple strategy to compute the SD-SPBs was outlined. The link between the SD-SPB corrections and the code multipath equations was established. As linear combinations of the multipath equations, the SD-SPB corrections can be directly affected by the unwanted effects of the multipath. Therefore, essential care needs to be taken in locating reference stations processing SPB corrections.

In order to reduce the code-dominated variance of the SD-SPB corrections, the data of extra antennas are incorporated into the model. As shown, the extra antennas give additional information on the SD-SPBs at the expense of additional unknowns, i.e. the array's DD ambiguities. After resolving the DD ambiguities of the array's data, the extra antennas do contribute to the precision of the SD-SPBs. With n being the number of all contributing antennas, the variance of the array-aided SD-SPB corrections is n times smaller than that of the single-antenna SD-SPB corrections. This precision improvement was also demonstrated by numerical results. As a consequence of which, the integer-recovered ambiguities of the user converge to integer values faster, upon increasing the number of aiding antennas.

Acknowledgments

The array-based experiment was conducted by Dr N Raziq and Dr B Padovan from Curtin University, Perth, Australia. This support is gratefully acknowledged.

Appendix A.

Proof of (9). As the number of observations in (6) is as many as the number of estimable parameters, the SD-SPB solution follows from

$$[\Lambda \otimes I_{m-1}]\,\widehat{\widetilde{\delta}} = -\underline{\phi}_1 + [e_2 \otimes I_{m-1}]\,\widehat{\underline{\rho}}_1 - [\mu \otimes I_{m-1}]\,\hat{\underline{I}}_1. \quad \text{(A.1)}$$

With regard to (8), pre-multiplying the preceding equation by $\Lambda^{-1} \otimes I_{m-1}$ gives (9). □

Proof of (25). Let $\sigma^2_{\hat{a}}$ be the variance of the multi-epoch solution of the ambiguity of the satellite pair $1s$ on frequency j. It is obtained as

$$\sigma^2_{\hat{a}} = \sigma^2_n \frac{1}{k_n \overline{w}^{1s}_{[k_n]}} \quad \text{(A.2)}$$

where σ^2_n is the variance of the corresponding single-epoch ambiguity solution, aided by the corrections of an array of n antennas. According to (A.2), the number of epochs, needed to achieve the variance $\sigma^2_{\hat{a}}$, follows as

$$k_n = \frac{\sigma^2_n}{\sigma^2_{\hat{a}}} \frac{1}{\overline{w}^{1s}_{[k_n]}} \quad \text{thus} \quad \frac{k_n}{k_1} = \frac{\sigma^2_n}{\sigma^2_1} \frac{\overline{w}^{1s}_{[k_1]}}{\overline{w}^{1s}_{[k_n]}} \quad \text{(A.3)}$$

The equality (25) is therefore proven if we demonstrate

$$\frac{\sigma^2_n}{\sigma^2_1} = \frac{n\alpha + 1}{n(1+\alpha)}. \quad \text{(A.4)}$$

Since, by definition, α is the variance-ratio of the data of the user antenna to that of the array's reference antenna, say $\sigma^2_{\hat{y}}$, one can obtain

$$\sigma^2_n = \alpha\sigma^2_{\hat{y}} + \frac{1}{n}\sigma^2_{\hat{y}} = \frac{1+n\alpha}{n}\sigma^2_{\hat{y}}. \quad \text{(A.5)}$$

The first term $\alpha\sigma^2_{\hat{y}}$ is the uncertainty due to the user data, while the second term $(1/n)\,\sigma^2_{\hat{y}}$ is the uncertainty due to the array-aided SD-SPB corrections. This proves (A.4). □

References

[1] Heroux P and Kouba J 1995 GPS precise point positioning with a difference *Geomatics 95 (Ottawa, June 1995)* pp 13–5

[2] Zumberge J F, Heflin M B, Jefferson D C, Watkins M M and Webb F H 1997 Precise point positioning for the efficient and robust analysis of GPS data from large networks *J. Geophys. Res.* **102** 5005–17

[3] Wielgosz P, Cellmer S, Rzepecka Z, Paziewski J and Grejner-Brzezinska D 2011 Troposphere modeling for precise GPS rapid static positioning in mountainous areas *Meas. Sci. Technol.* **22** 045101

[4] Hadas T, Kaplon J, Bosy J, Sierny J and Wilgan K 2013 Near-real-time regional troposphere models for the GNSS precise point positioning technique *Meas. Sci. Technol.* **24** 055003

[5] Leandro R F, Santos M C and Langley R B 2011 Analyzing GNSS data in precise point positioning software *GPS Solutions* **15** 1–3

[6] van Bree R J and Tiberius C C 2012 Real-time single-frequency precise point positioning: accuracy assessment *GPS Solutions* **16** 259–66

[7] Gabor M J and Nerem R S 2002 Satellite–satellite single-difference phase bias calibration as applied to ambiguity resolution *Navigation* **49** 223–42

[8] Ge M, Gendt G, Rothacher M, Shi C and Liu J 2008 Resolution of GPS carrier-phase ambiguities in precise point positioning (PPP) with daily observations *J. Geod.* **82** 389–99

[9] Laurichesse D, Mercier F, Berthias J, Broca P, Cerri L and CNES F 2009 Integer ambiguity resolution on undifferenced GPS phase measurements, Its application to PPP and satellite precise orbit determination *Navigation* **56** 135–49

[10] Collins P, Bisnath S, Lahaye F and Heroux P 2010 Undifferenced GPS ambiguity resolution using the decoupled clock model and ambiguity datum fixing *Navigation* **57** 123–35

[11] Teunissen P J G, Odijk D and Zhang B 2010 PPP-RTK: results of CORS network-based PPP with integer ambiguity resolution *J. Aeronaut. Astronaut. Aviat.* **42** 223–9

[12] Geng J, Shi C, Ge M, Dodson A H, Lou Y, Zhao Q and Liu J 2012 Improving the estimation of fractional-cycle biases for ambiguity resolution in precise point positioning *J. Geod.* **86** 579–89

[13] Loyer S, Perosanz F, Mercier F, Capdeville H and Marty J-C 2012 Zero-difference GPS ambiguity resolution at CNES-CLS IGS analysis center *J. Geod.* **86** 991–1003

[14] Henkel P, Wen Z and Gunther C 2010 Estimation of satellite, receiver biases on multiple Galileo frequencies with a Kalman filter *ION Proc. 2010 Int. Technical Meeting of The Institute of Navigation, CA (Portland, Sept. 2010)* (Manassas, VA: Institute of Navigation) pp 1067–74

[15] Wen Z, Henkel P and Gunther C 2011 Reliable estimation of phase biases of GPS satellites with a local reference network *2011 Proc. ELMAR, Croatia* (Piscataway, NJ: IEEE) pp 321–4

[16] Odijk D, Teunissen P J G and Zhang B 2012 Single-frequency integer ambiguity resolution enabled GPS precise point positioning *J. Surv. Eng.* **138** 193–202

[17] Li X and Zhang X 2012 Improving the estimation of uncalibrated fractional phase offsets for PPP ambiguity resolution *J. Navig.* **65** 513–29

[18] Zhang X, Li P and Guo F 2013 Ambiguity resolution in precise point positioning with hourly data for global single receiver *Adv. Space Res.* **51** 153–61

[19] Odijk D, Teunissen P J G and Khodabandeh A 2014 Single-frequency PPP-RTK: theory and experimental results *IAG Symp.* **139** 167–73

[20] Li X, Zhang X and Ge M 2011 Regional reference network augmented precise point positioning for instantaneous ambiguity resolution *J. Geod.* **85** 151–8

[21] Teunissen P J G 2012 A-PPP: array-aided precise point positioning with global navigation satellite systems *IEEE Trans. Signal Process.* **60** 2870–81

[22] Rao C R 1973 *Linear Statistical Inference and Its Applications* (New York: Wiley)

[23] Magnus J R and Neudecker H 2007 *Matrix Differential Calculus with Applications in Statistics and Econometrics* 3rd edn (New York: Wiley)

[24] Hofmann-Wellenhof B, Lichtenegger H and Wasle E 2008 *GNSS: Global Navigation Satellite Systems: GPS, Glonass, Galileo and More* (New York: Springer)

[25] Teunissen P J G 1985 Generalized inverses, adjustment, the datum problem and S-transformations *Optimization and Design of Geodetic Networks* ed E W Grafarend and F Sanso (Berlin: Springer) pp 11–55

[26] de Jonge P J 1998 A processing strategy for the application of the GPS in networks *PhD Thesis* Delft University of Technology (*Publication on Geodesy,* 46, Netherlands Geodetic Commission, Delft)

[27] Andreasson T B and Engman L 1999 Multipath at the SWEPOS stations *Evaluation of Eccsorb, a Microwave Absorbing Material, Reports in Geodesy, Geographical Information Systems* vol 2 (Sweden: National Land Survey)

[28] Leick A 2004 *GPS Satellite Surveying* 3rd edn (New York: Wiley)

[29] Euler H J and Goad C C 1991 On optimal filtering of GPS dual frequency observations without using orbit information *J. Geod.* **65** 130–43

[30] Teunissen P J G 1997 A canonical theory for short GPS baselines part II: the ambiguity precision and correlation *J. Geod.* **71** 389–401

6 Single-frequency PPP-RTK user performances

This chapter is covered by the following publication:

Odijk D., Teunissen P.J.G. and **Khodabandeh A.** (2014). Single-frequency PPP-RTK: theory and experimental results. International Association of Geodesy Symposium (IAG), 139:167–173, Springer.

Single-Frequency PPP-RTK: Theory and Experimental Results

Dennis Odijk, Peter J.G. Teunissen, and Amir Khodabandeh

Abstract

Integer ambiguity resolution enabled Precise (cm-level) Point Positioning (PPP) is feasible if corrections from a GPS network of CORS stations are applied to the single-receiver phase and code data of a user. The concept of PPP-RTK requires a proper definition and quality of the PPP-user network corrections, which are satellite clocks, satellite phase biases and ionospheric delays interpolated to the approximate location of the user. The availability of the satellite phase bias corrections enables the user to carry out integer resolution of ambiguities that are double-differenced, i.e., relative to those of the pivot receiver in the network. The availability of the interpolated ionospheric corrections is not absolutely required, however PPP-RTK for single-frequency users would virtually be impossible without them. A proper handling of the network corrections implies that the PPP-user should take their uncertainty into account as well. In order to limit the amount of information to be transmitted to the user, in this contribution we provide a closed-form analytical expression for the variance matrix of the network corrections which a single-frequency user can apply in his processing. Experimental results of single-frequency PPP-RTK for both a high-grade geodetic receiver as well as a low-grade mass-market receiver demonstrate that although single-epoch integer ambiguity resolution is not possible, single-frequency ambiguity resolution enabled cm-level PPP is feasible based on an accumulation of less than 10 min of observations plus network corrections on average.

Keywords

GPS • PPP-RTK • Single frequency • Integer ambiguity resolution • Closed-form variance matrix

1 Introduction

The technique of Precise Point Positioning (PPP) is based on GPS carrier phase and code (pseudo-range) observations of a single receiver, employing corrections for, among others, satellite orbits, clocks and ionospheric delays obtained from a worldwide network of GPS stations, for example the permanent GPS network of the International GNSS Service (IGS; Dow et al. (2009)). PPP was introduced in Zumberge et al. (1997) and the attainable instantaneous precision for a single-frequency user who employs global corrections is typically at the level of a few dm (van Bree and Tiberius 2012; Huisman et al. 2012).

The key to fast and cm-level PPP lies in resolving the ambiguities that are present in the phase data to integer values. Unfortunately, with the standard PPP technique this is not possible, because the ambiguities cannot be separated from the satellite hardware biases in the phase and code data. In this contribution we will present an approach that allows the single-receiver user to perform integer ambiguity resolution within short time spans and consequently enable

D. Odijk (✉) • P.J.G. Teunissen • A. Khodabandeh
Curtin University, GPO Box U1987, Perth, WA 6845, Australia
e-mail: d.odijk@curtin.edu.au

C. Rizos and P. Willis (eds.), *Earth on the Edge: Science for a Sustainable Planet*, International Association of Geodesy Symposia 139, DOI 10.1007/978-3-642-37222-3_75,

high-precision positioning. This PPP-RTK (Wuebbena et al. 2005) approach is like standard PPP based on applying corrections for satellite clocks and ionospheric delays, but, crucial to enable ambiguity resolution, are corrections for the satellite phase biases, provided that they are defined in an appropriate way.

Integer ambiguity resolution enabled PPP has been described earlier, see e.g. Laurichesse and Mercier (2007), Collins et al. (2008), Ge et al. (2008), Geng et al. (2011), Loyer et al. (2012). However, these approaches are all based on the ionosphere-free combination of dual-frequency GPS observations, requiring long convergence times (i.e. tens of minutes) for ambiguity resolution. Advantage of our PPP-RTK approach is that it is not only suitable for dual-frequency users (Teunissen et al. 2010), but also for those employing low-cost single-frequency receivers. Without alteration, our method is even applicable to multi-frequency (e.g. triple-frequency) receivers. Although multiple-frequency users can do without ionospheric corrections, they are essential to speed up integer ambiguity resolution for single-frequency users.

In this paper our PPP-RTK concept is demonstrated based on corrections determined from a regional CORS network with inter-station distances of less than 100 km. The advantage of such a relatively dense regional network is that the ionospheric corrections can be determined much more precise than by using a global network and this should benefit single-frequency applications. In this context we mention that the PPP-RTK concept in Li et al. (2011) as well as Trimble's commercial RTX service (Chen et al. 2011) also make use of a regional augmentation network; however they only present results for dual-frequency users. An important advantage of regionally augmented PPP-RTK over existing Network-RTK concepts (e.g. Vollath et al. (2000)) is that with PPP-RTK the correction information sent to users can be represented using a "state-space" approach (Wuebbena et al. 2005). This means that the different error components are represented individually and not lumped together which is the case with Network-RTK approaches. Hence, using a state-space representation the update rate of the information sent to the user is only high for highly variable parameters, such as satellite clocks and ionospheric delays, but can be lower for slower varying parameters (satellite phase biases). In case of Network-RTK the update rate of the correction information should be high, since all error terms are lumped together. Another advantage of the PPP-RTK concept is that there is a smooth transition to standard PPP if PPP-RTK ambiguity resolution is not possible, because the ambiguity-float PPP-RTK solution exactly corresponds to the standard PPP solution (this is not the case for Network-RTK).

In this paper it is assumed that a regional network provides corrections for satellite clocks, phase biases and ionospheric delays, but not for satellite orbits. These are computed by employing the IGS orbit information. By determining the satellite clocks based on a regional network, they are fully consistent with the satellite phase biases and ionospheric corrections, since these are determined from the same network. In addition to the corrections themselves, the PPP-RTK user needs to account for their uncertainty and in this contribution we present an easy-to-evaluate closed-form expression for the variance matrix of the network corrections.

The paper is organized as follows: The next section reviews the GPS phase and code observation equations, while the CORS network corrections that enable both regional PPP and PPP-RTK are discussed after that. Finally, results are presented of the performance of both techniques based on single-frequency GPS data.

2 GPS Phase and Code Observation Equations

Let us start by assuming a receiver r tracking dual-frequency GPS phase and code data. Since the focus of this paper is on the satellite-dependent effects, our starting point is formed by the between-satellite single differences (SD) of the phase and code observation equations from which all receiver-specific unknowns are removed, in units of distance:

$$\begin{aligned} E(\phi_{r,j}^{ps}) &= \rho_r^{ps} - (dt^{ps} + \delta_{,j}^{ps}) - \mu_j \imath_r^{ps} + \psi^{ps}\tau_r + \lambda_j M_{r,j}^{ps} \\ E(p_{r,j}^{ps}) &= \rho_r^{ps} - (dt^{ps} + d_{,j}^{ps}) + \mu_j \imath_r^{ps} + \psi^{ps}\tau_r \end{aligned} \tag{1}$$

These between-satellite single differences are formed between satellite s and a chosen pivot satellite p. It is assumed that the positions of these satellites are known. Furthermore, the symbols in Eq. (1) have the following meaning: $E(\cdot)$ denotes the mathematical expectation, $\phi_{r,j}^{ps}$ and $p_{r,j}^{ps}$ the SD observables for phase and code, respectively on frequency $j = 1, 2$, ρ_r^{ps} denotes the SD receiver-satellite range, dt^{ps} the SD satellite clock error, $\delta_{,j}^{ps}$ and $d_{,j}^{ps}$ the SD satellite phase and code hardware biases, $\imath_r^{ps}$ the SD ionospheric delay with $\mu_j = \lambda_j^2/\lambda_1^2$ its frequency-dependent coefficient, τ_r the zenith tropospheric delay (ZTD), with ψ^{ps} the SD mapping function, λ_j the wavelength, and $M_{r,j}^{ps}$ the SD phase ambiguity that consists of the initial phases of satellite plus an integer SD ambiguity, in units of cycle. All clock errors and hardware biases are given in units of distance. Both phase and code data are assumed to be a priori corrected for effects such as hydrostatic troposphere, phase center offsets, phase wind-up, solid earth tides, ocean loading, etc. More details on these corrections can be found in Kouba and Heroux (2001).

3 CORS-Based Single-Frequency PPP-RTK

In this section the corrections are discussed that need to be estimated from a CORS network in order for a user to carry out single-frequency PPP, as well as PPP-RTK. For PPP-RTK it is shown that by using satellite phase bias corrections with an appropriate definition the ambiguities for the user become integer.

3.1 Regional CORS Network Corrections

Regional CORS GPS network processing is based on the observation equations (1), keeping the positions fixed of both receivers (since these are precisely known), as well as of the satellites (from IGS orbit information). Unknown network parameters are then, in terms of between-satellite single differences: satellite clocks, satellite phase biases, ZTDs, ionospheric delays and phase ambiguities. Since the network model is not of full rank, it is only possible to estimate *combinations* of the individual parameters as given in Eq. (1). These combinations depend on the choice of *S-basis*, i.e., the minimum set of parameters that needs to be constrained to eliminate the rank deficiency (Lannes and Teunissen 2011). A particular choice was made in Teunissen et al. (2010); for this paper another S-basis is chosen, resulting in the following network observation equations, for $j = 1, 2$ frequencies and $r = 1, \ldots, n$ CORS stations:

$$\begin{aligned} E(\phi^{ps}_{r,j} - \rho^{ps}_r) &= -\widetilde{dt}^{ps} - \tilde{\delta}^{ps}_{,j} - \mu_j \tilde{\imath}^{ps}_r + \psi^{ps}\tilde{\tau}_r + \lambda_j \tilde{M}^{ps}_{r,j} \\ E(p^{ps}_{r,j} - \rho^{ps}_r) &= -\widetilde{dt}^{ps} + \mu_j \tilde{\imath}^{ps}_r + \psi^{ps}\tilde{\tau}_r \\ E(\imath^{ps}_r - \imath^{ps}_1) &= \tilde{\imath}^{ps}_r - \tilde{\imath}^{ps}_1, \quad \text{for } r = 2, \ldots, n \end{aligned} \tag{2}$$

As can be seen, in addition to the phase and code observation equations, constraints on the relative between-receiver ionospheric delays are incorporated in order to 'tune' the presence of the ionosphere in the model. The estimable parameter functions are denoted using the tilde on top of the symbol, where $\widetilde{dt}^{ps}$ denotes the SD satellite clock parameter, $\tilde{\delta}^{ps}_{,j}$ the estimable SD satellite phase bias parameter, $\tilde{\imath}^{ps}_r$ the estimable SD ionospheric delay parameter, $\tilde{\tau}_r$ the estimable ZTD parameter, and finally, $\tilde{M}^{ps}_{r,j}$ denotes the estimable SD ambiguity parameter. Most striking difference with existing approaches such as described by Laurichesse and Mercier (2007), Collins et al. (2008), Ge et al. (2008), Loyer et al. (2012) is that in the latter approaches the network processing is based on *elimination* of the ionospheric delays by using the ionosphere-free combination, whilst in Eq. (2) the ionospheric delays are explicitly solved as they are needed for the interpolation to provide to the user.

In addition to the functional relations as described in Eq. (2), for the network processing a stochastic model is used, capturing the noise of the observations:

$$D\left(\begin{bmatrix} \phi^{ps} \\ p^{ps} \\ \imath^{ps} \end{bmatrix}\right) = (q_p^2 + q_s^2)\begin{bmatrix} \begin{pmatrix} C_\phi & \\ & C_p \end{pmatrix} \otimes I_n & \\ & c_\imath^2 D_n^T D_n \end{bmatrix} \tag{3}$$

Here $D(\cdot)$ denotes the mathematical dispersion, and ϕ^{ps} and p^{ps} collect all dual-frequency phase and code observations, respectively of all receivers corresponding to one between-satellite single difference in one vector. In addition, $\imath^{ps}$ contains the between-receiver difference of the SD ionospheric pseudo-observations. Furthermore, $\otimes$ denotes the matrix Kronecker product, I_n the identity matrix of dimension n, e_n the n-vector with ones, and $D_n^T = [-e_{n-1}\ I_{n-1}]$, the between-receiver difference matrix. Both 2×2 cofactor matrices C_ϕ and C_p model the undifferenced precision of the dual-frequency phase and code observations in zenith, where $c_\imath^2$ denotes the undifferenced variance factor of the ionospheric pseudo observations in zenith as well. Through the factors q_p and q_s it is possible to model the elevation-dependency of the noise of the observations. It is finally remarked that the above stochastic model applies to just one between-satellite single difference. When between-satellite single differences are processed simultaneously the correlation between them is taken into account.

We will now discuss the estimable network parameters in more detail. Due to space limitation we will present these parameter functions without proof; this will be given elsewhere. In this paper we consider the regional CORS network to have inter-station distances below 100 km for which absolute ZTDs (per receiver) are poorly estimable, since all receivers in the network experience more or less an identical elevation to the same satellite. To solve this, we do not estimate the ZTD of the pivot receiver ($r = 1$) in the network, and parameterize all other ZTDs *relative* to that of the pivot receiver:

$$\tilde{\tau}_r = \tau_r - \tau_1, \quad r = 2, \ldots, n \tag{4}$$

The estimable *satellite clock* parameters can be shown to be a function of the 'true' satellite clocks, plus the code biases on L1 and L2, and the ZTD of the network's pivot receiver:

$$\widetilde{dt}^{ps} = dt^{ps} + d^{ps}_{,1} + \tfrac{\mu_1}{\mu_2 - \mu_1} DCB^{ps} - \psi^{ps}\tau_1 \tag{5}$$

Here $DCB^{ps} = d^{ps}_{,1} - d^{ps}_{,2}$ denotes the Differential Code Bias, see Schaer (1999). Although the estimable satellite clock is biased by the tropospheric delay of the pivot station in the network, this is *not* an issue for PPP-RTK users as we will show in the next subsection. The estimable *satellite phase bias* can be given by the following parameter function:

$$\tilde{\delta}^{ps}_{,j} = -\lambda_j \left[M^{ps}_{1,j} - \frac{1}{\lambda_j}(\delta^{ps}_{,j} - d^{ps}_{,1} - (\frac{\mu_j}{\mu_1}+1)\frac{\mu_1}{\mu_2-\mu_1}DCB^{ps}) \right] \quad (6)$$

This between-satellite phase bias parameter is a combination of the true between-satellite phase bias, biased by a combination of the satellite code biases on L1 and L2, plus the (non-integer) ambiguity of the network's pivot receiver. The estimable SD *ionospheric delay* for each of the network stations can be interpreted as the 'true' ionospheric delay, biased by a scaled SD differential code bias:

$$\tilde{\imath}^{ps}_r = \imath^{ps}_r + \frac{1}{\mu_2-\mu_1}DCB^{ps}, \quad r = 1, \ldots, n \quad (7)$$

The estimable *phase ambiguity* is—like the estimable ZTD parameter—the SD phase ambiguity of each receiver relative to the SD phase ambiguity of the pivot receiver in the network:

$$\tilde{M}^{ps}_{r,j} = M^{ps}_{r,j} - M^{ps}_{1,j} \quad (8)$$

Consequently, the estimable ambiguity parameter is a *double-differenced* ambiguity and thus integer, since the initial satellite phase biases that were present in the SD ambiguity terms get eliminated.

To enable PPP and/or PPP-RTK at the location of the user, the CORS network should broadcast at least the satellite clock parameters to the user. Furthermore, for users employing *single-frequency* receivers, the network should provide corrections for the ionosphere. For 'standard (global) PPP' these are often extracted from external Global Ionospheric Maps, but in presence of a dense regional CORS network a more sophisticated ionospheric product can be generated, in which the ionospheric delay is obtained from the network ionospheric delays by means of Ordinary Kriging interpolation, e.g., Wackernagel (2003). Then we can write for the network ionospheric correction, denoted as $\tilde{\imath}^{ps}_u$:

$$\tilde{\imath}^{ps}_u = h^T_u \left[\tilde{\imath}^{ps}_1, \ \ldots, \ \tilde{\imath}^{ps}_n\right]^T = \imath^{ps}_u + \frac{1}{\mu_2-\mu_1}DCB^{ps} \quad (9)$$

with $(\cdot)^T$ denoting a transposed vector. Furthermore, n-vector h_u denotes the Ordinary Kriging interpolation coefficient vector evaluated at the approximate user location for which holds that the entries sum up to 1 ($h^T_u e_n = 1$), and where $\imath^{ps}_u$ denotes the 'true' SD interpolated ionospheric delay at the approximate user location. Finally, to enable integer ambiguity resolution for the PPP user, the CORS network should provide corrections for the satellite phase bias parameters on the frequency corresponding to that of the single-frequency user. As a last remark, we emphasize that the network parameters should be transmitted to the users with the best possible precision, so after the network ambiguities are fixed to integers.

3.2 Regional Network-Based PPP and PPP-RTK

Before presenting the observation equations for PPP-RTK, a user can perform—similar to standard or 'global PPP'—'regional PPP' by correcting his phase and code observations by the ionosphere-free satellite clocks and interpolated ionospheric delay from the regional CORS network. The single-frequency (L1; $j = 1$) user thus applies the following corrections:

$$\Delta\tilde{\phi}^{ps}_{u,1} = \widetilde{dt}^{ps} + \mu_1\tilde{\imath}^{ps}_u; \quad \Delta\tilde{p}^{ps}_{u,1} = \widetilde{dt}^{ps} - \mu_1\tilde{\imath}^{ps}_u \quad (10)$$

With these corrections, the (linearized) single-frequency regional PPP observation equations read as follows:

$$\begin{aligned} E(\phi^{ps}_{u,1} + \Delta\tilde{\phi}^{ps}_{u,1}) &= -(\mathbf{u}^{ps}_u)^T x_u + \psi^{ps}\tilde{\tau}_u + \lambda_1\tilde{M}^{ps}_{u,1} \\ E(p^{ps}_{u,1} + \Delta\tilde{p}^{ps}_{u,1}) &= -(\mathbf{u}^{ps}_u)^T x_u + \psi^{ps}\tilde{\tau}_u \end{aligned} \quad (11)$$

where $\phi^{ps}_{u,1}$ and $p^{ps}_{u,1}$ denote the observed-minus-computed SD phase and code observables and $\mathbf{u}^{ps}_u$ the SD receiver-satellite line-of-sight vector. Satellite positions are held fixed; the user should compute them in the same way as the network. The following estimable parameters appear in these PPP observation equations: the user position x_u, the ZTD, which is defined relative to the network's pivot station, i.e., $\tilde{\tau}_u = \tau_u - \tau_1$, and an L1 phase ambiguity that is defined as follows:

$$\tilde{M}^{ps}_{u,1} = M^{ps}_{u,1} - \frac{1}{\lambda_1}(\delta^{ps}_{,1} - d^{ps}_{,1} - \frac{2\mu_1}{\mu_2-\mu_1}DCB^{ps}) \quad (12)$$

Thus, the estimable PPP ambiguity parameter is a combination of the original ambiguity term, lumped with phase and code satellite hardware biases. It can be shown that this ambiguity corresponds to the 'narrow-lane uncalibrated phase delay' parameter as used in Ge et al. (2008). Clearly, this parameter is *not* an integer.

Integer ambiguities become estimable when the PPP user applies the network's satellite bias corrections to his phase data. The observation equations then remain exactly the same as in Eq. (11), as well as the corrected code observations, however the correction to be applied to the phase observations is different:

$$\Delta\tilde{\phi}^{ps}_{u,1} = \widetilde{dt}^{ps} + \tilde{\delta}^{ps}_{,1} + \mu_1\tilde{\imath}^{ps}_u; \quad \Delta\tilde{p}^{ps}_{u,1} = \widetilde{dt}^{ps} - \mu_1\tilde{\imath}^{ps}_u \quad (13)$$

Since the satellite phase bias parameter contains the combined term $(\delta^{ps}_{,1} - d^{ps}_{,1} - \frac{2\mu_1}{\mu_2-\mu_1}DCB^{ps})$, see Eq. (6), this is exactly what is needed to remove the same term from Eq. (12), and the estimable ambiguity parameter becomes:

$$\tilde{M}^{ps}_{u,1} + \tfrac{1}{\lambda_1}\tilde{\delta}^{ps}_{,1} = M^{ps}_{u,1} - M^{ps}_{1,1} \;=\; \text{integer} \qquad (14)$$

Thus, the estimable PPP-RTK ambiguity parameter is the difference between the SD ambiguity of the PPP user and the SD ambiguity of the network's pivot station. This resulting parameter is consequently a *double-differenced* ambiguity and thus integer.

3.3 Regional PPP-RTK Correction Variance Matrix

The network corrections are stochastic and their variance matrix should be taken into account by the PPP-RTK user in order to have the best possible results for both his ambiguity resolution and positioning. In order to limit the amount of information sent to the user, we will present an easy-to-use *closed-form expression* for the network correction variance matrix such that a user can compute this matrix himself. For a between-satellite single-differenced pair of phase and code data, the variance matrix of the ambiguity-fixed network corrections that a single-frequency user needs to apply, can be shown to read as follows for a certain observation epoch:

$$D\left(\begin{bmatrix}\Delta\check{\tilde{\phi}}^{ps}_{u,1}\\ \Delta\check{\tilde{P}}^{ps}_{u,1}\end{bmatrix}\right) \triangleq$$
$$\underbrace{(q_p^2+q_s^2)\left[\frac{1}{n}\begin{pmatrix}c_\phi^2 & \\ & c_p^2\end{pmatrix} + c^2_{\check{I}|\rho}\left([h_u^T h_u]-\frac{1}{n}\right)\begin{pmatrix}-1\\1\end{pmatrix}\begin{pmatrix}-1\\1\end{pmatrix}^T\right]}_{Q_1}$$
$$+\;\underbrace{c_\tau^2(\psi^{ps})^2\left(\frac{c_{\check{I}\check{\rho}}}{c_{\check{\rho}}}\right)^2\left([h_u^T h_u]-\frac{1}{n}\right)\begin{pmatrix}-1\\1\end{pmatrix}\begin{pmatrix}-1\\1\end{pmatrix}^T}_{Q_2} \qquad (15)$$

where q_p and q_s are the factors to model satellite-elevation dependency, see Eq. (3), and c_ϕ and c_p the undifferenced standard deviations of the single-frequency phase and code data used in the network processing. These standard deviations plus the function to model the elevation dependency should be known by the user, as well as the number of CORS network stations n, plus their locations (in order to compute the interpolation vector h_u). It should be mentioned that the variance matrix as presented here is not the complete one of the actual PPP-RTK corrections, but the equivalent S-basis invariant form of it (this is why the equivalent sign has been used in Eq. (15)). While the PPP-RTK corrections themselves do depend on the choice of the network's pivot receiver (in this case receiver 1), it can be shown that only the S-invariant form of it is needed to properly weigh the corrections for position determination. Now we will take a closer look at the different components of this closed-form variance matrix.

In the first part of the variance matrix, i.e., Q_1 in Eq. (15), the variance factor $c^2_{\check{I}|\rho}$ reflects the precision with which the (ambiguity-fixed) ionospheric delays can be estimated in the CORS network. Assuming the precision of phase to be much better than of code, i.e., $c_\phi^2/c_p^2 \approx 0$, and for dual-frequency GPS CORS networks $c_\phi^2/c_i^2 \approx 0$, such that the square root of the variance factor can be approximated as:

$$c_{\check{I}|\rho} \approx c_\phi \frac{1}{\sqrt{\mu_1^2+\mu_2^2}} \approx 0.5 c_\phi, \;\text{ since }\; \mu_1 = 1,\; \mu_2 = (77/60)^2$$

Thus, the precision of the ambiguity-fixed network ionospheric delays is very high: about half the standard deviation of the undifferenced phase observations. The scalar $[h_u^T h_u]$ appears due to the interpolation of these network ionospheric delays, and it can be proved that $\frac{1}{n} \le [h_u^T h_u] \le 1$. This means that the factor $[h_u^T h_u] - \frac{1}{n}$ in Eq. (15) varies between 0 and $1 - \frac{1}{n}$.

The part Q_2 of Eq. (15) is due to the ZTD estimation in the network. The scalar c_τ^2 represents the variance factor with which the ZTD can be estimated in a standard *single point positioning* model, based on all satellites in view. It is possible to evaluate this standard deviation using a closed-form expression as well, by assuming that the elevation-dependency of the observation noise can be modeled as $q_i = 1/\sin\epsilon^i$, with ϵ^i the elevation of satellite $i = 1, \ldots, m$. In addition, if we approximate the tropospheric mapping function by the same, i.e., $\psi^i \approx 1/\sin\epsilon^i$, the user can apply the following approximation:

$$c_\tau \;\approx\; \sqrt{\frac{1}{m}\frac{\sum_{i=1}^m \sin^2\epsilon^i}{\sum_{i=1}^m(\sin\epsilon^i - \overline{\sin\epsilon})^2}} \;\text{ with }\; \overline{\sin\epsilon} = \frac{1}{m}\sum_{i=1}^m \sin\epsilon^i \qquad (16)$$

This factor does not vary much during a day; using a cut-off elevation of 10° and a number of GPS satellites varying between 6 and 9, c_τ typically varies between 0.8 and 2.4 with an average of 1.2. Furthermore, in part Q_2, $\frac{c_{\check{I}\check{\rho}}}{c_{\check{\rho}}}$ denotes the ratio of the covariance and the standard deviation with which the ionospheric delays and ranges can be estimated using the *geometry-free* single-baseline model, having the DD ambiguities fixed, see Odijk and Teunissen (2008). Using the same assumptions as done for $c_{\check{I}|\rho}$, it is possible to approximate this ratio as:

$$\frac{c_{\check{I}\check{\rho}}}{c_{\check{\rho}}} \approx c_\phi \frac{\mu_1+\mu_2}{(\mu_2-\mu_1)\sqrt{\mu_1^2+\mu_2^2}} \approx 2.1 c_\phi$$

so about twice the undifferenced phase standard deviation.

Thus, since both factors $c_{\check{I}|\rho}$ and $\frac{c_{\check{I}\check{\rho}}}{c_{\check{\rho}}}$ are governed by the phase precision, while the factors $[h_u^T h_u] - \frac{1}{n}$ and c_τ are always smaller or close to 1, it follows that the network correction for the PPP-RTK user's phase data has phase

precision (as it should be), while the PPP-RTK user's code correction is driven by the network's code noise (since c_p^2 in Eq. (15) is dominating over the phase-based terms).

4 Experimental Results of Regional PPP and PPP-RTK

In order to test the performance of our PPP-RTK concept, we determined corrections from a regional CORS network and applied these to single-frequency user data. The CORS network is depicted in Fig. 1 and consists of ($n = 4$) four stations at distances of about 60 km in Western Australia around Perth, all equipped with identical Trimble NetR5 receivers. The location at Curtin University Bentley campus (CUT0) was assigned as a (static) rover station. At this station, GPS data were collected using two receivers: a *high-grade* dual-frequency Trimble NetR9 receiver, plus a *low-grade* single-frequency u-blox AEK-4T receiver. For all CORS network stations dual-frequency phase and code observations have been collected above a cut-off elevation of 10° during the full day of 23 October 2010 with a sampling interval of 30 s.

4.1 Example of PPP-RTK Correction Variance Matrix

From the dual-frequency CORS network data precise estimates for satellite clock parameters, satellite phase bias parameters and interpolated ionospheric delays (for location CUT0) were obtained after network ambiguity resolution. In addition to the computation of these correction values, the closed-form expression as given in Eq. (15) has been employed to compute the variance matrix of the network corrections. As an example, for a particular between-satellite single difference (SD) at a particular epoch of the day, we present this variance matrix numerically. For this, the network processing has been done based on the following observable standard deviations (undifferenced and in zenith): $c_\phi = 2.5\,\text{mm}$, $c_p = 25\,\text{cm}$ and $c_\iota = 10\,\text{cm}$. In addition, the observations are weighted according to: $q_i = 1/\sin\epsilon^i$. The Kriging interpolation vector evaluated at CUT0 equals: $h_u^T = (-0.02, 0.24, 0.66, 0.12)$, based on station ordering: TORK–ROTT–MIDL–MDAH. At the particular epoch 8 satellites were tracked, resulting in $c_\tau \approx 1.1$. From these satellites we selected two satellites, one with $\epsilon^p = 56.7°$ and the other with $\epsilon^s = 27.1°$. For this pair $\psi^{ps} \approx -1.0$ and the two matrices in Eq. (15) are computed as:

$$Q_1 \approx \begin{bmatrix} 1.25\text{E}-5 & -2.72\text{E}-6 \\ -2.72\text{E}-6 & 0.098 \end{bmatrix},$$

$$Q_2 \approx \begin{bmatrix} 8.80\text{E}-6 & -8.80\text{E}-6 \\ -8.80\text{E}-6 & 8.80\text{E}-6 \end{bmatrix}$$

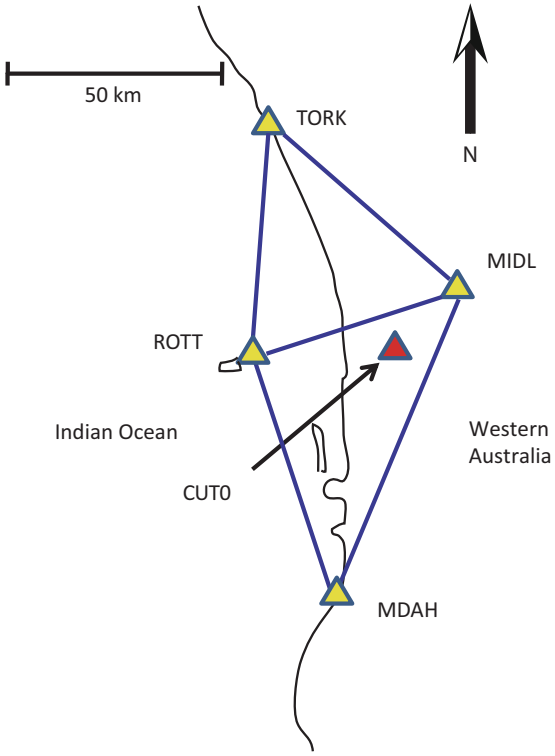

Fig. 1 CORS network (*yellow triangles*) used for generating the PPP (-RTK) products for user location CUT0 ((−32°, 116°); *red triangle*)

This results in the following variance matrix the PPP-RTK user needs to apply to account for the uncertainty of the network corrections at this epoch:

$$D\left(\begin{bmatrix} \check{\Delta\phi}_{u,1}^{ps} \\ \check{\Delta p}_{u,1}^{ps} \end{bmatrix}\right) \approx \begin{bmatrix} 2.13\text{E}-5 & -1.15\text{E}-5 \\ -1.15\text{E}-5 & 0.098 \end{bmatrix} \text{m}^2 \quad (17)$$

Thus, the phase correction is very precise, having a standard deviation of just 5 mm, while the standard deviation of the code correction is about 31 cm.

4.2 Performance of PPP-RTK at the User

In a next step the network corrections are applied to correct the user's single-frequency phase and code data and perform single-receiver ambiguity resolution and positioning. Due to the weakness of the single-epoch, single-frequency observation model (11), instantaneous or epoch-by-epoch ambiguity resolution was not feasible. However, successful ambiguity resolution was obtained by accumulating epochs in a Kalman filter incorporating the constancy of the ambiguities. In this

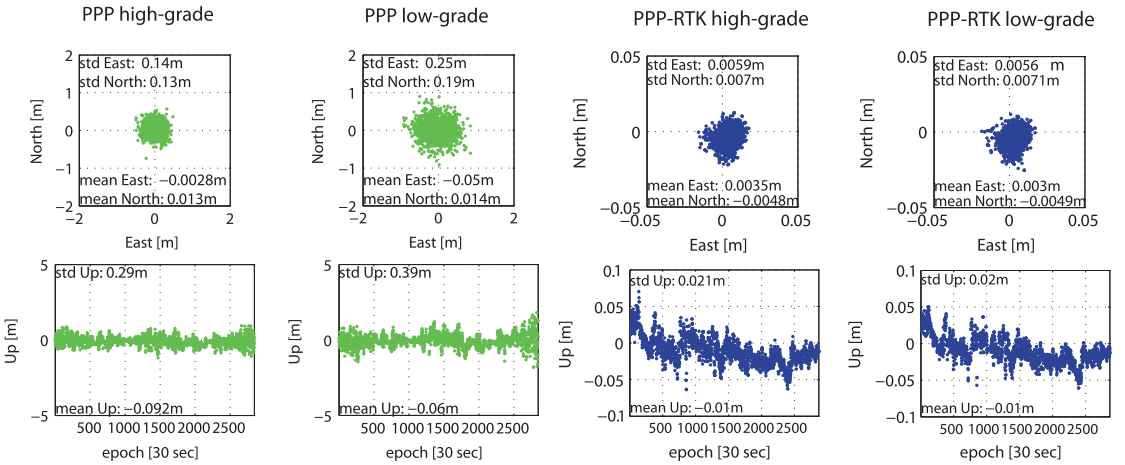

Fig. 2 PPP and PPP-RTK positioning results based on CORS-network corrected single-frequency GPS phase and code data. The left two graphs (*top*: North-East position scatter; *bottom*: Up position time series) correspond to PPP based on the high-grade receiver, while the two graphs second from left depict the PPP counterparts obtained using the data of the low-grade receiver. The *two columns* on the *right* side are those corresponding to PPP-RTK

way the average time to successfully resolve the integers is 2.5 min for the Trimble receiver and 4 min for the u-blox receiver. These short time spans could be achieved since—in contrast to current practice—the network corrections have been *weighted* in the processing, by applying the variance matrix of Eq. (15) for each epoch. On the other hand, the measurements were obtained in October 2010, during solar minimum and under relatively mild ionospheric conditions. However, to give an idea of the time to fix the ambiguities during more disturbed ionospheric conditions, we artificially increased the standard deviation of the ionospheric corrections by a factor 10. The resulting average time to fix the integers using these more uncertain network corrections increased to 6.5 min for the Trimble receiver and to 9.5 min for the u-blox receiver. So the mean time to fix is expected to be a factor 2–3 longer under a more disturbed ionosphere.

After ambiguity resolution, the rover position could be solved kinematically with a horizontal precision at sub-cm level, and a vertical precision of about 2 cm, for both types of receivers; see Fig. 2 (right two columns). The position errors are obtained by comparing the estimates with the known coordinates of station CUT0. To compare, the two left columns of Fig. 2 show the positioning results which would have been obtained *without* integer ambiguity resolution, i.e. 'regional single-frequency PPP', thus including interpolated ionospheric corrections, but without the phase data corrected for the satellite phase biases. In order to enable a fair comparison with PPP-RTK, the PPP results shown are based on a same number of epochs as was needed for PPP-RTK ambiguity resolution. It is stressed that apart from the satellite phase bias corrections, the assumptions underlying the PPP and PPP-RTK solutions are exactly the same (i.e. stochastic model of phase and code, initial receiver positions from standard single point positioning, number of satellites, etc.). The comparison clearly shows the impact of integer ambiguity resolution: the horizontal precision is improved from a level of a few dm (PPP) to sub-cm (PPP-RTK), while the vertical component improves from 3–4 dm (PPP) to about 2 cm (PPP-RTK). The difference in precision between PPP high-grade and PPP low-grade is mainly due to the lower quality of the code data for the u-blox receiver as compared to the Trimble receiver.

The accuracy of the PPP-RTK positioning results is in agreement of what can be expected if the integer ambiguities are resolved and all other biases have been properly taking into account: the phase data, having mm-precision (even for the low-cost receiver), start to act as if they are very precise code data, resulting in cm-precision or better. The horizontal sub-cm precision and vertical precision of a few cm is similar to the results described in e.g. Geng et al. (2011).

5 Conclusions

In this contribution the focus has been on integer ambiguity resolution enabled single-receiver Precise Point Positioning applications. While the observation model of this 'PPP-RTK' method is intrinsically the same as for 'standard PPP', the difference lies in the corrections applied to the user's phase data. Standard PPP is based on corrections for at least satellite clocks (in addition to the orbits), however the essential correction that enables integer ambiguity resolution is the

satellite phase bias parameter, which can be shown to be a combination of the (true) satellite phase bias, together with the (non-integer) ambiguity of the network's pivot station and dual-frequency satellite code biases. The PPP-RTK approach demonstrated in this paper is not only suitable for dual-frequency but also for single-frequency applications. In this paper we presented a closed-form expression which enables the single-frequency PPP-RTK user to computes the variance matrix of the network corrections by himself. Experimental results show that single-frequency PPP ambiguity resolution is feasible in less than 10 min, even using low-grade receivers. The kinematic position accuracy with the integer ambiguities fixed is at sub-cm level horizontally, and at the level of a few cm in the vertical direction.

Acknowledgements This work has been executed in the framework of the Positioning Program Project 1.01 of the Cooperative Research Centre for Spatial Information (CRC-SI2). Peter J.G. Teunissen is the recipient of an Australian Research Council (ARC) Federation Fellowship (project number FF0883188). The CORS network data in this study have been provided by the GPS Network Perth. All this support is gratefully acknowledged.

References

van Bree RJP, Tiberius CCJM (2012) Real-time single-frequency precise point positioning: accuracy assessment. GPS Solut 16(2):259–266

Chen X, Allison T, Cao W, Ferguson K, Gruenig S, Gromez V, Kipka A, Koehler J, Landau H, Leandro R, Lu G, Stolz R, Talbot N (2011) Trimble RTX, an innovative new approach for network RTK. In: Proceedings of ION GNSS-2011, pp 2214–2219, Portland, OR, 19–23 September 2011

Collins P, Lahaye F, Heroux P, Bisnath S (2008) Precise point positioning with ambiguity resolution using the decoupled clock model. In: Proceedings of ION GNSS-2008, pp 1315–1322, Savannah, GA, 16–19 September 2008

Dow JM, Neilan RE, Rizos C (2009) The international GNSS service in a changing landscape of global navigation satellite systems. J Geodes 83:191–198

Ge M, Gendt G, Rothacher M, Shi C, Liu J (2008) Resolution of GPS carrier-phase ambiguities in precise point positioning (PPP) with daily observations. J Geodes 82:389–399

Geng J, Teferle FN, Meng X, Dodson AH (2011) Towards PPP-RTK: ambiguity resolution in real-time precise point positioning. Adv Space Res 47:1664–1673

Huisman L, Teunissen PJG, Hu C (2012) GNSS precise point positioning in regional reference frames using real-time broadcast corrections. J Appl Geodes 6:15–23

Kouba J, Heroux P (2001) Precise point positioning using IGS orbit products. GPS Solut 5(2):12–28

Lannes A, Teunissen PJG (2011) GNSS algebraic structures. J Geodes 85:273–290

Laurichesse D, Mercier F (2007) Integer ambiguity resolution on undifferenced GPS phase measurements and its application to PPP. In: Proceedings of ION GNSS-2007, pp 839–848, Fort Worth, TX, 25–28 September 2007

Li X, Zhang X, Ge M (2011) Regional reference network augmented precise point positioning for instantaneous ambiguity resolution. J Geodes 85:151–158

Loyer S, Perosanz F, Mercier F, Capdeville H, Marty JC (2012) Zero difference GPS ambiguity resolution at CNES-CLS IGS analysis center. J Geodes. doi:10.1007/s00190-012-0559-2

Odijk D, Teunissen PJG (2008) ADOP in closed form for a hierarchy of multi-frequency single-baseline GNSS models. J Geodes 82:473–492

Schaer S (1999) Mapping and predicting the Earth's ionosphere using the global positioning system. Ph.D. thesis

Teunissen PJG, Odijk D, Zhang B (2010) PPP-RTK: results of CORS network-based PPP with integer ambiguity resolution. J Aeronaut Astronaut Aviat Ser A 42(4):223–230

Vollath U, Buecherl A, Landau H, Pagels C, Wagner B (2000) Multi-base RTK positioning using virtual reference stations. In: Proceedings of ION GPS-2000, pp 123–131, Salt Lake City, UT, 19–22 September 2000

Wackernagel H (2003) Multivariate geostatistics: an introduction with applications. Springer, Berlin

Wuebbena G, Schmitz M, Bagge A (2005) PPP-RTK: precise point positioning using state-space reprentation in RTK networks. In: Proceedings of ION GNSS-2005, pp 2584–2594, Long Beach, CA, 13–16 September 2005

Zumberge JF, Heflin MB, Jefferson DC, Watkins MM, Webb FH (1997) Precise point positioning for the efficient and robust analysis of GPS data from large networks. J Geophys Res 102:5005–5017

7 GPS+Galileo RTK user performances

This chapter is covered by the following publication:

Odijk D., Teunissen P.J.G. and **Khodabandeh A.** (2013). Galileo IOV RTK positioning: standalone and combined with GPS. Survey Review, Maney Publishing. UK.

Galileo IOV RTK positioning: standalone and combined with GPS

D. Odijk*[1], P. J. G. Teunissen[1,2] and A. Khodabandeh[1]

Results are presented of real time kinematic (RTK) positioning based on carrier phase and code (pseudorange) observations of the four Galileo In-Orbit Validation (IOV) satellites, as they were in orbit and transmitting navigation data at the time of writing this article (2013). These Galileo data were collected by multi-GNSS receivers operated by Curtin University and as such this article is one of the first presenting results of short baseline ambiguity resolution and positioning based on Galileo IOV observations. The results demonstrate that integer ambiguity resolution based on the four IOV satellites needs fewer than three minutes when at least observables from three frequencies are used. Combined with data of four GPS satellites even instantaneous (single epoch) ambiguity resolution is demonstrated, using only two frequencies per constellation (i.e. E1+E5a & L1+L2). We also show that at locations with obstructed satellite visibility, such that positioning based on either GPS-only or Galileo-only becomes impossible or only in a very inaccurate way, combined Galileo&GPS positioning is feasible, within 10 min if one frequency of each constellation is used and only 2 min time-to-fix the ambiguities based on observations of two frequencies of each constellation. It is furthermore demonstrated that this results in positions with centimetre level accuracy in the horizontal plane and sub-decimetre accuracy in the vertical direction.

Keywords: Galileo IOV, GPS, GNSS, Interoperability, RTK positioning, Ambiguity resolution, LAMBDA method

Introduction

Europe's global navigation satellite system (GNSS) Galileo is currently under development. At the moment of writing this article (2013) the project is in its In-Orbit Validation (IOV) phase. As part of this phase four IOV satellites have been launched (the first pair on 21 October 2011 and the second pair one year later, on 12 October 2012) and are in orbit. These first four IOV satellites have to demonstrate that the space and ground infrastructure of Galileo meet the requirements and they have to validate the system's design in advance of completing the full constellation [**1**]. The full Galileo constellation will consist of 30 satellites in three orbital planes, including three in-orbit spare ones. The first two satellites, IOV-PFM (PRN E11) and IOV-FM2 (PRN E12), began transmitting navigation messages in January 2013. The second pair of IOV satellites, IOV-FM3 (PRN E19) and IOV-FM4 (PRN E20) started to transmit their navigation messages in March 2013. Table 1 gives the frequencies/wavelengths of the Open Service signals that can be tracked from the Galileo IOV satellites, versus those of the signals that can be tracked from the satellites of the established Global Positioning System (GPS). It is assumed that data on the following Galileo frequencies are tracked: E1, E5a, E5b and E5. The E6 signal was not tracked by the receivers used in our analyses. We remark that this signal will not be part of Galileo's Open Service, as it will be encrypted for commercial purposes [**2**].

The Galileo E5 signal, with its Alternative Binary Offset Carrier (AltBOC) modulation, is an extra-wide-band signal having two components, E5a and E5b, and these can be received by tracking them as two independent BPSK(10) modulations, at centre frequencies 1176·45 and 1207·14 MHz. Second, the E5a and E5b bands can be tracked coherently as one signal, centred at the mean of the E5a and E5b frequencies, leading to high performance E5 observables [**3**]. The wideband E5 signal is expected to have a much better code (pseudorange) accuracy and multipath suppression as compared to its subcarriers E5a and E5b [**4**]. From Table 1, note that two of Galileo's frequency bands overlap GPS; as such, the Galileo E1 and E5a frequencies are identical to the L1 and L5 frequencies of GPS.

Since the first transmission of the Galileo IOV signals in December 2011, several research and industry groups have started to analyse and work with the signals [**5**]. First positioning results based on Galileo IOV data

[1]GNSS Research Centre Curtin University, GPO Box U1987 Perth, WA 6845, Australia
[2]Department of Geoscience and Remote Sensing, Delft University of Technology, PO Box 5048, 2628 CN Delft, The Netherlands

*Corresponding author, email d.odijk@curtin.edu.au

Received 17 April 2013; accepted 10 October 2013
DOI 10.1179/1752270613Y.0000000084

Table 1 Galileo versus GPS observables: frequencies and wavelengths

	Galileo frequencies				GPS frequencies		
	E1	E5a	E5b	E5	L1	L2	L5
Carrier frequency/MHz	1575·42	1176·45	1207·14	1191·795	1575·42	1227·60	1176·45
Carrier wavelength/cm	19·03	25·48	24·83	25·15	19·03	24·42	25·48

combined with GPS were presented in [**6**]; however the results were based on the first IOV satellite only. Precise point positioning based on the first two IOV satellites in combination with the two GIOVE satellites was demonstrated in [**7**], where they used satellite orbit and clock information from the Cooperative Network for GNSS Observation (CONGO; [**8**]). In a follow-up article [**9**] first results are given for single point positioning as well as relative phase based kinematic positioning based on the four Galileo IOV satellites. Again, orbits and clocks were determined from the CONGO network, and stations that are part of the Multi-GNSS Experiment (MGEX) of the International GNSS Service (IGS) [**10**].

This article focusses on high precision real time kinematic (RTK) positioning results based on data of the four IOV satellites for which their positions are computed using the broadcast navigation message data. Crucial to RTK positioning is a correct fixing of the carrier phase ambiguities, and, according to the authors' knowledge, results of Galileo IOV ambiguity resolution, standalone as well as with GPS, are described in an article for the very first time. The Galileo IOV data have been collected by the permanent multi-GNSS receivers operated by Curtin University in Perth, Western Australia. The focus of the article will be on the time needed to reliably fix the carrier phase ambiguities for different combinations of the Galileo frequencies. Integer ambiguity resolution is the prerequisite for precise positioning and hence should be as fast as possible. Results of ambiguity resolution and positioning were not only evaluated for Galileo IOV alone, but also when combined with GPS. This was done for two periods of ~2 h in which the four IOV satellites were simultaneously observed in Perth. These two datasets are separated by 10 days, corresponding to the period after which the four-satellite Galileo constellation is repeating itself [**11**]. In addition, combined Galileo&GPS positioning results will be presented for another dataset mimicking urban canyon conditions, such that it would not be possible to obtain precise positioning results based on data of one constellation only.

This article is set up as follows. The observation models underlying Galileo-only or GPS-only and combined Galileo&GPS as based on double differences are reviewed in the section on 'Single GNSS versus combined GPS&Galileo positioning model'. The section on 'Results of ambiguity resolution and precise positioning' presents results of ambiguity resolution and positioning based on these models, while the section on 'Conclusions' ends the article with conclusions.

Single GNSS versus combined GPS&Galileo positioning model

Single GNSS double differenced observation model

The double differenced (DD) observation equations for a single GNSS constellation short-baseline positioning model are given as follows, in linearised form, for a certain epoch i [**12**], [**13**]

$$\begin{aligned} E\{\Phi_j^{1_* s}(i)\} &= -[u^{1_* s}(i)]^T b(i) + \lambda_j a_j^{1_* s} \\ E\{p_j^{1_* s}(i)\} &= -[u^{1_* s}(i)]^T b(i) \end{aligned} \quad (1)$$

where $E\{\cdot\}$ denotes the mathematical expectation operator, $[\cdot]^T$ denotes the transpose, and where $(\cdot)_j^{1_* s} = (\cdot)_j^s - (\cdot)_j^{1_*}$ is used to denote a DD observable or variable between a pair of receivers (note: $(\cdot)_j^s$ denotes a between-receiver single-differenced observable) and a pair of satellites, denoted as $s = 2_*, \ldots, m_*$ (m_* denotes the number of satellites tracked), relative to a pivot satellite, denoted as 1_*. The asterisk (*) is introduced to distinguish between the constellations, i.e. * = G for GPS and * = E for Galileo. The frequency of the observables/variables is denoted using the index $j = 1_*, \ldots, f_*$, with f_* the number of frequencies. DD phase and code (observed-minus-computed) observables for each frequency are denoted as $j_j^{1_* s}(i)$ and $p_j^{1_* s}(i)$, both in distance units. Unknown parameters are first the 3D baseline vector for each epoch (so the receivers may be in motion), denoted as $b(i)$ (in distance units). The line-of-sight unit vectors between receiver and satellites are denoted as $u^s(i)$. In equation (1) they appear in between-satellite form and are denoted as $u^{1_* s}(i) = u^s(i) - u^{1_*}(i)$.

The second group of unknown parameters are the DD ambiguities for each frequency, denoted as $a_j^{1_* s}$, with the ambiguities in cycles. The DD ambiguities are integer and constant as long as no cycle slips occur. Their wavelengths are denoted as λ_j.

With a 'short' baseline we assume that the distance between the two GNSS receivers is at most about 10 km long, see e.g. [**14**]. This has the following consequences. First, the line-of-sight vectors can be taken identical for both receivers with respect to the same satellite. Second, errors in the satellite positions (that are assumed to be known in the baseline processing) can be safely ignored. Third, for short baselines the between-receiver differential atmospheric errors are so small that they can be ignored as well (under normal ionospheric conditions and in mid-latitude regions).

If we assume that the system of equations in equation (1) is set up for $i = 1, \ldots, k$ observation epochs and $j = 1_*, \ldots, f_*$ frequencies, the redundancy (number of observations minus number of parameters) of the single constellation DD model equals $f_*(m_* - 1)(2k - 1) - 3k$. This implies that if we have phase and code observations of at least one epoch ($k \geq 1$) and at least one frequency ($f_* \geq 1$), the number of satellites is required to be at least four ($m_* \geq 4$). We remark in this context that although the precision of the code data is much lower than of the phase data, they strengthen the observation model. Without code data, it is not possible to solve the model based on a single epoch of data, as there would be more

unknowns than observations using phase observations only.

Combined GPS&Galileo observation model

When GPS and Galileo observations are tracked by both receivers, the phase/code observation equations as in equation (1) can be set up for both systems, where they share the baseline components as common parameters. In such a combined observation model each of the systems defines its own pivot satellite to perform the differencing. This observation model will be referred to as the 'standard' GPS+Galileo model. However, GPS and Galileo have two identical frequencies (L1-E1 and L5-E5a) and we can take benefit of this. It is then possible to difference the Galileo observations at each identical frequency with respect to a pivot satellite of *GPS* [**15**]. In that case between-receiver differenced GPS-Galileo inter-system biases (ISB) may remain after performing the double differencing. In [**16**], [**17**] it is mentioned that these differential ISBs are due to a difference in receiver hardware biases between the GPS and Galileo signals. In [**18**] it was demonstrated that for baselines consisting of receiver pairs of the same manufacturer and type the differential ISBs are absent, while for pairs of mixed receivers they are present but very stable in time, such that they can be calibrated. Although these results were based on data using the GIOVE satellites, it is expected that a similar conclusion holds for the IOV satellites.

An alternative combined (linearised) system of DD GPS and Galileo observation equations, in which the Galileo phase and code data at identical frequencies are differenced relative to the GPS pivot satellite and corrected for differential ISBs, can now be given as follows:

$$
\begin{array}{lcll}
E\{\Phi_o^{1_G\,s}(i)\} & = & -[\mathbf{u}^{1_G\,s}(i)]^T\mathbf{b}(i) + \lambda_o a_o^{1_G\,s} & ; \text{ GPS identical frequencies} \\
E\{\Phi_j^{1_G\,s}(i)\} & = & -[\mathbf{u}^{1_G\,s}(i)]^T\mathbf{b}(i) + \lambda_j a_j^{1_G\,s} & ; \text{ GPS other frequencies} \\
E\{\Phi_o^{1_G 1_E}(i) - \lambda_o \hat{\delta}_o^{GE}\} & = & -[\mathbf{u}^{1_G 1_E}(i)]^T\mathbf{b}(i) + \lambda_o a_o^{1_G 1_E} & ; \text{ GPS}-\text{Galileo identical frequencies (pivot sats.)} \\
E\{\Phi_o^{1_G\,q}(i) - \lambda_o \hat{\delta}_o^{GE}\} & = & -[\mathbf{u}^{1_G\,q}(i)]^T\mathbf{b}(i) + \lambda_o a_o^{1_G\,q} & ; \text{ Galileo identical frequencies} \\
E\{\Phi_l^{1_E\,q}(i)\} & = & -[\mathbf{u}^{1_E\,q}(i)]^T\mathbf{b}(i) + \lambda_l a_l^{1_E\,q} & ; \text{ Galileo other frequencies} \\
E\{p_o^{1_G\,s}(i)\} & = & -[\mathbf{u}^{1_G\,s}(i)]^T\mathbf{b}(i) & ; \text{ GPS identical frequencies} \\
E\{p_j^{1_G\,s}(i)\} & = & -[\mathbf{u}^{1_G\,s}(i)]^T\mathbf{b}(i) & ; \text{ GPS other frequencies} \\
E\{p_o^{1_G 1_E}(i) - \hat{d}_o^{GE}\} & = & -[\mathbf{u}^{1_G 1_E}(i)]^T\mathbf{b}(i) & ; \text{ GPS - Galileo identical frequencies (pivot sats.)} \\
E\{p_o^{1_G\,q}(i) - \hat{d}_o^{GE}\} & = & -[\mathbf{u}^{1_G\,q}(i)]^T\mathbf{b}(i) & ; \text{ Galileo identical frequencies} \\
E\{p_l^{1_E\,q}(i)\} & = & -[\mathbf{u}^{1_E\,q}(i)]^T\mathbf{b}(i) & ; \text{ Galileo other frequencies}
\end{array}
\qquad (2)
$$

with the GPS satellite index $s=2_G,\ldots,\ m_G$ and the Galileo satellite index $q=2_E,\ldots,m_E$. Furthermore, the frequency indices are defined as follows: $o=1,\ \ldots,\ f$ for the identical frequencies between GPS and Galileo; $j=1_G,\ldots,f_G$ for the other GPS frequencies and $l=1_E,\ldots,f_E$ for the other Galileo frequencies. Thus, the notation f_S (with $S\in\{G,E\}$) is used here to denote the frequencies per constellation that are not identical, while for a single constellation it was used to denote the total number of frequencies per GNSS. For example, assume we have two GPS frequencies and three Galileo frequencies in the combined model of which one frequency is identical, we have $f=1$, $f_G=1$ and $f_E=2$. In case of the single constellation models we would have $f_G=2$ and $f_E=3$. The differential ISBs are defined as $\delta_o^{GE}=\delta_o^E-\delta_o^G$ for phase and as $d_o^{GE}=d_o^E-d_o^G$ for code, where δ_* and d_o^* denote the between-receiver differenced hardware phase and code delay per constellation. Thus, δ_o^{GE} and d_o^{GE} can be regarded as double differences with respect to the receivers and the different constellations. The corrections for these differential ISBs are denoted using the 'hat' sign in equation (2). While the DD ambiguities of the non-identical Galileo frequencies are relative to the Galileo pivot satellite, correction for the ISBs has as consequence that the DD ambiguities for the Galileo frequencies identical to those of GPS become relative to the pivot satellite of GPS.

The redundancy of the 'standard' combined model can be shown to read

$$[(f+f_G)(m_G-1)+(f+f_E)(m_E-1)](2k-1)-3k$$

Now, with at least one epoch ($k\geqslant 1$), as well as at least one frequency per system ($f+f_G\geqslant 1$ and $f+f_E\geqslant 1$), we have the requirement for the combined number of satellites that $m_G+m_E\geqslant 5$. This condition can be met with several combinations of GPS and Galileo satellites, as long there is at least one satellite of each system. In the alternative combined model (2) there is one phase and code observation more (per overlapping frequency and per epoch; thus $2fk$) than in the standard model. On the other hand, the number of additional unknowns in model (2) is of size f (the number of DD ambiguities between the pivot satellites of both systems). For the redundancy this means that it is increased with $f(2k-1)$ compared to the redundancy of the 'standard' GPS+Galileo model. This implies that if $f\geqslant 1$ we can do with one satellite less compared to the standard model, i.e. $m_G+m_E\geq 4$. This more relaxed requirement may be an advantage in areas with low satellite visibility (e.g. urban canyons).

Three-step procedure for solving relative GNSS model

To solve the relative receiver positions of the models in the previous subsections with high precision it is common to make use of the integer nature of the DD ambiguities. The model is then solved by means of a three-step procedure. In the first step the integer nature of the ambiguities is discarded and one performs a

standard least-squares adjustment. The solution is referred to as the 'float' solution, and is, for short timespans, governed by the precision of the code data (the phase data only start to contribute after the receiver-satellite geometry has changed sufficiently). In the second step the part of the float solution corresponding to the ambiguities is input for the LAMBDA method [**19**], which outputs an integer solution. It needs to be tested whether this integer solution can be accepted as the correct one with sufficient reliability. For this the fixed–failure rate ratio test (FFRT; [**20**]) is used, which also needs the second-best solution that is provided by the LAMBDA method, in addition to the 'best' or integer least-squares solution. After the integer ambiguities can be successfully resolved, in the third and final step another standard least-squares solution is carried out, with the ambiguities held fixed. The resulting position solution, often referred to as the 'fixed' solution, is then governed by the high precision of the phase data.

Results of ambiguity resolution and precise positioning

Selection of Galileo IOV and GPS data: datasets I and II

Galileo IOV and GPS data were collected by three multi-GNSS receivers permanently set up at Curtin University in Perth, Australia. Two Trimble TRM59800·00 geodetic antennas, with a short spacing of ~8·4 m, are connected to the roof of building 402 (see Fig. 1). One of the antennas is connected to a Trimble NetR9 receiver (CUTA), while the other antenna is connected to *two* receivers using a splitter: another Trimble NetR9 receiver (CUT0) and a Septentrio PolaRx4 receiver (CUT1). Both Trimble and Septentrio receivers collect Galileo data on four frequencies, and GPS data on three frequencies.

We first present ambiguity resolution and positioning results for a period of ~2 h during which the four Galileo IOV satellites were tracked above an elevation of 10°, i.e. for 20 March 2013 (04:05:30-06:00:00 GPST; where GPST stands for GPS Time), and compare these results for a period 10 days after, i.e. 30 March 2013 (03:24:00-05:18:30 GPST), when the Galileo constellation was the same to that of 20 March. These datasets are referred to as 'dataset I'. Figure 2 (left) depicts the sky plot for the 2 h periods during both days. In addition to the four Galileo satellites, the sky plot shows the tracks of four GPS satellites, which are used for the GPS-only computations and those combined with Galileo. Data of other than these four GPS satellites was collected as well, though not used in our computations; otherwise GPS would have a too dominant contribution to the combined solution. To have a 'fair' comparison we selected those four GPS satellites that were observed continuously during the 2 h timespan.

To get insight in the receiver-satellite geometry, Fig. 3 (left) shows the position dilution of precision (PDOP) values based on these four GPS satellites, as well as those based on the four Galileo IOV satellites, plus the PDOPs corresponding to combined Galileo&GPS. The PDOPs of GPS-only are very close to those of Galileo-only: while those of GPS have a mean of about 4, the Galileo-only PDOPs are just below this value. The combined Galileo&GPS case is most favourable in terms of receiver-satellite geometry, with PDOPs varying between

1 Trimble antennas on roof of Curtin University campus building 402, with inter-distance of ~8·4 m: CUTA and CUT0 are connected to Trimble NetR9 receivers, while CUT1 is connected to a Septentrio PolaRx4 receiver

a low 2 and 3. Besides PDOP values, Fig. 4 shows the DOPs for the east component (EDOP), the north component (NDOP) and the up or vertical component (VDOP). While the VDOP is in all cases (i.e. Galileo-only, GPS-only and Galileo&GPS) larger than the EDOP or NDOP during the 2 h timespan, note that for the Galileo-only case the NDOP is always larger than the EDOP.

In addition to the results based on a cut-off elevation of 10°, results are presented based on Galileo and GPS observations at a much higher cut-off elevation, i.e. 45°, to mimic 'urban canyon' conditions with obstructed satellite visibility at low elevations. These data are referred to as 'dataset II'. Figure 2 (right) shows the sky plot corresponding to a period of 1·3 h (17:54:00-19:13:00 GPST) on the day of 8 April 2013, during which two Galileo IOV satellites and three to four GPS satellites were available above this high elevation. Most of the time only three GPS satellites were tracked simultaneously; the required number of four GPS satellites needed for positioning was only available for 53% of the time. The accuracy of positioning based on these four GPS satellites would be very poor, because the receiver-satellite geometry turns out to be very bad, as indicated by the extremely large PDOP values in Fig. 3 (right). Although in the Galileo&GPS case at least 5 satellites are available all the time, which is sufficient for positioning, the PDOP of combined positioning still reaches up to values of 30, mainly close to epoch 50. Table 2 summarises the timespans and satellites that are used in datasets I and II.

Measuring performance of ambiguity resolution and positioning

Although both receivers of the baselines are stationary, in the processing the baseline coordinates are treated to be unlinked in time. The availability of these relative positions with high accuracy depends on the speed at which the ambiguities can be resolved to their correct integer values. Instantaneous (single epoch) ambiguity resolution is fastest, but can only be successful if the underlying model is strong enough. Otherwise, more epochs of data need to be processed in order for the float

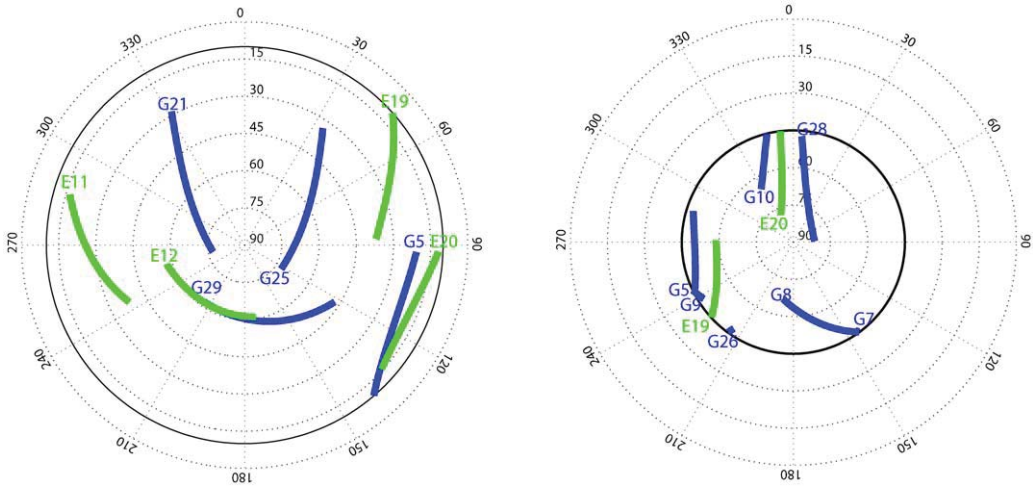

2 Left (dataset I): Galileo-IOV&GPS sky plot, based on 4 Galileo and 4 GPS satellites, above cut-off elevation of 10°, on 20/30 March 2013 at Curtin University, Perth, Australia; right (dataset II): Galileo-IOV&GPS sky plot, based on 2 Galileo and 3–4 GPS satellites (4 satellites only tracked for 53% of time), above cut-off elevation of 45°, on 8 April 2013; in both plots tracks of Galileo satellites are coloured green and those of GPS satellites are coloured blue

ambiguity solution to converge and integer estimation can be successful. The ambiguities are resolved successfully if the fixed failure rate ratio test is passed. In all computations a fixed failure rate of 0·001 was used. The time needed for correct integer ambiguity estimation will be referred to as 'time-to-fix-ambiguities' (TTFA). To assess the performance of the positioning, the estimated ambiguity-float and ambiguity fixed positions are compared to their given highly accurate benchmark positions. These benchmark positions are obtained from processing long time series of GPS data for the stations.

Stochastic model of Galileo IOV and GPS data

The stochastic model of the Galileo and GPS code data, as has been adopted in all computations in this article, is determined using variance-component estimation [**21**] based on the observation data of 20 and 30 March 2013, but then extended with one hour during which the four IOV satellites were visible as well, as to have more data to reliably estimate the variance components. Next to the variance components, also the (cross) covariances between the observables are estimated, which is in particular relevant for the Galileo E5a, E5b, and E5 observables, which are all derived from the same wideband signal.

Because of the known *a priori* coordinates of the short baselines, together with the cancelling of the differential atmospheric delays, the observables in DD mode can be treated as zero-mean random signals. Taking the exponential elevation weighting strategy [**22**], the weighted average of the squared elements of each observable type would then be referred to as an estimate

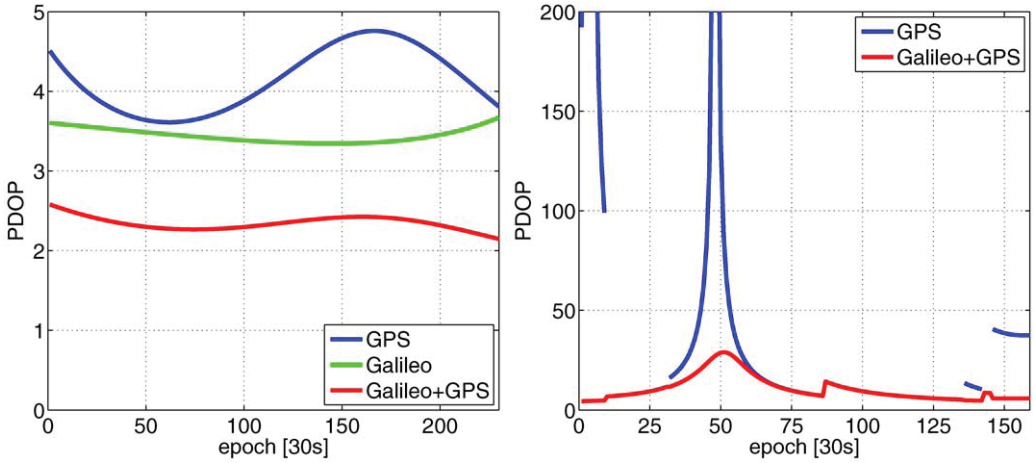

3 PDOPs based on GPS-only, Galileo-only and Galileo&GPS combined for dataset I (left) and for dataset II (right): for dataset I four GPS and four Galileo IOV satellites are used to compute the PDOPs, while in case of dataset II only two IOV satellites were tracked, so no PDOPs are computed for Galileo-only

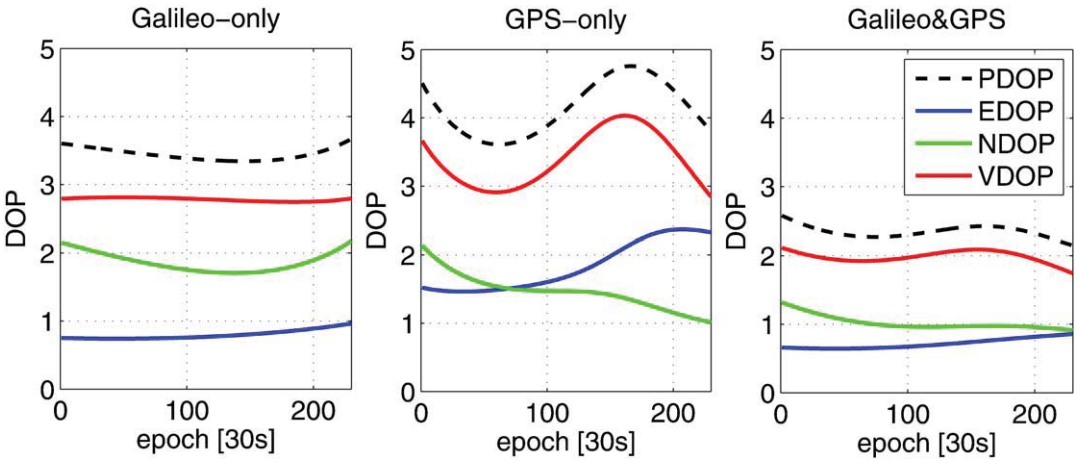

4 PDOPs, EDOPs, NDOPs and VDOPs for Galileo-only (left), GPS-only (middle) and Galileo&GPS (right) for dataset I, where 4 Galileo and 4 GPS satellites are used

of the observable type's variance. Similarly, the estimates of the cross-covariance between the observable types are computed through weighted averaging the product of their elements which, in turn, yields their estimated correlation coefficients.

Table 3 presents the estimated code standard deviations, referenced to zenith and in undifferenced mode, of the Galileo and GPS observables for both Trimble and Septentrio receivers. We remark that the GPS L5 frequency is not used in the computations since at the moment of writing this article (2013) it is transmitted by just three operational GPS satellites. Table 4 presents the results of the estimated (zenith-referenced) correlation coefficients of the Galileo code observables of the Trimble receivers. It can be seen that the results between the two days are very consistent with each other. Furthermore, the estimated correlation coefficients in Table 4 are reasonably small; the largest values of ~0·3 are the correlation coefficients between E5a and E5, as well as between E5b and E5. Based on these results, we believe that it is permitted to assume that the Galileo observables of different frequencies are uncorrelated. From the results it also followed that the code data of GPS can be assumed uncorrelated. For the correlation coefficients of the code data tracked by the Septentrio receiver a similar conclusion could be drawn as for the Trimble receivers. Concerning the phase data, based on the estimated variances it turned out that the undifferenced phase standard deviation for all observables could be set to a value of 3 mm (in zenith).

The estimated zenith-referenced standard deviations for phase and code are multiplied by an exponential function, cf. [**22**], as to model the precision as a function of elevation. In a next step the propagation law of variances is applied to compute the variance–covariance matrix of the DD observations.

Results dataset I: four satellites per constellation

For the two days forming dataset I the times to fix the integer ambiguities are evaluated for several cases: Galileo-only, GPS-only and Galileo&GPS combined. To quantify the benefit of additional frequencies, in the computations we started with single frequency cases and systematically added one frequency at a time. Figure 5 presents the mean convergence times to fix the ambiguities for the two baselines, i.e. CUT0-CUTA, consisting of identical Trimble receivers, and CUT1-CUTA, the mixed Septentrio-Trimble baseline. For the CUT0-CUTA baseline two times-to-fix are shown in Fig. 5: the first corresponding to 20 March and the second to 30 March. Unfortunately, the Septentrio receiver did not track data on the first day (20 March), so for the baseline CUT1-CUTA only the times-to-fix corresponding to 30 March is shown. For the CUT0-CUTA baseline it can be

Table 3 Standard deviations (in local zenith) for undifferenced Galileo and GPS code observables tracked by Trimble and Septentrio receivers

	E1	E5a	E5b	E5	L1	L2
Trimble/cm	25	20	25	10	25	30
Septentrio/cm	20	20	20	10	25	25

Table 2 Information on date, timespan, selection of Galileo and GPS satellites, cut-off elevation and sampling interval as used for datasets I and II

	Dataset I	Dataset II
Date and time	20 March 2013 (04:05:30-06:00:00 GPST) 30 March 2013 (03:24:00-05:18:30 GPST)	8 April 2013 (17:54:00–19:13:00 GPST)
Galileo satellites	E11-E12-E19-E20	E19-E20
GPS satellites	G5-G21-G25-G29	G5-G7-G8-G9-G10-G26-G28
Elevation cut-off	10°	45°
Sampling interval	30 s	30 s

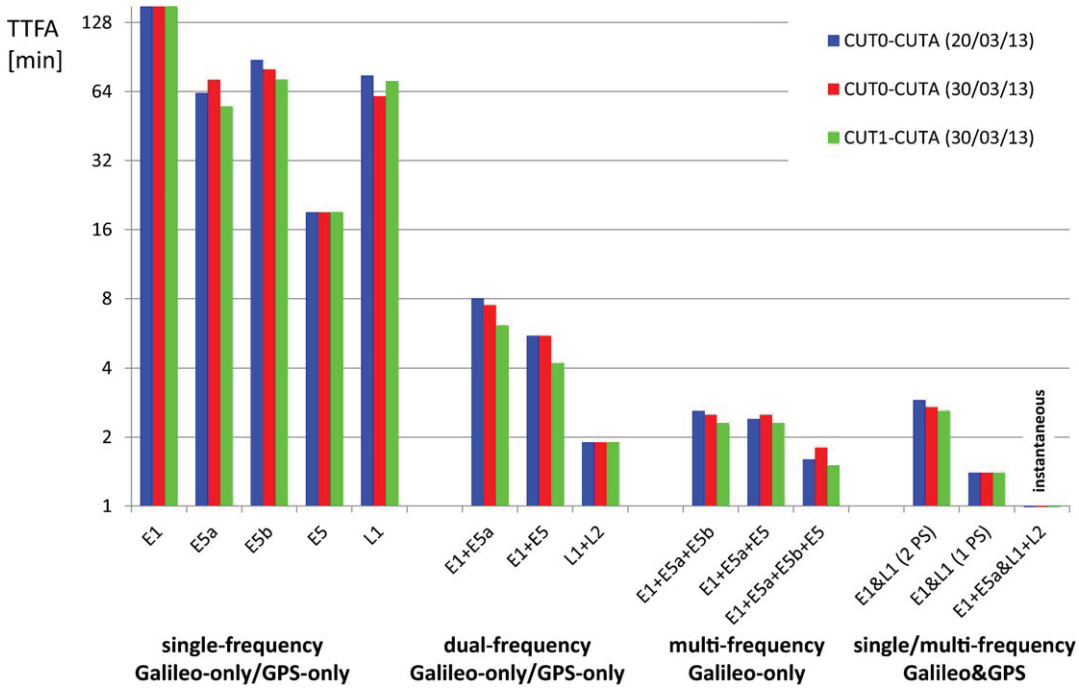

5 Mean times-to-fix-ambiguities (TTFA; in min) for different processing strategies based on 4-satellite Galileo IOV and 4-satellite GPS observations of dataset I, collected on baseline CUT0-CUTA on 20 March (blue bars) and 30 March (red bars) 2013, and on baseline CUT1-CUTA on 30 March 2013 (green bars): note that scaling of the y-axis is logarithmic; for single/multifrequency Galileo&GPS combined processing there are two single frequency strategies: first with pivot satellite (PS) for each constellation (E1&L1; 2 PS) and second with common pivot satellite for both Galileo and GPS (E1&L1; 1 PS); remark that for single frequency E1 and L1 cases ambiguity resolution could not be realised during full timespan; bars therefore take maximum value of y-axis; it is furthermore remarked that for multifrequency Galileo&GPS case mean time-to-fix-ambiguities is just based on single epoch (corresponds to 0·5 min) for both baselines during two days, which explains three small bars below 1 min value for E1 + E5a&L1 + L2

seen that the differences in times-to-fix between the two days are very small. Generally, the ambiguity convergence times for baseline CUT1-CUTA are slightly better than those of baseline CUT0-CUTA, which is attributed to the better code precision for some of the observables tracked by the Septentrio receiver (see Table 3).

Single constellation single frequency ambiguity resolution performance

As can be seen from Fig. 5, for both baselines the single constellation (i.e. Galileo-only or GPS-only) single frequency cases require the longest times-to-fix, which is due to the weakness of the underlying model, since satellite or frequency redundancy is absent. For the Galileo E1 observations even the 2 h timespan is insufficient to resolve the ambiguities. From GPS-only we know that single frequency ambiguity resolution is only expected to be successful with a large number of satellites [**23**], and thus only four visible satellites is simply too few. Comparing the Galileo-only E1 case with E5a, E5b and E5, it can be seen that E1 performs much worse (even the full 2 h timespan is still not enough for ambiguity resolution), as compared to the E5a, E5b and E5 frequencies. This result is due to the shorter wavelength of E1 (~19 cm) as compared to the other three (~25 cm), which led to a poorer float ambiguity solution for E1. The much better performance of E5 (~19 min time-to-fix) is attributed to the low code noise of this signal; a promising feature which was also emphasized in [**3**], although in that article simulated Galileo observations were used. The time-to-fix-ambiguities in case of GPS-only L1 are for the two baselines ~1 h, and this is much shorter than for the Galileo-only E1 case. At first sight, this better result for GPS-only may look surprising; since the precision of the E1 and L1 observations is comparable and the geometry based on the four GPS satellites is slightly poorer than based on the four Galileo satellites, as demonstrated by the higher PDOP values for GPS-only in Fig. 3. However, one has to keep in mind that it is not so much the instantaneous geometry that is relevant for ambiguity resolution, but more importantly is its change in time [**24**]. While the instantaneous geometry is poorer for GPS than for Galileo, the PDOP of GPS changes more than that of

Table 4 Estimated zenith-referenced cross-correlation coefficients of Galileo code observables, based on 3 h of Trimble data collected on 20 and 30 March 2013*

	E1/E5a	E1/E5b	E1/E5	E5a/E5b	E5a/E5	E5b/E5
20 March	0·09	0·08	0·06	0·06	0·32	0·26
30 March	0·11	0·05	0·10	0·11	0·28	0·29

*The standard deviation of the estimated correlations is ~0·04.

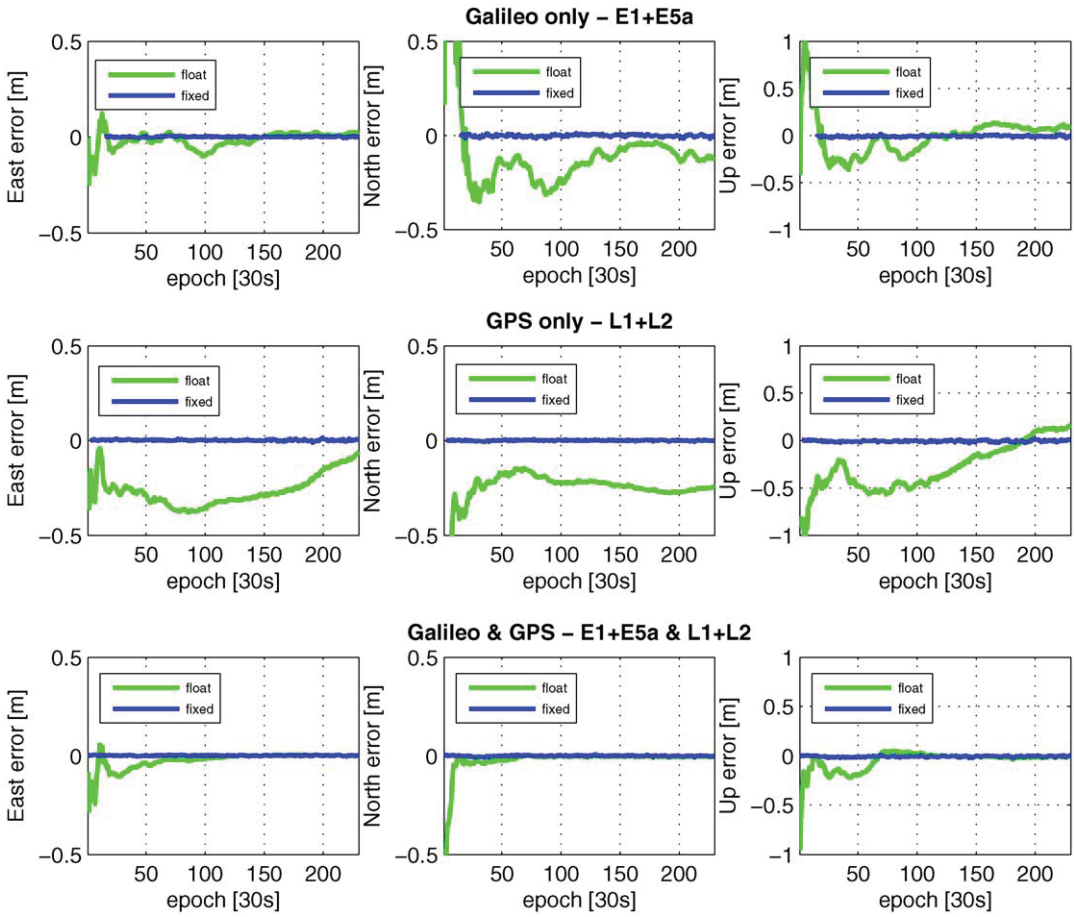

6 Dataset I: CUTA position (east-north-up) errors based on Galileo-only E1+E5a (top), GPS-only L1+L2 (middle) and Galileo&GPS E1+E5a & L1+L2 (bottom), estimated from CUT1-CUTA baseline: position errors based on float ambiguities are plotted in green; those based on fixed ambiguities are plotted in blue

Galileo, which remains at a more constant level during the 2 h timespan. This change of the geometry has a favourable effect on the precision of the float GPS ambiguities, leading to shorter times-to-fix as compared to the Galileo-only case, for which there is less change in receiver-satellite geometry.

Single constellation dual frequency ambiguity resolution performance

Adding a second frequency already improves the single constellation ambiguity times-to-fix considerably, to less than ten minutes for Galileo-only (E1+E5a and E1+E5, with a better performance for the second combination), and to even less than two minutes for GPS-only. The explanation for the better results in case of GPS-only is the same as in the single-frequency case.

Galileo-only triple and quadruple frequency ambiguity resolution performance

Before discussing the performance of combined Galileo &GPS ambiguity resolution and positioning, we will give results for Galileo-only ambiguity resolution when a third and fourth frequency are added. From Fig. 5 it follows that the addition of a third frequency still improves the ambiguity convergence time somewhat. For both baselines the time-to-fix is 2–3 min when based on either the E1+E5a+E5b observables, or the E1+E5a+E5 observables. The inclusion of the precise E5 observables does not have much influence in the triple-frequency performance compared to the use of E5b, as the times-to-fix are already at a fast level. Adding a fourth frequency (i.e. E1+E5a+E5b+E5) gives the best performance for Galileo-only: the mean time-to-fix-ambiguities is less than 2 min.

Galileo&GPS single/multifrequency ambiguity resolution performance

In the combined Galileo&GPS case, single frequency (E1&†L1) ambiguity resolution was first based on the 'standard' model with a pivot satellite for each constellation (see the section on 'Single GNSS versus combined GPS&Galileo positioning model'). For both baselines the resulting mean time-to-fix is less than three minutes. Compared to the single-system performances,

†The '&' symbol is used to list the observables of the combined Galileo&GPS constellations, whereas the '+' symbol is reserved to list the observables belonging to one constellation.

Table 5 Dataset I: position errors (mean and RMS error) for receiver CUTA, based on Galileo-only E1+E5a, GPS-only L1+L2 and Galileo&GPS E1+E5a & L1+L2, relative to *a priori* known values of position of receiver*

	Galileo only: E1+E5a		GPS only: L1+L2		Galileo&GPS: E1+E5a&L1+L2	
	Ambiguity float/cm	Ambiguity fixed/mm	Ambiguity float/cm	Ambiguity fixed/mm	Ambiguity float/cm	Ambiguity fixed/mm
East	Mean=−1	Mean=2	Mean=−26	Mean=1	Mean=−2	Mean=2
	RMS=5	RMS=3	RMS=28	RMS=4	RMS=5	RMS=2
North	Mean=−9	Mean=−1	Mean=−25	Mean=0	Mean=−3	Mean=0
	RMS=27	RMS=6	RMS=28	RMS=2	RMS=10	RMS=2
Up	Mean=0	Mean=−7	Mean=−29	Mean=−7	Mean=−5	Mean=−6
	RMS=22	RMS=10	RMS=38	RMS=10	RMS=12	RMS=9

*The position errors are computed for the case the ambiguities are float, as well as fixed. Time series of these position errors are depicted in Fig. 6.

which are on the order of one to a few hours, this is a tremendous improvement. An even further improvement is possible when instead of two pivot satellites only one is used; for the baseline CUT0-CUTA, consisting of identical Trimble receivers, differential ISBs can be assumed absent; however, for the baseline CUT1-CUTA, consisting of mixed receivers, we first determined the differential ISBs from another dataset. The differential phase ISB was estimated at −0·21 cycle, while the differential code ISB was estimated at an insignificant value close to zero, implying that it can be neglected for this combination of Septentrio and Trimble receivers. Thus only the phase data received an *a priori* ISB correction. From Fig. 5 it can be seen that the resulting performance of ambiguity resolution based on one pivot satellite is very similar for both baselines: the mean time-to-fix for the ambiguities is ~1·5 min, about half the time of the two-pivot-satellite case. In a next step, for the combined Galileo&GPS multifrequency case we processed two frequencies from both systems, i.e. E1+E5a and L1+L2. As can be expected, because of the strength of this model, its performance is best: for both baselines ambiguity resolution can be done successfully in an instantaneous way, thus based on a single epoch of data all the time.

Positioning performance

The above cases will now be used to assess the performance of the positioning. Figure 6 depicts the errors in east-north-up for the position solutions of CUTA, obtained from the Galileo E1+E5a, GPS L1+L2 and Galileo&GPS E1+E5a&L1+L2 processing of the CUT1-CUTA baseline, based on float as well as fixed ambiguities. These positioning results are plotted in multiepoch mode, where for the float solution use is made of the time constancy of the ambiguities. The fixed position errors are only plotted after the correct integer ambiguities have been estimated (in the Galileo-only case this takes more time than in the GPS-only and Galileo&GPS cases; this explains why the fixed curve starts 'later' in the Galileo-only case). The position errors are obtained by subtracting the position estimates from the precisely known benchmark coordinates. For each component the empirical mean and root-mean-square (RMS) error values are shown in Table 5. It can first be seen that in the Galileo-only case the east component is determined with a better precision than the north component: its RMS error values are 5 cm for float and 3 mm for fixed east; while the RMS error is a large 27 cm for float north and ~6 mm for fixed north. This better precision is east direction is due to the actual receiver-satellite geometry: in Fig. 4 (left) it can be seen that the EDOP in case of Galileo-only is smaller than the NDOP, indicating that the Galileo satellite distribution in east–west direction is much better than in north–south (as there are no satellites in the south). After ambiguity resolution however there is much less difference in the precision of east versus north: both are at sub-cm level. In the GPS-only L1+L2 case, there is less difference in precision level of east and north components. Although the float solution shows a large bias during the timespan (the coordinate estimates show a mean of ~30 cm in all three components), the results look much better after ambiguity resolution, with the means of the fixed components at the sub-cm level. The bottom three graphs of Fig. 6 depict the position errors for the combined Galileo&GPS case. Although ambiguity resolution can be done instantaneously in this case, the positioning results are plotted in multiepoch mode to compare them to the single constellation positioning results. From Table 5 it can be seen that the combined case results in the lowest RMS error values

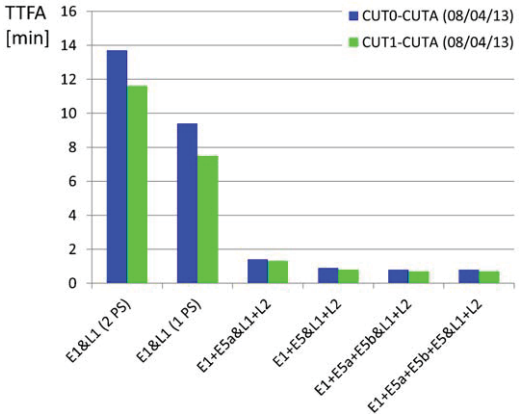

7 Mean times-to-fix-ambiguities (TTFA; in min) for different processing strategies based on 45° cut-off elevation Galileo&GPS observations of dataset II, collected on 8 April 2013 at baselines CUT0-CUTA (blue bars) and CUT1-CUTA (green bars); for single/multifrequency Galileo&GPS combined processing there are two single frequency strategies: first with pivot satellite for each constellation (E1&L1; 2 PS) and second with common pivot satellite for both Galileo and GPS (E1&L1; 1 PS)

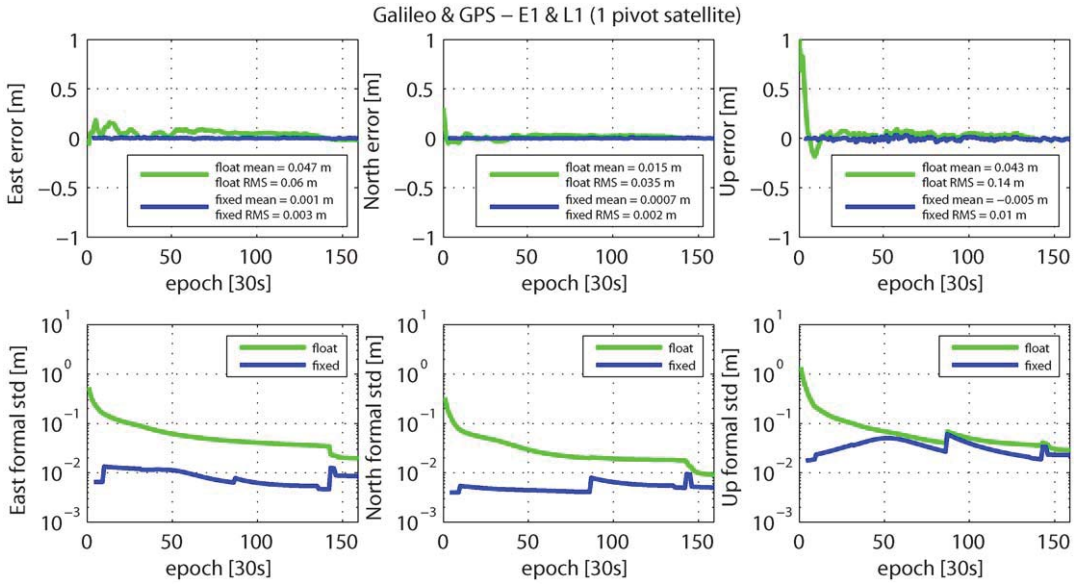

8 Dataset II: CUTA position (east-north-up) errors for Galileo&GPS E1&L1 with 1 pivot satellite (top) versus formal standard deviations, for float and fixed solutions (bottom), determined for baseline CUT1-CUTA

for float and fixed: the float RMS error is smaller than 12 cm and the fixed RMS error is below 1 cm, for all three components.

Results dataset II: 'urban canyon' conditions

For dataset II, where Galileo&GPS observations that are tracked above 45° elevation are used, we only present results of combined ambiguity resolution and positioning, because only two Galileo satellites were tracked and only four GPS satellites were available for half of the time (for the rest of the time just three GPS satellites), having a very poor geometry, see Fig. 3 (right).

Figure 7 presents the mean time-to-fix the ambiguities during the timespan, for the same short baselines as used in dataset I, i.e. CUT0-CUTA, formed by two Trimble receivers, and CUT1-CUTA, formed by a Septentrio and a Trimble receiver.

For the single frequency case, combining Galileo E1 with GPS L1, the processing was performed in two different ways: first, based on a pivot satellite per constellation (the 'standard' approach) and secondly, ignoring the differential ISBs for the CUT0-CUTA baseline, while applying differential ISB corrections to the CUT1-CUTA baseline, such that one pivot satellite (in this case of GPS) for both Galileo and GPS is sufficient. With two pivot satellites, the mean time-to-fix is in the range of 11–14 min, but this decreases to 7–10 min when one pivot satellite is used. These times are longer than for the similar cases in dataset I (see Fig. 5), but this is due to the fewer satellites we have in dataset II, resulting in a weaker model. Adding a frequency for both constellations (i.e. E1+E5a and L1+L2) significantly shortens the ambiguity convergence time, to just above 1 min for both baselines. Using the more precise E5, i.e. processing E1+E5 with L1+L2, improves ambiguity resolution, although the gain is only limited compared to the use of E5a: the mean time-to-fix is just below one minute for both baselines. While in case of dataset I instantaneous ambiguity resolution was feasible based on E1+E5a and L1+L2 observables, this is not possible for the current dataset as a result of the lack of satellite redundancy for many epochs. However, times-to-fix of less than one minute are promising for applications with obstructed satellite visibility. The addition of a third or even a fourth Galileo frequency does not further reduce the ambiguity convergence time, as compared to the case when two Galileo frequencies are used.

To illustrate the performance of the positioning based on a large cut-off elevation of 45°, Fig. 8 shows the east-north-up position errors for CUTA (relative to its precisely known coordinates), based on the Galileo&GPS single frequency processing applying one pivot satellite (of GPS) for both constellations (for baseline CUT1-CUTA). It can be seen that the north component is determined with a higher accuracy in terms of RMS errors, followed by east and up. This is due to the receiver-satellite geometry for this dataset, with a better distribution of satellites in north-south direction than in east-west (see the sky plot at the right in Fig. 2, showing that most satellites basically move in the north-south direction). Finally, we remark from Fig. 8 that the formal standard deviation of the up component reaches up to 8 cm after ambiguity fixing. This relatively poor height precision is due to the large cut-off elevation of 45°, resulting in a receiver-satellite geometry in which all satellites are relatively close to the zenith.

Conclusions

This article has presented results of carrier phase ambiguity resolution and high precision relative positioning based on real observation data of the four Galileo IOV satellites in orbit that were received beginning in March 2013. The positions of these Galileo satellites were computed using the ephemerides

transmitted in the navigation messages. The performance of LAMBDA based ambiguity resolution and positioning was tested for some short baselines for which the differential atmospheric delays and ephemeris errors can be safely ignored.

Although instantaneous (single epoch) ambiguity resolution based on just four satellites is not possible, as the underlying model is too weak, it was demonstrated that dual frequency Galileo-only ambiguity resolution needs less than ten minutes on average for the considered datasets. This mean time-to-fix was even reduced to less than 2 min using all four frequencies of Galileo's Open Service. Combined with dual frequency data of four GPS satellites successful instantaneous Galileo&GPS ambiguity resolution could be demonstrated using at least dual frequency Galileo data. The resulting (kinematic) positioning accuracy, based on fixed ambiguities, was at the few millimetre level horizontally and at the 1 cm level vertically, in terms of RMS errors. It is emphasised that these results are based on only four satellites of each constellation; in (future) practice the results will be even better when there are more Galileo satellites. From our analyses it could furthermore be demonstrated that the precision of the E5 code observables is much better than of the code observables at the other frequencies of Galileo's Open Service (i.e. E1, E5a and E5b).

The benefits of the combination of Galileo with GPS will become even more evident in areas with poor visibility at low elevations ('urban canyon'), such that insufficient (i.e. fewer than four) GPS satellites are available, or they have a poor receiver-satellite geometry. Mimicking such conditions by setting the elevation cut-off to 45° in our analyses, resulted in a mean ambiguity convergence time of only slightly more than one minute based on the combination of two frequencies of each constellation.

Acknowledgements

This research was carried out in the context of the Australian Space Research Program (ASRP) project 'Platform Technologies for Space, Atmosphere and Climate', as well as in the context of the Positioning Program Project 1·01 'New carrier phase processing strategies for achieving precise and reliable multi-satellite, multi-frequency GNSS/RNSS positioning in Australia' of the Cooperative Research Centre for Spatial Information (CRC-SI). The second author is the recipient of an Australian Research Council (ARC) Federation Fellowship (project number FF0883188). All this support is gratefully acknowledged.

References

1. European Space Agency (ESA), 2013. http://www.esa.int (consulted March 2013).
2. European Union, 2010. European GNSS (Galileo) Open Service – Signal in Space Interface Control Document. September 2010.
3. Simksy, A., Sleewaegen, J. M., Hollreiser, M., Crisci M., 2006. Performance assessment of Galileo ranging signals transmitted by GSTB-V2 satellites. *Proc. ION GNSS 2006*, Fort Worth, TX, 26–29 September: 1547–1559.
4. Diessongo, T. H., Schüler, T., Junker, S., 2013. Precise position determination using a Galileo E5 single-frequency receiver. *GPS Solutions*, doi: 10.1007/s10291-013-0311-2.
5. Galileo in its glory, 2012. *GPS World*, 23(1): 12–14.
6. Kassabian, N., Falco, G., Lo Presti, L., 2012. First joint GPS/IOV-PFM Galileo PVT estimation using carrier phase measurements. *Proc. European Navigation Conference (ENC) 2012*, Gdansk, Poland, 25–27 April.
7. Langley, R. B., Banville, S., Steigenberger, P., 2012. First results: precise positioning with Galileo prototype satellites. *GPS World*, 23(9): 45–49.
8. Montenbruck, O., Hauschild, A., Hessels, U., 2010. Characterization of GPS/GIOVE sensor stations in the CONGO network. *GPS Solutions*, 15(3), 193–205, doi: 10.1007/s10291-010-0182-8.
9. Steigenberger, P., Hugentobler, U., Montenbruck, O., 2013. First demonstration of Galileo-only positioning. *GPS World*, 24(2): 14–15.
10. International GNSS Service Multi-GNSS Experiment, 2013. http://igs.org/mgex (consulted April 2013).
11. Zandbergen, R., Dinwiddy, S., Hahn, J., Breeuwer, E., Blonski, D., 2004. Galileo orbit selection. *Proc. ION GNSS 2004*, Long Beach, CA, 21–24 September: 616–623.
12. Teunissen, P. J. G. and Kleusberg, A. (eds.) 1998. *GPS for Geodesy*, 2nd edn, Berlin/Heidelberg/New York, Springer-Verlag.
13. Hofmann-Wellenhof, B., Lichtenegger, H., Wasle, E., 2008. *GNSS – Global Navigation Satellite Systems, GPS, GLONASS, Galileo and more*, Wien/New York, Springer-Verlag.
14. Chang, X. W., Paige, C. C., Yin, L., 2004. Code and carrier phase based short baseline GPS positioning. *GPS Solutions*, 7(4): 230–240. DOI 10·1007/s10291-003-0077-z.
15. Julien, O., Alves, P., Cannon, M. E., Zhang, W. 2003. A tightly coupled GPS/Galileo combination for improved ambiguity resolution. *Proc. European Navigation Conference (ENC) 2003*, Graz, Austria, 22–25 April. Available at http://plan.geomatics.ucalgary.ca/papers/gnss2003_atightlycoupledgpsgalileo.pdf
16. Hegarty, C., Powers, E., Fonville, B., 2004a. Accounting for timing biases between GPS, modernized GPS, and Galileo signals. *Proc. 36th Annual Precise Time and Time Interval (PTTI) Meeting*, Washington, DC, 7–9 December: 307–317.
17. Hegarty, C., Powers, E., Fonville, B., 2004b. GPS + modernized GPS + Galileo. *GPS World*, 17(3): 49–54.
18. Odijk, D., and Teunissen, P. J. G., 2013. Characterization of between-receiver GPS-Galileo inter-system biases and their effect on mixed ambiguity resolution. *GPS Solutions*, 17(4): 521–533. DOI 10·1007/s10291-012-0298-0.
19. Teunissen, P. J. G., 1995. The least-squares ambiguity decorrelation adjustment: a method for fast GPS integer ambiguity estimation. *Journal of Geodesy*, 70(1–2): 65–82. DOI 10·1007/BF00863419.
20. Verhagen, S. and Teunissen, P. J. G., 2013. The ratio test for future GNSS ambiguity resolution. *GPS Solutions*, 17(4): 535–548. DOI 10·1007/s10291-012-0299-z.
21. Bona, P., 2000. Precision, cross correlation, and time correlation of GPS phase and code observations. *GPS Solutions*, 4(2): 3–13. DOI 10·1007/PL00012839.
22. Euler, H. J. and Goad, C. C., 1991. On optimal filtering of GPS dual-frequency observations without using orbit information. *Bull. Geod.*, 65: 130–143.
23. Verhagen, S., Odijk, D., Teunissen, P. J. G., Huisman, L., 2010. Performance improvement with low-cost multi-GNSS receivers. *Proc. 5th ESA workshop on Satellite Navigation User Equipment Technologies, NAVITEC 2010*, Noordwijk, The Netherlands, 8–10 December 2010.
24. Teunissen, P. J. G., 1997. A canonical theory for short GPS baselines. Part I: The baseline precision. *Journal of Geodesy*, 71(6): 320–336. DOI 10·1007/s001900050100.

8 GPS, Galileo, QZSS and IRNSS L5/E5a-signal performance

This chapter is covered by the following publication:

Nadarajah N., **Khodabandeh A.** and Teunissen P.J.G. (2015). Assessing the IRNSS L5-signal in combination with GPS, Galileo, and QZSS L5/E5a-signals for positioning and navigation. GPS Solutions, doi: 10.1007/s10291-015-0450 8.

GPS Solut
DOI 10.1007/s10291-015-0450-8

GNSS IN PROGRESS

Assessing the IRNSS L5-signal in combination with GPS, Galileo, and QZSS L5/E5a-signals for positioning and navigation

Nandakumaran Nadarajah[1] · Amir Khodabandeh[1] · Peter J. G. Teunissen[1,2]

Received: 16 January 2015 / Accepted: 11 March 2015

Abstract The Indian Regional Navigation Satellite System (IRNSS), which is being developed for positioning services in and around India, is the latest addition to the global family of satellite-based navigation systems. As IRNSS only shares the L5-frequency with GPS, the European Galileo, and the Japanese Quasi-Zenith Satellite System (QZSS), it has at least at present a limited interoperability with the existing systems. Noting that the L5-frequency capability is under development even for GPS, this contribution assesses the interoperability of the IRNSS L5-signal with the GPS, Galileo, and QZSS L5/E5a-signals for positioning and navigation using real data collected in Perth, Australia. First, the noise characteristic of the IRNSS L5-signal and its comparison with that of the GPS, Galileo, and QZSS L1/E1- and L5/E5a-signals is presented. Then, the L5-observables of combined systems (formed from IRNSS, GPS, Galileo, and QZSS) are assessed for real-time kinematic positioning using the standard LAMBDA method and for instantaneous attitude determination using the constrained LAMBDA method. The results show that the IRNSS L5-signal has comparable noise characteristics as that of the other L5/E5a-signals. For single-frequency carrier phase-based positioning and navigation, the results show better ambiguity resolution performance of L5/E5a-only processing than that of L1/E1-only processing.

✉ Nandakumaran Nadarajah
n.nadarajah@curtin.edu.au

[1] GNSS Research Centre, Curtin University, GPO Box U1987, Perth, WA 6845, Australia

[2] Delft Institute for Earth Observation and Space Systems, Delft University of Technology, PO Box 5048, 2600 GA Delft, The Netherlands

Published online: 19 March 2015

Keywords GPS · Galileo · QZSS · IRNSS · Attitude determination · Real-time kinematic (RTK) positioning

Introduction

The Indian Regional Navigation Satellite System (IRNSS) is the latest addition to the global family of satellite-based navigation systems. It is a regional system being developed by India for positioning services in and around India. The IRNSS will consist of three geosynchronous orbit (GEO) satellites and four inclined geosynchronous orbit (IGSO) satellites transmitting navigation signals in both the L5-band and the lower S-band, delivering an open standard positioning service (SPS) with a binary phase-shift key [BPSK(1)] modulation and a restricted/authorized service (RS) with a binary offset carrier [BOC(5,2)] modulation (ISRO 2014). The current constellation consists of two IGSO (IRNSS-1A/I1 and IRNSS-1B/I2) satellites and one GEO (IRNSS-1C/I3) satellite, which was only launched recently and is not yet transmitting navigation signals. Analyses in this contribution are based on the L5-observables of I1 and I2 tracked by Javad receivers at Curtin University, Perth, Australia, using a development firmware version (Javad 2014).

As the IRNSS only shares the L5-frequency with GPS, the European Galileo, and the Japanese Quasi-Zenith Satellite System (QZSS), IRNSS has a limited interoperability with these existing systems. Furthermore, the L5/E5a-frequency capability is currently under development even for GPS. Hence, only a few studies on L5/E5a-signal analyses have been reported in the literature. Noise characteristics of the GPS-L5- and Galileo-E5a-signals using a geometry-free approach have been reported in de Bakker et al. (2012). An analysis of precise point positioning using

GPS-L5-signals has been reported in Tegedor and Øvstedal (2014). At the time of writing (December 2014), all GPS Block IIF satellites were transmitting L5-signals, except G3, which was launched only recently. Three of the four Galileo In-Orbit Validation (IOV) satellites and one of the two full operational capability (FOC) satellites were transmitting E5a-signals, while J1, the only satellite of QZSS, is transmitting a L5-signal. Furthermore, only two Indian GAGAN satellites of four satellite-based augmentation systems (SBASs) satellites visible in the Western Australian region are transmitting L5-signals. Since the receivers used for this study were not enabled to track SBAS satellites, we focus on GPS, Galileo, QZSS, and IRNSS L5/E5a-signals. Moreover, the ranging observables of SBAS satellites are known to be more noisy than those of the other systems due to the narrow-band transmission (Nadarajah and Teunissen 2014).

Since the IRNSS satellites are a new addition to the family of navigation satellites and their signal description (ISRO 2014) was not available until recently, few studies on IRNSS have been reported in the literature. Apart from simulation-based studies (Sekar et al. 2012; Rethika et al. 2013; Rao 2013), the characterization and identification of IRNSS signals using real data from a 30-m high-gain antenna are reported in Thoelert et al. (2014). We assess the interoperability of the IRNSS L5-signal with the GPS, Galileo, and QZSS L5/E5a-signals for positioning and navigation. First, the noise characteristics of the IRNSS L5-signal and its comparison with that of the GPS, Galileo, and QZSS L1/E1- and L5/E5a-signals are presented. Using the least-squares variance component estimation method (Teunissen and Amiri-Simkooei 2008), it is shown that the noise characteristics of the IRNSS L5-signal are comparable with that of the other systems. Furthermore, the study also reveals that the L5/E5a code observables are less noisy than that of L1/E1 confirming higher received power and better signal design of L5/E5a (GPSD 2013, EU 2010, JAXA 2012, ISRO 2014).

Following the noise analysis, the performances of the L5-observables of combined systems, formed from IRNSS, GPS, Galileo, and QZSS, are assessed for instantaneous attitude determination using the constrained LAMBDA (C-LAMBDA) method (Teunissen 2010, Nadarajah et al. 2014b), as well as for real-time kinematic (RTK) positioning using the standard LAMBDA method. Since identical receivers were used in this study, inter-system biases (ISBs) (Odijk et al. 2012) among common frequency observables from different systems did not need to be explicitly modeled (Odijk and Teunissen 2013; Nadarajah et al. 2013). Hence, inter-system double differencing with a single pivot satellite for all systems, giving a higher level of redundancy than system-specific double differencing, is used. The results show that for single-frequency carrier phase-based positioning and navigation, a better ambiguity resolution performance is obtained with L5/E5a-only processing than with L1/E1-only processing.

Measurement campaign

The analyses are based on data collected from three GNSS stations (CUAA, CUBB, and SPA7) at Curtin University (Fig. 1) on December 6, 2014. All three stations are equipped with JAVAD TRE_G3TH_8 receivers and connected to TRM 59800.00 SCIS antennas tracking all systems except SBAS using a development firmware version (3.6.1b1-36-e202-local November 14, 2014) (Javad 2014). RINEX observations and navigation messages were extracted from JAVAD binary data using a modified version of the CONVBIN utility from the RTKLib open-source software package (Takasu 2007). For all satellites except the Galileo satellites, broadcast ephemeris data are used. For the Galileo satellites, precise orbit and clock products provided as a part of the international GNSS service multi-GNSS experiment (IGS-MGEX) campaign (Montenbruck et al. 2013) are used as receivers did not record broadcast ephemeris data for E18 during the period considered.

As shown in the skyplots of Fig. 2, the data include L5-observations from seven GPS Block IIF satellites (G1, G6, G9, G24, G25, G27, and G30), E5a-observables from three Galileo IOV satellites (E11, E12, and E19) and one Galileo FOC satellites (E18), L5-observables from two IRNSS satellites (I1 and I2), and L5-observables from QZSS satellite J1. As the current IRNSS satellites are in the western side of the proposed full IRNSS constellation, the Western Australian region currently has poor IRNSS satellite visibility with satellite elevation only going up to 30°. However, with upcoming launches of the IRNSS satellites for the eastern side of the proposed constellation, the Asia–Pacific region will have a better IRNSS satellite visibility. Figure 3 depicts satellite altitudes indicating near-circular orbits for all except QZSS satellite (J1), which is in a highly elliptical orbit (HEO), and the first Galileo FOC satellite (E18). The recent anomalous launch of E18 together with its twin Galileo FOC satellite resulted in an elongated orbit. Despite the non-nominal orbit, it is shown in the following sections that E18 (the first of two Galileo FOC satellites) can already be used for positioning and navigation.

Figure 4 shows the number of visible satellites with L5/E5a-signals and PDOP values for 10° elevation cutoff. The PDOP values are provided for only a brief period since L5/E5a-only standard positioning requires at least $3 + N_s$ satellites, where N_s is the number of satellite systems with at least one satellite.

Fig. 1 IRNSS L5-enabled GNSS stations at Curtin University comprise of JAVAD TRE_G3TH_8 receivers connected to TRM 59800.00 SCIS antennas. *Top* CUAA–CUBB. *Bottom* CUAA–SPA7

Characteristics of L5/E5a-observables

This section presents the noise characteristic of L5/E5a-observables based on observed carrier-to-noise-density ratio (C/N0) and using analyses with least-squares variance component estimation method (Teunissen and Amiri-Simkooei 2008). Figure 5 depicts the observed C/N0 of L1/E1-

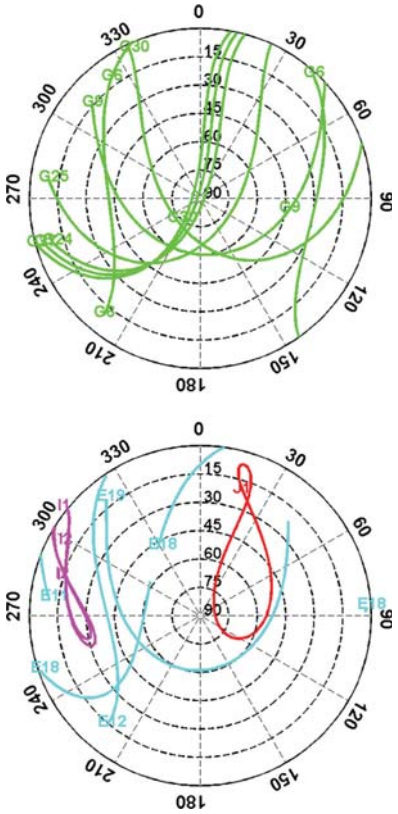

Fig. 2 Skyplot of GPS Block IIF, Galileo, QZSS, and IRNSS satellites with L5/E5a-signals observed at Perth, Australia, on December 6, 2014, with 0° elevation cutoff. *Top* GPS Block IIF. *Bottom* Galileo (*cyan*), QZSS (*red*), IRNSS (*magenta*)

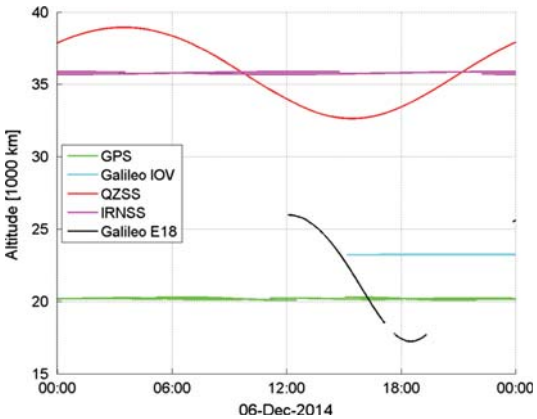

Fig. 3 Altitude of visible GPS, Galileo, QZSS, and IRNSS satellites with L5/E5a-signals tracked by JAVAD TRE_G3T_8 DELTA receiver connected to TRM59800.00 antenna at Perth, Australia, on December 6, 2014, with 0° elevation cutoff

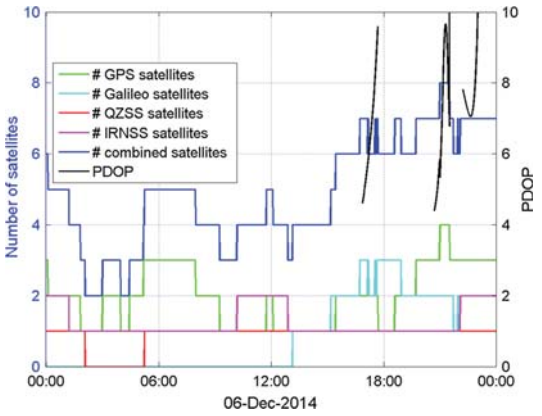

Fig. 4 Satellite visibility (number of satellites and PDOP) of GPS Block II, Galileo, QZSS, and IRNSS satellites with L5/E5a-signals tracked by JAVAD TRE_G3T DELTA receiver connected to TRM59800.00 antenna at Perth, Australia, on December 6, 2014, with 10° elevation cutoff. PDOP values are provided only for the epochs with enough satellites for L5/E5a-only standard positioning

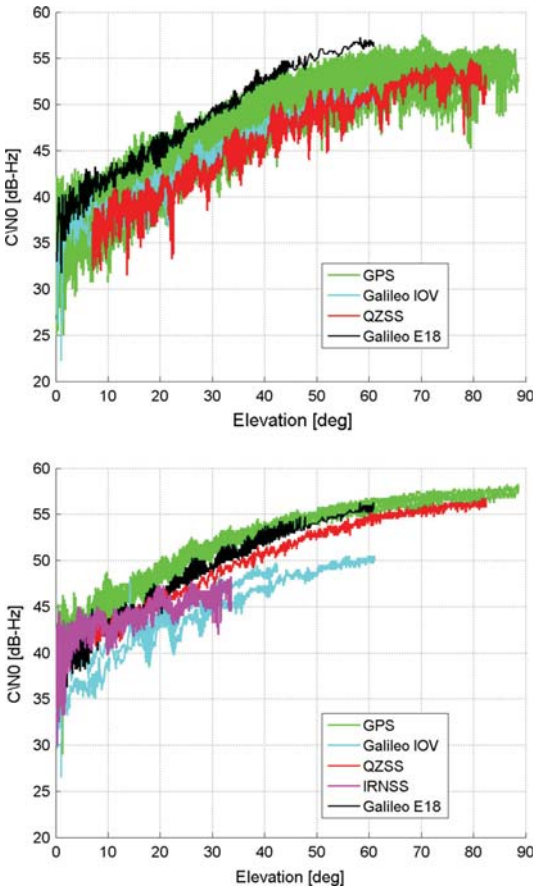

Fig. 5 Carrier-to-noise-density ratio (C/N0) for GPS, Galileo, QZSS, and IRNSS tracked by JAVAD TRE_G3T_8 DELTA receiver connected to TRM59800.00 antenna at Perth, Australia, on December 6, 2014. *Top* L1/E1-signal. *Bottom* L5/E5a-signal

and L5/E5a-signals. The GPS L5-signal, transmitted in a radio band dedicated for aviation safety services, has two codes (I5 and Q5) including a data-free channel (Q5), has higher transmission power than that of L1-signal, and has ten times higher chipping rate than that of C/A-signal (GPSD 2013). Hence, the L5-signal has better tracking noise performance than L1-signal.

Galileo E1-signal with a composite binary offset carrier (CBOC) modulation is expected to have better tracking noise performance compared to GPS L1-signal with the binary phase-shift keying (BPSK). Similarly, Galileo E5a-signal with an alternative BOC (AltBOC) modulation is expected to have a similar tracking noise performance as the new GPS L5-signal. After recent power anomaly in the fourth IOV satellite (FM4 or E20), however, the power on all of the IOV satellites has been reduced by 1.5 dB and E20 has only been transmitting E1-signal (Langley 2014). Hence, Galileo IOV signals have less C/N0 than expected. QZSS L1- and L5-signals have similar signal structures as the GPS counterparts and, hence, have similar tracking noise performance. IRNSS L5-signal has similar tracking noise performance as the other systems for lower elevation angles as observed in Perth, Australia.

Next, the noise characteristics of L5/E5a-observables are assessed using the observations from the short-baseline CUAA–CUBB (Fig. 1) with least-squares variance component estimation method. Since the differential atmospheric delays are absent for such a short baseline, the undifferenced least-squared residuals of the L1- and L5-observables are obtained for the geometry-fixed model with known receiver coordinates. Figure 6 shows the squared values of the stated residuals of the GPS L5- and IRNSS L5-code observables as functions of the satellite elevation. An elevation dependency of the stated residuals, whereby the magnitude of the residuals decreases as the elevation increases, can be seen.

To capture the aforementioned elevation dependency of the observables, we adopt the exponential elevation-weighting model (Euler and Goad 1991), where the standard deviation of the undifferenced observable ς is written as

$$\sigma_{\varsigma}(\theta) = \sigma_{\varsigma_0}\left(1 + 10\exp\left(\frac{-\theta}{10}\right)\right) \quad (1)$$

with θ being the elevation angle (in degrees) of the corresponding satellite, and σ_{ς_0} as the zenith-referenced standard deviation of the undifferenced observable ς.

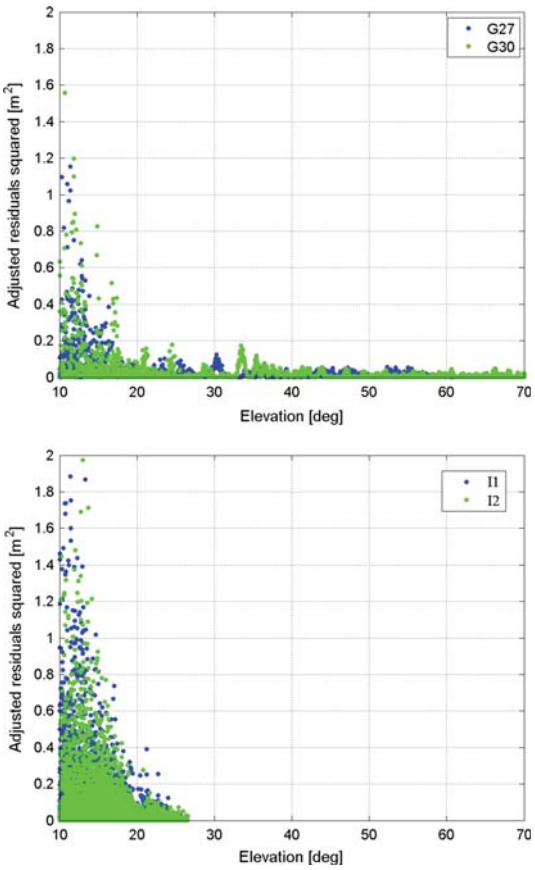

Fig. 6 *Squared values* of the undifferenced least-squared residuals of the L5-signal as function of the satellite elevation. *Top* GPS L5. *Bottom* IRNSS L5

Table 1 Estimated zenith-referenced standard deviation of the code observables in meters

Frequency	GPS	Galileo	QZSS	IRNSS
L1/E1	0.26	0.24	0.25	–
L5/E5a	0.19	0.18	0.18	0.20

The zenith-referenced standard deviations of the L1/E1- and L5/E5a-code observables are presented in Table 1. It is observed that while the zenith-referenced standard deviation is almost the same for different systems, the quality of the L5/E5a-code observables generally outperforms that of the L1/E1-code observables in the sense of delivering smaller standard deviations. This observation agrees well with signal characterization based on observed C/N0 in Fig. 5. However, the estimated zenith-referenced standard deviations of both L1/E1- and L5/E5a-phase observables have the same value, which is 1 mm, regardless of the system.

Performance of attitude determination and positioning

This section presents the performance of L5/E5a-only positioning comparing with that of L1/E1-only positioning. As the satellites with L5/E5a-signals are under development, L5/E5a-standard positioning is only available for a fraction of the period considered (Fig. 4). Hence, two distinct data intervals, whereby we have seven combined L5/E5a-signal-enabled satellites visible, are considered for L5/E5a-positioning analyses (Table 2). Since IRNSS satellites do not have signals in the L1/E1-band, L1-observations of GPS Block IIR satellites, namely G10, G11, and G13, are included in the L1/E1-positioning satellite set for a fair comparison of positioning performance between L1/E1 and L5/E5a. These GPS satellites are chosen such that both L1/E1- and L5/E5a-positioning satellite sets have similar satellite geometry (Figs. 7, 8).

Note that the first interval includes Galileo satellite E18, which is in a non-nominal orbit, and I1, which is the first of two current operational IRNSS satellites, while the second interval includes both operational IRNSS satellites (I1 and I2). In the following, the results of attitude determination and RTK positioning based on data at the rate of 1 Hz for the periods indicated in Table 2 consisting of about 6000 epochs are discussed. Since such a small sample size in a short period is possible with current constellations, the results of this contribution should be considered as an indicative first-hand assessment, but not as a fully fledged statistical analysis.

Since the baselines considered in this contribution consist of identical receiver–antenna pairs and the ISBs among common frequency observables from the receivers of the same type are known to be zero (Odijk et al. 2012; Odijk and Teunissen 2013), inter-system double differencing is used (Nadarajah et al. 2013; Nadarajah and Teunissen 2014, see for detailed formulation). This tightly combined observation model uses a single pivot satellite for all systems and yields a higher level of redundancy compared to system-specific double differencing. Note that the PDOP values in Fig. 8 correspond to tightly combined inter-system double differencing and differ from PDOP values depicted in Fig. 4, which are based on standard positioning estimating receiver clock per system in addition to position components.

For attitude determination, the baseline CUAA–CUBB with known baseline length is considered. Table 3 summarizes empirical instantaneous single-frequency ambiguity resolution success rates of L1/E1- and L5/E5a-processing. Here, the true ambiguities are computed using known antenna coordinates in WGS84 since the antennas used are part of Curtin's permanent stations. The higher

Table 2 Satellite sets used for performance analyses of positioning

Period	L1/E1 positioning	L5/E5a positioning
16:51:43–17:41:22	G1, (G11), G27, E12, E18, E19, J1	G1, G27, E12, E18, E19, J1, (I1)
22:13:01–23:01:19	G6, G9, (G10, G13), G30, E19, J1	G6, G9, G30, E19, J1, (I1, I2)

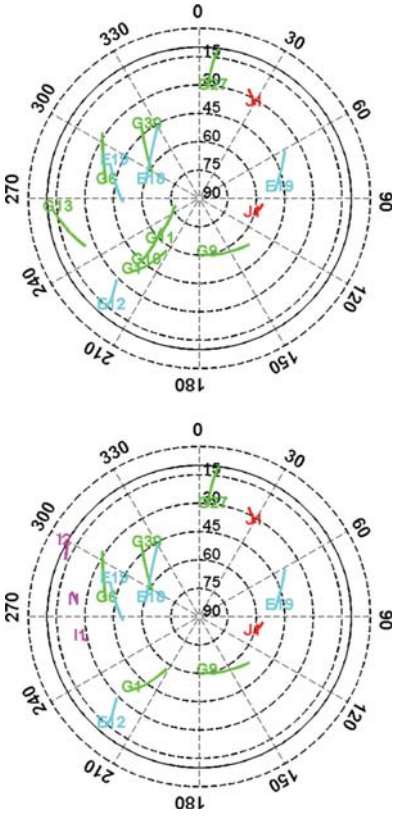

Fig. 7 Skyplot GPS (*green*), Galileo (*cyan*), QZSS (*red*), and IRNSS (*magenta*) satellites during the period considered for positioning performance. *Top* L1/E1 satellite set. *Bottom* L5/E5a satellite set

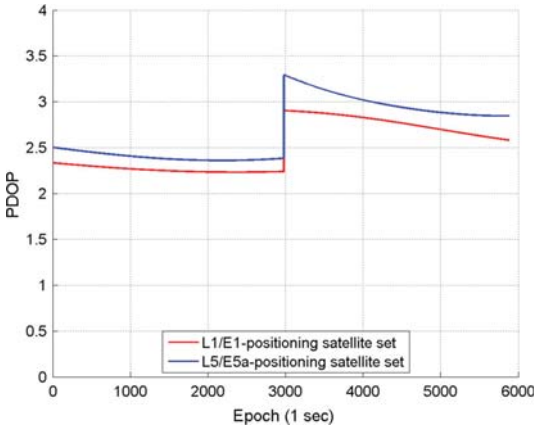

Fig. 8 PDOP values

Table 3 Empirical instantaneous single-frequency ambiguity resolution success rate in percent for attitude determination with static baseline CUAA–CUBB

Method	L1/E1 processing	L5/E5a processing
LAMBDA	77	95
C-LAMBDA	100	100

instantaneous ambiguity resolution success rate for L5/E5a-processing using the standard LAMBDA method (Teunissen 1995) compared to L1/E1-processing is due to perceived better tracking noise performance of L5/E5a-signals (Fig. 5; Table 1). The use of known baseline length information in C-LAMBDA method (Teunissen 2006, 2010) yields instantaneous attitude determination using even L1/E1-observables from the subset of all available satellites as chosen in Table 2. Figure 9 depicts the attitude angular time series, while Table 4 summarizes empirical angular standard deviations for both float and fixed solutions. The better float estimation accuracy for L5/E5a-processing reflects the better tracking noise performance of the L5/E5a-code observables (Table 1).

For RTK positioning, the short-baseline CUAA–SPA7 (Fig. 1) is considered with atmosphere-fixed model estimating only baseline components and ambiguities (Nadarajah et al. 2014a). Figure 10 depicts the position time series, while Table 5 summarizes empirical position standard deviations for both float and fixed solutions demonstrating the benefit of ambiguity fixing. The empirical instantaneous single-frequency ambiguity resolution success rates of L1/E1- and L5/E5a-processing are 74 and 96 %, respectively. The apparent outperformance of L5/E5a-processing in terms of ambiguity resolution and float estimation is due to better tracking noise performance of L5/E5a-signals (Fig. 5; Table 1).

Summary and conclusions

We presented an initial assessment of IRNSS L5-signal together with GPS, Galileo, and QZSS L5/E5a-signals for positioning and navigation. First, the noise characteristics of L5/E5a-signals were assessed based on observed carrier-

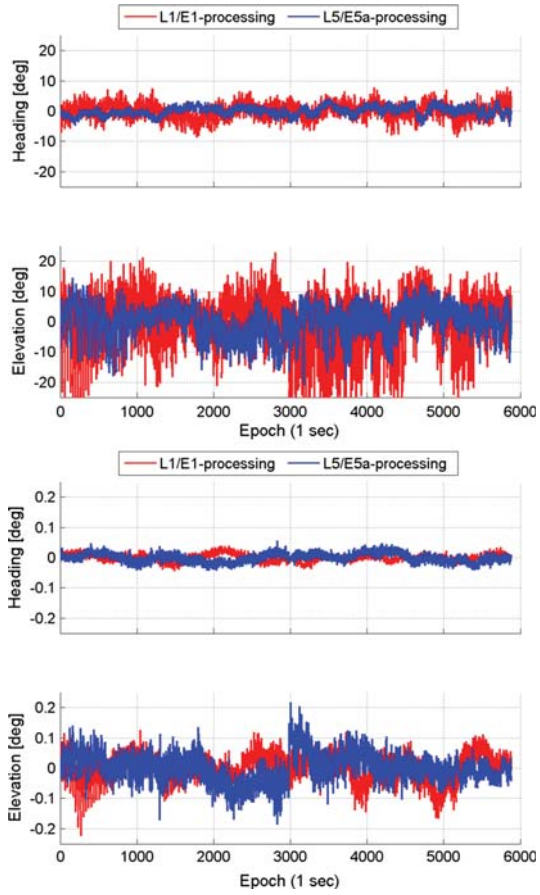

Fig. 9 Attitude angular time series based on single-frequency epoch-by-epoch processing of static baseline CUAA–CUBB. *Top two* ambiguity float solution. *Bottom two* ambiguity fixed solution

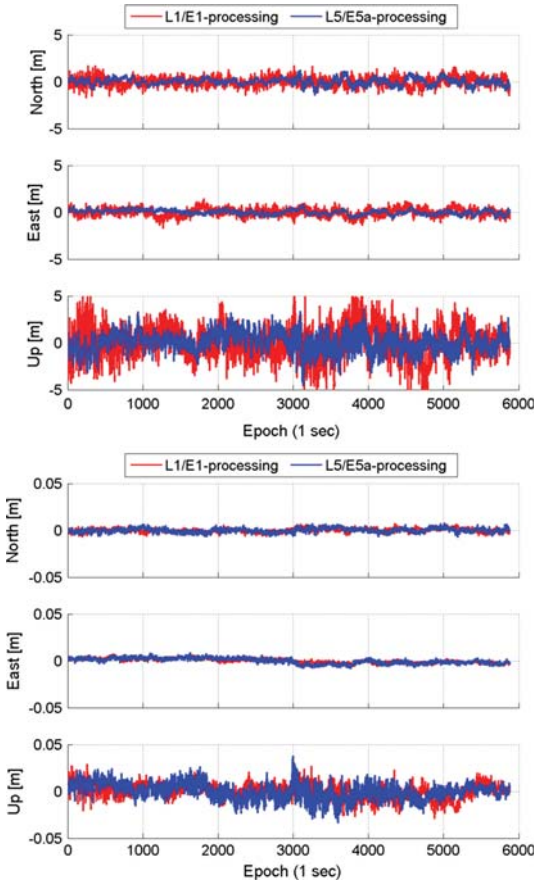

Fig. 10 Baseline component time series based on single-frequency epoch-by-epoch processing of static baseline CUAA–SPA7. *Top three* ambiguity float solution. *Bottom three* ambiguity fixed solution

Table 4 Empirical angular standard deviations in degrees of float and fixed (in brackets) solutions for instantaneous single-frequency attitude determination with static baseline CUAA–CUBB

	L1/E1 processing	L5/E5a processing
Heading	2.45 (0.01)	1.45 (0.01)
Elevation	8.60 (0.04)	5.36 (0.05)

Table 5 Empirical position standard deviations in centimeters of float and fixed (in brackets) solutions for instantaneous single-frequency RTK with static baseline CUAA–SPA7

	L1/E1 processing	L5/E5a processing
North	50 (0.2)	37 (0.2)
East	42 (0.2)	25 (0.3)
Up	170 (0.8)	103 (0.8)

to-noise-density ratio and variance component estimation indicating precise L5/E5a-code observables compared to L1/E1-code observables due to higher received power and better signal modulation. Furthermore, it has been observed that the performance of IRNSS L5-signal is comparable to that of L5/E5a-signals of other systems. With limited L5/E5a-capable satellite availability from current GNSS constellations, our analyses of L5/E5a-only attitude determination and RTK positioning indicated the superior performance of L5/E5a-only processing especially in terms of instantaneous ambiguity resolution compared to that of L1/E1-only processing. It was also demonstrated that recently deployed L5/E5a-capable satellites such as the first Galileo FOC satellite with non-nominal orbit and first two IRNSS satellites have already been contributing to

positioning and navigation. The full potential of L5/E5a-based positioning and navigation is, however, yet to be explored with the fully operational GPS L5-capability and the completion of other systems including Galileo, QZSS, and IRNSS in coming years. With the promising performance of L5/E5a-only processing, the development of L5/E5a-only receivers replacing current L1/E1-only low-cost receivers offering better positioning performance can be foreseeable.

Acknowledgments This work has been executed as part of the Positioning Program Project 1.01 "New carrier phase processing strategies for achieving precise and reliable multi-satellite, multi-frequency GNSS/RNSS positioning in Australia" of the Cooperative Research Centre for Spatial Information (CRC-SI). The third author P. J. G. Teunissen is the recipient of an Australian Research Council Federation Fellowship (Project Number FF0883188). A development version of firmware for JAVAD receivers was kindly provided by JAVAD GNSS Inc. All this support is gratefully acknowledged.

References

de Bakker PF, Tiberius CCJM, van der Marel H, van Bree RJP (2012) Short and zero baseline analysis of GPS L1 C/A, L5Q, GIOVE E1B, and E5aQ signals. GPS Solut 16:53–64

EU (2010) European GNSS (Galileo) open service: signal in space interface control document, Issue 1, Revision 1, European Union, Sep 2010

Euler H-J, Goad C (1991) On optimal filtering of GPS dual frequency observations without using orbit information. J Geod 65:130–143

GPSD (2013) Navstar GPS space segment/navigation user segment interfaces, Revision F (IS-GPS-200H:24-Sep-2013), global positioning system directorate

ISRO (2014). Indian regional navigation satellite system: signal in space ICD for standard positioning service, Version 1.0, ISRO Satellite Centre, Jun 2014

Javad (2014) Javad Delta multi-GNSS receiver. Personal communication, Dec 2014

JAXA (2012) Interface specification for QZSS, Japan Aerospace Exploration Agency

Langley RB (2014) ESA discusses Galileo satellite power loss, upcoming launch. http://gpsworld.com/esa-discusses-galileo-satellite-power-loss-upcoming-launch/, Aug 2014. Online; accessed: 06 Jan 2015

Montenbruck O, Steigenberger P, Khachikyan R, Weber R, Langley R, Mervart L, and Hugentobler U (2013) IGS-MGEX: preparing the ground for multi-constellation GNSS science, proceedings 4th international colloquium scientific and fundamental aspects of the galileo programme, Prague, Czech Republic, 4–6 Dec 2013, ESA-European GNSS Agency, pp 1–8

Nadarajah N, Teunissen PJG (2014) Instantaneous GPS/Galileo/QZSS/SBAS attitude determination: a single-frequency (L1/E1) robustness analysis under constrained environments. Navigation 61(1):65–75

Nadarajah N, Teunissen PJG, Raziq N (2013) Instantaneous GPS–Galileo attitude determination: single-frequency performance in satellite-deprived environments. IEEE Trans Veh Technol 62(7):2963–2976

Nadarajah N, Teunissen PJG, Sleewaegen J-M, Montenbruck O (2014a) The mixed-receiver BeiDou inter-satellite-type bias and its impact on RTK positioning. GPS Solut. doi:10.1007/s10291-014-0392-6

Nadarajah N, Teunissen PJG, Raziq N (2014b) Instantaneous BeiDou–GPS attitude determination: a performance analysis. Adv Space Res 54(5):851–862

Odijk D, Teunissen PJG (2013) Characterization of between-receiver GPS-Galileo inter-system biases and their effect on mixed ambiguity resolution. GPS Solut 17(4):521–533

Odijk D, Teunissen PJG, Huisman L (2012) First results of mixed GPS + GIOVE single-frequency RTK in Australia. J Spat Sci 57(1):3–18

Rao VG (2013) Proposed LOS fast TTFF signal design for IRNSS, PhD thesis, University of Calgary

Rethika T, Mishra S, Nirmala S, Rathnakara SC, Ganeshan AS (2013) Single frequency ionospheric error correction using coefficients generated from regional ionospheric data for IRNSS. Indian J Radio Space Phys 42(3):125–130

Sekar S, Sengupta S, and Bandyopadhyay K (2012) Spectral compatibility of BOC(5,2) modulation with existing GNSS signals, PLANS-2012 IEEE/ION, Myrtle Beach, SC, Apr 2012, pp 886–890

Takasu T (2007) RTKLIB: An open source program package for GNSS positioning, available online: www.rtklib.com

Tegedor J, Øvstedal O (2014) Triple carrier precise point positioning (PPP) using GPS L5. Surv Rev 46(337):288–297

Teunissen PJG (1995) The least-squares ambiguity decorrelation adjustment: a method for fast GPS integer ambiguity estimation. J Geod 70:65–82

Teunissen PJG (2006) The LAMBDA method for the GNSS compass. Artif Satell 41(3):89–103

Teunissen PJG (2010) Integer least-squares theory for the GNSS compass. J Geod 84(7):433–447

Teunissen PJG, Amiri-Simkooei A (2008) Least-squares variance component estimation. J Geod 82:65–82

Thoelert S, Montenbruck O, Meurer M (2014) IRNSS-1a: signal and clock characterization of the Indian regional navigation system. GPS Solut 18(1):147–152

Nandakumaran Nadarajah received his M.A.Sc and PhD in electrical and computer engineering from McMaster University, Canada. Currently, he is working as a research fellow at GNSS Research Centre, Curtin University. His research interests are in multi-GNSS attitude determination and relative navigation, signal processing, and target tracking.

Amir Khodabandeh received his M.Sc. degree in Geodesy from University of Tehran, Iran, in 2011. He is currently pursuing his PhD degree at the GNSS Research Centre, Curtin University. His research interests comprise estimation theory, GNSS precise positioning, and GNSS quality control.

Peter Teunissen is a Federation Fellow of the Australian Research Council (ARC), Professor of Geodesy and Navigation, Science Director of the Cooperative Research Centre for Spatial Information, and Head of CUT's Global Navigation Satellite System (GNSS) Research Centre. His current research focus is on modeling next-generation GNSS for relative navigation and attitude determination in space and air.

9 Impact of IAR on the PPP-RTK network parameters

This chapter is covered by the following publication:

Teunissen P.J.G. and **Khodabandeh A.** (2014b). Do GNSS parameters always benefit from integer ambiguity resolution? a PPP-RTK Network Scenario. ION GNSS+, 27:590–600. The Institute of Navigation, Florida.

Do GNSS parameters always benefit from integer ambiguity resolution? A PPP-RTK Network Scenario

P.J.G. Teunissen[1,2] and A. Khodabandeh[1]

[1]*GNSS Research Centre, Curtin University of Technology, Perth, Australia*

[2]*Geoscience and Remote Sensing, Delft University of Technology, The Netherlands*

Biography

Peter J.G. Teunissen is a Federation Fellow of the Australian Research Council, Professor of Geodesy and Navigation, Science Director of the Cooperative Research Centre for Spatial Information, and Head of Curtin's GNSS Research Centre. His current research focus is on modeling next-generation GNSS for relative navigation and attitude determination in space and air. Amir Khodabandeh is a PhD student at Curtin's GNSS Research Centre. His research interests comprise estimation theory, GNSS precise positioning and GNSS quality control.

Abstract

In this contribution we study the impact of integer ambiguity resolution (IAR) on the precision of GNSS estimable parameters. In doing so, a multivariate formulation of the GNSS undifferenced observation equations of a PPP-RTK network is presented, where appropriate one-to-one transformations to the parameters ease our analysis. Functions of the estimable slant ionospheric delays are shown to have distinct responses to IAR, ranging from zero (of a satellite-/receiver-averaged type) to very significant (of a double-differenced type). While the satellite-/receiver-averaged components of the estimable clocks and phase biases on a particular frequency remain unaffected after IAR, the precision of their single-differenced (SD) counterparts experiences improvement. In particular, the precision improvement gets larger as the geometry of the model gets weaker. This is, however, not the case with the wide-lane satellite phase biases, since their precision is almost insensitive to the geometry of the model. Supported by numerical results, our analytical expressions show that the precision improvement of the SD satellite clocks and phase biases increases as the number of stations increases. We also highlight the zero-correlation property between the double-differenced ambiguities and the code biases that get estimable on the third frequency and beyond.

1 Introduction

Integer ambiguity resolution (IAR) is considered by many to be the key to fast and precise GNSS parameter estimation. And indeed, carrier-phase based GNSS positioning can significantly benefit from fast and successful IAR [1–3]. There are however, next to the positioning parameters, several other types of GNSS parameters that are important for a range of different applications, like e.g. atmospheric sounding, time-transfer or instrumental calibration. This contribution will show, in a qualitative and quantitative sense, to what extent the GNSS parameters can benefit from integer ambiguity resolution. The results will show that different parameter types have very distinct responses to IAR, ranging from insignificant to very significant.

We consider an n-receiver network scenario for which the system of carrier-phase and code observation equations is formulated in undifferenced form. The advantage of such a formulation is that it still contains all estimable GNSS parameters [4], i.e. none are a priori eliminated, as would happen, for instance, if a double difference formulation was used. The following estimable GNSS parameter types are included in this study:

a) the geometry dependent parameters, i.e. coordinates and/or zenith tropospheric delays (ZTDs)

b) the slant ionospheric delays

c) the receiver and satellite clock parameters

d) the receiver and satellite phase biases

e) the receiver and satellite code biases

The geometry-dependent parameters of a) are included as reference, since it is known that their precision improves significantly by means of successful ambiguity resolution [1–3]. In case of instantaneous positioning, for

instance, the improvement can reach two orders of magnitude. The significance of knowing the impact of IAR on the other GNSS network parameters is as follows.

Ionosphere: As the slant ionospheric delays serve as inputs for ionospheric models (e.g. VTEC modelling [5]) or for PPP-RTK ionospheric correction generation [6, 7], it is important to know whether these inputs can benefit from IAR just like the geometry-dependent parameters do.

Timing: Estimating precise clock parameters is of great importance for timing and time-transfer applications [8]. It is therefore important to know under what circumstances (receiver and/or satellite) clocks' precision improvement can be realized by IAR.

PPP-RTK: Satellite clocks and satellite phase biases are essential components in the corrections provided to PPP-RTK users [9–11]. Can network ambiguity resolution improve these corrections, and if so, by how much?

Code biases: With the advent of triple-/quadruple-frequency data, the estimation of satellite code biases on the third/fourth frequency bands, next to the receiver code biases, becomes possible. It is then relevant to know whether one can improve this bias-calibration through IAR.

Our analyses will be based on the structure and content of the undifferenced full-rank GNSS network equations. It will allow us to determine analytical *gain numbers* [12] measuring the precision gain the estimator of the above mentioned GNSS network parameters experiences. With these measures we can then determine the impact that IAR has on each of the different parameter types mentioned under a)-e). This impact will be presented in a qualitative as well as quantitative sense. The qualitative formulation provides insight and understanding of the mechanisms of the individual impacts, while the numerical results allow one to measure their significance.

2 Multivariate GNSS network model

We consider the undifferenced (UD) GNSS network observation equations where the role of the observation matrix is taken by a multi-frequency phase and code data-set (see Figure 1). The 'observed-minus-computed' phase observations of m commonly-viewed satellites on frequency j ($j = 1,\ldots,f$), tracked by receiver r ($r = 1,\ldots,n$), are collected in the m-vector $\phi^S_{r,j} = [\phi^1_{r,j},\ldots,\phi^m_{r,j}]^T$. The fm-vector $\phi^S_r = [\phi^{S^T}_{r,1},\ldots,\phi^{S^T}_{r,f}]^T$ does therefore contain all the phase observations tracked by receiver r. The code observation vector p^S_r is defined similarly. With these in mind, the $fm \times n$ matrices of the network phase and code observations are structured as $\phi^S_R = [\phi^S_1,\ldots,\phi^S_n]$ and $p^S_R = [p^S_1,\ldots,p^S_n]$, respectively. A multivariate representation of the rank-deficient network observation equations reads then

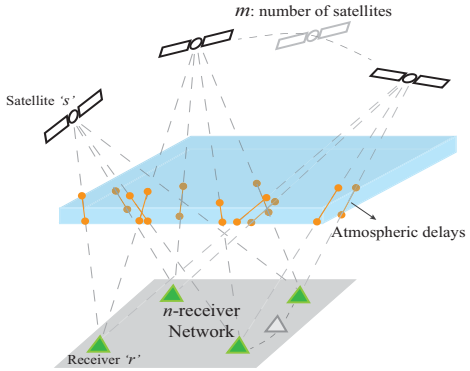

Figure 1. Schematic illustration of an n-receiver network tracking observables of m number of commonly-viewed satellites in the presence of atmospheric delays.

$$\begin{aligned} \mathsf{E}(\phi^S_R) &= [e_f \otimes I_m]\rho^S_R - [\mu \otimes I_m]\iota^S_R + [\Lambda \otimes I_m]a^S_R \\ \mathsf{E}(p^S_R) &= [e_f \otimes I_m]\rho^S_R + [\mu \otimes I_m]\iota^S_R + [I_f \otimes e_m]d_R - [I_f \otimes I_m]d^S e^T_n \end{aligned} \tag{1}$$

with I_f and e_f being, respectively, the identity matrix and the vector of ones, of size f. The columns of the $m \times n$ matrix ι^S_R are structured by the (first-order) slant ionospheric delays $\iota^S_r = [\iota^1_r,\ldots,\iota^m_r]^T$ ($r = 1,\ldots,n$). Likewise, the $m \times n$ matrix ρ^S_R of the non-dispersive parameters is ordered, while the $fm \times n$ ambiguity matrix a^S_R, in cycles, is ordered in the same way as ϕ^S_R. The $f \times n$ matrix d_R contain the receiver code biases, while and fm-vector d^S contain the satellite code biases. With λ_j as the wavelength on frequency j, the $f \times f$ diagonal matrix Λ and the f-vector μ, respectively, contain λ_j and $(\lambda^2_j/\lambda^2_1)$ ($j = 1,\ldots,f$). The symbol $\otimes$ is the Kronecker matrix product [13].

Assuming the precise orbital corrections are included in 'observed-minus-computed' observations, the non-dispersive matrix is, in turn, parametrized as $\rho^S_R = G\Delta x_R + e_m\, dt^T_R - dt^S e^T_n$, where Δx_R contains the receivers' position increments and/or the zenith tropospheric delays (ZTDs), with the geometry matrix G capturing the receiver-satellite unit vectors and/or the tropospheric mapping functions. The n-vector dt_R contains the receiver clock parameters, while the m-vector dt^S contains the satellite clock parameters. The real-valued ambiguity matrix is also parameterized as $a^S_R = z^S_R + [I_f \otimes e_m]\delta_R - \delta^S e^T_n$, where matrix z^S_R contains the *integer-valued* ambiguities, δ_R contains the non-integer receiver phase biases and δ^S contains the non-integer satellite phase biases.

Table 1. The dimensionless cofactor matrix $Q^o_{\tilde{X}\tilde{X}}$, in Eq. (5), chosen for the estimable functions. Typical diagonal elements of $Q^o_{\tilde{X}\tilde{X}}$ are also provided.

Estimable function		Cofactor matrix $Q^o_{\tilde{X}\tilde{X}}$	Typical diagonal elements*
Ionospheric delays	$\tilde{X} \mapsto \tilde{\imath}^S_R$	$I_n \otimes C_S$	$l^T(I_n \otimes C_S)l = 1$
SD receiver clocks	$\tilde{X} \mapsto d\tilde{t}_R$	$D_n^T D_n$	$l^T(D_n^T D_n)l = 2$
Satellite clocks	$\tilde{X} \mapsto d\tilde{t}^S$	C_S	$l^T(C_S)l = 1$
Frequency-combined satellite phase biases	$\tilde{X} \mapsto [q^T \otimes I_m]\,\tilde{\delta}^S$	C_S	$l^T(C_S)l = 1$

* The typical diagonal elements of the elevation-weighting matrix C_S are considered at *zenith*, thus being set to 1.

Applying an $\mathcal{S}$-system [14, 15] to the rank-deficient model (1), one can remove the underlying rank-deficiency and form a full-rank observation equations as

$$\begin{aligned} \mathsf{E}(\phi^S_R) &= [e_f \otimes I_m]\,\Delta\tilde{\rho}^S_R - [\mu \otimes I_m]\,\tilde{\imath}^S_R + [\Lambda \otimes I_m]\,\tilde{a}^S_R \\ \mathsf{E}(p^S_R) &= [e_f \otimes I_m]\,\Delta\tilde{\rho}^S_R + [\mu \otimes I_m]\,\tilde{\imath}^S_R + [E_f \otimes e_m]\,\tilde{d}_R - [E_f \otimes I_m]\,\tilde{d}^S e_n^T \end{aligned} \tag{2}$$

where the $f \times (f-2)$ matrix E_f follows by eliminating the first two columns of I_f. The $\check{\cdot}$-symbol refers to *estimable* quantities rather than their original versions. The following parameters are kept fixed as the $\mathcal{S}$-basis of the model:

- The receiver and satellite code biases on the first two frequencies $j = 1, 2$.
- The integer-valued ambiguities of the first receiver and of the first satellite.
- The receiver-specific parameters, i.e. the clock and phase/code biases, of the first receiver.
- In case of small-scale networks, the position and/or the ZTD of the first receiver.

As a consequence of the above $\mathcal{S}$-basis chosen:

- The clocks, phase/code biases, and the ionospheric delays are biased by the code biases on the first two frequencies.
- The satellite/receiver phase biases are further biased by the integer-valued ambiguities of the first receiver and of the first satellite. This makes the estimable double-differenced (DD) ambiguities $\tilde{a}^S_R$ appear in the model in a straightforward manner.
- The satellite-specific parameters are further biased by the receiver-specific parameters of the first receiver. Likewise, the receiver-specific parameters of the other receivers are biased by those of the first receiver.
- In case of small-scale networks, the satellite clocks are further biased by the position and/or the ZTD of the first receiver. This, in turn, make the *relative* positions (baselines) and/or the ZTDs estimable.

Let us now assume that the integer DD ambiguities

$$\tilde{a}^S_R = [I_f \otimes D_m^T]\,a^S_R D_n \tag{3}$$

are successfully resolved through IAR, where D_m and D_n refer to the between-satellite and between-receiver single-difference matrices, respectively [16]. Our task is to study the precision improvement of the estimable parameters as introduced in (2). Employing appropriate one-to-one transformations to the observations and parameters, we characterize the precision change from the float estimators (with $\hat{\cdot}$-symbol) to the fixed estimators (with $\check{\cdot}$-symbol). In doing so, the following variance matrices for the phase and code observations are adopted, respectively.

$$\begin{aligned} Q_{\phi^S_R \phi^S_R} &= I_n \otimes C_\phi \otimes C_S \\ Q_{p^S_R p^S_R} &= I_n \otimes C_p \otimes C_S \end{aligned} \tag{4}$$

The $m \times m$ matrix C_S captures the the satellite elevation dependency. The $f \times f$ positive-definite matrices C_ϕ and C_p are cofactor matrices of the phase and code observable types, respectively.

3 Impact of IAR on GNSS parameters

3.1 Gain numbers and float variance-ratios

In this section, the impact of IAR on the estimable parameters, given in (2), are analyzed by presenting their corresponding precision gain numbers [12]. Gain numbers measure the gain in the estimator's precision of the parameters due to ambiguity fixing. Next to the gain numbers, we also introduce the *float variance-ratios* measuring the variance-ratio of the float estimators. Given a typical estimable parameter matrix $\tilde{X}$ or its *vectorized* version $\mathrm{vec}(\tilde{X})$, the gain number γ and float variance-ratio F of

the linear function $l^T \mathrm{vec}(\tilde{X})$ are formally defined as

$$\gamma_{\tilde{X}}(l) = \frac{l^T Q_{\hat{\tilde{X}}\hat{\tilde{X}}} l}{l^T Q_{\check{\tilde{X}}\check{\tilde{X}}} l}, \qquad F_{\hat{\tilde{X}}}(l) = \frac{l^T Q_{\hat{\tilde{X}}\hat{\tilde{X}}} l}{l^T Q^o_{\check{\tilde{X}}\check{\tilde{X}}} l} \tag{5}$$

with $Q_{\hat{\tilde{X}}\hat{\tilde{X}}}$ and $Q_{\check{\tilde{X}}\check{\tilde{X}}}$ being the variance matrices of the float and fixed estimators $\mathrm{vec}(\hat{\tilde{X}})$ and $\mathrm{vec}(\check{\tilde{X}})$, respectively. The dimensionless cofactor matrix $Q^o_{\check{\tilde{X}}\check{\tilde{X}}}$ takes a certain structure for each estimable parameter (see Table 1). In case of the estimable satellite clocks for instance, the elevation-weighting matrix C_S takes the role of the cofactor $Q^o_{\check{\tilde{X}}\check{\tilde{X}}}$. Considering vector l as a canonical vector (i.e. a vector of zeros except one element equal to 1), the denominator $l^T Q^o_{\check{\tilde{X}}\check{\tilde{X}}} l$ of the float variance-ratio $F_{\hat{\tilde{X}}}(l)$ becomes 1 when the corresponding satellite is viewed at zenith. The satellite clocks' float variance-ratio $F_{\hat{d\tilde{t}}^S}(l)$ would therefore represent the variance of the float clock estimator of a particular satellite viewed at zenith. Having known the corresponding gain number $\gamma_{d\tilde{t}^S}(l)$, the variance of the *fixed* clock estimator of the satellite follows then by the ratio $[F_{\hat{d\tilde{t}}^S}(l)/\gamma_{d\tilde{t}^S}(l)]$.

It should be remarked that the gain number $\gamma_{\tilde{X}}(l)$ is *dimensionless*, while the float variance ratio $F_{\hat{\tilde{X}}}(l)$ would have the same dimension as that of $Q_{\hat{\tilde{X}}\hat{\tilde{X}}}$.

The gain number $\gamma_{\tilde{X}}(l)$ can take its *minimum* value '1' where no improvement in precision is experienced by IAR, or take unbounded values. As reference, it is well-known that the precision improvement of the geometry-dependent parameters (i.e. receivers' relative position and ZTDs) can reach two orders of magnitude, thereby generally having large gain numbers [12]. In the following we characterize the gain numbers corresponding to the other estimable parameters.

Our analytical presentation is accompanied by numerical results based on a 24-hour GPS satellite configuration visible in CUT00 (Curtin's permanent station, Perth, Australia), on 8 April, 2013. The number of network stations is set to $n = 10$, and the exponential satellite elevation weighting strategy is applied to form C_S [17]. The cofactor matrices of the dual-frequency GPS L1/L2 scenario are set to $C_p = \sigma_p^2 I_2$, $C_\phi = \sigma_\phi^2 I_2$, with $\sigma_p = 20$ cm, $\sigma_\phi = 2$ mm. The (co)variance-type scalars, given in Table 2, will appear in our forthcoming results. Our multi-epoch scenario is based on time-invariance of the ambiguity matrix a_R^S and the time-averaged geometry matrix G, with k being the number of all epochs involved.

3.2 Ionospheric delays' response to IAR

As previously stated, due to the $\mathcal{S}$-basis chosen, the estimable UD slant ionospheric delays $\tilde{\iota}_R^S$ comprises the true slant UD ionospheric delays as well as the between-frequency-difference of the receiver and satellite code biases on the first two frequencies $j = 1, 2$, i.e. the so-called differential code biases (DCBs). To get a better understanding of the impact of IAR, we decompose the estimable UD slant ionospheric delays into their (weighted) *satellite-/receiver-averaged* components and their DD components through the following one-to-one transformation

$$\begin{gathered} \tilde{\iota}_R^S = \left[e_m,\, D_m^{+T}\right] \begin{bmatrix} \tilde{\iota}_r^{\bar{s}} & \tilde{\iota}_{1R}^{\bar{s}} \\ \tilde{\iota}_r^{1S} & \tilde{\iota}_{1R}^{1S} \end{bmatrix} \begin{bmatrix} e_n^T \\ D_n^+ \end{bmatrix} \iff \\ \begin{bmatrix} (\frac{e_m^T Q_S^{-1}}{e_m^T Q_S^{-1} e_m}) \\ D_m^T \end{bmatrix} \tilde{\iota}_R^S \left[(\tfrac{e_n}{n}),\, D_n\right] = \begin{bmatrix} \tilde{\iota}_r^{\bar{s}} & \tilde{\iota}_{1R}^{\bar{s}} \\ \tilde{\iota}_r^{1S} & \tilde{\iota}_{1R}^{1S} \end{bmatrix} \end{gathered} \tag{6}$$

with $D_m^+ = (D_m^T Q_S D_m)^{-1} D_m^T Q_S$ and $D_n^+ = (D_n^T D_n)^{-1} D_n^T$. The satellite-/receiver-averaged components $\tilde{\iota}_r^{\bar{s}}$, $\tilde{\iota}_r^{1S}$, $\tilde{\iota}_{1R}^{\bar{s}}$ *always* require code data, irrespective of IAR. In other words, the integer-resolved DD phase observations cannot determine them. Therefore, these components experience no precision improvement after IAR. As shown in Table 3, the corresponding gain number takes its minimum value, i.e. $\gamma_{\tilde{\iota}_R^S} = 1$, while the corresponding float variance-ratio attains its maximum values, i.e. $F_{\hat{\tilde{\iota}}_R^S}(l) = c^2_{\tilde{\iota}_2}$. This corresponds to a float standard deviation of size $c_{\tilde{\iota}_2} \approx 44$ *cm* at zenith (GPS L1/L2 example) which gets even larger for lower satellites' elevation.

On the other hand however, any functions of the DD ionospheric delays $\tilde{\iota}_{1R}^{1S} = \iota_{1R}^{1S}$ can be solely determined by the integer-resolved DD phase observations, thus experiencing precision improvement of two orders of magnitude. Two important scenarios are considered, the strongest scenario, i.e. the *geometry-fixed* scenario where the relative

Table 2. (Co)Variance-type scalars as used in this contribution. The GPS L1/L2 example follows by setting $C_p = \sigma_p^2 I_2$, $C_\phi = \sigma_\phi^2 I_2$, with $\sigma_p = 20$ cm, $\sigma_\phi = 2$ mm.

	Float	Fixed	L1/L2 Example
$c^2_{\tilde{\rho}}$	$c^2_{\hat{\tilde{\rho}}} = \frac{h_{\tilde{\iota}\tilde{\iota}}}{h_{\hat{\rho}\hat{\rho}} h_{\tilde{\iota}\tilde{\iota}} - h^2_{\hat{\rho}\tilde{\iota}}}$	$c^2_{\check{\tilde{\rho}}} = \frac{h_{\tilde{\iota}\tilde{\iota}}}{h_{\hat{\rho}\hat{\rho}} h_{\tilde{\iota}\tilde{\iota}} - h^2_{\hat{\rho}\tilde{\iota}}}$	$c^2_{\tilde{\rho}} \approx 59.6^2$ cm^2 $c^2_{\tilde{\rho}} \approx 5.9^2$ mm^2
$c^2_{\tilde{\iota}}$	$c^2_{\hat{\tilde{\iota}}} = \frac{h_{\hat{\rho}\hat{\rho}}}{h_{\hat{\rho}\hat{\rho}} h_{\tilde{\iota}\tilde{\iota}} - h^2_{\hat{\rho}\tilde{\iota}}}$	$c^2_{\check{\tilde{\iota}}} = \frac{h_{\hat{\rho}\hat{\rho}}}{h_{\hat{\rho}\hat{\rho}} h_{\tilde{\iota}\tilde{\iota}} - h^2_{\hat{\rho}\tilde{\iota}}}$	$c^2_{\tilde{\iota}} \approx 43.7^2$ cm^2 $c^2_{\tilde{\iota}} \approx 4.4^2$ mm^2
$c^2_{\tilde{\iota}\|\tilde{\rho}}$	$c^2_{\hat{\tilde{\iota}}\|\tilde{\rho}} = \frac{1}{h_{\tilde{\iota}\tilde{\iota}}}$	$c^2_{\check{\tilde{\iota}}\|\tilde{\rho}} = \frac{1}{h_{\tilde{\iota}\tilde{\iota}}}$	$c^2_{\tilde{\iota}\|\tilde{\rho}} \approx 10.4^2$ cm^2 $c^2_{\tilde{\iota}\|\tilde{\rho}} \approx 1$ mm^2
$\frac{c_{\tilde{\rho}\tilde{\iota}}}{c^2_{\tilde{\rho}}}$	$\frac{c_{\hat{\tilde{\rho}}\hat{\tilde{\iota}}}}{c^2_{\hat{\tilde{\rho}}}} = \frac{h_{\hat{\rho}\tilde{\iota}}}{h_{\tilde{\iota}\tilde{\iota}}}$	$\frac{c_{\check{\tilde{\rho}}\check{\tilde{\iota}}}}{c^2_{\check{\tilde{\rho}}}} = \frac{h_{\hat{\rho}\tilde{\iota}}}{h_{\tilde{\iota}\tilde{\iota}}}$	$(c_{\hat{\rho}\tilde{\iota}}/c^2_{\hat{\rho}}) \approx -0.7131$ $(c_{\check{\rho}\tilde{\iota}}/c^2_{\check{\rho}}) \approx +0.7128$

$h_{\hat{\rho}\hat{\rho}} = e_f^T (C_\phi^{-1} + C_p^{-1}) e_f$, $h_{\hat{\rho}\tilde{\iota}} = e_f^T (C_\phi^{-1} - C_p^{-1})\mu$, $h_{\tilde{\iota}\tilde{\iota}} = \mu^T (C_\phi^{-1} + C_p^{-1})\mu$
$h_{\hat{\rho}\hat{\rho}} = e_f^T C_p^{-1} e_f$, $h_{\hat{\rho}\tilde{\iota}} = e_f^T C_p^{-1}\mu$, $h_{\tilde{\iota}\tilde{\iota}} = \mu^T C_p^{-1}\mu$

Table 3. Ranges of the estimable ionospheric gain number γ and float variance-ratio F for different scenarios. The scalar $c^2_{\tilde{\imath}_2}$ follows from $c^2_{\tilde{\imath}}$, given in Table 2, when the first two frequencies $j = 1,2$, are considered only.

Rec.-/Sat.-averaged:	$\gamma_{\tilde{\imath}^S_R}(l) = 1$	$F_{\tilde{\imath}^S_R}(l) = c^2_{\tilde{\imath}_2}$
Geometry-Fixed:	$1 = \gamma_{\tilde{\imath}^S_R}(l_{max}) \leq \gamma_{\tilde{\imath}^S_R}(l) \leq \gamma_{\tilde{\imath}^S_R}(l_{min}) = 1 + \frac{c^2_{\tilde{\imath}\|\rho} - c^2_{\tilde{\imath}\|\rho}}{k c^2_{\tilde{\imath}\|\rho}}$	$\frac{1}{k}(c^2_{\tilde{\imath}\|\rho} + [k-1]c^2_{\tilde{\imath}\|\rho}) = F_{\tilde{\imath}^S_R}(l_{min}) \leq F_{\tilde{\imath}^S_R}(l) \leq F_{\tilde{\imath}^S_R}(l_{max}) = c^2_{\tilde{\imath}_2}$
Geometry-Free:	$1 = \gamma_{\tilde{\imath}^S_R}(l_{max}) \leq \gamma_{\tilde{\imath}^S_R}(l) \leq \gamma_{\tilde{\imath}^S_R}(l_{min}) = 1 + \frac{c^2_{\tilde{\imath}} - c^2_{\tilde{\imath}}}{k c^2_{\tilde{\imath}}}$	$\frac{1}{k}(c^2_{\tilde{\imath}} + [k-1]c^2_{\tilde{\imath}}) = F_{\tilde{\imath}^S_R}(l_{min}) \leq F_{\tilde{\imath}^S_R}(l) \leq F_{\tilde{\imath}^S_R}(l_{max}) = c^2_{\tilde{\imath}_2}$

$l_{min} \in R(D_n \otimes D_m)$; $\quad l_{max} \in R(e_n \otimes I_m) \cup R(I_n \otimes C_S^{-1} e_m)$

receivers' positions/ZTDs are assumed known, and the weakest scenario, i.e. the *geometry-free* scenario where the geometry-parametrization $G\Delta x_R$ does not apply to the non-dispersive matrix ρ^S_R. As presented in Table 3, once the DD functions $l^T_{min}\text{vec}(\tilde{\imath}^S_R)$ are considered, the single-epoch ($k = 1$) float variance-ratio gets minimum and identical to $F_{\tilde{\imath}^S_R}(l_{min}) = c^2_{\tilde{\imath}\|\rho} \approx 10^2\ cm^2$ (geometry-fixed) and $F_{\tilde{\imath}^S_R}(l_{min}) = c^2_{\tilde{\imath}} \approx 44^2\ cm^2$ (geometry-free). In this case, the corresponding gain number becomes maximum and identical to to $\gamma_{\tilde{\imath}^S_R}(l_{min}) = (c^2_{\tilde{\imath}\|\rho}/c^2_{\tilde{\imath}\|\rho}) \approx 100^2$ (geometry-fixed) and $\gamma_{\tilde{\imath}^S_R}(l_{min}) = (c^2_{\tilde{\imath}}/c^2_{\tilde{\imath}}) \approx 100^2$ (geometry-free). This namely means, in case of the geometry-free scenario, that the standard deviation of size $c_{\tilde{\imath}} \approx 44\ cm$, at zenith, would reduce to $c_{\tilde{\imath}} \approx 4.4\ mm$ after IAR.

The single-epoch float-to-fixed standard deviation ratio of any linear function of the estimable slant ionospheric delays do therefore lie between 1 and 100. Figure 2 shows the formal standard deviation of the single-epoch UD (left-panel) and between-satellite single-differenced (SD) (right-panel) slant ionospheric delays before and after IAR over time. The corresponding float-to-fixed standard deviation ratio has been also presented. In contrast to the spectacular precision improvement of the DD ionospheric delays, the precision improvement of the UD ionospheric delays is rather marginal. The explanation for this difference lies in the fact that the ionospheric delays' estimator is built up by those of the DD components and of the satellite-/receiver-average components. After IAR, although the DD components become of the phase-level precision, the code-based precision of the satellite-/receiver-average components remains unchanged. This relatively poor code-based precision does therefore prohibit the gain to reach the two orders of the magnitude level.

Table 3 also characterizes the role of the number of epochs k in governing the ionospheric gain number and the float variance-ratio. While the float variance-ratio gets smaller over epochs, the gain in precision improvement due to IAR gets smaller as well. For sufficiently large number epochs, the minimum float variance-ratio becomes of the phase-level precision, the corresponding gain number tends to 1. This makes sense, as in that case, the time-constant DD ambiguities get precise enough so that no IAR is needed.

3.3 Receiver clocks' response to IAR

The estimable receiver clock parameters are composed of the *between-receiver* SD true receiver clock parameters as well as the between-receiver SD *ionosphere-free* components of the receiver code biases on the first two frequencies $j = 1,2$. Given the calibrated ionosphere-free components of the receiver code biases [18, 19], the estimable receiver clock parameters would then serve as input in the GNSS-based time transfer applications. The corresponding gain number and float variance-ratio can be shown to be the *same* for any function $l^T d\tilde{\imath}_R$ which are given by

$$\begin{aligned} \gamma_{d\tilde{\imath}_R}(l) &= 1 + \frac{c^2_{\tilde{\rho}} - c^2_{\tilde{\rho}}}{k c^2_{\hat{\rho}_2} \tan^2\theta + c^2_{\tilde{\rho}}} \\ F_{d\hat{\imath}_R}(l) &= \tfrac{1}{m^*}(c^2_{\hat{\rho}_2} + \frac{c^2_{\tilde{\rho}}}{k \tan^2\theta}) \end{aligned} \qquad (7)$$

with $m^* = e_m^T C_S^{-1} e_m$. The angle θ ($0 \leq \theta \leq 90^\circ$) measures the *degree of dependence* between vector e_m and the geometric matrix G [20].

While being independent of the number of stations n, the preceding gain number and float variance-ratio do depend on the number of satellites m and the elevation-weighting matrix C_S, characterized in the denominator (m^*), the number of epochs k, and the degree of dependence angle θ. Two extreme cases follows from (7). Firstly, we consider the perfect geometry case, i.e. when the vector e_m is orthogonal to the geometry matrix G ($\theta = 90^\circ$). This leads to $\gamma_{d\tilde{\imath}_R}(l) = 1$ and $F_{d\hat{\imath}_R}(l) = (c^2_{\hat{\rho}_2}/m^*)$. This namely means that there is *no* receiver clocks' precision improvement due to IAR. In this case, similar to the geometry-fixed scenario, the estimable receiver clocks do indeed get *uncorrelated* with the DD ambiguities, thus experiencing no precision gain by IAR.

Secondly, we consider the case where a *geometry defect* takes place. In that case, matrix $[e_m,\ G]$ is singular leading

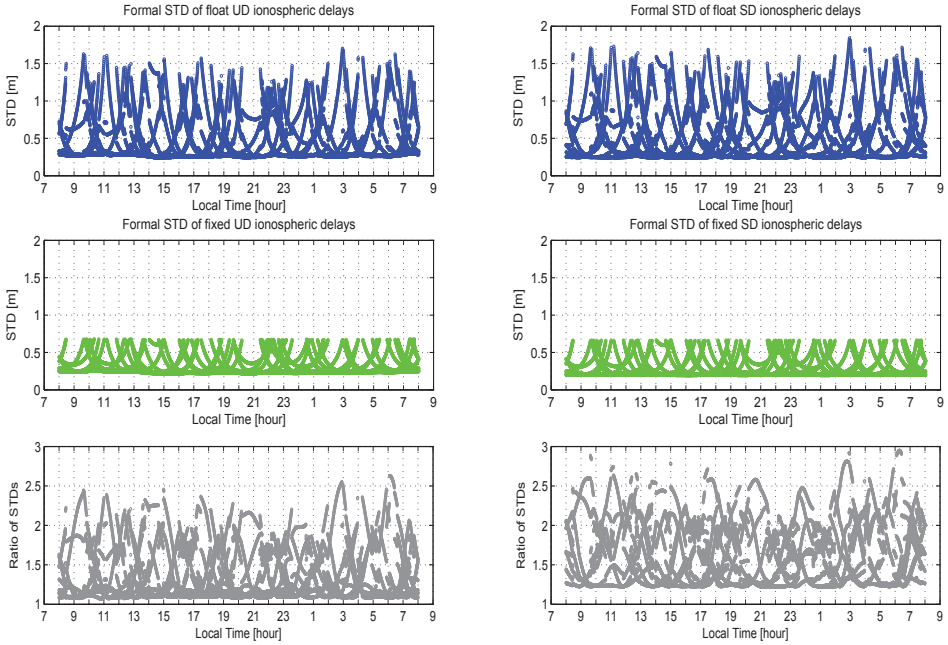

Figure 2. *Left-panel*: Impact of IAR on the single-epoch estimable UD slant ionospheric delays, *right-panel*: on their between-satellite SD versions (Geometry-based, ZTD-estimation only). Formal standard deviation (STD), in meters, before IAR (*top*), after IAR (*middle*), and float-to-fixed STD ratio (*bottom*). The number of stations is set to $n = 10$.

to $\theta = 0$, thus $F_{d\hat{l}_R}(l) \to \infty$. While the estimable receiver clocks are poorly estimable, the corresponding gain number attains its maximum value, i.e. $F_{d\hat{l}_R}(l) = (c^2_{\hat{\rho}}/c^2_{\tilde{\rho}}) \approx 100^2$. One can then infer that the weaker the geometry (i.e. the more the dependency between e_m and G), the smaller the angle θ, thus the larger the estimable receiver clock's precision gain is experienced through IAR.

Figure 3 shows the formal standard deviation of the single-epoch receiver clock parameters before and after IAR over time. The results are accompanied by the number of visible satellites (red lines). One can clearly observe the dependency of the float standard deviation on the number of satellites. The standard deviation *generally* increases as the number of satellite decreases. There are, however, a few occasions in which the standard deviation is not too large when the number satellites are minimum, see e.g. the interval around 11:00 am. In those occasions the receiver-satellite geometry is thus rather strong leading to not-too-large values. As more number of satellites, viewed by the network, causes rather wide dispersion in the geometry matrix G, the degree of dependence angle θ gets far different from zero leading to smaller gain numbers. This issue is clearly observed in Figure 3 where the float-to-fixed standard deviations generally gets smaller when the number of satellites increases.

To conclude this subsection, two important remarks must be made. First, for sufficiently large number of epochs, the float variance-ratio becomes almost identical to its geometry-fixed counterpart, namely $F_{d\hat{l}_R}(l) = (c^2_{\hat{\rho}_2}/m^*)$. In that case, the corresponding gain number becomes equal to 1, i.e. no precision gain is experienced by IAR. Second, we consider the receiver clocks' precision after successful IAR. The corresponding fixed variance-ratio follows as

$$\frac{F_{d\hat{l}_R}(l)}{\gamma_{d\tilde{l}_R}(l)} = \frac{1}{m^*}(c^2_{\hat{\rho}_2} + \frac{c^2_{\tilde{\rho}}}{k\tan^2\theta}) \approx \frac{1}{m^*}c^2_{\hat{\rho}_2} \qquad (8)$$

where the approximation is made by neglecting the small value $c^2_{\tilde{\rho}}$ and assuming $\tan^2\theta$ to be bounded. Thus after successful IAR, the receiver clocks' precision becomes almost identical to its geometry-fixed float counterpart if the geometry-defect would not take place, i.e. $\tan^2\theta$ takes finite values.

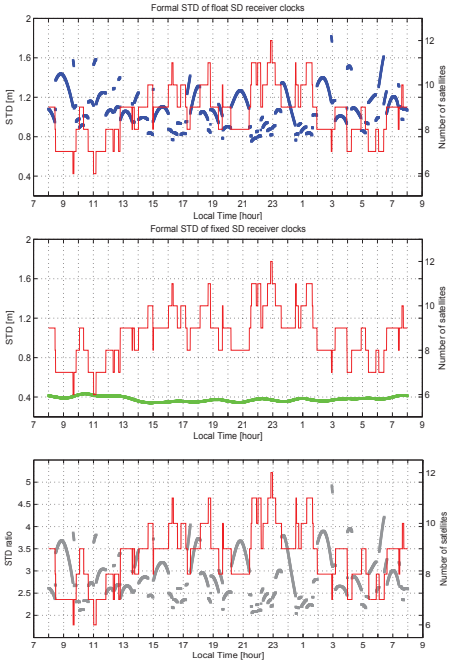

Figure 3. Impact of IAR on the single-epoch estimable SD receiver clocks (Geometry-based, ZTD-estimation only). Formal standard deviation (STD), in meters, before IAR (*top*), after IAR (*middle*), and float-to-fixed STD ratio (*bottom*). The number of satellites is depicted in red. The number of stations is set to $n = 10$.

3.4 PPP-RTK parameters' response to IAR

Estimable satellite clocks

We now consider the estimable satellite clocks and phase biases, where their between-satellite SD versions are essential components in the corrections provided to PPP-RTK users [9–11]. Similar to the estimable ionospheric delays, one can decompose the estimable satellite clocks and phase biases into their *satellite-averaged* components and between-satellite SD components (cf. 6). The satellite-averaged components always require code data to be determined. These components do therefore experience no precision improvement due to IAR. Let us now restrict ourselves to the between-satellite SD components. We begin with those of the estimable satellite clocks, i.e. $l_{min}^T d\tilde{t}^S$ (Table 4). Using the same analogy with the estimable receiver clocks, in the geometry-fixed case, the satellite clocks (and thus their SD functions) get uncorrelated with the DD ambiguities, thereby experiencing *no* improvement by IAR, i.e. $\gamma_{d\tilde{t}^S}(l) = 1$. On the other hand, when the geometry-dependent parameters are to be estimated (geometry-based scenario), the maximum precision gain is experienced, if the absence of satellite redundancy takes place. This is the case when the geometry matrix $[e_m,\ G]$ becomes a square matrix. Table 4 presents the ranges of the satellite clock gain number and float variance-ratio for different scenarios. It is not difficult to verify that the maximum value of the satellite clock gain number is bounded above and approximated by

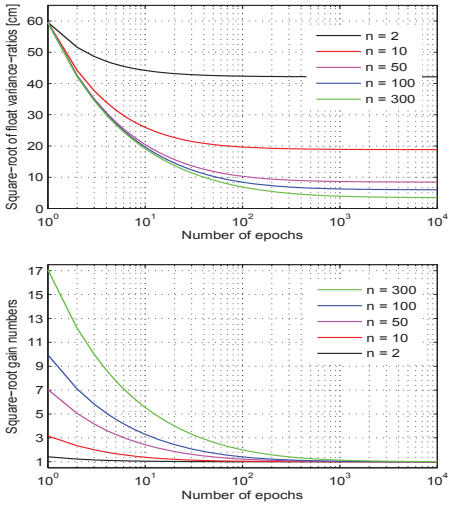

Figure 4. The square-root of the *minimum* float variance-ratio $F_{d\hat{t}^S}(l_{min})$ (top) and the corresponding gain numbers $\gamma_{d\tilde{t}^S}(l_{min})$ of the estimable satellite clocks (bottom) as function of number of epochs 'k' for different numbers of stations 'n', geometry-based scenario.

$$\gamma_{d\tilde{t}^S}(l) \leq 1 + \frac{n-1}{k} \tag{9}$$

In the single-epoch case ($k = 1$), the preceding maximum gain number is approximated by the number of stations n. Thus the more the number of stations, the larger satellite clocks' precision gain due to IAR is experienced. Shown in Figure 4 are the square-roots of the minimum float variance-ratio $F_{d\hat{t}^S}(l_{min})$ and the corresponding gain numbers $\gamma_{d\tilde{t}^S}(l_{min})$ as functions of the number of epochs for different numbers of stations. In the single-epoch case, GPS L1/L2 example, the minimum float variance-ratio becomes $F_{d\hat{t}^S}(l_{min}) = c^2_{\hat{\rho}_2}$ which correspond to a float standard deviation of the SD satellite clocks of size $\sqrt{2}c_{\hat{\rho}_2} \approx 85\ cm$, at zenith. The value gets even larger for lower

Table 4. Ranges of the estimable satellite clock gain number γ and float variance-ratio F for different scenarios. The scalar $c^2_{\hat{\rho}_2}$ follows from $c^2_{\hat{\rho}}$, given in Table 2, when the first two frequencies $j = 1,2$, are considered only.

Satellite-averaged:	$\gamma_{\hat{d}\bar{s}}(l) = 1$	$F_{\hat{d}\bar{s}}(l) = c^2_{\hat{\rho}_2}$
Geometry-Fixed:	$\gamma_{\hat{d}\bar{s}}(l) = 1$	$\frac{1}{n}c^2_{\hat{\rho}_2} = F_{\hat{d}\bar{s}}(l_{min}) \le F_{\hat{d}\bar{s}}(l) \le F_{\hat{d}\bar{s}}(l_{max}) = c^2_{\hat{\rho}_2}$
Geometry-Based:	$1 = \gamma_{\hat{d}\bar{s}}(l_{max}) \le \gamma_{\hat{d}\bar{s}}(l) \le \gamma_{\hat{d}\bar{s}}(l_{min}) = 1 + \frac{[n-1](c^2_{\hat{\rho}} - c^2_{\hat{\rho}})}{kc^2_{\hat{\rho}_2} + [n-1]c^2_{\hat{\rho}}}$	$\frac{1}{kn}(kc^2_{\hat{\rho}_2} + [n-1]c^2_{\hat{\rho}}) = F_{\hat{d}\bar{s}}(l_{min}) \le F_{\hat{d}\bar{s}}(l) \le F_{\hat{d}\bar{s}}(l_{max}) = c^2_{\hat{\rho}_2}$
Geometry-Free:	$1 = \gamma_{\hat{d}\bar{s}}(l_{max}) \le \gamma_{\hat{d}\bar{s}}(l) \le \gamma_{\hat{d}\bar{s}}(l_{min}) = 1 + \frac{[n-1](c^2_{\hat{\rho}} - c^2_{\hat{\rho}})}{kc^2_{\hat{\rho}_2} + k[n-1]c^2_{\hat{\rho}}}$	$\frac{1}{kn}(kc^2_{\hat{\rho}_2} + [n-1]c^2_{\hat{\rho}} + [k-1][n-1]c^2_{\hat{\rho}}) = F_{\hat{d}\bar{s}}(l_{min}) \le F_{\hat{d}\bar{s}}(l) \le F_{\hat{d}\bar{s}}(l_{max}) = c^2_{\hat{\rho}_2}$

$l_{min} \in R(D_m)$; $\quad l_{max} \in R(C_S^{-1}e_m)$

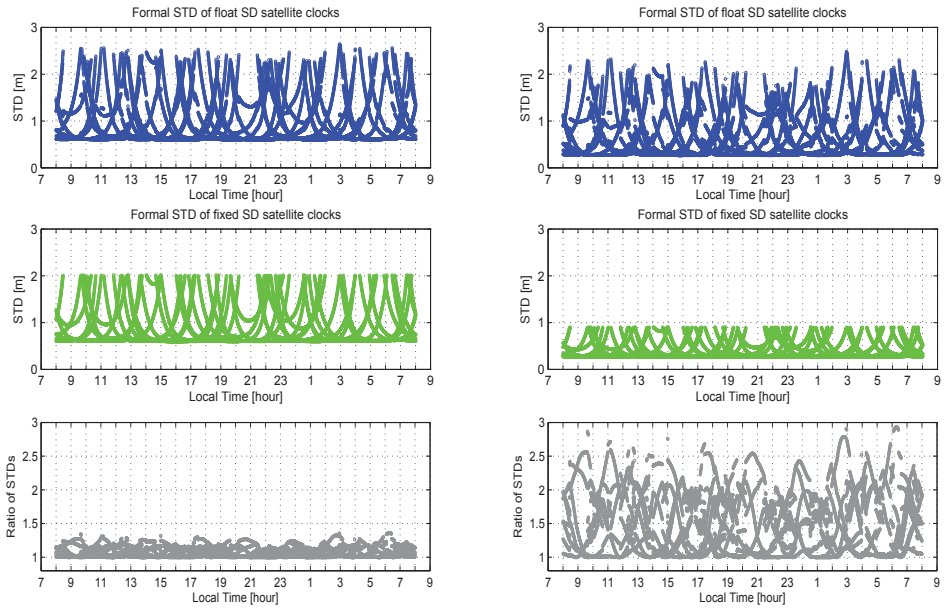

Figure 5. Impact of IAR on the single-epoch estimable SD satellite clocks (Geometry-based, ZTD-estimation only), for $n = 2$ (*left-panel*) and for $n = 10$ (*right-panel*). Formal standard deviation (STD), in meters, before IAR (*top*), after IAR (*middle*), and float-to-fixed STD ratio (*bottom*).

satellites' elevation. As shown, the float variance-ratio decrease over epochs faster for a more number of stations. Would one further apply IAR, the value decreases again faster for more number of stations.

Figure 5 shows the formal standard deviation of the single-epoch SD satellite clock parameters before and after IAR over time for $n = 2$ (left-panel) and for $n = 10$ (right-panel). The corresponding float-to-fixed standard deviation ratio has been also given. Being in agreement with the analytical results, it is observed that float-to-fixed standard deviation ratio gets larger by increasing the number stations from $n = 2$ to $n = 10$.

Estimable satellite phase biases

In case of the estimable satellite phase biases, we consider their *frequency-combined* versions $[q^T \otimes I_m]\tilde{\delta}^S$. The f-vector q characterizes the combination sought. For instance by taking q a canonical vector (a vector of zeros, except the j^{th} element equal to 1), the estimable satellite phase biases on frequency j is then considered.

Table 5 presents the ranges of the satellite phase bias gain number and float variance-ratio for different scenarios. In a similar way to that of the satellite clocks, one can verify that the maximum value of the satellite phase bias gain

Table 5. Ranges of the estimable satellite phase bias gain number γ and float variance-ratio F for different scenarios.

Sat.-averaged:	$\gamma_{\hat{\delta}^s}(q\otimes l)=1$	$F_{\hat{\delta}^s}(q\otimes l)=q^T(Q_2+Q_{\hat{\rho}_2})q$
Geometry-Fixed:	$q^T\Lambda^{-1}\mu=0;\quad \gamma_{\hat{\delta}^s}(q\otimes l)\approx 1$ $q^T\Lambda^{-1}e_\mu=0;\quad 1\le\gamma_{\hat{\delta}^s}(q\otimes l)\le 1+\frac{n-1}{k}$	$\frac{1}{n}q^T(Q_2+Q_{\hat{\rho}_2})q+[\frac{n-1}{kn}]q^TQq=F_{\hat{\delta}^s}(q\otimes l_{min})\le F_{\hat{\delta}^s}(q\otimes l)\le F_{\hat{\delta}^s}(q\otimes l_{max})=q^T(Q_2+Q_{\hat{\rho}_2})q$
Geometry-Free:	$1\le\gamma_{\hat{\delta}^s}(q\otimes l)\le 1+\frac{n-1}{k}$	$\frac{1}{n}q^T(Q_2+Q_{\hat{\rho}_2})q+[\frac{n-1}{kn}]q^T(Q+Q_{\hat{\rho}})q=F_{\hat{\delta}^s}(q\otimes l_{min})\le F_{\hat{\delta}^s}(q\otimes l)\le F_{\hat{\delta}^s}(q\otimes l_{max})=q^T(Q_2+Q_{\hat{\rho}_2})q$

$l_{min}\in R(D_m);\quad l_{max}\in R(C_S^{-1}e_m);\quad e_\mu=e_f-(c_{\hat{\rho}\hat{1}}/c_{\hat{\rho}}^2)\mu$

$Q_2=\Lambda^{-1}(C_\phi+c_{\hat{1}|\hat{\rho}_2}^2\mu\mu^T)\Lambda^{-1};\ Q=\Lambda^{-1}(C_\phi+c_{\hat{1}|\hat{\rho}}^2\mu\mu^T)\Lambda^{-1};\quad Q_{\hat{\rho}_2}=c_{\hat{\rho}_2}^2\,\Lambda^{-1}e_\mu e_\mu^T\Lambda^{-1};\ Q_{\hat{\rho}}=c_{\hat{\rho}}^2\Lambda^{-1}e_\mu e_\mu^T\Lambda^{-1}$

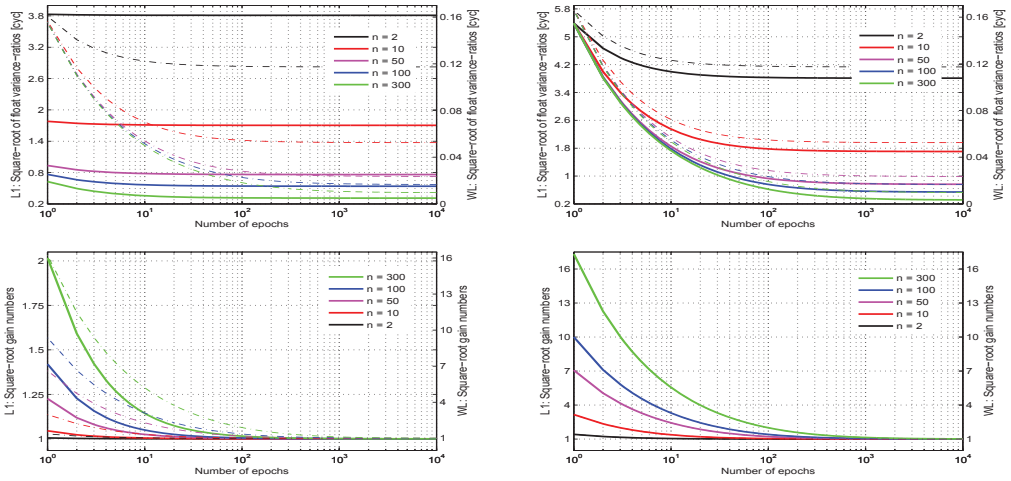

Figure 6. The square-root of the *minimum* float variance-ratio $F_{\hat{\delta}^s}(l_{min})$ (top) and the corresponding gain numbers of the estimable satellite phase biases $\gamma_{\hat{\delta}^s}(l_{min})$ (bottom) as function of number of epochs 'k' for different numbers of stations 'n', geometry-fixed scenario (left-panel) and geometry-free scenario (right-panel). The thick lines correspond to the GPS L1 phase biases, while the dashed lines correspond to the GPS wide-lane (i.e L1-L2) phase biases.

number is bounded above and approximated by

$$\gamma_{\hat{\delta}^s}(q\otimes l)\le 1+\frac{n-1}{k} \tag{10}$$

Thus the more the number of stations, the larger satellite clocks' precision gain due to IAR is experienced. The response to IAR is, however, quite distinct for different scenarios and frequency combinations. To make this issue more apparent, we consider our GPS dual-frequency example with the L1 and wide-lane combinations that are characterized by $q_{L1}=[1,0]^T$ and $q_{WL}=[1,-1]^T$, respectively. Figure 6 presents the square-roots of the minimum float variance-ratio $F_{\hat{\delta}^s}(l_{min})$ and the corresponding gain numbers $\gamma_{\hat{\delta}^s}(l_{min})$ as functions of the number of epochs for different numbers of stations. This has been done for both the L1 (thick lines) and wide-lane (dashed lines) estimable phase biases, the geometry-fixed scenario (left-panel) and the geometry-free scenario (right-panel). It is observed that the wide-lane estimable phase biases have almost the *same* signature in both the scenarios showing very less dependency on the geometry of the model. While the square-roots of their minimum float variance-ratio is already very small (about $0.16[cycle]$, single-epoch case), they can further considerably be improved by IAR (about 7 times smaller, single-epoch case, $n=50$). On the other hand however, the signature of the L1 estimable phase biases do highly depend on the geometry of the model. In case of the geometry-fixed scenario, the square-roots of the corresponding gain number is rather small and hardly increases as the number of stations increases (about 1.2, single-epoch case, $n=50$). Quite differently, in case of the geometry-free scenario, the square-roots of the corresponding gain number is considerable and gets larger as the number of stations increases (about 7, single-epoch case, $n=50$).

3.5 Estimable code biases' response to IAR

We conclude this section by discussing the impact of IAR on the estimable code biases. Since the code biases on the first two frequencies are fully absorbed by the ionospheric delays and the clock parameters, the estimable code biases only show up themselves on the third frequency and beyond. They are the true code biases on $j \geq 3$, biased by functions of the true code biases on first two frequencies. While the estimable receiver code biases can be used for the calibration purposes, the estimable satellite code biases must be integrated by the satellite clocks and phase biases as the corrections of the *multi-frequency* PPP-RTK users. It can be shown that the estimable code biases are *uncorrelated* with the DD ambiguities, thus no precision improvement is realized due to IAR. This namely yields

$$\gamma_{\tilde{d}_R}(l) = 1; \qquad \gamma_{\tilde{d}^S}(l) = 1 \tag{11}$$

Therefore, if one is interested to determine the estimable code biases, no additional IAR step is required.

4 Summary and conclusions

Presenting a multivariate formulation of the network observation equations, we studied the impact of IAR on the precision of GNSS estimable parameters using appropriate one-to-one transformations (cf. 6). In case of the estimable ionospheric delays, the (weighted) satellite-/receiver-averaged components $\tilde{\mathfrak{i}}_r^{\bar{s}}$, $\tilde{\mathfrak{i}}_r^{1\bar{S}}$, $\tilde{\mathfrak{i}}_{1R}^{\bar{s}}$ remain unaffected after IAR, as they are solely determined by the code data and cannot be determined by the integer-resolved DD phase data. On the other hand, the DD component $\tilde{\mathfrak{i}}_{1R}^{1S}$ experiences precision improvement of two orders of magnitude. Being functions of the aforementioned four constituent components, the precision improvement of the UD and SD ionospheric delays is not as spectacular as that of their DD counterparts, since the relatively poor code-based precision of the unaffected components $\tilde{\mathfrak{i}}_r^{\bar{s}}$, $\tilde{\mathfrak{i}}_r^{1\bar{S}}$, $\tilde{\mathfrak{i}}_{1R}^{\bar{s}}$ prohibits the precision gain to reach two orders of magnitude level.

In case of the estimable receiver clocks $d\tilde{t}_R$, we formulated the corresponding gain number and float variance-ratio as functions of the number satellites/elevation-weights, the number of epochs, and the degree of dependence angle characterizing the strength of the geometry of the model (cf. 7). In agreement with the analytical expressions, the corresponding numerical results highlight that the weaker the geometrical strength, the larger the precision gain is experienced through IAR.

In case of the estimable satellite clocks and phase biases, the (weighted) satellite-averaged components remain unaffected after IAR. As essential elements in the PPP-RTK corrections, the between-satellite SD components do, however, generally experience precision improvement through IAR. The precision gain gets larger as the number of stations increases. While the variance of the float wide-lane satellite phase biases is almost insensitive to the geometry of the model and already very small, that of the satellite clocks and phase biases on a particular frequency highly depends on the geometry of the model. Similar to the receiver clocks, the weaker the geometrical strength, the larger the precision gain is experienced.

Finally we considered the impact of IAR on the estimable code biases that are present on the third frequency and beyond. Being uncorrelated with the DD ambiguities, no precision improvement is realized due to IAR. One can therefore be exempted from the additional IAR step, if these types of biases would be of interest.

Acknowledgements

The first author is the recipient of an Australian Research Council (ARC) Federation Fellowship (project number FF0883188). This support is gratefully acknowledged.

References

[1] P. J. G. Teunissen, P. J. de Jonge, and C. C. J. M. Tiberius, "Performance of the LAMBDA method for fast GPS ambiguity resolution," *Navigation*, vol. 44, no. 3, pages 373–383, 1997.

[2] C. C. J. M. Tiberius and P. J. de Jonge, "Fast positioning using the LAMBDA method," in *Proceedings of the 4th International Symposium on Differential Satellite Navigation Systems,Bergen, Norway, 24-28 April*, vol. 30, Citeseer, 1995.

[3] S. Han, "Quality-control issues relating to instantaneous ambiguity resolution for real-time GPS kinematic positioning," *J. Geod.*, vol. 71, no. 6, pages 351–361, 1997.

[4] P. J. G. Teunissen, "The least-squares ambiguity decorrelation adjustment: a method for fast GPS integer ambiguity estimation," *J. Geod.*, vol. 70, no. 1-2, pages 65–82, 1995.

[5] S. Schaer, G. Beutler, L. Mervart, M. Rothacher, and U. Wild, "Global and regional ionosphere models using the GPS double difference phase observable," in *Proceedings of the IGS Workshop on Special Topics on New Directions*, (77-92 Potsdam, Germany, May 15–27), 1995.

[6] X. Li, X. Zhang, and M. Ge, "Regional reference network augmented precise point positioning for in-

stantaneous ambiguity resolution," *J. Geod.*, vol. 85, no. 3, pages 151–158, 2011.

[7] D. Odijk, P. J. G. Teunissen, and A. Khodabandeh, "Single-Frequency PPP-RTK: Theory and Experimental Results," *IAG Symp*, vol. 139, pages 167–173, 2014.

[8] J. Delporte, F. Mercier, D. Laurichesse, and O. Galy, "Fixing integer ambiguities for GPS carrier phase time transfer," in *Frequency Control Symposium, 2007 Joint with the 21st European Frequency and Time Forum. IEEE International*, pages 927–932, IEEE, 2007.

[9] P. J. G. Teunissen, D. Odijk, and B. Zhang, "PPP-RTK: Results of CORS Network-Based PPP with Integer Ambiguity Resolution," *J. Aeronaut. Astronaut. Aviat.*, vol. 42, no. 4, pages 223–229, 2010.

[10] P. Collins, S. Bisnath, F. Lahaye, and P. Heroux, "Undifferenced GPS ambiguity resolution using the decoupled clock model and ambiguity datum fixing," *Navigation*, vol. 57, no. 2, pages 123–135, 2010.

[11] J. Geng, C. Shi, M. Ge, A. H. Dodson, Y. Lou, Q. Zhao, and J. Liu, "Improving the estimation of fractional-cycle biases for ambiguity resolution in precise point positioning," *J. Geod.*, vol. 86, no. 8, pages 579–589, 2012.

[12] P. J. G. Teunissen, "A canonical theory for short GPS baselines. Part I: The baseline precision," *J. Geod.*, vol. 71, no. 6, pages 320–336, 1997.

[13] C. R. Rao, *Linear statistical inference and its applications*, vol. 2nd ed. John Wiley & Sons, 1973.

[14] P. J. G. Teunissen, "Generalized inverses, adjustment, the datum problem and S-transformations," in *Optimization and Design of Geodetic Networks* (E. W. Grafarend and F. Sanso, eds.), pages 11–55, Springer, Berlin, 1985.

[15] P. J. de Jonge, *A processing strategy for the application of the GPS in networks*. PhD thesis, Delft University of Technology, Publication on Geodesy, 46, Netherlands Geodetic Commission, Delft, 1998.

[16] P. J. G. Teunissen, "GPS double difference statistics: with and without using satellite geometry," *J. Geod.*, vol. 71, no. 3, pages 137–148, 1997.

[17] H. J. Euler and C. C. Goad, "On optimal filtering of GPS dual frequency observations without using orbit information," *J. Geod.*, vol. 65, no. 2, pages 130–143, 1991.

[18] G. Petit, Z. Jiang, P. Uhrich, and F. Taris, "Differential calibration of Ashtech Z12-T receivers for accurate time comparisons," in *Proc. 14th European Frequency and Time Forum (Turin)*, pages 40–4, 2000.

[19] J. Plumb, K. M. Larson, J. White, and E. Powers, "Absolute calibration of a geodetic time transfer system," *IEEE Trans. Ultrason. Ferroelectr. Freq. Control*, vol. 52, no. 11, pages 1904–1911, 2005.

[20] P. J. G. Teunissen, *Adjustment theory: an introduction*. Delft University Press, 2000. Series on Mathematical Geodesy and Positioning.

10 Single-Epoch Integrity Monitoring in Array-based PPP-RTK

This chapter is covered by the following publication:

Khodabandeh A. and Teunissen P.J.G. (2014b). Single-Epoch GNSS Array Integrity: an Analytical Study. International Association of Geodesy Symposium (IAG), Springer, Accepted for publication.

VIII Hotine-Marussi Symposium on Mathematical Geodesy manuscript No.
(will be inserted by the editor)

Single-Epoch GNSS Array Integrity: an Analytical Study

A. Khodabandeh · P.J.G. Teunissen

Received: date / Accepted: date

Abstract In this contribution we analyze the integrity of the GNSS array model through the so-called uniformly most powerful invariant (UMPI) test-statistics and their corresponding minimal detectable biases (MDBs). The model considered is characterized by multiple receivers/satellites with known coordinates where the multi-frequency carrier-phase and pseudo-range observables are subject to atmospheric (ionospheric and tropospheric) delays, receiver and satellite clock biases, as well as instrumental delays. Highlighting the role played by the model's misclosures, analytical multivariate expressions of a few leading test-statistics together with their MDBs are studied that are further accompanied by numerical results of the three GNSSs GPS, Galileo and BeiDou.

Keywords Uniformly Most Powerful Invariant (UMPI) test-statistic · Minimal Detectable Bias (MDB) · GNSS misclosures · Array model · Integrity

1 Introduction

The notion of the GNSS array model, here, refers to an array of antennas tracking the multi-frequency carrier-phase/pseudo-range observables in the presence of atmospheric effects. The coordinates of antennas and satellites are assumed to be known. The definition presented is rather general in the sense that even the medium-scale control networks can also be considered as an array. Examples of such are the continuously operating reference station (CORS) networks sending corrections to the RTK- and/or PPP-RTK users (de Jonge, 1998; Odijk et al, 2014), a set of antennas mounted on rigid platforms improving the position/attitude of points in its vicinity (Teunissen, 2010, 2012), and the ground based augmentation systems (GBASs) supporting safe flight procedures such as landing, departure and surface operations at an airport (Khanafseh et al, 2012; Giorgi et al, 2012). Despite their different applications, all of the aforementioned arrays are, however, utilized for the purpose of the *same* functionality, that is, providing accurate corrections for the users. Ensuring the integrity and reliability of the corrections, even at the pre-analysis level, is therefore of great importance, see e.g., Teunissen (1998); Teunissen and de Bakker (2012).

Integrity monitoring and quality control of the GNSS array model is the topic of this contribution. We confine our study to the *single-epoch* scenario as it is indeed the ultimate goal of the near real-time applications and, at the same time, brings us conservative thresholds of the reliability measures of the corresponding multi-epoch scenario. Our strategy commences with the model's misclosures. Although the GNSS misclosures can be treated as diagnostic tools in their own right, we make use of certain linear functions of them to formulate the UMPI test-statistics which give rise to the highest probability of the detection for a class of critical regions. For an overview of the underlying principles of the UMPI test, see Arnold (1981), and for its applications to hypothesis testing in linear models, see e.g. Teunissen (2000).

The test-statistics to be studied are 1) the array-, antenna- and satellite-detectors in which the overall/local validity of the model is tested, 2) the celebrated *w*-test-statistic for the purpose of outlier identification and 3) the atmospheric detectors well suited to the small-scale arrays. The detectabil-

A. Khodabandeh
GNSS Research Centre, Department of Spatial Sciences, Curtin University of Technology, Perth, Australia
E-mail: amir.khodabandeh@curtin.edu.au

P.J.G. Teunissen
GNSS Research Centre, Department of Spatial Sciences, Curtin University of Technology, Perth, Australia; Department of Geoscience and Remote Sensing, Delft University of Technology, Delft, The Netherlands
E-mail: p.teunissen@curtin.edu.au

ity of the tests is formulated via the corresponding MDBs where the associated numerical illustrations, emphasized on the three GNSSs GPS, Galileo and BeiDou, are also given.

2 Array model and the GNSS misclosures

Consider a single antenna, say antenna r ($r = 1,\dots,n$), that tracks s number of commonly-viewed satellites on frequency j ($j = 1,\dots,f$). One can then put the corresponding *undifferenced* carrier-phase observations on each frequency, as the s-vectors $\phi_{r,j}$ ($j = 1,\dots,f$), into a higher-dimensioned vector $\phi_r = [\phi_{r,1}^T,\dots,\phi_{r,f}^T]^T$. Doing the same to the pseudo-range observations p_r and collecting observations of all n antennas, the final $sf \times n$ matrices of carrier-phase and pseudo-range data of the array can be, respectively, formulated as

$$\Phi = [\phi_1,\dots,\phi_n], \quad P = [p_1,\dots,p_n]$$

The satellite-/receiver-dependent biases are, respectively, canceled out by applying the between-receiver single-differenced (SD) operator D_n and the between-satellite SD operator D_s (Teunissen, 1997). The multivariate representation of the double-differenced (DD) observation equations of the array model, under the null hypothesis H_o, reads then

$$\begin{aligned} \mathsf{E}\{(I_f \otimes D_s^T)\Phi\, D_n\} &= (e_f \otimes D_s^T g)\, \tau^T D_n - (\mu \otimes I_{s-1})\, D_s^T\, \imath\, D_n + (\Lambda \otimes I_{s-1})\, Z \\ \mathsf{E}\{(I_f \otimes D_s^T)P\, D_n\} &= (e_f \otimes D_s^T g)\, \tau^T D_n + (\mu \otimes I_{s-1})\, D_s^T\, \imath\, D_n \end{aligned} \tag{1}$$

$$\begin{aligned} \mathsf{D}\{vec[(I_f \otimes D_s^T)\Phi\, D_n]\} &= D_n^T D_n \otimes Q_\phi \otimes D_s^T W_s^{-1} D_s \\ \mathsf{D}\{vec[(I_f \otimes D_s^T)P\, D_n]\} &= D_n^T D_n \otimes Q_p \otimes D_s^T W_s^{-1} D_s \end{aligned} \tag{2}$$

where the s-vector g contains functions mapping the slant tropospheric delays (STDs) onto the zenith tropospheric delays (ZTDs) $\tau = [\tau_1,\dots,\ \tau_n]^T$. The $s \times n$ matrix $\imath$ is introduced as $\imath = [\imath_1,\dots,\imath_n]$, with $\imath_r$ being the s-vector of the (first-order) slant ionospheric delays of antenna r. The f-vector μ contains the ionospheric coefficients $\mu_j = \lambda_j^2/\lambda_1^2$, with λ_j being the wavelengths positioned on the $f \times f$ diagonal matrix Λ. The matrix Z contains the integer-valued DD ambiguities. The $f \times f$ positive-definite matrices Q_ϕ and Q_p are the cofactor matrices of the phase and pseudo-range observable-type. The $s \times s$ diagonal matrix W_s captures the satellite elevation dependency of the observations. I and e, respectively, denote the identity matrix and the vector of ones, where the subscripts indicate their size. The operator $\otimes$ denotes the Kronecker product. $\mathsf{E}\{.\}$ and $\mathsf{D}\{.\}$ are the mathematical expectation and dispersion operators, respectively. The operator $vec[.]$ vectorizes the associated matrix.

Using model (1) and (2), we are interested to check the validity of the model against unaccounted effects. To do so, we therefore work with the conditioned equations of (1) and the corresponding misclosures. The idea to employ the conditioned equations rather than the commonly-used observation equations is motivated by the desire to characterize the intrinsic behavior of the array model in relation to the possible misspecifications. This is indeed realized by forming the GNSS misclosures showing the contribution of the observations to the redundancy of the model.

2.1 GNSS-based decoupled misclosures

Although the misclosures of (1) can be formed in many different ways, we form those that are group-wise *uncorrelated* and at the same time have easy interpretations. The GNSS-based decoupled misclosures, in case of the ambiguity-float scenario, are introduced as follows (cf. Appendix)

$$\begin{aligned} &\textit{i: Frequency-differenced misclosures:} \\ &M_1 = [(D_f^T \mu)^{\perp^T} D_f^T \otimes c_{d|\tau}^2 \bar{g}^T W_s]\ P\, D_n \\ &\textit{ii: Atmosphere-free misclosures:} \\ &M_2 = [\mu^{\perp^T} \otimes (D_s^T g)^{\perp^T} D_s^T]\ P\, D_n \end{aligned} \tag{3}$$

where $(.)^\perp$ denotes the orthogonal complement basis matrix. We introduce the s-vector $\bar{g} = g + (c_{d\tau}/c_\tau^2)e_s$, in which the satellite-domain (co)variance-type scalars $c_{d|\tau}^2$, $c_{d\tau}$ and c_τ^2 are computed as

$$\begin{aligned} c_\tau^2 &= \frac{e_s^T W_s e_s}{[e_s^T W_s e_s][g^T W_s g] - [g^T W_s e_s]^2} \\ c_{d\tau} &= \frac{-g^T W_s e_s}{[e_s^T W_s e_s][g^T W_s g] - [g^T W_s e_s]^2}, \quad c_{d|\tau}^2 = \frac{1}{e_s^T W_s e_s} \end{aligned} \tag{4}$$

With regard to (3), M_1 and M_2, respectively, contribute to the model's redundancy of size $(f-2)$ and $(f-1)(s-2)$ per baseline. After fixing ambiguities, similar expressions can be obtained for the phase and phase-and-code misclosures.

2.2 Atmosphere-aided decoupled misclosures

The GNSS-based misclosures, presented in (3), contain the *complete* information needed to check and to study the quality of the observation matrices Φ and P in (1). One may, however, strengthen the model by using a-priori atmospheric information, i.e. the spatial dependency of the atmospheric delays. In case of not-too-large arrays, the differential atmospheric delays, with amount of uncertainty, would thus play the role of pseudo-observables as

$$\begin{aligned} &\mathsf{E}\{D_s^T \imath\, D_n\} = D_s^T \imath\, D_n, \text{ with } \mathsf{D}\{D_s^T \imath\, D_n\} = \sigma_\imath^2\, D_n^T D_n \otimes D_s^T W_s^{-1} D_s \\ &\mathsf{E}\{D_n^T \tau\} = D_n^T \tau, \qquad \text{with } \mathsf{D}\{D_n^T \tau\} = \sigma_\tau^2\, D_n^T D_n \end{aligned} \tag{5}$$

with $\sigma_\imath^2$ and σ_τ^2 being the a-priori ionospheric and tropospheric variances, respectively.

Appending the preceding equations to (1) does increase the redundancy of the model by comparing the GNSS-based estimators of the differential atmospheric delays with their pseudo-observable ones (s redundant observations per baseline). This, in a similar way to (3), provides us with the atmosphere-aided misclosures.

3 UMPI test-statistics and their MDBs

Given the GNSS decoupled misclosures introduced in the previous section, we are now in a position to form various test-statistics.

Theorem 1 (UMPI test-statistic and its MDB) *Let the alternative hypothesis H_a be related to the null hypothesis H_o as $\mathsf{E}\{vec[Y]|H_a\} = \mathsf{E}\{vec[Y]|H_o\} + C_Y\nabla$, where the q-vector of misspecifications ∇ is linked to the observations by the full-rank design matrix C_Y. Given a representation for the model's misclosures as $M = B^T vec[Y]$ under H_o, the UMPI test-statistic T_q and its MDB are respectively given by*

$$T_q = \frac{tr\{Q_{MM}^{-1} P_{C_M} MM^T\}}{tr\{P_{C_M}\}} \tag{6}$$

$$||\nabla|| = \sqrt{\frac{\nu_{q,\alpha,\gamma}}{d_Y^T C_M^T Q_{MM}^{-1} C_M d_Y}}, \quad \nabla = ||\nabla|| d_Y \tag{7}$$

where $Q_{MM} = \mathsf{D}\{M\}$ and $C_M = B^T C_Y$, with the projector $P_{C_M} = C_M(C_M^T Q_{MM}^{-1} C_M)^{-1} C_M^T Q_{MM}^{-1}$. The scalar $\nu_{q,\alpha,\gamma}$ is the χ^2-noncentrality parameter to be determined by the power of the test γ and the probability of false alarm α. The operator $tr\{.\}$ denotes the trace of a matrix, whereas $||.||^2 = (.)^T(.)$ is the squared-norm of a vector.

Proof see Appendix. □

The above theorem shows how the multivariate representation of the UMPI test-statistic is realized through the model's misclosures and the type of misspecifications, i.e. C_Y. We remark that the test-statistic T_q follows central and noncentral F-distribution under H_o and H_a, respectively, that is, $T_q|H_o \sim F(q,\infty,0)$ and $T_q|H_a \sim F(q,\infty,\nu)$, with the first two arguments q, ∞ being the degrees of freedom and ν the noncentrality parameter.

As to the GNSS array model, one may formulate a rather general structure for the misspecification design matrix C_Y at the *undifferenced* level. The following structure has been adopted in this study

$$\mathsf{E}\{\tilde{Y}|H_a\} = \mathsf{E}\{\tilde{Y}|H_o\} + (C_f \otimes C_s)\,\nabla\, C_n^T \tag{8}$$

where the full-rank matrices C_f, C_s and C_n specify the type of misspecification ∇ in the frequency-, satellite- and antenna-domain, respectively. The role of the *atmosphere-corrected* observation matrix $\tilde{Y}$ can be taken by $\tilde{P}$ and $\tilde{\Phi}$ or both of them, in which we define

$$\begin{aligned} \tilde{P} &= P - (e_f \otimes g)\tau - (\mu \otimes I_s)\iota \\ \tilde{\Phi} &= \Phi - (e_f \otimes g)\tau + (\mu \otimes I_s)\iota \end{aligned} \tag{9}$$

MDB-parametrization: In general there is no unique solution for the MDB of the misspecifications of a *multi dimensional* type. This issue can be properly circumvented through an MDB-parametrization as follows

$$\nabla = ||vec[\nabla]||\,(d_f \otimes d_s)\, d_n^T \tag{10}$$

with d_f, d_s and d_n being, respectively, the frequency-, satellite- and antenna-domain vectors such that their resultant vector $d_n \otimes d_f \otimes d_s$ is of length 1, i.e. a direction vector.

In the following, a few important test-statistics, together with their MDBs, will be specialized by setting C_f, C_s and C_n in (8) to certain structures.

3.1 Array-, Antenna- and Satellite-detectors

First one needs to check the validity of the array model against any type of misspecification that might potentially occur. The stated validity can be either of an *overall* type or of a *local* type. The overall validity of the model is tested through the array-detector characterized by the following setting

$$\textit{array-detector:} \quad C_f \mapsto I_f, \quad C_s \mapsto D_s, \quad C_n \mapsto D_n \tag{11}$$

Depending on the a-priori atmospheric variances σ_ι^2 and σ_τ^2, several expressions can be formulated. In case of atmosphere-fixed scenario, i.e. $\sigma_\iota^2 = 0$ and $\sigma_\tau^2 = 0$, the array-detector can be shown to take the following form (cf. Appendix)

$$T_q = \tfrac{1}{q} tr\{[Q_p^{-1} \otimes W_s P_{e_s}^{\perp}]\, \tilde{P} P_{D_n} \tilde{P}^T\} + \tfrac{1}{q} tr\{[Q_\phi^{-1} \otimes W_s P_{e_s}^{\perp}]\, \tilde{\Phi} P_{D_n} \tilde{\Phi}^T\} \tag{12}$$

with the projectors $P_{e_s}^{\perp} = I_s - c_{d|\tau}^2 e_s e_s^T W_s$ and $P_{D_n} = I_n - (1/n) e_n e_n^T$. The degrees of freedom q is determined upon choosing the following scenarios

$$\begin{aligned} &\textit{codeless data}\ (Q_p^{-1} = 0): && \Rightarrow q = f(s-1)(n-1) \\ &\textit{phaseless data}\ (Q_\phi^{-1} = 0): && \Rightarrow q = f(s-1)(n-1) \\ &\textit{code+phase data}: && \Rightarrow q = 2f(s-1)(n-1) \end{aligned} \tag{13}$$

The corresponding MDB, in accordance with (7), reads

$$||vec[\nabla]|| = \frac{\nu_{q,\alpha,\gamma}^{\frac{1}{2}}}{\sqrt{[d_f^T (Q_p^{-1} + Q_\phi^{-1}) d_f][d_s^T D_s^T W_s P_{e_s}^{\perp} D_s d_s][d_n^T D_n^T P_{D_n} D_n d_n]}} \tag{14}$$

Clearly a judgment on the size of the MDB cannot be easily made since it depends on the three vectors d_f, d_s and d_n. Keeping fixed two vectors out of which however, one can still gain information on the sensitivity of the MDB to the contributing factors like the number of frequencies/satellites and the quality of the observables. This idea leads to locally validate the model by testing observations of a particular antenna and/or those of a particular satellite. We can therefore characterize the antenna-/satellite-detector upon the following setting

$$\begin{aligned} &\textit{antenna-detector:} && C_f \mapsto I_f, \quad C_s \mapsto D_s, \quad C_n \mapsto u_r^n \\ &\textit{satellite-detector:} && C_f \mapsto I_f, \quad C_s \mapsto u_i^s, \quad C_n \mapsto D_n \end{aligned} \tag{15}$$

where u_r^n denotes the canonical n-vector containing zeros except the r^{th} element equal to one. The canonical vector u_i^s is defined similarly. With this setting, in an analogous way to (11) and (12), expressions of the stated test-statistics as well as their MDBs can be obtained. For the atmosphere-fixed case, the degrees of freedoms of the antenna-/satellite-detector are $q = f(s-1)$ and $q = f(n-1)$, respectively.

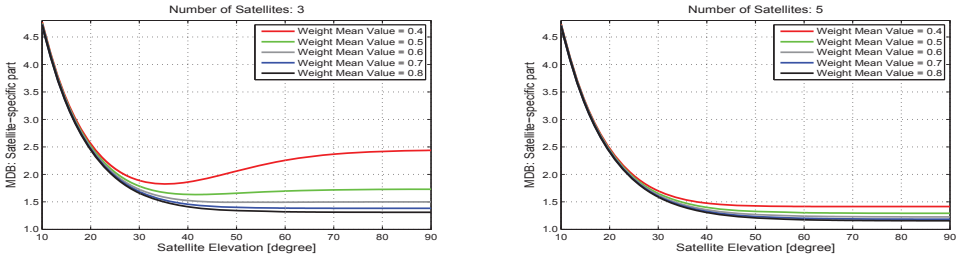

Fig. 1 Satellite-specific part of the outlier MDBs as function of the satellite elevation for different satellite configuration. The overall satellite configuration has been characterized by the weight mean value '$\bar{w}$'.

3.2 *w*-test-statistic and the MDB of single outliers

We now focus our attention to the well-known *w*-test-statistic employed for the purpose of identification of a single erroneous observation (Baarda, 1968). The structure of C_Y is then set to

$$\textit{w-test-statistic:} \quad C_f \mapsto u_j^f, \quad C_s \mapsto u_i^s, \quad C_n \mapsto u_r^n \qquad (16)$$

Similar to the array-detector, depending on the scenarios considered, several expressions can be given to the *w*-test-statistic. The structures of the corresponding MDB do however follow the same pattern. Let us, for the moment, consider STDs rather than ZTDs in the model. The code-outlier MDB can be shown to read as

$$||vec[\nabla]||_{STD} = v_{1,\alpha,\gamma}^{\frac{1}{2}} \times [\tfrac{n}{n-1}]^{\frac{1}{2}} \times [w^i(1-[\tfrac{w^i}{\bar{w}}]\tfrac{1}{s})]^{-\frac{1}{2}} \times [\tfrac{\sigma_{\hat{p}_j}^2}{1-(\sigma_{\hat{p}_j}^2/\sigma_{\hat{p}_j}^2)}]^{\frac{1}{2}} \qquad (17)$$

Four contributing elements show up themselves in the above MDB that are described in the following:

Noncentrality parameter $v_{1,\alpha,\gamma}$: Given the fixed probability of false alarm α, the χ^2-noncentrality parameter increases as the power of the test γ increases. In other words, for a given fixed model and a fixed α, the higher the power of the test is sought, the larger the MDB becomes.

Antenna-specific part $[n/(n-1)]^{\frac{1}{2}}$: This clearly shows that an increase in the number of antennas n could decrease the size of the outlier MDB considerably, would one, in the beginning, consider a *limited* number of antennas (e.g. $n = 2$ or $n = 3$). However, the stated MDB *does not* significantly decrease in size by adding an extra antenna when dealing with an array of a *large* number of antennas.

Satellite-specific part $[w^i(1-[\frac{w^i}{\bar{w}}]\frac{1}{s})]^{-\frac{1}{2}}$: This term depends on three factors, namely, 1) the elevation-dependent weight w^i of an individual satellite, say i, 2) the mean value of w^i ($i = 1,\ldots,s$) denoted by $\bar{w}$, and 3) the number of common satellites s. In this study, we make use of the exponential elevation weighting strategy to form the diagonal elements of matrix W_s, i.e. w^i (Euler and Goad, 1991)

$$w^i = [1 + 10\exp(-\frac{\varepsilon^i}{10^\circ})]^{-2}, \quad i = 1,\ldots,s \qquad (18)$$

where ε^i is the elevation of satellite i [degree] with respect to the reference antenna. Note that the elevation-dependent weight w^i should not be confused with the *w*-test-statistic.

Fig. 1 depicts the satellite-specific part as function of the elevation of an individual satellite. The graphs have been presented for different values of $\bar{w}$ reflecting the overall configuration of the satellites with respect to the array ($0.4 \leq \bar{w} \leq 0.8$). This has been done for two cases, the case where the number of satellites is $s = 3$ (left-panel) and the other one with $s = 5$ (right-panel). As shown, the size of the MDB of an outlier, occurred in a single observation of satellites of *low elevation* (e.g. $10^\circ \leq \varepsilon^i \leq 20^\circ$), is governed by the elevation of the corresponding satellite only, irrespective of the number/configuation of the satellites. In case of satellites of a higher elevation, the scenario would change as the number of satellites starts taking an active role as well. Considering a limited number of common satellites, it is interestingly observed that the MDB does not *generally* decrease as the elevation of the corresponding satellite increases (see the red thick line in Fig. 1, left-panel). In this case, in addition to the satellite elevation, the overall satellite configuration would also contribute to the size of the MDB. The stated contribution does however get insignificant once the number of satellite increases (see Fig. 1, right-panel). In the situations where the number of satellites is large enough (e.g. more than 5), one can therefore simply consider the elevation of each satellite *individually* to analyze the corresponding outlier MDB.

Frequency-specific part $[\sigma_{p_j}^2/(1-(\sigma_{\hat{p}_j}/\sigma_{p_j})^2)]^{\frac{1}{2}}$: In addition to the variance of an individual pseudo-range observable-type $\sigma_{p_j}^2$, this term is also dependent on the variance of the *adjusted* observable-type denoted by $\sigma_{\hat{p}_j}^2$. This quantity in turn is a function of the a-priori atmospheric variances, the quality of the other pseudo-range observable-types through Q_p and the ionospheric vector μ.

Fig. 2 shows the frequency-specific part as function of the inter-station distance for the three GNSSs GPS, Galileo and BeiDou. In order to link the inter-station distance to the ionospheric variance σ_ι^2, use has been made of that given in

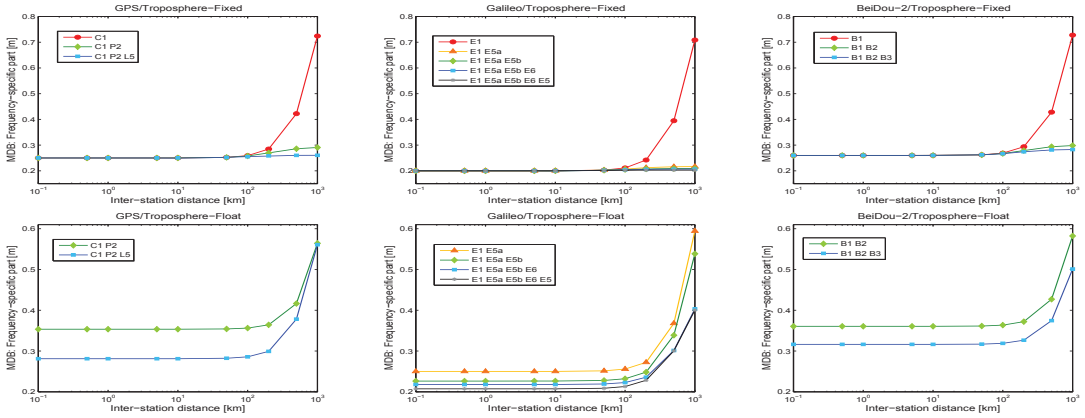

Fig. 2 Frequency-specific part of the code-outlier MDBs [m] as function of the inter-station distance [km] for three GNSSs GPS (right), Galileo (middle), and BeiDou (left): *troposphere-fixed scenario (top-panel), troposphere-float scenario (bottom-panel)*

Schaffrin and Bock (1988). The graphs have been plotted for the troposphere-fixed case $\sigma_\tau^2 = 0$ (top-panel) as well as the troposphere-float case $\sigma_\tau^2 \to \infty$ (bottom-panel). As shown, the frequency-specific part behaves almost unchanged up to a certain inter-station distance (in this study around 100 [km]). In contrast to the single-frequency data (red dots), the MDB associated with the multi-frequency data does not significantly change as the inter-station distance increases (troposphere-fixed case). Because of the dispersive nature of the ionospheric effects (i.e. dependency on the frequencies), the *GNSS-based* misclosures would, in addition to the atmosphere-aided ones, also contribute to the *w*-test-statistic, whereas they do vanish in case of single-frequency data (cf.-(3)). It is also important to note that there is no redundancy in the single-frequency troposphere-float scenario, thus giving rise to infinite MDBs. The single-frequency case is therefore excluded from the graphs of the bottom-panel. We remark, due to a generally better precision of the Galileo's signals, that the associated results illustrate a superior performance to those of GPS and BeiDou. The pseudo-range zenith-referenced standard deviation is taken as 25 [cm] for GPS/BeiDou, and as 20 [cm] for Galileo .

Similar to the satellite-specific part, as the model gets stronger (i.e. $\sigma_{\hat{p}_j}^2 \approx 0$), one can only consider the quality of that individual observable-type on frequency j (i.e. $\sigma_{p_j}^2$). As an example, for an array of 4 antennas with the probability of false alarm $\alpha = 0.01$, the code-outlier MDB is about 79 [cm] ($\gamma = 0.8$) and 89 [cm] ($\gamma = 0.9$). In case of phase-slip MDB of two successive epochs, the MDB is about 3.9 [mm] ($\gamma = 0.8$) and 4.4 [mm] ($\gamma = 0.9$). The zenith-referenced standard deviations of the pseudo-range and carrier-phase observables are, respectively, set to $\sigma_{p_j} = 20$ [cm] and $\sigma_{\phi_j} = 1$ [mm].

MDB reduction-factor: from the STD-based model to the ZTD-based model

As stated so far, the MDB given in (17) refers to the STD-based model. One can now ask to what extent the MDB decreases by mapping the STDs to their ZTDs. Following the same procedure as before, the MDB of the ZTD-based model can be formulated that reveals the gain in terms of the reduction of the MDB. Although in addition to the number of frequencies/satellites, the stated reduction-factor does also depend on the tropospheric mapping functions g and the elevation-dependent weight matrix W_s (see Fig. 3), one can however present a *rule-of-thumb* expression as its rough value, namely (ionosphere-fixed scenario)

$$\begin{aligned} &\textit{Before ambiguity-fixing} \\ &\frac{||vec[\nabla]||_{STD}}{||vec[\nabla]||_{ZTD}} \approx [1 + \tfrac{1}{f-1}(\tfrac{s-2}{s-1})]^{\frac{1}{2}} \\ &\textit{After ambiguity-fixing} \\ &\frac{||vec[\nabla]||_{STD}}{||vec[\nabla]||_{ZTD}} \approx 1 \end{aligned} \tag{19}$$

According to the above equations, before fixing ambiguities the reduction-factor is mostly governed by the number of

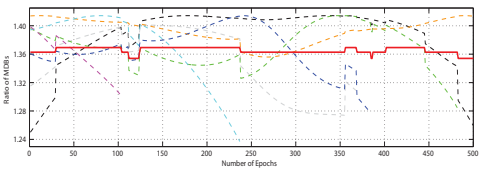

Fig. 3 Reduction-factors (ambiguity-float) of the code-outlier MDB (dashed lines) due to mapping the slant tropospheric delays (STDs) to their zenith counterparts (ZTDs) compared to the *rule-of-thumb* formula (red thick line) over time (a GPS data-set). Different colors have been used for different satellites.

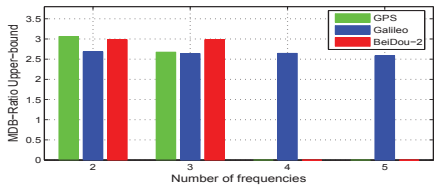

Fig. 4 Upper bounds of the reduction-factor of the ionospheric MDB due to excluding zenith tropospheric delays (ZTDs) from the underlying model for three GNSSs GPS (green bars), Galileo (blue bars), and BeiDou (red bars)

frequencies f but not too much by the number satellites s. As the number frequency increases, the gain in terms of MDB reduction gets less. After fixing ambiguities, the reduction-factor becomes almost 1 meaning that the code-outlier MDB remains almost unchanged by even strengthening the model through mapping the tropospheric delays to their ZTDs.

3.3 Atmospheric detectors and their MDBs

In most applications dealing with the small-scale arrays, one needs to check as to whether there are significant dispersive/nondispersive effects or not. Taking the atmosphere-fixed scenario as the null hypothesis, the atmospheric detectors are defined as

$$\begin{aligned} &\textit{tropospheric-detector: } C_f \mapsto e_f, C_s \mapsto g, \quad C_n \mapsto D_n \\ &\textit{ionospheric-detector: } \quad C_f \mapsto \mu, \; C_s \mapsto D_s, C_n \mapsto D_n \end{aligned} \tag{20}$$

Despite the complexity of the atmospheric MDBs, we can evaluate them in a *relative* sense. For instance, one can analyze the reduction of the ionospheric MDB when the differential ZTDs are assumed to be a-priori known via the following bounds (codeless data)

$$1 \leq \frac{||vec[\nabla]||_\tau}{||vec[\nabla]||} \leq [1+\frac{\bar{\mu}^2}{\sigma_\mu^2}]^{\frac{1}{2}} \tag{21}$$

with $\bar{\mu} = (1/f)\sum_{j=1}^{f}\mu_j$ and $\sigma_\mu^2 = (1/f)\sum_{j=1}^{f}(\mu_j - \bar{\mu})^2$. The ionospheric MDBs with and without ZTDs are denoted by $||vec[\nabla]||_\tau$ and $||vec[\nabla]||$, respectively.

According to (21), the detectability of the differential ionosphere can get better at most $[1+(\bar{\mu}/\sigma_\mu)^2]^{\frac{1}{2}}$ times, if one excludes the differential ZTDs from the model. For the current systems, the stated value is around 3 (cf. Fig. 4).

4 Concluding remarks

In this contribution, the UMPI test-statistics as well as their MDBs, associated with the array model, were studied. With the aid of the GNSS decoupled misclosures, a few important examples such as the array-detector, w-test-statistic and the ionospheric-detector were discussed. In particular, we showed that as the model gets stronger, one can simply, in case of outlier's MDB, analyze the single-channel/frequency scenario instead.

Acknowledgements P.J.G. Teunissen is the recipient of an Australian Research Council Federation Fellowship (project number FF0883188).

Appendix

Proof of (3) The model's misclosures, forming the condition equations, can be formulated through pre-multiplying the corresponding observation vector by an orthogonal complement basis matrix of the design matrix (Teunissen, 2000). In case of the single-epoch ambiguity-float scenario, the carrier-phase observations are all reserved to determine the DD ambiguities, thus leaving the code observations to contribute to the redundancy of the model. Given the observations equations (1), the code-only design matrix A, together with its orthogonal complement basis matrix B, can therefore be expressed as (per baseline)

$$\begin{aligned} &A \mapsto [\, e_f \otimes D_s^T g \;,\; \mu \otimes I_{s-1}\,] \Rightarrow \\ &\qquad B^T \mapsto \begin{bmatrix} (D_f^T\mu)^{\perp T} D_f^T \otimes c_{d|\tau}^2 g^T D_s (D_s^T W_s^{-1} D_s)^{-1} \\ \mu^{\perp T} \otimes (D_s^T g)^{\perp T} \end{bmatrix} \end{aligned} \tag{22}$$

from which (3) follows. That the misclosures M_1 and M_2 are mutually uncorrelated follows from the identities $D_s^T\bar{g} = D_s^T g$, and $(D_s^T g)^{\perp T} D_s^T g = 0$. □

Proof of Theorem 1 Equation (6) is indeed another expression of the UMPI test-statistic T_q presented in Teunissen (2000). In terms of the model's misclosures M, T_q and its MDB-squared $||\nabla||^2$ read

$$T_q = \frac{1}{q} M^T Q_{MM}^{-1} P_{C_M} M \tag{23}$$

$$||\nabla||^2 = \frac{v_{q,\alpha,\gamma}}{d_Y^T C_M^T Q_{MM}^{-1} C_M d_Y} \tag{24}$$

To complete the proof, we thus need to show

$$\begin{aligned} &tr(Q_{MM}^{-1} P_{C_M} M M^T) = M^T Q_{MM}^{-1} P_{C_M} M, \\ &tr(P_{C_M}) = q \end{aligned} \tag{25}$$

The first expression follows from the trace-property $tr(UV) = tr(VU)$ for any matrices U and V of an appropriate size, and the fact that the trace of a scalar is equal to the scalar itself. The second expression follows from the equality between the trace of a projector and its rank, that is

$$tr(P_{C_M}) = rank(P_{C_M}) = q, \tag{26}$$

since $rank(C_M) = q$. □

Proof of (12) In case of the atmosphere-fixed scenario, no differential atmospheric delays are to be estimated, i.e. $\mu =$

0 and $g = 0$. This yields $\mu^{\perp} = I_f$ and $(D_s^T g)^{\perp} = I_{s-1}$. According to (3), the frequency-difference misclosures M_1 vanishes, and the vectorized version of the atmosphere-free misclosures M_2 takes the following form

$$M_{\tilde{p}} = [D_n^T \otimes I_f \otimes D_s^T] vec[\tilde{P}] \tag{27}$$

with the variance matrix (cf. (2))

$$Q_{M_{\tilde{p}} M_{\tilde{p}}} = D_n^T D_n \otimes Q_p \otimes D_s^T W_s^{-1} D_s \tag{28}$$

Upon choosing the array-detector structure (11), matrix C_M of $M_{\tilde{p}}$, introduced in Theorem 1, reads then

$$C_{M_{\tilde{p}}} = D_n^T D_n \otimes I_f \otimes D_s^T D_s \tag{29}$$

Similar expressions are formulated for the carrier-phase observations $\tilde{\Phi}$, in case the ambiguities are fixed to their integers. The structures of $M_{\tilde{\phi}}$, $Q_{M_{\tilde{\phi}} M_{\tilde{\phi}}}$ and $C_{M_{\tilde{p}}}$ are thus identical to those of $\tilde{P}$. Substituting $M = [M_{\tilde{p}}^T, M_{\tilde{\phi}}^T]^T$,

$$Q_{MM} = \begin{bmatrix} Q_{M_{\tilde{p}} M_{\tilde{p}}} & 0 \\ 0 & Q_{M_{\tilde{\phi}} M_{\tilde{\phi}}} \end{bmatrix}, \quad C_M = \begin{bmatrix} C_{M_{\tilde{p}}} & 0 \\ 0 & C_{M_{\tilde{\phi}}} \end{bmatrix}, \tag{30}$$

an application of Theorem 1 gives (cf. (6))

$$T_q = \frac{tr\{Q^{-1}_{M_{\tilde{p}} M_{\tilde{p}}} P_{C_{M_{\tilde{p}}}} M_{\tilde{p}} M_{\tilde{p}}^T\} + tr\{Q^{-1}_{M_{\tilde{\phi}} M_{\tilde{\phi}}} P_{C_{M_{\tilde{\phi}}}} M_{\tilde{\phi}} M_{\tilde{\phi}}^T\}}{tr\{P_{C_{M_{\tilde{p}}}}\} + tr\{P_{C_{M_{\tilde{\phi}}}}\}} \tag{31}$$

The proof follows then from

$$P_{C_{M_{\tilde{\phi}}}} = P_{C_{M_{\tilde{p}}}} = I_{n-1} \otimes I_f \otimes I_{s-1}, \tag{32}$$

and

$$\begin{aligned} tr\{Q^{-1}_{M_{\tilde{p}} M_{\tilde{p}}} M_{\tilde{p}} M_{\tilde{p}}^T\} &= tr\{[Q_p^{-1} \otimes W_s P_{e_s}^{\perp}]\, \tilde{P} P_{D_n} \tilde{P}^T\}, \\ tr\{Q^{-1}_{M_{\tilde{\phi}} M_{\tilde{\phi}}} M_{\tilde{\phi}} M_{\tilde{\phi}}^T\} &= tr\{[Q_{\phi}^{-1} \otimes W_s P_{e_s}^{\perp}]\, \tilde{\Phi} P_{D_n} \tilde{\Phi}^T\} \end{aligned} \tag{33}$$

with the projectors $P_{e_s}^{\perp} = W_s^{-1} D_s (D_s^T W_s^{-1} D_s)^{-1} D_s^T$, and $P_{D_n} = D_n (D_n^T D_n)^{-1} D_n^T$.

The proof of (14), (17), (19) and (21) goes along the same lines as the proof of (12). □

References

Arnold SF (1981) The theory of linear models and multivariate analysis, vol 2. Wiley New York

Baarda W (1968) A testing procedure for use in geodetic networks. Tech. rep., Netherlands Geodetic Commission, Publ. on Geodesy, New Series, Vol. 2(5), Delft

Euler HJ, Goad CC (1991) On optimal filtering of GPS dual frequency observations without using orbit information. J Geod 65(2):130–143

Giorgi G, Henkel P, Gunther C (2012) Testing of a statistical approach for local ionospheric disturbances detection. In: Position Location and Navigation Symp (PLANS), 2012, IEEE, pp 167–173

de Jonge PJ (1998) A processing strategy for the application of the GPS in networks. PhD thesis, Delft University of Technology, Publication on Geodesy, 46, Netherlands Geodetic Commission, Delft

Khanafseh S, Pullen S, Warburton J (2012) Carrier phase ionospheric gradient ground monitor for GBAS with experimental validation. Navigation 59(1):51–60

Odijk D, Teunissen PJG, Khodabandeh A (2014) Single-Frequency PPP-RTK: Theory and Experimental Results. IAG Symp 139:167–173

Schaffrin B, Bock Y (1988) A unified scheme for processing GPS dual-band phase observations. Bulletin Geodesique 62(2):142–160

Teunissen PJG (1997) GPS double difference statistics: with and without using satellite geometry. J Geod 71(3):137–148

Teunissen PJG (1998) Minimal detectable biases of GPS data. J Geod 72(4):236–244

Teunissen PJG (2000) Testing theory: an introduction. Delft University Press, series on Mathematical Geodesy and Positioning

Teunissen PJG (2010) Integer least-squares theory for the GNSS compass. J Geod 84(7):433–447

Teunissen PJG (2012) A-PPP: Array-Aided Precise Point Positioning with Global Navigation Satellite Systems. Signal Processing, IEEE Transactions on 60(6):2870–2881

Teunissen PJG, de Bakker PF (2012) Single-receiver single-channel multi-frequency GNSS integrity: outliers, slips, and ionospheric disturbances. J Geod 87(2):161–177

11 A recursive MMSE filter (Part 1: Basic Concepts and Principles)

This chapter is covered by the following publication:

Teunissen P.J.G. and **Khodabandeh A.** (2013) BLUE, BLUP and the Kalman filter: some new results. Journal of Geodesy, 87(5):461–473

J Geod (2013) 87:461–473
DOI 10.1007/s00190-013-0623-6

ORIGINAL ARTICLE

BLUE, BLUP and the Kalman filter: some new results

P. J. G. Teunissen · A. Khodabandeh

Received: 26 October 2012 / Accepted: 2 February 2013 / Published online: 23 February 2013

Abstract In this contribution, we extend 'Kalman-filter' theory by introducing a new BLUE–BLUP recursion of the partitioned measurement and dynamic models. Instead of working with known state-vector means, we relax the model and assume these means to be unknown. The recursive BLUP is derived from first principles, in which a prominent role is played by the model's misclosures. As a consequence of the mean state-vector relaxing assumption, the recursion does away with the usual need of having to specify the initial state-vector variance matrix. Next to the recursive BLUP, we introduce, for the same model, the recursive BLUE. This extension is another consequence of assuming the state-vector means unknown. In the standard Kalman filter set-up with known state-vector means, such difference between estimation and prediction does not occur. It is shown how the two intertwined recursions can be combined into one general BLUE–BLUP recursion, the outputs of which produce for every epoch, in parallel, the BLUP for the random state-vector and the BLUE for the mean of the state-vector.

Keywords Best linear unbiased estimation (BLUE) · Best linear unbiased prediction (BLUP) · Minimum mean squared error (MMSE) · Misclosures · Kalman filter · BLUE–BLUP recursion

P. J. G. Teunissen · A. Khodabandeh (✉)
Department of Spatial Sciences, GNSS Research Centre,
Curtin University of Technology, Perth, Australia
e-mail: amir.khodabandeh@curtin.edu.au

P. J. G. Teunissen
Department of Geoscience and Remote Sensing,
Delft University of Technology, Delft, The Netherlands
e-mail: p.teunissen@curtin.edu.au

1 Introduction

To determine best estimators or best predictors, the minimum mean squared error (MMSE) criterion is often used. Different MMSE predictors exist however. They depend on the class of functions for which the MMSE principle is applied. Examples of different MMSE predictors are the conditional mean as best predictor (BP), the best linear predictor (BLP), the best integer equivariant predictor (BIEP), or the best linear unbiased predictor (BLUP), see e.g. Goldberger (1962), Anderson and Moore (1979), Stark and Woods (1986), Sanso (1986), Simon (2006), Teunissen (2007). Although the same principle is applied, these MMSE predictors all have different performances.

In the literature, the Kalman filter is derived as either a BP or a BLP, see e.g. Kalman (1960), Gelb (1974), Kailath (1981), Candy (1986), Brammer and Siffling (1989), Jazwinski (1991), Gibbs (2011). Both these predictors, BP and BLP, require the mean of the to-be-predicted random vector to be known. This is why in the derivation of the Kalman filter one usually assumes the mean of the random initial state-vector to be known, see for instance the contributions by Sorenson (1966, p. 222), Maybeck (1979, p. 204), Anderson and Moore (1979, p. 15), Stark and Woods (1986, p. 393), Bar-Shalom and Li (1993, p. 209), Kailath et al. (2000, p. 311), Simon (2006, p. 125), and Grewal and Andrews (2008, p. 138).

Despite the BLP approach, it is indeed sometimes acknowledged that the mean of the initial state-vector is not known. The approach then taken is to treat the initial state-vector as being *diffuse*, meaning that its variance matrix tends to infinity, see e.g. Harvey and Phillips (1979), Ansley and Kohn (1985), de Jong (1991). The proposed approach in practice is then to initialize the Kalman filter with a sufficiently 'large' variance matrix. With such an approach,

however, the Kalman filter is still derived and presented within the BLP context.

We believe that the BLP derivation of the Kalman filter is not appropriate in case the mean of the random state-vector is unknown, a situation that applies to many, perhaps even most, engineering applications. Not the BLP principle, but the BLUP principle should be applied in case the mean state-vectors are unknown. In this contribution, we derive and present the recursive BLUP from first principles and show how such an approach does away with the need to assume the mean and variance matrix of the initial state-vector to be known.

Next to the recursive BLUP, we also present, for the same model, the recursive best linear unbiased estimator (BLUE). To appreciate the difference with the recursive BLUP, it is important to make a sharp distinction between prediction and estimation. We speak of prediction if observables are used to guess the outcome of a random vector and we speak of estimation if the observables are used to guess the value of an unknown nonrandom vector.

Our development of the BLUE–BLUP recursion is an extention of standard 'Kalman filter' theory. This extension is a consequence of our relaxing assumptions that the means of the random state-vectors are unknown. Since these means are assumed unknown, the problem of estimation can be addressed as well. In the standard Kalman filter set-up with known state-vector means, this difference between estimation and prediction does not occur since one is then only left with BLP instead of with BLUP of the state-vectors.

This contribution is organized as follows. In Sect. 2, we briefly review the necessary ingredients of prediction and estimation for linear models. Essential in our presentation is the role given to the misclosures of the linear model. We treat prediction and estimation on an equal footing and show how predictors and estimators are driven by the way misclosures are mapped. We also show how the BLUE and BLUP can be decomposed into misclosures and any LUE or LUP. This decomposition forms the basis for our development of the BLUE–BLUP recursion in later sections.

In Sect. 3, we present the general BLUE–BLUP measurement update equations for a time series of vectorial observables. Through a one-to-one mapping, it is shown how the sequential prediction errors of the misclosures form the basis of the predicted residuals. No assumptions are here yet made on the structure of the variance–covariance matrices.

In Sect. 4, we develop the BLUP recursion for the partitioned measurement and dynamic models that form the basis of the standard Kalman filter. Instead of the standard assumption of known mean state-vectors, we assume the means of the random state-vectors to be unknown. Through this relaxation the initialization issue gets resolved, whereby it is shown that the variance matrix of the initial state-vector is not needed anymore. In Sect. 5, we extend standard 'Kalman-filter' theory further by introducing, next to the BLUP recursion, the BLUE recursion of the means of the random state-vectors. It is shown how the two recursions are intertwined and how their difference is driven by the presence of system noise. Finally, we show how the two recursions can be combined into one general BLUE–BLUP recursion. It outputs for every epoch, in parallel, the BLUP for the random state-vector and the BLUE for the mean of this state-vector.

We make use of the following notation: we use the underscore to denote a random vector. Thus $\underline{x}$ is random, while x is not. $\mathsf{E}(\cdot)$ and $\mathsf{D}(\cdot)$ denote the expectation and dispersion operator, while $\mathsf{C}(\cdot,\cdot)$ denotes the covariance operator. The norm of a vector is denoted as $||\cdot||$. Thus $||\cdot||^2 = (\cdot)^T(\cdot)$.

2 Estimation and prediction in linear models

2.1 Estimation and prediction

As our point of departure, we take the following linear model of observation equations

$$\underline{y} = Ax + \underline{e} \tag{1}$$

with mean and dispersion

$$\mathsf{E}(\underline{e}) = 0\ ,\ \mathsf{D}(\underline{y}) = \mathsf{D}(\underline{e}) = Q_{yy}$$

where $\underline{y} \in \mathbb{R}^m$ is the random vector of observables and $x \in \mathbb{R}^n$ is the nonrandom vector of unknown parameters. The known matrix A, of order $m \times n$, is assumed to be of full column rank, and the variance matrix Q_{yy} is assumed to be positive definite.

The aims are to *estimate* a linear function of x, or, to *predict* the outcome of a random vector having a mean that is a linear function of x. The to-be-estimated linear function is given as

$$\bar{z} = A_z x, \tag{2}$$

with known $k \times n$ matrix A_z. The to-be-predicted random vector is given as

$$\underline{z} = A_z x + \underline{e}_z, \quad \text{with} \quad \mathsf{E}(\underline{e}_z) = 0 \tag{3}$$

This random vector is assumed to be stochastically related to $\underline{y}$. Their joint variance matrix is assumed given as

$$\mathsf{D}\left(\begin{bmatrix}\underline{y}\\ \underline{z}\end{bmatrix}\right) = \begin{bmatrix} Q_{yy} & Q_{yz} \\ Q_{zy} & Q_{zz}\end{bmatrix} \tag{4}$$

For our further development, the following canonical form of the linear model (1) is very helpful.

Lemma 1 (Linear model in canonical form) *Define the transformed vector of observables as* $[\underline{\hat{x}}^T, \underline{u}^T]^T = T\underline{y}$, *with transformation matrix* $T = [A^{+T}, B]^T$, *least-squares*

inverse $A^+ = (A^T Q_{yy}^{-1} A)^{-1} A^T Q_{yy}^{-1}$ *and where* B *is a basis matrix of the null space of* A^T*, i.e.* $A^T B = 0$*. Then*

$$\mathsf{E}\left(\begin{bmatrix}\underline{\hat{x}}\\ \underline{u}\end{bmatrix}\right) = \begin{bmatrix}I_n\\ 0\end{bmatrix} x, \quad \mathsf{D}\left(\begin{bmatrix}\underline{\hat{x}}\\ \underline{u}\end{bmatrix}\right) = \begin{bmatrix}Q_{\hat{x}\hat{x}} & 0\\ 0 & Q_{uu}\end{bmatrix} \tag{5}$$

Proof The mean and dispersion of (5) follow from an application of the mean and variance propagation laws to $T\underline{y}$. That the linear model (5) stands in a one-to-one relation with the original linear model formulation (1) follows from the invertibility of $T = [A^{+T}, B]^T \Leftrightarrow T^{-1} = [A, B^{+T}]$, with least-squares inverse $B^+ = (B^T Q_{yy} B)^{-1} B^T Q_{yy}$. □

With the above canonical form, the design matrix has the simple form $[I_n, 0]^T$, while the dispersion has become block diagonal. As $\underline{\hat{x}}$ and $\underline{u}$ stand in one-to-one correspondence with $\underline{y}$, while $\underline{\hat{x}}$ has the unity-matrix as design matrix and itself is uncorrelated with the zero-mean vector $\underline{u}$, one may expect that $\underline{\hat{x}}$ contains the full information for the determination of x. And indeed, $\underline{\hat{x}} = A^+\underline{y} \in \mathbb{R}^n$ is recognized as the BLUE of x, while $\underline{u} = B^T\underline{y} \in \mathbb{R}^{m-n}$ is recognized as the vector of *misclosures* (Teunissen 2000). The dimension of the vector of misclosures is equal to the redundancy, $r = m - n$, i.e. the vector of misclosures only exists in the presence of redundancy ($r > 0$). Note that the vector of misclosures is not unique, since for any invertible matrix L, the vector $\underline{v} = L\underline{u}$ is again a vector of misclosures, i.e. both B and BL^T are basis matrices of the null space of A^T.

The advantage of the decomposition $\underline{y} = T^{-1}[\underline{\hat{x}}^T, \underline{u}^T]^T$ is that it enables finding simple representations of estimators and predictors. The following lemma gives such representation for linear unbiased estimators/predictors of $\bar{z}$ and $\underline{z}$, respectively.

Lemma 2 (Linear unbiased estimation/prediction) *A linear function* $F\underline{y} + f_0$*, satisfying the condition* $\mathsf{E}(F\underline{y} + f_0) = A_z x$ *for all* x*, is called a linear unbiased estimator (LUE) of* $\bar{z} = A_z x$*, or a linear unbiased predictor (LUP) of* $\underline{z} = \bar{z} + \underline{e}_z$*. Any such LUE or LUP can be represented as*

$$\text{LUE/LUP} = A_z\underline{\hat{x}} + J\underline{u}, \text{ for some } J \in \mathbb{R}^{k\times r} \tag{6}$$

Proof With $\mathsf{E}(\underline{y}) = Ax$, the unbiasedness condition $\mathsf{E}(F\underline{y} + f_0) = A_z x, \forall x \in \mathbb{R}^n$, is fulfilled by setting $f_0 = 0$ and $FA = A_z$. Given the matrix equation $FA = A_z$, the general solution for F is given by the sum of a particular solution and the homogeneous solution. A particular solution is given by $A_z A^+$, while the homogeneous solution is provided by JB^T, for some matrix $J \in \mathbb{R}^{k\times r}$. Therefore, $F = A_z A^+ + JB^T$. Equation (6) follows then by substituting the result into $\text{LUE} = F\underline{y}$. □

The above representation shows that LUEs and LUPs differ only through their linear functions of the misclosure vector $\underline{u}$. Hence, it is through the choice of matrix J that specific LUEs and LUPs can be identified.

2.2 MMSE estimation/prediction and misclosures

To determine best estimators/predictors, the minimum mean squared error (MMSE) criterion is used. In case no restrictions are placed on the class of predictors, the best predictor of $\underline{z}$ in the MMSE sense is given by the conditional mean,

$$\text{BP} = \mathsf{E}(\underline{z}|\underline{y}) \tag{7}$$

[see e.g. Anderson and Moore (1979); Maybeck (1979); Teunissen et al. (2005)]. The BP is unbiased, but generally nonlinear, with exemptions, for instance in the Gaussian case. In case $\underline{y}$ and $\underline{z}$ are jointly Gaussian, the BP becomes linear and identical to the best linear predictor,

$$\text{BLP} = \bar{z} + Q_{zy} Q_{yy}^{-1}(\underline{y} - \bar{y}) \tag{8}$$

where $\bar{y}$ and $\bar{z}$ denote the mean of $\underline{y}$ and $\underline{z}$, respectively [see e.g. Bar-Shalom and Li (1993); Kailath et al. (2000); Teunissen (2008)]. Although the BLP is linear, it still requires knowledge of the means $\bar{y}$ and $\bar{z}$. These means are however unknown, since x is assumed unknown in case of the linear model (1). Instead of working within the unconstrained class of linear functions, we therefore work in the more restricted class as specified by the representation (6). To determine the best estimator/predictor within this class, use is made of the following lemma.

Lemma 3 (Minimum mean squared norm) *Let* $\underline{\varepsilon} \in \mathbb{R}^k$ *and* $\underline{u} \in \mathbb{R}^r$ *be given random vectors, with* $\mathsf{E}(\underline{u}) = 0$*. Then,*

$$\underline{\hat{\varepsilon}} = \underline{\varepsilon} - Q_{\varepsilon u} Q_{uu}^{-1}\underline{u} \tag{9}$$

has smallest mean squared norm within the class of random vectors $\underline{\varepsilon}_J = \underline{\varepsilon} + J\underline{u}$*,* $J \in \mathbb{R}^{k\times r}$*, i.e.*

$$\mathsf{E}||\underline{\hat{\varepsilon}}||^2 \le \mathsf{E}||\underline{\varepsilon}_J||^2 \ , \ \forall J \in \mathbb{R}^{k\times r} \tag{10}$$

Proof Since $\underline{\hat{\varepsilon}} = \underline{\varepsilon} - Q_{\varepsilon u} Q_{uu}^{-1}\underline{u}$ is uncorrelated with $\underline{u}$, we have the 'sum-of-squares' decomposition

$$\begin{aligned}\mathsf{E}||\underline{\varepsilon} + J\underline{u}||^2 &= \mathsf{E}||\underline{\varepsilon} - Q_{\varepsilon u} Q_{uu}^{-1}\underline{u} + (J + Q_{\varepsilon u} Q_{uu}^{-1})\underline{u}||^2\\ &= \mathsf{E}||\underline{\hat{\varepsilon}}||^2 + \mathsf{E}||(J + Q_{\varepsilon u} Q_{uu}^{-1})\underline{u}||^2\end{aligned}$$

from which (10) follows. □

This lemma shows that the mean squared norm of a random vector cannot be made smaller by adding uncorrelated linear functions of zero mean random vectors. We now use this lemma to determine the best estimator and the best predictor within the class of LUEs and LUPs, respectively.

Theorem 1 (BLUE/BLUP) *For any LUE of* $\bar{z}$*, with estimation error* $\underline{\varepsilon}_{\text{LUE}} = \bar{z} - \text{LUE}$*, and any LUP of* $\underline{z}$*, with prediction error* $\underline{\varepsilon}_{\text{LUP}} = \underline{z} - \text{LUP}$*, the BLUE and BLUP can be computed as*

$$\begin{bmatrix}\text{BLUE}\\ \text{BLUP}\end{bmatrix} = \begin{bmatrix}\text{LUE}\\ \text{LUP}\end{bmatrix} + Q_{\varepsilon u} Q_{uu}^{-1}\underline{u} \ , \ \underline{\varepsilon} = \begin{bmatrix}\underline{\varepsilon}_{LUE}\\ \underline{\varepsilon}_{LUP}\end{bmatrix} \tag{11}$$

Proof Consider a certain fixed LUP. Since the BLUP is a LUP, it follows from Lemma 2 that the BLUP can be written as BLUP = LUP + Ju for some J. Hence, their prediction errors, $\varepsilon_{\text{BLUP}} = \underline{z} - \text{BLUP}$ and $\varepsilon_{\text{LUP}} = \underline{z} - \text{LUP}$, are related as $\underline{\varepsilon}_{\text{BLUP}} = \underline{\varepsilon}_{\text{LUP}} - J\underline{u}$. According to Lemma 3 (cf. 9), J must be chosen as $J = Q_{\varepsilon_{\text{LUP}},u} Q_{uu}^{-1}$ for $\mathsf{E}||\underline{\varepsilon}_{\text{BLUP}}||^2$ to be minimal. This proves the BLUP-part of (11). The proof of the BLUE part goes likewise. □

This result clearly shows the important role that is played by the vector of misclosures $\underline{u}$, both in best estimating $\bar{z}$ and in best predicting $\underline{z}$. In Sect. 5, we present the recursive counterpart of the above BLUE–BLUP expression.

The relations between the error covariance matrices are readily obtained from (11) through an application of the (co)variance propagation law. They are summarized in the following corollary.

Corollary 1 (Error covariance matrices) *The error covariance matrices of estimation and prediction satisfy:*

$$\begin{aligned} \mathsf{C}(\underline{\varepsilon}_{\text{BLUE}}, \underline{\varepsilon}_{\text{BLUP}}) &= \mathsf{C}(\underline{\varepsilon}_{\text{LUE}}, \underline{\varepsilon}_{\text{LUP}}) - Q_{\varepsilon_{\text{LUE}}u} Q_{uu}^{-1} Q_{u\varepsilon_{\text{LUP}}} \\ \mathsf{C}(\underline{\varepsilon}_{\text{BLUE}}, \underline{\varepsilon}_{\text{BLUP}}) &= \mathsf{C}(\underline{\varepsilon}_{\text{BLUE}}, \underline{\varepsilon}_{\text{LUP}}) = \mathsf{C}(\underline{\varepsilon}_{\text{LUE}}, \underline{\varepsilon}_{\text{BLUP}}) \\ \mathsf{C}(\underline{\varepsilon}_{\text{BLUE}}, \underline{u}) &= \mathsf{C}(\underline{\varepsilon}_{\text{BLUP}}, \underline{u}) = 0 \end{aligned} \tag{12}$$

This result shows that the misclosures are uncorrelated with both the best estimation errors and the best prediction errors.

2.3 From LUE to BLUE

As a direct consequence of the above theorem we have the following simple relationship between the BLUE and any LUE.

Corollary 2 (BLUE–LUE formula) *The BLUE and its variance matrix are related to that of any arbitrary LUE as*

$$\begin{aligned} \text{BLUE} &= \text{LUE} - Q_{\text{LUE},u} Q_{uu}^{-1} \underline{u} \\ Q_{\text{BLUE, BLUE}} &= Q_{\text{LUE, LUE}} - Q_{\text{LUE},u} Q_{uu}^{-1} Q_{u,\text{LUE}} \end{aligned} \tag{13}$$

Proof Since $\bar{z}$ is nonrandom, it follows from $\underline{\varepsilon}_{\text{LUE}} = \bar{z} - \text{LUE}$ that $\mathsf{C}(\underline{\varepsilon}_{\text{LUE}}, \underline{u}) = -\mathsf{C}(\text{LUE}, \underline{u})$. Substitution into (11) proves the first equation of (13). The second equation follows from an application of the variance propagation law, thereby making use of the fact that the misclosures are not correlated with the estimation error $\underline{\varepsilon}_{\text{BLUE}}$ (cf. 12) and thus also not with the BLUE itself, $\mathsf{C}(\text{BLUE}, \underline{u}) = 0$. □

This simple BLUE–LUE relation will be very useful in our later derivations of the recursive BLUE and the recursive BLUP. Here, three examples are given to see the BLUE–LUE relation at work.

Example 1 (Least-squares as LUE) The least-squares estimator $\text{LSE} = (A^T W A)^{-1} A^T W \underline{y}$ is a LUE of x. Hence, according to (13) the BLUE of $\hat{x}$ can be expressed in the LSE as

$$\text{BLUE} = \text{LSE} - Q_{\text{LSE},u} Q_{uu}^{-1} \underline{u} \tag{14}$$

which is identical to the LSE with $W = Q_{yy}^{-1}$.

Example 2 (Conditional adjustment) Consider the model of condition equations

$$B^T \mathsf{E}(\underline{y}) = 0 \tag{15}$$

It is the implicit formulation of the parametric model of observation equations $\mathsf{E}(\underline{y}) = Ax$. Since $\underline{y}$ is a LUE of $\mathsf{E}(\underline{y})$, the BLUE of $\mathsf{E}(\underline{y})$ can be written according to the BLUE–LUE formula (13) as $\underline{\hat{y}} = \underline{y} - Q_{yu} Q_{uu}^{-1} \underline{u}$. Substitution of $\underline{u} = B^T \underline{y}$ gives

$$\underline{\hat{y}} = \underline{y} - Q_{yy} B (B^T Q_{yy} B)^{-1} B^T \underline{y} \tag{16}$$

which is the BLUE of $\mathsf{E}(\underline{y})$ expressed in the design matrix B of the conditional model.

Example 3 (Tienstra's phased adjustment) Consider the partitioned model of condition equations

$$\begin{bmatrix} B_{[i-1]}^T \\ B_i^T \end{bmatrix} \mathsf{E}(\underline{y}) = \begin{bmatrix} 0 \\ 0 \end{bmatrix} \tag{17}$$

with the corresponding partitioned misclosure vector $\underline{u}_{[i]} = [\underline{u}_{[i-1]}^T,\ \underline{u}_i^T]^T$. Then, the BLUE of $\mathsf{E}(\underline{y})$ based on the first set of conditions $B_{[i-1]}^T \mathsf{E}(\underline{y})$, denoted as $\underline{\hat{y}}_{[i-1]}$, is a LUE of $\mathsf{E}(\underline{y})$ for the complete set of conditions. Hence, we have

$$\underline{\hat{y}}_{[i]} = \underline{\hat{y}}_{[i-1]} - Q_{\hat{y}_{[i-1]}u_{[i]}} Q_{u_{[i]}u_{[i]}}^{-1} \underline{u}_{[i]} \tag{18}$$

Since $\underline{\hat{y}}_{[i-1]}$ is uncorrelated with $\underline{u}_{[i-1]}$, it follows upon choosing the respresentation of the vector of misclosures as $\underline{u}_{[i]} = [\underline{u}_{[i-1]}^T,\ (B_i^T \underline{\hat{y}}_{[i-1]})^T]^T$ that

$$\underline{\hat{y}}_{[i]} = \underline{\hat{y}}_{[i-1]} - Q_{\hat{y}_{[i-1]}\hat{y}_{[i-1]}} B_i (B_i^T Q_{\hat{y}_{[i-1]}\hat{y}_{[i-1]}} B_i)^{-1} B_i^T \underline{\hat{y}}_{[i-1]} \tag{19}$$

This is Tienstra's formula for adjustment in phases (Tienstra 1956).

2.4 From LUP to BLUP

Similar to the BLUE–LUE relation, we have the following counterpart for prediction.

Corollary 3 (BLUP–LUP formula) *The BLUP, its error variance matrix and its variance matrix are related to that of any arbitrary LUP as*

$$\begin{aligned} \text{BLUP} &= \text{LUP} + Q_{z-\text{LUP},u} Q_{uu}^{-1} \underline{u} \\ Q_{\varepsilon_{\text{BLUP}}\varepsilon_{\text{BLUP}}} &= Q_{\varepsilon_{\text{LUP}}\varepsilon_{\text{LUP}}} - Q_{\varepsilon_{\text{LUP}},u} Q_{uu}^{-1} Q_{u,\varepsilon_{\text{LUP}}} \\ Q_{\text{BLUP, BLUP}} &= Q_{\text{LUP, LUP}} - Q_{\text{LUP},u} Q_{uu}^{-1} Q_{u,\text{LUP}} + Q_{zu} Q_{uu}^{-1} Q_{uz} \end{aligned} \tag{20}$$

Proof The first equation follows from (11), while the second and third follow from an application of the variance propagation law, thereby making use of the zero-covariance property (12). □

Note that $Q_{\varepsilon_{\text{BLUP}}\varepsilon_{\text{BLUP}}}$ and $Q_{\text{BLUP, BLUP}}$ are two different variance matrices. The first is the variance matrix of the prediction error $\underline{\varepsilon}_{\text{BLUP}} = \underline{z} - \text{BLUP}$, thus describing the MMSE quality of the predictor. The second does *not* describe the quality of prediction, but instead the precision of the predictor, i.e. the mean squared difference between the predictor and $\bar{z}$, instead of between the predictor and $\underline{z}$. In case of estimation, this difference is absent as we have $Q_{\varepsilon_{\text{BLUE}}\varepsilon_{\text{BLUE}}} = Q_{\text{BLUE, BLUE}}$ (cf 13).

From the above corollary we can also directly obtain the BLUP-BLUE relation.

Corollary 4 (BLUP-BLUE formula) *The BLUP, its error variance matrix and its variance matrix are related to that of the BLUE as*

$$\begin{aligned} \text{BLUP} &= \text{BLUE} + Q_{zu}Q_{uu}^{-1}\underline{u} \\ Q_{\varepsilon_{\text{BLUP}}\varepsilon_{\text{BLUP}}} &= Q_{z-\text{BLUE},z-\text{BLUE}} - Q_{zu}Q_{uu}^{-1}Q_{uz} \\ Q_{\text{BLUP, BLUP}} &= Q_{\text{BLUE, BLUE}} + Q_{zu}Q_{uu}^{-1}Q_{uz} \end{aligned} \tag{21}$$

Proof Since $C(\text{BLUE}, \underline{u}) = 0$ and the BLUE, like any other LUE, is a LUP, (21) follows immediately from (20). □

Here, three examples are given to see the above BLUP-relations at work.

Example 4 (The BLUPs of $\underline{y}$ and $\underline{e}$) The BLUP of $\underline{y} = Ax + \underline{e}$ is the BLUE of Ax plus the BLUP of $\underline{e}$. The BLUP of $\underline{e}$ is $\hat{\underline{e}} = Q_{yu}Q_{uu}^{-1}\underline{u}$. Substitution of $\underline{u} = B^T\underline{y}$ gives

$$\hat{\underline{e}} = Q_{yy}B(B^TQ_{yy}B)^{-1}B^T\underline{y} = \underline{y} - \hat{\underline{y}} \tag{22}$$

If we add the BLUE of $\mathsf{E}(\underline{y}) = Ax$, which is $\hat{\underline{y}} = A\hat{\underline{x}}$, we get the BLUP of $\underline{y}$ as $\underline{y} = A\hat{\underline{x}} + \hat{\underline{e}}$. Hence the BLUP of $\underline{y}$ is $\underline{y}$ itself. This is the *reproducing property* of best prediction, i.e. the best prediction of an observable is the observable itself.

Example 5 (Equality of BLUP and BLUE) We now consider $\underline{y} = A\underline{x} + \underline{n}$ in which $\underline{x}$ and $\underline{n}$ are random vectors having means $\mathsf{E}(\underline{x}) = x$ and $\mathsf{E}(\underline{n}) = 0$, respectively. The mean of $\underline{x}$ is assumed unknown. To bring the observation equations into the standard form of (1), we write

$$\underline{y} = Ax + \underline{e}\ , \text{with } \underline{e} = A(\underline{x} - x) + \underline{n} \tag{23}$$

Note that the misclosure vector does not depend on $\underline{x}$, but only on the measurement noise vector $\underline{n}$, i.e. $\underline{u} = B^T\underline{y} = B^T\underline{n}$. Let $\hat{\underline{x}} = A^+\underline{y}$ be the BLUE of x. Then according to (21), the BLUP of $\underline{x}$ and its error variance matrix are given as

$$\begin{aligned} \text{BLUP} &= \hat{\underline{x}} + Q_{xu}Q_{uu}^{-1}\underline{u} \\ Q_{\varepsilon_{\text{BLUP}}\varepsilon_{\text{BLUP}}} &= Q_{x-\hat{x},x-\hat{x}} - Q_{xu}Q_{uu}^{-1}Q_{ux} \end{aligned} \tag{24}$$

This shows, since $Q_{xu} = Q_{xn}B$, that the BLUP of $\underline{x}$ becomes identical to the BLUE of x if $\mathsf{C}(\underline{x}, \underline{n}) = 0$, i.e. when $\underline{x}$ and $\underline{n}$ are uncorrelated. The error variance matrix reduces then to

$$Q_{\varepsilon_{\text{BLUP}}\varepsilon_{\text{BLUP}}} = Q_{x-\hat{x},x-\hat{x}} = Q_{\hat{x}\hat{x}} - Q_{xx} \tag{25}$$

since $\mathsf{C}(\hat{\underline{x}}, \underline{x}) = \mathsf{C}(A^+\underline{y}, \underline{x}) = \mathsf{C}(\underline{x} + A^+\underline{n}, \underline{x}) = Q_{xx}$. The fact that BLUP=BLUE in this case does not mean that the two have the same quality. The BLUP should be judged as a predictor through its error variance matrix (25), whereas the BLUE should be judged as an estimator through its variance matrix $Q_{\hat{x}\hat{x}}$. We come back to the BLUE–BLUP relation when we consider their recursive forms in the next sections.

Example 6 (BLUP and BLP compared) Using $\text{BLUE} = A_z\hat{\underline{x}}$ and $Q_{zu}Q_{uu}^{-1}\underline{u} = Q_{zy}B(B^TQ_{yy}B)^{-1}B^T\underline{y} = Q_{zy}Q_{yy}^{-1}(\underline{y} - \hat{\underline{y}})$, we may write the first equation of (21) as

$$\text{BLUP} = A_z\hat{\underline{x}} + Q_{zy}Q_{yy}^{-1}(\underline{y} - \hat{\underline{y}}) \tag{26}$$

This expression makes an easy comparison with the BLP in (8) possible. It shows that the BLUP can be obtained from the BLP expression by replacing the means $\bar{z}$ and $\bar{y}$ by their BLUEs. The price to pay for such replacement lies in the larger mean squared errors. The prediction error variance matrices of the BLP and the BLUP are namely given as

$$\begin{aligned} \mathsf{C}(\underline{\varepsilon}_{\text{BLP}}, \underline{\varepsilon}_{\text{BLP}}) &= Q_{zz} - Q_{zy}Q_{yy}^{-1}Q_{yz} \\ \mathsf{C}(\underline{\varepsilon}_{\text{BLUP}}, \underline{\varepsilon}_{\text{BLUP}}) &= \mathsf{C}(\underline{\varepsilon}_{\text{BLP}}, \underline{\varepsilon}_{\text{BLP}}) + A_{z|y}Q_{\hat{x}\hat{x}}A_{z|y}^T \end{aligned} \tag{27}$$

with $A_{z|y} = A_z - Q_{zy}Q_{yy}^{-1}A$. Another consequence of estimating the unknown means in case of the BLUP is that

$$\mathsf{C}(\underline{\varepsilon}_{\text{BLUP}}, \underline{y}) \neq 0, \text{ but } \mathsf{C}(\underline{\varepsilon}_{\text{BLUP}}, \underline{u}) = 0 \tag{28}$$

while $\mathsf{C}(\underline{\varepsilon}_{\text{BLP}}, \underline{y}) = 0$.

For a quick reference, a summary of the estimation–prediction relations is given in Table 1.

3 BLUE and BLUP measurement update equations

We now generalize the single observational vector $\underline{y}$ to a time series of vectorial observables, $\underline{y}_0, \ldots, \underline{y}_t$, of which the means are assumed to be linearly related to the mean of $\underline{z}$. The index refers to the time instant the data are collected.

The data are collected with the purpose of predicting $\underline{z}$ and estimating $\bar{z} = \mathsf{E}(\underline{z})$. To show how estimation and prediction are affected by the inclusion of a new observation vector $\underline{y}_i$, we present the BLUE and BLUP measurement update equations. No assumptions are yet made on the dispersion of the observables. From now on we denote a BLUE with the $\hat{\cdot}$-symbol and a BLUP with the $\breve{\cdot}$-symbol. To show on which set of observables estimation and prediction are based, we use the notations $\hat{\underline{z}}_{|[i-1]}$ and $\breve{\underline{z}}_{|[i-1]}$ when based on $\underline{y}_{[i-1]} = [\underline{y}_0^T, \ldots, \underline{y}_{i-1}^T]^T$.

Table 1 Estimation and prediction compared for linear models

$\hat{\underline{x}} = A^+ \underline{y}$, $\underline{u} = B^T \underline{y}$	Estimation	Prediction
Class representation	LUE $= A_z \hat{\underline{x}} + J\underline{u}$ for some J	LUP $= A_z \hat{\underline{x}} + H\underline{u}$ for some H
Best member	$BLUE = A_z \hat{\underline{x}}$	BLUP $= A_z \hat{\underline{x}} + Q_{zu} Q_{uu}^{-1} \underline{u}$
BLUE–LUE (BLUP–LUP) formula	BLUE = LUE $- Q_{\mathrm{LUE},u} Q_{uu}^{-1} \underline{u}$	BLUP = LUP $+ Q_{z-\mathrm{LUP},u} Q_{uu}^{-1} \underline{u}$
BLUE (BLUP) variance matrix	$Q_{\mathrm{BLUE,\,BLUE}} = Q_{\mathrm{LUE,\,LUE}} - Q_{\mathrm{LUE},u} Q_{uu}^{-1} Q_{u,\mathrm{LUE}}$	$Q_{\mathrm{BLUP,\,BLUP}} = Q_{\mathrm{LUP,\,LUP}} - Q_{\mathrm{LUP},u} Q_{uu}^{-1} Q_{u,\mathrm{LUP}} + Q_{z,u} Q_{uu}^{-1} Q_{u,z}$
Error variance matrix	$Q_{\varepsilon_{\mathrm{BLUE}}\varepsilon_{\mathrm{BLUE}}} = Q_{\mathrm{LUE,\,LUE}} - Q_{\mathrm{LUE},u} Q_{uu}^{-1} Q_{u,\mathrm{LUE}}$	$Q_{\varepsilon_{\mathrm{BLUP}}\varepsilon_{\mathrm{BLUP}}} = Q_{z-\mathrm{LUP},z-\mathrm{LUP}} - Q_{z-\mathrm{LUP},u} Q_{uu}^{-1} Q_{u,z-\mathrm{LUP}}$
Error covariance matrices	$C(\underline{\varepsilon}_{\mathrm{BLUE}}, \underline{u}) = 0$, $C(\underline{\varepsilon}_{\mathrm{BLUE}}, \mathrm{BLUE}) = C(\underline{\varepsilon}_{\mathrm{BLUE}}, \mathrm{BLUP})$	$C(\underline{\varepsilon}_{\mathrm{BLUP}}, \underline{u}) = 0$, $C(\underline{\varepsilon}_{\mathrm{BLUP}}, \mathrm{BLUE}) = C(\underline{\varepsilon}_{\mathrm{BLUE}}, \mathrm{BLUP})$

3.1 Uncorrelated misclosures and the statistics of the block-triangular decomposition

In the results up to now, we have emphasized the role played by the vector of misclosures $\underline{u}$, both in estimation and in prediction. We also pointed out that the vector of misclosures is not unique. Any one-to-one transformation of $\underline{u}$ produces again a vector of misclosures. Despite this nonuniqueness, the BLUE and BLUP are unique, i.e. they are invariant for any regular transformation of the vector of misclosures. This is illustrated by the identity

$$Q_{zu} Q_{uu}^{-1} \underline{u} = Q_{zv} Q_{vv}^{-1} \underline{v} \tag{29}$$

which holds for any $\underline{v} = L\underline{u}$ with invertible L.

The freedom we have in choosing the vector of misclosures makes it possible to choose a vector of misclosures with (block)diagonal variance matrix, e.g. such that they become uncorrelated from epoch to epoch. This is attractive as it generally simplifies computations. In case Q_{vv} is (block)diagonal, the multi-epoch inversion can be achieved through an epoch-by-epoch inversion of lower dimensioned matrices,

$$Q_{zv} Q_{vv}^{-1} \underline{v} = \sum_{j=1}^{t} Q_{zv_j} Q_{v_j v_j}^{-1} \underline{v}_j \tag{30}$$

Although there are different ways of making a variance matrix (block)diagonal, it is the triangular decomposition that is particularly suited for the sequential treatment of the measurement update equations. The following lemma provides the statistical properties of the transformed misclosures that correspond to the triangular decomposition of the original misclosures' variance matrix.

Lemma 4 (Uncorrelated misclosures) *Consider the partitioned misclosure vector* $\underline{u}_{[i]} = [\underline{u}_{[i-1]}^T, \underline{u}_i^T]^T$, $i = 1, 2, \ldots$, *with* $\underline{u}_{[0]} = \underline{u}_0$, *and define* $\underline{v}_{[i]} = [\underline{v}_{[i-1]}^T, \underline{v}_i^T]^T$, $i = 1, 2, \ldots$ *as*

$$\begin{bmatrix} \underline{v}_{[i-1]} \\ \underline{v}_i \end{bmatrix} = \begin{bmatrix} L_{[i-1]} & 0 \\ -Q_{u_i u_{[i-1]}} Q_{u_{[i-1]} u_{[i-1]}}^{-1} & I \end{bmatrix} \begin{bmatrix} \underline{u}_{[i-1]} \\ \underline{u}_i \end{bmatrix} \tag{31}$$

with $L_{[0]} = I$. *Then*

(a) $\underline{v}_i = \underline{u}_i - \breve{\underline{u}}_{i|[i-1]}$ *is the sequential predictor error of* $\underline{u}_i$
(b) $\underline{v}_{[i]} = L_{[i]} \underline{u}_{[i]}$, *with* $L_{[i]}$ *unit lower (block)triangular*
(c) $Q_{v_{[i]} v_{[i]}} = \mathrm{blockdiag}(Q_{v_0 v_0}, \ldots, Q_{v_i v_i})$

Proof (*a*) The BLUP of $\underline{u}_i$ based on the previous misclosure vector $\underline{u}_{[i-1]}$ is $\breve{\underline{u}}_{i|[i-1]} = Q_{u_i u_{[i-1]}} Q_{u_{[i-1]} u_{[i-1]}}^{-1} \underline{u}_{[i-1]}$. Hence, $\underline{v}_i = \underline{u}_i - \breve{\underline{u}}_{i|[i-1]}$ is the corresponding prediction error. (*b*) The transformation matrix $L_{[i]}$ of (31) is lower triangular with 1's on the diagonal. (*c*) We have $\mathsf{C}(\underline{v}_i, \underline{u}_{[i-1]}) = \mathsf{C}(\underline{u}_i - \breve{\underline{u}}_{i|[i-1]}, \underline{u}_{[i-1]}) = 0$, since the BLUP prediction error is uncorrelated with its misclosure vector. Substitution of $\underline{u}_{[i-1]} = L_{[i-1]}^{-1} \underline{v}_{[i-1]}$ gives $\mathsf{C}(\underline{v}_i, \underline{v}_{[i-1]}) = 0$. Hence, the variance matrix of $\underline{v}_{[i]}$ is block diagonal. □

As the above result shows, the random vectors $\underline{v}_i$, $i = 0, 1, \ldots$, are uncorrelated misclosures and at the same time sequential prediction errors of their correlated counterparts.

3.2 Measurement update equations

We are now in a position to use the misclosure vector $\underline{v}_{[i]} = [\underline{v}_{[i-1]}^T, \underline{v}_i^T]^T$ and the blockdiagonal structure of its variance matrix, $Q_{v_{[i]} v_{[i]}} = \mathrm{blockdiag}(Q_{v_{[i-1]} v_{[i-1]}}, Q_{v_i v_i})$, to formulate the BLUE and BLUP measurement update equations.

Lemma 5 (BLUE–BLUP measurement update) *Given the new observation vector* $\underline{y}_i$, *the BLUE* $\hat{\underline{z}}_{|[i-1]}$ *and BLUP* $\breve{\underline{z}}_{|[i-1]}$ *of* $\bar{z}$ *and* $\underline{z}$, *respectively, are updated as*

$$\begin{aligned} \hat{\underline{z}}_{|[i]} &= \hat{\underline{z}}_{|[i-1]} - Q_{\hat{z}_{|[i-1]} v_i} Q_{v_i v_i}^{-1} \underline{v}_i, \\ Q_{\hat{z}_{|[i]} \hat{z}_{|[i]}} &= Q_{\hat{z}_{|[i-1]} \hat{z}_{|[i-1]}} - Q_{\hat{z}_{|[i-1]} v_i} Q_{v_i v_i}^{-1} Q_{v_i \hat{z}_{|[i-1]}} \end{aligned} \tag{32}$$

and

$$\begin{aligned} \breve{\underline{z}}_{|[i]} &= \breve{\underline{z}}_{|[i-1]} + Q_{z-\breve{z}_{|[i-1]}, v_i} Q_{v_i v_i}^{-1} \underline{v}_i, \\ P_{\breve{z}_{|[i]} \breve{z}_{|[i]}} &= P_{\breve{z}_{|[i-1]} \breve{z}_{|[i-1]}} - Q_{z-\breve{z}_{|[i-1]}, v_i} Q_{v_i v_i}^{-1} Q_{v_i, z-\breve{z}_{|[i-1]}} \end{aligned} \tag{33}$$

Proof Since the BLUE $\hat{\underline{z}}_{|[i-1]}$ is a LUE where it is based on $\underline{y}_{[i]}$, we can apply the BLUE–LUE formula of Corollary 1, and obtain

$$\hat{\underline{z}}_{|[i]} = \hat{\underline{z}}_{|[i-1]} - Q_{\hat{z}_{|[i-1]}v_{[i]}} Q^{-1}_{v_{[i]}v_{[i]}} \underline{v}_{[i]},$$
$$Q_{\hat{z}_{|[i]}\hat{z}_{|[i]}} = Q_{\hat{z}_{|[i-1]}\hat{z}_{|[i-1]}} - Q_{\hat{z}_{|[i-1]}v_{[i]}} Q^{-1}_{v_{[i]}v_{[i]}} Q_{v_{[i]}\hat{z}_{|[i-1]}} \quad (34)$$

With $\mathsf{C}(\hat{\underline{z}}_{|[i-1]}, \underline{v}_{[i-1]}) = 0$ and the blockdiagonality of $Q_{v_{[i]}v_{[i]}}$, the above equation simplifies to Eq. (32). The proof for the predictor goes likewise. □

As the lemma shows, the contribution to the difference between two succeeding estimators and their respective predictors, $\hat{\underline{z}}_{|[i]}$ and $\hat{\underline{z}}_{|[i-1]}$ or $\check{\underline{z}}_{|[i]}$ and $\check{\underline{z}}_{|[i-1]}$, is provided by $\underline{v}_i$. Since $\underline{v}_i$ is uncorrelated with $\underline{v}_{[i-1]} = L_{[i-1]}u_{[i-1]}$, it cannot be predicted by the previous information, and therefore, it contains truly *new* information. The term *innovation* for $\underline{v}_i$ was first independently introduced, in case of stationary time series, by Bode and Shannon (1950) and Zadeh and Ragazzini (1950), and later further used for known-mean, non-stationary time series by Kailath (1968).

3.3 Partitioned linear model and predicted residuals

Note that the results of the above two Lemmas 4 and 5 do not depend on the linear model structure of the observables. We now introduce this structure by means of the partitioned linear model

$$\begin{bmatrix} \underline{y}_{[i-1]} \\ \underline{y}_i \end{bmatrix} = \begin{bmatrix} A_{[i-1]} \\ A_i \end{bmatrix} x + \begin{bmatrix} \underline{e}_{[i-1]} \\ \underline{e}_i \end{bmatrix} \quad (35)$$

with mean and dispersion

$$\mathsf{E}\left(\begin{bmatrix} \underline{e}_{[i-1]} \\ \underline{e}_i \end{bmatrix}\right) = \begin{bmatrix} 0 \\ 0 \end{bmatrix}, \ \mathsf{D}\left(\begin{bmatrix} \underline{y}_{[i-1]} \\ \underline{y}_i \end{bmatrix}\right) = \begin{bmatrix} Q_{y_{[i-1]}y_{[i-1]}} & Q_{y_{[i-1]}y_i} \\ Q_{y_i y_{[i-1]}} & Q_{y_i y_i} \end{bmatrix}$$

We make use of this structure to get a further interpretation of the innovation vector $\underline{v}_i$.

Lemma 6 (Estimation and prediction residuals) *Let the transpose of the basis matrix $B_{[i]}$ of the null space of $A^T_{[i]} = [A^T_{[i-1]}, A^T_i]$ be chosen as*

$$B^T_{[i]} = \begin{bmatrix} B^T_{[i-1]} & 0 \\ -A_i A^+_{[i-1]} & I \end{bmatrix} \quad (36)$$

with $A^+_{[i-1]} = \left(A^T_{[i-1]} Q^{-1}_{y_{[i-1]}y_{[i-1]}} A_{[i-1]}\right)^{-1} A^T_{[i-1]} Q^{-1}_{y_{[i-1]}y_{[i-1]}}$. *Then*

$$\begin{aligned} &(a)\ \underline{u}_i = \underline{y}_i - \hat{\underline{y}}_{i|[i-1]} \\ &(b)\ \underline{v}_i = \underline{y}_i - \check{\underline{y}}_{i|[i-1]} \end{aligned} \quad (37)$$

with BLUE $\hat{\underline{y}}_{i|[i-1]} = A_i \hat{\underline{x}}_{|[i-1]}$ *and BLUP* $\check{\underline{y}}_{i|[i-1]} = \hat{\underline{y}}_{i|[i-1]} + Q_{y_i u_{[i-1]}} Q^{-1}_{u_{[i-1]}u_{[i-1]}} \underline{u}_{[i-1]}$.

Proof (*a*) With (36), it follows from $\underline{u}_{[i]} = B^T_{[i]} \underline{y}_{[i]} = [\underline{u}^T_{[i-1]}, \underline{u}^T_i]^T$ that $\underline{u}_i = \underline{y}_i - A_i A^+_{[i-1]} y_{[i-1]}$. Hence, with $\hat{\underline{y}}_{i|[i-1]} = A_i \hat{\underline{x}}_{|[i-1]}$ and $\hat{\underline{x}}_{|[i-1]} = A^+_{[i-1]} y_{[i-1]}$ the result follows. (*b*) Since $\mathsf{C}(\hat{\underline{x}}_{|[i-1]}, \underline{u}_{[i-1]}) = 0$, we have $\mathsf{C}(\underline{u}_i, \underline{u}_{[i-1]}) = \mathsf{C}(\underline{y}_i - A_i \hat{\underline{x}}_{|[i-1]}, \underline{u}_{[i-1]}) = \mathsf{C}(\underline{y}_i, \underline{u}_{[i-1]})$ and thus $Q_{u_i,u_{[i-1]}} = Q_{y_i,u_{[i-1]}}$. We may therefore write $\check{\underline{u}}_{i|[i-1]} = Q_{y_i u_{[i-1]}} Q^{-1}_{u_{[i-1]}u_{[i-1]}} \underline{u}_{[i-1]}$. Substitution into $\underline{v}_i = \underline{u}_i - \check{\underline{u}}_{i|[i-1]}$ gives, with $\underline{u}_i = \underline{y}_i - \hat{\underline{y}}_{i|[i-1]}$ and $\check{\underline{y}}_{i|[i-1]} = \hat{\underline{y}}_{i|[i-1]} + Q_{y_i u_{[i-1]}} Q^{-1}_{u_{[i-1]}u_{[i-1]}} \underline{u}_{[i-1]}$, the stated result. □

The above result (37) shows that the innovation vector $\underline{v}_i$ is not only the sequential prediction error of $\underline{u}_i$ (cf. Lemma 4), but also, in case the basis matrix is chosen as (36), that of the observation vector $\underline{y}_i$. The innovation vector $\underline{v}_i$ will therefore from now on be referred to as the *predicted residual* of $\underline{y}_i$.

Note, since $Q_{y_i u_{[i-1]}} = 0$ if $\mathsf{C}(\underline{y}_i, \underline{y}_j) = 0$, $i \neq j$, that the estimator and predictor coincide, $\hat{\underline{y}}_{i|[i-1]} = \check{\underline{y}}_{i|[i-1]}$, if the observables are uncorrelated. In that case, we have $\underline{u}_i = \underline{v}_i = \underline{y}_i - A_i \hat{\underline{x}}_{|[i-1]}$.

Example 7 (Recursive least-squares estimation) If we assume uncorrelated observation vectors $\underline{y}_i$, i.e. $\mathsf{C}(\underline{y}_i, \underline{y}_j) = 0$, $i \neq j$, and take $A_z = I$, then (32) reduces, with $\underline{v}_i = \underline{y}_i - A_i \hat{\underline{x}}_{|[i-1]}$ and $Q_{\hat{x}_{|[i-1]}v_i} = -Q_{\hat{x}_{[i-1]}\hat{x}_{[i-1]}} A^T_i$, to the well-known recursive least-squares solution

$$\hat{\underline{x}}_{|[i]} = \hat{\underline{x}}_{|[i-1]} + Q_{\hat{x}_{|[i-1]}\hat{x}_{[i-1]}} A^T_i Q^{-1}_{v_i v_i} (\underline{y}_i - A_i \hat{\underline{x}}_{|[i-1]}) \quad (38)$$

4 Recursive BLUP and the Kalman filter

We now consider as partitioned model the measurement and dynamic models that form the basis of the well-known recursive Kalman filter. However, instead of the standard assumption that the means of the random state-vectors are known, we assume them to be unknown. Since the model can be brought into the linear model form, the BLUE and BLUP results of the previous sections directly apply. The recursive BLUP is shown to follow the Kalman filter updates, albeit with an initialization that is different from that of the known-mean, standard Kalman filter.

4.1 Model assumptions

First, we state the assumptions concerning the measurement and dynamic models.

The measurement model The link between the random vector of observables $\underline{y}_i$ and the random state-vector $\underline{x}_i$ is assumed given as

$$\underline{y}_i = A_i \underline{x}_i + \underline{n}_i, \ i = 0, 1, \ldots, t, \quad (39)$$

together with

$$\mathsf{E}(\underline{x}_0) = x_0 \text{ (unknown)}, \quad \mathsf{E}(\underline{n}_i) = 0, \quad (40)$$

and

$$\mathsf{C}(\underline{x}_0, \underline{n}_i) = 0, \quad \mathsf{C}(\underline{n}_i, \underline{n}_j) = R_i \delta_{i,j}, \ i = 0, 1, \ldots, t \quad (41)$$

with $\delta_{i,j}$ being the Kronecker delta. Thus, the zero-mean measurement noise $\underline{n}_i$ is assumed to be uncorrelated in time and to be uncorrelated with the initial state-vector $\underline{x}_0$.

The dynamic model The linear dynamic model, describing the time evolution of the random state-vector $\underline{x}_i$, is given as

$$\underline{x}_i = \Phi_{i,i-1}\underline{x}_{i-1} + \underline{d}_i,\ i = 1, 2, \ldots, t \tag{42}$$

with

$$\mathsf{E}(\underline{d}_i) = 0,\ \mathsf{C}(\underline{x}_0, \underline{d}_i) = 0, \tag{43}$$

$$\mathsf{C}(\underline{d}_i, \underline{n}_j) = 0,\ \mathsf{C}(\underline{d}_i, \underline{d}_j) = S_i\delta_{i,j},\ i, j = 1, 2, \ldots, t \tag{44}$$

where $\Phi_{i,i-1}$ denotes the transition matrix and the random vector $\underline{d}_i$ is the system noise. The system noise $\underline{d}_i$ is thus also assumed to have a zero mean, to be uncorrelated in time and to be uncorrelated with the initial state-vector and the measurement noise.

The above model equations are formulated on an epoch-by-epoch basis (cf. 39 and 42). To establish the link with the linear model formulation as used in the previous sections, one can obtain the corresponding multi-epoch linear model of (39) and (42) by defining the observation vector as $\underline{y} = [\underline{y}_0^T,\ \underline{y}_1^T,\ , \ldots, \underline{y}_t^T]^T$. This is shown in Table 2. Hence, we can now directly apply the BLUE–BLUP results of the previous sections for predicting the random state-vector $\underline{x}_t$ and estimating its unknown mean $\mathsf{E}(\underline{x}_t) = x_t$. From now on we denote the variance matrix of the BLUE $\hat{\underline{x}}_{t|[t]}$ with $Q_{t|[t]}$, whereas the *error* variance matrix of the BLUP $\check{\underline{x}}_{t|[t]}$ is denoted by $P_{t|[t]}$. Similar notation is employed for $Q_{t|[t-1]}$ and $P_{t|[t-1]}$. We start with the initialization, i.e. the case $t = 0$, where we assume that the data vector $\underline{y}_0$ contains the complete information content to determine the unknown mean x_0, i.e. A_0 is of full column rank.

4.2 Initialization

For $t = 0$, we have the linear model $\underline{y}_0 = A_0\underline{x}_0 + \underline{n}_0$, which may also be written as $\underline{y}_0 = A_0x_0 + \underline{e}_0$, with $\underline{e}_0 = A_0(\underline{x}_0 - x_0) + \underline{n}_0$. In general the BLUE of x_0 differs from the BLUP of $\underline{x}_0$. In our case, however, the two coincide. As shown in Example 5, the predictor and estimator, and their (error) variance matrices, are simply related as

$$\check{\underline{x}}_{0|0} = \hat{\underline{x}}_{0|0} \quad \text{and} \quad P_{0|0} = Q_{0|0} - Q_{x_0x_0} \tag{45}$$

when $\underline{x}_0$ and $\underline{n}_0$ are assumed uncorrelated. In the next lemma, these expressions are further worked out in A_0, R_0 and $Q_{x_0x_0}$.

Lemma 7 (BLUE–BLUP initialization) *Let the linear model at time $t = 0$ be given as $\underline{y}_0 = A_0\underline{x}_0 + \underline{n}_0$, with unknown mean state-vector $\mathsf{E}(\underline{x}_0) = x_0$, zero-mean noise vector $\mathsf{E}(\underline{n}_0) = 0$ and variance matrix $Q_{y_0y_0} = A_0Q_{x_0x_0}A_0^T + R_0$.*

Table 2 Linear model formulation for estimation and prediction

Linear model	Linear model form of (39) and (42)
Model eqs.	$\begin{bmatrix}\underline{y}\\ \underline{z}\end{bmatrix} = \begin{bmatrix}A\\ A_z\end{bmatrix}x + \begin{bmatrix}\underline{e}\\ \underline{e}_z\end{bmatrix}$
Mean, Dispersion	$\mathsf{E}\left(\begin{bmatrix}\underline{e}\\ \underline{e}_z\end{bmatrix}\right) = \begin{bmatrix}0\\ 0\end{bmatrix}, \mathsf{D}\left(\begin{bmatrix}\underline{y}\\ \underline{z}\end{bmatrix}\right) = \begin{bmatrix}Q_{ee} & Q_{ee_z}\\ Q_{e_ze} & Q_{e_ze_z}\end{bmatrix}$
BLUE of $\underline{z}$	$\hat{\underline{z}} = A_z\hat{\underline{x}} = A_z(A^TQ_{yy}^{-1}A)^{-1}A^TQ_{yy}^{-1}\underline{y}$
BLUP of $\underline{z}$	$\check{\underline{z}} = A_z\hat{\underline{x}} + Q_{zy}Q_{yy}^{-1}(\underline{y} - A\hat{\underline{x}})$

$$y = \left[\underline{y}_0^T,\ \underline{y}_1^T,\ \ldots,\ \underline{y}_t^T\right]^T,\ A = \left[A_0^T,\ (A_1\Phi_{1,0})^T,\ \ldots,\ (A_t\Phi_{t,0})^T\right]^T,$$

$$\underline{e} = \left[\{A_0(\underline{x}_0 - x_0) + \underline{n}_0\}^T, [A_1\{\Phi_{1,0}(\underline{x}_0 - x_0) + \underline{d}_1\} + \underline{n}_1]^T, \ldots, [A_t\{\Phi_{t,0}(\underline{x}_0 - x_0) + \textstyle\sum_{i=1}^{t}\Phi_{t,i}\,\underline{d}_i\} + \underline{n}_t]^T\right]^T$$

$$\underline{z} = \underline{x}_t,\ A_z = \Phi_{t,0},\ \underline{e}_z = \Phi_{t,0}(\underline{x}_0 - x_0) + \textstyle\sum_{i=1}^{t}\Phi_{t,i}\,\underline{d}_i$$

$$Q_{ee} = \begin{bmatrix} A_0Q_{x_0x_0}A_0^T + R_0 & \cdots & A_1(\Phi_{1,0}Q_{x_0x_0}\Phi_{1,0}^T + S_1)A_1^T + R_1 & \\ \vdots & & \vdots & \ddots \\ A_t\Phi_{t,0}Q_{x_0x_0}A_0^T & \cdots & A_t(\Phi_{t,0}Q_{x_0x_0}\Phi_{1,0}^T + \Phi_{t,1}S_1)A_1^T & \cdots\ A_t(\Phi_{t,0}Q_{x_0x_0}\Phi_{t,0}^T + \textstyle\sum_{i=1}^{t}\Phi_{t,i}S_i\Phi_{t,i}^T)A_t^T + R_t \end{bmatrix}$$

$$Q_{e_ze} = \left[\Phi_{t,0}Q_{x_0x_0}A_0^T, (\Phi_{t,0}Q_{x_0x_0}\Phi_{1,0}^T + \Phi_{t,1}S_1)A_1^T, \ldots, (\Phi_{t,0}Q_{x_0x_0}\Phi_{t,0}^T + \textstyle\sum_{i=1}^{t}\Phi_{t,i}S_i\Phi_{t,i}^T)A_t^T\right]$$

$$Q_{e_ze_z} = \Phi_{t,0}Q_{x_0x_0}\Phi_{t,0}^T + \textstyle\sum_{i=1}^{t}\Phi_{t,i}S_i\Phi_{t,i}^T$$

Recursive BLUE of x_t : $\hat{\underline{x}}_{t|t} = \hat{\underline{x}}_{t|t-1} + \ldots$ (cf. 60, 61, 62)

Recursive BLUP of $\underline{x}_t$: $\check{\underline{x}}_{t|t} = \check{\underline{x}}_{t|t-1} + \ldots$ (cf. 50, 51, 52)

Then, the BLUE of x_0 is equal to the BLUP of $\underline{x}_0$ and given as

$$\hat{\underline{x}}_{0|0} = \check{\underline{x}}_{0|0} = (A_0^T R_0^{-1} A_0)^{-1} A_0^T R_0^{-1} \underline{y}_0 \tag{46}$$

with (error)variance matrices

$$\begin{aligned} Q_{0|0} &= (A^T R_0^{-1} A_0)^{-1} + Q_{x_0 x_0} \\ P_{0|0} &= (A_0^T R_0^{-1} A_0)^{-1} \end{aligned} \tag{47}$$

Proof The equality of the BLUE and BLUP in (46) is due to the zero correlation between state-vector and measurement noise vector. That R_0^{-1}, instead of $Q_{y_0 y_0}^{-1}$, may be used as weight matrix in the least-squares formula of (46) follows from the matrix identity $(A_0^T Q_{y_0 y_0}^{-1} A_0)^{-1} A_0^T Q_{y_0 y_0}^{-1} \underline{y}_0 = (A_0^T R_0^{-1} A_0)^{-1} A_0^T R_0^{-1} \underline{y}_0$ for $Q_{y_0 y_0} = A_0 Q_{x_0 x_0} A_0^T + R_0$. Application of the (co)variance propagation law to (46) gives the (error)variance matrices of (47). □

As the above result shows, the BLUP of $\underline{x}_0$ is independent of its variance matrix $Q_{x_0 x_0}$. This variance matrix is therefore not needed for the initialization. It is not needed for computing $\check{\underline{x}}_{0|0}$, nor for its error variance matrix $P_{0|0}$. This is a marked difference with the standard formulation of the Kalman filter where the mean of the state-vector is assumed known. In that case, prediction is based on the BLP and the initialization takes the form

$$\check{x}_{0|0}^{\mathrm{BLP}} = \mathsf{E}(\underline{x}_0), \quad P_{0|0}^{\mathrm{BLP}} = \mathsf{C}(\underline{x}_0 - \check{x}_{0|0}^{\mathrm{BLP}}, \underline{x}_0 - \check{x}_{0|0}^{\mathrm{BLP}}) = Q_{x_0 x_0} \tag{48}$$

Hence, in that case the known mean is taken as the initial prediction of the random state-vector. As a consequence, the variance matrix $Q_{x_0 x_0}$ is then needed as it equals the error variance matrix.

Although $Q_{x_0 x_0}$ is not needed for the BLUP, the above lemma shows that it is needed for the BLUE. Not so much for computing the BLUE, but for describing its quality by means of its variance matrix $Q_{0|0}$.

4.3 Recursive BLUP

Recursion of the BLUP $\check{\underline{x}}_{t|[t]}$ is possible since the predictors of the zero-mean measurement and system noise are identically zero, $\check{\underline{n}}_{t|[t-1]} = 0$ and $\check{\underline{d}}_{t|[t-1]} = 0$. This is a consequence of having measurement noise and system noise that are both uncorrelated with the observables and state-vectors of the previous epochs. They are thus also uncorrelated with the predicted residuals of these epochs.

Since $\check{\underline{d}}_{t|[t-1]} = 0$, the predictor $\check{\underline{x}}_{t|[t-1]}$ can be computed directly from $\check{\underline{x}}_{t-1|[t-1]}$, thus providing the time update. Similarly, since $\check{\underline{n}}_{t|[t-1]} = 0$, the predicted residual $\underline{v}_t = \underline{y}_t - \check{\underline{y}}_{t|[t-1]}$ can be computed directly from $\underline{y}_t$ and $\check{\underline{x}}_{t|[t-1]}$, thus providing, in combination with (33), the measurement update of $\check{\underline{x}}_{t|[t-1]}$.

Lemma 8 (Predicted residuals) *For the measurement and dynamic model (39) and (42), the predicted residual vector and its variance matrix are given as*

$$\begin{aligned} \underline{v}_t &= \underline{y}_t - A_t \check{\underline{x}}_{t|[t-1]} \\ Q_{v_t v_t} &= R_t + A_t P_{t|[t-1]} A_t^T \end{aligned} \tag{49}$$

Proof As the BLUP of a linear function is the linear function of the BLUP, the BLUP of $\underline{y}_t = A_t \underline{x}_t + \underline{n}_t$ is $\check{\underline{y}}_{t|[t-1]} = A_t \check{\underline{x}}_{t|[t-1]} + \check{\underline{n}}_{t|[t-1]}$, with $\check{\underline{n}}_{t|[t-1]} = 0$, since $\underline{n}_t$ is zero mean and uncorrelated with the previous predicted residuals. Substitution of $\check{\underline{y}}_{t|[t-1]} = A_t \check{\underline{x}}_{t|[t-1]}$ into $\underline{v}_t = \underline{y}_t - \check{\underline{y}}_{t|[t-1]}$ proves the first equation of (49). The second equation follows from an application of the variance propagation law to $\underline{v}_t = A_t(\underline{x}_t - \check{\underline{x}}_{t|[t-1]}) + \underline{n}_t$. □

The steps for the recursion of $\check{\underline{x}}_{t|t}$ can now be summarized as follows.

Theorem 2 (a) (Recursive BLUP) *The three steps of the recursive state-vector prediction are given as*

$$\begin{aligned} \textit{Initialization:}\quad \check{\underline{x}}_{0|0} &= (A_0^T R_0^{-1} A_0)^{-1} A_0^T R_0^{-1} \underline{y}_0, \\ P_{0|0} &= (A_0^T R_0^{-1} A_0)^{-1} \end{aligned} \tag{50}$$

$$\begin{aligned} \textit{Time update:}\quad \check{\underline{x}}_{t|[t-1]} &= \Phi_{t,t-1} \check{\underline{x}}_{t-1|[t-1]}, \\ P_{t|[t-1]} &= \Phi_{t,t-1} P_{t-1|[t-1]} \Phi_{t,t-1}^T + S_t \end{aligned} \tag{51}$$

$$\begin{aligned} \textit{Measurement update:}\quad \check{\underline{x}}_{t|[t]} &= \check{\underline{x}}_{t|[t-1]} + K_t \underline{v}_t, \\ P_{t|[t]} &= P_{t|[t-1]} - K_t Q_{v_t v_t} K_t^T \end{aligned} \tag{52}$$

with gain matrix $K_t = P_{t|[t-1]} A_t^T Q_{v_t v_t}^{-1}$.

Proof The *initialization* was already proven in (46) and (47). To find the *time update*, we determine the BLUP of $\underline{x}_t = \Phi_{t,t-1} \underline{x}_{t-1} + \underline{d}_t$ as $\check{\underline{x}}_{t|[t-1]} = \Phi_{t,t-1} \check{\underline{x}}_{t-1|[t-1]} + \check{\underline{d}}_{t|[t-1]}$, with $\check{\underline{d}}_{t|[t-1]} = 0$, since $\underline{d}_t$ is zero mean and uncorrelated with the previous predicted residuals. This proves the first equation of (51). The second expression follows by applying the variance propagation law to $\underline{x}_t - \check{\underline{x}}_{t|[t-1]} = \Phi_{t,t-1}(\underline{x}_{t-1} - \check{\underline{x}}_{t-1|[t-1]}) + \underline{d}_t$ and using the relation $\mathsf{C}(\underline{x}_{t-1} - \check{\underline{x}}_{t-1|[t-1]}, \underline{d}_t) = 0$. To determine the *measurement update*, we apply (33), noting that for $\underline{z} = \underline{x}_t$, we need the covariance matrix $\mathsf{C}(\underline{x}_t - \check{\underline{x}}_{t|[t-1]}, v_t)$. With $\underline{v}_t = A_t(\underline{x}_t - \check{\underline{x}}_{t|[t-1]}) + \underline{n}_t$, this gives $\mathsf{C}(\underline{x}_t - \check{\underline{x}}_{t|[t-1]}, v_t) = P_{t|[t-1]} A_t^T$. Substitution into (33) proves (52). □

This result shows that apart from the initialization, the structure of the recursive BLUP is identical to that of the Kalman filter. Although the two expressions of the initialization (50) may suggest otherwise, it is important to note that $P_{0|0}$ is *not* the variance matrix of $\check{\underline{x}}_{0|0}$, but rather its *error* variance matrix. The variance matrix of $\underline{y}_0$ is namely not R_0,

but $A_0 Q_{x_0x_0} A_0^T + R_0$. The variance matrix of $\check{\underline{x}}_{0|0}$ is therefore equal to the sum $Q_{x_0x_0} + P_{0|0}$ and not equal to $P_{0|0}$.

As already pointed out earlier, the BLUP-initialization does not require the variance matrix $Q_{x_0x_0}$ of the initial state-vector $\underline{x}_0$. In fact, as the theorem now shows, this variance matrix is not needed at all. Hence, $Q_{x_0x_0}$ can take *any* value (e.g. 0 or ∞) without it having any effect on the result and quality of the recursive BLUP. This is in marked contrast to the standard Kalman filter.

5 The BLUE–BLUP recursion

Next to the prediction, we now present the recursive BLUE solution. This extension of the 'Kalman-filter' theory is a consequence of our relaxing assumptions that the means of the random state-vectors are unknown. In the standard Kalman filter set-up with known state-vector means, this difference between estimation and prediction does not occur since one is then only left with BLP instead of with BLUP of the state-vectors.

5.1 Time evolution of the error covariances

In order to develop the recursion for the BLUE $\hat{\underline{x}}_{t|[t-1]}$, we first determine the time evolution of the BLUE–BLUP error covariance matrices

$$\begin{aligned} C_{t|[t]} &= \mathsf{C}(x_t - \hat{\underline{x}}_{t|[t]}, \underline{x}_t - \check{\underline{x}}_{t|[t]}) \quad \text{and} \\ C_{t|[t-1]} &= \mathsf{C}(x_t - \hat{\underline{x}}_{t|[t-1]}, \underline{x}_t - \check{\underline{x}}_{t|[t-1]}) \end{aligned} \tag{53}$$

The following lemma shows how these error covariance matrices can be computed recursively.

Lemma 9 (BLUE–BLUP error covariance) *The time evolution of the error covariance matrices $C_{t|[t]}$ and $C_{t|[t-1]}$ is given as:*

$$\textit{Initialization:} \quad C_{0|0} = P_{0|0} \tag{54}$$

$$\textit{Time update:} \quad C_{t|[t-1]} = \Phi_{t,t-1} C_{t-1|[t-1]} \Phi_{t,t-1}^T \tag{55}$$

$$\textit{Measurement update:} \quad C_{t|[t]} = C_{t|[t-1]}(I - K_t A_t)^T \tag{56}$$

Proof For the *initialization* ($t = 0$) we have $C_{0|0} = \mathsf{C}(x_0 - \hat{\underline{x}}_{0|0}, \underline{x}_0 - \check{\underline{x}}_{0|0}) = Q_{0|0} - Q_{x_0x_0} = P_{0|0}$, since $\hat{\underline{x}}_{0|0} = \check{\underline{x}}_{0|0}$ and $\mathsf{C}(\hat{\underline{x}}_{0|0}, \underline{x}_0) = \mathsf{C}(\underline{x}_0, \underline{x}_0)$. This proves (54). For the *time update* we have, with $\hat{\underline{\varepsilon}}_{t|[t-1]} = x_t - \hat{\underline{x}}_{t|[t-1]}$ and $\check{\underline{\varepsilon}}_{t|[t-1]} = \underline{x}_t - \check{\underline{x}}_{t|[t-1]}$, that

$$\begin{aligned} C_{t|[t-1]} &= \mathsf{C}(\hat{\underline{\varepsilon}}_{t|[t-1]}, \check{\underline{\varepsilon}}_{t|[t-1]}) \\ &= \mathsf{C}(\Phi_{t,t-1}\hat{\underline{\varepsilon}}_{t-1|[t-1]}, \Phi_{t,t-1}\check{\underline{\varepsilon}}_{t-1|[t-1]} + \underline{d}_t) \\ &= \Phi_{t,t-1} C_{t-1|[t-1]} \Phi_{t,t-1}^T \end{aligned} \tag{57}$$

which proves (55). To prove the *measurement update*, we make use of Corollary 1. Since $\hat{\underline{\varepsilon}}_{t|[t-1]}$ and $\check{\underline{\varepsilon}}_{t|[t-1]}$ are both uncorrelated with $\underline{v}_i$ for $i < t$, it follows from Corollary 1, with $\hat{\underline{\varepsilon}}_{t|[t]} = x_t - \hat{\underline{x}}_{t|[t]}$ and $\check{\underline{\varepsilon}}_{t|[t]} = \underline{x}_t - \check{\underline{x}}_{t|[t]}$, that

$$\begin{aligned} \mathsf{C}(\hat{\underline{\varepsilon}}_{t|[t]}, \check{\underline{\varepsilon}}_{t|[t]}) &= \mathsf{C}(\hat{\underline{\varepsilon}}_{t|[t-1]}, \check{\underline{\varepsilon}}_{t|[t-1]}) \\ &\quad - \mathsf{C}(\hat{\underline{\varepsilon}}_{t|[t-1]}, \underline{v}_t) Q_{v_tv_t}^{-1} \mathsf{C}(\check{\underline{\varepsilon}}_{t|[t-1]}, \underline{v}_t)^T \end{aligned} \tag{58}$$

Furthermore we have, with $\underline{v}_t = A_t \check{\underline{\varepsilon}}_{t|[t-1]} + \underline{n}_t$,

$$\begin{aligned} \mathsf{C}(\hat{\underline{\varepsilon}}_{t|[t-1]}, \underline{v}_t) &= \mathsf{C}(\hat{\underline{\varepsilon}}_{t|[t-1]}, \check{\underline{\varepsilon}}_{t|[t-1]}) A_t^T = C_{t|[t-1]} A_t^T \\ \mathsf{C}(\check{\underline{\varepsilon}}_{t|[t-1]}, \underline{v}_t) &= \mathsf{C}(\check{\underline{\varepsilon}}_{t|[t-1]}, \check{\underline{\varepsilon}}_{t|[t-1]}) A_t^T = P_{t|[t-1]} A_t^T \end{aligned} \tag{59}$$

Substitution into (58) gives the measurement update of the error covariance matrix as $C_{t|[t]} = C_{t|[t-1]}(I - A_t^T Q_{v_tv_t}^{-1} A_t P_{t|[t-1]})$, which proves (56). □

5.2 Recursive BLUE

With the help of the recursion of these error covariance matrices, it becomes possible to set up the recursion for the BLUE of the mean state-vectors $x_t = \mathsf{E}(\underline{x}_t)$.

Theorem 2 (b) (Recursive BLUE) *The three steps of the recursive mean state-vector estimation are given as*

$$\begin{aligned} \textit{Initialization:} \quad & \hat{\underline{x}}_{0|0} = (A_0^T R_0^{-1} A_0)^{-1} A_0^T R_0^{-1} \underline{y}_0, \\ & Q_{0|0} = Q_{x_0x_0} + P_{0|0} \end{aligned} \tag{60}$$

$$\begin{aligned} \textit{Time update:} \quad & \hat{\underline{x}}_{t|[t-1]} = \Phi_{t,t-1} \hat{\underline{x}}_{t-1|[t-1]}, \\ & Q_{t|[t-1]} = \Phi_{t,t-1} Q_{t-1|[t-1]} \Phi_{t,t-1}^T \end{aligned} \tag{61}$$

$$\begin{aligned} \textit{Measurement update:} \quad & \hat{\underline{x}}_{t|[t]} = \hat{\underline{x}}_{t|[t-1]} + G_t \underline{v}_t, \\ & Q_{t|[t]} = Q_{t|[t-1]} - G_t Q_{v_tv_t} G_t^T \end{aligned} \tag{62}$$

with gain matrix $G_t = C_{t|[t-1]} A_t^T Q_{v_tv_t}^{-1}$.

Proof The *initialization* was already proven in (46) and (47). Since the BLUE of a linear function is the linear function of the BLUE, also the *time update* (61) directly follows.To determine the *measurement update*, we apply (32), noting that for $\bar{z} = \mathsf{E}(\underline{x}_t)$, we need the covariance matrix $\mathsf{C}(x_t - \hat{\underline{x}}_{t|[t-1]}, v_t)$. With $\underline{v}_t = A_t(\underline{x}_t - \check{\underline{x}}_{t|[t-1]}) + \underline{n}_t$, this gives $\mathsf{C}(x_t - \hat{\underline{x}}_{t|[t-1]}, v_t) = C_{t|[t-1]} A_t^T$. Substitution into (32) proves (62). □

Compare this BLUE recursion with the BLUP recursion of Theorem 2(a). Both look very similar. They have the same structure and they even have the same initialization ($\hat{\underline{x}}_{0|0} = \check{\underline{x}}_{0|0}$) and the same time update ($\hat{\underline{x}}_{t|[t-1]} = \Phi_{t,t-1}\hat{\underline{x}}_{t-1|[t-1]}$ versus $\check{\underline{x}}_{t|[t-1]} = \Phi_{t,t-1}\check{\underline{x}}_{t-1|[t-1]}$). They differ however in the variance matrices and in their measurement updates. In case of the BLUP, the error variance matrix $P_{t|[t-1]}$ is used both in the computation of the gain K_t and in the quality evaluation of the predictor. In case of the BLUE, however, the quality of the estimator $\hat{\underline{x}}_{t|[t-1]}$ is described by $Q_{t|[t-1]}$,

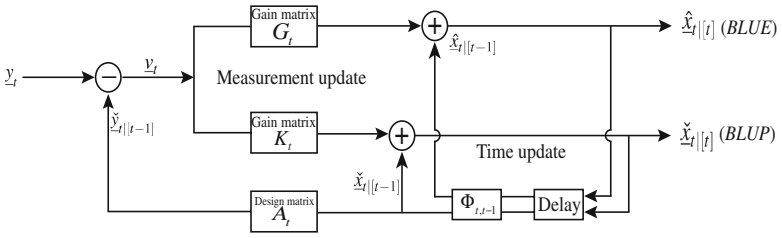

Fig. 1 Block diagram of the recursive BLUE–BLUP method with measurement and time updates

whereas the gain is computed from the error covariance matrix $C_{t|[t-1]}$.

As another important difference, note that in contrast to the BLUP recursion, the BLUE recursion cannot stand on its own. It requires the predicted residuals $\underline{v}_t$ and therefore the BLUP $\check{\underline{x}}_{t|[t-1]}$. Figure 1 shows the block diagram of the BLUE–BLUP recursion. The input is $\underline{y}_t$ and the outputs are the BLUE $\hat{\underline{x}}_{t|[t]}$ and the BLUP $\check{\underline{x}}_{t|[t]}$. The block diagram shows that estimation and prediction have the time update in common, but not the measurement update. The two measurement updates are fed with the same predicted residual, but have different gains. Their gain matrices are related as

$$G_t = C_{t|[t-1]} P_{t|[t-1]}^{-1} K_t \tag{63}$$

Let us now compare the two recursions with regards to their need of knowing $Q_{x_0x_0}$, the variance matrix of the initial state-vector $\underline{x}_0$. We already pointed out that this matrix does not play a role at all in the BLUP-recursion (cf. Theorem 2 (a)). It does however seem to play a role in the BLUE recursion, as it shows up in its initialization (60). A closer study of the mechanism of the BLUE recursion shows however that $Q_{x_0x_0}$ has also no effect on the outcomes of the BLUE. The gain matrix of the BLUE recursion is namely not driven by the variance matrix $Q_{t|[t-1]}$, but by the error covariance matrix $C_{t|[t-1]}$, which itself does not depend on $Q_{x_0x_0}$ (cf. Lemma 9). Hence, the only role played by $Q_{x_0x_0}$ lies in describing how the uncertainty of $\underline{x}_0$ contributes to the uncertainty of the estimators at the various epochs. Working with a model with unknown, but deterministic initial state-vector, i.e. $Q_{x_0x_0} = 0$, will therefore produce the same state-vector estimate as obtained when working with a random initial state-vector with unknown mean. Only the variance matrices of the two solutions will differ, since the latter is impacted by the randomness of the initial state-vector.

A further comparison between the two recursions shows that the difference between the BLUE and the BLUP is only driven by the system noise. Since both have the same initialization and the same time update, the difference between the two only starts to be felt in the measurement update of epoch $t = 1$. The measurement updates differ, since the gain matrices differ, $G_t \neq K_t$ (cf. 63). These gain matrices are the same however, in case $C_{t|[t-1]} = P_{t|[t-1]}$, which is the case when the system noise is absent. We therefore have the following result.

Corollary 5 (BLUE=BLUP) *The recursive BLUP becomes identical to the recursive BLUE, in case system noise is absent, i.e. if $S_t = 0$ for all t, then*

$$\hat{\underline{x}}_{t|[t]} = \check{\underline{x}}_{t|[t]} \quad \text{and} \quad \hat{\underline{x}}_{t|[t-1]} = \check{\underline{x}}_{t|[t-1]} \tag{64}$$

for all t.

Thus, in all cases where system noise is present the recursive BLUE will give an output different from that of the recursive BLUP.

5.3 Recursive BLUE–BLUP

Since the BLUE and BLUP recursions have the same structure and are both based on the same predicted residuals, one can combine them into one recursion. For that purpose, we denote the BLUE–BLUP state-vector and its error variance matrix as

$$\tilde{\underline{x}}_{t|[t-1]} = \begin{bmatrix} \hat{\underline{x}}_{t|[t-1]} \\ \check{\underline{x}}_{t|[t-1]} \end{bmatrix}, \quad \tilde{P}_{t|[t-1]} = \begin{bmatrix} Q_{t|[t-1]} & C_{t|[t-1]} \\ C_{t|[t-1]}^T & P_{t|[t-1]} \end{bmatrix} \tag{65}$$

with a likewise definition for $\tilde{\underline{x}}_{t|[t]}$ and $\tilde{P}_{t|[t]}$. Thus combining the recursions, the combined results of Theorems 2 (a) and (b) can be summarized as follows.

Theorem 2 (Recursive BLUE–BLUP) *The three steps of the BLUE–BLUP recursion are given as*

$$\begin{aligned} \textit{Initialization:}\ & \tilde{\underline{x}}_{0|0} = E\hat{\underline{x}}_{0|0}, \\ & \tilde{P}_{0|0} = E P_{0|0} E^T + \tilde{Q}_{x_0x_0} \end{aligned} \tag{66}$$

with $E = [I_n, I_n]^T$ and $\tilde{Q}_{x_0x_0} = \text{blockdiag}(Q_{x_0x_0}, 0)$.

$$\begin{aligned} \textit{Time update:}\ & \tilde{\underline{x}}_{t|[t-1]} = \tilde{\Phi}_{t,t-1} \tilde{\underline{x}}_{t-1|[t-1]}, \\ & \tilde{P}_{t|[t-1]} = \tilde{\Phi}_{t,t-1} \tilde{P}_{t-1|[t-1]} \tilde{\Phi}_{t,t-1}^T + \tilde{S}_t \end{aligned} \tag{67}$$

with transition matrix $\tilde{\Phi}_{t,t-1} = \text{blockdiag}(\Phi_{t,t-1}, \Phi_{t,t-1})$ and system noise variance matrix $\tilde{S}_t = \text{blockdiag}(0, S_t)$.

$$\begin{aligned} \textit{Measurement update:}\ & \\ & \tilde{\underline{x}}_{t|[t]} = \tilde{\underline{x}}_{t|[t-1]} + \tilde{K}_t \underline{v}_t, \\ & \tilde{P}_{t|[t]} = \tilde{P}_{t|[t-1]} - \tilde{K}_t Q_{v_t v_t} \tilde{K}_t^T \end{aligned} \tag{68}$$

Table 3 The three steps of the BLUE–BLUP recursion compared

	Estimation	Prediction
Initialization	$\hat{\underline{x}}_{0\|0} = (A_0^T R_0^{-1} A_0)^{-1} A_0^T R_0^{-1} \underline{y}_0$	$\check{\underline{x}}_{0\|0} = \hat{\underline{x}}_{0\|0} = (A_0^T R_0^{-1} A_0)^{-1} A_0^T R_0^{-1} \underline{y}_0$
	$Q_{0\|0} = Q_{x_0 x_0} + (A_0^T R_0^{-1} A_0)^{-1}$	$P_{0\|0} = (A_0^T R_0^{-1} A_0)^{-1}$
Time update	$\hat{\underline{x}}_{t\|[t-1]} = \Phi_{t,t-1} \hat{\underline{x}}_{t-1\|[t-1]}$	$\check{\underline{x}}_{t\|[t-1]} = \Phi_{t,t-1} \check{\underline{x}}_{t-1\|[t-1]}$
	$Q_{t\|[t-1]} = \Phi_{t,t-1} Q_{t-1\|[t-1]} \Phi_{t,t-1}^T$	$P_{t\|[t-1]} = \Phi_{t,t-1} P_{t-1\|[t-1]} \Phi_{t,t-1}^T + S_t$
Measurement update	$\hat{\underline{x}}_{t\|[t]} = \hat{\underline{x}}_{t\|[t-1]} + C_{t\|[t-1]} A_t^T Q_{\underline{v}_t \underline{v}_t}^{-1} \underline{v}_t$	$\check{\underline{x}}_{t\|[t]} = \check{\underline{x}}_{t\|[t-1]} + P_{t\|[t-1]} A_t^T Q_{\underline{v}_t \underline{v}_t}^{-1} \underline{v}_t$
	$Q_{t\|[t]} = Q_{t\|[t-1]} - C_{t\|[t-1]} A_t^T Q_{\underline{v}_t \underline{v}_t}^{-1} A_t C_{t\|[t-1]}^T$	$P_{t\|[t]} = P_{t\|[t-1]} - P_{t\|[t-1]} A_t^T Q_{\underline{v}_t \underline{v}_t}^{-1} A_t P_{t\|[t-1]}$

with predicted residual $\underline{v}_t = \underline{y}_t - \tilde{A}_t \check{\underline{x}}_{t|[t-1]}$, $\tilde{A}_t = A_t[0, I_n]$, *and gain matrix* $\bar{K}_t = \tilde{P}_{t|[t-1]} \tilde{A}_t^T Q_{\underline{v}_t \underline{v}_t}^{-1}$.

This result shows how the recursive BLUE and the recursive BLUP can be mechanized into one single recursion. This result is therefore the recursive formulation of the BLUE–BLUP expression given in Theorem 1. With this extention of the standard 'Kalman filter' theory, we are thus also able to recursively compute the best estimate of the unknown mean state-vector, instead of only the best prediction of the random state-vector outcome.

In analogy with Kalman filter-based smoothing, it also possible to develop the BLUE–BLUP smoothing solution. For the BLUE part, smoothing is rather straightforward, since $\hat{\underline{x}}_{t|[s]} = \Phi_{t,s} \hat{\underline{x}}_{s|[s]}$ and $Q_{t|[s]} = \Phi_{t,s} Q_{s|[s]} \Phi_{t,s}^T$. For the BLUP part, the smoothing will resemble the standard smoothing methods, like fixed-point, fixed-interval or fixed-lag smoothing, see e.g. (Gelb 1974; Maybeck 1979; Jazwinski 1991; Gibbs 2011).

6 Summary and conclusions

In this contribution, the BLUE–BLUP recursion of the partitioned measurement and dynamic models was introduced (see Table 3). It extends 'Kalman-filter' theory by replacing the BLP approach with the BLUP, thereby relaxing the assumptions on the state-vector means. It was argued that the BLUP approach is often more appropriate, since in many, if not most, applications the means of the state-vectors are indeed unknown.

The recursive BLUP was derived from first principles, thereby making use of an earlier derived decomposition of the BLUP into misclosures and any LUP. The role of the misclosures was emphasized and it was shown how they form the basis for constructing the predicted residuals. It was also shown how the recursive BLUP, as a consequence of the relaxing assumption on the state-vector means, does away with the need of having to specify the initial state-vector variance matrix.

Next to the recursive BLUP, we introduced, for the same model, the recursive BLUE. This extension is new and another consequence of assuming the state-vector means unknown. In the standard Kalman filter set-up with known state-vector means, such difference between estimation and prediction does not occur since one is then only left with BLP instead of with BLUP of the state-vectors.

Finally, it was shown how the two intertwined recursions can be combined into one general BLUE–BLUP recursion. The recursion outputs for every epoch, in parallel, the BLUP for the random state-vector and the BLUE for the mean of the state-vector (cf. the block diagram of Fig. 1).

Acknowledgments P.J.G. Teunissen is the recipient of an Australian Research Council Federation Fellowship (project number FF0883188). The research of A. Khodabandeh was carried out whilst a Curtin International Research Scholar at Curtin's GNSS Research Centre. All this support is gratefully acknowledged.

References

Anderson BDO, Moore JB (1979) Optimal filtering, vol 11. Prentice-hall, Englewood Cliffs

Ansley CF, Kohn R (1985) Estimation, filtering, and smoothing in state space models with incompletely specified initial conditions. Ann Stat 13(4):1286–1316

Bar-Shalom Y, Li X (1993) Estimation and tracking—principles, techniques, and software. Artech House, Inc., Norwood

Bode H, Shannon C (1950) A simplified derivation of linear least square smoothing and prediction theory. Proc IRE 38(4):417–425

Brammer K, Siffling G (1989) Kalman-Bucy filters. Artech House, Norwood

Candy J (1986) Signal processing: model based approach. McGraw-Hill, Inc, New York

Gelb A (1974) Applied optimal estimation. MIT Press, Cambridge

Gibbs B (2011) Advanced Kalman filtering, least-squares and modeling: a practical handbook. Wiley, New York

Goldberger A (1962) Best linear unbiased prediction in the generalized linear regression model. J Am Stat Assoc 57(298):369–375

Grewal MS, Andrews AP (2008) Kalman filtering: theory and practice using MATLAB, 3rd edn. Wiley, New York

Harvey AC, Phillips GDA (1979) Maximum likelihood estimation of regression models with autoregressive-moving average disturbances. Biometrika 66(1):49–58

Jazwinski A (1991) Stochastic processes and filtering theory. Dover Publications, New York

de Jong P (1991) The diffuse Kalman filter. Ann Stat 19(2):1073–1083

Kailath T (1968) An innovations approach to least-squares estimation—part I: Linear filtering in additive white noise. IEEE Trans Autom Control 13(6):646–655

Kailath T (1981) Lectures on Wiener and Kalman filtering. Springer, Berlin
Kailath T, Sayed AH, Hassibi B (2000) Linear estimation. Prentice-Hall, Englewood Cliffs
Kalman RE (1960) A new approach to linear filtering and prediction problems. J Basic Eng 82(1):35–45
Maybeck P (1979) Stochastic models, estimation, and control, vol 1. Academic Press, Waltham, republished 1994
Sanso F (1986) Statistical methods in physical geodesy. In: Sunkel H (ed) Mathematical and numerical techniques in physical geodesy. Lecture notes in earth sciences, vol 7. Springer, Berlin, pp 49–155
Simon D (2006) Optimal state estimation: Kalman, H [infinity] and nonlinear approaches. Wiley, New York
Sorenson HW (1966) Kalman filtering techniques. In: Leondes CT (ed) Advances in control systems: theory and applications, vol 3. pp 219–292
Stark H, Woods J (1986) Probability, random processes, and estimation theory for engineers. Prentice-Hall, Englewood Cliffs
Teunissen PJG (2000) Adjustment theory: an introduction. In: Series on Mathematical Geodesy and Positioning. Delft University Press
Teunissen PJG (2007) Best prediction in linear models with mixed integer/real unknowns: theory and application. J Geod 81(12):759–780
Teunissen PJG (2008) On a stronger-than-best property for best prediction. J Geod 82(3):167–175
Teunissen PJG, Simons DG, Tiberius CCJM (2005) Probability and observation theory. Delft University, Faculty of Aerospace Engineering, Delft University of Technology, lecture notes AE2-E01
Tienstra J (1956) Theory of the adjustment of normally distributed observation. Argus, Amsterdam
Zadeh LA, Ragazzini JR (1950) An extension of Wiener's theory of prediction. J Appl Phys 21(7):645–655

12 A recursive MMSE filter (Part 2: Relation to the Kalman filter)

This chapter is covered by the following publication:

Khodabandeh A. and Teunissen P.J.G. (2014c). A recursive linear MMSE filter for dynamic systems with unknown state vector means. International Journal on Geomathematics, 5:17–31, Springer

Int J Geomath
DOI 10.1007/s13137-014-0058-0

ORIGINAL PAPER

A recursive linear MMSE filter for dynamic systems with unknown state vector means

Amir Khodabandeh · Peter J. G. Teunissen

Received: 18 December 2013 / Accepted: 30 January 2014

Abstract In this contribution we extend Kalman-filter theory by introducing a new recursive linear minimum mean squared error (MMSE) filter for dynamic systems with unknown state-vector means. The recursive filter enables the joint MMSE prediction and estimation of the random state vectors and their unknown means, respectively. We show how the new filter reduces to the Kalman-filter in case the state-vector means are known and we discuss the fundamentally different roles played by the intitialization of the two filters.

Keywords Minimum mean squared error (MMSE) · Best linear unbiased estimation (BLUE) · Best linear unbiased prediction (BLUP) · Kalman filter · BLUE-BLUP recursion

Mathematics Subject Classification 60G25 · 60G35 · 93E11

1 Introduction

The minimum mean squared error (MMSE) criterion is a popular criterion for determining estimators and predictors. Depending on the class of functions considered, different MMSE predictors exist. The conditional mean achieves the smallest MSE

A. Khodabandeh · P. J. G. Teunissen
Department of Spatial Sciences, GNSS Research Centre,
Curtin University of Technology, Perth, Australia
e-mail: amir.khodabandeh@curtin.edu.au

P. J. G. Teunissen (✉)
Department of Geoscience and Remote Sensing,
Delft University of Technology, Delft, The Netherlands
e-mail: p.teunissen@curtin.edu.au

Published online: 05 March 2014

and is therefore the best predictor (BP) of all. Within the class of linear functions however, it is the best linear predictor (BLP) that achieves the smallest MSE.

The Kalman filter is a recursive MMSE filter, which has found a widespread usage in various Earth science disciplines (Grafarend 1976; Sanso 1980; Bertino et al. 2002; Marx and Potthast 2012). It is used, for example, in deformation and earth-orientation studies (Gross et al. 1998; Ince and Sahin 2000), in physical and space geodesy (Grafarend and Rapp 1984; Sanso 1986; Herring et al. 1990), and in hydrology and atmospheric studies (Ferraresi et al. 1996; Cao et al. 2006; Acharya et al. 2011).

In the literature, the recursive Kalman-filter is derived as either a BP or a BLP, see e.g., Kalman (1960); Gelb (1974); Kailath (1981); Candy (1986); Brammer and Siffling (1989); Jazwinski (1991); Gibbs (2011). Both these predictors however, require the mean of the to-be-predicted random vector to be known. This is why in the derivation of the Kalman filter the mean of the random initial state-vector is assumed known, see e.g., Sorenson (1966, p. 222), Kailath (1974, p. 148), Maybeck (1979, p. 204), Anderson and Moore (1979, p. 15), Stark and Woods (1986, p. 393), Bar-Shalom and Li (1993, p. 209), Kailath et al. (2000, p. 311), Christensen (2001, p. 261), Simon (2006, p. 125), Grewal and Andrews (2008, p. 138). Hence, the BP, the BLP, nor the Kalman filter, are applicable in case the mean of the random state vector is unknown.

As shown in Teunissen and Khodabandeh (2013), one can do away with this need to have the means known. In this contribution we build on that fact and develop from first principles the recursive linear MMSE filter for dynamic systems with unknown state vector means. This filter generalizes standard Kalman filter theory and it enables the joint recursive prediction and estimation of the random state vector and its unknown mean, respectively. In the standard Kalman filter set-up, with known state-vector means, this difference between estimation and prediction does not occur since one is then only left with predicting the outcomes of the random state vectors. The generalized filter links BLUE-BLUP with BLP and shows how the outcomes of the BLUE-BLUP recursions can be directly used in tandem to obtain those of the standard Kalman filter as special case.

This contribution is organized as follows. In Sect. 2, we briefly review the necessary ingredients of prediction and estimation for linear models. We use the misclosure vector of the linear model as an ancillary statistic to give a useful joint representation for the best linear unbiased estimator (BLUE) and the best linear unbiased predictor (BLUP). This representation is used in Sect. 3 to derive our recursive linear MMSE filter for dynamic models with unknown state vector means. In Sect. 4 we show how this generalized filter specializes to that of the Kalman filter in case the state-vector means are known. It demonstrates how the different recursions are related and interacting, and in what way their quality descriptions differ. We discuss the role of system noise and that of the error-covariance matrices in the generalized filter. Hereby we also discuss the fundamentally different role played by the initialization of the two filters.

Throughout this contribution, the estimator and the predictor are distinguished by the $\hat{}$-symbol and $\check{}$-symbol, respectively, while the joint estimator-predictor is denoted by using the $\tilde{}$-symbol. Random variates are indicated by an underscore. Thus $\underline{x}$ is random, while x is not. $\mathsf{E}(.)$, $\mathsf{C}(.,.)$ and $\mathsf{D}(.)$ denote the expectation, covariance and

dispersion operators, respectively. Thus $\mathsf{E}([\underline{x}-\mathsf{E}(\underline{x})][\underline{x}-\mathsf{E}(\underline{x})]^T) = \mathsf{C}(\underline{x}, \underline{x}) = \mathsf{D}(\underline{x})$. The norm of a vector is denoted as $||.||$. Thus $||.||^2 = (.)^T(.)$.

2 Estimation and prediction in linear models

2.1 Linear unbiased statistics

Consider the linear model

$$\begin{bmatrix} \underline{y} \\ \underline{z} \end{bmatrix} = \begin{bmatrix} A \\ A_z \end{bmatrix} x + \begin{bmatrix} \underline{e} \\ \underline{e}_z \end{bmatrix} \tag{1}$$

with known matrices $A \in \mathbb{R}^{m\times n}$, $A_z \in \mathbb{R}^{k\times n}$, zero-mean $\mathsf{E}([\underline{e}^T\, \underline{e}_z^T]^T) = 0$, and known dispersion

$$\mathsf{D}\left(\begin{bmatrix} \underline{y} \\ \underline{z} \end{bmatrix}\right) = \begin{bmatrix} Q_{yy} & Q_{yz} \\ Q_{zy} & Q_{zz} \end{bmatrix} \tag{2}$$

It is assumed that $\text{rank}A = n$, Q_{yy} is positive definite and the nonrandom vector $x \in \mathbb{R}^n$ is unknown.

It is our aim to use a linear unbiased statistic of $\underline{y}$ to *estimate* the unknown mean $\bar{z} = A_z x$ and to *predict* the outcome of $\underline{z} = \bar{z} + \underline{e}_z$. In order to perform the estimation and prediction jointly, we define the target vector $\underline{\mathscr{Z}} = [\bar{z}^T, \underline{z}^T]^T$.

Let $\mathscr{G}(\underline{y}) = F\underline{y} + f$ and $\mathscr{G}_J(\underline{y}) = F_J\underline{y} + f_J$ be two arbitrary linear unbiased statistics for $\underline{\mathscr{Z}}$. Then it follows from the condition of unbiasedness that the expectation of their difference satisfies $\mathsf{E}(\mathscr{G}_J(\underline{y}) - \mathscr{G}(\underline{y})) = (F_J - F)Ax + (f_J - f) = 0$ for all x. Hence,

$$F_J = F + JB^T, \quad \text{and} \quad f_J = f \tag{3}$$

for some matrix $J \in \mathbb{R}^{2k\times(m-n)}$, where B is an $m \times (m-n)$ basis matrix of the orthogonal complement of the range space of A, $B^TA = 0$, or equivalently, B is a basis matrix of the null space of A^T. Using the above representation, we arrive at the following lemma.

Lemma 1 *Let the misclosure of $\underline{y}$ be given as $\underline{v} = B^T\underline{y}$, with B a basis matrix of the null space of A^T. Then any two linear unbiased statistics $\mathscr{G}_J(\underline{y})$ and $\mathscr{G}(\underline{y})$ for $\underline{\mathscr{Z}}$, are related as*

$$\mathscr{G}_J(\underline{y}) = \mathscr{G}(\underline{y}) + J\underline{v}, \quad \text{for some } J \in \mathbb{R}^{2k\times(m-n)}. \tag{4}$$

This lemma shows that any two linear unbiased statistics differ only by a linear function of the random misclosure vector $\underline{v}$.

2.2 MMSE-estimator and predictor

We now use representation (4) to establish the connection between any arbitrary linear unbiased statistic and the one achieving the minimum mean squared error (MMSE). The error vector $\underline{\epsilon}_J = \underline{\mathscr{Z}} - \mathscr{G}_J(\underline{y})$, of which the squared norm is to be minimized, consists of the *estimation error* as well as the *prediction error*. One may then, through the choice of matrix $J \in \mathbb{R}^{2k\times r}$, minimize the mean squared norm of the error vector $\underline{\epsilon}_J$ to obtain the joint MMSE estimator/predictor $\underline{\tilde{\mathscr{Z}}} = [\underline{\hat{z}}^T, \underline{\check{z}}^T]^T$. Recall that its two components, $\underline{\hat{z}}$ and $\underline{\check{z}}$, respectively, are referred to as the best linear unbiased estimator (BLUE) and the best linear unbiased predictor (BLUP), see e.g.,Goldberger (1962); Anderson and Moore (1979); Stark and Woods (1986); Simon (2006); Teunissen (2007). The idea is finalized in the following theorem.

Theorem 1 *Let $\mathscr{G}(\underline{y})$ be an arbitrary linear unbiased statistic for $\underline{\mathscr{Z}}$. Then the joint BLUE-BLUP of $\underline{\mathscr{Z}}$ can be computed as*

$$\underline{\tilde{\mathscr{Z}}} = \mathscr{G}(\underline{y}) + Q_{\epsilon v} Q_{vv}^{-1} \underline{v} \tag{5}$$

with $\underline{\epsilon} = \underline{\mathscr{Z}} - \mathscr{G}(\underline{y})$.

Proof Since $\mathscr{G}_J(\underline{y}) = \mathscr{G}(\underline{y}) + J\underline{v}$ for some $J \in \mathbb{R}^{2k\times(m-n)}$, then $\mathsf{E}||\underline{\epsilon}_J||^2 = \mathsf{E}||\underline{\epsilon} - J\underline{v}||^2$. This can be further decomposed as

$$\begin{aligned}\mathsf{E}||\underline{\epsilon} - J\underline{v}||^2 &= \mathsf{E}||\underline{\epsilon} - Q_{\epsilon v}Q_{vv}^{-1}\underline{v} - (J - Q_{\epsilon v}Q_{vv}^{-1})\underline{v}||^2 \\ &= \mathsf{E}||\underline{\epsilon} - Q_{\epsilon v}Q_{vv}^{-1}\underline{v}||^2 + \mathsf{E}||(J - Q_{\epsilon v}Q_{vv}^{-1})\underline{v}||^2\end{aligned}$$

since $\underline{\epsilon} - Q_{\epsilon v}Q_{vv}^{-1}\underline{v}$ is uncorrelated with $\underline{v}$. By setting $J - Q_{\epsilon v}Q_{vv}^{-1} = 0$, $\mathsf{E}||\underline{\epsilon}_J||^2$ attains its minimum, which proves the claim. □

Theorem 1 implies that the joint BLUE-BLUP error vector $\underline{\tilde{\epsilon}} = \underline{\mathscr{Z}} - \underline{\tilde{\mathscr{Z}}}$ is *uncorrelated* with the misclosure vector $\underline{v}$, i.e. $\mathsf{C}(\underline{\tilde{\epsilon}}, \underline{v}) = 0$.

3 BLUE-BLUP recursion

In this section the recursive formulation of Theorem 1 is presented. It is based on the measurement- and dynamic model that forms the basis of the Kalman-filter. However, instead of the standard assumption of known state-vector means, we assume the means to be *unknown*.

3.1 Model assumptions

First we state the assumptions concerning the measurement- and dynamic model. Accordingly, the observational vector $\underline{y}$ is generalized to a time series of vectorial observables, $\underline{y}_1, \ldots, \underline{y}_t$. Here the role of the to-be-predicted vector $\underline{z}$ is taken by the state-vector $\underline{x}_t$. Hence, it is our aim to estimate the unknown state vector mean

$x_t = \mathsf{E}(\underline{x}_t)$ and to predict the outcome of the random state-vector $\underline{x}_t$. It will be shown how such joint estimation/prediction can be performed recursively.

The dynamic model The linear dynamic model, describing the time-evolution of the random state-vector $\underline{x}_i$, is given as

$$\underline{x}_i = \Phi_{i,i-1}\underline{x}_{i-1} + \underline{d}_i,\ i = 1, 2, \ldots, t \tag{6}$$

with

$$\mathsf{E}(\underline{x}_0) = x_0 \text{ (unknown)}, \quad \mathsf{D}(\underline{x}_0) = Q_{x_0 x_0} \tag{7}$$

and

$$\mathsf{E}(\underline{d}_i) = 0,\ \mathsf{C}(\underline{d}_i, \underline{d}_j) = S_i \delta_{i,j},\ \mathsf{C}(\underline{d}_i, \underline{x}_0) = 0 \tag{8}$$

for $i, j = 1, 2, \ldots, t$, with $\delta_{i,j}$ being the Kronecker delta, and where the $n \times n$ nonsingular matrix $\Phi_{i,i-1}$ denotes the transition matrix and the random vector $\underline{d}_i$ is the system noise. The system noise $\underline{d}_i$ is thus assumed to have a zero mean, to be uncorrelated in time and to be uncorrelated with the initial state-vector $\underline{x}_0$. The transition matrix from epoch j to i is denoted as $\Phi_{i,j}$. Thus $\Phi_{i,j}^{-1} = \Phi_{j,i}$ and $\Phi_{i,i} = I_n$, the identity matrix of size n.

The measurement model The link between the random vector of observables $\underline{y}_i \in \mathbb{R}^{m_i}$ and the random state-vector $\underline{x}_i \in \mathbb{R}^n$ is assumed given as

$$\underline{y}_i = A_i \underline{x}_i + \underline{n}_i,\ i = 1, 2, \ldots, t, \tag{9}$$

with

$$\mathsf{E}(\underline{n}_i) = 0,\ \mathsf{C}(\underline{n}_i, \underline{n}_j) = R_i \delta_{i,j} \tag{10}$$

and

$$\mathsf{C}(\underline{n}_i, \underline{x}_0) = 0,\ \mathsf{C}(\underline{n}_i, \underline{d}_j) = 0 \tag{11}$$

for $i, j = 1, 2, \ldots, t$. Thus the zero-mean measurement noise $\underline{n}_i$ is assumed to be uncorrelated in time and to be uncorrelated with the initial state-vector $\underline{x}_0$ and the system noise $\underline{d}_i$. Matrix A_1 of (9) is assumed to be of full column rank.

3.2 The three-step recursion

In the following, to show on which set of observables estimation/prediction are based, we use the notation $\tilde{\underline{x}}_{t|[\tau]} = [\hat{\underline{x}}_{t|[\tau]}^T,\ \check{\underline{x}}_{t|[\tau]}^T]^T$ when based on $\underline{y}_{[\tau]} = [\underline{y}_1^T, \ldots, \underline{y}_\tau^T]^T$. The variance matrix of the joint estimation-prediction error

$$\tilde{\underline{\varepsilon}}_{t|[\tau]} = [(x_t - \hat{\underline{x}}_{t|[\tau]})^T,\ (\underline{x}_t - \check{\underline{x}}_{t|[\tau]})^T]^T,$$

will be denoted by $\tilde{P}_{t|[\tau]}$.

Before forming the recursive counterpart of Theorem 1, an appropriate representation of the random misclosure vector $\underline{v}$, defined in lemma 1, must be formulated.

Lemma 2 *Let the linear model* $\mathsf{E}(\underline{y}_{[t]}) = A_{[t],\tau}x_\tau,\ t = 1, 2, \ldots,$ *be structured by those given in* (6) *and* (9). *That is,* $\underline{y}_{[t]} = [\underline{y}^T_{[t-1]},\ \underline{y}^T_t]^T$, $A_{[t],\tau} = [A^T_{[t-1],\tau},\ A^T_{t,\tau}]^T$ *with* $A_{i,\tau} = A_i\Phi_{i,\tau}$. *Then there exists a representation of* $\underline{v}_{[t]} = B^T_{[t]}\underline{y}_{[t]}$ *as*

$$\underline{v}_{[t]} = \begin{bmatrix} \underline{v}_{[t-1]} \\ \underline{v}_t \end{bmatrix} = \begin{bmatrix} B^T_{[t-1]}\underline{y}_{[t-1]} \\ \underline{y}_t - A_t\underline{\check{x}}_{t|[t-1]} \end{bmatrix} \tag{12}$$

with $B_{[t-1]}$ *and* $B_{[t]}$ *being basis matrices of the null spaces of* $A^T_{[t-1],t}$ *and* $A^T_{[t],t}$, *respectively.*

Proof Matrix $B^T_{[t]}$ can be represented as

$$B^T_{[t]} = \begin{bmatrix} B^T_{[t-1]} & 0 \\ -A_tA^-_{[t-1],t} & I \end{bmatrix}, \quad t = 2, 3, \ldots \tag{13}$$

where $A^-_{[t-1],t}$ denotes an arbitrary left-inverse of $A_{[t-1],t}$, i.e. $A^-_{[t-1],t}A_{[t-1],t} = I_n$. Hence,

$$B^T_{[t]}\underline{y}_{[t]} = \left[[B^T_{[t-1]}\underline{y}_{[t-1]}]^T, [\underline{y}_t - A_tA^-_{[t-1],t}\underline{y}_{[t-1]}]^T\right]^T \tag{14}$$

The lemma is proven if $A^-_{[t-1],t}$ can be chosen such that $A^-_{[t-1],t}\underline{y}_{[t-1]}$ is the BLUP of $\underline{x}_t$ based on $\underline{y}_{[t-1]}$. Let $A^-_{[t-1],t}$ therefore be of the form

$$A^-_{[t-1],t} = A^+_{[t-1],t} + HB^T_{[t-1]} \tag{15}$$

for some H and where $A^+_{[t-1],t}$ is another left-inverse of $A_{[t-1],t}$. Then, since $A^+_{[t-1],t}\underline{y}_{[t-1]}$ is a linear unbiased statistic for x_t based on $\underline{y}_{[t-1]}$, it follows from Theorem 1 that matrix H can always be chosen such that $A^-_{[t-1],t}\underline{y}_{[t-1]} = \underline{\check{x}}_{t|[t-1]}$. □

We are now in a position to present the three-step procedure of the BLUE-BLUP recursion. In each step, use is made of Theorem 1, i.e. the MMSE-estimator/predictor is obtained from the sum of an unbiased linear statistic $\mathscr{G}$ and a linear function of $\underline{v}_{[t]}$ in (12).

Initialization ($t = 1$) We start with $\underline{y}_1 = A_1\underline{x}_1 + \underline{n}_1$. Since the random vector $\underline{v}_1 = B^T_1\underline{y}_1 = B^T_1\underline{n}_1$ is uncorrelated with the state-vector $\underline{x}_1$, we choose the following linear unbiased statistic

$$\mathscr{G}(\underline{y}_1) \mapsto U(A^T_1R^{-1}_1A_1)^{-1}A^T_1R^{-1}_1\underline{y}_1 \tag{16}$$

with $U = [I_n, I_n]^T$.

Using the identity $B_1^T A_1 = 0$, the zero-covariance property $\mathsf{C}(A_1^T R_1^{-1} \underline{y}_1, \underline{v}_1) = 0$ follows as well. Thus the joint estimation-prediction error $[x_1^T, \underline{x}_1^T]^T - \mathscr{G}(\underline{y}_1)$ is uncorrelated with $\underline{v}_1$, meaning that the proposed statistic $\mathscr{G}(\underline{y}_1)$ itself is the joint BLUE-BLUP $\tilde{\underline{x}}_{1|1} = [\hat{\underline{x}}_{1|1}^T, \check{\underline{x}}_{1|1}^T]^T$. The error variance matrix $\tilde{P}_{1|1}$ also follows by an application of the variance propagation law to

$$\tilde{\underline{\epsilon}}_{1|1} = U(\underline{x}_1 - \hat{\underline{x}}_{1|1}) + [I_n, 0]^T (x_1 - \underline{x}_1)$$

This, together with $Q_{x_1 x_1} = \Phi_{1,0} Q_{x_0 x_0} \Phi_{1,0}^T + S_1$, results in

$$\tilde{P}_{1|1} = U(A_1^T R_1^{-1} A_1)^{-1} U^T + \text{blockdiag}(Q_{x_1 x_1}, 0), \tag{17}$$

since $\mathsf{D}(\underline{x}_1 - \hat{\underline{x}}_{1|1}) = (A_1^T R_1^{-1} A_1)^{-1}$ and $\mathsf{C}(\underline{x}_1, \underline{x}_1 - \hat{\underline{x}}_{1|1}) = 0$

Time update In case of the time update step, we set $\mathscr{G}$ as

$$\mathscr{G}(\underline{y}_{[t-1]}) \mapsto \tilde{\Phi}_{t,t-1} \tilde{\underline{x}}_{t-1|[t-1]} \tag{18}$$

with $\tilde{\Phi}_{t,t-1} = \text{blockdiag}(\Phi_{t,t-1}, \Phi_{t,t-1})$. The corresponding joint estimation-prediction error can be expressed as

$$[x_t^T, \underline{x}_t^T]^T - \mathscr{G}(\underline{y}_{[t-1]}) = \tilde{\Phi}_{t,t-1} \tilde{\underline{\epsilon}}_{t-1|[t-1]} + [0, I_n]^T \underline{d}_t. \tag{19}$$

The estimation-prediction error $\tilde{\underline{\epsilon}}_{t-1|[t-1]}$ is uncorrelated with $\underline{v}_{[t-1]}$ of (12) (cf. Theorem 1). Given the assumptions (8), (10) and (11), the system noise $\underline{d}_t$ is also uncorrelated with the previous observables, thus with any linear functions thereof, i.e. $\mathsf{C}(\underline{d}_t, \underline{v}_{[t-1]}) = 0$. This confirms the zero-covariance property between the estimation-prediction error (19) and $\underline{v}_{[t-1]}$. The BLUE-BLUP time-update is thus nothing else but the statistic given in (18).

With $\mathsf{C}(\tilde{\underline{\epsilon}}_{t-1|[t-1]}, \underline{d}_t) = 0$, the error variance matrix $\tilde{P}_{t|[t-1]}$ is obtained by applying the variance propagation law to the representation of $\tilde{\underline{\epsilon}}_{t|[t-1]}$ given in (19). This yields

$$\tilde{P}_{t|[t-1]} = \tilde{\Phi}_{t,t-1} \tilde{P}_{t-1|[t-1]} \tilde{\Phi}_{t,t-1}^T + \text{blockdiag}(0, S_t) \tag{20}$$

Measurement update For the measurement-update, the BLUE-BLUP based on the data vector $\underline{y}_{[t-1]}$ is taken as the linear unbiased statistic of the data vector $\underline{y}_{[t]}$, that is

$$\mathscr{G}(\underline{y}_{[t]}) \mapsto \tilde{\underline{x}}_{t|[t-1]} \tag{21}$$

Now we make use of the representation of (12) by which $\underline{v}_t$ can also be re-written as

$$\underline{v}_t = \tilde{A}_t \tilde{\underline{\epsilon}}_{t|[t-1]} + \underline{n}_t, \quad \text{with} \quad \tilde{A}_t = A_t [0, I_n] \tag{22}$$

Given the assumptions (8), (10) and (11), the measurement noise $\underline{n}_t$ is uncorrelated with the previous observables and the state-vectors. This, together with (22), yields $\mathsf{C}(\tilde{\underline{\epsilon}}_{t|[t-1]}, \underline{v}_t) = \tilde{P}_{t|[t-1]}\tilde{A}_t^T$. Combining the results with $\mathsf{C}(\tilde{\underline{\epsilon}}_{t|[t-1]}, \underline{v}_{[t-1]}) = 0$, an application of Theorem 1 gives finally

$$\tilde{\underline{x}}_{t|[t]} = \mathscr{G}(\underline{y}_{[t]}) + \tilde{P}_{t|[t-1]}\tilde{A}_t^T Q_{v_t v_t}^{-1}\underline{v}_t \tag{23}$$

With $\mathsf{C}(\tilde{\underline{\epsilon}}_{t|[t-1]}, \underline{n}_t) = 0$, an application of the variance propagation law to (22) provides the following expression of the variance matrix $Q_{v_t v_t}$

$$Q_{v_t v_t} = R_t + \tilde{A}_t \tilde{P}_{t|[t-1]}\tilde{A}_t^T \tag{24}$$

Using the identity $\tilde{\underline{\epsilon}}_{t|[t]} = \tilde{\underline{\epsilon}}_{t|[t-1]} - \tilde{P}_{t|[t-1]}\tilde{A}_t^T Q_{v_t v_t}^{-1}\underline{v}_t$, the error variance matrix $\tilde{P}_{t|[t]}$ reads

$$\tilde{P}_{t|[t]} = \tilde{P}_{t|[t-1]} - \tilde{P}_{t|[t-1]}\tilde{A}_t^T Q_{v_t v_t}^{-1}\tilde{A}_t \tilde{P}_{t|[t-1]} \tag{25}$$

since $\mathsf{C}(\tilde{\underline{\epsilon}}_{t|[t-1]}, \underline{v}_t) = \tilde{P}_{t|[t-1]}\tilde{A}_t^T$.

The structure of the above recursive procedure has been summarized in Theorem 2.

Theorem 2 (Recursive BLUE-BLUP) *The three steps of the BLUE-BLUP recursion are given as follows.*

Initialization:

$$\begin{aligned} \tilde{\underline{x}}_{1|1} &= U\hat{\underline{x}}_{1|1}, \\ \tilde{P}_{1|1} &= U P_{1|1} U^T + \tilde{Q}_{x_1 x_1} \end{aligned} \tag{26}$$

with $U = [I_n, I_n]^T$, $\hat{\underline{x}}_{1|1} = (A_1^T R_1^{-1} A_1)^{-1} A_1^T R_1^{-1}\underline{y}_1$, $P_{1|1} = (A_1^T R_1^{-1} A_1)^{-1}$, *and* $\tilde{Q}_{x_1 x_1} = blockdiag(Q_{x_1 x_1}, 0)$.

Time-update:

$$\begin{aligned} \tilde{\underline{x}}_{t|[t-1]} &= \tilde{\Phi}_{t,t-1}\tilde{\underline{x}}_{t-1|[t-1]}, \\ \tilde{P}_{t|[t-1]} &= \tilde{\Phi}_{t,t-1}\tilde{P}_{t-1|[t-1]}\tilde{\Phi}_{t,t-1}^T + \tilde{S}_t \end{aligned} \tag{27}$$

with transition matrix $\tilde{\Phi}_{t,t-1} = blockdiag(\Phi_{t,t-1}, \Phi_{t,t-1})$ *and system noise variance matrix* $\tilde{S}_t = blockdiag(0, S_t)$.

Measurement-update:

$$\begin{aligned} \tilde{\underline{x}}_{t|[t]} &= \tilde{\underline{x}}_{t|[t-1]} + \tilde{K}_t\underline{v}_t, \\ \tilde{P}_{t|[t]} &= (I_{2n} - \tilde{K}_t\tilde{A}_t)\tilde{P}_{t|[t-1]} \end{aligned} \tag{28}$$

with $\underline{v}_t = \underline{y}_t - \tilde{A}_t\tilde{\underline{x}}_{t|[t-1]}$, $\tilde{A}_t = A_t[0, I_n]$, $Q_{v_t v_t} = R_t + A_t P_{t|[t-1]}A_t^T$, *and gain matrix* $\tilde{K}_t = \tilde{P}_{t|[t-1]}\tilde{A}_t^T Q_{v_t v_t}^{-1}$. $\diamond$

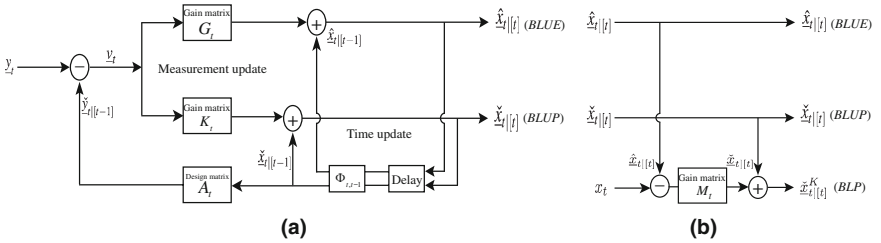

Fig. 1 **a** BLUE-BLUP recursion: measurement- and time-update, with gain matrices $G_t = C_{t|[t-1]}A_t^T Q_{v_t v_t}^{-1}$ and $K_t = P_{t|[t-1]}A_t^T Q_{v_t v_t}^{-1}$; **b** BLP from the BLUE and BLUP, with gain matrix $M_t = C_{t|[t]}Q_{t|[t]}^{-1}$

With the use of the partitioning $\tilde{\underline{x}}_{t|[t]} = (\hat{\underline{x}}_{t|[t]}^T, \check{\underline{x}}_{t|[t]}^T)^T$ and $\tilde{K}_t = (G_t^T, K_t^T)^T$, the mechanism of the BLUE-BLUP recursion is illustrated with the block diagram given in Fig. 1a. It shows that, in contrast to the BLUP recursion, the BLUE-part of the BLUE-BLUP recursion cannot stand on its own. It requires $\underline{v}_t = \underline{y}_t - A_t\check{\underline{x}}_{t|[t-1]}$, and therefore the BLUP $\check{\underline{x}}_{t|[t-1]}$.

3.3 Role of the system noise

As the expressions of (26) and (27) show, the BLUE and BLUP both have the same initialization ($\hat{\underline{x}}_{1|1} = \check{\underline{x}}_{1|1}$) and the same time-update structure ($\tilde{\Phi}_{t,t-1} = \text{blockdiag}(\Phi_{t,t-1}, \Phi_{t,t-1})$). They differ however in their error variance matrices, which in turn makes their measurement-updates different. As the structure of $\tilde{P}_{t|[t-1]}$ in (27) shows, the difference between the BLUE and the BLUP is only driven by the system noise. This difference starts to be felt in the measurement-update of the time instance $t = 2$, where the corresponding BLUE/BLUP components of the partitioned gain matrix $\tilde{K}_t = [G_t^T,\ K_t^T]^T$ start deviating from each other (i.e. $G_t \neq K_t$). Would the system noises be absent (i.e. $S_t = 0\ \forall t$), then $G_t = K_t,\ \forall t$, thus making the outcomes of the recursive BLUE identical to that of the recursive BLUP.

Example As illustration of the stated system noise role, we consider as example an observed time-series of random-walk noise with unknown trend. The underlying model follows from (9) and (6) by setting ($n = 1$)

$$A_t = 1, \quad \Phi_{t,t-1} = 1, \quad \forall\, t \tag{29}$$

We further assume the variance of the system noise to be related by that of the measurement noise, say σ^2, via the nonnegative scalar α as

$$R_t = \sigma^2, \quad S_t = \alpha\,\sigma^2, \quad \forall\, t \tag{30}$$

Employing the BLUE-BLUP recursion, the estimation and prediction gain values can be shown to read

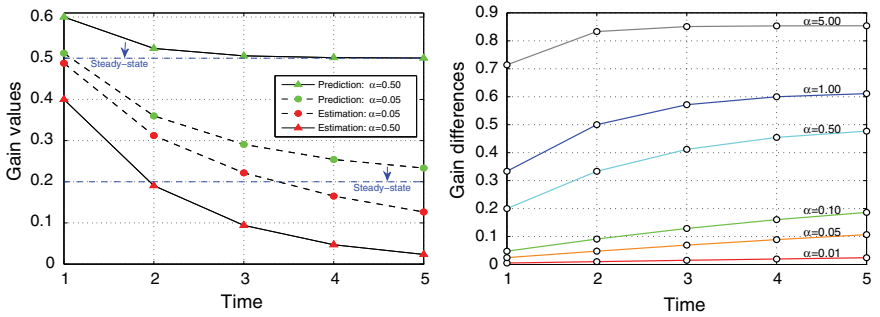

Fig. 2 *Left-panel*: Estimation gain values (*in red*) versus their prediction counterparts (*in green*) for two different values of $\alpha = 0.50$ (*triangles*) and $\alpha = 0.05$ (*circles*) over time. *Right-panel*: The difference in the gain values (i.e. $K_t - G_t$) for different values of α over time (color figure online)

$$G_t = \frac{1}{\sum_{i=1}^{t} w_i}, \quad K_t = \frac{w_t}{\sum_{i=1}^{t} w_i} \tag{31}$$

where the nonnegative weights w_t, $t = 1, 2, \ldots$, as polynomials of α, are computed as

$$w_1 = 1 + \alpha, \quad w_t = w_{t-1} + \alpha \sum_{i=1}^{t-1} w_i, \quad t = 2, 3, \ldots \tag{32}$$

Figure 2 shows the gain values (and their difference) for different values of α. As shown, the difference between the two gain values is insignificant for small values of α, while the gain values deviate from each other by increasing α (right-panel).

The identities in (31) show that the estimation gain values, in this example, get smaller faster than their prediction counterparts, that is $G_t \leq K_t$ (see also Fig. 2, left-panel).This can be explained as follows. As stated, the estimation target vector is the unknown mean x_t which, in this example, does not change over time (i.e. $\Phi_{t,t-1} = 1$). Therefore, as the information content in the data vectors $\underline{y}_t$ is accumulated, the gain in improving the estimator due to the upcoming data gets less. In case of prediction however, the target vector is an outcome of the state-vector $\underline{x}_t$. Thus the gain in improving the predictor does generally rely on the observables in time. In the extreme case when the time instance tends to infinity, the *steady-state* gain values follow, namely

$$\lim_{t\to\infty} G_t = 0, \quad \lim_{t\to\infty} K_t = \frac{1}{2}(\sqrt{\alpha^2 + 4\alpha} - \alpha) \tag{33}$$

According to (33), as the filter converges to its steady-state form, the BLUE $\hat{\underline{x}}_{t|[t]}$ does not improve any more by accumulating further data. In case of prediction however, the constant gain values are generally different from zero meaning that the BLUP $\check{\underline{x}}_{t|[t]}$ still benefits from the further data. The steady-state error variance matrix of the joint BLUE-BLUP reads similarly

$$\lim_{t\to\infty} \tilde{P}_{t|[t]} = \begin{bmatrix} \sigma_{x_1}^2 & 0 \\ 0 & 0 \end{bmatrix} + \frac{1}{2}(\sqrt{\alpha^2+4\alpha} - \alpha) \begin{bmatrix} \sigma^2 & 0 \\ 0 & \sigma^2 \end{bmatrix} \tag{34}$$

with $\sigma_{x_1}^2 = \sigma_{x_0}^2 + \alpha\sigma^2$ being the variance of the state-vector $\underline{x}_1$.

3.4 Role of the estimation-error variance matrix

To appreciate the contribution to the BLUE-BLUP recursion of the entries of the joint estimation-prediction error variance matrices, we partition $\tilde{P}_{t|[t]}$ as

$$\tilde{P}_{t|[t]} = \begin{bmatrix} Q_{t|[t]} & C_{t|[t]} \\ C_{t|[t]}^T & P_{t|[t]} \end{bmatrix}, \quad t = 1, 2, \ldots \tag{35}$$

with $Q_{t|[t]} = \mathsf{D}(x_t - \hat{\underline{x}}_{t|[t]})$ and $P_{t|[t]} = \mathsf{D}(\underline{x}_t - \check{\underline{x}}_{t|[t]})$, the error-variance matrices of estimation and prediction, and $C_{t|[t]} = \mathsf{C}(x_t - \hat{\underline{x}}_{t|[t]}, \underline{x}_t - \check{\underline{x}}_{t|[t]})$ their error cross-covariance. A similar partitioning is used for $\tilde{P}_{t|[t-1]}$. From Theorem 2 follows then:

Initialization:

$$\begin{aligned} P_{1|1} &= (A_1^T R_1^{-1} A_1)^{-1}, \\ C_{1|1}^T &= P_{1|1}, \\ Q_{1|1} &= P_{1|1} + Q_{x_1x_1} \end{aligned} \tag{36}$$

Time-update:

$$\begin{aligned} P_{t|[t-1]} &= \Phi_{t,t-1} P_{t-1|[t-1]} \Phi_{t,t-1}^T + S_t, \\ C_{t|[t-1]}^T &= \Phi_{t,t-1} C_{t-1|[t-1]}^T \Phi_{t,t-1}^T, \\ Q_{t|[t-1]} &= \Phi_{t,t-1} Q_{t-1|[t-1]} \Phi_{t,t-1}^T \end{aligned} \tag{37}$$

Measurement-update:

$$\begin{aligned} P_{t|[t]} &= (I_n - K_t A_t) P_{t|[t-1]}, \\ C_{t|[t]}^T &= (I_n - K_t A_t) C_{t|[t-1]}^T, \\ Q_{t|[t]} &= Q_{t|[t-1]} - G_t A_t C_{t|[t-1]}^T \end{aligned} \tag{38}$$

with the gain matrices $G_t = C_{t|[t-1]} A_t^T Q_{v_t v_t}^{-1}$ and $K_t = P_{t|[t-1]} A_t^T Q_{v_t v_t}^{-1}$. This shows that the P- and C-matrices are not impacted by the error-estimation variance matrices Q. In particular note, that neither the estimation gain matrix G_t, nor the prediction gain matrix K_t, depend on the initial uncertainty $\mathsf{D}(\underline{x}_1) = Q_{x_1x_1}$. This implies that the numerical sampling outcome of the BLUE-BLUP recursion is invariant for changes in $Q_{x_1x_1}$. This variance matrix, and therefore also $Q_{x_0x_0}$ and S_1, are thus not needed for computing the BLUE-BLUP outcomes $\hat{x}_{t|[t]}$ and $\check{x}_{t|[t]}$. The only role played by $Q_{x_1x_1}$ lies in describing how the uncertainty of $\underline{x}_1$ contributes to the uncertainty of the estimators at various time instances.

4 Relation to the Kalman filter

In this section we show how the BLUE-BLUP recursion specializes to that of the Kalman-filter in case the state-vector means are known.

4.1 From BLUE-BLUP to the BLP recursion

Let the mean $\mathsf{E}(\underline{x}_0) = x_0$ (cf. (7)) be known. Then $\mathsf{E}(\underline{x}_t) = x_t$ is known for all times, since $x_i = \Phi_{i,i-1}x_{i-1},\ i = 1, 2, \ldots, t$. With all state-vector means known, the need for estimation disappears and the mean squared error of prediction can be improved. Hence, the BLP can now take over from the BLUE-BLUP. The BLP of $\underline{x}_t$, when based on $\underline{y}_1, \ldots, \underline{y}_\tau$, is denoted as $\underline{\check{x}}^K_{t|[\tau]}$ and its error variance matrix is denoted as $P^K_{t|[\tau]}$.

Lemma 3 (BLUE-BLUP and BLP) *In the presence of data, the BLP $\underline{\check{x}}^K_{t|[\tau]}$ and its error variance matrix $P^K_{t|[\tau]}$ can be expressed in the BLUE $\underline{\hat{x}}_{t|\tau}$ and BLUP $\underline{\check{x}}_{t|\tau}$, and their error variance matrices $P_{t|\tau}$ and $Q_{t|\tau}$, as*

$$\begin{aligned} &(i)\ \ \underline{\check{x}}^K_{t|[\tau]} = \underline{\check{x}}_{t|[\tau]} + C^T_{t|[\tau]}Q^{-1}_{t|[\tau]}(x_t - \underline{\hat{x}}_{t|[\tau]}) \\ &(ii)\ P^K_{t|[\tau]} = P_{t|[\tau]} - C^T_{t|[\tau]}Q^{-1}_{t|[\tau]}C_{t|[\tau]} \end{aligned} \tag{39}$$

In the absence of data, the BLP of $\underline{x}_t$ is given as $\underline{\check{x}}^K_{t|[0]} = x_t$, with error variance matrix $P^K_{t|[0]} = Q_{x_t x_t}$.

Proof We first prove (i). With the mean $\mathsf{E}(\underline{x}_t) = x_t$ known, the misclosure vector $\underline{v}_{[\tau]}$ extends to $\underline{v}'_{[\tau]} = [\underline{v}^T_{[\tau]}, (x_t - \underline{\hat{x}}_{t|[\tau]})^T]^T$. Note, since $\mathsf{C}(\underline{v}_{[\tau]}, \underline{\hat{x}}_{t|[\tau]}) = 0$, that the variance matrix of $\underline{v}'_{[\tau]}$ is blockdiagional. To determine the MMSE-predictor $\underline{\check{x}}^K_{t|[\tau]}$, we apply Theorem 1. Accordingly, using $\mathscr{G}(\underline{y}_{[\tau]}) \mapsto \underline{\check{x}}_{t|[\tau]}$ as the linear unbiased statistic, we get

$$\begin{aligned} \underline{\check{x}}^K_{t|[\tau]} &= \underline{\check{x}}_{t|[\tau]} + \mathsf{C}(\underline{x}_t - \underline{\check{x}}_{t|[\tau]}, \underline{v}'_{[\tau]})Q^{-1}_{\underline{v}'_{[\tau]}\underline{v}'_{[\tau]}}\underline{v}'_{[\tau]} \\ &= \underline{\check{x}}_{t|[\tau]} + \mathsf{C}(\underline{x}_t - \underline{\check{x}}_{t|[\tau]}, x_t - \underline{\hat{x}}_{t|[\tau]})Q^{-1}_{t|[\tau]}(x_t - \underline{\hat{x}}_{t|[\tau]}) \end{aligned} \tag{40}$$

since $Q_{\underline{v}'_{[\tau]}\underline{v}'_{[\tau]}}$ is blockdiagonal and $\mathsf{C}(\underline{x}_t - \underline{\check{x}}_{t|[\tau]}, \underline{v}_{[\tau]}) = 0$. The result (i) now follows, since $C_{t|[\tau]} = \mathsf{C}(x_t - \underline{\hat{x}}_{t|[\tau]}, \underline{x}_t - \underline{\check{x}}_{t|[\tau]})$ by definition.

To prove (ii), recall that the MMSE prediction error is uncorrelated with the misclosure vector (cf. Theorem 1). Hence, the prediction error of $\underline{\check{x}}^K_{t|[\tau]}$ is uncorrelated with $\underline{v}'_{[\tau]}$ and thus also with $x_t - \underline{\hat{x}}_{t|[\tau]}$. With $\mathsf{C}(\underline{x}_t - \underline{\check{x}}^K_{t|[\tau]}, x_t - \underline{\hat{x}}_{t|[\tau]}) = 0$ and (i), the variance matrix of $\underline{x}_t - \underline{\check{x}}^K_{t|[\tau]}$ follows as given in (ii). □

This lemma shows how the BLP can be obtained from the BLUE, the BLUP and the known state-vector mean x_t. This is illustrated in the block diagram given in Fig. 1 (b). As the BLP makes use of the known mean x_t, it is a better predictor than the BLUP, i.e. $P^K_{t|[\tau]} \leq P_{t|[\tau]}$ (cf. (39)). Also note that the BLP prediction error is uncorrelated with the BLUE estimation error, i.e. $\mathsf{C}(\underline{x}_t - \underline{\check{x}}^K_{t|[\tau]}, x_t - \underline{\hat{x}}_{t|[\tau]}) = 0$.

We now use the above lemma to determine the recursive form of the BLP $\underline{\check{x}}^K_{t|[\tau]}$, thus giving the Kalman filter. This will also show how the Kalman gain matrix K^K_t is formed from the gain matrices K_t, G_t and M_t (cf. Fig. 1).

Lemma 4 (The Kalman Filter) *The three steps of the BLP recursion are given as follows.*

Initialization:

$$\begin{aligned} \check{x}^K_{0|0} &= \mathsf{E}(\underline{x}_0) = x_0, \\ P^K_{0|0} &= \mathsf{D}(\underline{x}_0 - \check{x}^K_{0|0}) = Q_{x_0 x_0} \end{aligned} \tag{41}$$

Time-update:

$$\begin{aligned} \underline{\check{x}}^K_{t|[t-1]} &= \Phi_{t,t-1}\underline{\check{x}}^K_{t-1|[t-1]} \\ P^K_{t|[t-1]} &= \Phi_{t,t-1}P^K_{t-1|[t-1]}\Phi^T_{t,t-1} + S_t \end{aligned} \tag{42}$$

Measurement-update:

$$\begin{aligned} \underline{\check{x}}^K_{t|[t]} &= \underline{\check{x}}^K_{t|[t-1]} + K^K_t \underline{v}^K_t \\ P^K_{t|[t]} &= (I_n - K^K_t A_t)P^K_{t|[t-1]} \end{aligned} \tag{43}$$

with $\underline{v}^K_t = \underline{y}_t - A_t\underline{\check{x}}^K_{t|[t-1]}$, $Q_{v^K_t v^K_t} = R_t + A_t P^K_{t|[t-1]}A^T_t$, *and Kalman gain matrix*

$$\begin{aligned} K^K_t &= K_t - M_t G_t \\ &= P^K_{t|[t-1]}A^T_t Q^{-1}_{v^K_t v^K_t} \end{aligned} \tag{44}$$

Proof As the mean x_0 is known, the best predictor of $\underline{x}_0$ in the absence of data is the mean. Hence, the initialization is given as in (41). To prove the time-update (42), first note that

$$\begin{aligned} \underline{\check{x}}_{t|[t-1]} &= \Phi_{t,t-1}\underline{\check{x}}_{t-1|[t-1]} \\ (x_t - \underline{\hat{x}}_{t|[t-1]}) &= \Phi_{t,t-1}(x_{t-1} - \underline{\hat{x}}_{t-1|[t-1]}) \\ C^T_{t|[t-1]}Q^{-1}_{t|[t-1]} &= \Phi_{t,t-1}(C^T_{t-1|[t-1]}Q^{-1}_{t-1|[t-1]})\Phi^{-1}_{t,t-1} \end{aligned} \tag{45}$$

where the last equation follows from (37). Substitution of (45) into the expression of (39) for $\tau = t-1$, gives $\underline{\check{x}}^K_{t,|[t-1]} = \Phi_{t,t-1}[\underline{\check{x}}_{t-1|[t-1]} + C^T_{t-1|[t-1]}Q^{-1}_{t-1|[t-1]}(x_{t-1} - \underline{\hat{x}}_{t-1|[t-1]})] = \Phi_{t,t-1}\underline{\check{x}}^K_{t-1|[t-1]}$, and thus the time-update (42). To prove (43), we first substitute $\underline{\check{x}}_{t|[t]} = \underline{\check{x}}_{t|[t-1]} + K_t\underline{v}_t$, $\underline{\hat{x}}_{t|[t]} = \underline{\hat{x}}_{t|[t-1]} + G_t\underline{v}_t$, and $M_t = C^T_{t|[t]}Q^{-1}_{t|[t]}$ into $\underline{\check{x}}^K_{t|[t]} = \underline{\check{x}}_{t|[t]} + C^T_{t|[t]}Q^{-1}_{t|[t]}(x_t - \underline{\hat{x}}_{t|[t]})$ (cf. (39) for $\tau = t$). This gives

$$\underline{\check{x}}^K_{t|[t]} = \underline{\check{x}}_{t|[t-1]} + (K_t - M_t G_t)\underline{v}_t + C^T_{t|[t]}Q^{-1}_{t|[t]}(x_t - \underline{\hat{x}}_{t|[t-1]}) \tag{46}$$

From the last two expressions of (38) follows

$$C^T_{t|[t]}Q^{-1}_{t|[t]} = [I_n - (K_t - M_tG_t)A_t]C^T_{t|[t-1]}Q^{-1}_{t|[t-1]} \tag{47}$$

Substitution into (46) gives, with (39) for $\tau = t - 1$,

$$\underset{\sim}{\check{x}}^K_{t|[t]} = \underset{\sim}{\check{x}}^K_{t|[t-1]} + (K_t - M_tG_t)[\underline{v}_t - A_t(\underset{\sim}{\check{x}}^K_{t|[t-1]} - \underset{\sim}{\check{x}}_{t|[t-1]})] \tag{48}$$

from which the measurement update (43), with gain matrix (44), follows. □

Apart from the initialization, the recursive structure of the Kalman filter is the same as that of the BLUE-BLUP recursion. The initialization is different as the Kalman filter assumes the state-vector means known. The estimation of the mean $\mathsf{E}(\underline{x}_t) = x_t$ is therefore not needed and the initialization can start with the known mean $\mathsf{E}(\underline{x}_0) = x_0$. As a consequence, the initial uncertainty needs to be specified through $Q_{x_0x_0}$ (cf. (41)), which takes the role of the error variance matrix $P^K_{0|0}$. The BLUE-BLUP initialization however, does not require this variance matrix. As shown earlier, the BLUE-BLUP outcomes, $\hat{x}_{t|[t]}$ and $\check{x}_{t|[t]}$, do not depend on $Q_{x_0x_0}$. Hence, with the BLUE-BLUP recursion, the same results are obtained, irrespective of the choice made for this variance matrix. This is in marked contrast to the Kalman filter where the results are affected by $P^K_{0|0} = Q_{x_0x_0}$.

5 Conclusion

In this contribution we introduced a new recursive filter that does away with the need to have the state vector means of a dynamic system known. The recursive filter enables the joint linear MMSE prediction and estimation of the random state vectors and their unknown means, respectively (cf. Fig. 1). We discussed the role of the system noise and of the estimation-error variance matrix in the joint prediction and estimation of the filter. We showed how the filter specialize to the Kalman-filter in case the state-vector means are known and determined the relation between their respective error variance matrices and gain matrices. We also discussed the fundamentally different roles played by the intitialization of the two filters. In particular, it was shown that for the new filter the initial variance-matrix $Q_{x_0x_0}$ need not be known, this in contrast to the Kalman-filter.

References

Acharya, R., Roy, B., Sivaraman, M., Dasgupta, A.: Estimation of equatorial electrojet from total electron content at geomagnetic equator using Kalman filter. Adv. Space Res. **47**(6), 938–944 (2011)

Anderson, B.D.O., Moore, J.B.: Optimal Filtering, vol. 11. Prentice-hall Englewood Cliffs, New Jersey (1979)

Bar-Shalom, Y., Li, X.: Estimation and Tracking-Principles, Techniques, and Software. Artech House Inc, Norwood (1993)

Bertino, L., Evensen, G., Wackernagel, H.: Combining geostatistics and Kalman filtering for data assimilation in an estuarine system. Inverse Probl. **18**(1), 1 (2002)

Brammer, K., Siffling, G.: Kalman-Bucy Filters. Artech Hous, Norwood (1989)

Candy, J.: Signal Processing: Model Based Approach. McGraw-Hill Inc, New York (1986)
Cao, Y., Chen, Y., Li, P.: Wet refractivity tomography with an improved Kalman-filter method. Adv. Atmos. Sci. **23**, 693–699 (2006)
Christensen R (2001) Advanced Linear Modeling: Multivariate, Time Series, and Spatial Data; Nonparametric Regression and Response Surface Maximization, 2nd edn. Springer, Heidelberg
Ferraresi, M., Todini, E., Vignoli, R.: A solution to the inverse problem in groundwater hydrology based on Kalman filtering. J. Hydrol. **175**(1), 567–581 (1996)
Gelb, A.: Applied Optimal Estimation. MIT Press, Cambridge (1974)
Gibbs, B.: Advanced Kalman Filtering, Least-squares and Modeling. A Practical Handbook. Wiley, New York (2011)
Goldberger, A.: Best linear unbiased prediction in the generalized linear regression model. J. Am. Stat. Assoc. **57**(298), 369–375 (1962)
Grafarend, E.W.: Geodetic applications of stochastic processes. Phys. Earth Planet. Inter. **12**(2), 151–179 (1976)
Grafarend, E.W., Rapp, R.H.: Advances in Geodesy: selected papers from reviews of Geophysics and Space Physics. American Geophysical Union 1, Washington DC (1984)
Grewal, M.S., Andrews, A.P.: Kalman Filtering; Theory and Practice Using MATLAB, 3rd edn. Wiley, New York (2008)
Gross, R.S., Eubanks, T.M., Steppe, J.A., Freedman, A.P., Dickey, J.O., Runge, T.F.: A Kalman-filter-based approach to combining independent Earth-orientation series. J. Geod. **72**(4), 215–235 (1998)
Herring, T.A., Davis, J.L., Shapiro, I.I.: Geodesy by radio interferometry: the application of Kalman filtering to the analysis of very long baseline interferometry data. J. Geophys. Res (1978–2012) **95**(B8), 12561–12581 (1990)
Ince, C.D., Sahin, M.: Real-time deformation monitoring with GPS and Kalman Filter. Earth Planets Space **52**(10), 837–840 (2000)
Jazwinski, A.: Stochastic Processes and Filtering Theory. Dover Publications, New York (1991)
Kailath, T.: A view of three decades of linear filtering theory. IEEE Trans. Inf. Theory **20**(2), 146–181 (1974)
Kailath, T.: Lectures on Wiener and Kalman Filtering, p. 140. Springer, Heidelberg (1981)
Kailath, T., Sayed, A.H., Hassibi, B.: Linear Estimation. Prentice-Hall, New Jersey (2000)
Kalman, R.E.: A new approach to linear filtering and prediction problems. J. Basic Eng. **82**(1), 35–45 (1960)
Marx, B.A., Potthast, R.W.E.: On instabilities in data assimilation algorithms. GEM-Int. J. Geomath. **3**(2), 253–278 (2012)
Maybeck, P.: Stochastic Models, Estimation, and Control, vol. 1, Academic Press, Massachusetts (1979)
Sanso, F.: The minimum mean square estimation error principle in physical geodesy (stochastic and non-stochastic interpretation). Boll. Geod. Sci. Affi. **39**(2), 112–129 (1980)
Sanso, F.: Statistical methods in physical geodesy. In: Sunkel, H. (ed.) Mathematical and Numerical Techniques in Physical Geodesy. Lecture Notes in Earth Sciences, vol. 7, pp. 49–155. Springer, Berlin (1986)
Simon, D.: Optimal state estimation: Kalman, H (infinity) and Nonlinear Approaches. Wiley, Hoboken (2006)
Sorenson, H.W.: Kalman filtering techniques. In: Leondes, C.T., (ed.) Advances in Control Systems Theory and Applications, **3**, 219–292 (1966)
Stark, H., Woods, J.: Probability, Random Processes, and Estimation Theory for Engineers. Prentice-Hall Englewood Cliffs, New Jersey (1986)
Teunissen, P.J.G.: Best prediction in linear models with mixed integer/real unknowns: theory and application. J. Geod. **81**(12), 759–780 (2007)
Teunissen, P.J.G., Khodabandeh, A.: BLUE, BLUP and the Kalman filter: some new results. J. Geod. **87**(5), 1–13 (2013)

REFRENCES

Allison T (1991) Multi-observable processing techniques for precise relative positioning. In: Proceedings ION GPS-91. Albuquerque, New Mexico, 11–13 September, pp 715–725

Anderson BDO, Moore JB (1979) Optimal filtering, vol 11. Prentice hall, Englewood Cliffs

Ansley CF, Kohn R (1985) Estimation, filtering, and smoothing in state space models with incompletely specified initial conditions. Ann Stat 13(4):1286–1316

Baarda W (1973) S-transformations and criterion matrices. Tech. rep., Netherlands Geodetic Commission, Publ. on Geodesy, NewSeries, vol 5(1), Delft

Bar-Shalom Y, Li X (1993) Estimation and tracking—principles, techniques, and software. Artech House, Inc., Norwood

Bertiger W, Desai SD, Haines B, Harvey N, Moore AW, Owen S,Weiss JP (2010) Single receiver phase ambiguity resolution with GPS data. J Geod 84(5):327–337

Beutler G, Bock H, Dach R, Fridez P, Gade A, Hugentobler U, Jaggi A, Meindl M, Mervart L, Prange L, Schaer S, Springer T, Urschl P, Walser P (2007) Bernese GPS software version 5.0. Astron. Inst., Univ. of Bern, Bern, Switzerland

Bisnath S, Collins P (2012) Recent developments in precise point positioning. Geomatica 66(2):103–111

Bisnath S, Gao Y (2008) Current state of precise point positioning and future prospects and limitations. In: Observing our changing earth, IAG Symp 133:615–623

Blewitt G (1989) Carrier phase ambiguity resolution for the Global Positioning System applied to geodetic baselines up to 2000 km. Journal of Geophysical Research, 94(B8).

Bode H, Shannon C (1950) A simplified derivation of linear least square smoothing and prediction theory. Proc IRE 38(4):417–425

Brammer K, Siffling G (1989) Kalman-Bucy filters. Artech House, Norwood

Candy J (1986) Signal processing: model based approach. McGraw-Hill, Inc, New York

Collins P (2008) Isolating and estimating undifferenced GPS integer ambiguities. In: Proceedings ION NTM, pp 720–732

Collins P, Lahaye F, Heroux P, Bisnath S (2008) Precise point positioning with ambiguity resolution using the decoupled clock model. In: Proceedings of the 21st international technical meeting of the satellite division of the Institute of Navigation (ION GNSS 2008), pp 1315–1322

de Jong P (1991) The diffuse Kalman filter. Ann Stat 19(2):1073–1083

de Jonge PJ (1998) A processing strategy for the application of the GPS in networks. PhD thesis, Delft University of Technology, Publication on Geodesy, 46, Netherlands Geodetic Commission, Delft

Frei E, and Beutler G (1990) Rapid Static Positioning Based on the Fast Ambiguity Resolution Approach FARA: Theory and First Results. Manuscripta Geodaetica, 15(6).

Ge M, Gendt G, Rothacher M, Shi C, Liu J (2008) Resolution of GPS carrier-phase ambiguities in precise point positioning (PPP) with daily observations. J Geod 82(7):389–399

Gelb A (1974) Applied optimal estimation. MIT Press, Cambridge

Geng J (2011) Rapid integer ambiguity resolution in GPS precise point positioning. PhD thesis, University of Nottingham, UK

Geng J, Bock Y (2013) Triple-frequency GPS precise point positioning with rapid ambiguity resolution. J Geod 87(5):449–460
Geng J, Meng X, Dodson A, Teferle F (2010) Integer ambiguity resolution in precise point positioning: method comparison. J Geod 84(9):569–581

Geng J, Teferle FN, Meng X, Dodson AH (2011) Towards PPP-RTK: ambiguity resolution in real-time precise point positioning. Adv Space Res 47(10):1664–1673

Geng J, Shi C, Ge M, Dodson AH, Lou Y, Zhao Q, Liu J (2012) Improving the estimation of fractional-cycle biases for ambiguity resolution in precise point positioning. J Geod 86(8):579–589

Gibbs B (2011) Advanced Kalman filtering, least-squares and modeling: a practical handbook. Wiley, New York

Goldberger A (1962) Best linear unbiased prediction in the generalized linear regression model. J Am Stat Assoc 57(298):369–375

Grafarend, EW (1976) Geodetic applications of stochastic processes. Phys. Earth Planet. Inter. **12**(2), 151–179

Grafarend, EW, Rapp, RH (1984) Advances in Geodesy: selected papers from reviews of Geophysics and Space Physics. American Geophysical Union 1, Washington DC

Grejner-Brzezinska DA, Wielgosz P, Kashani I, Smith DA, Spencer PS, Robertson DS, Mader GL, et al (2004) An analysis of the effects of different network-based ionosphere estimation models on rover positioning accuracy. J GPS 3(1-2):115–131

Grejner-Brzezinska DA, Kashani I, Wielgosz P, Smith DA, Spencer PS, Robertson DS, Mader GL (2007) Efficiency and reliability of ambiguity resolution in network-based real-time kinematic GPS. J Surv Eng 133(2):56–65

Grewal MS, Andrews AP (2008) Kalman filtering: theory and practice using MATLAB, 3rd edn. Wiley, New York

Harvey AC, Phillips GDA (1979) Maximum likelihood estimation of regression models with autoregressive-moving average disturbances. Biometrika 66(1):49–58

Henkel P, Wen Z and Gunther C (2010) Estimation of satellite, receiver biases on multiple Galileo frequencies with a Kalman filter. ION Proc. 2010 Int. Technical Meeting of The Institute of Navigation, CA (Portland, Sept. 2010)

Heroux P, Kouba J (1995) GPS precise point positioning with a difference. In: Paper presented at Geomatics 95, Ottawa, Ontario, Canada, 13-15 June

Hernandez-Pajares M, Juan JM, Sanz J, Colombo OL (2000) Application of ionospheric tomography to real-time GPS carrier-phase ambiguities resolution, at scales of 400–1,000 km and with high geomagnetic activity. Geophys Res Lett 27(13):2009–2012

Heroux P and Kouba J (1995) GPS precise point positioning with a difference. Geomatics 95 *(*Ottawa, June 1995*)* pp 13–5

Hofmann-Wellenhof B, Lichtenegger H,Wasle E (2008) GNSS: global navigation satellite systems: GPS, Glonass, Galileo, and more. Springer, New York

Jazwinski A (1991) Stochastic processes and filtering theory. Dover Publications, New York

Jonkman N, Teunissen P, Joosten P, Odijk D (2000) GNSS long baseline ambiguity resolution: impact of a third navigation frequency. In: Geodesy Beyond 2000, IAG Symp 121, pp 349–354

Kailath T (1968) An innovations approach to least-squares estimation— part I: Linear filtering in additive white noise. IEEE Trans Autom Control 13(6):646–655

Kailath T (1981) Lectures on Wiener and Kalman filtering. Springer, Berlin

KailathT, Sayed AH, Hassibi B (2000) Linear estimation. Prentice-Hall, Englewood Cliffs

Kalman RE (1960) A new approach to linear filtering and prediction problems. J Basic Eng 82(1):35–45

Khodabandeh A (2014) Array-aided single-differenced satellite phase bias determination: methodology and results. ION GNSS+, 27:2523–2532. The Institute of Navigation, Florida, USA.

Khodabandeh A and Teunissen PJG (2014a) Array-based satellite phase bias sensing: theory and GPS/BeiDou/QZSS results. Meas. Sci. Technol., 25,095801 (11pp). UK.

Khodabandeh A and Teunissen PJG (2014b) Single-epoch GNSS array integrity: an analytical study. IAG Symp 142, accepted for publication

Khodabandeh A and Teunissen PJG (2014c) A recursive linear MMSE filter for dynamic systems with unknown state vector means. International Journal on Geomathematics, 5:17–31, Springer.

Kouba J, Heroux P (2001) Precise point positioning using IGS orbit and clock products. GPS solut 5(2):12–28

Lannes A, Prieur JL (2013) Calibration of the clock-phase biases of GNSS networks: the closure-ambiguity approach. J Geod 87(8):709–731

Lannes A, Teunissen PJG (2011) GNSS algebraic structures. J Geod 85(5):273–290

Laurichesse D (2011) The CNES real-time PPP with undifferenced integer ambiguity resolution demonstrator. In: Proceedings of the ION GNSS, pp 654–662

Laurichesse D, Mercier F (2007) Integer ambiguity resolution on undifferenced GPS phase measurements and its application to PPP. In: Proceedings of the 20th international technical meeting of the satellite division of the Institute of Navigation (ION GNSS 2007), pp 839–848

Laurichesse D, Mercier F, Berthias J, Broca P, Cerri L, CNES F (2009) Integer ambiguity resolution on undifferenced GPS phase measurements and its application to PPP and satellite precise orbit determination. Navigation 56(2):135–149

Leandro RF, Santos MC and Langley RB (2011) Analyzing GNSS data in precise point positioning software. GPS Solutions **15** 1–3

Li B, Shen Y, Feng Y, Gao W, Yang L (2014) GNSS ambiguity resolution with controllable failure rate for long baseline network RTK. J Geod 88(2):99–112

Li T, Wang J, Laurichesse D (2013a) Modeling and quality control for reliable precise point positioning integer ambiguity resolution with GNSS modernization. GPS Solut, pp 1–14

Li X, Ge M, Zhang H, Wickert J (2013b) A method for improving uncalibrated phase delay estimation and ambiguity-fixing in realtime precise point positioning. J Geod 87(5):405–416

Li X, Ge M, Lu C, Zhang Y, Wang R, Wickert J, Schuh H (2014) High-rate GPS seismology using real-time precise point positioning with ambiguity resolution. Geoscience and remote sensing, IEEE transactions on, pp 1–15. doi:10.1109/TGRS.2013.2295373

Loyer S, Perosanz F, Mercier F, Capdeville H, Marty JC (2012) Zero-difference GPS ambiguity resolution at CNES-CLS IGS analysis center. J Geod 86(11):991–1003

Maybeck P (1979) Stochastic models, estimation, and control, vol 1. Academic Press, Waltham, republished 1994

Mervart L, Lukes Z, Rocken C, Iwabuchi T (2008) Precise point positioning with ambiguity resolution in real-time. In: Proceedings of ION GNSS, pp 397–405

Mervart L, Rocken C, Iwabuchi T, Lukes Z, Kanzaki M (2013) Precise point positioning with fast ambiguity resolution-prerequisites, algorithms and performance. In: Proceedings of ION GNSS, pp 1176–1185

Odijk D (2002) Fast precise GPS positioning in the presence of ionospheric delays. Ph.D. thesis, Delft University of Technology, Publication on Geodesy, 52, Netherlands, Geodetic Commission, Delft

Odijk D, Teunissen PJG (2008) ADOP in closed form for a hierarchy of multi-frequency single-baseline GNSSmodels. J Geod 82(8):473–492

Odijk D, Teunissen PJG, Zhang B (2012) Single-frequency integer ambiguity resolution enabled GPS precise point positioning. J Survey Eng 138(4):193–202

Odijk D, Teunissen PJG and Khodabandeh A (2013) Galileo IOV RTK positioning: standalone and combined with GPS. Survey Review, Maney Publishing. UK.

Odijk D, Arora BS, Teunissen PJG (2014a) Predicting the success rate of long-baseline GPS + Galileo (partial) ambiguity resolution. J Navigation 1–17. doi:10.1017/S037346331400006X

Odijk D, Teunissen PJG, Khodabandeh A (2014b) Single-frequency PPP-RTK: theory and experimental results. IAG Symp Earth Edge: Sci Sustain Planet 139:571 578

Rao CR (1973) Linear statistical inference and its applications, vol 2. Wiley, New Jersey

Sanso F (1986) Statistical methods in physical geodesy. In: Sunkel H (ed) Mathematical and numerical techniques in physical geodesy. Lecture notes in earth sciences, vol 7. Springer, Berlin, pp 49–155

Shi J (2012) Precise point positioning integer ambiguity resolution with decoupled clocks. PhD thesis, University of Calgary, Canada Shi J, Gao Y (2013) A comparison of three PPP integer ambiguity resolution methods. GPS Solut (published online)

Simon D (2006) Optimal state estimation: Kalman, H [infinity] and nonlinear approaches. Wiley, New York

Sorenson HW (1966) Kalman filtering techniques. In: Leondes CT (ed) Advances in control systems: theory and applications, vol 3. pp 219–292

Stark H, Woods J (1986) Probability, random processes, and estimation theory for engineers. Prentice-Hall, Englewood Cliffs

Schaer S (1999) Mapping and predicting the Earths ionosphere using the Global Positioning System. PhD thesis, University of Bern, Bern, Switzerland

Teunissen PJG (1985) Generalized inverses, adjustment, the datum problem and S-transformations. In: Grafarend EW, Sanso F (eds) Optimization and design of geodetic networks. Springer, Berlin

Teunissen PJG (1993) Least-Squares Estimation of the Integer GPS ambiguities. Invited Lecture, Section IV Theory and Methodology, IAG General Meeting, Beijing, China, August.

Teunissen PJG (1995) The least-squares ambiguity decorrelation adjustment: a method for fast GPS integer ambiguity estimation. J Geod 70(1–2):65–82

Teunissen PJG (1997a) A canonical theory for shortGPS baselines. Part I: the baseline precision. J Geod 71(6):320–336

Teunissen PJG (1997b) A canonical theory for short GPS baselines. Part IV: precision versus reliability. J Geod 71(9):513–525

Teunissen PJG (1997c) The geometry-free GPS ambiguity search space with a weighted ionosphere. J Geod 71(6):370–383

Teunissen PJG (1997d) On the GPS widelane and its decorrelating property. J Geod 71(9):577–587

Teunissen PJG (1998) Success probability of integer GPS ambiguity rounding and bootstrapping. J Geod 72(10):606–612

Teunissen PJG, Kleusberg A (1998) GPS for geodesy, 2nd edn. Springer, Berlin

Teunissen PJG (1999) An optimality property of the integer least-squares estimator. J Geod 73(11):587–593

Teunissen PJG (2000) Adjustment theory: an introduction. Delft University Press, series on Mathematical Geodesy and Positioning

Teunissen PJG (2000) Testing theory: an introduction. Delft University Press, series on Mathematical Geodesy and Positioning

Teunissen PJG (2002) The parameter distributions of the integer GPS model. J Geod 76(1):41–48

Teunissen PJG (2007) Best prediction in linear models with mixed integer/real unknowns: theory and application. J Geod 81(12):759–780

Teunissen PJG (2008) On a stronger-than-best property for best prediction. J Geod 82(3):167–175

Teunissen PJG (2012) A-PPP: array-aided precise point positioning with global navigation satellite systems. Signal Process IEEE Trans 60(6):2870–2881

Teunissen PJG, de Bakker PF (2012) Single-receiver single-channel multi-frequency GNSS integrity: outliers, slips, and ionospheric disturbances. J Geod 1–17

Teunissen PJG, Khodabandeh A (2013) BLUE, BLUP and the Kalman filter: some new results. J Geod 87(5):461–473

Teunissen PJG, Odijk D, Zhang B (2010) PPP-RTK: results of CORS network-based PPP with integer ambiguity resolution. J Aeronaut, Astronaut Aviat 42(4):223–229

Teunissen PJG and Khodabandeh A (2014a) Review and Principles of PPP-RTK Methods. J Geod, Springer, doi: 10.1007/s00190-014-0771-3.

Teunissen PJG and Khodabandeh A (2014b) Do GNSS parameters always benefit from integer ambiguity resolution? a PPP-RTK Network Scenario. ION GNSS+, 27:590–600. The Institute of Navigation, Florida, USA.

Tienstra J (1956) Theory of the adjustment of normally distributed observation. Argus, Amsterdam

van Bree RJ and Tiberius CC (2012) Real-time single-frequency precise point positioning: accuracy assessment. GPS Solutions **16** 259–66

van der Marel, H. (1998). Virtual GPS reference stations in the Netherlands, Proceedings of the 11th International Technical Meeting of the Satellite Division of the Institute of Navigation, ION GPS-1998, Nashville, USA, September 15-18, 49-58.

Verhagen S (2002) Studying the Performance of Global Navigation Satellite Systems: a New Software Tool. GPS world 13(6):60–65

Wielgosz P, Krankowski A, Sieradzki R, Grejner-Brzezinska DA (2008) Application of predictive regional ionosphere model to medium range RTK positioning. Acta Geophysica 56(4):1147– 1161

Wielgosz P, Cellmer S, Rzepecka Z, Paziewski J and Grejner-Brzezinska D (2011) Troposphere modeling for precise GPS rapid static positioning in mountainous areas. Meas. Sci. Technol. **22** 045101

Wubbena G (1989) The GPS adjustment software package-GEONAP-concepts and models. In: International geodetic symposium on satellite positioning l, Las Cruces, New Mexico, 13–17 March, pp 452–461

Wubbena G, Schmitz M, Bagg A (2005) PPP-RTK: precise point positioning using state-space representation in RTK networks. In: Proceedings of ION GNSS, pp 13–16

Zadeh LA, Ragazzini JR (1950) An extension of Wiener's theory of prediction. J Appl Phys 21(7):645–655

Zhang B, Teunissen PJG, Odijk D (2011) A novel un-differenced PPPRTK concept. J Navig 64(S1):S180–S191

Zhang X, Li P (2013) Assessment of correct fixing rate for precise point positioning ambiguity resolution on a global scale. J Geod 87(6):579–589

Zumberge JF,Heflin MB, Jefferson DC,Watkins MM,Webb FH (1997) Precise point positioning for the efficient and robust analysis of GPS data from large networks. J Geophys Res 102:5005–5017

APPENDIX A COPYRIGHT PERMISSION STATEMENTS

I warrant that I have obtained, where necessary, permission from the copyright owners to use any third-party copyright material reproduced in this thesis, or to use any of my own published work (e.g. journal articles) in which the copyright is held by another party (e.g. publisher, co-author). These permissions are all attached below

Amir Khodabandeh

Permissions of the following **Springer** publications are attached in the forthcoming pages:

1) Teunissen P.J.G. and Khodabandeh A. (2014a). Review and Principles of PPP-RTK Methods. Journal of Geodesy, **Springer**, doi: 10.1007/s00190-014-0771-3.

2) Odijk D., Teunissen P.J.G. and Khodabandeh **A.** (2014). Single-frequency PPP-RTK: theory and experimental results. International Association of Geodesy Symposium (IAG), 139:167–173, **Springer**.

3) Teunissen P.J.G. and Khodabandeh A. (2013) BLUE, BLUP and the Kalman filter: some new results. Journal of Geodesy, 87(5):461–473, **Springer**.

4) Khodabandeh A. and Teunissen P.J.G. (2014c). A recursive linear MMSE filter for dynamic systems with unknown state vector means. International Journal on Geomathematics, 5:17–31, **Springer**.

5) Nadarajah N., Khodabandeh A. and Teunissen P.J.G. (2015). Assessing the IRNSS L5-signal in combination with GPS, Galileo, and QZSS L5/E5a-signals for positioning and navigation. GPS Solutions, **Springer**, doi: 10.1007/s10291-015-0450-8.

6) Khodabandeh A. and Teunissen P.J.G. (2014b). Single-Epoch GNSS Array Integrity: an Analytical Study. International Association of Geodesy Symposium (IAG), **Springer**, Accepted for publication.

7) Khodabandeh A. and Teunissen P.J.G. (2015). An Analytical Study of PPP-RTK Corrections: Precision, Correlation and User-Impact. Journal of Geodesy, doi: 10.1007/s00190-015-0838-9, **Springer**.

SPRINGER LICENSE
TERMS AND CONDITIONS

Jan 29, 2015

This is a License Agreement between Amir Khodabandeh ("You") and Springer ("Springer") provided by Copyright Clearance Center ("CCC"). The license consists of your order details, the terms and conditions provided by Springer, and the payment terms and conditions.

All payments must be made in full to CCC. For payment instructions, please see information listed at the bottom of this form.

License Number	3558020523121
License date	Jan 29, 2015
Licensed content publisher	Springer
Licensed content publication	Journal of Geodesy
Licensed content title	Review and principles of PPP-RTK methods
Licensed content author	P. J. G. Teunissen
Licensed content date	Jan 1, 2014
Type of Use	Book/Textbook
Requestor type	Publisher
Publisher	Not listed below
Portion	Full text
Format	Print and Electronic
Will you be translating?	No
Print run	20
Author of this Springer article	Yes and you are the sole author of the new work
Order reference number	None
Title of new book	Precise Multi-GNSS Point Positioning: Theory, Algorithm and Data Analysis
Author of new book	Amir Khodabandeh
Expected publication date of new book	Mar 2015
Estimated size of new book (pages)	100
Total	0.00 USD
Terms and Conditions	

Introduction

The publisher for this copyrighted material is Springer Science + Business Media. By clicking "accept" in connection with completing this licensing transaction, you agree that the following terms and conditions apply to this transaction (along with the Billing and Payment terms and conditions established by Copyright Clearance Center, Inc. ("CCC"), at the time that you opened your Rightslink account and that are available at any time at http://myaccount.copyright.com).

Warranties
Springer Science + Business Media makes no representations or warranties with respect to the licensed material.

Indemnity
You hereby indemnify and agree to hold harmless Springer Science + Business Media and CCC, and their respective officers, directors, employees and agents, from and against any and all claims arising out of your use of the licensed material other than as specifically authorized pursuant to this license.

No Transfer of License
This license is personal to you and may not be sublicensed, assigned, or transferred by you to any other person without Springer Science + Business Media's written permission.

No Amendment Except in Writing
This license may not be amended except in a writing signed by both parties (or, in the case of Springer Science + Business Media, by CCC on Springer Science + Business Media's behalf).

Objection to Contrary Terms
Springer Science + Business Media hereby objects to any terms contained in any purchase order, acknowledgment, check endorsement or other writing prepared by you, which terms are inconsistent with these terms and conditions or CCC's Billing and Payment terms and conditions. These terms and conditions, together with CCC's Billing and Payment terms and conditions (which are incorporated herein), comprise the entire agreement between you and Springer Science + Business Media (and CCC) concerning this licensing transaction. In the event of any conflict between your obligations established by these terms and conditions and those established by CCC's Billing and Payment terms and conditions, these terms and conditions shall control.

Jurisdiction
All disputes that may arise in connection with this present License, or the breach thereof, shall be settled exclusively by the country's law in which the work was originally published.

Other terms and conditions:

v1.3

SPRINGER LICENSE
TERMS AND CONDITIONS

Jan 28, 2015

This is a License Agreement between Amir Khodabandeh ("You") and Springer ("Springer") provided by Copyright Clearance Center ("CCC"). The license consists of your order details, the terms and conditions provided by Springer, and the payment terms and conditions.

All payments must be made in full to CCC. For payment instructions, please see information listed at the bottom of this form.

License Number	3557971461597
License date	Jan 28, 2015
Licensed content publisher	Springer
Licensed content publication	Springer eBook
Licensed content title	Single-Frequency PPP-RTK: Theory and Experimental Results
Licensed content author	Dennis Odijk
Licensed content date	Jan 1, 2014
Type of Use	Book/Textbook
Requestor type	Publisher
Publisher	Not listed below
Portion	Full text
Format	Print and Electronic
Will you be translating?	No
Print run	20
Author of this Springer article	Yes and you are the sole author of the new work
Order reference number	None
Title of new book	Precise Multi-GNSS Point Positioning: Theory, Algorithm and Data Analysis
Author of new book	Amir Khodabandeh
Expected publication date of new book	Mar 2015
Estimated size of new book (pages)	100
Total	0.00 USD
Terms and Conditions	

Introduction

The publisher for this copyrighted material is Springer Science + Business Media. By clicking "accept" in connection with completing this licensing transaction, you agree that the following terms and conditions apply to this transaction (along with the Billing and Payment terms and conditions established by Copyright Clearance Center, Inc. ("CCC"), at the time that you opened your Rightslink account and that are available at any time at http://myaccount.copyright.com).

Warranties
Springer Science + Business Media makes no representations or warranties with respect to the licensed material.

Indemnity
You hereby indemnify and agree to hold harmless Springer Science + Business Media and CCC, and their respective officers, directors, employees and agents, from and against any and all claims arising out of your use of the licensed material other than as specifically authorized pursuant to this license.

No Transfer of License
This license is personal to you and may not be sublicensed, assigned, or transferred by you to any other person without Springer Science + Business Media's written permission.

No Amendment Except in Writing
This license may not be amended except in a writing signed by both parties (or, in the case of Springer Science + Business Media, by CCC on Springer Science + Business Media's behalf).

Objection to Contrary Terms
Springer Science + Business Media hereby objects to any terms contained in any purchase order, acknowledgment, check endorsement or other writing prepared by you, which terms are inconsistent with these terms and conditions or CCC's Billing and Payment terms and conditions. These terms and conditions, together with CCC's Billing and Payment terms and conditions (which are incorporated herein), comprise the entire agreement between you and Springer Science + Business Media (and CCC) concerning this licensing transaction. In the event of any conflict between your obligations established by these terms and conditions and those established by CCC's Billing and Payment terms and conditions, these terms and conditions shall control.

Jurisdiction
All disputes that may arise in connection with this present License, or the breach thereof, shall be settled exclusively by the country's law in which the work was originally published.

Other terms and conditions:

v1.3

SPRINGER LICENSE
TERMS AND CONDITIONS

Jan 28, 2015

This is a License Agreement between Amir Khodabandeh ("You") and Springer ("Springer") provided by Copyright Clearance Center ("CCC"). The license consists of your order details, the terms and conditions provided by Springer, and the payment terms and conditions.

All payments must be made in full to CCC. For payment instructions, please see information listed at the bottom of this form.

License Number	3557970758490
License date	Jan 28, 2015
Licensed content publisher	Springer
Licensed content publication	Journal of Geodesy
Licensed content title	BLUE, BLUP and the Kalman filter: some new results
Licensed content author	P. J. G. Teunissen
Licensed content date	Jan 1, 2013
Volume number	87
Issue number	5
Type of Use	Book/Textbook
Requestor type	Publisher
Publisher	Not listed below
Portion	Full text
Format	Print and Electronic
Will you be translating?	No
Print run	20
Author of this Springer article	Yes and you are the sole author of the new work
Order reference number	None
Title of new book	Precise Multi-GNSS Point Positioning: Theory, Algorithm and Data Analysis
Author of new book	Amir Khodabandeh
Expected publication date of new book	Mar 2015
Estimated size of new book (pages)	100
Total	0.00 USD
Terms and Conditions	

Introduction

The publisher for this copyrighted material is Springer Science + Business Media. By clicking "accept" in connection with completing this licensing transaction, you agree that the following terms

"With kind permission from Springer Science+Business Media: <book/journal title, chapter/article title, volume, year of publication, page, name(s) of author(s), figure number(s), and any original (first) copyright notice displayed with material>."

Warranties
Springer Science + Business Media makes no representations or warranties with respect to the licensed material.

Indemnity
You hereby indemnify and agree to hold harmless Springer Science + Business Media and CCC, and their respective officers, directors, employees and agents, from and against any and all claims arising out of your use of the licensed material other than as specifically authorized pursuant to this license.

No Transfer of License
This license is personal to you and may not be sublicensed, assigned, or transferred by you to any other person without Springer Science + Business Media's written permission.

No Amendment Except in Writing
This license may not be amended except in a writing signed by both parties (or, in the case of Springer Science + Business Media, by CCC on Springer Science + Business Media's behalf).

Objection to Contrary Terms
Springer Science + Business Media hereby objects to any terms contained in any purchase order, acknowledgment, check endorsement or other writing prepared by you, which terms are inconsistent with these terms and conditions or CCC's Billing and Payment terms and conditions. These terms and conditions, together with CCC's Billing and Payment terms and conditions (which are incorporated herein), comprise the entire agreement between you and Springer Science + Business Media (and CCC) concerning this licensing transaction. In the event of any conflict between your obligations established by these terms and conditions and those established by CCC's Billing and Payment terms and conditions, these terms and conditions shall control.

Jurisdiction
All disputes that may arise in connection with this present License, or the breach thereof, shall be settled exclusively by the country's law in which the work was originally published.

Other terms and conditions:

v1.3

SPRINGER LICENSE
TERMS AND CONDITIONS

Jan 28, 2015

This is a License Agreement between Amir Khodabandeh ("You") and Springer ("Springer") provided by Copyright Clearance Center ("CCC"). The license consists of your order details, the terms and conditions provided by Springer, and the payment terms and conditions.

All payments must be made in full to CCC. For payment instructions, please see information listed at the bottom of this form.

License Number	3557960998218
License date	Jan 28, 2015
Licensed content publisher	Springer
Licensed content publication	GEM - International Journal on Geomathematics
Licensed content title	A recursive linear MMSE filter for dynamic systems with unknown state vector means
Licensed content author	Amir Khodabandeh
Licensed content date	Jan 1, 2014
Volume number	5
Issue number	1
Type of Use	Book/Textbook
Requestor type	Publisher
Publisher	Not listed below
Portion	Full text
Format	Print and Electronic
Will you be translating?	No
Print run	20
Author of this Springer article	Yes and you are the sole author of the new work
Order reference number	None
Title of new book	Precise Multi-GNSS Point Positioning: Theory, Algorithm and Data Analysis
Author of new book	Amir Khodabandeh
Expected publication date of new book	Mar 2015
Estimated size of new book (pages)	100
Total	0.00 USD
Terms and Conditions	

Introduction

The publisher for this copyrighted material is Springer Science + Business Media. By clicking "accept" in connection with completing this licensing transaction, you agree that the following terms

"With kind permission from Springer Science+Business Media: <book/journal title, chapter/article title, volume, year of publication, page, name(s) of author(s), figure number(s), and any original (first) copyright notice displayed with material>."

Warranties
Springer Science + Business Media makes no representations or warranties with respect to the licensed material.

Indemnity
You hereby indemnify and agree to hold harmless Springer Science + Business Media and CCC, and their respective officers, directors, employees and agents, from and against any and all claims arising out of your use of the licensed material other than as specifically authorized pursuant to this license.

No Transfer of License
This license is personal to you and may not be sublicensed, assigned, or transferred by you to any other person without Springer Science + Business Media's written permission.

No Amendment Except in Writing
This license may not be amended except in a writing signed by both parties (or, in the case of Springer Science + Business Media, by CCC on Springer Science + Business Media's behalf).

Objection to Contrary Terms
Springer Science + Business Media hereby objects to any terms contained in any purchase order, acknowledgment, check endorsement or other writing prepared by you, which terms are inconsistent with these terms and conditions or CCC's Billing and Payment terms and conditions. These terms and conditions, together with CCC's Billing and Payment terms and conditions (which are incorporated herein), comprise the entire agreement between you and Springer Science + Business Media (and CCC) concerning this licensing transaction. In the event of any conflict between your obligations established by these terms and conditions and those established by CCC's Billing and Payment terms and conditions, these terms and conditions shall control.

Jurisdiction
All disputes that may arise in connection with this present License, or the breach thereof, shall be settled exclusively by the country's law in which the work was originally published.

Other terms and conditions:

v1.3

SPRINGER LICENSE
TERMS AND CONDITIONS

Mar 27, 2015

This is a License Agreement between Amir Khodabandeh ("You") and Springer ("Springer") provided by Copyright Clearance Center ("CCC"). The license consists of your order details, the terms and conditions provided by Springer, and the payment terms and conditions.

All payments must be made in full to CCC. For payment instructions, please see information listed at the bottom of this form.

License Number	3596890719670
License date	Mar 27, 2015
Licensed content publisher	Springer
Licensed content publication	GPS Solutions
Licensed content title	Assessing the IRNSS L5-signal in combination with GPS, Galileo, and QZSS L5/E5a-signals for positioning and navigation
Licensed content author	Nandakumaran Nadarajah
Licensed content date	Jan 1, 2015
Type of Use	Book/Textbook
Requestor type	Publisher
Publisher	Not listed below
Portion	Full text
Format	Print and Electronic
Will you be translating?	No
Print run	20
Author of this Springer article	Yes and you are the sole author of the new work
Order reference number	None
Title of new book	Precise Multi-GNSS Point Positioning : Theory, Algorithm and Data Analysis
Author of new book	Amir Khodabandeh
Expected publication date of new book	Mar 2015
Estimated size of new book (pages)	100
Total	0.00 USD
Terms and Conditions	

Introduction

The publisher for this copyrighted material is Springer Science + Business Media. By clicking "accept" in connection with completing this licensing transaction, you agree that the following terms and conditions apply to this transaction (along with the Billing and Payment terms and conditions established by Copyright Clearance Center, Inc. ("CCC"), at the time that you opened your Rightslink account and that are available at any time at http://myaccount.copyright.com).

Springer Science + Business Media makes no representations or warranties with respect to the licensed material.

Indemnity
You hereby indemnify and agree to hold harmless Springer Science + Business Media and CCC, and their respective officers, directors, employees and agents, from and against any and all claims arising out of your use of the licensed material other than as specifically authorized pursuant to this license.

No Transfer of License
This license is personal to you and may not be sublicensed, assigned, or transferred by you to any other person without Springer Science + Business Media's written permission.

No Amendment Except in Writing
This license may not be amended except in a writing signed by both parties (or, in the case of Springer Science + Business Media, by CCC on Springer Science + Business Media's behalf).

Objection to Contrary Terms
Springer Science + Business Media hereby objects to any terms contained in any purchase order, acknowledgment, check endorsement or other writing prepared by you, which terms are inconsistent with these terms and conditions or CCC's Billing and Payment terms and conditions. These terms and conditions, together with CCC's Billing and Payment terms and conditions (which are incorporated herein), comprise the entire agreement between you and Springer Science + Business Media (and CCC) concerning this licensing transaction. In the event of any conflict between your obligations established by these terms and conditions and those established by CCC's Billing and Payment terms and conditions, these terms and conditions shall control.

Jurisdiction
All disputes that may arise in connection with this present License, or the breach thereof, shall be settled exclusively by the country's law in which the work was originally published.

Other terms and conditions:

v1.3

Amir Khodabandeh

Subject: FW: Request for copyright permission

From: Springer, Permissions [mailto:permissions.springer@spi-global.com]
Sent: Thursday, 29 January 2015 2:04 PM
To: Amir Khodabandeh
Subject: RE: Request for copyright permission

Dear Amir Khodabandeh,

Thank you for your request.

For all articles where the copyright is held by us, we allow that the material is used for the habilitation thesis, and with a maximum of 100 extra copies [paper]. In addition, the author is allowed to self-archive an author-created version of his thesis on his own website and his university's repository; however he may not use the publisher's PDF version of the article.

It is up to your decision whether this article is published with open access. This means that copyright remains with the authors. The article is then published under the Creative Commons Attribution-NonCommercial license, which allows all users to read, copy, distribute and create new works for non-commercial use of the material, as long as the original work is quoted.

I hope this information helps you to finish the "My publication" process.

Sincerely,

Springer
Rights and Permissions
Springer Science+Business Media
Tiergartenstr. 17
69121 Heidelberg
Germany

From: Amir Khodabandeh [mailto:Amir.Khodabandeh@curtin.edu.au]
Sent: Thursday, January 29, 2015 6:55 AM
To: Springer, Permissions
Subject: Request for copyright permission

Dear Springer team,

Herewith I kindly request for copyright permission of my accepted conference paper in IAG symposium 142 (see the attached file).

Best regards,

SPRINGER LICENSE
TERMS AND CONDITIONS

Aug 08, 2015

This is a License Agreement between Amir Khodabandeh ("You") and Springer ("Springer") provided by Copyright Clearance Center ("CCC"). The license consists of your order details, the terms and conditions provided by Springer, and the payment terms and conditions.

All payments must be made in full to CCC. For payment instructions, please see information listed at the bottom of this form.

License Number	3684200397745
License date	Aug 08, 2015
Licensed content publisher	Springer
Licensed content publication	Journal of Geodesy
Licensed content title	An analytical study of PPP-RTK corrections: precision, correlation and user-impact
Licensed content author	A. Khodabandeh
Licensed content date	Jan 1, 2015
Type of Use	Book/Textbook
Requestor type	Publisher
Publisher	Not listed
Portion	Full text
Format	Print and Electronic
Will you be translating?	No
Print run	20
Author of this Springer article	Yes and you are the sole author of the new work
Order reference number	None
Title of new book	Precise Multi-GNSS Point Positioning: Theory, Algorithm and Data Analysis
Author of new book	Amir Khodabandeh
Expected publication date of new book	Aug 2015
Estimated size of new book (pages)	100
Total	0.00 USD
Terms and Conditions	

Introduction

The publisher for this copyrighted material is Springer Science + Business Media. By clicking "accept" in connection with completing this licensing transaction, you agree that the following terms and conditions apply to this transaction (along with the Billing and Payment

material was originally published. Where wording is within brackets, please include verbatim.

"With kind permission from Springer Science+Business Media: <book/journal title, chapter/article title, volume, year of publication, page, name(s) of author(s), figure number(s), and any original (first) copyright notice displayed with material>."

Warranties
Springer Science + Business Media makes no representations or warranties with respect to the licensed material.

Indemnity
You hereby indemnify and agree to hold harmless Springer Science + Business Media and CCC, and their respective officers, directors, employees and agents, from and against any and all claims arising out of your use of the licensed material other than as specifically authorized pursuant to this license.

No Transfer of License
This license is personal to you and may not be sublicensed, assigned, or transferred by you to any other person without Springer Science + Business Media's written permission.

No Amendment Except in Writing
This license may not be amended except in a writing signed by both parties (or, in the case of Springer Science + Business Media, by CCC on Springer Science + Business Media's behalf).

Objection to Contrary Terms
Springer Science + Business Media hereby objects to any terms contained in any purchase order, acknowledgment, check endorsement or other writing prepared by you, which terms are inconsistent with these terms and conditions or CCC's Billing and Payment terms and conditions. These terms and conditions, together with CCC's Billing and Payment terms and conditions (which are incorporated herein), comprise the entire agreement between you and Springer Science + Business Media (and CCC) concerning this licensing transaction. In the event of any conflict between your obligations established by these terms and conditions and those established by CCC's Billing and Payment terms and conditions, these terms and conditions shall control.

Jurisdiction
All disputes that may arise in connection with this present License, or the breach thereof, shall be settled exclusively by the country's law in which the work was originally published.

Other terms and conditions:

v1.3

Permissions of the following '**The Institute of Navigation'** publications are attached in the forthcoming pages:

1) Khodabandeh A. (2014). Array-aided single-differenced satellite phase bias determination: methodology and results. ION GNSS+, 27:2523–2532. **The Institute of Navigation**, Florida, USA. *Best Student Paper Award*

2) Teunissen P.J.G. and Khodabandeh A. (2014b). Do GNSS parameters always benefit from integer ambiguity resolution? a PPP-RTK Network Scenario. ION GNSS+, 27:590–600. **The Institute of Navigation**, Florida.

THE INSTITUTE OF NAVIGATION

COPYRIGHT RELEASE FORM

ION PROCEEDINGS

Signing of "Statement A" or "Statement B" is required except that employees of governments other than the U.S. Government may submit equivalent statements. It is essential that The Institute of Navigation (ION) and its agents or assignees have the right of publication and reproduction.

Proceedings to Appear in: **ION GNSS+ 2014**

Session Number & Title: E4: High Precision GNSS Positioning

Paper Title *(exactly as it appears on the paper)*:

Array-aided single-differenced satellite phase bias determination: methodology and results

Author(s) & Affiliation(s) *(in the exact order they appear on the paper)*: Amir Khodabandeh

GNSS Research Centre, Curtin University of Technology, Perth, Australia

Primary Author Address:

GNSS Research Centre, Curtin University of Technology, Perth, Australia

Phone/Fax/E-Mail: amir.khodabandeh@curtin.edu.au

STATEMENT A:

The undersigned "Copyright Owner," desiring to publish a paper (the "Paper") in ION Proceedings and/or through other publications of The Institute of Navigation ("ION"), hereby grants to ION the following rights in exchange for good and valuable consideration:

1.) the exclusive, royalty-free right of first publication of the above Paper throughout the world as part of the proceedings named above and;
2.) a non-exclusive, perpetual, royalty-free, worldwide license to reprint and/or provide in electronic format the above Paper, either in excerpt, in summary, or in completed form, for free or in exchange for a fee.

Copyright Owner reserves all rights not specifically granted to ION herein and has the right after the Paper has been published, to reprint the Work in any publication, provided that the terms of such republication do not conflict with this license. Copyright Owner agrees to include the proper credit to ION for prior publication of the Paper in any reprint of the Paper in a publication, including date (month and year) and location (city and state) of the meeting at which the paper was presented.

Copyright Owner warrants that the Paper is original with him/her, that its publication will not infringe the rights of others, that the Paper is factually accurate and contains no defamatory or otherwise unlawful material, and that Copyright Owner has full power to make this agreement. Copyright Owner further warrants that the Paper has not been published elsewhere in whole or in part (except as set out in a rider attached thereto if applicable) and that no agreement to publish the Paper or any part or version thereof is outstanding. Should the Paper contain any material which requires permission for inclusion in the Paper, Copyright Owner agrees to obtain such permission in writing and provide a copy of such permission to ION.

1. Amir Khodabandeh — PRIMARY AUTHOR'S SIGNATURE

Curtin University of Technology — EMPLOYER FOR WHOM WORK WAS PERFORMED

AUTHORIZED SIGNATURE

15 August 2014 — DATE FORM SIGNED

STATEMENT B:

This will certify that all authors of the above Paper are employees of the U.S. Government and that the authors created the Paper as part of their employment and that the Paper is therefore not subject to U.S. Copyright protection.

2. _____ PRIMARY AUTHOR'S SIGNATURE

_____ EMPLOYER FOR WHOM WORK WAS PERFORMED

_____ AUTHORIZED SIGNATURE

_____ DATE FORM SIGNED

Crown Copyright Certification (where applicable)

This will certify that all authors of the Work are employees of the British or applicable Commonwealth Government and prepared the Work in connection with their official duties. As such, the Work is subject to Crown Copyright and is not assigned to the ION as set forth above. The Undersigned acknowledges, however, that the ION has the right to publish, distribute and reprint the Work in all forms and media.

3. _____ AUTHORIZED SIGNATURE

_____ DATE FORM SIGNED

(Authors who are British or applicable Commonwealth Government employees should also sign line (1) above to indicate their acceptance of all terms other than the copyright transfer.)

THE INSTITUTE OF NAVIGATION

COPYRIGHT RELEASE FORM

ION PROCEEDINGS

Signing of "Statement A" or "Statement B" is required except that employees of governments other than the U.S. Government may submit equivalent statements. It is essential that The Institute of Navigation (ION) and its agents or assignees have the right of publication and reproduction.

Proceedings to Appear in: **ION GNSS+ 2014**

Session Number & Title: B2: High Precision GNSS

Paper Title *(exactly as it appears on the paper)*:

Do GNSS parameters always benefit from integer ambiguity resolution? A PPP-RTK Network Scenario

Author(s) & Affiliation(s) *(in the exact order they appear on the paper)*: P.J.G. Teunissen and A. Khodabandeh

GNSS Research Centre, Curtin University of Technology, Perth, Australia

Primary Author Address:

GNSS Research Centre, Curtin University of Technology, Perth, Australia

Phone/Fax/E-Mail: p.teunissen@curtin.edu.au

STATEMENT A:

The undersigned "Copyright Owner," desiring to publish a paper (the "Paper") in ION Proceedings and/or through other publications of The Institute of Navigation ("ION"), hereby grants to ION the following rights in exchange for good and valuable consideration:

1.) the exclusive, royalty-free right of first publication of the above Paper throughout the world as part of the proceedings named above and;
2.) a non-exclusive, perpetual, royalty-free, worldwide license to reprint and/or provide in electronic format the above Paper, either in excerpt, in summary, or in completed form, for free or in exchange for a fee.

Copyright Owner reserves all rights not specifically granted to ION herein and has the right after the Paper has been published, to reprint the Work in any publication, provided that the terms of such republication do not conflict with this license. Copyright Owner agrees to include the proper credit to ION for prior publication of the Paper in any reprint of the Paper in a publication, including date (month and year) and location (city and state) of the meeting at which the paper was presented.

Copyright Owner warrants that the Paper is original with him/her, that its publication will not infringe the rights of others, that the Paper is factually accurate and contains no defamatory or otherwise unlawful material, and that Copyright Owner has full power to make this agreement. Copyright Owner further warrants that the Paper has not been published elsewhere in whole or in part (except as set out in a rider attached thereto if applicable) and that no agreement to publish the Paper or any part or version thereof is outstanding. Should the Paper contain any material which requires permission for inclusion in the Paper, Copyright Owner agrees to obtain such permission in writing and provide a copy of such permission to ION.

1. Peter J.G. Teunissen	Curtin University of Technology
PRIMARY AUTHOR'S SIGNATURE	EMPLOYER FOR WHOM WORK WAS PERFORMED
	15 August 2014
AUTHORIZED SIGNATURE	DATE FORM SIGNED

STATEMENT B:

This will certify that all authors of the above Paper are employees of the U.S. Government and that the authors created the Paper as part of their employment and that the Paper is therefore not subject to U.S. Copyright protection.

2.	
PRIMARY AUTHOR'S SIGNATURE	EMPLOYER FOR WHOM WORK WAS PERFORMED
AUTHORIZED SIGNATURE	DATE FORM SIGNED

Crown Copyright Certification (where applicable)

This will certify that all authors of the Work are employees of the British or applicable Commonwealth Government and prepared the Work in connection with their official duties. As such, the Work is subject to Crown Copyright and is not assigned to the ION as set forth above. The Undersigned acknowledges, however, that the ION has the right to publish, distribute and reprint the Work in all forms and media.

3.	
AUTHORIZED SIGNATURE	DATE FORM SIGNED

(Authors who are British or applicable Commonwealth Government employees should also sign line (1) above to indicate their acceptance of all terms other than the copyright transfer.)

Permission of the following '**Maney Publishing'** publication is attached in the forthcoming pages:

Odijk D., Teunissen P.J.G., and Khodabandeh A. (2013). Galileo IOV RTK positioning: standalone and combined with GPS. Survey Review, **Maney Publishing**. UK.

Copyright & Permissions

It is important to have a reasonable and defensible copyright and permissions policies in order to protect the rights of the authors and societies whom we serve, whilst disseminating knowledge and scholarship as widely as possible.

The following information applies to Maney's subscription journals. Authors wishing to publish a gold (immediate) open access (OA) article should refer to information on open access publication.

Maney monitors policies in order to comply with funder OA mandates. Further information about compliance is available on our open access funding policies page.

Jump to:

Author resources menu

Author home

Preparation

Submission

After acceptance

Article promotion

Publishing ethics

Copyright & permissions

Supporting resources

Language editing

Using Editorial Manager

Open access publication

Assignment of copyright

It is a condition of publication that, on acceptance of the article by the journal editor, copyright must be assigned to the publisher or to the society or professional organisation for which Maney publishes the journal.

An Assignment of Copyright Form will be issued with author proofs or can be downloaded from an individual journal's instructions for authors.

Authors submitting via the Editorial Manager online system will need to upload a scanned, signed Assignment of Copyright form or, if appropriate, licence to publish with the revised version of their article.

It may be that the author is not able to make the assignment:

- If it is appropriate, the author's employer may sign this agreement. The employer may reserve the right to use the article for internal or promotion purposes (by indicating on this agreement), and reserve all rights other than copyright.
- If the author is a UK Government employee, TSO will grant a non-exclusive licence to publish the article in the journal in any medium or form provided that Crown Copyright and user rights (including patent rights) are reserved.
- If the author is a US Government employee and the work was done in that capacity, the assignment applies only to the extent allowed by US law.

In these cases, the use of a 'licence to publish', rather than the standard copyright agreement, can be discussed with the academic editor and managing editor of the journal.

The author(s) of papers retain their moral rights under the terms of the Copyright Designs and Patents Act 1988 to be identified as the author(s) of the article. Maney ensures that your moral rights are asserted as part of that act.

Author images
If authors wish to retain copyright of their own images in their article, this can be accommodated. Authors wishing to retain the copyright in an image should indicate this by adding into the figure caption wording such as "© [Author name]" or "Copyright [Author name]". This will ensure that anyone who may subsequently want to reference the work, or reuse the image, will know who owns the copyright and therefore who to contact for further permission.

Using images from Google
Authors may use Google Maps/Google Earth images in articles (where necessary) subject to the guidelines published by Google. Full acknowledgement must be given in the caption credit.

Using images and other content from the internet
Sometimes copyright laws apply to the internet more rigorously than for other media. Authors must check the terms and conditions of the website and/or the copyright disclaimer. If these items are not visible please do not assume that re-using content is acceptable.

The rights of authors to reuse their own work

Authors can use their articles for a range of scholarly purposes without seeking additional permission from Maney, so long as no commercial use is made of the article.

The following table shows the authors right to reuse their article. These rights apply for Maney authors who publish their article in a subscription journal. A full acknowledgment and link to the final published version should always be included.

	Pre-print	Post-print	Eprint
Share with colleagues and research associates	Y	Y	Y
Put on their personal or institutional website or distribute via social media	Y	N	N
Post (archive) in an institutional or subject based repository	Y	Y (embargoed)	N
Use for teaching purposes in the author's institution	Y	Y	Y
Use at a conference	Y	Y	N
Include in a thesis or dissertation	Y	Y	N
Use for commercial purposes	N	N	N

Definitions:
Pre-print: original manuscript before peer-review and editing
Post-print: final accepted version (i.e. after peer-review but without Maney editing and typesetting)
Eprint: final paginated version published in the journal
Embargo periods: 12 months for STEM (science, technology, engineering and medicine) and 24 months for HSS (humanities and social sciences) journals

For gold (immediate) OA articles, reuse for both authors and readers are defined by the author's choice of Creative Commons user license options.

Inclusion in an institutional or subject-based repository

Authors may post a copy of their pre-print on a non-commercial institutional repository but archiving a post-print is **subject to an embargo period** as above and as specified in the individual journal's instructions for authors, from the date of publication, as long as:

- full acknowledgement is made of the Journal issue in which the article is published
- there is a link to the published online version of the article on Maney's chosen online hosting platform, to the Journal, and the Publisher's website at www.maneypublishing.com, and any other information specified in the copyright transfer statement
- no commercial use is made of the article

Authors will receive an Eprint (PDF file) of the final published version of their article that they may forward and share with all co-authors, and other research associates.

Additionally, Maney may grant permission for an author to use sections of a Maney-published article in a thesis, research article or book chapter, subject to proper acknowledgement of the original article. However, we reserve the right to charge a third party that intends to make a commercial gain from any reuse.

Maney will never unreasonably withhold permission for an author to republish his or her own material, subject to acknowledgement of the original place of publication. In all cases the author should contact the Copyright Clearance Center (CCC), who act on behalf of the copyright holders. Orders can be placed either online at www.copyright.com, by email at info@copyright.com or by phone at +1-855-239-3415 or +1-978-750-8400

Permission guidelines for Maney authors

Authors who wish to reproduce sections of text, data or figures from previously published sources, or where copyright is owned by a third party, must obtain written permission from the copyright holder and any other interested party. Please note that all sources must be credited in the article regardless of whether or not permission is required.

Authors should obtain permission to use items in their article ensuring they explicitly obtain permission for all three of the following:

- all geographical regions of the world
- in all formats, including electronic
- in perpetuity

Authors may use the permissions form template and cover letter. Note that many publishers now deal with copyright permissions requests online via Rightslink (a permissions link is usually provided from the abstract page of the article in question).

The author should fill in the details of the article, and the journal that the article is being submitted to, and obtain a signature on the permission letter. Many copyright owners prefer to provide their own letter of permission, and this is acceptable as long as the three stipulations of **geography, format and perpetuity of reuse** (see above) are included.

For further information contact Maney's Permissions Department: permissions@maneypublishing.com.

Obtaining permission to re-use Maney material

Any reuse or reproduction from Maney's publications, except for the purposes of review or 'fair dealing', must have the permission of the copyright holder.

Requests for such permission should be addressed to the Copyright Clearance Center (CCC), who act on behalf of the copyright holders. Orders can be placed online at www.copyright.com, or contact the CCC by email at info@copyright.com or by phone at +1-855-239-3415 or +1-978-750-8400.

In all cases, the name of the journal should be mentioned. Please include details about who you are, the material that you wish to use, and the purpose for which use is requested; for example, to republish in a journal, book, thesis or dissertation, including in any electronic format.

Maney is a member of STM and permissions are granted according to the Guidelines offered by this organisation.

Translation requests

Any party wishing to translate an article published in one of Maney's journals or one of our books should also contact the Copyright Clearance Center (CCC), who act on behalf of the copyright holders. Orders can be placed either online at www.copyright.com, by email at info@copyright.com or by phone at +1-855-239-3415 or +1-978-750-8400

Educational photocopying

For users in North America, permission is granted by the copyright owner for libraries and others registered with the Copyright Clearance Center (CCC) to make copies of any articles in Maney published journals. Payment should be sent direct to CCC, 22 Rosewood Drive, Danvers, MA 01923, USA.

In the UK, the Copyright Licensing Agency, cla@cla.co.uk, is mandated to grant permission to make copies.

Intranet and controlled access

Those wishing to make material available online via secure networks or to a restricted readership should contact the Copyright Clearance Center (CCC), who act on behalf of the copyright holders. Orders can be placed either online at www.copyright.com, by email at info@copyright.com or by phone at +1-855-239-3415 or +1-978-750-8400

Permission of the following ‘**IOP’** publication is attached in the forthcoming pages:

Khodabandeh A. and Teunissen P.J.G. (2014a). Array-based satellite phase bias sensing: theory and GPS/BeiDou/QZSS results. Measurement Science and Technology, 25,095801 (11pp). **IOP**, UK.

Assignment of copyright and publication agreement - IOP Publishing Limited

IOP Publishing Limited ("IOP") agrees to publish:

Manuscript Title: Array-based satellite phase bias sensing: theory and GPS/BeiDou/QZSS results (the "Article") written by

Names of all authors: Khodabandeh, Amir; Teunissen, P ("the Named Authors") in the following journal Measurement Science and Technology ("the Journal")

Name of Institution(s) (if applicable – see Important Information above):

Curtin University **("the Institution")**

IOP Ref: MST-101038

Part 1 - Subscription Copyright Assignment

Assignment of copyright to IOP

1.1 Upon acceptance for publication, in consideration for publication of the Article by IOP, the Named Authors of the Article shall assign to IOP with full title guarantee the entire copyright in all original material published as part of the Article (which expression includes but is not limited to the text, abstract, tables, figures and graphs, video abstracts and other multimedia content but excludes any other item referred to as supplementary material) throughout the world for the full term of copyright (including any extensions or renewals thereof) for all media and formats, whether known or unknown. For the avoidance of doubt, copyright does not subsist in any fundamental data underlying the Article and nothing in this Agreement is intended to limit access to or use of such data.

1.2 If any of the Named Authors are Government employees who produced the Article in the course of their duties, in consideration for publication such Named Authors and the relevant originating department or agency shall grant IOP a royalty-free non-exclusive worldwide licence for the full term of copyright (including any extensions or renewals thereof) for all media and formats, whether known or unknown, to do in relation to the Article all acts restricted by copyright worldwide. This shall include, but not be limited to, including the Article (or part thereof) on IOP's own websites (such as insights and labtalk) and/or on third party websites.

1.3 In consideration for publication, the Named Authors shall grant IOP a royalty-free non-exclusive worldwide freely transferrable licence for the full term of copyright (including any extensions or renewals thereof) to do in relation to any supplementary material not deemed to be part of the Article all acts restricted by copyright worldwide. This shall include, but not be limited to, including the supplementary material (or part thereof) on IOP's own websites (such as insights and labtalk) and/or on third party websites.

1.4 Each of the Named Authors consents to the publication and processing by IOP of their email addresses.

Representations and warranties

2.1 The Corresponding Author and/or the Named Authors (as appropriate) represent and warrant that:

2.1.1 the Article is the original work of the Named Authors;

2.1.2 the Article has not been published previously in any form, other than as part of the Named

Authors' research theses or dissertations (which fact has been notified to IOP in writing) or as a pre-print, for example on the arXiv.org service;

2.1.3 each of the Named Authors has made a material contribution to the conception and/or writing of the Article, has received the final version of the Article, has agreed to its submission on the terms contained herein and takes responsibility for it and submission has been approved as necessary by the authorities at the establishment where the research was carried out;

2.1.4 the Corresponding Author completes and returns this agreement as authorised agent for and on behalf of all the Named Authors and has the full power to enter into this agreement and to make the grants and assignments it contains;

2.1.5 the Article has not been and shall not be submitted to another publisher prior to withdrawal or rejection by IOP;

2.1.6 the Article does not infringe any third party rights, it contains nothing libellous or unlawful, all factual statements are to the best of the Named Authors' knowledge true or based on valid research conducted according to accepted norms and all required permissions have been obtained in writing; and

2.1.7 the Article expressly acknowledges any third party funding and/or potential conflicts of interest.
2.2 The Named Authors indemnify and will keep indemnified IOP and its affiliates, parent company, subsidiaries, directors, officers, servants, employees, agents and shareholders against all actions, claims, costs, demands, expenses and other liabilities suffered or incurred by IOP as a result of and/or arising from IOP's exploitation (or exploitation by third parties authorised by IOP) of the Article where such claim arises out of any breach by any of the Named Authors of the representations and/or warranties in this section 2.

The Named Authors' rights

3.1 IOP grants the Named Authors the rights specified in paragraphs 3.2, 3.3 and 3.4. All such rights must be exercised solely for non-commercial purposes. Where possible, any use should display citation information and IOP's copyright notice, and, for electronic use, best efforts must be made to include a link to the online abstract in the Journal. Exercise of the rights in paragraphs 3.3 and 3.4 must not use the final published IOP format but the Named Authors' own format (which may include amendments made following peer review but not any editing, typesetting or other changes made by IOP) (the "Accepted Manuscript") and must be accompanied by the following statement of provenance:

'This is an author-created, un-copyedited version of an article accepted for publication in Measurement Science and Technology. IOP Publishing Ltd is not responsible for any errors or omissions in this version of the manuscript or any version derived from it. The Version of Record is available online at [insert DOI].'

3.2 The rights are:

3.2.1 To make copies of the Article (all or part) for teaching purposes;

3.2.2 To include the Article (all or part) in a research thesis or dissertation;

3.2.3 To make oral presentation of the Article (all or part) and to include a summary and/or highlights of it in papers distributed at such presentations or in conference proceedings; and

3.2.4 To include figures and text falling within the quota outlined in the STM Permissions Guidelines (http://www.stm-assoc.org/permissions-guidelines/) at the relevant time in force from the Article in new works created or co-created by any of the Named Authors.
For the avoidance of doubt, the Named Authors retain all proprietary rights in the Article other than copyright.

3.3 Additional rights of the Named Authors are to:

3.3.1 Use the Accepted Manuscript (all or part) without modification in personal compilations of the Named Authors' own works (provided not created by a third party publisher); and

3.3.2 Include the Accepted Manuscript (all or part) on the Named Authors' own personal websites.
3.4 In addition to the above, following the expiry of a period of 12 months from the date of publication of the Article by IOP (the "Embargo Period"), the Named Authors may:

3.4.1 Include the Accepted Manuscript (all or part) on websites of the institution (including its repository) where the Named Authors worked when research for the Article was carried out; and

3.4.2 Include the Accepted Manuscript (all or part) on third party websites including e-print servers, but not on other publishers' websites. Further information is included on the web page http://authors.iop.org/atom/help.nsf/LookupJournalSpecific/WebPermissionsFAQ~**
3.5 Notwithstanding the provisions of paragraph 3.4 above, and until any change to IOP policy, which change will be included within the copyright information on IOP's website, an exception to the Embargo Period is that the Named Authors may at any time, including prior to publication by IOP of the Article, submit the Accepted Manuscript to the e-print service at arXiv.org subject to a non-exclusive, perpetual licence.

Miscellaneous

4. To the extent that there are moral rights in the Article, all the Named Authors expressly reserve and assert their moral rights to be identified as the authors of the Article.

5. The Named Authors shall execute such further documents, and take such actions and do such things, as may be requested by IOP at IOP's reasonable expense to give full effect to the terms of this agreement.

6. For the avoidance of doubt, the grants and assignment envisaged herein shall become effective only upon acceptance by IOP of the Article for publication. In the event that the Article is withdrawn prior to acceptance, or is rejected, this agreement shall have no effect and no party shall be bound by it.

7. This agreement shall be governed by English Law and subject to the non-exclusive jurisdiction of the English Courts.

Confirmation

8. By typing the Corresponding Author's name into the box at Part 3 below and clicking "Submit", the Named Authors agree to these terms.

Part 2 - Open Access Copyright Assignment
Assignment of copyright to IOP

1.1 Upon acceptance for publication, in consideration for publication of the Article by IOP, the Named Authors of the Article shall assign to IOP with full title guarantee the entire copyright in all original material published as part of the Article (which expression includes but is not limited to the text, abstract, tables, figures and graphs, video abstracts and other multimedia content but excludes any other item referred to as supplementary material) throughout the world for the full term of copyright (including any extensions or renewals thereof) for all media and formats, whether known or unknown. For the avoidance of doubt, copyright does not subsist in any fundamental data underlying the Article and nothing in this agreement is intended to limit access to or use of such data.

1.2 If any of the Named Authors are Government employees who produced the Article in the course of their duties, in consideration for publication such Named Authors and the relevant originating department or agency shall grant IOP a royalty-free non-exclusive worldwide licence for the full term of copyright (including any extensions or renewals thereof) for all media and formats, whether known or unknown, to do in relation to the Article all acts restricted by copyright worldwide. This shall include, but not be limited to, including the Article (or part thereof) on IOP's own websites (such as insights and labtalk) and/or on third party websites.

1.3 In consideration for publication, the Named Authors shall grant IOP a royalty-free non-exclusive worldwide freely transferrable licence for the full term of copyright (including any extensions or renewals thereof) to do in relation to any supplementary material not deemed to be part of the Article all acts restricted by copyright worldwide. This shall include, but not be limited to, including the supplementary material (or part thereof) on IOP's own websites (such as insights and labtalk) and/or on third party websites.

1.4 Each of the Named Authors consents to the publication and processing by IOP of their email addresses.

Representations and warranties

2.1 The Corresponding Author and/or the Named Authors (as appropriate) represent and warrant that:

2.1.1 the Article is the original work of the Named Authors;

2.1.2 the Article has not been published previously in any form, other than as part of the Named Authors' research theses or dissertations (which fact has been notified to IOP in writing) or as a pre-print, for example on the arXiv.org service;

2.1.3 each of the Named Authors has made a material contribution to the conception and/or writing of the Article, has received the final version of the Article, has agreed to its submission on the terms contained herein and takes responsibility for it and submission has been approved as necessary by the authorities at the establishment where the research was carried out;

2.1.4 the Corresponding Author completes and returns this agreement as authorised agent for and on behalf of all the Named Authors and has the full power to enter into this agreement and to make the grants and assignments it contains;

2.1.5 the Article has not been and shall not be submitted to another publisher prior to withdrawal or rejection by IOP;

2.1.6 the Article does not infringe any third party rights, it contains nothing libellous or unlawful, all factual statements are to the best of the Named Authors' knowledge true or based on valid research conducted according to accepted norms and all required permissions have been obtained in writing; and

2.1.7 the Article explicitly acknowledges any third party funding and/or potential conflicts of interest.

2.2 The Named Authors indemnify and will keep indemnified IOP and its affiliates, parent company, subsidiaries, directors, officers, servants, employees, agents and shareholders against all actions, claims, costs, demands, expenses and other liabilities suffered or incurred by IOP as a result of and/or arising from IOP's exploitation (or exploitation by third parties authorised by IOP) of the Article where such claim arises out of any breach by any of the Named Authors of the representations and/or warranties in this section 2.

The Named Authors' rights

3.1 The Named Authors and all third parties will have the rights to use the Article as described in the Creative Commons Attribution 3.0 Unported licence (http://creativecommons.org/licenses/by/3.0/). These rights allow users to copy, distribute and display the published version of the Article and create derivative works, subject to appropriate attribution.

3.2 Where the Article is used in accordance with 3.1 above, the following attribution shall be included:
Article title
Named Authors
DOI
"This article was first published in Measurement Science and Technology by IOP Publishing, which maintains the Version of Record".

Miscellaneous

4. To the extent that there are moral rights in the Article, all the Named Authors expressly reserve and assert their moral rights to be identified as the authors of the Article.

5. The Named Authors shall execute such further documents, and take such actions and do such things, as may be requested by IOP at IOP's reasonable expense to give full effect to the terms of this agreement.

6. For the avoidance of doubt, the grants and assignment envisaged herein shall become effective only upon acceptance by IOP of the Article for publication. In the event that the Article is withdrawn prior to acceptance, or is rejected, this agreement shall have no effect and no party shall be bound by it.

7. This agreement shall be governed by English Law and subject to the non-exclusive jurisdiction of the English Courts.

Confirmation

8. By typing the Corresponding Author's name into the box at Part 3 below and clicking "Submit", the Named Authors agree to all these terms.

Part 3 – Confirmation and Execution

Please tick the box below to confirm the basis upon which you, as the Corresponding Author, on behalf of all the Named Authors, are submitting the Article to IOP.

Subscription Copyright Assignment – Part 1 Applies

Type your name here:

Amir Khodabandeh (the "Corresponding Author")

req Date:
30-Apr-2014

By clicking "Submit" and typing your name above, you shall be assumed to have read and understood all of the terms and conditions of the relevant part of this agreement and you will be agreeing to all of the terms and conditions and assignment (as the case may be) detailed above.

APPENDIX B STATEMENT OF CONTRIBUTIONS BY OTHERS

This thesis presents 1 single-author, 4 first-author, 4 second-author, and 2 third-author papers that have been published in journals and conference proceedings. In this Appendix, author's and co-authors' contributions for these papers are stated and singed.

To Whom It May Concern,

I, Amir Khodabandeh, wrote the manuscripts, derived the analytical expressions, and provided the multi-GNSS numerical results by my own software. In case of the co-authored publications, Prof Peter J.G. Teunissen provided their comments as to improve the manuscripts for submission. All the above holds for the following publications:

1) Khodabandeh A. (2014). Array-aided single-differenced satellite phase bias determination: methodology and results. ION GNSS+, 27:2523–2532. The Institute of Navigation, Florida, USA.

2) Khodabandeh A. and Teunissen P.J.G. (2014a). Array-based satellite phase bias sensing: theory and GPS/BeiDou/QZSS results. Meas. Sci. Technol., 25,095801 (11pp). UK.

3) Khodabandeh A. and Teunissen P.J.G. (2014c). A recursive linear MMSE filter for dynamic systems with unknown state vector means. International Journal on Geomathematics, 5:17–31, Springer.

4) Khodabandeh A. and Teunissen P.J.G. (2014b). Single-Epoch GNSS Array Integrity: an Analytical Study. International Association of Geodesy Symposium (IAG), Springer, Accepted for publication.

5) Teunissen P.J.G. and Khodabandeh A. (2014b). Do GNSS parameters always benefit from integer ambiguity resolution? a PPP-RTK Network Scenario. ION GNSS+, 27:590–600. The Institute of Navigation, Florida.

6) Khodabandeh A. and Teunissen P.J.G. (2015). An Analytical Study of PPP-RTK Corrections: Precision, Correlation and User-Impact. Journal of Geodesy, doi: 10.1007/s00190-015-0838-9, Springer.

And, I, Amir Khodabandeh, wrote the main material of the following publications, including the underlying theory and analytical derivations. The first author is Prof Peter J.G. Teunissen who wrote the final organization of the manuscripts:

7) Teunissen P.J.G. and Khodabandeh A. (2013) BLUE, BLUP and the Kalman filter: some new results. Journal of Geodesy 87(5):461–473, Springer.

8) Teunissen P.J.G. and Khodabandeh A. (2014a). Review and Principles of PPP-RTK Methods. Journal of Geodesy, Springer.

And, I, Amir Khodabandeh, contributed to a part of the analytical derivations and numerical results of the following publications. The first authors, where applicable, are Dr Dennis Odijk and Dr Nandakumaran Nadarajah who wrote the manuscripts, and Prof Peter J.G. Teunissen provided his comments to the manuscript before submission:

9) Odijk D., Teunissen P.J.G. and Khodabandeh A. (2014). Single-frequency PPP-RTK: theory and experimental results. International Association of Geodesy Symposium (IAG), 139:167–173, Springer.

10) Odijk D., Teunissen P.J.G. and Khodabandeh A. (2013). Galileo IOV RTK positioning: standalone and combined with GPS. Survey Review, Maney Publishing. UK.

11) Nadarajah N., Khodabandeh A. and Teunissen P.J.G. (2015). Assessing the IRNSS L5-signal in combination with GPS, Galileo, and QZSS L5/E5a-signals for positioning and navigation. GPS Solutions, Springer.

Amir Khodabandeh _____

I, as a Co-Author, endorse that this level of contributions by the candidate indicated above is appropriate.

Peter J.G. Teunissen _____

Dennis Odijk _____

Nandakumaran Nadarajah _____

APPENDIX C PROOF OF PEER-REVIEWED AND ACCEPTED PUBLICATIONS

Provided below is the proof that the conference publications:

1) Khodabandeh A. (2014). Array-aided single-differenced satellite phase bias determination: methodology and results. ION GNSS+, 27:2523–2532. The Institute of Navigation, Florida, USA.

2) Khodabandeh A. and Teunissen P.J.G. (2014b). Single-Epoch GNSS Array Integrity: an Analytical Study. International Association of Geodesy Symposium (IAG), Springer, Accepted for publication.

3) Teunissen P.J.G. and Khodabandeh A. (2014b). Do GNSS parameters always benefit from integer ambiguity resolution? a PPP-RTK Network Scenario. ION GNSS+, 27:590–600. The Institute of Navigation, Florida.

were published in peer-reviewed conference proceedings and accepted respectively.

Amir Khodabandeh

From: Meetings <meetings@ion.org>
Sent: Monday, 3 March 2014 11:58 PM
To: Amir Khodabandeh
Cc: Peter Teunissen
Subject: ION GNSS+ 2014 Student Paper Award

March 3, 2013

Mr. Amir Khodabandeh
Curtin University of Technology
GNSS Research Centre, Dept. of Spatial Sciences
GPO BOX U1987
Perth, a 6845, AUSTRALIA

Sent Via E-mail (Original will be sent via air mail next week)

Dear Mr. Khodabandeh,

It is my pleasure to inform you that your paper "***Array-aided Single-differenced Satellite Phase bias determination: Methodology and Results***" have been selected by the ION GNSS+ 2014 Student Award Committee to be presented at the ION GNSS+ 2014 Conference, September 08-12, 2014 in Tampa, Florida. Details for the presentation and travel sponsorship are as follows:

Paper Title: Array-aided Single-differenced Satellite Phase bias Determination: Methodology and Results
Session: TBD

Below are some important details concerning the meeting, your travel arrangements, and final paper publication guidelines. I would encourage you to get an early start of making your arrangements to attend the conference and pay special attention to the mandatory deadlines.

WHAT YOU RECEIVE:

Your award includes:

1. Travel award funds (according to the published schedule and based on the country in which the school resides) upon the Institute's receipt of valid visa copy.
2. A complimentary **FULL** conference registration that includes all conference meals and a copy of the proceedings.
3. Publication of your technical paper in the conference proceedings.
4. Awards certificate and acknowledgement of your accomplishment at the ION GNSS+ Awards Luncheon.

Travel Award Funds: Student travel awards provide a flat rate of travel subsidy based on the country in which the sponsoring school is located as follows:

U.S. Schools:	*$1,300*
Canadian Schools:	*$1,500*
U.K./Western European Schools:	*$2,000*
Brazilian Schools:	*$2,200*
Chinese/Korean/Japanese Schools	*$2,300*
Australian Schools:	*$2,500*

Other: qualify for special arrangements

You, or your school, is responsible to make ALL travel arrangements (including airline and individual hotel reservations). Due to U.S. tax laws travel funds will NOT be payable to an individual. Travel funds shall be remitted directly to the sponsored student's academic institution after the ION National Office receives proof of visa/passport (if applicable). There will be no exceptions made to this policy. Travel costs that exceed the published amount shall be borne by the student. The university shall retain funds in excess of actual student's travel. **Funds are not transferable and shall be returned to the ION if for any reason the student winner named on this letter is unable to attend**. Failure to do so would affect the acceptance of future papers submitted for consideration under the student awards program.

ION GNSS+ Meeting Registration:

You will be receiving a **full complimentary meeting registration**. This includes all sessions, conference events, meals served at the conference, and a copy of the proceedings. You will receive an electronic registration confirmation letter from our meeting registration department this summer.

Publication of Your Paper in GNSS+ Meeting Proceedings:

You will receive a link to the online authors' kit via e-mail from Miriam Lewis. Please review it thoroughly as it contains information on the formatting of your paper for publication in the official ION GNSS+ conference proceedings. Your final formatted paper must be received at the National Office in proper form no later than August 22, 2014.

The author's kit also contains additional requirements for the publication of your paper. Note that your paper must be presented to be included in the proceedings. You will also find information on what audio-visual equipment will be made available to you for your oral presentation and you will be provided information on the speaker's breakfast (which you are required to attend the morning of your presentation).

YOU ARE RESPONSIBLE FOR/TO:

As a GNSS student award winner you are responsible for/required to:

1. Fax or e-mail a copy of your visa or valid passport to my attention at the National Office at +1-703-366-2724.
2. Attend the **Speakers Breakfast** on the morning of your presentation.
3. Present your paper at the time scheduled per the published conference program.
4. Participate in all three days of the conference's technical program/commercial exhibit.
5. You are **REQUIRED** to attend the **Friday Awards Luncheon**. Failure to attend this event will jeopardize future student papers being accepted from your school.

Obtain a Visa:

We recommend that you apply for your visa at least three months in advance. Currently there is a mandatory security check period of 30 days for people whose passports are issued from several countries. U.S. consular offices now interview most applicants as part of the application process. Please ensure you arrive at the embassy with all required documentation at the time of your interview.

You will find an original visa letter for use in making your visa application enclosed. Please take this visa letter with you to the embassy when making your visa application.

IMPORTANT!!! A faxed copy of your visa must be received no later than August 30. If your visa is not received by August 30 your travel award will be terminated and your paper will be automatically canceled and withdrawn from the conference. If you are not a U.S./Canadian citizen, you are required to obtain a visa prior to the Institute issuing you any sponsorship funds. No exceptions will be made to this policy. After your visa has been issued please fax or e-mail a copy at +1-703-366-2724. Once the copy of your visa has been received you will be eligible to receive travel funds.

To Whom Travel Award Funds Shall Be Sent:

All travel award funds will be made payable to your university. Please provide your university department's full mailing address. All checks will be mailed via standard airmail. Travel funds shall be issued with a check written in U.S. dollars and drawn on a U.S. bank. There will be no exceptions made to these policies.

At the GNSS Meeting YOU are REQUIRED to:

- Attend the **Speakers Breakfast** on the morning of your presentation.
- Present your paper at the original time in which it has been scheduled per the conference program.
- Participate in all three days of the conference's technical program/commercial exhibit (Wednesday through Friday).
- Attend the **Friday Awards Luncheon on Friday, September 12** from noon-2 p.m.

I hope this memo has answered most of your questions. **Remember to make your visa application right away and fax or e-mail valid visa no later than August 30** to avoid the cancellation of your paper and discontinuation of your sponsorship. Let us know if you have any questions.

Sincerely,

Lisa Beaty
Executive Director
Phone: +1-703-366-2723
E-mail: Lbeaty@ion.org

Enc: Visa Invitation Letter

CC: Faculty Representative
Dr. Peter J.G. Teunissen

Amir Khodabandeh

From: meetings@ion.org
Sent: Saturday, 3 May 2014 12:03 AM
To: Amir Khodabandeh
Subject: GNSS+ 2014 Acceptance Notification

Dear Amir Khodabandeh:

Your abstract, titled **"Array-aided Single-Differenced Satellite Phase Bias Determination: Methodology and Results,"** has been accepted for the ION GNSS+ 2014 Conference, taking place September 8-12, 2014, at the Tampa Convention Center, Tampa, Florida.

Your abstract has been assigned to Session E4: High Precision GNSS Positioning, scheduled for Thursday, September 11, 2014. You can view the full program online at: ion.org/gnss/program.cfm

Please confirm that you have been notified of the acceptance of your abstract. Click here to confirm that you have received this acceptance notice.

You can also confirm by signing in to the ION Abstract Management Portal at www.ion.org/abstracts

Please review your paper title and author list carefully to ensure that all of the information is correct. You may use the ION Abstract Management Portal to make edits to the title of your paper, the authors listed, and your abstract text. You can also upload your conference paper and/or make changes to your conference paper. Any changes made online before August 22, 2014 will be reflected in the on-site printed conference program. NOTE: Papers not representative of the original abstract submitted will NOT be included in the conference proceedings, and this may affect the acceptance of future abstracts.

Papers desiring peer review (only applies to papers in the Advanced Multisensor Navigation Track and the Advanced Algorithms and Methods Track) must be uploaded in final form to the ION's Abstract Management Portal (AMP) by July 15. Papers not received in final form by July 15, will not be eligible for peer review.

The Author's Kit (revised for this year) with all necessary information for authors is available online at the GNSS+ Author Resource Center at: http://www.ion.org/gnss/author-resource-center.cfm. This provides all the information you need to prepare your paper for submission, and to create a dynamic presentation at your session. The Author Resource Center includes:

- Important Dates and Deadlines
- Speaker Breakfast Information (attendance is mandatory)
- Presentation Instructions
- Paper Preparation Instructions for Compliant Files
- Instructions for Uploading Your Final Paper Electronically
- Helpful Tips on Promoting Your Presentation
- Forms, Documents and Templates

Your completed manuscript is due no later than August 22, 2014. Corrected manuscripts will be accepted through September 22, 2014. Papers submitted after September 22 will not be accepted.

You are encouraged to contact your session chairs, preferably by e-mail, at your earliest opportunity. Please keep them updated on your status; they are your first points of contact for any questions you might have. If for any reason you are not able to make contact with your session chair, please do not hesitate to contact me.

Best Regards,
Miriam Lewis
ION Author Liaison
Phone: 703-366-2723
E-mail: meetings@ion.org

Amir Khodabandeh

Subject: GNSS+ 2014 Paper - Recommended for NAVIGATION

From: Miriam Lewis [mailto:mlewis@ion.org]
Sent: Tuesday, 4 November 2014 3:02 AM
To: Amir Khodabandeh
Subject: GNSS+ 2014 Paper - Recommended for Consideration in NAVIGATION

Dear Mr. Khodabandeh,

A paper that you recently authored at the **GNSS+ 2014 Conference** last September in Tampa, Florida, entitled "**Do GNSS Parameters Always Benefit from Integer Ambiguity Resolution? A PPP-RTK Network Scenario**" was recommended/accepted by the Session Chairs for consideration in the ION journal NAVIGATION.

The Editor of NAVIGATION, Dr. Boris Pervan would like to invite you to submit your paper for potential publication. If you are interested, please enter your paper electronically at your earliest convenience at the following link: http://mc.manuscriptcentral.com/navigation Once entered into the system, your paper will go through the journal's normal peer review process. Please make sure the paper is formatted following NAVIGATION guidelines found on your left side of the sign in Navigation page. For your convenience, here is the link http://onlinelibrary.wiley.com/journal/10.1002/%28ISSN%292161-4296/homepage/ForAuthors.html Please let me know if you have any questions.

Best Regards,

Miriam Lewis
Program/Author Liaison & Executive Assistant
The Institute of Navigation
8551 Rixlew Lane, Ste. 360
Manassas, VA 20109
Office: 703-366-2723
Direct: 703-636-0580
Fax: 703-366-2724

Amir Khodabandeh

Subject: IAGS: Your manuscript entitled Single-Epoch GNSS Array Integrity: An Analytical Study

-----Original Message-----
From: em.iags.3e8.368996.53347545@editorialmanager.com
[mailto:em.iags.3e8.368996.53347545@editorialmanager.com] On Behalf Of Pascal Willis
Sent: Friday, 18 October 2013 10:56 PM
To: Amir Khodabandeh
Subject: IAGS: Your manuscript entitled Single-Epoch GNSS Array Integrity: An Analytical Study

CC: willis@ipgp.fr

*** PLEASE ACKNOWLEDGE RECEIPT TO willis@ipgp.fr *** DO NOT USE REPLY

PW/IAGS 13.1341

Ref.: Ms. No. IAGS-D-13-00016
Single-Epoch GNSS Array Integrity: An Analytical Study International Association of Geodesy Symposia

Dear Mr. Khodabandeh,

Reviewers have now commented on your paper. You will see that they are advising that you revise your manuscript.

I then invite you to prepare and submit a revision.

For your information, a major revision means that your future revised manuscript will be sent back with the rebuttal letter to at least one of the reviewers.

The reviewers' comments can be found at the end of this email or can be accessed by following the provided link.

This is your login information:
Your username is: Amirlio
Your password is: 314271brain

When revising your work, please submit a list of changes or a rebuttal against each point which is being raised when you submit the revised manuscript.

Your revision is due by 17-11-2013.

To submit a revision, go to http://iags.edmgr.com/ and log in as an Author. You will see a menu item called 'Submissions Needing Revision'. You will find your submission record there.

Yours sincerely

Pascal Willis, Ph.D.-habil.
Editor-in-Chief
International Association of Geodesy Symposia

Amir Khodabandeh

From: em.iags.3e8.37861b.03d591c7@editorialmanager.com on behalf of Pascal Willis <willis@ipgp.fr>
Sent: Monday, 2 December 2013 9:21 PM
To: Amir Khodabandeh
Subject: IAGS: Your manuscript entitled Single-Epoch GNSS Array Integrity: an Analytical Study

CC: willis@ipgp.fr

PW/IAGS 13.1909

Ref.: Ms. No. IAGS-D-13-00016R1
Single-Epoch GNSS Array Integrity: an Analytical Study International Association of Geodesy Symposia

Dear Mr. Khodabandeh,

I am pleased to inform you that your work has now been accepted for publication in International Association of Geodesy Symposia.

Thank you for submitting your work to this journal.

With kind regards

Pascal Willis, Ph.D.-habil.
Editor-in-Chief
International Association of Geodesy Symposia